BIOACTIVE COMPOUNDS WITH POTENTIAL MEDICINAL PROPERTIES DERIVED FROM FUNGI: RECENT AND FUTURE DEVELOPMENTS IN MICROBIAL BIOTECHNOLOGY

EDITED BY: Paola Angelini, Ahmed M. Abdel-Azeem and Carolina Elena Girometta

PUBLISHED IN: Frontiers in Microbiology and Frontiers in Bioengineering and Biotechnology

frontiers Research Topics

ISSN 1664-8714
ISBN 978-2-88974-566-1
DOI 10.3389/978-2-88974-566-1

About Frontiers

Frontiers is more than just an open-access publisher of scholarly articles: it is a pioneering approach to the world of academia, radically improving the way scholarly research is managed. The grand vision of Frontiers is a world where all people have an equal opportunity to seek, share and generate knowledge. Frontiers provides immediate and permanent online open access to all its publications, but this alone is not enough to realize our grand goals.

Frontiers Journal Series

The Frontiers Journal Series is a multi-tier and interdisciplinary set of open-access, online journals, promising a paradigm shift from the current review, selection and dissemination processes in academic publishing. All Frontiers journals are driven by researchers for researchers; therefore, they constitute a service to the scholarly community. At the same time, the Frontiers Journal Series operates on a revolutionary invention, the tiered publishing system, initially addressing specific communities of scholars, and gradually climbing up to broader public understanding, thus serving the interests of the lay society, too.

Dedication to Quality

Each Frontiers article is a landmark of the highest quality, thanks to genuinely collaborative interactions between authors and review editors, who include some of the world's best academicians. Research must be certified by peers before entering a stream of knowledge that may eventually reach the public - and shape society; therefore, Frontiers only applies the most rigorous and unbiased reviews.
Frontiers revolutionizes research publishing by freely delivering the most outstanding research, evaluated with no bias from both the academic and social point of view. By applying the most advanced information technologies, Frontiers is catapulting scholarly publishing into a new generation.

What are Frontiers Research Topics?

Frontiers Research Topics are very popular trademarks of the Frontiers Journals Series: they are collections of at least ten articles, all centered on a particular subject. With their unique mix of varied contributions from Original Research to Review Articles, Frontiers Research Topics unify the most influential researchers, the latest key findings and historical advances in a hot research area! Find out more on how to host your own Frontiers Research Topic or contribute to one as an author by contacting the Frontiers Editorial Office: frontiersin.org/about/contact

BIOACTIVE COMPOUNDS WITH POTENTIAL MEDICINAL PROPERTIES DERIVED FROM FUNGI: RECENT AND FUTURE DEVELOPMENTS IN MICROBIAL BIOTECHNOLOGY

Topic Editors:
Paola Angelini, University of Perugia, Italy
Ahmed M. Abdel-Azeem, Suez Canal University, Egypt
Carolina Elena Girometta, University of Pavia, Italy

Citation: Angelini, P., Abdel-Azeem, A. M., Girometta, C. E., eds. (2022). Bioactive Compounds With Potential Medicinal Properties Derived From Fungi: Recent and Future Developments in Microbial Biotechnology. Lausanne: Frontiers Media SA. doi: 10.3389/978-2-88974-566-1

Table of Contents

frontiers in Microbiology

EDITORIAL
published: 01 February 2022
doi: 10.3389/fmicb.2022.837586

Editorial: Bioactive Compounds With Potential Medicinal Properties Derived From Fungi: Recent and Future Developments in Microbial Biotechnology

Paola Angelini[1]*, *Ahmed M. Abdel-Azeem*[2] and *Carolina Elena Gorometta*[3]*

[1] Department of Chemistry, Biology and Biotechnology, University of Perugia, Perugia, Italy, [2] Department of Botany and Microbiology, Faculty of Science, Suez Canal University, Ismailia, Egypt, [3] Department of Earth and Environmental Sciences (DSTA), University of Pavia, Pavia, Italy

Keywords: amazonian fungi, Ascomycota, Basidiomycota, biological activities, Chinese medicinal preparation, crude extract, marine fungi, secondary metabolites

Editorial on the Research Topic

Editorial: Bioactive Compounds With Potential Medicinal Properties Derived From Fungi: Recent and Future Developments in Microbial Biotechnology

OPEN ACCESS

Edited and reviewed by:
Eric Altermann, AgResearch Ltd., New Zealand

***Correspondence:**
Paola Angelini
paola.angelini@unipg.it
Carolina Elena Gorometta
carolinaelena.gorometta@unipv.it

Specialty section:
This article was submitted to Microbiotechnology, a section of the journal Frontiers in Microbiology

Received: *16 December 2021*
Accepted: *06 January 2022*
Published: *01 February 2022*

Citation:
Angelini P, Abdel-Azeem AM and Gorometta CE (2022) Editorial: Bioactive Compounds With Potential Medicinal Properties Derived From Fungi: Recent and Future Developments in Microbial Biotechnology. Front. Microbiol. 13:837586. doi: 10.3389/fmicb.2022.837586

The continuous exploration of new sources for drugs and bioactive compounds has never ceased to delve into the fungal kingdom. Indeed, it has entered profoundly into the widest range of environments on Earth as well as into the chemical structure of compounds and the molecular mechanisms underlying metabolism regulation.

It can be demonstrated once more that varying points of view within the scientific community can still be held whilst retaining consistency along several research paths, allowing the gradual convergence in obtaining solutions.

The work by Ding et al. is a perfectly serendipitous combination of molecular biology, organic chemistry, and plant pathology that starts from the transcription regulation to discover new compounds with antifungal activities. In this study we find a focus on polyketides, which is the most represented category of the secondary metabolism in Ascomycota unlikely terpenoids, whose deputed portion of the genome is significantly larger in Basidiomycota. However, Ascomycota have to date included the major model organisms in this concern, thus Shi et al. provide us with the discovery and characterization of six new tremulane sesquiterpenoids from *Pseudogymnoascus* sp. showing good potential against human cancer cell lines. Analogously, Ge et al. deal with new enantiomers of a NOR-bisabolane derivative and two new phthalides by *Penicillium chrysogenum* and suggest applications of these compounds against some important fungal phytopathogens. Further on, Pan et al. report four new indole-terpenoids with anti-inflammatory activities from *Penicillium* sp., and find a species from the poorly known Genus *Pseudogymnoascus* besides the model-species for biosynthetic pathways *P. chrysogenum*, to witness that new frontiers in mycology are to be conquered in both.

Several works in this issue share another common feature: their fungal sources come from the sea. "Marine" fungi are indeed related to different habitats. They can be isolated from the sea but actually their life is not actually dependent on this environment. However, in the sea they find peculiar niches which are likely to stimulate the adaptation of unknown strains against a range of bacteria including human pathogens. Thus, Wang et al. report a sponge-associated *Cymostachys* sp.

from a marine mesophotic zone; the above mentioned Ge et al. have also achieved their strain from a marine environment as well as Jenssen et al., who also tested their strain against several human melanoma, hepatocellular carcinoma, and non-malignant lung fibroblast cell lines. This latter work introduces us to fungi which are to be regarded as more strictly related to the marine environments around the world. Further on, Pang et al. report the antibacterial activity of a *Penicillium* strain from tides.

In addition to the sea, the endophytic niche is another enormous and still widely unexplored source of fungal diversity and bioactive resources. Endophytes are difficult and sometimes ambiguous to define, creeping in a shadow zone among saprotrophism, mutualism, and potential parasitism—opportunism, basically. The endophytism topic meets the marine fungi topic when dealing with fungi hosted by algae, as Sahoo et al. have shown. Another topic that merits attention is the great potential of chitosan in biomaterials. Fungi are a major source of chitosan that is easily obtained from chitin; here, Li et al. describe the joint application of chitosan-based hydrogel and algal extracts to treat cutaneous wounds in mice without inducing excessive inflammatory response.

Returning to the endophytes, besides the mere search for new bioactive compounds, the study of fungal metabolites contributes to understanding the complex relationship between host and fungus as a stepping stone to improve the bioactivity itself, as reported by Charria-Girón et al. Moreover, this study highlights the importance of the valorization and preservation of the biodiversity in fragile habitats such as the tropical montane rainforest in Colombia.

The endophytism topic also entails the topic of the rhizosphere fungal community, including, according to Ding et al., genera like *Trichoderma*. Zhang et al. consider *Trichoderma* "a treasure house of structurally diverse secondary metabolites," since it is an evergreen model for studies about fungal metabolite diversity. The plethora of bioactive compounds from *Trichoderma* species has current and potential applications in medicine and toxicology as well as in agriculture, phytopathology, and other fields.

The invisible role of fungi in the environmental equilibrium, even against invasive allochthonous parasites, is brought to our attention by Rodrigues de Oliveira et al. through their work on the larvicidal activities of fungal strains isolated from water against *Aedes aegypti* in the Amazonas. From outdoor water to controlled fermentation tanks for traditional or innovative products, this study reminds us that interspecific and intraspecific metabolic features produce a unique profile in the substrate. Simply due to the potential bioactivity of its component, such a profile must be handled very carefully. Thus, Xie et al. describe the evolution in the community participating in the fermentation process of the Chinese medicinal preparation of "Lianzhifan solution" as well as the evolution of its chemical profile. Notably, two species deserving particular attention are pointed out as key actors in the fermentation: *Aspergillus niger* and *Penicillium expansum*, which are typically double-edged swords due to their biotechnological as well as toxicological potential.

When dealing with bioactive compounds, the basic aims of the work may be multiple: research, separation, and structural characterization of new compounds; qualitative and quantitative exploration of the bioactivity on specific targets, without exact discrimination of the bioactive molecules acting on these; and both the matters together.

In this issue, four articles rely on the latter approach by either dealing with bacteria, virus, other competitor fungi, or animal parasites. For example, Grey et al. deal with the need of new antibiotics against *Mycobacteria*—also including *Mycobacterium tuberculosis* complex—by applying a screening of fungal species, even phylogenetically distant from each other, which may show antibacterial activity. In order to achieve this, the authors propose a medium-throughput bioluminescence-based assay, without regard to the exact identification of the molecule(s) responsible for the desired result, at least in this stage of the work. It is evident in such an approach that the fungal bioactivity is often the result of a wide range of compounds acting altogether. Above all, the challenge of fungal metabolites to analytics and structural chemistry is notable and full of technical difficulties. When they are not fully known, these compounds are often unknown to the libraries and their standards are really difficult to achieve. The same species can shift from certain metabolites to others depending on the growth stage and, of course, on the strain. The frontier is therefore still wide and open for scientists. In this issue, seven articles brought their contribution to the identification of new molecules. The readers will therefore find inspiration from the innovative combinations of methods for a multi-focus approach: HPLC and spectroscopic and spectrometric data furtherly supported by X-ray crystallography for Wang et al.; high resolution mass spectrometer (HRMS), NMR, and electronic circular dichroism (ECD) for Ding et al.; ECD spectra are the striking tool for Shi et al. as well as for Pan et al. and Pang et al. to confirm the potential of this technique; Ge et al. also adopt ECD besides 1D/2D NMR and ESI-MS; quite similarly, Jenssen et al. work by 1D/2D NMR and HRMS.

Last but not least, the challenge posed by the research and characterization of bioactive compounds cannot cast a shadow over another apparently minor topic that is far from being an aristocratic and sterile issue: the exact identification and taxonomic placement of the species and strains under examination. This is another story made of non-negligible endeavor and workload; no surprise if one cannot focus on both simultaneously. This expertise is often different from the one of bioactive compound explorers. This is not a limitation, this is just a confirmation of the African proverb: "If you want to go fast, go alone. If you want to go far, go together."

AUTHOR CONTRIBUTIONS

PA first conceived and outlined the general topics of this special issue as well as the draft of the editorial. PA, CG, and AA-A contributed together to select and tailor the topics, to actively manage the papers as guest editors, that is by overseeing the special topic, to contribute to the editorial revision and final approval, and contributed to the writing of this

editorial. All authors contributed to the article and approved the submitted version.

ACKNOWLEDGMENTS

The editors wish to thank all the reviewers who kindly consented to give us part of their working time to make this issue possible by carefully examining one or more papers.

Conflict of Interest: The authors declare that the research was conducted in the absence of any commercial or financial relationships that could be construed as a potential conflict of interest.

Publisher's Note: All claims expressed in this article are solely those of the authors and do not necessarily represent those of their affiliated organizations, or those of the publisher, the editors and the reviewers. Any product that may be evaluated in this article, or claim that may be made by its manufacturer, is not guaranteed or endorsed by the publisher.

frontiers in Microbiology

ORIGINAL RESEARCH
published: 23 December 2020
doi: 10.3389/fmicb.2020.622785

Overexpression of Global Regulator Talae1 Leads to the Discovery of New Antifungal Polyketides From Endophytic Fungus *Trichoderma afroharzianum*

Zhuang Ding[1], Xiao Wang[1], Fan-Dong Kong[2], Hui-Ming Huang[3], Yan-Na Zhao[1], Min Liu[1], Zheng-Ping Wang[1] and Jun Han[1]*

[1]Institute of BioPharmaceutical Research, Liaocheng University, Liaocheng, China, [2]Hainan Key Laboratory for Research and Development of Natural Product From Li Folk Medicine, Institute of Tropical Bioscience and Biotechnology, Chinese Academy of Tropical Agriculture Sciences, Haikou, China, [3]School of Life Sciences, Liaocheng University, Liaocheng, China

OPEN ACCESS

Edited by:
Paola Angelini, University of Perugia, Italy

Reviewed by:
Weaam Ebrahim, Mansoura University, Egypt
Liwei Wang, Hangzhou Normal University, China
Chunyuan Li, South China Agricultural University, China

***Correspondence:**
Zhuang Ding
dingzhuang@lcu.edu.cn

Specialty section:
This article was submitted to Microbiotechnology, a section of the journal Frontiers in Microbiology

Received: *29 October 2020*
Accepted: *04 December 2020*
Published: *23 December 2020*

Citation:
Ding Z, Wang X, Kong F-D, Huang H-M, Zhao Y-N, Liu M, Wang Z-P and Han J (2020) Overexpression of Global Regulator Talae1 Leads to the Discovery of New Antifungal Polyketides From Endophytic Fungus Trichoderma afroharzianum. Front. Microbiol. 11:622785. doi: 10.3389/fmicb.2020.622785

Transcription regulation caused by global regulators exerts important effects on fungal secondary metabolism. By overexpression of the global regulator Talae1 in a *Ficus elastica*-associated fungus *Trichoderma afroharzianum*, two structurally new polyketides (**1** and **2**) that were newly produced in the transformant were isolated and identified. Their structures, including the absolute configurations, were elucidated through a combination of high resolution mass spectrometer (HRMS), NMR, and electronic circular dichroism (ECD) calculations. The growth inhibitory activities of compounds **1** and **2** were evaluated against four bacteria and six plant-pathogenic fungi. Compound **1** showed the highest antifungal activity against *Botrytis cinerea* and *Fusarium oxysporum* f. sp. *nicotianae* with MIC of 8 μg/ml. To the best of our knowledge, this is the first study to report on the application of the global regulator in *T. afroharzianum* to activate the biosynthesis of bioactive secondary metabolites.

Keywords: global regulator, LaeA, polyketides, antifungal activity, endophytic fungi, *Trichoderma afroharzianum*

INTRODUCTION

The genus *Trichoderma* is a ubiquitous fungal group comprising of more than 340 species (Zeng and Zhuang, 2019). Some *Trichoderma* species are widely used in agriculture as biological control agents to prevent the growth of other phytopathogenic fungi and to promote the development of crop plants (Benítez et al., 2004; Reino et al., 2008). The genus *Trichoderma* has been reported to be an excellent producer of bioactivity secondary metabolites (SMs). Several hundreds of SMs, including polyketides, non-ribosomal peptides, terpenoids, and alkaloids, have been identified and isolated in *Trichoderma* species and strains from different environments (Reino et al., 2008; Degenkolb et al., 2015; Li et al., 2019). Some of the SMs are considered to play a significant role in stimulating plant growth or providing defense against plant pathogens (Vinale et al., 2008).

Recent genome sequencing of many fungal species has revealed that most of the biosynthetic gene clusters (BGCs) are cryptic or lowly expressed under general culture conditions

(Rutledge and Challis, 2015; Wu et al., 2020). Similarly, although diverse metabolites have been discovered from the genus *Trichoderma*, genome sequencing has revealed that there are more BGCs than we have discovered (Mukherjee et al., 2013; Zeilinger et al., 2016), suggesting that the potential of *Trichoderma* fungi to produce more undetected metabolites has hidden and needs to be activated.

To activate the cryptic biosynthetic potential and reveal more SMs, several strategies, such as ribosome engineering, transcriptional regulation, epigenetic perturbation, and heterologous expression, have been developed (Wiemann and Keller, 2014; Wu et al., 2016). Besides, the manipulation of global transcriptional regulators is also reported to be a feasible strategy for the activation of cryptic BGCs. The LaeA protein was first discovered as a global regulator of secondary metabolism in *Aspergillus nidulans* (Bok and Keller, 2004). Because of sequence similarity to histone methyltransferases, LaeA may achieve global transcriptional regulation by influencing chromatin modification (Brakhage, 2013). Reyes-Dominguez et al. (2010) reported that LaeA reversed the repressive chromatin structure caused by some negative regulators, resulting in the activation of BGCs in *A. nidulans*. Furthermore, LaeA is conserved in filamentous fungi, and thus its gene homologs are found in other filamentous fungi including *Aspergillus carbonarius* (Linde et al., 2016), *Aspergillus fumisynnematus* (Hong et al., 2015), *Alternaria alternata* (Estiarte et al., 2016), *Fusarium verticillioides* (Butchko et al., 2012), *Monascus ruber* (Liu et al., 2016), and *Penicillium chrysogenum* (Kosalková et al., 2009) and *Penicillium brocae* (Wang et al., 2020). Numerous studies have also determined that the presence of LaeA facilitates the expression of multiple BGCs. For instance, Jiang et al. (2016) reported that overexpression of *laeA* in *Chaetomium globosum* upregulated the expression of chaetoglobosin BGC and led to the discovery of a new cytochalasan. Yu et al. (2019) reported the discovery of a series of sorbicillinoids including two new ones by overexpression of laeA in *Penicillium dipodomyis*. Thus, overexpression of LaeA is considered as a useful strategy in activating silent biosynthetic pathways and promoting the discovery of novel SMs in fungi.

Endophytic fungi are increasingly recognized as a significant reservoir of bioactive metabolites (Chandra, 2012; Wu et al., 2016). Due to the absence of a simulated ecological environment, the BGCs of endophytic fungi are not effectively expressed under standard laboratory conditions, thus reducing the probability of detecting new SMs (Mao et al., 2015). In our previous research work, the endophytic fungus *Trichoderma afroharzianum* Fes1712 isolated from rubber tree *Ficus elastica* was shown to produce novel isocoumarin analogues (Ding et al., 2019). To further activate its chemical potential, we constructed a *laeA*-like gene (*talae1*) overexpression transformant of *T. afroharzianum* and investigated the effect of *laeA*-like gene overexpression on secondary metabolic profile. Chemical analysis of SMs produced by the overexpression strain led to the discovery of two new polyketides (**1**, **2**). In this study, structural elucidation and biological evaluation of the two new compounds are presented.

MATERIALS AND METHODS

General Experimental Procedures

DNA restriction enzymes were purchased from Transgen Biotech Co., LTD (Beijing, China). Polymerase chain reaction (PCR) was performed using TransStart® Fastpfu Fly DNA Polymerase (Transgen Biotech, Beijing, China). Optical rotations were measured on a P-1020 digital polarimeter (JASCO Corporation, Tokyo, Japan). ECD spectra were recorded on a JASCO J-815 spectropolarimeter (JASCO Corporation). UV spectra were recorded on Waters 2487 (Waters Corporation, Milford, MA, United States). HRESIMS and ESIMS spectra were measured on Thermo Scientific LTQ Orbitrap XL mass spectrometer (Thermo Fisher Scientific). NMR spectra were recorded on Agilent 500 MHz DD2 spectrometer (Agilent Technologies Inc., Santa Clara, CA, United States). Semi-preparative HPLC was performed using a YMC Pack ODS-A column (250 × 10 mm, 5 μm, 3 ml/min, YMC Co., Ltd., Kyoto, Japan). Column chromatography was performed on silica gel (200–300 mesh, Qingdao Marine Chemical Inc., Qingdao, China) and Sephadex LH-20 (GE Healthcare, Uppsala, Sweden).

Fungal Material

The fungal wild strain Fes1712 (WT) was originally isolated from fresh leaves of *F. elastica* collected from Liaocheng University Arboretum, Liaocheng, Shandong Province of China and identified as *T. afroharzianum* based on *tef1* and *rpb2* sequences (Chaverri et al., 2015; **Supplementary Figure S1**).

Generation of the OE::Talae1 Strain

Because the genomic sequence of *T. afroharzianum* Fes1712 is currently unknown, the genomic sequence of *Trichoderma harzianum* CBS 226.95 was used for gene selection and initial primer design. A *laeA*-like gene was identified using Local-Blast with *A. nidulans* LaeA gene (AN0807) as the query. The two pairs of specific primers, including two inner primers (Ta85012iF/R) with terminal XbaI and EcoRV restriction sites, were used as primers of the nested-PCR amplification of *talae1* from genomic DNA of strain Fes1712. The PCR product of the *talae1* gene was digested using endonucleases and inserted into the same restriction site of the pZeo vector (Tang et al., 2017) to create pZeo-talae1 (**Supplementary Figure S2**). The *talae1* gene from strain Fes1712 was sequenced by Sangon Biotech (Shanghai, China) and deposited in the GenBank Database under the accession numbers MT313929. The overexpression vector pZeo-talae1 comprised of a continuous expression cassette, including the PgpdA promoter, *talae1* gene, and TtrpC terminator, and two selection markers (ampicillin resistance gene for selection of *Escherichia coli* strain and bleomycin resistance gene for the Fes1712 transformant). The recombinant vector was transformed into *E. coli* strain Trans1-T1 to extract plasmids for transformation. The extracted plasmids were then transferred into WT yielding a transformant with overexpressed *talae1* gene (*OE::Talae1*) by PEG-mediated protoplast transformation (Tang et al., 2017), while the control transformant was also generated using a vacant pZeo.

The transformants were selected and purified in the presence of bleomycin. The genotype of the overexpression transformant was confirmed by diagnostic PCR (**Supplementary Figure S3**). The oligonucleotide sequences for PCR primers are presented in **Supplementary Table S1**.

Culture, Fermentation, and Extraction

For SMs production, the overexpression transformant and control transformant were cultured on PDA medium (PDA, 20% potato, 2% dextrose, and 1.5% agar) at 28°C for 5 days. They were then inoculated into 1 L Erlenmeyer flasks, each containing 80 g of rice and 120 ml distilled water and incubated at 28°C under static conditions. After 15 days, the fermented substrate in each flask was broken using a disperser (T18, IKA, Germany) and extracted three times with 200 ml MeOH. The liquid layers were collected and evaporated to remove MeOH. The residual extract was suspended in H_2O and extracted three times with an equal volume of EtOAc. The EtOAc layers were separated and evaporated under reduced pressure to yield the solid extract.

Purification

The extract from the overexpression transformant (6.7 g) was applied on silica gel using a step gradient elution with petroleum ether−EtOAc (*v*/*v* 10:1, 5:1, 2:1, 1:1, 1:3) and EtOAc−MeOH (*v*/*v* 10:1, 3:1, 1:1, 0:1) to give nine fractions (Fr. 1–9). Fraction 7 was fractionated on MPLC (60–100% MeOH/H_2O, 45 min) to give five fractions (Fr. 7.1–7.5). Fraction 7.3 and Fraction 7.4 were further purified by semipreparative HPLC eluting with 70% MeOH−H_2O to obtain compound **1** (9.0 mg) and **2** (4.5 mg).

Compound **1**: white amorphous powder; $[\alpha]^{20}_{D}$ − 36.1 (*c* 0.10, MeOH); ECD (MeOH) λ_{max} (Δε) 304 (+2.01), 233 (−10.55) nm; UV (MeOH) λ_{max} (log ε) 299 (2.01), 210 (3.14) nm; positive HR-ESI-MS (*m/z*): 263.1282 $[M + H]^+$ (calcd. for $C_{15}H_{19}O_4$, 263.1283; **Supplementary Figure S5**); ^1H and ^{13}C NMR data, see **Table 1** and **Supplementary Figures S6–S11**.

Compound **2**: white amorphous powder; $[\alpha]^{20}_{D}$ − 44.2 (*c* 0.10, MeOH); ECD (MeOH) λ_{max} (Δε) 304 (+2.52), 235 (−9.74) nm; UV (MeOH) λ_{max} (log ε) 300 (2.10), 210 (3.15) nm; positive HR-ESI-MS (*m/z*): 277.1435 $[M + H]^+$ (calcd. for $C_{16}H_{21}O_4$, 277.1439; **Supplementary Figure S12**); ^1H and ^{13}C NMR data, see **Table 1** and **Supplementary Figures S13–S18**.

Bioactivity Assay

Antimicrobial activities of the isolated compounds were evaluated against four bacteria (*Bacillus subtilis* CMCC 63501, *E. coli* CMCC 44102, *Pseudomonas aeruginosa* CMCC 10104, and *Staphylococcus aureus* CMCC 26003) and six plant-pathogenic fungi (*A. alternata* ACCC 36110, *Botrytis cinerea* ACCC 36028, *Colletotrichum lagenarium* ACCC 30016, *Fusarium oxysporum* f. sp. *nicotianae* TRICAAS 0101, *Gaeumannomyces graminis* var. *graminis* TRICAAS 0191, and *Thielaviopsis basicola* TRICAAS 0207) using the 96-well plate microdilution method (Zhang et al., 2019).

TABLE 1 | ^1H and ^{13}C NMR data of the compounds **1** and **2** (500 MHz in CD_3OD); δ in p.p.m., *J* in Hz.

Position	Compound (1)		Compound (2)	
	δ_C, type	δ_H, (*J* in Hz)	δ_C, type	δ_H, (*J* in Hz)
1	106.8, CH	6.29, *s*	106.6, CH	6.35, *s*
2	154.0, Cq		154.0, Cq	
3	111.8, Cq		112.0, Cq	
4	153.5, Cq		153.6, Cq	
5	114.9, Cq		115.3, Cq	
6	134.1, Cq		131.6, Cq	
7	76.6, CH	5.33, *s*	85.7, CH	4.98, *s*
8	199.1, Cq		197.6, Cq	
9	122.6, CH	6.12, *d*, (15.3)	122.7, CH	6.17, *d*, (15.3)
10	143.5, CH	7.24, *dd*, (15.3, 10.5)	143.6, CH	7.23, *dd*, (15.3, 10.6)
11	130.0, CH	6.21, *dd*, (15.5, 10.5)	130.0, CH	6.21, *dd*, (15.5, 10.6)
12	141.3, CH	6.25, *dq*, (15.5, 6.4)	141.3, CH	6.25, *dq*, (15.5, 6.2)
13	17.4, CH_3	1.81, *d*, (6.4)	17.4, CH_3	1.82, *d*, (6.2)
14	7.6, CH_3	2.06, *s*	7.6, CH_3	2.06, *s*
15	10.2, CH_3	2.16, *s*	10.3, CH_3	2.13, *s*
7-OCH_3			55.6, CH_3	3.30, *s*

The phytopathogenic fungi were provided and deposited by the Tobacco Research Institute of the Chinese Academy of Agricultural Sciences, Qingdao, China. The tested compounds were prepared as 2-fold dilutions with DMSO and added (10 μl) to each well, containing the spore suspension (10^6 CFU/ml, 10 μl) and culture medium (180 μl, Luria-Bertani medium for bacteria, potato dextrose medium for fungi), to obtain a final concentration of between 512 μg/ml to 1 μg/ml. After adequate mixing, the assay plates were incubated in the dark for 24–72 h at 30°C. The minimal inhibitory concentration (MIC) was determined as the lowest concentration at which no growth of pathogen was observed. Chloramphenicol and prochloraz were used as positive controls for antibacterial and antifungal assays, respectively. All tests were performed in triplicate.

RESULTS AND DISCUSSION

Genome Mining and Overexpression of Talae1

A *laeA*-like gene was identified in the genomic sequence of *T. harzianum* CBS 226.95 using Local-blast. In the genomic sequence of *T. harzianum* CBS 226.95, the *laeA*-like gene is designated as M431DRAFT_85012 (DOE Joint Genome Institute). Subsequently, we designed special primers to clone *talae1* ORF from the genomic DNA of strain Fes1712 *via* nested-PCR. The obtained PCR fragment was 1,228 bp in size, and the predicted coding sequence was 999 bp, encoding a 332-residue polypeptide. Sequence analysis *via* InterProScan indicated that *talae1* protein was an S-adenosyl-L-methionine-dependent methyltransferase, which is consistent with the function of LaeA. BLAST analysis indicated that Talae1 protein had 73.9, 68.1, 57.1, and 56.8% sequence identity to Lae1 (XP_006966726.1) of *Trichoderma reesei*

(Seiboth et al., 2012), Lae1 (XP_013938600.1) of *Trichoderma atroviride* (Aghcheh et al., 2013), LaeA (XP_018233436.1) of *F. oxysporum* (López-Berges et al., 2014), and Lae1 (XP_018742755.1) of *F. verticillioides* (Butchko et al., 2012), respectively (**Figure 1**).

To examine the effect of *talae1* gene overexpression on secondary metabolism in strain Fes1712, *OE::Talae1* transformant and control transformant were constructed and cultured on rice medium at 28°C for 15 days under static conditions. Real time PCR was performed to determine the difference in the transcriptional levels of *talae1* gene between the *OE::Talae1* and control transformants. Results indicated that the transcriptional level of *talae1* gene was 7.7-fold upregulated in *OE::Talae1* transformant (**Supplementary Figure S4**). The fermentation products were extracted and analyzed using HPLC. *OE::Talae1* transformant showed an obvious change in the secondary metabolic profile, evidenced by the emergence of several new peaks (**Figure 2**), compared with that of the control transformant. Purification of the new peaks led to the isolation of two relatively high-yield compounds **1** and **2** (**Figure 3**).

Structure Elucidation of the New Compounds

Compound **1** was obtained as a white amorphous powder. The molecular formula $C_{15}H_{18}O_4$ was determined by the positive HRESIMS *m/z* 263.1282 ($[M + H]^+$, calcd. 263.1283), indicating 7 degrees of unsaturation. The ^{1}H NMR spectrum of **1** revealed signals for five olefinic protons (δ_H 7.24, 6.29, 6.25, 6.21, and 6.12), an oxymethine (δ_H 5.33), and three methyl groups (δ_H 2.16, 2.06, and 1.81). While the ^{13}C NMR, DEPT, and HSQC spectra exhibited the presence of 15 carbon resonance signals, including one conjugated ketone carbonyl (δ_C 199.1), nine olefinic or aromatic carbons with five protonated, one oxymethine ($\delta_{C/H}$ 76.6/5.33), and three methyls ($\delta_{C/H}$ 17.4/1.81, 10.2/2.16, and 7.6/2.06; **Table 1**). Analysis of the 2D NMR data of **1** revealed contiguous COSY correlations extending from H-9 to

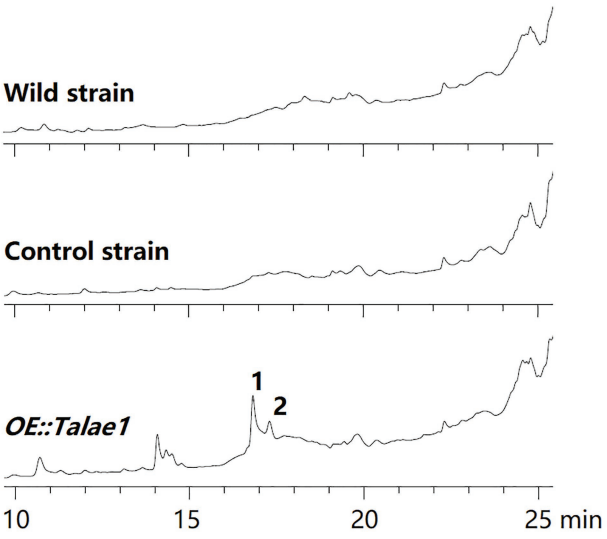

FIGURE 2 | Comparative analysis of secondary metabolite HPLC profiles of *OE::Talae1* and control transformants. The numbers represent the compounds isolated from the *OE::Talae1* transformant. Detection was carried out at 210 nm.

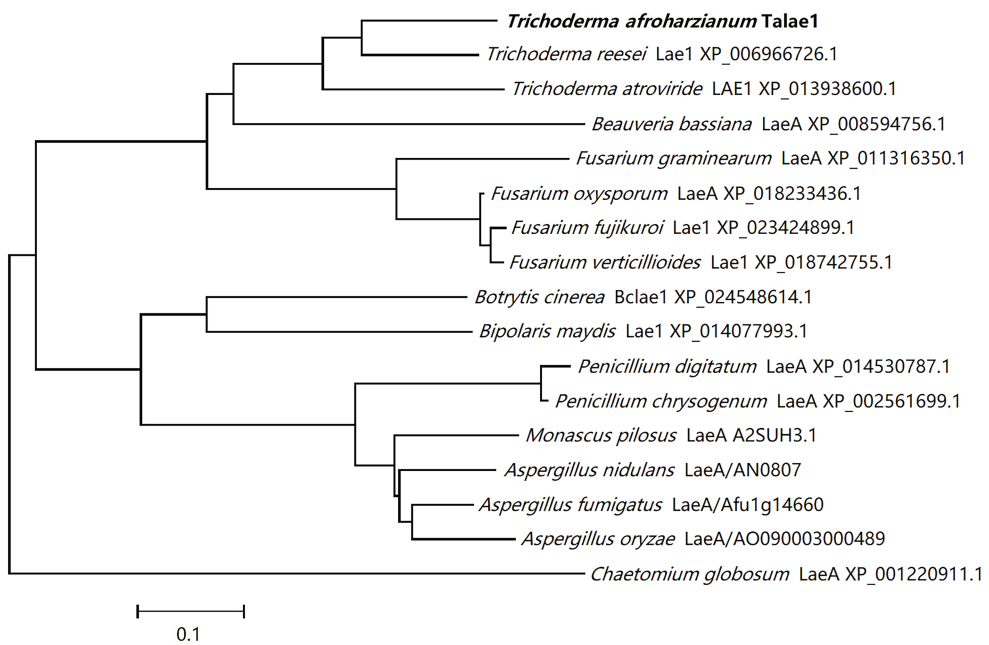

FIGURE 1 | Phylogenetic tree analyses of Talae1 and its homologs from different species. Branch lengths are in proportion to distance.

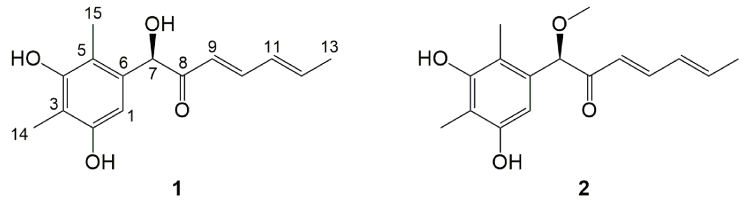

FIGURE 3 | Structures of compounds **1** and **2** from the *OE::Talae1* transformant.

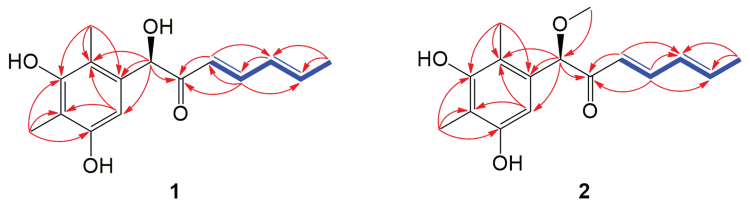

FIGURE 4 | Key COSY (bold blue lines) and HMBC (red arrows) correlations of the compounds **1** and **2**.

H-13, as well as heteronuclear multiple bond correlation (HMBC) correlation from H-10, H-9, and the oxymethine proton H-7 to C-8 carbonyl, indicating the presence of a 1-hydroxyhepta-3,5-dien-2-one side chain (**Figure 4**). The large *J* values of H-9/H-10 (*J* = 15.3 Hz) and H-11/H-12 (*J* = 15.5 Hz) revealed the *E*-configuration of the Δ^{10} and Δ^{12} double bonds (**Figure 4**). HMBC correlations from H_3-15 to C-5, C-6, and the hydroxylated aromatic carbon C-4, from H_3-14 to C-3 and the two hydroxylated aromatic carbons C-4 and C-2, and from the aromatic proton H-1 to C-3 and C-5 collectively led to the construction of the penta-substituted benzene core structure of compound **1** as shown in **Figure 4**. The presence of C-6/C-7 linkage between the penta-substituted benzene core structure and the 1-hydroxyhepta-3,5-dien-2-one side chain was demonstrated by HMBC correlations from H-7 to C-1, C-5, and C-6. To determine the absolute configuration of C-7 in **1**, the ECD spectrum of **1** was calculated using the time-dependent density functional theory (TD-DFT) at the B3LYP/6-31 + G (d) level using the Gaussian 09 program (Frisch et al., 2009). The result showed that the experimental ECD spectrum of **1** was in good agreement with the calculated ECD spectrum of (7*R*)-**1** (**Figure 5**), designating the absolute configuration of C-7 as *R*. Thus, compound **1** was determined to be (*R*,3*E*,5*E*)-1-(3,5-dihydroxy-2,4-dimethylphenyl)-1-hydroxyhepta-3,5-dien-2-one.

Compound **2** was isolated as a white amorphous powder with the molecular formula $C_{16}H_{20}O_4$ determined based on HRESIMS (*m/z* 277.1413 $[M + H]^+$), with an additional CH_3 group compared to **1**. The 1D and 2D NMR data of compound **2** showed close similarity to those of **1**, with the only distinction attributable to the presence of a methoxy signal at $\delta_{H/C}$ 3.30/55.6 in **2** (**Table 1**). The key HMBC correlation from H_3-16 (δ 3.67) to the oxymethine carbon C-7 (δ 172.1) indicated that the hydroxyl group at C-7 in **1** was methylated in **2**. The absolute configuration of C-7 in **2** was determined to be similar

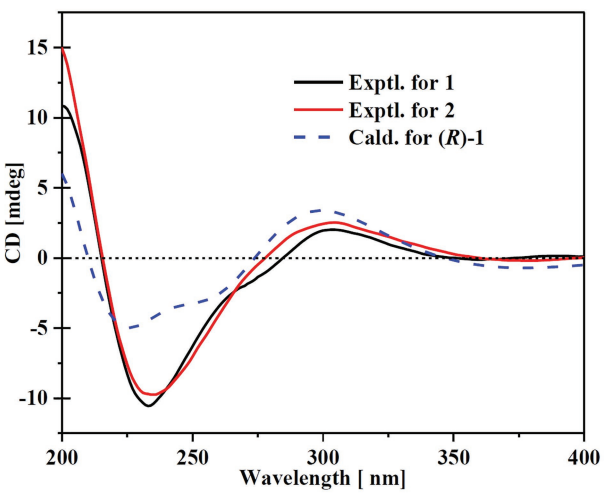

FIGURE 5 | Experimental ECD of the compounds **1** and **2** and the calculated spectrum for (7*R*)**-1**.

to that of **1** based on ECD spectra (**Figure 5**). Therefore, the structure of compound **2** was determined to be (*R*,3*E*,5*E*)-1-(3,5-dihydroxy-2,4-dimethylphenyl)-1-methoxyhepta-3,5-dien-2-one.

Plausible Biogenetic Pathways Proposed for 1 and 2

A plausible biosynthetic pathway for **1** and **2** is proposed as shown in **Figure 6**. The polyketide chain primed with one acetyl-CoA starter unit and six malonyl-CoA extender units was selectively enolized, hydroxylated, methylated, cyclized, and finally released as the intermediate **a** (Wu et al., 2019).

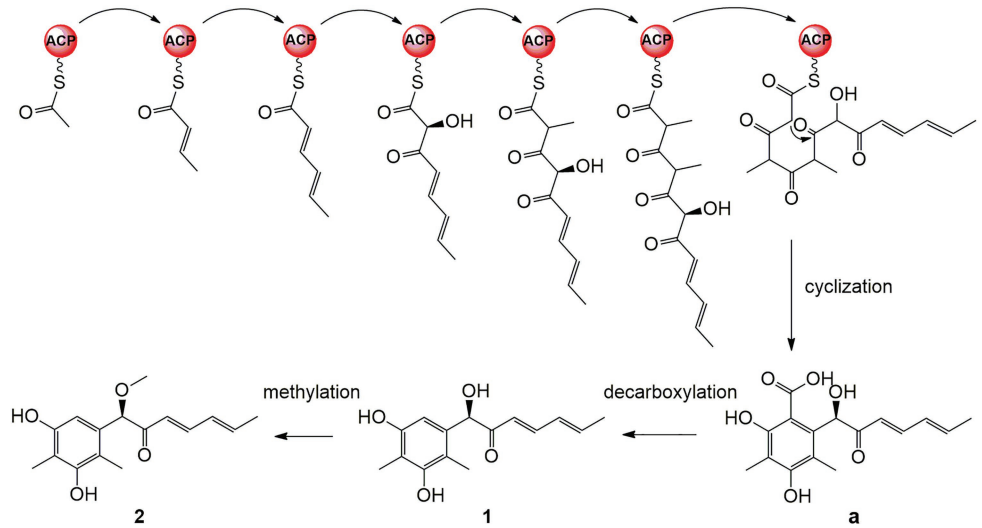

FIGURE 6 | Plausible biosynthetic pathway for **1** and **2**.

TABLE 2 | Antimicrobial activities of the compounds **1** and **2** (MIC, μg/ml).

Compound	Bacteria[a]				Fungi[b]					
	Bs	*Ec*	*Pa*	*Sa*	*Aa*	*Bc*	*Cl*	*Fo*	*Gg*	*Tb*
1	>256	256	256	>256	>256	8	32	8	>256	>256
2	>256	256	256	>256	>256	16	32	16	>256	>256
Ch[c]	2	1	4	2						
Pr[d]					16	8	16	8	4	8

[a]*Bs, Bacillus subtilis; Ec, Escherichia coli; Pa, Pseudomonas aeruginosa; Sa, Staphylococcus aureus.*

[b]*Aa, Alternaria alternata; Bc, Botrytis cinerea; Cl, Colletotrichum lagenarium; Fo, Fusarium oxysporum f. sp. nicotianae; Gg, Gaeumannomyces graminis var. graminis; Tb, Thielaviopsis basicola.*

[c]*Ch, positive control, chloromycetin.*

[d]*Pr, positive control, prochloraz.*

Compounds **1** and **2** are proposed to be generated by further decarboxylation and O-methylation (Shaw et al., 2015; Lebe and Cox, 2019).

Bioactivity Assay

The newly produced compounds **1** and **2** were evaluated for antifungal activity against four bacteria and six plant-pathogenic fungi were tested. As shown in **Table 2**, compounds **1** and **2** showed selective antifungal activity with MIC values ranging from 8 to 32 μg/ml. Compound **1** displayed the highest growth inhibitory activity with MIC values of 8, 8, and 32 toward *B. cinerea*, *F. oxysporum* f. sp. *nicotianae*, and *C. lagenarium*, respectively. The genus *Trichoderma* has been shown to produce numerous polyketides with various bioactivities (Reino et al., 2008; Harned and Volp, 2011). For instance, fungal species of the *Trichoderma* genus are known to be the main producers of sorbicillin family (Harned and Volp, 2011; Derntl et al., 2017), which are structurally similar to the compounds **1** and **2**. Reátegui et al. (2006) have reported antifungal activity of sorbicillin analogues against *Aspergillus flavus* and *Fusarium verticillioides*. Besides, the compounds **1** and **2** also showed weak antibacterial activity against Gram-positive bacteria *S. aureus*.

CONCLUSION

In summary, overexpression of the global regulator Talae1 upregulated the production of SMs in an endophytic fungus *T. afroharzianum*, and two new polyketides (**1** and **2**) were isolated and identified from overexpression transformant. These results indicate that the global regulator Talae1 is involved in secondary metabolic regulation of *T. afroharzianum* and affects the biosynthesis of a series of antifungal polyketides. This study also demonstrates that genetic manipulation of the global regulator presents a promising approach for activating new SMs and improving the metabolic potential of biocontrol fungi.

DATA AVAILABILITY STATEMENT

The datasets presented in this study can be found in online repositories. The names of the repository/repositories and

accession number(s) can be found in the article/ **Supplementary Material**.

AUTHOR CONTRIBUTIONS

ZD conceived and designed the experiments, prepared the manuscript, and was involved in isolation of compounds. XW and H-MH performed genetic manipulation, strain fermentation, and extraction. F-DK contributed to determinate the structures of isolated compounds. Y-NZ and ML contributed to bioactivity assay. Z-PW and JH supervised the work and revised the manuscript. All authors contributed to the article and approved the submitted version.

FUNDING

This work was financially supported by the Natural Science Foundation of Shandong Province (ZR2017BB077 and ZR2018BH043) and Tai-Shan Scholar Foundation of Shandong Province (319190201).

SUPPLEMENTARY MATERIAL

The Supplementary Material for this article can be found online at: https://www.frontiersin.org/articles/10.3389/fmicb.2020.622785/full#supplementary-material

REFERENCES

Aghcheh, R. K., Druzhinina, I. S., and Kubicek, C. P. (2013). The putative protein methyltransferase LAE1 of *Trichoderma atroviride* is a key regulator of asexual development and mycoparasitism. *PLoS One* 8:e67144. doi: 10.1371/journal.pone.0067144

Benítez, T., Rincón, A. M., Limón, M. C., and Codón, A. C. (2004). Biocontrol mechanisms of *Trichoderma* strains. *Int. Microbiol.* 7, 249–260. doi: 10.2436/im.v7i4.9480

Bok, J. W., and Keller, N. P. (2004). LaeA, a regulator of secondary metabolism in *Aspergillus* spp. *Eukaryot. Cell* 3, 527–535. doi: 10.1128/ec.3.2.527-535.2004

Brakhage, A. A. (2013). Regulation of fungal secondary metabolism. *Nat. Rev. Microbiol.* 11, 21–32. doi: 10.1038/nrmicro2916

Butchko, R. A. E., Brown, D. W., Busman, M., Tudzynski, B., and Wiemann, P. (2012). Lae1 regulates expression of multiple secondary metabolite gene clusters in *Fusarium verticillioides*. *Fungal Genet. Biol.* 49, 602–612. doi: 10.1016/j.fgb.2012.06.003

Chandra, S. (2012). Endophytic fungi: novel sources of anticancer lead molecules. *Appl. Microbiol. Biotechnol.* 95, 47–59. doi: 10.1007/s00253-012-4128-7

Chaverri, P., Branco-Rocha, F., Jaklitsch, W., Gazis, R., Degenkolb, T., and Samuels, G. J. (2015). Systematics of the *Trichoderma harzianum* species complex and the re-identification of commercial biocontrol strains. *Mycologia* 107, 558–590. doi: 10.3852/14-147

Degenkolb, T., Nielsen, K. F., Dieckmann, R., Branco-Rocha, F., Chaverri, P., Samuels, G. J., et al. (2015). Peptaibol, secondary-metabolite, and hydrophobin pattern of commercial biocontrol agents formulated with species of the *Trichoderma harzianum* complex. *Chem. Biodivers.* 12, 662–684. doi: 10.1002/cbdv.201400300

Derntl, C., Guzmán-Chávez, F., Mello-de-Sousa, T. M., Busse, H. -J., Driessen, A. J. M., Mach, R. L., et al. (2017). In vivo study of the sorbicillinoid gene cluster in *Trichoderma reesei*. *Front. Microbiol.* 8:2037. doi: 10.3389/fmicb.2017.02037

Ding, Z., Tao, T., Wang, L., Zhao, Y., Huang, H., Zhang, D., et al. (2019). Bioprospecting of novel and bioactive metabolites from endophytic fungi isolated from rubber tree *Ficus elastica* leaves. *J. Microbiol. Biotechnol.* 29, 731–738. doi: 10.4014/jmb.1901.01015

Estiarte, N., Lawrence, C. B., Sanchis, V., Ramos, A. J., and Crespo-Sempere, A. (2016). LaeA and VeA are involved in growth morphology, asexual development, and mycotoxin production in *Alternaria alternata*. *Int. J. Food Microbiol.* 238, 153–164. doi: 10.1016/j.ijfoodmicro.2016.09.003

Frisch, M. J., Trucks, G. W., Schlegel, H. B., Scuseria, G. E., Robb, M. A., Cheeseman, J. R., et al. (2009). Gaussian 09, Revision A.1, Gaussian, Inc., Wallingford, CT.

Harned, A. M., and Volp, K. A. (2011). The sorbicillinoid family of natural products: isolation, biosynthesis, and synthetic studies. *Nat. Prod. Rep.* 28, 1790–1810. doi: 10.1039/c1np00039j

Hong, E. J., Kim, N. K., Lee, D., Kim, W. G., and Lee, I. (2015). Overexpression of the *laeA* gene leads to increased production of cyclopiazonic acid in *Aspergillus fumisynnematus*. *Fungal Biol.* 119, 973–983. doi: 10.1016/j.funbio.2015.06.006

Jiang, T., Wang, M., Li, L., Si, J., Song, B., Zhou, C., et al. (2016). Overexpression of the global regulator LaeA in *Chaetomium globosum* leads to the biosynthesis of chaetoglobosin Z. *J. Nat. Prod.* 79, 2487–2494. doi: 10.1021/acs.jnatprod.6b00333

Kosalková, K., García-Estrada, C., Ullán, R. V., Godio, R. P., Feltrer, R., Teijeira, F., et al. (2009). The global regulator LaeA controls penicillin biosynthesis, pigmentation and sporulation, but not roquefortine C synthesis in *Penicillium chrysogenum*. *Biochimie* 91, 214–225. doi: 10.1016/j.biochi.2008.09.004

Lebe, K. E., and Cox, R. J. (2019). O-methylation steps during strobilurin and bolineol biosynthesis. *RSC Adv.* 9, 31527–31531. doi: 10.1039/c9ra06412e

Li, M. F., Li, G. H., and Zhang, K. Q. (2019). Non-volatile metabolites from *Trichoderma* spp. *Metabolites* 9:58. doi: 10.3390/metabo9030058

Linde, T., Zoglowek, M., Lübeck, M., Frisvad, J. C., and Lübeck, P. S. (2016). The global regulator LaeA controls production of citric acidand endoglucanases in *Aspergillus carbonarius*. *J. Ind. Microbiol. Biotechnol.* 43, 1139–1147. doi: 10.1007/s10295-016-1781-3

Liu, Q., Cai, L., Shao, Y., Zhou, Y., Li, M., Wang, X., et al. (2016). Inactivation of the global regulator LaeA in *Monascus ruber* results in a species-dependent response in sporulation and secondary metabolism. *Fungal Biol.* 120, 297–305. doi: 10.1016/j.funbio.2015.10.008

López-Berges, M. S., Schäefer, K., Hera, C., and Pietro, A. D. (2014). Combinatorial function of velvet and AreA in transcriptional regulation of nitrate utilization and secondary metabolism. *Fungal Genet. Biol.* 62, 78–84. doi: 10.1016/j.fgb.2013.11.002

Mao, X. M., Xu, W., Li, D., Yin, W. B., Chooi, Y. H., Li, Y. Q., et al. (2015). Epigenetic genome mining of an endophytic fungus leads to the pleiotropic biosynthesis of natural products. *Angew. Chem. Int. Ed.* 54, 7592–7596. doi: 10.1002/anie.201502452

Mukherjee, P. K., Horwitz, B. A., Herrera-Estrella, A., Schmoll, M., and Kenerley, C. M. (2013). *Trichoderma* research in the genome era. *Annu. Rev. Phytopathol.* 51, 105–129. doi: 10.1146/annurev-phyto-082712-102353

Reátegui, R. F., Wicklow, D. T., and Gloer, J. B. (2006). Phaeofurans and sorbicillin analogues from a fungicolous *Phaeoacremonium* species (NRRL 32148). *J. Nat. Prod.* 69, 113–117. doi: 10.1021/np0504199

Reino, J. L., Guerrero, R. F., Hernández-Galán, R., and Collado, I. G. (2008). Secondary metabolites from species of the biocontrol agent *Trichoderma*. *Phytochem. Rev.* 7, 89–123. doi: 10.1007/s11101-006-9032-2

Reyes-Dominguez, Y., Bok, J. W., Berger, H., Shwab, E. K., Basheer, A., Gallmetzer, A., et al. (2010). Heterochromatic marks are associated with the repression of secondary metabolism clusters in *Aspergillus nidulans*. *Mol. Microbiol.* 76, 1376–1386. doi: 10.1111/j.1365-2958.2010.07051.x

Rutledge, P. J., and Challis, G. L. (2015). Discovery of microbial natural products by activation of silent biosynthetic gene clusters. *Nat. Rev. Microbiol.* 13, 509–523. doi: 10.1038/nrmicro3496

Seiboth, B., Karimi, R. A., Phatale, P. A., Linke, R., Hartl, L., Sauer, D. G., et al. (2012). The putative protein methyltransferase LAE1 controls cellulase gene expression in *Trichoderma reesei*. *Mol. Microbiol.* 84, 1150–1164. doi: 10.1111/j.1365-2958.2012.08083.x

Shaw, J. J., Spakowicz, D. J., Dalal, R. S., Davis, J. H., Lehr, N. A., Dunican, B. F., et al. (2015). Biosynthesis and genomic analysis of

medium-chain hydrocarbon production by the endophytic fungal isolate *Nigrograna mackinnonii* E5202H. *Appl. Microbiol. Biotechnol.* 99, 3715–3728. doi: 10.1007/s00253-014-6206-5

Tang, M. C., Cui, X., He, X., Ding, Z., Zhu, T., Tang, Y., et al. (2017). Late-stage terpene cyclization by an integral membrane cyclase in the biosynthesis of isoprenoid epoxycyclohexenone natural products. *Org. Lett.* 19, 5376–5379. doi: 10.1021/acs.orglett.7b02653

Vinale, F., Sivasithamparam, K., Ghisalberti, E. L., Marra, R., Barbetti, M. J., Li, H., et al. (2008). A novel role for *Trichoderma* secondary metabolites in the interactions with plants. *Physiol. Mol. Plant Pathol.* 72, 80–86. doi: 10.1016/j.pmpp.2008.05.005

Wang, L., Zhang, X., Zhang, K., Zhang, X., Zhu, T., Che, Q., et al. (2020). Overexpression of global regulator PbrlaeA leads to the discovery of new polyketide in fungus *Penicillium brocae* HDN-12-143. *Front. Chem.* 8:270. doi: 10.3389/fchem.2020.00270

Wiemann, P., and Keller, N. P. (2014). Strategies for mining fungal natural products. *J. Ind. Microbiol. Biotechnol.* 41, 301–313. doi: 10.1007/s10295-013-1366-3

Wu, J. S., Shi, X. H., Zhang, Y. H., Yu, J. Y., Fu, X. M., Li, X., et al. (2019). Co-cultivation with 5-azacytidine induced new metabolites from the zoanthid-derived fungus *Cochliobolus lunatus*. *Front. Chem.* 7:763. doi: 10.3389/fchem.2019.00763

Wu, J. S., Yao, G. S., Shi, X. H., Rehman, S. U., Xu, Y., Fu, X. M., et al. (2020). Epigenetic agents trigger the production of bioactive nucleoside derivatives and bisabolane sesquiterpenes from the marine-derived fungus *Aspergillus versicolor*. *Front. Microbiol.* 11:85. doi: 10.3389/fmicb.2020.00085

Wu, G., Zhou, H., Zhang, P., Wang, X., Li, W., Zhang, W., et al. (2016). Polyketide production of pestaloficiols and macrodiolide ficiolides revealed by manipulations of epigenetic regulators in an endophytic fungus. *Org. Lett.* 18, 1832–1835. doi: 10.1021/acs.orglett.6b00562

Yu, J., Han, H., Zhang, X., Ma, C., Sun, C., Che, Q., et al. (2019). Discovery of two new sorbicillinoids by overexpression of the global regulator LaeA in a marine-derived fungus *Penicillium dipodomyis* YJ-11. *Mar. Drugs* 17:446. doi: 10.3390/md17080446

Zeilinger, S., Gruber, S., Bansal, R., and Mukherjee, P. K. (2016). Secondary metabolism in *Trichoderma*—chemistry meets genomics. *Fungal Biol. Rev.* 30, 74–90. doi: 10.1016/j.fbr.2016.05.001

Zeng, Z. Q., and Zhuang, W. Y. (2019). Two new species and a new Chinese record of *Hypocreaceae* as evidenced by morphological and molecular data. *Mycobiology* 47, 280–291. doi: 10.1080/12298093.2019.1641062

Zhang, P., Yuan, X. L., Du, Y. M., Zhang, H. B., Shen, G. M., Zhang, Z. F., et al. (2019). Angularly prenylated indole alkaloids with antimicrobial and insecticidal activities from an endophytic fungus *Fusarium sambucinum* TE-6L. *J. Agric. Food Chem.* 67, 11994–12001. doi: 10.1021/acs.jafc.9b05827

Conflict of Interest: The authors declare that the research was conducted in the absence of any commercial or financial relationships that could be construed as a potential conflict of interest.

frontiers in Microbiology

ORIGINAL RESEARCH
published: 22 February 2021
doi: 10.3389/fmicb.2021.638610

Discovery of Cymopolyphenols A–F From a Marine Mesophotic Zone *Aaptos* Sponge-Associated Fungus *Cymostachys* sp. NBUF082

Tingting Wang[1], Jing Zhou[1], Jiabin Zou[1], Yutong Shi[1], Wenli Zhou[2], Peng Shao[2], Tianze Yu[3], Wei Cui[3], Xiaohui Li[1], Xingxin Wu[4], Jing Ye[4], Xiaojun Yan[1], C. Benjamin Naman[1], J. Enrico H. Lazaro[5] and Shan He[1]**

[1]Li Dak Sum Marine Biopharmaceutical Research Center, Department of Marine Pharmacy, College of Food and Pharmaceutical Sciences, Ningbo University, Ningbo, China, [2]College of Fisheries, Tianjin Agricultural University, Tianjin, China, [3]Zhejiang Provincial Key Laboratory of Pathophysiology, School of Medicine, Ningbo University, Ningbo, China, [4]State Key Laboratory of Pharmaceutical Biotechnology, School of Life Sciences, Nanjing University, Nanjing, China, [5]National Institute of Molecular Biology and Biotechnology, University of the Philippines Diliman, Quezon, Philippines

Mesophotic coral ecosystems (MCEs) have complex but understudied biodiversity, especially for natural products discovery. Untargeted metabolomics research on 80 extracts prepared from marine sponge-associated fungi, half from shallow reefs (<30 m) and half from MCEs (30–150 m), facilitated prioritization for further study a *Cymostachys* fungus from a 103 m deep *Aaptos* sponge. LC-MS target-directed isolation yielded a series of new compounds, cymopolyphenols A–F (**1**–**6**), and two known phenylspirodrimanes, F1839-I (**7**) and stachybotrylactone (**8**). This is the first report of natural products from the recently described genus, *Cymostachys*. Compounds **1**–**6** and **8** contain a dihydroisobenzofuran moiety, and **4**–**6** are low-order polymers of **1** with novel scaffolds. The structures of the compounds were established by spectroscopic and spectrometric data interpretation, with further support from X-ray crystallography studies of **3** and **4**. Compound **3** undergoes facile racemization in solution and was found to crystalize as a racemic mixture. Compound **5** was also obtained in racemic form, and after chiral chromatography, both separated enantiomers racemized in solution by a presumed keto-enol tautomerization. Compounds **1** and **3**–**6** were found to be weakly antimicrobial (MIC 16–64 μg/ml) *in vitro* against several Gram-positive and Gram-negative human or aquatic pathogens, compound **5** was shown to chelate iron *in vitro* at 10 μM, and **8** activated plant disease resistance *in vivo* in a transgenic model organism.

Keywords: mesophotic coral ecosystems, twilight zone, sponges, fungi, sponge-associated fungi, natural products, polyphenols, dihydroisobenzofuran

OPEN ACCESS

Edited by:
Carolina Elena Girometta, University of Pavia, Italy

Reviewed by:
Yonghong Liu, Chinese Academy of Sciences (CAS), China
Pramod B. Shinde, Central Salt & Marine Chemicals Research Institute (CSIR), India

***Correspondence:**
C. Benjamin Naman
bnaman@nbu.edu.cn; bnaman@ucsd.edu
Shan He
heshan@nbu.edu.cn

Specialty section:
This article was submitted to Microbiotechnology, a section of the journal Frontiers in Microbiology

Received: *07 December 2020*
Accepted: *29 January 2021*
Published: *22 February 2021*

Citation:
Wang T, Zhou J, Zou J, Shi Y, Zhou W, Shao P, Yu T, Cui W, Li X, Wu X, Ye J, Yan X, Naman CB, Lazaro JEH and He S (2021) Discovery of Cymopolyphenols A–F From a Marine Mesophotic Zone Aaptos Sponge-Associated Fungus Cymostachys sp. NBUF082. Front. Microbiol. 12:638610. doi: 10.3389/fmicb.2021.638610

INTRODUCTION

Natural products research has long been instrumental in generating lead molecules for drug discovery, and many natural products have reached the clinic without structural modification by medicinal chemistry (Cragg et al., 2009; Lachance et al., 2012; Agarwal et al., 2020; Newman and Cragg, 2020). For decades, scientists have followed the adage that studying biodiversity leads to chemodiversity, and the continued exploration of environmental niches and different branches of life has been fruitful (Suffness and Douros, 1981). Studies of marine organisms were at one point considered to be pioneering, and now thousands of marine natural products have been reported. These have provided a resource for drug development and, "as shown at the global marine pharmaceutical pipeline website,[1] there are currently nine approved marine-derived pharmaceuticals, and an additional 31 compounds are either in Phase I, II, and III of *clinical* pharmaceutical development" (Mayer et al., 2020).

In the ocean, mesophotic coral ecosystems (MCEs, also known as twilight zone reefs) that range from 30 to 150 m deep represent an understudied environmental frontier for the collection of sponges and other macroscopic organisms that harbor diverse microbes (Olson and Kellogg, 2010; Weiss, 2017). It was reported that MCEs represent approximately 80% of coral reef habitat worldwide, yet very little is known about these deep habitats comparing to shallow reefs (Pyle and Copus, 2019). The biodiversity found in MCEs appears to differ significantly from that of shallow reefs, but a small fraction of life present there has been categorized taxonomically or examined in natural products research due to technical challenges (Sinniger et al., 2016; Lesser et al., 2018; Rocha et al., 2018). One strategy to access this resource is the investigation of assemblages produced from dredging, but this practice is extremely damaging to the environment (Machida et al., 2014; Pedrosa et al., 2020). Because most everything comes up broken into pieces, it is also challenging to determine the producing organism of any molecules discovered, e.g., by analytical comparison with extracts of sorted and identified biomass fragments (Machida et al., 2014; Pedrosa et al., 2020). More natural product studies have thus been reported on mesophotic zone organisms after being collected by a remotely operated vehicle (ROV) or autonomous underwater vehicle (AUV). However, this practice is very costly and usually reserved for studying the much deeper bathypelagic and abyssopelagic zones, or even hadopelagic trenches (Schupp et al., 2009). Scientific SCUBA diving to the mesophotic zone is preferable, but carries many challenges including the need for mixed gases, multiple tanks, and/or rebreather apparatus, and relatively few divers are trained for such depths. There are additionally dramatic safety limitations, including short working time at depth, long decompression stops to return to the surface, and risks of nitrogen narcosis and oxygen toxicity. Still, technical scientific diving is more eco-friendly than dredging and more cost-effective and efficient than using an ROV or AUV for sample collection.

A previous preliminary survey of mesophotic zone organisms from Guam reported that "extracts from the twilight zone sponges and gorgonians resulted in an astonishing 72% hit rate" using *in vitro* cancer chemopreventive and antiproliferative bioassays and already yielded some new natural products (Schupp et al., 2009; Wright et al., 2012). While many researchers have studied macroscopic marine organisms, some natural products they discovered have been suspected or shown to be produced by associated microorganisms (Hirata and Uemura, 1986; Still et al., 2014; McCauley et al., 2020; Newman and Cragg, 2020). Recently, the multinational EU-funded program, TASCMAR (Tools And Strategies to access original bioactive compounds by Cultivating MARine invertebrates and associated symbionts[2]), has begun to harness of the microbial diversity of some mesophotic zone invertebrates for the purpose of natural products discovery projects, and these have reported new bioactive molecules from interesting microbes (Le Goff et al., 2019; Nikolaivits et al., 2019; Letsiou et al., 2020).

Fungal metabolism is well-characterized as being diverse, and often leads to natural products with useful pharmacological activities, but may require efforts to activate in laboratory cultures as exemplified by the "One Strain, MAny Compounds" (OSMAC) approach (Keller, 2019). It is now typical to cultivate in a laboratory the microbes found associated with sponges, especially fungi, and then reproducibly access the biosynthetic potential of these organisms under different conditions (Li and Wang, 2009; Zhang et al., 2020). Meanwhile, it is understood that mesophotic zone organisms represent a vastly unexplored biological diversity with great potential for natural products drug discovery. In the current study, sample prioritization was achieved by the OSMAC strategy combined with LC-MS/MS molecular networking (Wang et al., 2016) of organic extracts produced from 40 cultured fungi isolated from mesophotic zone sponges and 40 more from shallow reef sponges collected by scientific diving. This allowed a *Cymostachys* fungus to be selected for further study based on the observed production of then-hypothesized and now-demonstrated new natural products of interest.

The genus *Cymostachys* was only recently described, and no earlier literature exists on the natural products chemistry of any species therein (Lombard et al., 2016). *Cymostachys* is closely related to the genus *Stachybotrys*, and the latter has been extensively studied for its natural product chemistry (Wang et al., 2015; Zhao et al., 2017; Jagels et al., 2019; Zheng et al., 2019). For example, compounds **7** and **8** (**Figure 1**) were both originally discovered from *Stachybotrys* fungi (Ayer and Miao, 1993; Sakai et al., 1995; Zhao et al., 2017). The organism prioritization, targeted compound isolation and characterization of new molecules for ongoing natural product drug discovery efforts are described herein.

MATERIALS AND METHODS

General Experimental Procedures

Optical rotations were acquired on a JASCO P-2000 automatic polarimeter in MeOH at 20°C. NMR spectra were recorded

[1]https://www.midwestern.edu/departments/marinepharmacology.xml

[2]http://www.tascmar.eu/

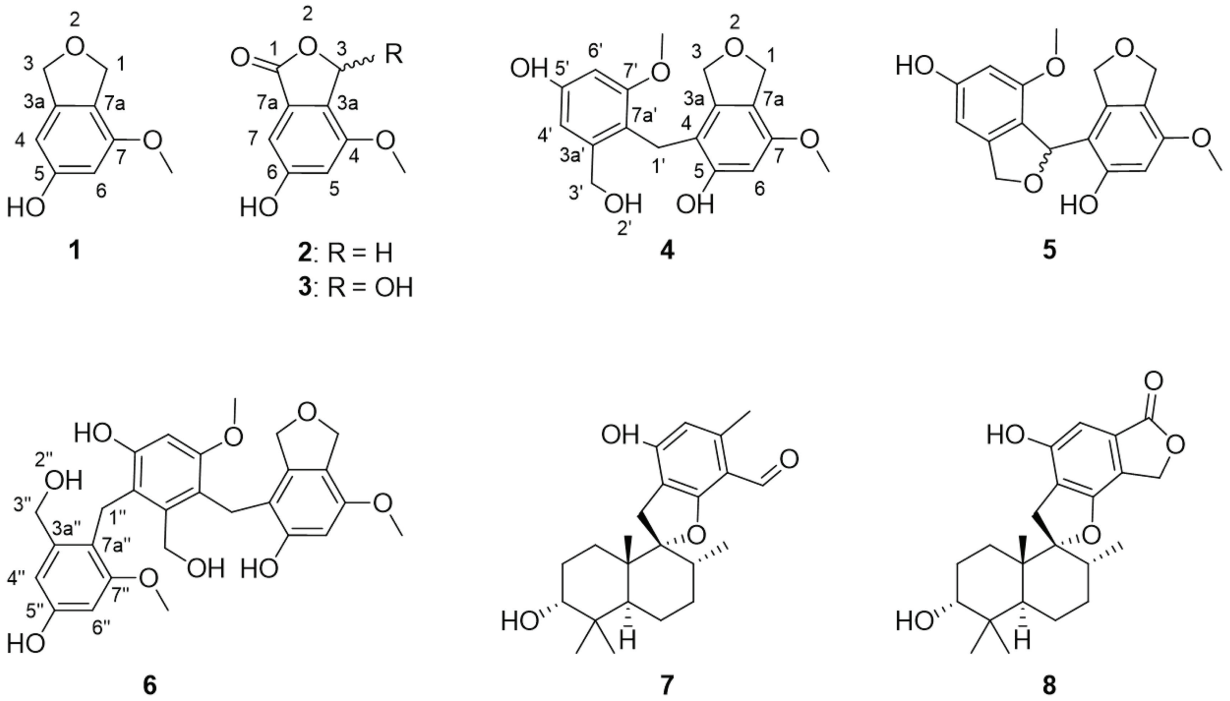

FIGURE 1 | Structures of compounds **1–8**, here discovered from *Cymostachys* sp. NBUF082. Compounds **7** and **8** were previously reported from *Stachybotrys* fungi.

on a Bruker AVANCE NEO 600 spectrometer with a 5 mm inverse detection triple resonance (H-C/N/D) cryoprobe having z-gradients, and Bruker AVANCE 500 spectrometer with a 5 mm double resonance broadband room temperature probe. Spectra were collected using standard Bruker pulse programs, and chemical shifts were recorded relative to the solvent peak in DMSO-d_6 (δ_H 2.50 and δ_C 39.52). High-resolution electrospray ionization mass spectra (HRESIMS) were measured on an Agilent (Santa Clara, CA, United States) 6545 Q-TOF instrument. Reversed-phase HPLC purification was performed using a Waters HPLC equipped with a 1525 binary pump, and a Thermo Scientific (Waltham, MA, United States) ODS-2 Hypersil column (5 μm, 250 mm × 10 mm). Analytical chiral HPLC was performed using a Waters HPLC equipped with a 1525 binary pump and a Sepax Technologies (Newark, Delaware, United States) Chiralomix SA column (5 μm, 250 mm × 4.6 mm). Normal phase column chromatography and thin-layer chromatography were accomplished using coarse (200–300 mesh) and fine GF254 (10–20 μm) silica, respectively (Qingdao Marine Chemical Company, China). Sephadex LH-20 (Pharmacia Biotech, Sweden) was used for gel filtration chromatography, and YMC*GEL ODS-A (AA12S50; YMC Co., Ltd., Japan) was used for reverse phase column chromatography. Biological assays were read for absorbance determination on a Thermo Scientific Multiskan GO microplate spectrophotometer.

Organism Collection and Identification

The fungi evaluated in this study were isolated from sponges collected in a shallow water reef and the deeper MCEs near Apo Island, Negros Oriental, Philippines (9°04'40.6"N 123°15'57.3"E and 9°04'33.0"N 123°15'59.1"E) by scientific technical SCUBA diving in October 2018. The details of specific sponge identification and sampling depths are listed in **Supplementary Table S1**. The fresh inner tissue of the each sponge was sliced and stuck on petri dishes containing modified Czapek's medium (sucrose 3.0 g, Na_2NO_3 3.0 g, $MgSO_4{\cdot}7H_2O$ 0.5 g, $FeSO_4{\cdot}7H_2O$ 0.001 g, KH_2PO_4 1.0 g, KCl 0.5 g, yeast extract 1.0 g, kanamycin 150 mg, ampicillin sodium 150 mg, sea salt 35.0 g, agar powder 20.0 g, and H_2O up to a total volume of 1 L), modified potato dextrose agar (modified PDA: potato 20.0 g, glucose 2.0 g, kanamycin 150 mg, ampicillin sodium 150 mg, sea salt 35.0 g, agar powder 20.0 g, and H_2O up to a total volume of 1 L), and modified martin medium (peptone 10.0 g, yeast extract 20.0 g, sucrose 1.0 g, KH_2PO_4 1.0 g, $MgSO_4$ 0.5 g, kanamycin 150 mg, ampicillin sodium 150 mg, sea salt 35.0 g, agar powder 20.0 g, and H_2O up to a total volume of 1 L). Two weeks later, fungal colonies on the plates were picked and purified on petri dishes containing PDA (glucose 20.0 g, potato 200 g, sea salt 35.0 g, agar powder 20.0 g, and H_2O up to a total volume of 1 L). Voucher specimens were deposited at the College of Food and Pharmaceutical Sciences, Ningbo University, Ningbo, China, available from SH.

The fungal strain studied most extensively in this work, NBUF082, was inoculated at three points on PDA and cultivated at 28°C for 5 days. The fungal colonies were fast-growing and flocculated, and they turned from white to light brown color on cultivation day 5. The reverse side of the medium was fawn-colored and non-extravasated. The strain was able to

be identified as belonging to the genus *Cymostachys* according to its morphological traits (Lin et al., 2016), and sequence analysis of the ITS region (GenBank accession no. MW077215) as described previously (Henríquez et al., 2014; Lombard et al., 2016). Two other fungi were isolated from the same *Aaptos* sponge in addition to *Cymostachys* sp. NBUF082. These were identified as belonging to genera *Roussoella* and *Aspergillus*, respectively, based on morphological traits and sequence analysis of the ITS region (Henríquez et al., 2014).

Small-Scale Cultivation, Extraction, and Molecular Networking

Inspired by the OSMAC strategy, the obtained sponge-derived fungi were each cultured separately in three different types of media, potato dextrose broth (PDB: glucose 20.0 g, potato 200.0 g, sea salt 35.0 g, and H_2O up to a total volume of 1 L), Czapek-Dox medium (sucrose 30.0 g, Na_2NO_3 3.0 g, $MgSO_4{\cdot}7H_2O$ 0.5 g, $FeSO_4{\cdot}7H_2O$ 0.001 g, KH_2PO_4 1.0 g, KCl 0.5 g, yeast extract 1.0 g, sea salt 35.0 g, and H_2O up to a total volume of 1 L), and modified Martin medium (peptone 10.0 g, yeast extract 20.0 g, sucrose 10.0 g, KH_2PO_4 1.0 g, $MgSO_4$ 0.5 g, sea salt 35.0 g, and H_2O up to a total volume of 1 L). The fungal mycelia on petri-dishes were cut into squares (0.5 cm^3 × 0.5 cm^3 × 0.5 cm^3) and incubated into 1 L Erlenmeyer flasks containing 400 ml of above-mentioned medium. The cultures were incubated for 15 days at 28°C with agitation (120 rpm), and then extracted with EtOAc (v/v, 1:1) three times each. The crude extracts were concentrated under vacuum with rotary evaporators.

The extracts were dissolved in MeOH to final concentrations of 1 mg/ml and preprocessed by 0.22 μm membrane filtration. A 3 μl aliquot of each sample was injected into the LC-HRESIMS and eluted at 0.8 ml/min (MeOH/H_2O with 0.1% formic acid, v/v, 30%→99%): 30% for 5 min to 99% in 17 min, held for 3 min, to 30% in 1 min, and held for 4 min. The mass spectrometer was set to observe m/z 190–2000 in positive ESI mode and with an automated data-dependent MS/MS scan enabled. The resulting data were uploaded to the Global Natural Product Social Molecular Networking web interface (GNPS[3]), and the results were used to generate molecular network diagrams using the freely available open source visualization software, Cytoscape.[4]

Large-Scale Fermentation, Extraction, and Isolation

The *Cymostachys* fungus of interest was scaled up in culture size for chemical investigation. First, it was cultivated on potato dextrose agar (PDA) at 28°C for 7 days. The mycelia on PDA in petri dishes were cut into squares (0.5 cm^3 × 0.5 cm^3 × 0.5 cm^3) and incubated into 280 L × 1 L Erlenmeyer flasks, each containing 400 ml PDB medium (80 g potato dextrose, 8 g glucose, 14.0 g sea salt, and 400 ml H_2O). The cultures were incubated for 15 days at 28°C with agitation (120 rpm) and then extracted with EtOAc (v/v, 1:1) for three times.

[3]http://gnps.ucsd.edu/
[4]https://cytoscape.org/

The combined organic phase was concentrated under reduced pressure to give 350 g (partially wet weight) of crude extract, which was subjected to column chromatography (CC) over silica gel (PE/EtOAc, v/v, 100:0→0:100 then EtOAc/MeOH v/v, 100:0→0:100) to give 10 fractions (Fr.1–Fr.10). Of these, Fr.5, which eluted from the column with 1:1 PE/EtOAc, v/v, was separated with Sephadex LH-20 in MeOH to yield 15 subfractions (Fr.5.1–Fr.5.15). Fr.5.13 was further purified by RP-HPLC with CH_3CN/H_2O (45:55, 2 ml/min) to afford compounds **4** (t_R = 48 min, 11.3 mg), **5** (t_R = 42 min, 12.2 mg), and **6** (t_R = 57 min, 5.7 mg). Crude Fr.6, which eluted from the column with EtOAc, was chromatographed again with silica gel (PE/EtOAc, v/v, 100:0→0:100 then EtOAc/MeOH v/v, 100:0→0:100) to afford 10 subfractions (Fr.6.1–Fr.6.10). Fr.6.6 and Fr.6.7, which both eluted with EtOAc, were subjected to RP-HPLC to yield compounds **7** (t_R = 30 min, 3.4 mg) and **8** (t_R = 39 min, 14.6 mg) by elution with CH_3CN/H_2O (42:58, 2 ml/min) and CH_3CN/H_2O (45:55, 2 ml/min), respectively. Fr. 6.8, which was eluted from the column by 40:1 EtOAc/MeOH, v/v, was separated with Sephadex LH-20 in MeOH to yield 15 subfractions (Fr.6.8.1–Fr.6.8.15). Further purification of Fr.6.8.8 *via* RP-HPLC (CH_3CN/H_2O, 36:64, 2 ml/min) afforded compounds **1** (t_R = 28 min, 10.2 mg) and **2** (t_R = 30 min, 0.8 mg). Fr. 6.9, which was eluted from the column by 20:1 EtOAc/MeOH, v/v, was separated with Sephadex LH-20 in MeOH to yield fifteen subfractions (Fr.6.9.1–Fr.6.9.15). Subfraction Fr.6.9.5 yielded **3** (t_R = 25 min, 10.0 mg) after being subjected to RP-HPLC (CH_3CN/H_2O, 50:50, 2 ml/min).

Isolated Materials (New Natural Products)

Cymopolyphenol A (**1**): White powder; UV (MeOH) λ_{max} (log ε) = 280 (3.74) nm; for ^1H NMR and ^{13}C NMR data

TABLE 1 | ^1H and ^{13}C NMR spectroscopic data for **1**–**3** in DMSO-d_6[a].

Position	1		2		3	
	δ_C, type	δ_H (*J* in Hz)	δ_C, type	δ_H (*J* in Hz)	δ_C, type	δ_H (*J* in Hz)
1	70.9, CH_2	4.84 t (2.3)	170.8, C		168.1, C	
3	73.1, CH_2	4.88 t (2.3)	68.0, CH_2	5.23 s	102.0, CH	6.44 s
3a	141.5, C		125.9, C		122.5, C	
4	99.7, CH	6.26 s[b]	154.9, C		156.1, C	
5	159.1, C		105.0, CH	6.75 d (1.8)	105.2, CH	6.75 d (1.8)
6	97.7, CH	6.27 s[b]	160.3, C		161.8, C	
7	154.3, C		101.4, CH	6.71 d (1.8)	101.6, CH	6.70 d (1.8)
7a	116.3, C		127.2, C		129.2, C	
7-OCH_3	55.0, CH_3	3.71 s				
4-OCH_3			55.8, CH_3	3.83 s	55.8, CH_3	3.83 s
5-OH		9.46 br s				
6-OH				10.21 br s		10.39 s

[a]*Data recorded at 298 K, 600 MHz (^1H) and 150 MHz (^{13}C). Assignments supported by 2D NMR.*
[b]*Partially overlapped.*

see **Table 1**; HR-ESI-MS [M + H]$^+$ *m/z* 167.0706 (calcd. for $C_9H_{11}O_3$, 167.0703).

Cymopolyphenol B (**2**): White powder; UV (MeOH) λ_{max} (log ε) = 285 (3.08) nm; for ^{1}H NMR and ^{13}C NMR data see **Table 1**; HR-ESI-MS [M + H]$^+$ *m/z* 181.0500 (calcd. for $C_9H_9O_4$, 181.0495).

Cymopolyphenol C (**3**): Colorless prisms; $[\alpha]_D^{25}$ 0 (*c* 0.1, MeOH); UV (MeOH) λ_{max} (log ε) = 285 (3.11) nm; for ^{1}H NMR and ^{13}C NMR data see **Table 1**; HR-ESI-MS [M + H]$^+$ *m/z* 197.0453 (calcd. for $C_9H_9O_5$, 197.0444).

Cymopolyphenol D (**4**): Colorless prisms; UV (MeOH) λ_{max} (log ε) = 290 (3.66); for ^{1}H NMR and ^{13}C NMR data see **Table 2**; HR-ESI-MS [M + Na]$^+$ *m/z* 355.1159 (calcd. for $C_{18}H_{20}O_6Na$, 355.1152).

Cymopolyphenol E (**5**): Light brown powder; $[\alpha]_D^{25}$ 0 (*c* 0.1, MeOH); UV (MeOH) λ_{max} (log ε) = 285 (3.82) nm; for ^{1}H NMR and ^{13}C NMR data see **Table 2**; HR-ESI-MS [M + Na]$^+$ *m/z* 353.0997 (calcd. for $C_{18}H_{18}O_6Na$, 353.0996).

Cymopolyphenol F (**6**): White powder; UV (MeOH) λ_{max} (log ε) = 285 (3.81) nm; for ^{1}H NMR and ^{13}C NMR data see **Table 2**; HR-ESI-MS [M + Na]$^+$ *m/z* 521.1790 (calcd. for $C_{27}H_{30}O_9Na$, 521.1782).

TABLE 2 | ^{1}H and ^{13}C NMR Spectroscopic Data for **4**–**6** in DMSO-d_6[a].

Position	4		5		6	
	δ_C, type	δ_H (*J* in Hz)	δ_C, type	δ_H (*J* in Hz)	δ_C, type	δ_H (*J* in Hz)
1	70.3, CH_2	4.70 t (2.4)	70.2, CH_2	4.72 m	70.1, CH_2	4.67 t (2.3)
3	71.8, CH_2	4.16 t (2.4)	71.6, CH_2	4.49 br d (12.7)	71.9, CH_2	4.00 t (2.3)
				3.99 br d (12.7)		
3a	139.5, C		140.0, C		139.5, C	
4	112.8, C		114.3, C		114.1, C	
5	155.6, C		156.2, C		155.4, C	
6	97.7, CH	6.37 s	97.8, CH	6.36 s	97.6, CH	6.38 s
7	151.4, C		153.0, C		151.2, C	
7a	116.4, C		116.6, C		116.2, C	
5-OH		9.43 s		9.45 s		
7-OCH_3	54.9, CH_3	3.678 s[b]	54.9, CH_3	3.71 s	54.8, CH_3	3.68 s
1'	21.1, CH_2	3.674 br s[b]	76.4, CH	6.41 dd (3.0, 1.9)	22.6, CH_2	3.84 s[c]
3'	60.0, CH_2	4.23 s	72.4, CH_2	5.00 dd (12.4, 3.0)	57.1, CH_2	4.39 s
				4.84 dd (12.4, 1.9)		
3a'	143.3, C		142.4, C		141.2, C	
4'	105.3, CH	6.52 d (2.4)	99.3, CH	6.27 d (1.8)	119.0, C	
5'	156.7, C		159.3, C		154.8, C	
6'	96.9, CH	6.28 d (2.4)	97.9, CH	6.23 d (1.8)	98.0, CH	6.30 s
7'	158.2, C		154.9, C		156.0, C	
7a'	114.2, C		117.8, C		117.0, C	
5'-OH		9.23 s		9.49 s		
7'-OCH_3	55.3, CH_3	3.682[b] s	55.2, CH_3	3.52 s	55.0, CH_3	3.61 s
1''					22.4, CH_2	3.76 s[c]
3''					61.1, CH_2	4.54 s
3a''					142.2, C	
4''					105.9, CH	6.44 d (2.4)
5''					155.8, C	
6''					97.3, CH	6.14 d (2.4)
7''					158.2, C	
7a''					117.3, C	
7''-OCH_3					54.5, CH_3	3.35 s

[a]*Data recorded at 298 K, 600 MHz (^{1}H) and 150 MHz (^{13}C) or 500 MHz (^{1}H) and 125 MHz (^{13}C). Assignments supported by 2D NMR.*
[b]*Signals partially overlapped.*
[c]*Might be interchanged.*

Single Crystal X-ray Diffraction Analysis

The crystals obtained for **3** and **4** were evaluated on a Bruker APEX-II CCD diffractometer through Ga Kα (λ = 1.34139 Å). The structures were solved by direct methods (SHELXT-2014) and refined *via* full-matrix least-squares difference Fourier techniques using SHELXL-2018/3. Crystallographic data for the structures reported in this paper have been deposited with the Cambridge Crystallographic Data Centre. Copies of the data can be obtained, free of charge, on application to the Director, CCDC, 12 Union Road, Cambridge CB2 1EZ, United Kingdom (fax: +44-(0)1223-336033 or e-mail: deposit@ccdc.cam.ac.uk).

Crystallographic data for **3**: $C_9H_8O_5$, M_r = 196.15, prism from MeOH/H_2O (50:1), space group Cc, *a* = 3.8907(3) Å, *b* = 15.5114(11) Å, *c* = 13.8032(10) Å, *V* = 827.53(11) Å^3, *Z* = 4, μ = 0.718 mm^{-1}, *F*(000) = 408.0; crystal size: 0.120 mm^3 × 0.110 mm^3 × 0.090 mm^3; 1,478 unique reflections with 1,368 obeying the $I \geq 2\sigma(I)$; *R* = 0.0336(1368), *wR*2 = 0.0849(1478), *S* = 1.055; supplementary publication no. CCDC-2027079.

Crystallographic data for **4**: $C_{18}H_{20}O_6$, M_r = 332.34, prism from MeOH/DCM (40:1), space group P_{-1}, *a* = 4.8536(2) Å, *b* = 11.5267(5) Å, *c* = 14.9026(7) Å, *V* = 769.37(6) Å^3, *Z* = 2, μ = 0.572 mm^{-1}, *F*(000) = 352.0; crystal size: 0.120 mm^3 × 0.110 mm^3 × 0.080 mm^3; 2,792 unique reflections with 2,287 obeying the $I \geq 2\sigma(I)$; *R* = 0.0377(2287), *wR*2 = 0.1016(2792), *S* = 1.030; supplementary publication no. CCDC-2019163.

In vitro Cytotoxicity Test Protocols

Compounds **1** and **3**–**8** were tested in serial dilutions from the maximum concentration of 20 μM for their inhibition toward CCRF-CEM human T lymphoblast cells *via* lactate dehydrogenase testing and U87 human glioblastoma with MTT according to published protocols (Boudreau et al., 2012; Williams et al., 2017).

In vitro Antimicrobial Assay Protocols

Antibacterial susceptibility was tested against several Gram-positive and Gram-negative human or aquatic pathogens, namely *Pseudoalteromonas carrageenovora*, *Vibrio shilanii*, *V. scophthalmi*,

V. alginolyticus, *Salmonella typhi*, *Pseudomonas aeruginosa*, *Staphylococcus aureus*, and *Bacillus pumilus*. Compounds **1** and **3–8** were dissolved in DMSO and tested at a concentration of 64, 32, 16, 8, and 4 μg/ml according to a published protocol (CLSI, 2018; Bibi et al., 2020). Briefly, the bacteria were grown in MH medium (beef powder 6.0 g, soluble starch 1.5 g, acid hydrolyzed casein 17.5 g, and H_2O up to a total volume of 1 L) for 24 h at 28°C with agitation (180 rpm), then diluted with sterile MH medium to match 0.5 McFarland standard. 100 μl of each bacteria supernatant, 100 μl MH medium with 0.001% 2,3,5-triphenyltetrazolium chloride (an indicator of viable bacteria), together with test or control materials were incubated in 96-well plates. The treated bacteria were cultured statically at 28°C for 24 h, then the inhibition data were recorded optically. Norfloxacin (from Shanghai Yuanye Bio-Technology Co., Ltd.) was used as positive control, and this was dissolved in DMSO at the same concentrations as the tested compounds. Blank media with the same volume of DMSO as the test samples was used as the negative control.

Iron Chelation Evaluation

Ferrozine can chelate Fe^{2+} to afford a complex with an absorbance at 562 nm, which allows for a facile chemical assay that was repeated according to published protocols (Da Lozzo et al., 2002; Azran et al., 2015). In brief, the reaction system on a 96-well plate was composed of 160 μl CH_3COONa (100 mM), 40 μl $FeCl_2$ (1.5 mg/ml), and 10 μl of compounds **1** and **3–8** (0.3, 1, 3, and 10 μM), separately. At the same concentrations, EDTA, a known chelator of Fe^{2+} was used as a positive control. The reaction medium, CH_3COONa (100 mM), was used as a negative control. Following sample addition and 30-min light-proof standing, 10 μl ferrozine (40 mM) was added and the absorbance at 562 nm was collected after another 5-min light-proof standing.

In vivo Activation of the GUS Reporter in PR1::GUS Transgenic *Arabidopsis thaliana* Plants

Following a published method (Wang et al., 2018), clean *Arabidopsis thaliana* seeds ProPR1::GUS (purchased from Arabidopsis Biological Resource Center) were sown in Murashige and Skoog medium (PhytoTechnology Laboratories, United States), with or without added individual compounds **1** and **3–8** at 10 μM and maintained at 4°C. After 3 days, the culture conditions were altered to 22°C with a 16 h light/8 h dark photoperiod. After another 10 days, the plants were dyed in GUS histochemical staining stock at 37°C for 3 h, and the chlorophyll of the plants were washed with 70% ethanol. Observation and photo documentation of the results were carried out with an optical microscope.

RESULTS AND DISCUSSION

Sample Prioritization

From a series of sponges that were collected at diverse depths of 7–103 m (**Supplementary Table S1**), some 80 fungal strains were isolated in laboratory culture by conventional methods (Höller et al., 2000; Liu et al., 2019). The fungal strains were divided into two groups of each $n = 40$, representing shallow reef and MCE origins of the sponges that yielded the isolated microbial samples. Each strain ($n = 80$) was cultivated in small-scale replicates using three different types of growth media to evaluate their secondary metabolite production potential by the OSMAC approach. Organic extracts were prepared from all 240 strain-media combination cultures and evaluated by TLC. The most natural product-rich culture of each strain was selected for further evaluation by untargeted LC-MS/MS analysis ($n = 80$). All obtained data were analyzed together using the Global Natural Product Social Molecular Networking (GNPS) web interface (Wang et al., 2016). A molecular network was prepared and annotated (**Figure 2**), from which it was obvious that the extracts of fungal strains prepared from MCE sponge samples were largely distinct from their shallow water counterparts. Although this remains a relatively small sample set of $n = 40$ per group, the major compositional difference between the MCE and shallow reef samples here analyzed is postulated to be a widespread phenomenon. Further sample collections and laboratory investigations are planned for evaluating this hypothesis.

One organism from the MCE subset of the above strain library was selected for further study in part because the morphology of the producing organism separated it from typically studied genera of fungal natural product producers. Upon close examination of the literature, it was determined that the morphology of strain NBUF082 matched what was described for the genus *Cymostachys* when it was established in recent reports, and it was also conclusively identified as a *Cymostachys* sp. by the ITS region sequence of this organism (Lin et al., 2016; Lombard et al., 2016). Although *Cymostachys* is closely related to the genus *Stachybotrys*, only the latter has been extensively studied for its natural product chemistry (Wang et al., 2015; Zhao et al., 2017; Jagels et al., 2019; Zheng et al., 2019). In contrast, no natural products reported from *Cymostachys* could be found at the onset of this study, and it was proposed that this organism could produce new and interesting natural products chemistry.

Furthermore, the result of using the OSMAC approach to screen the 240 strain x culture condition set of combinations showed that the *Cymostachys* sp. NBUF082 was a moderately high yielding producer of natural products when grown on potato dextrose agar (PDA). With this media, the organism generated 451.8 mg/L organic extract, compared with a range from about 5 mg/L to 1 g/L for other strain x culture condition combinations. When the extract from this sample was evaluated by LC-MS/MS molecular networking, it was selected for further study based on the observation of several distinct molecules compared to the remainder of the data set. The nodes in the network owing to this sample have been colored green in **Figure 2** to show how it stood out from all the 40 shallow reef and the remaining 39 MCE originating sponge-derived fungi. Many more broadly distributed metabolites and molecular feature node clusters were observed to be shared between data sets resulting from shallow and MCE samples, and these are apparent as split-color pie graph nodes in **Figure 2**.

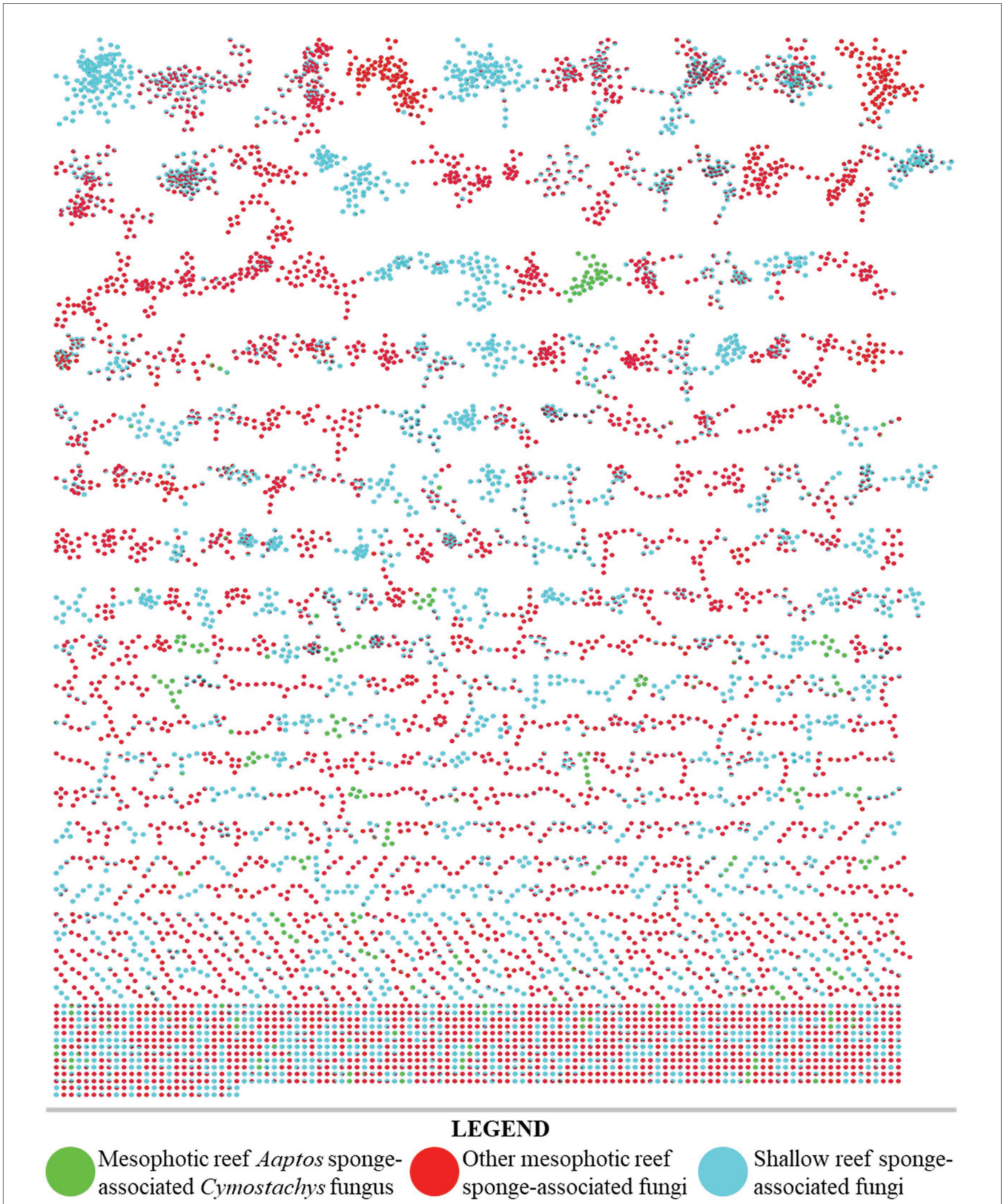

FIGURE 2 | LC–MS/MS derived molecular network of organic extracts produced from 80 fungal cultures (40 from shallow reef sponges, 40 from mesophotic zone sponges). Single node clusters, or self-loop nodes, were excluded for brevity.

Some metabolites were found to be more broadly distributed, but exclusively observed in the same depth-based subsets, and these were purposefully overlooked for prioritization in this research study. For example, metabolites coming from two or more shallow-derived samples and not the MCE subset were lumped together (shown in only blue in **Figure 2**) and avoided for targeted isolation here, as were those resulting from two or more MCE-derived samples but not the shallow subset (shown in only red in **Figure 2**). The prioritized fungal strain, *Cymostachys* sp. NBUF082, was cultivated in large-scale for natural product discovery. Some other fungal samples along with their OSMAC culture conditions from the 240 combination set were also considered to be chemically interesting, and these were ranked lower in priority to be investigated and reported on in due time.

Structure Elucidation

Compound **1** was obtained as a white powder and assigned the molecular formula $C_9H_{10}O_3$ based on a proton adduct peak in the HRESIMS spectrum at *m/z* 167.0706 $[M + H]^+$ (calcd. for $C_9H_{11}O_3$, 167.0703). This formula indicated that **1** possessed five degrees of unsaturation. The ^1H and ^{13}C NMR data of **1** (**Table 1**) demonstrated the existence of one methoxy group (δ_H 3.71, δ_C 55.0; 7-*O*-CH_3), two oxygenated methylenes (δ_H 4.84, δ_c 70.9; CH_2-1 and δ_H 4.88, δ_C 73.1; CH_2-3), two aromatic methines (δ_H 6.26, δ_C 99.7; CH-4 and δ_H 6.27, δ_C 97.7; CH-6), and four nonprotonated sp^2 carbons (δ_C 141.5; C-3a, δ_C 159.1; C-5, δ_C 154.3; C-7, and δ_C 116.3; C-7a). A substituted phenolic group was deduced from the 1D NMR data, which accounted for four of five required degrees of unsaturation. The downfield protons CH_2-1 and CH_2-3 exhibited long range coupling with each other (J = 2.3 Hz), as is typical for the methylene units of a dihydroisobenzofuran, and the dihydrofuran subunit accounted for the last degree of unsaturation required for **1**. Observed correlations in the ^1H-^{13}C HMBC spectrum for H-1 with C-3, C-3a, and C-7, H-4 with C-3 and C-7a, H-6 with C-4 and C-7a, the protons of 7-*O*-CH_3 with C-7, and of 5-OH with C-4 and C-6 (**Figure 3**) were used to determine the substitution pattern for the aromatic ring. Altogether, this established the structure of **1** as 7-methoxy-1,3-dihydroisobenzofuran-5-ol, a new fungal natural product here named cymopolyphenol A, which is a methoxy analog of the 1,3-dihydroisobenzofuran-4,6-diol previously reported from *Neolentinus lepideus* (Li et al., 2013).

Compound **2** was also obtained as a white powder. The molecular formula of **2** was determined to have two less hydrogen atoms and one more oxygen than **1**, or $C_9H_8O_4$, after observation of the proton adduct peak in the HRESIMS spectrum at *m/z* 181.0500 $[M + H]^+$ (calcd. for $C_9H_9O_4$, 181.0495). This formula requires six degrees of unsaturation, which is one more than **1** has. The ^1H and ^{13}C NMR spectra of **2** resemble those of **1**, except that the absence of one oxygenated methylene group accompanied the addition of a carbonyl at δ_C 170.8 (C-1) for **2** (note that different carbon numbering schemes emerged for **1** and **2** due to the priority

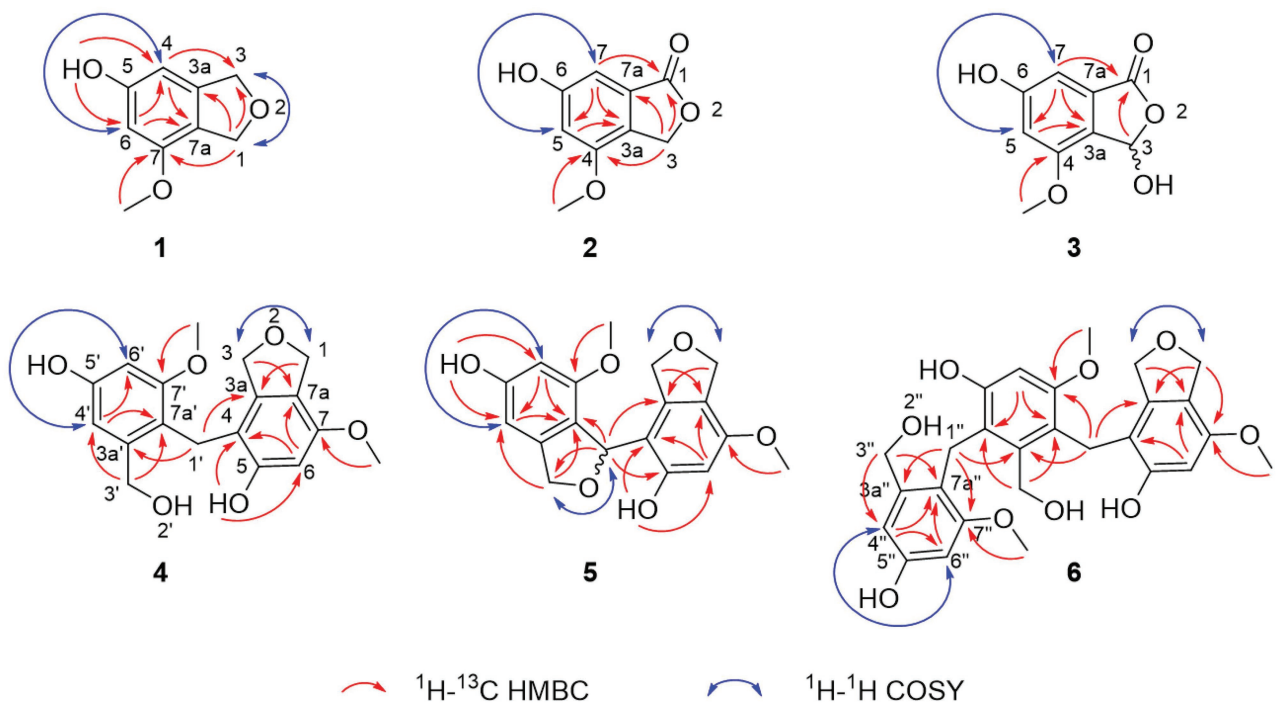

FIGURE 3 | Selected correlations used to determine the planar structures of cymopolyphenols A-F **(1–6)**. Red single-sided arrows represent cross peaks from the ^{1}H-^{13}C HMBC spectrum. Blue double-sided arrows show protons correlated in the ^{1}H-^{1}H COSY spectrum, and long-range *J* coupling that was determined for each from the ^{1}H spectrum.

of this carbonyl), and the long range coupling observed for CH_2-1 in **1** was not observed for the corresponding CH_2-3 in **2** (**Table 1**). The ^{1}H-^{13}C HSQC and HMBC spectra of **1** and **2** were also similar, and key correlations from H-3 to C-4 and H-7 to C-1 (**Figure 3**) led to the structure elucidation of **2** as an analog of **1** with C-3 being oxidized to an ester carbonyl and re-numbered as C-1. The incremented oxidation state of C-1 in **2** satisfied the difference in molecular formula and the corresponding additional unsaturation required compared to **1**, as well as an observed respective upfield shift of C-7a and downfield shifts of H-7, C-3a, C-5, and C-7. It was considered that the alternative position on the hydrofuran ring in **2** might instead be the oxidized carbon in the furan-1(3*H*)-one ring, if some 4-bond HMBC correlations were observed. However, the corresponding compound with C-1 bearing the lactone carbonyl adjacent the methoxy group rather than the phenyl proton has been reported in the literature as an intermediate in the total synthesis of notholaenic acid, and this alternative compound (measured in the same NMR solvent) has spectroscopic data that is distinct from **2** (El-Feraly et al., 1985). Thus compound **2** was established as 6-hydroxy-4-methoxyisobenzofuran-1(3*H*)-one, a new fungal natural product congener of the sparalides reported from *Sparassis crispa* (Wulf.) (Bang et al., 2017), here named as cymopolyphenol B.

Compound **3** was purified in crystalline form as colorless prisms. The molecular formula for this compound was obtained as $C_9H_8O_5$ due to the proton adduct peak observed in the HRESIMS at *m/z* 197.0453 $[M + H]^+$ (calcd. for $C_9H_9O_5$, 197.0444). Compared with compound **2**, this requires the same six degrees of unsaturation but one additional oxygen atom. The NMR data of **2** and **3** are quite similar (**Table 1**), with the noteworthy difference being that the oxygenated methylene of **2** (δ_H 5.23, δ_c 68.0; CH_2-3) was absent in **3**, and instead a significantly deshielded oxygenated methine group was observed (δ_H 6.44, δ_c 102.0; CH-3). The HSQC and ^{1}H-^{13}C HMBC spectra of **2** and **3** were also otherwise similar, and key correlations from H-3 to C-1 and H-7 to C-1 (**Figure 3**) led to the structure elucidation of **3** as an analog of **2** with C-3 being oxidized as a hemiacetal. Since this compound was obtained in crystalline form and is relatively devoid of signals in the ^{1}H NMR spectrum, it was decided to investigate the configuration of C-3 by X-ray crystallography rather than using a Mosher ester analysis. The crystallographic study of **3** confirmed the planar structure of this molecule (**Figure 4**). It was also found that this material was obtained in crystalline form as a racemic mixture, as indicated by the non-centrosymmetric space group *Cc* that would be invalid if **3** were enantio-pure (Parsons, 2017). The optical rotation measured for **3** $\{[\alpha]_D^{25}$ (*c* 0.1, MeOH)$\}$ was also zero, further supporting the assignment of the racemic mixture. This likely resulted from keto-enol tautomerization or lactone ring opening and re-closure in solution and during the extraction and purification process rather than non-stereospecific biosynthesis. The instability of **3** was further noted with the observation of an impurity of the proposedly 3-*O*-methyl analog in the NMR spectra measured first in CD_3OD (then diluted in MeOH for sample transfer) and later in DMSO-d_6, since corresponding peaks were not in the HRESIMS, nor was this impurity observed in the same sample by X-ray crystallography. The new natural product, **3**, was in summary established as 3,6-dihydroxy-4-methoxyisobenzofuran-1(3*H*)-one, here named as cymopolyphenol C.

Compound **4** was afforded in crystalline form as colorless prisms. The molecular formula was determined to be $C_{18}H_{20}O_6$ from its sodium adduct peak at *m/z* 355.1159 $[M + Na]^+$ (calcd. for $C_{18}H_{20}O_6Na$, 355.1152) in the HRESIMS. This formula calls for nine degrees of unsaturation. The ^{1}H and ^{13}C NMR data (**Table 2**) revealed that **4** possesses two methoxy groups (δ_H 3.678, δ_C 54.9; 7-*O*-CH_3; and δ_H 3.682, δ_C 55.3; 7'-*O*-CH_3), one aliphatic methylene (δ_H 3.674, δ_C 21.1; CH_2-1'), three oxygenated methylenes (δ_H 4.70, δ_C 70.3; CH_2-1, δ_H 4.16, δ_C 71.8; CH_2-3, and δ_H 4.23, δ_C 60.0; CH_2-3'), three aromatic methines (δ_H 6.37, δ_C 97.7; CH-6, δ_H 6.52, δ_C 105.3; CH-4' and δ_H 6.28, δ_C 96.9; CH-6′), and nine nonprotonated sp^2 carbons [δ_C 139.5 (C-3a), 112.8 (C-4), 155.6 (C-5), 151.4 (C-7), 116.4 (C-7a), 143.3 (C-3a'), 156.7 (C-5'), 158.2 (C-7'), and 114.2 (C-7a')]. From the NMR data, several key features from compounds **1**–**3** were observed in **4**. The HMBC correlations from H-1 to C-3a, from H-3 to C-7a, from 5-OH to C-4 and C-6, from H-6 to C-4 and C-7a, and 7-*O*-CH_3 to C-7, together with the long-range spin system of H-1 and H-3 (*J* = 2.4 Hz) indicated a

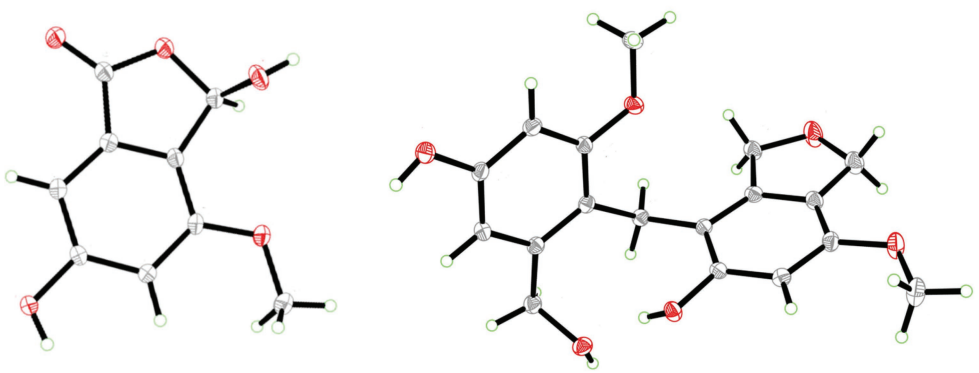

FIGURE 4 | X-ray ORTEP drawings of compounds **3** (left) and **4** (right).

7-methoxy-1,3-dihydroisobenzofuran-5-ol moiety in **4**. Inspection of the remaining NMR signals led to the establishment of a related tetra-substituted phenolic moiety that is representative of a ring opening between C-1 and O-2 in the dihydrofuran subunit of compound **1**, here presumed to be a monomeric subunit of **4**. The open-ring and closed-ring subunits mentioned above were determined to be connected from methylene C-1' to the nonprotonated aromatic C-4, with evidence of HMBC correlations from H-1' to both C-3a and C-3a'. The structure of **4** was thus established as a homodimer of 7-methoxy-1,3-dihydroisobenzofuran-5-ol (**1**) with ring opening between C-1' and O-2'. Compound **4** is here named as cymopolyphenol D, systematically 4-[4-hydroxy-2-(hydroxymethyl)-6-methoxybenzyl]-7-methoxy-1,3-dihydroisobenzofuran-5-ol. The structure of this new natural product was further confirmed by single-crystal X-ray diffraction analysis (**Figure 4**).

Compound **5** was isolated as a light-brown powder. The molecular formula of **5** was established as $C_{18}H_{18}O_6$ based on a sodium adduct peak observed in the HRESIMS at *m/z* 353.0997 $[M + Na]^+$ (calcd. for $C_{18}H_{18}O_6Na$, 353.0996). This formula requires 10 degrees of unsaturation, or one more than for the structure of **4**. Comparison of the ^1H and ^{13}C NMR data (**Table 2**) for **5** with those of **4** showed strong similarities except for the presence in **5** of one additional oxymethine (δ_H 6.41, δ_C 76.4; C-1') that accompanied the absence of an aliphatic methylene from **4**. Furthermore, the oxymethine C-1' exhibited long range coupling (J = 3.0, 1.9 Hz) with the diastereotopic protons of oxymethylene C-3′ [δ_H 5.00 (dd, J = 12.4, 3.0 Hz) and 4.84 (dd, J = 12.4, 1.9 Hz), δ_C 72.4], which was consistent with the protons of C-1 and C-3 coupling in compounds **1** and **4**, while the corresponding groups (C-1' and C-3') were not coupled and were observed as singlets in **4** (**Figure 3**). It was accordingly suggested that **5** is an analog of **4**, and another homodimer of **1**, but with both dihydroisobenzofuran subunits intact. This proposal accounted for the additional degree of unsaturation required for **5**, and was further supported in concept and attachment point by the HMBC correlations from H-1' to C-3a, C-5, and C-7a'. Therefore, the structure of **5** was established as a new homodimer of 7-methoxy-1,3-dihydroisobenzofuran-5-ol (**1**), as shown. Since C-1' is a chiral center, the optical rotation of **5** was measured, and this compound was found to be racemic {$[\alpha]_D^{25}$ 0 (*c* 0.1, MeOH)}. It was attempted to purify the enantiomers of **5** by HPLC using a chiral column, but the completely resolved separated peaks were found upon reinjection to have undergone racemization in solution. Accordingly, this racemic mixture (**5**) was assigned the common name cympolyphenol E and systematic name 7,7'-dimethoxy-1,1',3,3'-tetrahydro-[1,4'-biisobenzofuran]-5,5'-diol.

Compound **6** was obtained as a white powder and found to have the molecular formula $C_{27}H_{30}O_9$ based on the observed sodium adduct peak at *m/z* 521.1790 in the HRESIMS (calcd. For $C_{27}H_{30}O_9Na$, 521.1782). The NMR data of **6** had the hallmarks of both **4** and **5** (**Table 2**), and indicated the presence of one 7-methoxy-1,3-dihydroisobenzofuran-5-ol and two 3-(hydroxymethyl)-5-methoxyphenol moieties as monomeric substructures presumably all derived from **1**. The structural subunits were able to be connected unequivocally from C-1' to C-4 and C-1'' to C-4' by the observation of HMBC correlations from H-1' to C-3a, C-3a', and C-7' along with those from H-1'' to C-3a', C-3a'', and C-7'' (**Figure 3**). The structure of **6** was thus established as a homotrimer of 7-methoxy-1,3-dihydroisobenzofuran-5-ol (**1**), with one intact dihydroisobenzofuran moiety at the terminal monomeric subunit, as shown. This achiral molecule was assigned the common name of cymopolyphenol F, or 4-(4-hydroxy-3-(4-hydroxy-2-(hydroxymethyl)-6-methoxybenzyl)-2-(hydroxymethyl)-6-methoxybenzyl)-7-methoxy-1,3-dihydroisobenzofuran-5-ol.

It was considered whether compounds **4**–**6**, representing low-order polymers of **1**, might be extraction artifacts as opposed to biosynthetic products of fungal metabolism. These molecules could be biosynthesized *de novo*, using **1** as an intermediate, through radical coupling, or by acid/base reactions *via* a quinone methide pathway catalyzed by fungal enzymes. Alternatively, the compounds might be generated incidentally by the extraction and isolation protocol. However, the corresponding LC-MS peaks for these compounds were observed in the crude extract prior to purification by the relatively harsher conditions of repeated chromatographic separation. Furthermore, preliminary attempts to chemically synthesize compounds **4**–**6** from **1** at identical medium PDB used in scale-up fermentation, acid (pH = 4.0) and base (pH = 10.0) solvents at 28°C with agitation (120 rpm) for 15 days were unsuccessful.

Compounds **7** and **8** were identified as previously described molecules, respectively F1839-I and stachybotrylactone, by comparison of obtained NMR, MS, and optical rotation data with literature values (Ayer and Miao, 1993; Sakai et al., 1995; Zhao et al., 2017). Interestingly, stachybotrylactone was established at the time of its discovery as a spontaneous Cannizzaro reaction degradation product of the related molecule, stachybotrydial (Ayer and Miao, 1993). However, this known phenylspirodrimane fungal natural product contains as a substructure one of the new molecules here reported, **2**.

Biological Evaluation

Compound **2** was not obtained in sufficient quantity for biological testing in the present study. However, the purified compounds **1** and **3**–**8** were tested *in vitro* with a small array of bioassays to evaluate their potential for use in medicine, agriculture, aquaculture, or other biotechnology applications. For example, *in vitro* against the U87 human glioblastoma and CCRF-CEM human T lymphoblast cell lines, none of the tested compounds were found to be antiproliferative or cytotoxic (IC_{50} > 20 μM). Accordingly, these compounds were evaluated for activity against an array of aquatic and human pathogens including Gram-negative and Gram-positive bacteria: *P. carrageenovora*, *V. shilanii*, *V. scophthalmi*, *V. alginolyticus*, *S. typhi*, *P. aeruginosa*, *S. aureus*, and *B. pumilus*. Compounds **1** and **3**–**6** were found to be weakly antimicrobial (MIC 16–64 μg/ml) *in vitro* against some of these pathogens, as detailed in **Table 3**. While these compounds are not active against the human pathogens at concentrations with pharmaceutical relevance, it is of interest to find selective agents for the potential treatment of aquatic

TABLE 3 | *In vitro* antimicrobial activity observed for **1** and **3–8**.

Cpd	Minimum inhibition concentration (MIC, μg/ml)							
	Pseudoalteromonas carrageenovora	*Vibrio shilanii*	*Vibrio scophthalmi*	*Vibrio alginolyticus*	*Salmonella typhi*	*Pseudomonas aeruginosa*	*Staphylococcus aureus*	*Bacillus pumilus*
1	>64	>64	>64	64	>64	>64	>64	>64
3	32	>64	64	64	32	64	>64	>64
4	32	32	32	64	64	64	>64	>64
5	64	>64	>64	>64	>64	>64	32	>64
6	32	32	16	64	32	64	>64	>64
7	>64	>64	>64	>64	>64	>64	>64	>64
8	>64	>64	>64	>64	>64	>64	>64	>64
PC[a]	0.5	1	2	1	1	1	1	1
NC[b]	>64	>64	>64	>64	>64	>64	>64	>64

[a]*PC: norfloxacin, used as a positive control. The MIC of this compound was not tested below 0.5 μg/ml in this experiment, but it has been shown to be active ≤ 0.125 μg/ml in all organisms tested by the same experiment conducted at a different time.*
[b]*NC: blank media, used as a negative control.*

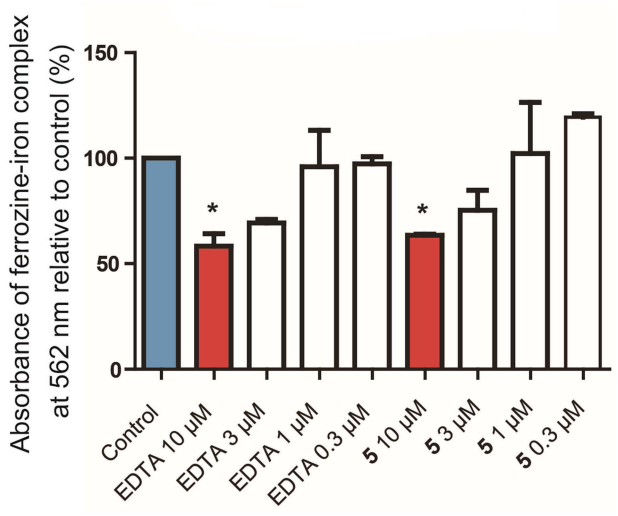

FIGURE 5 | *In vitro* chelation of **5** to Fe^{2+} in a ferrozine-based chemical assay. Control: Blank media, sodium acetate in water, used as a negative control. EDTA: Ethylenediaminetetraacetate, used as a positive control. *$p < 0.05$ vs. control.

pathogens for use in preventing economic losses in the aquaculture industry without risking the induction of drug resistance in human pathogens. Compounds **4** and **6** were the most active tested against the aquatic pathogens, which may indicate an ecological role of these new natural products and potential direction for further development based on the same scaffolds.

Due to the amount of oxygen atoms in the isolated compounds, especially **4**–**6**, it was considered whether these molecules could chelate iron. The chelation of iron by secondary metabolites has ecological implications, e.g., with siderophores, and can also play a role in various aspects of human health. For example, the deposition of iron in nerves causes oxidative stress and inflammation, leading to the kind of nerve damage that can be found in traumatic brain injury, Alzheimer's disease, and Parkinson's disease. When the pure molecules were tested in a ferrozine Fe^{2+} chelation chemical assay, it was found that compound **5** concentration-dependently chelated iron (**Figure 5**) with nearly the same efficacy at 10 μM as the positive control, ethylenediaminetetraacetate (EDTA). Interestingly, compound **4** was inactive in the same assay at 10 μM. This suggests that while the flexibility afforded to **4** by its structural subunits being linked with the C-1' methylene group rather than the C-1' dihydroisofuran methine in **5** may give it preferential antibacterial activity, the relatively locked conformation of **5** is more suitable for iron chelation. This also suggests that iron chelation is not the primary mechanism of antibiotic action of **4**.

Finally, the compounds were evaluated with an *in vivo* assay of inducing disease resistance in plants using the PR1::GUS transgenic model organism, *A. thaliana*. Pathogenesis-related protein 1 (PR1) is correlated to plant disease resistance, and β-glucuronidase (GUS) is attached as a reporter gene (Van Loon, 1997; Koornneef et al., 2008). As shown in **Figure 6**, plants treated with compound **8** at 10 μM were found to accumulate PR1, indicating the potential of this molecule to enhance plant disease resistance. The remaining compounds, including the close structural analog, **7**, were not found to activate PR1 in the same test model at 10 μM. This newly discovered function of **8** merits further investigation of structurally related molecules in this and similar ecological studies.

CONCLUSION

From preliminary MS/MS-based molecular networking analysis of 80 extracts prepared from marine sponge-associated fungal cultures, half from shallow reefs and half from MCEs, it was found that the extracts of fungal strains prepared from mesophotic zone sponge samples contained different chemistry than their shallow water counterparts. It is hypothesized that this is a representative phenomenon that should encourage the further chemical investigation of mesophotic zone organisms, and the

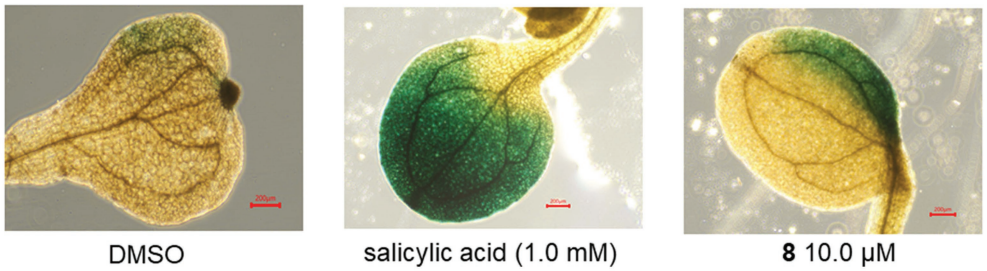

FIGURE 6 | *In vivo* activation of the GUS reporter in PR1::GUS transgenic *Arabidopsis thaliana* plants. DMSO was used as a negative control. Salicylic acid was used as a positive control.

purposeful generation and analysis of a larger data set is planned. The investigation of a prioritized *Cymostachys* fungus that was isolated from its association with a 103 m deep *Aaptos* sponge led to the discovery and structural characterization of a new series of compounds, cymopolyphenols A–F (**1**–**6**) along with the known fungal natural products F1839-I (**7**) and stachybotrylactone (**8**). Compounds **1**–**6** and **8** all contain a dihydroisobenzofuran skeleton, and **4**–**6** appear to be low-order polymers of **1** that present new scaffolds. Structural analogs of these compounds with different oxidation states, increased order of polymerization, and methylation patterns are predicted to emerge from future research on related organisms.

Compounds **1**–**6** are hydrogen deficient molecules, and each has a proton-to-heavy-atom ratio under 1, yet the structures of these molecules were able to be established by spectroscopic and spectrometric data interpretation. This fortuitous occurrence was due in equal parts to the dispersion of signals in the ^{1}H NMR spectrum without significant overlapping, and the distribution of the associated hydrogen atoms throughout the molecules that allowed for informative long-range correlations to be observed. Still, further support for all the structures was garnered from the X-ray crystallographic study of 3 and **4**. Compounds **1** and **3**–**6** were found to be weakly antimicrobial (MIC 16–64 μg/ml) *in vitro* against several Gram-positive and Gram-negative human or aquatic pathogens. These data are not suggestive of a meaningful lead for pharmaceutical development, but could potentially be useful in the development of aquaculture treatments or represent clues to an ecological role of the compounds.

DATA AVAILABILITY STATEMENT

The datasets presented in this study can be found in online repositories. The names of the repository/repositories and accession number(s) can be found in the article/**Supplementary Material**.

AUTHOR CONTRIBUTIONS

All authors conceived the research, analyzed the data, contributed to the study, and approved the final version of the manuscript. TW, JZh, JZo, YS, PS, TY, XL, and JY carried out the experiments. WZ, WC, XW, XY, CN, JL, and SH revised the manuscript.

FUNDING

This study was supported by the National Key Research and Development Program of China, funded through MOST (the Ministry of Science and Technology of China; grant 2018YFC0310900 to XY, CN, and SH), NSFC (the National Natural Science Foundation of China; grant 41906093 to TW, 41776168 to SH, and 81850410553 and 82050410451 to CN), the Natural Science Foundation of Zhejiang Province (grant LGF21D060003 to TW), Ningbo Public Service Platform for High-Value Utilization of Marine Biological Resources (grant NBHY-2017-P2 to SH), Research Fund for Science in Ningbo University (XYL20021 to TW), the National 111 Project of China (D16013), and the Li Dak Sum Yip Yio Chin Kenneth Li Marine Biopharmaceutical Development Fund of Ningbo University.

ACKNOWLEDGMENTS

We are grateful to Ting Han from Blue Flag Diving Club, for technical diving and collection of the sponges used for mycology in this research.

SUPPLEMENTARY MATERIAL

The Supplementary Material for this article can be found online at: https://www.frontiersin.org/articles/10.3389/fmicb.2021.638610/full#supplementary-material

REFERENCES

Agarwal, G., Carcache, P. J. B., Addo, E. M., and Kinghorn, A. D. (2020). Current status and contemporary approaches to the discovery of antitumor agents from higher plants. *Biotechnol. Adv.* 38:107337. doi: 10.1016/j.biotechadv.2019.01.004

Ayer, W. A., and Miao, S. (1993). Secondary metabolites of the aspen fungus *Stachybotrys cylindrospora*. *Can. J. Chem.* 71, 487–493. doi: 10.1139/v93-069

Azran, S., Danino, O., Förster, D., Kenigsberg, S., Reiser, G., Dixit, M., et al. (2015). Identification of highly promising antioxidants/neuroprotectants based on nucleoside 5'-phosphorothioate scaffold. Synthesis, activity, and

mechanisms of action. *J. Med. Chem.* 58, 8427–8443. doi: 10.1021/acs.jmedchem.5b00575

Bang, S., Chae, H. S., Lee, C., Choi, H. G., Ryu, J., Li, W., et al. (2017). New aromatic compounds from the fruiting body of *Sparassis crispa* (Wulf.) and their inhibitory activities on proprotein convertase subtilisin/kexin type 9 mRNA expression. *J. Agric. Food Chem.* 65, 6152–6157. doi: 10.1021/acs.jafc.7b02657

Bibi, F., Yasir, M., Al-Sofyani, A., Naseer, M. I., and Azhar, E. I. (2020). Antimicrobial activity of bacteria from marine sponge *Suberea mollis* and bioactive metabolites of *Vibrio* sp. EA348. *Saudi. J. Biol. Sci.* 27, 1139–1147. doi: 10.1016/j.sjbs.2020.02.002

Boudreau, P. D., Byrum, T., Liu, W. T., Dorrestein, P. C., and Gerwick, W. H. (2012). Viequeamide A, a cytotoxic member of the kulolide superfamily of cyclic depsipeptides from a marine button Cyanobacterium. *J. Nat. Prod.* 75, 1560–1570. doi: 10.1021/np300321b

CLSI (2018). *Methods for dilution antimicrobial susceptibility tests for bacteria that grow aerobically. 11th Edn.* Wayne, PA: Clinical and Laboratory Standards Institute.

Cragg, G. M., Grothaus, P. G., and Newman, D. J. (2009). Impact of natural products on developing new anti-cancer agents. *Chem. Rev.* 109, 3012–3043. doi: 10.1021/cr900019j

Da Lozzo, E. J., Mangrich, A. S., Rocha, M. E. M., de Oliveira, M. B. M., and Carnieri, E. G. S. (2002). Effects of citrinin on iron-redox cycle. *Cell Biochem. Funct.* 20, 19–29. doi: 10.1002/cbf.931

El-Feraly, F. S., Cheatham, S. F., and McChesney, J. D. (1985). Total synthesis of notholaenic acid. *J. Nat. Prod.* 48, 293–298. doi: 10.1021/np50038a015

Henríquez, M., Vergara, K., Norambuena, J., Beiza, A., Maza, F., Ubilla, P., et al. (2014). Diversity of cultivable fungi associated with Antarctic marine sponges and screening for their antimicrobial, antitumoral and antioxidant potential. *World J. Microbiol. Biotechnol.* 30, 65–76. doi: 10.1007/s11274-013-1418-x

Hirata, Y., and Uemura, D. (1986). Halichondrins—antitumor polyether macrolides from a marine sponge. *Pure Appl. Chem.* 58, 701–710. doi: 10.1351/pac198658050701

Höller, U., Wright, A. D., Matthee, G. F., Konig, G. M., Draeger, S., Aust, H. J., et al. (2000). Fungi from marine sponges: diversity, biological activity and secondary metabolites. *Mycol. Res.* 104, 1354–1365. doi: 10.1017/S0953756200003117

Jagels, A., Lindemann, V., Ulrich, S., Gottschalk, C., Cramer, B., Hübner, F., et al. (2019). Exploring secondary metabolite profiles of *Stachybotrys* spp. by LC-MS/MS. *Toxins* 11:133. doi: 10.3390/toxins11030133

Keller, N. P. (2019). Fungal secondary metabolism: regulation, function and drug discovery. *Nat. Rev. Microbiol.* 17, 167–180. doi: 10.1038/s41579-018-0121-1

Koornneef, A., Verhage, A., Leon-Reyes, A., Snetselaar, R., Van Loon, L. C., and Pieterse, C. M. J. (2008). Towards a reporter system to identify regulators of cross-talk between salicylate and jasmonate signaling pathways in *Arabidopsis*. *Plant Signal. Behav.* 3, 543–546. doi: 10.4161/psb.3.8.6151

Lachance, H., Wetzel, S., Kumar, K., and Waldmann, H. (2012). Charting, navigating, and populating natural product chemical space for drug discovery. *J. Med. Chem.* 55, 5989–6001. doi: 10.1021/jm300288g

Le Goff, G., Lopes, P., Arcile, G., Vlachou, P., Van Elslande, E., Retailleau, P., et al. (2019). Impact of the cultivation technique on the production of secondary metabolites by *Chrysosporium lobatum* TM-237-S5, isolated from the sponge *Acanthella cavernosa*. *Mar. Drugs* 17:678. doi: 10.3390/md17120678

Lesser, M. P., Slattery, M., and Mobley, C. D. (2018). Biodiversity and functional ecology of mesophotic coral reefs. *Annu. Rev. Ecol. Evol. Syst.* 49, 49–71. doi: 10.1146/annurev-ecolsys-110617-062423

Letsiou, S., Bakea, A., Le Goff, G., Lopes, P., Gardikis, K., Weis, M., et al. (2020). Marine fungus *Aspergillus chevalieri* TM2-S6 extract protects skin fibroblasts from oxidative stress. *Mar. Drugs* 18:460. doi: 10.3390/md18090460

Li, Y. X., Bao, L., Song, B., Han, J. J., Li, H. R., Zhao, F., et al. (2013). A new benzoquinone and a new benzofuran from the edible mushroom *Neolentinus lepideus* and their inhibitory activity in NO production inhibition assay. *Food Chem.* 141, 1614–1618. doi: 10.1016/j.foodchem.2013.04.133

Li, Q., and Wang, G. (2009). Diversity of fungal isolates from three Hawaiian marine sponges. *Microbiol. Res.* 164, 233–241. doi: 10.1016/j.micres.2007.07.002

Lin, C. G., McKenzie, E. H. C., Bhat, D. J., Ran, S. F., Chen, Y., Hyde, K. D., et al. (2016). *Stachybotrys*-like taxa from karst areas and a checklist of *Stachybotrys*-like species from Thailand. *Mycosphere* 7, 1273–1291. doi: 10.5943/mycosphere/7/9/3

Liu, N., Peng, S., Yang, J., Cong, Z., Lin, X., Liao, S., et al. (2019). Structurally diverse sesquiterpenoids and polyketides from a sponge-associated fungus *Aspergillus sydowii* SCSIO41301. *Fitoterapia* 135, 27–32. doi: 10.1016/j.fitote.2019.03.031

Lombard, L., Houbraken, J., Decock, C., Samson, R. A., Meijer, M., Réblová, M., et al. (2016). Generic hyper-diversity in *Stachybotriaceae*. *Persoonia Mol. Phylogeny Evol. Fungi* 36, 156–246. doi: 10.3767/003158516X691582

Machida, K., Abe, T., Arai, D., Okamoto, M., Shimizu, I., de Voogd, N. J., et al. (2014). Cinanthrenol A, an estrogenic steroid containing phenanthrene nucleus, from a marine sponge *Cinachyrella* sp. *Org. Lett.* 16, 1539–1541. doi: 10.1021/ol5000023

Mayer, A. M. S., Guerrero, A. J., Rodríguez, A. D., Taglialatela-Scafati, O., Nakamura, F., and Fusetani, N. (2020). Marine pharmacology in 2014–2015: Marine compounds with antibacterial, antidiabetic, antifungal, anti-inflammatory, antiprotozoal, antituberculosis, antiviral, and anthelmintic activities; affecting the immune and nervous systems, and other miscellaneous mechanisms of action. *Mar. Drugs* 18:5. doi: 10.3390/md18010005

McCauley, E. P., Piña, I. C., Thompson, A. D., Bashir, K., Weinberg, M., Kurz, S. L., et al. (2020). Highlights of marine natural products having parallel scaffolds found from marine-derived bacteria, sponges, and tunicates. *J. Antibiot.* 73, 504–525. doi: 10.1038/s41429-020-0330-5

Newman, D. J., and Cragg, G. M. (2020). Natural products as sources of new drugs over the nearly four decades from 01/1981 to 09/2019. *J. Nat. Prod.* 83, 770–803. doi: 10.1021/acs.jnatprod.9b01285

Nikolaivits, E., Agrafiotis, A., Termentzi, A., Machera, K., Le Goff, G., Álvarez, P., et al. (2019). Unraveling the detoxification mechanism of 2,4-dichlorophenol by marine-derived mesophotic symbiotic fungi isolated from marine invertebrates. *Mar. Drugs* 17:564. doi: 10.3390/md17100564

Olson, J. B., and Kellogg, C. A. (2010). Microbial ecology of corals, sponges, and algae in mesophotic coral environments. *FEMS Microbiol. Ecol.* 73, 17–30. doi: 10.1111/j.1574-6941.2010.00862.x

Parsons, S. (2017). Determination of absolute configuration using X-ray diffraction. *Tetrahedron Asymmetry* 28, 1304–1313. doi: 10.1016/j.tetasy.2017.08.018

Pedrosa, R., Gaudêncio, P. S., and Vasconcelos, V. (2020). XVI international symposium on marine natural products |XI European conference on marine natural products. *Mar. Drugs* 18:40. doi: 10.3390/md18010040

Pyle, R. L., and Copus, J. M. (2019). "Mesophotic coral ecosystems: introduction and overview" in *Mesophotic coral ecosystems*. eds. Y. Loya, K. A. Puglise and T. Bridge (Springer: New York), 3–27.

Rocha, L. A., Pinheiro, H. T., Shepherd, B., Papastamatiou, Y. P., Luiz, O. J., Pyle, R. L., et al. (2018). Mesophotic coral ecosystems are threatened and ecologically distinct from shallow water reefs. *Science* 361, 281–284. doi: 10.1126/science.aaq1614

Sakai, K., Watanabe, K., Masuda, K., Tsuji, M., Hasumi, K., and Endo, A. (1995). Isolation, characterization and biological activities of novel triprenyl phenols as pancreatic cholesterol esterase inhibitors produced by *Stachybotrys* sp. F-1839. *J. Antibiot.* 48, 447–456. doi: 10.7164/antibiotics.48.447

Schupp, P. J., Kohlert-Schupp, C., Whitefield, S., Engemann, A., Rohde, S., Hemscheidt, T., et al. (2009). Cancer chemopreventive and anticancer evaluation of extracts and fractions from marine macro- and micro-organisms collected from twilight zone waters around Guam. *Nat. Prod. Commun.* 4, 1717–1728. doi: 10.1177/1934578X0900401222

Sinniger, F., Ballantine, D. L., Bejarano, I., Colin, P. L., Pochon, X., Pomponi, S. A., et al. (2016). "Biodiversity of mesophotic coral ecosystems" in *Mesophotic coral ecosystems—A lifeboat for coral reefs?* eds. E. K. Baker, K. Puglise and P. Harris (Arendal, Nairobi and Arendal: The United Nations Environment Programme and GRID), 50–62.

Still, P. C., Johnson, T. A., Theodore, C. M., Loveridge, S. T., and Crews, P. (2014). Scrutinizing the scaffolds of marine biosynthetics from different source organisms: Gram-negative cultured bacterial products enter center stage. *J. Nat. Prod.* 77, 690–702. doi: 10.1021/np500041x

Suffness, M., and Douros, J. D. (1981). Discovery of antitumor agents from natural sources. *Trends Pharmacol. Sci.* 2, 307–310. doi: 10.1016/0165-6147(81)90349-7

Van Loon, L. C. (1997). Induced resistance in plants and the role of pathogenesis-related proteins. *Eur. J. Plant Pathol.* 103, 753–765. doi: 10.1023/A:1008638109140

Wang, M., Carver, J. J., Phelan, V. V., Sanchez, L. M., Garg, N., Peng, Y., et al. (2016). Sharing and community curation of mass spectrometry data with Global Natural Products Social Molecular Networking. *Nat. Biotechnol.* 34, 828–837. doi: 10.1038/nbt.3597

Wang, A., Xu, Y., Gao, Y., Huang, Q., Luo, X., An, H., et al. (2015). Chemical and bioactive diversities of the genera *Stachybotrys* and *Memnoniella* secondary metabolites. *Phytochem. Rev.* 14, 623–655. doi: 10.1007/s11101-014-9365-1

Wang, S., Zheng, Y., Gu, C., He, C., Yang, M., Zhang, X., et al. (2018). *Bacillus cereus* AR156 activates defense responses to *Pseudomonas syringae* pv *tomato* in *Arabidopsis thaliana* similarly to flg22. *Mol. Plant-Microbe Interact.* 31, 311–322. doi: 10.1094/MPMI-10-17-0240-R

Weiss, K. R. (2017). Into the twilight zone. *Science* 355, 900–904. doi: 10.1126/science.355.6328.900

Williams, R. B., Martin, S. M., Lawrence, J. A., Norman, V. L., O'Neil-Johnson, M., Eldridge, G. R., et al. (2017). Isolation and identification of the novel tubulin polymerization inhibitor bifidenon. *J. Nat. Prod.* 80, 616–624. doi: 10.1021/acs.jnatprod.6b00893

Wright, A. D., Schupp, P. J., Schrör, J.-P., Engemann, A., Rohde, S., Kelman, D., et al. (2012). Twilight zone sponges from Guam yield theonellin isocyanate and psammaplysins I and J. *J. Nat. Prod.* 75, 502–506. doi: 10.1021/np200939d

Zhang, B., Zhang, T., Xu, J., Lu, J., Qiu, P., Wang, T., et al. (2020). Marine sponge-associated fungi as potential novel bioactive natural product sources for drug discovery: a review. *Mini Rev. Med. Chem.* 20, 1966–2010. doi: 10.2174/1389557520666200826123248

Zhao, J., Feng, J., Tan, Z., Liu, J., Zhao, J., Chen, R., et al. (2017). Stachybotrysins A−G, phenylspirodrimane derivatives from the fungus *Stachybotrys chartarum*. *J. Nat. Prod.* 80, 1819–1826. doi: 10.1021/acs.jnatprod.7b00014

Zheng, H., Zhang, Z., Liu, D. Z., and Yu, Z. F. (2019). *Memnoniella sinensis* sp. nov., a new species from China and a key to species of the genus. *Int. J. Syst. Evol. Microbiol.* 69, 3161–3169. doi: 10.1099/ijsem.0.003605

Conflict of Interest: The authors declare that the research was conducted in the absence of any commercial or financial relationships that could be construed as a potential conflict of interest.

frontiers in Microbiology

ORIGINAL RESEARCH
published: 11 June 2021
doi: 10.3389/fmicb.2021.688202

Sesquiterpenoids From the Antarctic Fungus *Pseudogymnoascus* sp. HSX2#-11

*Ting Shi[1], Xiang-Qian Li[1,2], Li Zheng[3,4], Ya-Hui Zhang[5,6], Jia-Jia Dai[1], Er-Lei Shang[7], Yan-Yan Yu[1], Yi-Ting Zhang[1], Wen-Peng Hu[1] and Da-Yong Shi[1,2]**

[1] State Key Laboratory of Microbial Technology, Institute of Microbial Technology, Shandong University, Qingdao, China, [2] Laboratory for Marine Drugs and Bioproducts of Qingdao National Laboratory for Marine Science and Technology, Qingdao, China, [3] Key Laboratory of Marine Eco-Environmental Science and Technology, First Institute of Oceanography, Ministry of Natural Resources, Qingdao, China, [4] Laboratory for Marine Ecology and Environmental Science, Qingdao Pilot National Laboratory for Marine Science and Technology, Qingdao, China, [5] Key Laboratory of Marine Drugs, The Ministry of Education of China, School of Medicine and Pharmacy, Ocean University of China, Qingdao, China, [6] Laboratory for Marine Drugs and Bioproducts, Qingdao National Laboratory for Marine Science and Technology, Qingdao, China, [7] State Key Laboratory of Pharmaceutical Biotechnology, School of Life Sciences, Nanjing University, Nanjing, China

The fungal strains *Pseudogymnoascus* are a kind of psychrophilic pathogenic fungi that are ubiquitously distributed in Antarctica, while the studies of their secondary metabolites are infrequent. Systematic research of the metabolites of the fungus *Pseudogymnoascus* sp. HSX2#-11 led to the isolation of six new tremulane sesquiterpenoids pseudotremulanes A–F (**1**–**6**), combined with one known analog 11,12-epoxy-12β-hydroxy-1-tremulen-5-one (**7**), and five known steroids (**8**–**12**). The absolute configurations of the new compounds (**1**–**6**) were elucidated by their ECD spectra and ECD calculations. Compounds **1**–**7** were proved to be isomeride structures with the same chemical formula. Compounds **1**/**2**, **3**/**4**, **1**/**4**, and **2**/**3** were identified as four pairs of epimerides at the locations of C-3, C-3, C-9, and C-9, respectively. Compounds **8** and **9** exhibited cytotoxic activities against human breast cancer (MDA-MB-231), colorectal cancer (HCT116), and hepatoma (HepG2) cell lines. Compounds **9** and **10** also showed antibacterial activities against marine fouling bacteria *Aeromonas salmonicida*. This is the first time to find terpenoids and steroids in the fungal genus *Pseudogymnoascus*.

Keywords: Antarctic fungus, *Pseudogymnoascus* sp. HSX2#-11, sesquiterpenoids, steroids, cytotoxicity, antibacterial activity

OPEN ACCESS

Edited by:
Carolina Elena Girometta, University of Pavia, Italy

Reviewed by:
Fei Cao, Hebei University, China
Madhuree Kumari, Indian Institute of Science (IISc), India

***Correspondence:**
Da-Yong Shi
shidayong@sdu.edu.cn

Specialty section:
This article was submitted to Microbiotechnology, a section of the journal Frontiers in Microbiology

Received: *30 March 2021*
Accepted: *06 May 2021*
Published: *11 June 2021*

Citation:
Shi T, Li X-Q, Zheng L, Zhang Y-H, Dai J-J, Shang E-L, Yu Y-Y, Zhang Y-T, Hu W-P and Shi D-Y (2021) Sesquiterpenoids From the Antarctic Fungus Pseudogymnoascus sp. HSX2#-11. Front. Microbiol. 12:688202. doi: 10.3389/fmicb.2021.688202

INTRODUCTION

Tremulanes, a family of sesquiterpenoids with characteristic structures of 5/7 fused bicyclic system, were rarely discovered in nature until 2015 (Guo et al., 2016). However, from 2016 to 2020, about 60 tremulane derivatives were found (Guo et al., 2016; Isaka et al., 2016; Wu, 2016; Chen et al., 2017, 2018; Cong et al., 2020; Wang et al., 2017, 2020; Ding et al., 2018, 2019, 2020a,b; Zhou et al., 2018; Duan et al., 2019; Wu et al., 2019, 2020; He et al., 2020; Lee et al., 2020; Shi et al., 2020; Sun C.-T. et al., 2020), and the number is twice as many as before. Most of them were isolated from the cultures of the basidiomycetes *Irpex lacteus* (Chen et al., 2018, 2020; Ding et al., 2018, 2019, 2020a,b;

Zhou et al., 2018; Duan et al., 2019; Wu et al., 2019; Shi et al., 2020; Sun C.-T. et al., 2020; Wang et al., 2020). All the tremulanes isolated from 2016 to 2020 were derived from fungi, except one derivative, which was obtained from a traditional Chinese medicine tabasheer (Wu, 2016). Some of them were discovered to have different bioactivities, such as tremutin A with the inhibition of the lipopolysaccharide-induced proliferation of B lymphocyte cells (Wang et al., 2020), and 5-demethyl conocenol C showed antifungal activities (Wu et al., 2019).

The extreme environments of Antarctica, including cold, dry climate and intense solar radiations, have nurtured a number of unique microbial resources (Cong et al., 2020). It has been proved that Antarctic microorganisms, especially fungi, have the potential capacity to produce novel secondary metabolites to adapt to the harsh environments (Kwon et al., 2017; Rusman et al., 2018; Yu et al., 2019; Sun C. et al., 2020). *Pseudogymnoascus* are known as a kind of psychrophilic pathogenic fungi with ubiquitous distribution in Antarctica (Rosa et al., 2020; Santos et al., 2020; Martorell et al., 2021). These fungal strains have been proved to have the abilities to produce cold-adapted enzymes to adapt severe cold Antarctic environment (Loperena et al., 2012; Poveda et al., 2018). *Pseudogymnoascus* can be antagonistic fungi against potato scab pathogens from potato field soils (Tagawa et al., 2010) and have been certified to be one of the predominant microbial colonizers in the root endosphere and rhizosphere of turfgrass systems (Xia et al., 2021). The extracts of some of *Pseudogymnoascus* strains exhibit potent bioactivities, such as antimicrobial, herbicidal, and antitumoral activities (Henríquez et al., 2014; Gonçalves et al., 2015; Gomes et al., 2018; Ferrarezi et al., 2019). However, only four studies have been done on the secondary metabolites of the genus *Pseudogymnoascus* until now, as far as we know, and most of the obtained structures focus on polyketides, showing antimicrobial activities (Figueroa et al., 2015; Guo et al., 2019; Fujita et al., 2021; Shi et al., 2021). Rare studies about the secondary metabolites of these fungi enlighten that there is latent space for searching novel compounds. *Pseudogymnoascus* sp. HSX2#-11 was an Antarctic fungus isolated from a soil sample of the Fields Peninsula, which can produce abundant and various secondary metabolites, according to our previous research on the fingerprint spectrum and molecular network of its ethyl acetate extract of the fermentation broth (Shi et al., 2021). Further chemical investigation resulted in the isolation and identification of six new tremulane sesquiterpenoids, pseudotremulanes A–F (**1**–**6**), together with one known analog 11,12-epoxy-12β-hydroxy-1-tremulen-5-one (**7**; Zhou et al., 2008), and five known steroids, ganodermasides A (**8**), B (**9**), and D (**10**; Weng et al., 2010, 2011), ergosterol (**11**; Feng et al., 2010), and dankasterone B (**12**; Amagata et al., 2007; **Figure 1**). Compounds **8** and **9** exhibited cytotoxicities against human breast cancer cell line MDA-MB-231, colorectal cancer cell line HCT116, and hepatoma cell line HepG2 (**Table 3**). Compounds **9** and **10** showed antibacterial activity against marine fouling bacteria *Aeromonas salmonicida*. Here, we address the isolation, structure elucidation, and biological activity evaluation of the isolated compounds.

EXPERIMENTAL SECTION

General Experimental Procedures

Optical rotations were measured on a JASCO P-1020 digital polarimeter (JASCO, Japan). The UV spectrum was recorded using an Implen Gmbh NanoPhotometer N50 Touch (Implen, Germany). ECD spectra were obtained on a Jasco J-815-150S circular dichroism spectrometer (JASCO, Japan). NMR spectra were recorded on a Bruker AVANCE NEO (Bruker, Switzerland) at 600 MHz for ^{1}H and 150 MHz for ^{13}C in $CDCl_3$. Chemical shifts δ were recorded in ppm using TMS as the internal standard. HR-APCI-MS spectra were measured on a Thermo Scientific LTQ Orbitrap XL spectrometer (Thermo Fisher Scientific, Bremen, Germany). HPLC separation was performed using a Hitachi Primaide Organizer Semi-HPLC system (Hitachi High Technologies, Tokyo, Japan) coupled with a Hitachi Primaide 1430 photodiodearray detector (Hitachi High Technologies, Tokyo, Japan). A Kromasil C_{18} semi-preparative HPLC column (250 × 10 mm, 5 μm; Eka Nobel, Bohus, Sweden) was used. Silica gel (200–300 mesh; Qingdao Marine Chemical Group Co., Qingdao, China) and Sephadex LH-20 (Amersham Biosciences Inc., Piscataway, NJ, United States) were used for column chromatography (CC). Precoated silica gel GF254 plates (20 × 20 cm, Yantai Zifu Chemical Group Co., Yantai, China).

Fungal Materials

The soil samples were collected in ice-free areas (about 10 cm underground) of the Fields Peninsula using sterile spatulas and sterilized WhirlPak bags (Sigma-Aldrich, United States), and were transported to the lab in sealed foam package with dry ice added by airplane, at the Chinese 35th Antarctic expedition in 2019. The fungus *Pseudogymnoascus* sp. HSX2#-11 was isolated from a soil sample from Fields Peninsula. The strain was deposited at −80°C in the State Key Laboratory of Microbial Technology, Institute of Microbial Technology, Shandong University, Qingdao, China.

The identification of the fungal strain HSX2#-11 was conducted by the analysis of the 28S rRNA gene sequence. The fresh fungal mycelium (about 1.00 mg) was dispersed in a 50 μl lysis buffer for the microorganisms to direct PCR (Takara, Cat# 9164), saved in metal bath (Yooning, China) at 100°C for 30 min to extract its genomic DNA as the template DNA. The PCRs were performed in a final volume of 50 μl, which was composed of the template DNA (3 μl), ITS1 (1 μl), ITS4 (1 μl), PrimeSTAR® Max DNA Polymerase (25 μl, Takara, Cat# R045A), and ultrapure water (20 μl), under the following procedures: (1) initial denaturation at 98°C for 5 min; (2) denaturation at 98°C for 30 s; (3) annealing at 55°C for 30 s; (4) extension at 72°C for 1 min; and (5) final extension at 72°C for 10 min. Steps 2–4 were repeated 30 times. The PCR products were then submitted for sequencing (BGI, China) with the primers ITS1 and ITS4. The sequence of HSX2#-11 was searched in the NCBI nucleotide collection database through the BLAST program. The phylogenetic tree of the top 20 most similar to this fungal sequence identified the strain HSX2#-11 as

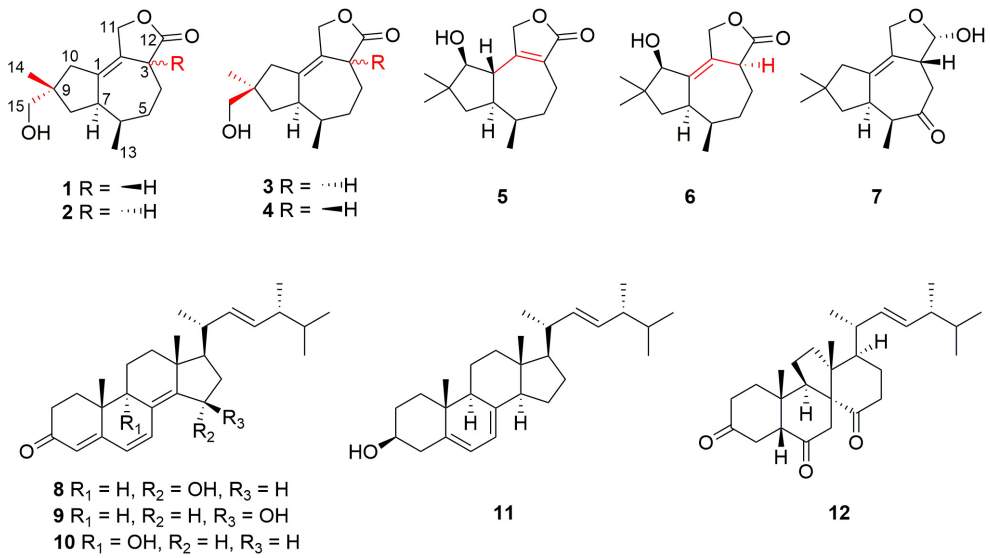

FIGURE 1 | Structures of compounds **1**–**12**.

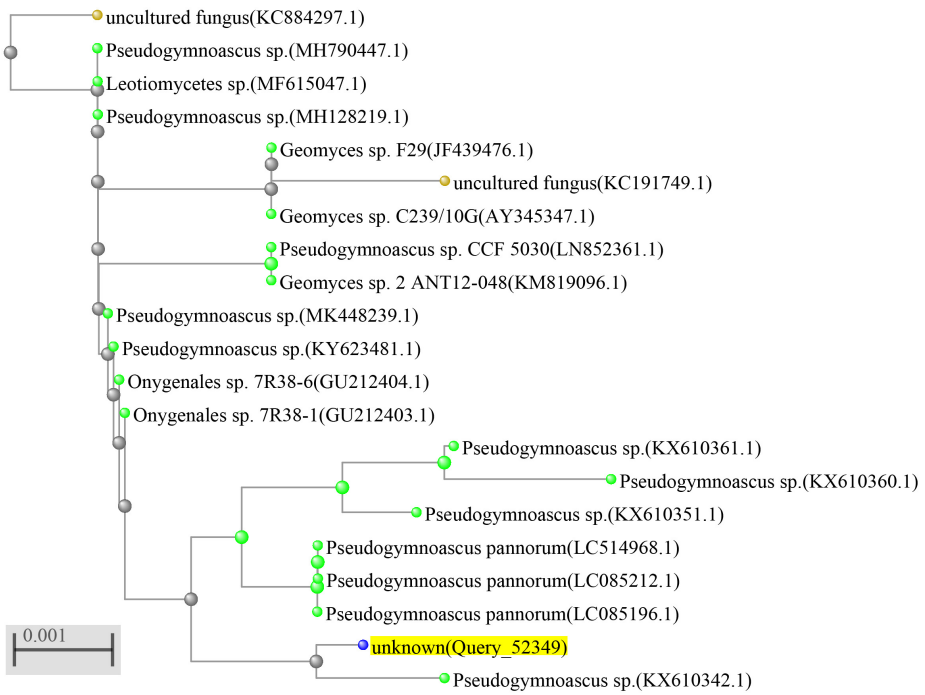

FIGURE 2 | Phylogenetic tree of the fungus *Pseudogymnoascus* sp. HSX2#-11.

a *Pseudogymnoascus* sp. (**Figure 2**), with GenBank (NCBI) accession number MT367223.1.

Extraction and Isolation

The fungal strain *Pseudogymnoascus* sp. HSX2#-11 was fermented in a PDA liquid medium in 200 Erlenmeyer flasks (300 ml in each 1,000-ml flask) at 16°C in air condition room for 45 days. The culture (60 L) was filtered to separate the broth from the mycelia. Then the mycelia were extracted three times with EtOAc (3 × 4,000 ml) and then repeatedly extracted with CH_2Cl_2–MeOH (v/v, 1:1) three times (3 × 4,000 ml). The broth was extracted repeatedly with EtOAc (3 × 60 L) to get the EtOAc layer. All the extracts were combined and then evaporated to dryness under reduced pressure to afford a residue (71.5 g). The residue was subjected to vacuum liquid chromatography on silica gel using step gradient elution

with EtOAc–petroleum ether (PE; 0–100%) and then with MeOH–EtOAc (0–100%) to afford eight fractions (Fr.1–Fr.8). Fr.2 was the pure compound **11** (89.7 mg). Fr.3 was first subjected to the gradient elution of ODS CC with MeOH in H_2O (10–100%) and then purified by using semipreparative HPLC on an ODS column (Kromasil C_{18}, 250 × 10 mm, 5 μm, 2 ml/min) eluted with 85% MeOH–H_2O to give compound **12** (2.7 mg). Fr.4 was isolated by CC on Sephadex LH-20 eluted with CH_2Cl_2–MeOH (v/v, 1:1) to afford two fractions (Fr.4.1, Fr.4.2). Fr.4.1 was subjected to silica gel CC eluting with EtOAc–PE (0–50%) to get three fractions (Fr.4.1.1–4.1.3). Fr.4.1.1 was first purified by HPLC eluted with 60% MeOH–H_2O to give compound **7** (1.9 mg), and then purified by HPLC eluted with 40% MeCN–H_2O to afford **5** (0.1 mg) and **6** (0.2 mg). Fr.4.1.2 was subjected on HPLC eluting with 35% MeCN–H_2O to give **1** (0.7 mg) and **2** (0.7 mg). Fr.4.1.3 was separated on HPLC eluting with 30% MeCN–H_2O to get **3** (0.6 mg) and **4** (0.5 mg). Fr.4.2 was first separated on silica gel CC eluting with EtOAc–PE (0–50%), and then purified by HPLC eluting with 75% MeOH–H_2O to gain **8** (13.6 mg), **10** (3.1 mg), and **9** (11.1 mg).

Pseudotremulane A (**1**): colorless oil; $[\alpha]_D^{20}$ + 8.6 (*c* 0.058, MeOH); UV (CH_2Cl_2) λ_{max} (log ε): 224 (4.90) nm; CD (3.4 mM, MeOH) λ_{max} ($\Delta\varepsilon$) 204 (+9.51), 230 (−4.31) nm; ^{1}H and ^{13}C NMR data, see **Tables 1**, **2**; HR-APCI-MS m/z 251.1641 $[M + H]^+$ (calcd for $C_{15}H_{23}O_3$, 251.1642).

Pseudotremulane B (**2**): colorless oil; $[\alpha]_D^{20}$ + 13.9 (*c* 0.058, MeOH); UV (CH_2Cl_2) λ_{max} (log ε): 223 (4.82); CD (3.4 mM, MeOH) λ_{max} ($\Delta\varepsilon$) 223 (+4.80) nm; ^{1}H and ^{13}C NMR data, see **Tables 1**, **2**; HR-APCI-MS m/z 251.1641 $[M + H]^+$ (calcd for $C_{15}H_{23}O_3$, 251.1642).

Pseudotremulane C (**3**): colorless oil; $[\alpha]_D^{20}$ + 20.6 (*c* 0.050, MeOH); UV (CH_2Cl_2) λ_{max} (log ε): 228 (4.48); CD (4.0 mM, MeOH) λ_{max} ($\Delta\varepsilon$) 217 (+3.05) nm; ^{1}H and ^{13}C NMR data, see **Tables 1**, **2**; HR-APCI-MS m/z 251.1642 $[M + H]^+$ (calcd for $C_{15}H_{23}O_3$, 251.1642).

Pseudotremulane D (**4**): colorless oil; $[\alpha]_D^{20}$ + 8.5 (*c* 0.042, MeOH); UV (CH_2Cl_2) λ_{max} (log ε): 223 (4.88); CD (2.4 mM, MeOH) λ_{max} ($\Delta\varepsilon$) 205 (+13.51), 232 (−5.56) nm; ^{1}H and ^{13}C NMR data, see **Tables 1**, **2**; HR-APCI-MS m/z 251.1641 $[M + H]^+$ (calcd for $C_{15}H_{23}O_3$, 251.1642).

Pseudotremulane E (**5**): colorless oil; $[\alpha]_D^{20}$ −75.0 (*c* 0.008, MeOH); UV (CH_2Cl_2) λ_{max} (log ε): 224 (5.51); CD (1.2 mM, MeOH) λ_{max} ($\Delta\varepsilon$) 222 (−0.29), 247 (+1.29) nm; ^{1}H and ^{13}C NMR data, see **Tables 1**, **2**; HR-APCI-MS m/z 251.1638 $[M + H]^+$ (calcd for $C_{15}H_{23}O_3$, 251.1642).

Pseudotremulane F (**6**): colorless oil; $[\alpha]_D^{20}$ + 7.9 (*c* 0.017, MeOH); UV (CH_2Cl_2) λ_{max} (log ε): 221 (5.17); CD (6.0 mM, MeOH) λ_{max} ($\Delta\varepsilon$) 223 (+4.29) nm; ^{1}H and ^{13}C NMR data, see **Tables 1**, **2**; HR-APCI-MS m/z 251.1641 $[M + H]^+$ (calcd for $C_{15}H_{23}O_3$, 251.1642).

Cytotoxicity Assays

Cytotoxicities against human breast cancer (MDA-MB-231), colorectal cancer (HCT116), lung carcinoma (A549), pancreatic carcinoma (PANC-1), and hepatoma (HepG2) cell lines were evaluated using the SRB method (Skehan et al., 1990). Adriamycin was used as a positive control. The cell lines of MDA-MB-231, HCT116, A549, PANC-1, and HepG2 in the logarithmic growth phase were seeded into 96-well plates with 5,000 cells/well (100 μl/well), respectively. After 24 h of culture, the isolated compounds to be tested were added (the final concentration was shown in **Supplementary Table 1**), and three replicates were set for each concentration. The dosage of DMSO in the solvent control group was 0.1% of the maximum dose used in the test group. After 72 h of drug treatment, 10% (m/v) of cold trichloroacetic acid was added to each well to fix the cells. After SRB staining, 150 μl/well Tris solution was added to determine the optic density (OD) values at 515 nm on a microplate reader (TriStar^2 S LB 942 Multimode Reader, Berthold Technologies, Germany). The inhibition rates of the tumor cell growth were calculated by the following formula:

$$\text{Inhibition rate } (\%) = \left(\text{OD}_{\text{DMSO}} - \text{OD}_{\text{compound}}\right) / \text{OD}_{\text{DMSO}} \times 100$$

The IC_{50} values were calculated using the method of log (inhibitor) vs. normalized response in the software package GraphPad Prism 5.

Antibacterial Activity Assays

The antibacterial activities were evaluated by the conventional broth dilution assay (Appendino et al., 2008). Nine marine fouling bacteria, *Pseudomonas fulva*, *Aeromonas hydrophila*, *A. salmonicida*, *Vibrio anguillarum*, *V. harveyi*, *Photobacterium halotolerans*, *P. angustum*, *Enterobacter cloacae*, and *E. hormaechei*, were used, and cipofloxacin was used as a positive control. The initial screening of antibacterial activity assays was tested in a 96-well plate. Each well contained 198 μl tested bacterial suspension (2–5 × 10^5 CFU/ml in LB broth) and 2 μl compound (final concentration was 20 μM). Three replicates were performed. The plates were incubated at 37°C for 24 h, and then the OD values were tested at 600 nm in a microplate reader (TriStar^2 S LB 942 Multimode Reader, Berthold Technologies, Germany). The inhibitory rates were calculated according to the following formula:

$$\text{Inhibition rate } (\%) = \left(\text{OD}_{\text{DMSO}} - \text{OD}_{\text{compound}}\right) / \text{OD}_{\text{DMSO}} \times 100$$

The MIC values of some active target compounds were evaluated using the twofold serial dilution method. The concentrations of the compounds ranged from 100 to 6.25 μM. The other steps were the same as in the primary screening. The MIC values were calculated using the method of log (inhibitor) vs. normalized response in the software package GraphPad Prism 5.

RESULTS

Structure Elucidations of Isolated Compounds

Pseudotremulane A (**1**) was obtained as a colorless oil. Its molecular formula, $C_{15}H_{22}O_3$, was determined by the

TABLE 1 | ^{1}H NMR data of compounds **1**–**6** in $CDCl_3$ at 600 MHz.

No.	1	2	3	4	5	6
1					2.71, t (10.5)	
3	3.03–2.99, m	3.14–3.08, m	3.15, d (12.1)	3.03, d (12.2)		3.16, dt (12.1, 2.8)
4	2.23, dd (13.5, 6.1)	1.95, ddt (14.0, 5.3, 2.7)	1.96, ddt (13.3, 5.5, 2.8)	2.25, dd (14.1, 6.2)	2.47, d (16.9)	2.01–1.96, m
	1.75, dd (13.5, 6.2)	1.62, ddd (14.0, 12.5, 2.1)	1.63, ddd (13.3, 12.1, 2.1)	1.88–1.78, m	2.38–2.29, m	1.65, d (13.2)
5	2.05, dd (14.2, 8.5)	2.03–1.98, m	2.04–1.99, m	2.11–2.04, m	1.71–1.62, m	2.05–2.02, m
	1.47, td (14.2, 6.2)	1.77, dt (13.5, 2.7)	1.81–1.79, m	1.49, dt (13.3, 6.2)		1.79, t (13.2)
6	2.11–2.07, m	1.91–1.86, m	1.91, dq (7.0, 3.0)	2.17–2.11, m	2.08–2.00, m	1.96–1.91, m
7	3.10–3.03, m	2.89–2.83, m	2.98–2.92, m	3.16, br s	2.08–2.00, m	2.91–2.86, m
8	1.82–1.77, m	1.82–1.79, m	1.58, t (12.0)	1.60, t (12.0)	1.60–1.56, m	1.69, d (12.0)
	1.41, t (12.5)	1.40, dd (13.3, 10.7)	1.50, dd (12.0, 8.4)	1.42, dd (12.0, 7.3)	1.53–1.50, m	1.46, dd (12.0, 8.1)
10	2.32, d (17.5)	2.13, d (16.1)	2.07, d (15.7)	2.17–2.11, m	3.64, dd (10.5, 6.2)	3.73, s
	1.90, d (17.5)	1.86–1.82, m	1.85–1.81, m	2.11–2.04, m		
11	4.67, d (10.3)	4.75, d (13.2)	4.75, d (13.3)	4.67, d (12.0)	4.91, d (17.8)	5.00, d (13.6)
	4.65, d (10.3)	4.69, d (13.2)	4.68, d (13.3)	4.62, d (12.0)	4.81, d (17.8)	4.88, d (13.6)
13	0.93, d (7.2)	0.88, d (6.9)	0.86, d (7.0)	0.93, d (7.1)	0.96, d (5.8)	0.91, d (7.0)
14	1.11, s	1.12, s	0.92, s	1.06, s	0.95, s	1.07, s
15	3.46, d (10.6)	3.30, d (10.6)	3.52, s	3.49, s	1.07, s	0.82, s
	3.39, d (10.6)	3.26, d (10.6)				

TABLE 2 | ^{13}C NMR data of compounds **1**–**6** in $CDCl_3$ at 150 MHz.

No.	1	2	3	4	5	6
1	138.5, C	138.8, C	138.4, C	138.0, C	45.0, CH	140.8, C
2	125.0, C	125.6, C	125.8, C	125.2, C	162.9, C	132.6, C
3	43.56, CH	44.5, CH	44.6, CH	43.6, CH	128.8, C	44.7, CH
4	26.5, CH_2	22.7, CH_2	22.6, CH_2	26.5, CH_2	20.1, CH_2	22.2, CH_2
5	33.1, CH_2	36.9, CH_2	36.9, CH_2	33.2, CH_2	33.5, CH_2	36.9, CH_2
6	32.7, CH	31.5, CH	31.5, CH	32.6, CH	32.7, CH	30.7, CH
7	43.59, CH	48.4, CH	47.7, CH	43.2, CH	41.5, CH	47.5, CH
8	40.8, CH_2	40.1, CH_2	39.7, CH_2	40.6, CH_2	42.3, CH_2	41.1, CH_2
9	42.6, C	43.8, C	43.9, C	42.8, C	39.0, C	42.6, C
10	41.2, CH_2	41.5, CH_2	41.6, CH2	41.1, CH_2	83.6, CH	80.1, CH
11	69.20, CH_2	69.6, CH_2	69.6, CH2	69.2, CH_2	71.1, CH_2	68.9, CH2
12	177.8, C	179.3, C	179.3, C	177.8, C	175.3, C	178.6, C
13	17.5, CH_3	12.0, CH_3	12.1, CH_3	17.7, CH_3	12.1, CH_3	12.9, CH_3
14	24.3, CH_3	23.6, CH_3	22.7, CH_3	23.2, CH_3	23.9, CH_3	22.1, CH_3
15	69.18, CH_2	68.9, CH_2	71.2, CH_2	71.5, CH_2	29.1, CH_3	25.7, CH_3

TABLE 3 | Cytotoxicities (IC_{50}, μM) of compounds **8** and **9**.

Compounds	8	9
MDA-MB-231	30 ± 2.0	27 ± 1.7
A549	>40	>40
HCT116	25 ± 1.5	23 ± 0.93
HepG2	21 ± 1.0	23 ± 1.3
PANC-1	>40	>40

HR-APCI-MS spectrum (**Supplementary Figure 7**), with five degrees of unsaturation. The analysis of ^{1}H NMR and ^{13}C NMR spectra (**Supplementary Figures 1**, **2**) combined with the HSQC spectrum (**Supplementary Figure 3**) of **1** indicated two methyl signals at δ_H 0.93 (3H, d, 7.2 Hz), δ_C 17.5; δ_H 1.11 (3H, s), δ_C 24.3, six methylenes, including two oxygenated methylenes at δ_H 3.39 (1H, d, 10.6 Hz), 3.46 (1H, d, 10.6 Hz), δ_C 69.18; δ_H 4.65 (1H, d, 10.3 Hz), 4.67 (1H, d, 10.3 Hz), δ_C 69.20, three methines, and four quaternary carbon signals, including two olefinic carbons at δ_C 125.0 and δ_C 138.5, and one ester group at δ_C 177.8, which represented two degrees of unsaturation (**Tables 1**, **2**). The other degrees of unsaturation revealed that there had been three rings in the structure of **1**. These data suggested that **1** was tremulane-type sesquiterpenoid similar to 11,12-epoxy-12β-hydroxy-1-tremulen-5-one (**7**; Zhou et al., 2008). There had been three obvious differences between **1** and **7**. The disappeared ketone carbonyl in **7** was replaced by the arisen methylene at C-5 in **1** (**Tables 1**, **2**); this was further confirmed by the key HMBC correlation from H-13 to C-5 (**Figure 3**). The HMBC correlations from H-11 to C-12, and H-4 to C-12 indicated the

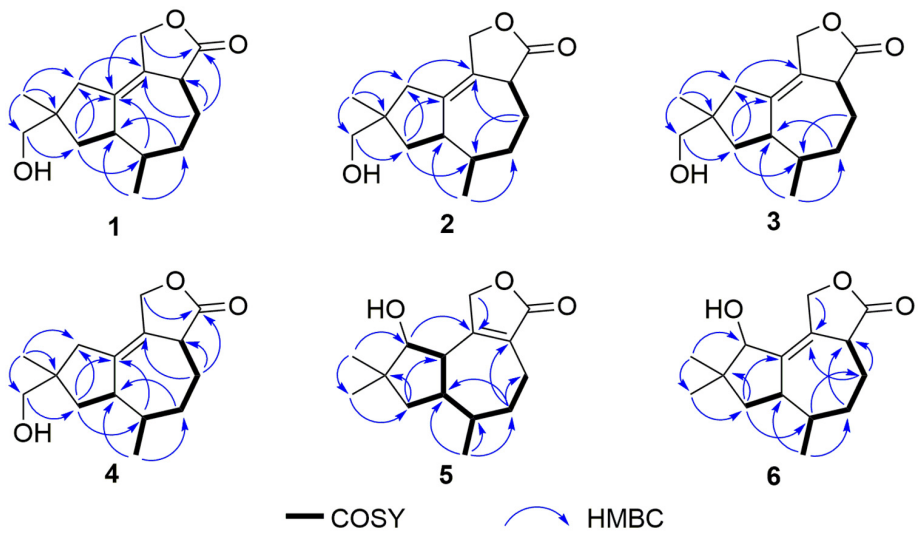

FIGURE 3 | Key COSY and HMBC correlations of compounds **1**–**6**.

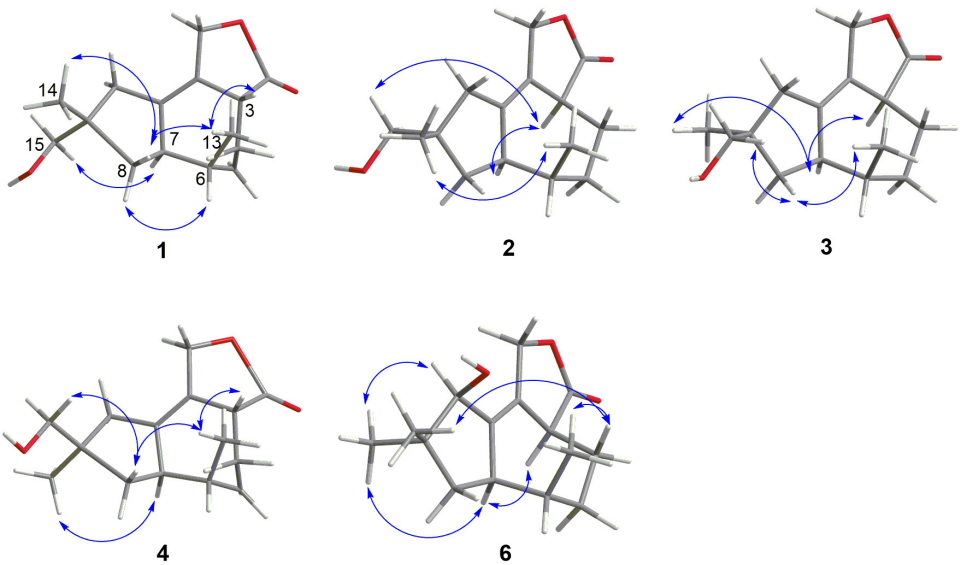

FIGURE 4 | Key NOESY correlations of compounds **1**–**4** and **6**.

ester group carbon at C-12 (**Figure 3**). The lower field shift of C-15 data (**Tables 1**, **2**) compared with those of **7**, combined with the HMBC correlations from H-15 to C-8, and H-14 to C-15 elucidated the oxidation of C-15 (**Figure 3**). Thus, the planer structure of **1** was unambiguously confirmed. The relative configurations of **1** were determined by NOESY spectra analysis (**Supplementary Figure 6**). The NOESY correlations between H-14 and H-8b, H-8b and H-13, and H-13 and H-3 indicated that H-14, H-13, and H-3 were in the same orientation (**Figure 4**). The other orientation of H-6, H-7, and H-15 was suggested by the NOESY cross-peaks of H-6/H-8a and H-7/H-15 (**Figure 4**). Therefore, the relative configurations of **1** were assigned as 3*R**,6*R**,7*R**,9*S**.

Pseudotremulane B (**2**) was gained as a colorless oil, with the molecular formula of $C_{15}H_{22}O_3$ determined by HR-APCI-MS indicating five degrees of unsaturation and had the same molecular formula as **1** (**Supplementary Figure 14**). The ^{1}H and ^{13}C NMR data of **2** were very similar to those of **1** (**Tables 1**, **2**). The downfield shift of C-2, C-3, C-5, C-7, C-9, C-11, and C-12 and the high-field shift of C-4, C-6, C-8, C-13, and C-14 in ^{13}C NMR suggested the difference configurations between **1** and **2**. The NOESY cross-peaks of H-15/H-3 and H-3/H-7 declared that H-3, H-7, and H-15 were in the same face (**Figure 4**). The NOESY correlation of H-13 and H-14 indicated that H-13 and H-14 were in another face. Therefore, the relative configurations of **2** were assigned as 3*S**,6*R**,7*R**,9*S**.

Pseudotremulane C (**3**) was acquired as a colorless oil. The HR-APCI-MS of **3** exhibited the same molecular formula with **1** and **2** (**Supplementary Figure 21**). The strong similar ^{1}H and ^{13}C NMR data between **2** and **3** (**Tables 1**, **2**) suggested that they shared the same planer structures. The high-field shift of C-14 and the downfield shift of C-15 (**Table 2**) revealed the difference configurations of C-9 of **2** and **3**. The α-orientation of H-3, H-7, and H-14 was determined by the NOESY correlations of H-3/H-7 and H-7/H-14 (**Figure 4**). The β-orientation of H-13 and H-15 was determined by the NOESY cross-peaks of H-13/H-8a and H-8a/H-15 (**Figure 4**). Compounds **2** and **3** were a pair of epimeride at the location of C-9.

Pseudotremulane D (**4**) was obtained as a colorless oil, with the same molecular formula with **1**–**3**, according the analysis of its HR-APCI-MS spectrum (**Supplementary Figure 28**). Careful analysis of the ^{1}H and ^{13}C NMR data of **1** and **4** indicated that they had the same planer structures. The difference configurations of C-9 of **1** and **4** were determined by the high-field shift of C-14 and the downfield shift of C-15 (**Table 2**). The NOESY correlations of H-3/H-13, H-13/H-8a, and H-8a/H-15 (**Figure 4**) revealed the β-orientation of H-3, H-13, and H-15. The α-orientation of H-7 and H-14 was proved by the NOESY cross-peak of H-7/H-14 (**Figure 4**). Compounds **1** and **4** were a pair of epimeride at the location of C-9.

Pseudotremulane E (**5**) was obtained as a colorless oil. Its molecular formula was the same as **1**–**4**, as suggested by HR-APCI-MS (**Supplementary Figure 35**). The NMR spectra of **5** revealed the presence of three methyls, four methylenes (one oxygenated), four methines (one oxygenated), and four quaternary carbons (one ester group carbon, two olefinic, and one sp^3 quaternary carbon; **Supplementary Figures 29**–**31**). These characteristic NMR spectroscopic data of **5** showed similarities with those of 11,12-epoxy-12β-hydroxy-1-tremulen-5-one (**7**; Zhou et al., 2008). Compared with **7**, the disappeared ketone at C-5 was substituted by methylene [δ_H 1.71–1.62 (2H, m), δ_C 33.5] in **5** (**Tables 1**, **2**), elucidated by the ^{1}H-^{1}H COSY correlations of H-6/H-5 and H-5/H-4, and further confirmed by the HMBC correlations from H-13 to C-5, and H-5 to C-3, C-4, and C-7 (**Figure 3**). The position of the double bond was changed from C-1/C-2 in **7** into C-2/C-3 in **5**, proved by the ^{1}H-^{1}H COSY cross-peak of H-1/H-7 and the HMBC signals of H-10/C-2, H-11/C-2, and H-5/C-3 (**Figure 3**). The absence of carbonyl carbon (δ_C 175.3) in **5** and the disappeared oxygenated methine at C-12 in **7**, combined with the molecular formula of **5**, revealed that there had been an ester group at C-12 in **5**. The large coupling constants of H-1/H-10 (J = 11.0 Hz) and H-1/H-7 (J = 11.0 Hz) revealed the β-orientation of H-1 and the α-orientation of H-7 and H-10 (**Table 1**). The overlapped ^{1}H NMR signals of H-6/H-7 and H-13/H-14 increased the difficulties to decide the configurations of **5** (**Table 1**). However, based on biogenetic considerations, H-13 was proposed to have β-orientation be the same with **1**–**6.**

Pseudotremulane F (**6**) was isolated as a colorless oil. The same molecular formula of $C_{15}H_{22}O_3$ was determined by the HR-APCI-MS spectrum (**Supplementary Figure 42**). The three methyls, four methylenes (one oxygenated), four methines (one oxygenated), and four quaternary carbons (one ester group carbon, two olefinic, and one sp^3 quaternary carbon) exhibited

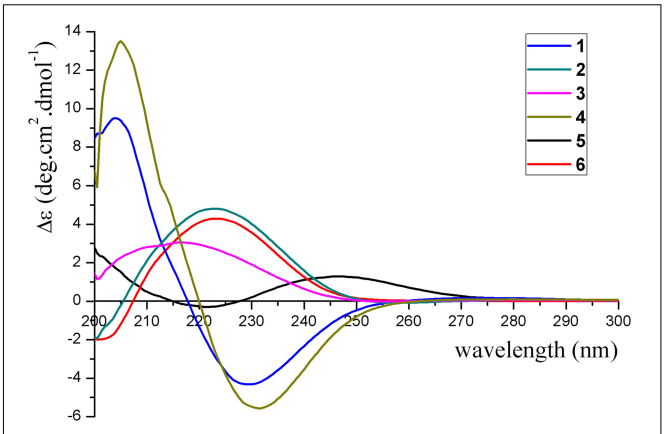

FIGURE 5 | Experimental ECD spectra of compounds **1**–**6**.

in the NMR spectra (**Supplementary Figures 29**–**31**), indicating the similar structures of **6** and **5**. The most obvious differences of ^{13}C NMR data between **6** and **5** were the downfield shift of C-1 (δ_C 140.8 in **6** *vs* δ_C 45.0 in **5**) and the high-field shift of C-2 (δ_C 132.6 in **6** *vs* δ_C 162.9 in **5**) and C-3 (δ_C 44.7 in **6** *vs* δ_C 128.8 in **5**; **Table 2**), elucidating that the olefinic bond location was changed from C-2/C-3 in **5** into C-1/C-2 in **6**. This was further confirmed by the HMBC correlations from H-11 to C-2, H-4 to C-2, and H-8 to C-1 (**Figure 3**). The β-orientation of H-13 and H-14 was revealed by the NOESY cross-peaks of H-13/H-4b and H-4b/H-14, and the α-orientation of H-3, H-7, H-15, and H-10 was suggested by the NOESY correlations of H-3/H-7, H-7/H-15, and H-15/H-10 (**Figure 4**).

The absolute configurations of **1**–**6** were determined by their ECD spectra (**Figure 5**) and were further confirmed by ECD calculations. The experimental ECD spectrum of **1** exhibited a negative cotton effect at 230 nm. According to the π-π^* CD octant rule for olefins (Guo et al., 2016), the negative cotton effect at 230 nm was caused by ester carbonyl (C-12) and oxymethene (C-11) lying in the negative contribution region (**Figure 5**). Combined with the relative configuration conclusions, the absolute configurations of **1** were established as 3*R*,6*R*,7*R*,9*S*, and named as pseudotremulane A. The similar ECD spectra of **4** and **5** with the negative cotton effects at 232 and 222 nm (**Figure 5**), respectively, indicated the absolute configurations of 3*R*,6*R*,7*R*,9*R*–**4** and 1*S*,6*R*,7*R*,10*S*–**5**. The positive cotton effects of the ECD spectra of compounds **2** (223 nm), **3** (217 nm), and **6** (223 nm) elucidated the absolute configurations of 3*S*,6*R*,7*R*,9*S*–**2**, 3*S*,6*R*,7*R*,9*R*–**3**, and 3*S*,6*R*,7*R*,10*R*–**6** (**Figure 5**). Thus, the structures compounds **2**–**6** were completely confirmed and named as pseudotremulanes B-F, respectively.

To further conform these results, the theoretical ECDs of compounds **1**–**6** (**Figure 6**) were calculated to compare with their experimental ECD spectra (Mazzeo et al., 2013; Cao et al., 2020). The MMFF94S method was used to conformational searches of **1a**–**6a** to obtain the lowest energy conformers with relative energies between 0 and 10 kcal/mol. Gaussian 09 package was used to optimize the searched conformations. The first optimization was set at the gas-phase RB3LYP/6-31G(d) level to

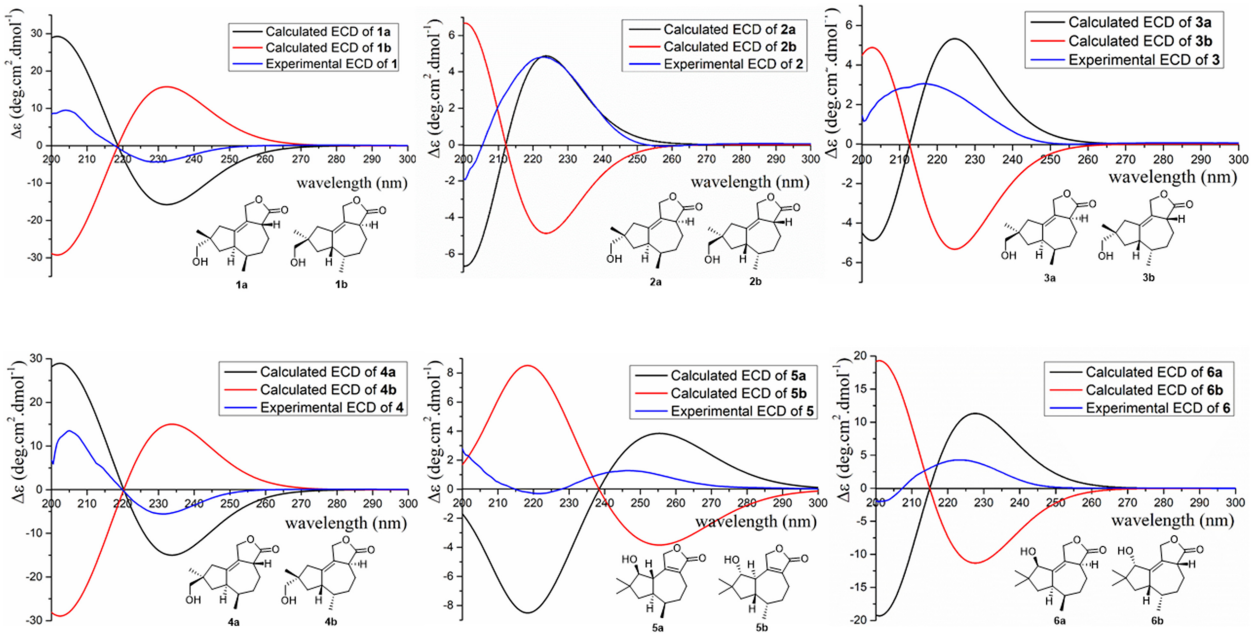

FIGURE 6 | Experimental and calculated ECD of compounds **1**–**6**.

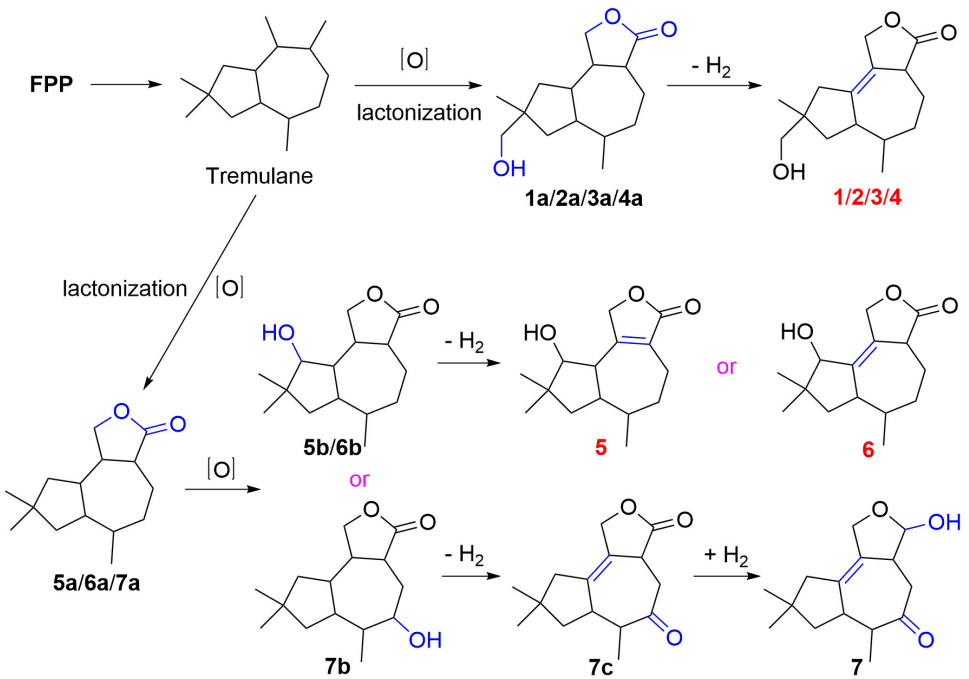

FIGURE 7 | Proposed biosynthetic pathway for **1**–**7**.

get preferential conformations with the relative energies less than 2.5 kcal/mol. Then the conformers were optimized again at the set of gas-phase B3LYP/6-311 + G(d). The total 60 electronic excited states were calculated at the set of gas-phase RB3LYP/6-311 + + G(2d,p). Boltzmann statistics were used to simulate ECD with a standard deviation of σ 0.4 eV. The theoretical ECD spectra of **1b**–**6b** were obtained by directly reversing the spectra of **1a**–**6a**, respectively. The results exhibited that the experimental ECDs of **1**–**6** were matched well with the calculated ECDs of **1a**–**6a**, respectively, which further verified the absolute structures of

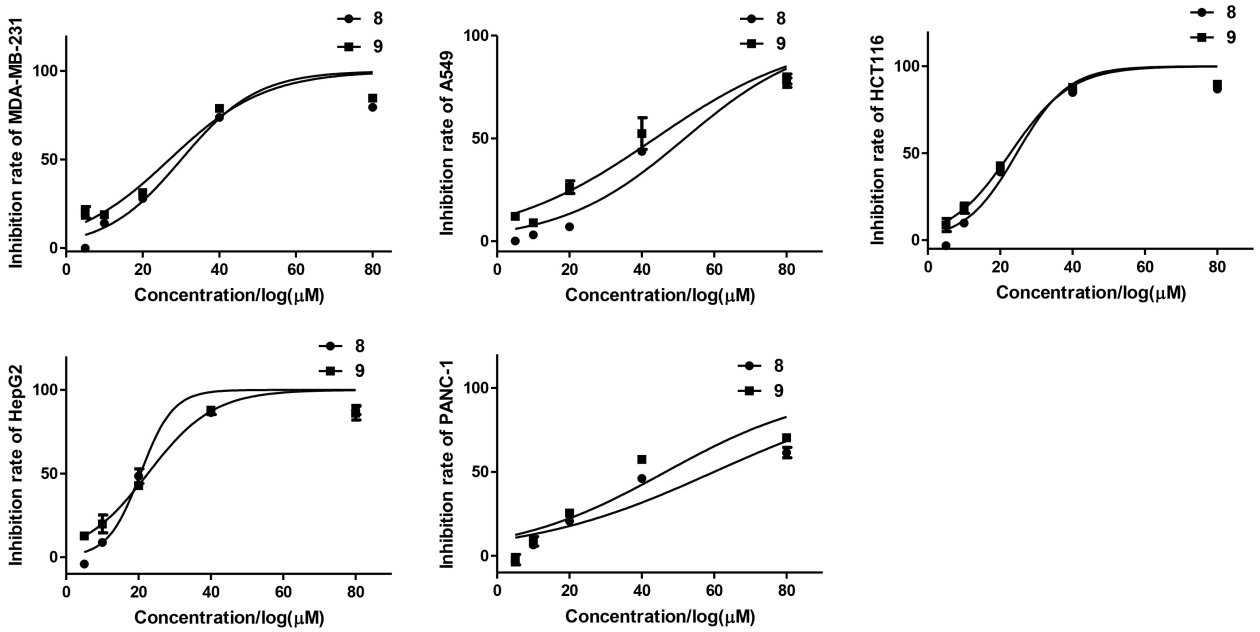

FIGURE 8 | Inhibition rates of tested cell lines of compounds **8** and **9**.

1–**6** (**Figure 6**). Interestingly, compounds **1**/**2**, **3**/**4**, **1**/**4**, and **2**/**3** were identified as four pairs of epimeride at the locations of C-3, C-3, C-9, and C-9, respectively.

The structures of **7**–**12** were determined as 11,12-epoxy-12β-hydroxy-1-tremulen-5-one (Zhou et al., 2008), ganodermasides A, B, and D (Weng et al., 2010, 2011), ergosterol (Feng et al., 2010), and dankasterone B (Amagata et al., 2007), respectively, by comparing their NMR data with those in the literature.

Proposed Biosynthetic Pathway for 1–7

Compounds **1**–**7** could derive from tremulane, a 5/7 endocyclic system sesquiterpenoid (**Figure 7**; He et al., 2020; Wang et al., 2020). As exhibited in **Figure 7**, compounds **1**–**7** could be obtained after a series of oxidation, lactonization, dehydrogenation, and revivification of tremulane. The intermediate products **1a**/**2a**/**3a**/**4a** were obtained after the oxidation of tremulane at C-11, C-12, and C-15 and lactonization at C-11 and C-12. Then the dehydrogenation of the intermediate products at C-1 and C-2 acquired the compounds **1**–**4**. Similarly, compounds **5**, **6**, and **7c** were gained from tremulane after the reactions of oxidation, lactonization, and dehydrogenation. Compound **7** was obtained from the revivification of **7c**.

Bioactivity Evaluations of Isolated Compounds

All the isolated compounds (**1**–**12**) were evaluated for their cytotoxic activities against five human cancer cell lines (MDA-MB-231, HCT116, HepG2, A549, and PANC-1). Compounds **8** and **9** exhibited cytotoxicities against MDA-MB-231, HCT116, and HepG2 cell lines with the IC_{50} values ranging from 21 to 30 μM (**Table 3** and **Figure 8**).

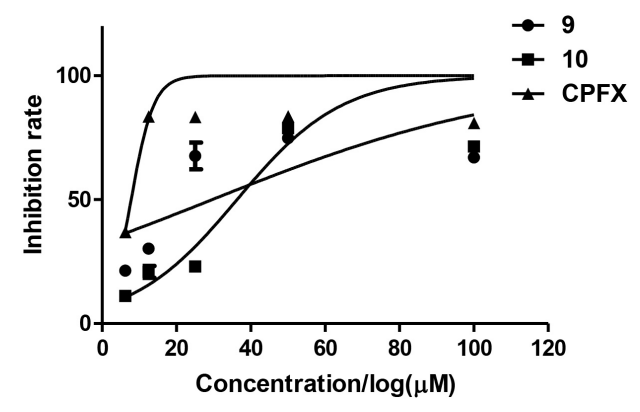

FIGURE 9 | Inhibition rates of *A. salmonicida* of compounds **9** and **10**.

The antibacterial activities of the isolated compounds (**1**–**12**) were also evaluated against nine marine fouling bacteria *P. fulva*, *A. hydrophila*, *A. salmonicida*, *V. anguillarum*, *V. harveyi*, *P. halotolerans*, *P. angustum*, *E. cloacae*, and *E. hormaechei*. Compounds **9** and **10** showed antibacterial activities against marine fouling bacteria *A. salmonicida* with the MIC values of 30 and 36 μM, respectively (**Figure 9**). The MIC value of the positive control ciprofloxacin (CPFX) was 7.8 μM (**Figure 9**).

CONCLUSION

In summary, six new tremulane sesquiterpenoids, pseudotremulanes A–F (**1**–**6**), together with one known analog, 11,12-epoxy-12β-hydroxy-1-tremulen-5-one (**7**), and

five known steroids, ganodermasides A (**8**), B (**9**), and D (**10**), ergosterol (**11**), and dankasterone B (**12**), were isolated from the Antarctic-derived fungus *Pseudogymnoascus* sp. HSX2#-11. Compounds **1**–**7** were proved to be isomeride structures with the same chemical formula. Compounds **1** and **2**, **3** and **4**, **1** and **4**, and **2** and **3** were identified as four pairs of epimeride at the locations of C-3, C-3, C-9, and C-9, respectively. Compounds **8** and **9** exhibited cytotoxicities against MDA-MB-231, HCT116, and HepG2 cell lines. Compounds **9** and **10** showed antibacterial activities against marine fouling bacteria *A. salmonicida*. This is the first time to discover terpenoids and steroids from the fungal genus *Pseudogymnoascus*. Our chemical investigation of the Antarctic fungus *Pseudogymnoascus* sp. HSX2#-11 enriches the chemical diversity of this fungal species.

DISCUSSION

The genus *Pseudogymnoascus* as a kind of psychrophilic pathogenic fungi is widely distributed in Antarctica (Rosa et al., 2020; Santos et al., 2020; Martorell et al., 2021). *Pseudogymnoascus* can be one of the antagonistic fungi against potato scab pathogens from potato field soils, which could be used as potential agents to control potato scab disease (Tagawa et al., 2010). *Pseudogymnoascus* spp. has been certified to be one of the predominant microbial colonizers in the root endosphere and rhizosphere of turfgrass systems (Xia et al., 2021). The extracts of some *Pseudogymnoascus* strains exhibit potent bioactivities, such as antimicrobial, herbicidal, and antitumoral activities (Henríquez et al., 2014; Gonçalves et al., 2015; Gomes et al., 2018; Ferrarezi et al., 2019). To the best of our knowledge, only 22 natural products, including 6 new compounds, were discovered from *Pseudogymnoascus* up to now (Figueroa et al., 2015; Guo et al., 2019; Fujita et al., 2021; Shi et al., 2021). More than 70% of the previously isolated structures belong to polyketides; others are alkaloids (13.6%), benzene derivative (9.1%), and fatty acid (4.5%). Our research isolated 12 natural products (**1**–**12**), including 6 new compounds (**1**–**6**), from the fungus *Pseudogymnoascus* 2#-11. All of the isolated compounds are first obtained from the genus *Pseudogymnoascus*. This is the first time to discover terpenoids and steroids from the genus *Pseudogymnoascus*. The whole number of the fungal strain secondary metabolites increased by 35%, and the number of their new compounds is doubled. This greatly enriches the number and diversity of natural products of the genus *Pseudogymnoascus*. Except for antimicrobial activities of some of the previously obtained polyketides (Figueroa et al., 2015; Fujita et al., 2021; Shi et al., 2021), no other activities were found in *Pseudogymnoascus* in previous studies. This study is the first to identify secondary metabolites with cytotoxic activities (**8** and **9**) in *Pseudogymnoascus*.

The isolated new sesquiterpenoids (**1**–**6**), with characteristic structures of 5/7 fused bicyclic system, belong to the family of tremulanes. Tremulane derivatives have been found from cultures of *Phellinus tremulae* (Ayer and Cruz, 1993), *P. igniarius* (Liu et al., 2007; Wu et al., 2020), *Conocybe siliginea* (Zhou et al., 2008; Wu et al., 2010; He et al., 2020), *Huperzia serrata* (Ying et al., 2013), *Flavodon flavus* (Isaka et al., 2016), *Coriolopsis* sp. (Chen et al., 2017), *Colletotrichum capsici* (Wang et al., 2017), *I. lacteus* (Chen et al., 2018, 2020; Ding et al., 2018, 2019, 2020a,b; Zhou et al., 2018; Duan et al., 2019; Wu et al., 2019; Shi et al., 2020; Sun C.-T. et al., 2020; Wang et al., 2020), and *Gymnopilus junonius* (Lee et al., 2020). This is the first time to find tremulane derivatives from *Pseudogymnoascus*.

DATA AVAILABILITY STATEMENT

The datasets presented in this study can be found in online repositories. The names of the repository/repositories and accession number(s) can be found in the article/ **Supplementary Material**.

AUTHOR CONTRIBUTIONS

TS contributed to experimental design and operation, data analysis, and manuscript preparation. X-QL contributed to manuscript revision. LZ supported the sample of the Antarctic soil. Y-HZ contributed to ECD calculations. J-JD contributed to activity evaluations. E-LS contributed to software drawing guidance. Y-YY, Y-TZ, and W-PH contributed to activity evaluations. D-YS was the project leader organizing and guiding the experiments. All authors contributed to the article and approved the submitted version.

FUNDING

This work was supported by the Natural Science Foundation of Shandong Province of China (No. ZR2020QD111); the China Postdoctoral Science Foundation (No. 2019M662378); the National Program for Support of Top-notch Young Professionals; the Fund of Taishan Scholar Project; The Shandong Provincial Natural Science Foundation for Distinguished Young Scholars (JQ201722); the Qingdao Science and Technology Benefit People Demonstration Guide Special Project (20-3-4-20-nsh); and the Fundamental Research Funds of Shandong University (2020GN033).

ACKNOWLEDGMENTS

We would like to thank Antarctic Great Wall National Observation and Research Station of Polar Ecosystem for sample collection; Jing-Yao Qu, Jing Zhu, and Zhi-Feng Li in MS, and Hai-Yan Sui in NMR for help and guidance from State Key Laboratory of Microbial Technology of Shandong University.

SUPPLEMENTARY MATERIAL

The Supplementary Material for this article can be found online at: https://www.frontiersin.org/articles/10.3389/fmicb.2021.688202/full#supplementary-material

REFERENCES

Amagata, T., Tanaka, M., Yamada, T., Doi, M., Minoura, K., Ohishi, H., et al. (2007). Variation in cytostatic constituents of a sponge-derived *Gymnascella dankaliensis* by manipulating the carbon source. *J. Nat. Prod.* 70, 1731–1740. doi: 10.1021/np070165m

Appendino, G., Gibbons, S., Giana, A., Pagani, A., Grassi, G., Stavri, M., et al. (2008). Antibacterial cannabinoids from *Cannabis sativa*: a structure-activity study. *J. Nat. Prod.* 71, 1427–1430.

Ayer, W. A., and Cruz, E. R. (1993). The tremulanes, a new group of sesquiterpenes from the aspen rotting fungus *Phellinus tremulae*. *J. Org. Chem.* 58, 7529–7534.

Cao, F., Meng, Z.-H., Wang, P., Luo, D.-Q., and Zhu, H.-J. (2020). Dipleosporalones A and B, dimeric azaphilones from a marine-derived *Pleosporales* sp. fungus. *J. Nat. Prod.* 83, 1283–1287.

Chen, H.-P., Ji, X., Li, Z.-H., Feng, T., and Liu, J.-K. (2020). Irlactane and tremulane sesquiterpenes from the cultures of the medicinal fungus *Irpex lacteus* HFG1102. *Nat. Prod. Bioprospect.* 10, 89–100. doi: 10.1007/s13659-020-00239-z

Chen, H.-P., Zhao, Z.-Z., Li, Z.-H., Feng, T., and Liu, J.-K. (2018). Seco-tremulane sesquiterpenoids from the cultures of the medicinal Fungus *Irpex lacteus* HFG1102. *Nat. Prod. Bioprospect.* 8, 113–119. doi: 10.1007/s13659-018-0157-y

Chen, L.-L., Kong, F.-D., Wang, P., Yuan, J.-Z., Guo, Z.-K., Wang, H., et al. (2017). Two new tremulane sesquiterpenes from a mangrove endophytic fungus. *Coriolopsis* sp. J5. *Chin. Chem. Lett.* 28, 222–225. doi: 10.1016/j.cclet.2016.07.019

Cong, B., Yin, X., Deng, A., Shen, J., and Yang, H. (2020). Diversity of cultivable microbes from soil of the Fildes Peninsula, Antarctica, and their potential application. *Front. Microbiol.* 11:570836. doi: 10.3389/fmicb.2020.570836

Ding, J.-H., Li, Z.-H., Feng, T., and Liu, J.-K. (2018). Tremulane sesquiterpenes from cultures of the basidiomycete *Irpex lacteus*. *Fitoterapia* 125, 245–248. doi: 10.1016/j.fitote.2017.12.001

Ding, J.-H., Li, Z.-H., Feng, T., and Liu, J.-K. (2019). A new tremulane sesquiterpenoid from the fungus *Irpex lacteus*. *Nat. Prod. Res.* 33, 316–320. doi: 10.1080/14786419.2018.1448816

Ding, J.-H., Li, Z.-H., Feng, T., and Liu, J.-K. (2020a). A sesquiterpene lactone from *Irpex lacteus*. *Chem. Nat. Compd.* 56, 403–405. doi: 10.1007/s10600-020-03047-6

Ding, J.-H., Li, Z.-H., Feng, T., and Liu, J.-K. (2020b). Two new sesquiterpenes from cultures of the fungus *Irpex lacteus*. *J. Asian Nat. Prod. Res.* 23, 348–352. doi: 10.1080/10286020.2020.1737857

Duan, X.-X., Qin, D., Song, H.-C., Gao, T.-C., Zuo, S.-H., Yan, X., et al. (2019). Irpexlacte A-D, four new bioactive metabolites of endophytic fungus *Irpex lacteus* DR10-1 from the waterlogging tolerant plant *Distylium chinense*. *Phytochem. Lett.* 32, 151–156. doi: 10.1016/j.phytol.2019.06.001

Feng, N., Zhang, J., Tang, Q., Hao, R., Liu, Y., Yang, Y., et al. (2010). Steroids from fruiting bodies of *Coprinus comatus* and their inhibition to tumor cell proliferation. *Junwu Xuebao* 29, 249–253.

Ferrarezi, J. H., Dos Santos, J. A., Sette, L. D., Ferreira, H., and Sass, D. C. (2019). Anti-*Xanthomonas* activity of Antarctic fungi crude extracts. *Afr. J. Biotechnol.* 18, 713–718. doi: 10.5897/ajb2019.16886

Figueroa, L., Jiménez, C., Rodríguez, J., Areche, C., Chávez, R., Henríquez, M., et al. (2015). 3-Nitroasterric acid derivatives from an Antarctic sponge-derived *Pseudogymnoascus* sp. fungus. *J. Nat. Prod.* 78, 919–923.

Fujita, K., Ikuta, M., Nishimura, S., Sugiyama, R., Yoshimura, A., and Kakeya, H. (2021). Amphiol, an antifungal fungal pigment from *Pseudogymnoascus* sp. PF1464. . *J. Nat. Prod.* 84, 986–992. doi: 10.1021/acs.jnatprod.0c01010

Gomes, E. C. Q., Godinho, V. M., Silva, D. A. S., de Paula, M. T. R., Vitoreli, G. A., Zani, C. L., et al. (2018). Cultivable fungi present in Antarctic soils: taxonomy, phylogeny, diversity, and bioprospecting of antiparasitic and herbicidal metabolites. *Extremophiles* 22, 381–393. doi: 10.1007/s00792-018-1003-1

Gonçalves, V. N., Carvalho, C. R., Johann, S., Mendes, G., Alves, T. M. A., and Zani, C. L. (2015). Antibacterial, antifungal and antiprotozoal activities of fungal communities present in different substrates from Antarctica. *Polar Biol.* 38, 1143–1152. doi: 10.1007/s00300-015-1672-5

Guo, Y.-Z., Wei, Q., Gao, J., Liu, B.-Y., Zhang, T., Hua, H.-M., et al. (2019). Metabolites of the psychrophilic fungus *Pseudogymnoascus pannorum*. *Nat. Prod. Res. Dev.* 31, 446–449.

Guo, Z., Li, X., Zhang, L., Feng, Z., Deng, Z., He, H., et al. (2016). Cytotoxic tremulanes and 5,6-secotremulanes, four new sesquiterpenoids from a plant-associated fungus X1-2. *Nat. Prod. Res.* 30, 2582–2589. doi: 10.1080/14786419.2015.1135140

He, J., Pu, C.-J., Wang, M., Li, Z.-H., Feng, T., Zhao, D.-K., et al. (2020). Conosiligins A-D, ring-rearranged tremulane sesquiterpenoids from *Conocybe siliginea*. *J. Nat. Prod.* 83, 2743–2748. doi: 10.1021/acs.jnatprod.0c00681

Henríquez, M., Vergara, K., Norambuena, J., Beiza, A., Maza, F., Ubilla, P., et al. (2014). Diversity of cultivable fungi associated with Antarctic marine sponges and screening for their antimicrobial, antitumoral and antioxidant potential. *World J. Microbiol. Biotechnol.* 30, 65–76. doi: 10.1007/s11274-013-1418-x

Isaka, M., Palasarn, S., Supothina, S., Srichomthong, K., and Choeyklin, R. (2016). Seco-tremulanes from cultures of the basidiomycete *Flavodon flavus* BCC 17421. *Helv. Chim. Acta* 99, 232–236. doi: 10.1002/hlca.201500249

Kwon, J., Lee, H., Ko, W., Kim, D. C., Kim, K. W., Kwon, H. C., et al. (2017). Chemical constituents isolated from Antarctic marine-derived *Aspergillus* sp. SF-5976 and their anti-inflammatory effects in LPS-stimulated RAW 264.7 and BV2 cells. *Tetrahedron* 73, 3905–3912.

Lee, S., Ryoo, R., Choi, J. H., Kim, J.-H., Kim, S.-H., and Kim, K. H. (2020). Trichothecene and tremulane sesquiterpenes from a hallucinogenic mushroom *Gymnopilus junonius* and their cytotoxicity. *Arch. Pharm. Res.* 43, 214–223. doi: 10.1007/s12272-020-01213-6

Liu, D. Z., Wang, F., and Liu, J. K. (2007). Sesquiterpenes from cultures of the basidiomycete *Conocybe siliginea*. *J. Nat. Prod.* 70, 1503–1506.

Loperena, L., Soria, V., Varela, H., Lupo, S., Bergalli, A., Guigou, M., et al. (2012). Extracellular enzymes produced by microorganisms isolated from maritime Antarctica. *World J. Microbiol. Biotechnol.* 28, 2249–2256. doi: 10.1007/s11274-012-1032-3

Martorell, M. M., Lannert, M., Matula, C. V., Quartino, M. L., de Figueroa, L. I. C., MacCormack, W. P., et al. (2021). Studies toward the comprehension of fungal-macroalgae interaction in cold marine regions from a biotechnological perspective. *Fungal Biol.* 125, 218–230. doi: 10.1016/j.funbio.2020.11.003

Mazzeo, G., Santoro, E., Andolfi, A., Cimmino, A., Troselj, P., Petrovic, A. G., et al. (2013). Absolute configurations of fungal and plant metabolites by chiroptical methods. ORD, ECD, and VCD studies on phyllostin, scytolide, and oxysporone. *J. Nat. Prod.* 76, 588–599.

Poveda, G., Gil-Durán, C., Vaca, I., Levicán, G., and Chávez, R. (2018). Coldactive pectinolytic activity produced by flamentous fungi associated with Antarctic marine sponges. *Biol. Res.* 51:28. doi: 10.1186/s40659-018-0177-4

Rosa, L. H., Pinto, O. H. B., Convey, P., Carvalho-Silva, M., Rosa, C. A., and Camara, P. E. A. S. (2020). DNA metabarcoding to assess the diversity of airborne fungi present over Keller Peninsula, King George Island, Antarctica. *Microb. Ecol.* doi: 10.1007/s00248-020-01627-1 [Online ahead of Print].

Rusman, Y., Held, B. W., Blanchette, R. A., He, Y., and Salomon, C. E. (2018). Cadopherone and colomitide polyketides from *Cadophora* wood-rot fungi associated with historic expedition huts in Antarctica. *Phytochemistry* 148:1.

Santos, J. A. D., Meyer, E., and Sette, L. D. (2020). Fungal community in antarctic soil along the retreating Collins Glacier (Fildes Peninsula, King George Island). *Microorganisms* 8:1145. doi: 10.3390/microorganisms8081145

Shi, L.-J., Wu, Y.-M., Yang, X.-Q., Xu, T.-T., Yang, S., Wang, X.-Y., et al. (2020). The cocultured *Nigrospora oryzae* and *Collectotrichum gloeosporioides*, *Irpex lacteus*, and the plant host *Dendrobium officinale* bidirectionally regulate the production of phytotoxins by anti-phytopathogenic metabolites. *J. Nat. Prod.* 83, 1374–1382. doi: 10.1021/acs.jnatprod.0c00036

Shi, T., Yu, Y.-Y., Dai, J.-J., Zhang, Y.-T., Hu, W.-P., Zheng, L., et al. (2021). New Polyketides from the Antarctic Fungus Pseudogymnoascus sp. HSX2#-11. *Mar. Drugs* 19:168.

Skehan, P., Storeng, R., Scudiero, D., Monks, A., Mcmahon, J., Vistica, D., et al. (1990). New colorimetric cytotoxicity assay for anticancer-drug screening. *J. Natl. Cancer Inst.* 82:1107.

Sun, C.-T., Wang, J.-P., Shu, Y., Cai, X.-Y., Hu, J.-T., Zhang, S.-Q., et al. (2020). A new tremulane sesquiterpene from *Irpex lacteus* by solid-state fermentation. *Nat. Prod. Res.* 1–6. doi: 10.1080/14786419.2020.1806272 [Online ahead of print].

Sun, C., Zhang, Z., Ren, Z., Yu, L., and Zhu, T. (2020). Antibacterial cyclic tripeptides from Antarctica-sponge-derived fungus *Aspergillus insulicola* HDN151418. *Mar. Drugs* 18:532.

Tagawa, M., Tamaki, H., Manome, A., Koyama, O., and Kamagata, Y. (2010). Isolation and characterization of antagonistic fungi against potato scab pathogens from potato field soils. *FEMS Microbiol. Lett.* 305, 136–142. doi: 10.1111/j.1574-6968.2010.01928.x

Wang, F., Ma, H., Hu, Z., Jiang, J., Zhu, H., Cheng, L., et al. (2017). Secondary metabolites from *Colletotrichum capsici*, an endophytic fungus derived from *Siegesbeckia pubescens Makino*. *Nat. Prod. Res.* 31, 1849–1854. doi: 10.1080/14786419.2016.1261346

Wang, M., Du, J.-X., Yang, H.-X., Dai, Q., Liu, Y.-P., He, J., et al. (2020). Sesquiterpenoids from cultures of the basidiomycetes *Irpex lacteus*. *J. Nat. Prod.* 83, 1524–1531. doi: 10.1021/acs.jnatprod.9b01177

Weng, Y., Lu, J., Xiang, L., Matsuura, A., Zhang, Y., Huang, Q., et al. (2011). Ganodermasides C and D, two new anti-aging ergosterols from spores of the medicinal mushroom *Ganoderma lucidum*. *Biosci. Biotechnol. Biochem.* 75, 800–803. doi: 10.1271/bbb.100918

Weng, Y., Xiang, L., Matsuura, A., Zhang, Y., Huang, Q., and Qi, J. (2010). Ganodermasides A and B, two novel anti-aging ergosterols from spores of a medicinal mushroom *Ganoderma lucidum* on yeast via UTH1 gene. *Bioorg. Med. Chem.* 18, 999–1002. doi: 10.1016/j.bmc.2009.12.070

Wu, G. (2016). Pharmaceutical composition of citicoline sodium and medicinal application thereof. China Patent No. 105753681A, Jul 13, Jiangsu, China.

Wu, P.-F., Ding, R., Tan, R., Liu, J., Hu, E.-M., Li, C.-Y., et al. (2020). Sesquiterpenes from cultures of the fungus *Phellinus igniarius* and their cytotoxicities. *Fitoterapia* 140:104415. doi: 10.1016/j.fitote.2019.104415

Wu, X., Lin, S., Zhu, C., Yue, Z., Yu, Y., Zhao, F., et al. (2010). Homo- and heptanorsterols and tremulane sesquiterpenes from cultures of *Phellinus igniarius*. *J. Nat. Prod.* 73, 1294–1300.

Wu, Y.-M., Zhou, Q.-Y., Yang, X.-Q., Luo, Y.-J., Qian, J.-J., Liu, S.-X., et al. (2019). Induction of antiphytopathogenic metabolite and squalene production and phytotoxin elimination by adjustment of the mode of fermentation in cocultures of phytopathogenic *Nigrospora oryzae* and *Irpex lacteus*. *J. Agric. Food Chem.* 67, 11877–11882. doi: 10.1021/acs.jafc.9b04209

Xia, Q., Rufty, T., and Shi, W. (2021). Predominant microbial colonizers in the root endosphere and rhizosphere of turfgrass systems: *Pseudomonas veronii*, *Janthinobacterium lividum*, and *Pseudogymnoascus* spp. *Front. Microbiol.* 12:643904. doi: 10.3389/fmicb.2021.643904

Ying, Y. M., Shan, W. G., Zhang, L. W., and Zhan, Z. J. (2013). Ceriponols A–K, tremulane sesquitepenes from *Ceriporia lacerate* HS-ZJUT-C13A, a fungal endophyte of *Huperzia serrata*. *Phytochemistry* 95, 360–367.

Yu, G., Sun, Z., Peng, J., Zhu, M., Che, Q., Zhang, G., et al. (2019). Secondary metabolites produced by combined culture of *Penicillium crustosum* and a *Xylaria* sp. *J. Nat. Prod.* 82, 2013–2017.

Zhou, Q.-Y., Yang, X.-Q., Zhang, Z.-X., Wang, B.-Y., Hu, M., Yang, Y.-B., et al. (2018). New azaphilones and tremulane sesquiterpene from endophytic *Nigrospora oryzae* cocultured with *Irpex lacteus*. *Fitoterapia* 130, 26–30. doi: 10.1016/j.fitote.2018.07.018

Zhou, Z.-Y., Tang, J.-G., Wang, F., Dong, Z.-J., and Liu, J.-K. (2008). Sesquiterpenes and aliphatic diketones from cultures of the basidiomycete *Conocybe siliginea*. *J. Nat. Prod.* 71, 1423–1426. doi: 10.1021/np8002657

Conflict of Interest: The authors declare that the research was conducted in the absence of any commercial or financial relationships that could be construed as a potential conflict of interest.

frontiers in Microbiology

ORIGINAL RESEARCH
published: 14 June 2021
doi: 10.3389/fmicb.2021.650177

Diversity of Marine Macro-Algicolous Endophytic Fungi and Cytotoxic Potential of *Biscogniauxia petrensis* Metabolites Against Cancer Cell Lines

*Subhadarsini Sahoo, Kamalraj Subban and Jayabaskaran Chelliah**

Department of Biochemistry, Indian Institute of Science, Bengaluru, India

OPEN ACCESS

Edited by:
Paola Angelini,
University of Perugia, Italy

Reviewed by:
Weaam Ebrahim,
Mansoura University, Egypt
Sundeep Jaglan,
Indian Institute of Integrative Medicine (CSIR), India
Dian Handayani,
University of Andalas, Indonesia
Dinkar Sahal,
International Centre for Genetic Engineering and Biotechnology (India), India

***Correspondence:**
Jayabaskaran Chelliah
cjb@iisc.ac.in

Specialty section:
This article was submitted to Microbiotechnology, a section of the journal Frontiers in Microbiology

Received: *06 January 2021*
Accepted: *13 May 2021*
Published: *14 June 2021*

Citation:
Sahoo S, Subban K and Chelliah J (2021) Diversity of Marine Macro-Algicolous Endophytic Fungi and Cytotoxic Potential of Biscogniauxia petrensis Metabolites Against Cancer Cell Lines. Front. Microbiol. 12:650177. doi: 10.3389/fmicb.2021.650177

Hypersaline environments are known to support diverse fungal species from various orders. The production of secondary metabolites is one of the strategies that fungi adopt to thrive under such extreme environments, bringing up the stress tolerance response. Some such unique secondary metabolites also exhibit clinical significance. The increasing prevalence of drug resistance in cancer therapy demands further exploration of these novel bioactive compounds as cancer therapeutics. In the present study, a total of 31 endophytic fungi harboring inside red, green, and brown marine algae have been isolated and identified. The maximum likelihood analysis and diversity indices of fungal endophytes revealed the phylogenetic relationship and species richness. The genus *Aspergillus* was found to be the dominating fungus, followed by *Cladosporium* spp. All the isolated endophytic fungal extracts were tested for their cytotoxicity against HeLa and A431 cancer cell lines. Nine isolates were further analyzed for their cytotoxic activity from the culture filtrate and mycelia extract. Among these isolates, *Biscogniauxia petrensis* showed potential cytotoxicity with CC_{50} values of 18.04 and 24.85 μg/ml against HeLa and A431 cells, respectively. Furthermore, the media and solvent extraction optimization revealed the highest cytotoxic active compounds in ethyl acetate extract from the potato dextrose yeast extract broth medium. The compound-induced cell death *via* apoptosis was 50–60 and 45% when assayed using propidium iodide-live/dead and loss of mitochondrial membrane potential assay, respectively, in HeLa cells. Four bioactive fractions (bioassay-based) were obtained and analyzed using chromatography and spectroscopy. This study reports, for the first time, the cytotoxic activity of an endophytic fungal community that was isolated from marine macro-algae in the Rameswaram coastal region of Tamil Nadu, India. In addition, *B. petrensis* is a prominent apoptotic agent, which can be used in pharmaceutical applications as a therapeutic.

Keywords: biodiversity, algicolous fungi, cytotoxicity, *Biscogniauxia petrensis*, secondary metabolites

INTRODUCTION

Cancer is one of the major causes of illness and death globally (Nagai and Kim, 2017). The current cancer treatments comprise of surgery and radiation, followed by chemotherapy. The most extensively used treatment is chemotherapy; however, the routine use of chemically synthesized anticancer drugs suppresses the immune system. This necessitates the development of anticancer drugs which can control cancer progression in a better way. Moreover, the requirement for new and highly effective compounds which can provide assistance and relief in all aspects of human illnesses is ever growing. Therefore, the discovery of new drugs from natural sources has been the focus of research works (Wright, 2019). In this context, marine fungi are being considered as a new and promising source of bioactive compounds (Deshmukh et al., 2018).

It has been reported that there has been a lack of study on endophytic fungi's applications in the pharmaceutical field (Sarasan et al., 2017). The marine macro-algae-associated endophytic fungi have the capability to produce novel secondary molecules, as they survive in special ecological niches of inexorable stress (prolonged periods of exposure to sunlight, sharp variation in moisture, large salt concentration, changing tides, abundant microorganisms, and insect herbivores) (Schulz and Boyle, 2005). Even though the relationship between host and endophyte is poorly understood, it has been observed that microbial endophytes enhance host fitness by producing bioactive compounds, which improve their survival against pathogens and environmental stresses and promote host growth. These active metabolites are the target of current research in drug discovery (Pietra, 1997; Strobel and Daisy, 2003; Debbab et al., 2011). Thus, an enormous chance to discover novel compounds from less-investigated marine endophytic fungi (Guo et al., 2008; Aly et al., 2011) and marine fungi has been largely neglected for many decades (Imhoff, 2016). Recently, endophytic fungi have been recognized as an important and novel resource of natural bioactive products, especially for their anticancer properties for therapeutic purposes (Jeewon et al., 2019).

The marine algae-associated endophytic fungi have already been reported in many countries such as Germany, China, Israel, Italy, United States, and South Africa (Nguyen et al., 2013; de Felício et al., 2015; Zhang et al., 2016). Moreover, such fungi and their bioactive compounds have been reported from many regions in India (Sarasan et al., 2020). A total of 199 different compounds isolated from marine fungi have shown considerable promise as cytotoxic agents (Deshmukh et al., 2017). A previous study also reported that 45 endophytic fungi have been isolated from the red macro-alga; among these, the ethyl acetate extracts of *Penicillium decaturense* showed cytotoxicity, with IC_{50} values of 20.93, 6.63, and 3.78 μg/ml, against cell lines SF-295, HCT-8, and HL-60, respectively. *Penicillium waksmanii* possessed IC_{50} values of 14.57, 4.38, and 11.73 μg/ml against SF-295, HCT-8, and HL-60 cell lines. Both strains displayed antibacterial activities, with minimum inhibitory concentration > 400 μg/ml (de Felício et al., 2015). In this context, it is necessary to study marine endophytes extensively for several therapeutic purposes. Several lines of evidence suggest that algae-associated endophytes are an outstanding source of bioactive metabolites from *Cephalosporium*, *Penicillium*, *Aspergillus, Strobilurus*, *Tolypocladium*, and *Chaetomium* (Gouda et al., 2016; Blunt et al., 2017; Shirley et al., 2018).

From this point of view, as part of our continuing search for novel cytotoxic compounds, it was found that crude ethyl acetate (EtOAc) extract has potent anticancer metabolites from algae-associated endophytes such as *Talaromyces purpureogenus* and *Aspergillus unguis* (AG1.2) from the coastal regions of Goa and Kerala (Kumari et al., 2018; Kamat et al., 2020). It has been reported that there is increasing pressure, due to temperature, high salinity, and environmental pollution, on the natural resources with rich marine algae biodiversity in Rameswaram (Thirunavukkarasu et al., 2012; Bhagyaraj and Kunchithapatham, 2016). Interestingly, another study reported and showed the distribution and diversity of endophytic fungi in 10 seagrasses by morphological taxonomy approaches in the Bay of Bengal waters at Rameswaram (Venkatachalam et al., 2015b). To the best of the authors' knowledge, cytotoxicity against cancer cell lines has not yet been reported from algae-associated endophytic fungi from the Mandapam region of Tamil Nadu; chitinase and xylanase activities have been documented (Thirunavukkarasu et al., 2015; Venkatachalam et al., 2015a). Therefore, continuing the search for potent algae-associated endophytic fungi from the unexplored marine region of Rameswaram, the authors sought to isolate and identify such fungi to explore potentially cytotoxic metabolites and their apoptotic activity in cancerous cells.

MATERIALS AND METHODS

Chemicals and Reagents Used for This Study

Sodium hypochlorite, cetyltrimethylammonium bromide (CTAB), phenol, ethidium bromide, Dulbecco's modified eagle's medium, and dimethyl sulfoxide (DMSO) were purchased from Sigma Aldrich. Potato dextrose agar (PDA) and potato dextrose broth (PDB) were procured from HiMedia. Streptomycin, penicillin, and MTT were obtained from SRL-Ranbaxy. The plasticware for mammalian cell cultures was purchased from Corning and TPP. Isoamyl alcohol and ammonium acetate were purchased from SDFCL (SD- Fine Chemicals). Magnesium chloride ($MgCl_2$), dNTP, and Taq polymerase were purchased from Thermo Fisher Scientific, Bangalore. Fetal bovine serum and trypsin-ethylenediaminetetraacetic acid (EDTA) were procured from GIBCO-BRL. The analytical thin-layer chromatography (TLC) sheets (silica gel 60 GF254 with aluminum support) were acquired from Merck-Millipore. Ethanol was procured from Analytical Reagents. Ethyl acetate was purchased from Merck. The water used was deionized using a Millipore (Milli-Q) system.

Collection of Marine Algae and Isolation of Endophytic Fungi

Marie fungi/microorganisms have, to a great extent, been dismissed indeed in spite of the fact that it is evaluated that

more than 10,000 prominent marine fungi are less investigated in comparison to their earth-bound partners (Jones, 2011; Deshmukh et al., 2018).

In the current research scenario, algae-associated endophytic fungi (Molinski et al., 2009) are under focus. A total of 18 different marine macro-algal species were collected from the intertidal zone at four locations, namely, Pamban, Kilakarai, Thonithurai, and Seeniappa Dargah in the high-salinity area of Gulf of Mannar, Rameswaram at 9.2876° N, 79.3129° E in Tamil Nadu; these are listed in **Table 1**. All the collected algae were identified based on morphological characteristics by an algae expert and according to Bhagyaraj and Kunchithapatham (2016). The healthy, mature, and undamaged algae were collected and transported to the laboratory in suitable sterile containers with seawater and processed within 24 h to isolate the endophytic fungi.

All the algal samples were washed thoroughly under running tap water, and each sample (pieces of algae) was further cut into small segments of approximately 0.5 cm and rinsed three times with sterile sea water to eliminate adherent surface debris. Then, each sample was immersed in 70% ethanol for 60–120 s for surface sterilization, followed by immersion in 4% sodium hypochlorite (NaOCl) for 60 s and washing with sterile distilled water for 10 s, separately as earlier reported (Kjer et al., 2010; Suryanarayanan et al., 2010). The samples were semi-dried with sterile tissue paper and carefully placed over the surface of a petri dish containing fresh PDA medium prepared with ASW (Holler et al., 2000). Another batch of PDA medium was prepared in sterile distilled water, and all plates were supplemented with 250 mg/L of streptomycin. The petri dishes were sealed with parafilm, labeled, and stored at 25°C under 12 h of light followed by 12 h of darkness (Suryanarayanan et al., 2010) for 4–15 days. The petri dishes were observed once every day, and the endophytes grown out of the segments were further sub-cultured in new fresh PDA plates to get pure fungal isolates. These isolates were segregated based on culture characteristics such as growth, colony surface morphology, and pigmentation (Bhagyaraj and Kunchithapatham, 2016). All the isolated fungi were sub-cultured in PDA slants, allowed to grow for 7–14 days, and stored at 4°C for future use.

TABLE 1 | List of the collected algae from the Gulf of Mannar, Rameswaram, Tamil Nadu, India.

S. no.	Algae code	Marine algae	Collection site
Green algae			
1	GCSS	*Gracilaria crassa*	Thonithurai
2	HCSS	*Halimeda gracilis*	Kilakarai
3	CRSS	*Caulerpa racemosa*	Pamban
4	CSSS	*Caulerpa scafeliformis*	Seeniappa Dargah
5	CASS	*Chaetomorpha antennina*	Thonithurai
6	CTSS	*Caulerpa taxifolia*	Thonithurai
7	HMSS	*Halimeda macroloba*	Pamban
8	CPeSS	*Caulerpa peltata*	Kilakarai
9	EFSS	*Enteromorpha flexuosa*	Seeniappa Dargah
Brown algae			
10	PTSS	*Padina tetrastromatica*	Kilakarai
11	TCSS	*Turbinaria conoides*	Kilakarai
12	SMSS	*Sargassum myriocystum*	Pamban
13	SMaSS	*Stochospermum marginatum*	Pamban
14	DDSS	*Dictyota dichotoma*	Thonithurai
Red algae			
15	GCSS	*Gracilaria corticata*	Pamban
16	HFSS	*Halymenia floresia*	Seeniappa Dargah
17	ASSS	*Acanthophora spicifera*	Seeniappa Dargah
18	CPSS	*Champia parvula*	Thonithurai

Identification of Isolated Endophytic Fungi

All the isolated different morphotypes of endophytic fungi were identified by molecular techniques. To identify the fungal isolates, each fungus was cultured in PDB medium for 7 days, and genomic DNA was isolated from fresh mycelium using the phenol–chloroform–CTAB method (Moller et al., 1992). The isolated genomic DNA was quantified using NANODROP (Thermo, United States), and the quality was assessed by visualization on 0.8% agarose gel. The isolated genomic DNA was used as a template for PCR to amplify the ITS1 and ITS2 regions using the universal primers ITS1 (CTTGGTCATTTAGAGGAAGTAA) and ITS4 [CAGACTT (G/A) TA (C/T) ATGGTCCAG], respectively. The PCR reaction mixture and amplification conditions were chosen according to the description by White et al. (1990); the reaction was carried out in a thermocycler (Techne, TC-512, United Kingdom). The PCR-amplified products were examined for purity and amplicon size by visualization on 1% agarose gel. The respective PCR product was purified (Thermo Scientific GeneJET Gel Extraction Kit) and sequenced using Sanger's method, and a similarity of ITS gene sequences search was performed using GenBank Basic Local Alignment Search Tool for nucleotide (BLASTn) (Altschul et al., 1990). Based on the search identity and taxonomic status, the fungi were identified.

Diversity, Species Richness, and Phylogenetic Analysis of Endophytic Fungi

The colonization frequency (CF) of each fungal isolate was observed, and the percentage of colonization frequency (CF%) was calculated. Furthermore, the Menhinick's index (I Mn), occurrence of each fungal species, and species richness for each group of algae (red, green, and brown) were calculated using the formulae given below:

$$\mathrm{CF\%} = \frac{\text{Number of colonies isolated per species}}{\text{Number of segments screened}} \times 100$$

$$\text{Species richness} = \frac{\text{Number of species obtained per group of algae}}{\text{Total number of species obtained}}$$

$$\text{I Mn} = \frac{S}{\sqrt{N}}$$

where S = number of species and N = total number of individuals.

In addition, diversity indices such as Simpson's index and Shannon diversity index were calculated using the EstimateSWin910 software (Colwell and Elsensohn, 2014).

For phylogenetic analysis, similar ITS sequences of the fungal isolates were obtained from GenBank through BLASTn analysis. Furthermore, the sequences were subjected to multiple sequence alignment by the ClustalW program, and gaps were removed from the sequences. The highly relevant sequences were used for construction of the phylogenetic tree using maximum parsimony by the MEGA 6 software (Tamura et al., 2013); *Amanita muscaria* was used as an outgroup for the phylogenetic tree.

Cultivation of Endophytic Fungi and Preparation of Culture Extract

The endophytic fungi were inoculated in the center of petri dishes containing PDA medium and incubated at 25 ± 2°C in the dark for 7 days. The pure mycelia of each fungus (fresh; 12 plugs of 9 mm) were inoculated in a 1,000-ml flask containing 300 ml of PDB and kept in the dark at 25 ± 2°C for 21 days. On completion of 21 days, the entire culture was passed through two layers of cheesecloth to separate the mycelia and the culture filtrate. The mycelia were crushed in a sterile mortar and pestle with liquid nitrogen to obtain powder. The mycelia powder and culture filtrate were mixed together in the form of a suspension (heterogeneous mixture) in which the mycelia powder was floating around freely in the culture filtrate. The internal phase (mycelia solid powder) is dispersed throughout the external phase (liquid culture filtrate) by mechanical agitation using a shaker at 200 rpm for 12 h with the double volume of suspending solvent ethyl acetate. Furthermore, ethyl acetate solvent extract was separated from the culture filtrate and filtrated to remove the mycelia fine debris. The solvent was removed from the organic extract using a rotary evaporator (IKA RV 10 digital, Sweden). The fungal metabolites were highly concentrated under speed vacuum at 35°C (LABCONCO, United States) and stored at −20°C for further experimental use.

Cancer Cell Lines and Their Maintenance

HeLa (Human cervical adenocarcinoma), A431 (skin cancer cells), HepG2 (human liver cancer cell line), MCF-7 (breast cancer cells), and HEK (human embryonic kidney) cell lines were procured from the National Centre for Cell Science (NCCS), Pune. They were maintained in Dulbecco's modified eagle's medium supplemented with 10% fetal bovine serum, penicillin (100 IU ml-1), and streptomycin (100 IU ml-1) in a humidified 5% CO_2 atmosphere at 37°C for experiments.

Cytotoxic Activity of Fungal Extracts Against Human Cancer Cells

The cytotoxicity of fungal secondary metabolites against both HeLa, A431 cancer cell lines, and normal healthy cells (HEK) was assessed using the MTT assay (Mosmann, 1983). For the study, approximately 1×10^4 cells per well were seeded in a 96-well plate and allowed to acclimatize overnight. Then, the cells were treated with fungal extract (5, 25, 50, and 100 μg/ml) prepared using 4% DMSO and filtered by syringe filters (0.22 μm) for a period of 24 h at 37°C in a CO_2 incubator. At post-treatment, 20 μl of 5 mg/ml MTT solution was added to each well of the 96-well plate and further incubated for 3 h. After incubation, the medium was discarded, and the formazan crystals formed were dissolved by adding 200 μl of DMSO. The optical density (OD) was measured at 570 nm using a microplate reader (VersaMax™ Tunable Microplate Reader, United States). The percentage of cytotoxicity exhibited by the cancer cells upon treatment with each fungal extract was evaluated using the following formula: cytotoxicity (%) = [1 – (OD of treated cells/OD of untreated cells) × 100]. Then, 50% of cytotoxic concentration CC_{50} was calculated for each fungal extract, and the selective index (SI) was analyzed using the formula: CC_{50} of normal healthy cells (HEK) / CC_{50} of cancer cells.

Preparation of Culture Filtrate and Mycelial Extract for Cytotoxic Assay

To find out whether the cytotoxic metabolites are bound with mycelia or secreted into the culture filtrate, the ethyl acetate extract of the mycelium and the culture filtrate were tested separately for cytotoxicity on both HeLa and A431 cancer cell lines. For this purpose, the selected fungi were cultured in 1,000-ml flasks containing 300 ml of PDB medium and incubated in the dark at 25 ± 2°C for 21 days. After 21 days, the culture was harvested by filtration through two layers of cheesecloth to separate the mycelia and the culture filtrate. The mycelia were dried at 60°C overnight, and their dry weight was determined. Then, the mycelia were powdered using liquid nitrogen, and the intracellular metabolites were extracted with a 5X volume of ethyl acetate, whereas the culture filtrate was extracted using double the volume of ethyl acetate (Dhayanithy et al., 2019). The organic phase was collected by a separating funnel and evaporated to dryness using a vacuum rotary evaporator at 45°C. Each fungal dry solid residue of mycelia and culture filtrate extract was quantified and prepared to test the cytotoxicity.

Characterization of *Biscogniauxia petrensis*

The endophytic fungal isolate *B. petrensis* was inoculated in petri dishes containing fresh PDA medium and incubated at 25 ± 2°C in the dark for 7 days. The mycelia pattern and conidial morphology were characterized using a phase-contrast light microscope (Zeiss AX10 Imager A2, Zeiss, Germany). Thirty to 50 conidia were studied to confirm the species level.

Cytotoxic Potential of *B. petrensis* Metabolites Using Different Media and Solvents

A proven fact is that the media used for cultivation also plays an important role in the production of secondary metabolites by the fungus (Bode et al., 2002). Hence, in the present study, *B. petrensis* was further subjected to optimization in 11 different

liquid media (**Supplementary Table 1**). The four agar plugs containing *B. petrensis* mycelia (9 mm) were inoculated in 500-ml flasks containing 100 ml of different media separately. All the flasks were incubated in dark condition at 25 ± 2°C for 21 days. Then, the cultures were harvested, and metabolites from the culture filtrate and the mycelia were extracted separately using ethyl acetate. Each fungal extract was assayed for cytotoxicity at a concentration of 25 μg/ml on HeLa and A431 cells using the MTT assay. Furthermore, to find out the cytotoxic effect of different organic solvent extracts of *B. petrensis*, the culture was inoculated in 1,000-ml flasks containing 300 ml of potato dextrose yeast extract broth (PDYEB) medium. The cultures were grown for 21 days and harvested. The mycelia, culture filtrate, and total culture were extracted separately using five different solvents, namely, ethyl acetate, dichloromethane, chloroform, hexane, and diethyl ether. The solvents were completely removed under reduced pressure using a rotary evaporator. The organic solvent extracts were prepared (25 μg/ml) and tested for anticancer activity against A431 and HeLa cell lines.

Live/Dead Viability Assay

Propidium iodide (PI), a fluorescent dye, binds to DNA by intercalating between the bases and is commonly used to detect dead cells in a population, as it is not permeable in live cells. To observe the cytotoxic effect of EtOAc extracts of mycelia and culture filtrate on HeLa cells, a PI live/dead assay was performed as reported earlier (Chakravarthi et al., 2013). For this purpose, HeLa cells (2.5×10^4/ml) were seeded in a 24-well culture plate and allowed to adhere overnight. Furthermore, the cells were treated with two different concentrations (25 and 50 μg/ml) of *B. petrensis* culture filtrate extract (BpCFE) and mycelial extract (BpME) prepared using 4% DMSO for 24 h. After incubation, the cells were trypsinized and centrifuged (3,000 rpm, 3 min), and the pellet was washed twice with ice-cold × 1 PBS. The untreated cells were taken as control, and paclitaxel (12 nM)-treated cells served as a positive control. The cells were then stained with PI for 30 min at 37°C and analyzed by fluorescence-activated cell sorting (FACS) in a CytoFlex flow cytometer (Beckman coulter-CytoFLEX S). The percentage of live and dead cells was calculated using the CytExpert software.

Measurement of Mitochondrial Membrane Potential Using JC-1 Staining

The mitochondrial membrane potential test was done with JC-1 (5,5′,6,6′-tetrachloro-1,1′,3,3′-tetraethylbenzimidazolcarbocyanine iodide) staining as described earlier (Cossarizza et al., 1993). For the experiment, 5×10^4 HeLa cells were seeded per well in a 24-well plate and kept overnight. Then, the cells were treated with 25 μg/ml of BpME and BpCFE for 24 h. At post-treatment, 0.2 μM of JC-1 dye was added into the untreated and treated cells. The untreated cells were considered as control, while the 2,4-DNP (1 μM)-treated cells acted as positive control. The plates were incubated under dark conditions at 37°C for 15 min. Then, the cells were harvested, washed twice with ice cold × 1 PBS, and analyzed in a FACS instrument (Beckman coulter-CytoFLEX S). The percentage of cell population was calculated using the CytExpert software.

Cell Cycle Analysis

The cell cycle was studied by flow cytometry as described earlier (Sowmya et al., 2015). The HeLa cells were seeded (1×10^5 per well) in 12-well plates treated with 25 μg/ml ethyl acetate extract of BpME and BpCFE for 12 h. Then, the cells (in the 12-well plates) were rinsed with PBS, detached with trypsin-EDTA at room temperature, and centrifuged at 3,000 rpm for 5 min. The cells were washed twice with PBS, re-suspended in 1 ml of ice-cold PBS, 0.1% Triton X-100, and 0.1 mg/ml RNase, and incubated for 3 h at 37°C. Propidium iodide (50 mg/ml) was added, and incubation was continued for 15 min. After incubation, the cell suspension was analyzed using FACS (Beckman coulter-CytoFLEX S), and the data was plotted using the CytExpert software to determine the percentage of cells in each phase of the cell cycle (G0, G1, S, and G2M).

Chemical Analysis of Bioactive Extracts From *B. petrensis*

Separation of the Bioactive Extract and Determination of Cytotoxic Activity

Thin-layer chromatography was carried out using pre-coated TLC silica sheets 60 F 254. The ethyl acetates BpME and BpCFE were dissolved in methanol and spotted on the TLC sheets separately. The TLC chromatogram was developed with an optimized solvent system, namely, ethyl acetate/chloroform/methanol (80:12.5:7.5, v/v/v). The developed chromatogram was detected under white light and ultraviolet (UV) lamp at 254 and 366 nm, respectively. The R_f value of each band was determined, and the band characters were noted. Furthermore, preparative TLC silica gel glass plates (1 mm in thickness) were used to get the bioactive metabolites in large amounts with the same solvent system as mentioned above. All the bands were carefully scraped off from the plates with silica gel, and the compounds of each band were eluted from silica by dissolving in methanol and centrifugation at 5,000 rpm for 3 min. The elute was collected carefully without disturbing the settled silica. The eluted compounds were further purified using a silica gel column (Qiagen, RNeasy mini Column), concentrated under vacuum in a pre-weighed vial, and evaporated using a Speed Vac at 35°C (LABCONCO, United States). The yields of the compounds were noted and tested for cytotoxicity against HeLa, A431, MCF-7, HepG2, and HEK cells using the MTT assay.

UV Spectroscopy and High-Performance Liquid Chromatographic Analysis

The four purified bioactive fractions were processed to determine their absorption maxima by using an ultraviolet/visible (UV/vis) spectrophotometer (Shimadzu UV–vis spectrophotometer, United States). A graph of wavelength *versus* optical density was plotted to determine λ-max. Finally, the active compounds were also checked for their purity and retention time using high-performance liquid chromatography (HPLC). The purity of the bioactive compounds (C2, C5, M3, and M4) from *B. petrensis*

extracts was determined using an Agilent 1120 HPLC system with a photo iodide array detector measuring absorbance at 282, 270, 273, and 266 nm, respectively. A Phenomenex Luna C18 (5 μm, 250 × 4.6 mm) column was used in combination with the isocratic elution of the mobile phase consisting of 30% acetonitrile and 70% water. The flow rate of the mobile phase was set at 0.3 ml min^{-1}. The purity and retention time of the purified metabolites present in the culture filtrate and mycelial extracts were analyzed.

LC-ESI-MS/MS Analysis With MetFrag Tandem MS/MS Databases

Liquid chromatography with mass spectrometry (LC/MS) provides abundant information about molecular mass for the structural elucidation of compounds when tandem mass spectrometry (MS^n) is applied. Therefore, the active extracts and four purified compounds were subjected to liquid chromatography–electrospray ionization–tandem mass spectrometry (LC–ESI–MS/MS) for analysis. The fungal extracts were filtered through 0.22-μm polyvinylidene fluoride filters before injecting into the column; 20 μl of each sample was injected. The analysis was performed using the Dionex Ultimate 3000 Micro LC instrument fitted with an analytical column Agilent Poroshell 120 (4.6 × 150 mm) SB-C18 and 2.7 μm particle size and a guard column. The mobile phase consisted of water/acetonitrile (75:25, v/v), and separation was performed using iso-gradient elution with a flow rate of 0.3 ml/min and column temperature of 40°C. The Rt value of the purified compound was compared with the chromatogram of an active fungal extract to confirm its presence. ESI–MS/MS was performed using the instrument ESI-Qtof (Impact HD from Bruker) in the positive mode. An acquisition range from 50 to 1,700 m/z at a spectral rate of 1 Hz was used. The LC–MS interface was used for electrospray ionization. The mass spectrometry data was analyzed using the Bruker Compass Data Analysis software (version 4.3; Bruker Daltonics, Bremen, Germany). The MetFrag1web tool (version 2.1) was used to compare the fragment patterns of fragmented ions with existing databases such as PubChem, ChemSpider, and KEGG (Tapfuma et al., 2019).

Statistical Analysis

The statistical values were represented by the mean of three replicates and their standard deviations (mean ± SD). All the statistical analyses were done using Microsoft Excel (Redmond, WA) and the GraphPad Prism software (version 5.03).

RESULTS

Identification of Marine Algae-Associated Endophytic Fungi

In this study, 31 different endophytic fungi were isolated from 18 marine macro-algae (**Figure 1** and **Supplementary Figure 1**) by culturing them on a PDA medium prepared with and without artificial salt. The fungal isolates were identified based on different morphological features and molecular taxonomy using ITS gene sequences from the PCR-amplified products (**Supplementary Figure 2**). The obtained ITS sequences were compared with existing ITS sequences in the GenBank repository to identify the fungi. The names of the fungal isolates were obtained and confirmed according to 99.9% similarity in the GenBank database. Furthermore, the sequences, along with detailed descriptions of the endophytic fungi and their hosts, were submitted to the National Center for Biotechnology Information (NCBI) GenBank; the obtained accession numbers are mentioned in **Table 2**.

Diversity and Phylogenetic Study of Endophytic Fungi

Forty-seven endophytic fungal isolates were obtained from green algae, 26 from brown algae, and 23 from red algae. Interestingly, the *Aspergillus* genus was found to be dominant among the fungal isolates, exhibiting seven different species followed by three species of *Cladosporium*. Two species each of *Periconia* and *Aschotricha* were obtained, and the rest of the 13 genera were represented by only one species each (**Table 2**). The Shannon and Simpson's index values were found to be 3, 2.5, and 2.58 and 15.77, 9.45, and 9.46 for green, brown, and red algae, respectively. This shows that the diversity of fungal endophytes in red and brown algae was high in comparison to that in green algae. The species richness of endophytic fungi was highest in red algae (6) but similar in brown and green algae (5 and 5.22, respectively), as shown in **Supplementary Table 2**. Nevertheless, it can be claimed that brown algae represent more diverse forms of fungal species as the number of host algae was less in brown (five) than in green (nine) algae. Furthermore, a phylogenetic tree has been constructed with ITS 1/5.8S rDNA/ITS 2 sequences using the MEGA6 software. This phylogenetic tree gives the evolutionary relationship between different endophytic fungi distinguished by a monophyletic group in different subclades from the outgroup (*Amanita*), as shown in **Supplementary Figure 3**.

Cytotoxic Potential of Marine Endophytic Fungi

From the results of the MTT assay of 31 fungal extracts, the percentage of cytotoxicity was observed at a dose-dependent manner in both HeLa and A431 cells (**Figures 2A,B**). Though all the fungal extracts showed cytotoxicity against both cancer cells, a significant cytotoxicity was observed in the extracts of nine fungi, namely, *Periconia byssoides*, *Coniochaeta* sp., *C. cladosporioides*, *Biscogniauxia petrensis*, *Nigrospora oryzae*, *Gymnascella aurantiaca*, *Gliomastix murorum*, *Nectria dematicosa*, and *Ascotricha sinuosa*. The 50% cytotoxicity concentration (CC_{50}) values for cancer cells (HeLa and A431) and normal healthy cells, along with their selectivity index, are mentioned in **Supplementary Table 3**. The cytotoxic effect of five fungal extracts, namely, *Amesia atrobrunnea*, *Aspergillus niger*, *Hortaea werneckii*, *Aspergillus amoenus*, and *Periconia celaeidis*, was marginal at lower doses, while it was notable at higher concentrations. The results also showed that HeLa cells were more sensitive than A431; 10–20% cell death was observed at 5 μg/ml in HeLa but not in A431.

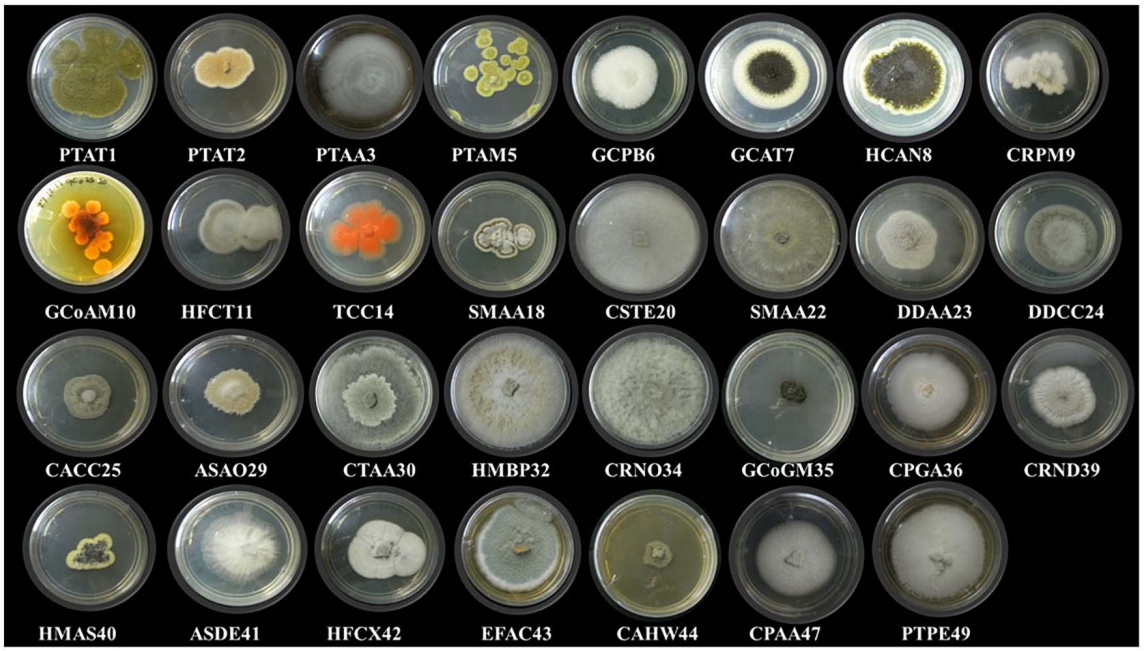

FIGURE 1 | Different endophytic fungi (morpho species) isolated from marine brown, green, and red algae.

Furthermore, the mycelial and culture filtrate extracts of the nine potent fungi were tested separately for their cytotoxic activities in HeLa and A431 cells. Interestingly, both the mycelial and culture filtrate extracts of *B. petrensis* showed 70% cytotoxicity on cancer cells. The mycelial extracts of six fungi showed 60% cytotoxicity, but their culture filtrate extracts were not very effective and showed less than 40% cytotoxicity. It was also observed that the extracts of *Periconia byssoides* were not effective on A431, but its mycelial extracts exhibited 70% activity on HeLa cells (**Figures 3A,B**). The culture filtrate extract of *G. aurantiaca* had no inhibitory effect on either HeLa or A431 cells, whereas its mycelial extract showed 50% cytotoxicity in both cells. The fungal biomass and yield of extracts were also measured; this clearly presented *B. petrensis* as the most prominent candidate compared to other fungi, with the highest biomass of 9 g (mycelial dry weight) and yields of 533 mg total extract, 733 mg mycelial extract, and 1 g culture filtrate extract obtained per liter of culture. Although the biomass and yield of extract from *P. byssoides* were of notable quantity, the cytotoxic activity was not considerable against A431 cell line. The other seven endophytic fungi showed less biomass and yield of secondary metabolites (**Supplementary Figure 4**).

Biscogniauxia petrensis and Cytotoxic Effect of Different Media and Organic Solvent Extracts

Biscogniauxia petrensis grew 80–85 mm in diameter on the PDA medium within 7 days with a cottony to wooly texture, whitish to light pink color, and with aerial mycelia. It showed dark-colored pigmentation in both solid and broth cultures (**Figures 4A,B**). The microscopic images showed the hyphae as brown, septate, and abundantly branched aerial mycelium. The conidiospores were yellow to light brown in color, measuring 4 to 5 μm in length, and were composed of a main axis along with one or more branches. The conidia were holoblastic, unicellular, smooth ovoid to clavate, and 5.3–7.1 μm in diameter, with an obtuse tip and acute truncated base (**Figures 4C–F**). The rarely seen chlamydospores were globose, 5–7 μm, dark brown, thick-walled, and attached with mycelia with a basal stalk (**Figure 4G**). The cytotoxicity assay of *B. petrensis* extracts obtained from 11 different culture media against HeLa and A431 cells was observed. The mycelia and culture filtrate extracts of PDYEB media showed a prominent cytotoxicity of 50–60% on both cancer cells. In the case of PDB and MB media mycelial extracts, 40–50% of cell death was observed in HeLa, while it was below 40% in A431. In addition, it was observed that the culture filtrate extracts of *B. petrensis* from S7 media was more effective on A431 (60%) in comparison to HeLa (30%). The other media extracts of *B. petrensis* showed an almost similar cytotoxicity in the range of 20–40% in HeLa and A431 cells (**Figures 5A,B**). In the optimization of different solvents, the ethyl acetate extracts of *B. petrensis* showed the highest cytotoxicity against both HeLa and A431 cells in the mycelial (84 and 77%), culture filtrate (74 and 83%), and total culture extracts (58 and 63%), respectively. Moreover, the mycelial extracts of dichloromethane and diethyl ether also exhibited notable cytotoxicity against HeLa cells. The mycelial chloroform extract exhibited moderate cytotoxicity on both cell lines. Ethyl acetate was found to be the most suitable out of five organic solvents, namely, hexane, diethyl ether, chloroform, ethyl acetate, and dichloromethane (**Supplementary Figures 5A–C**).

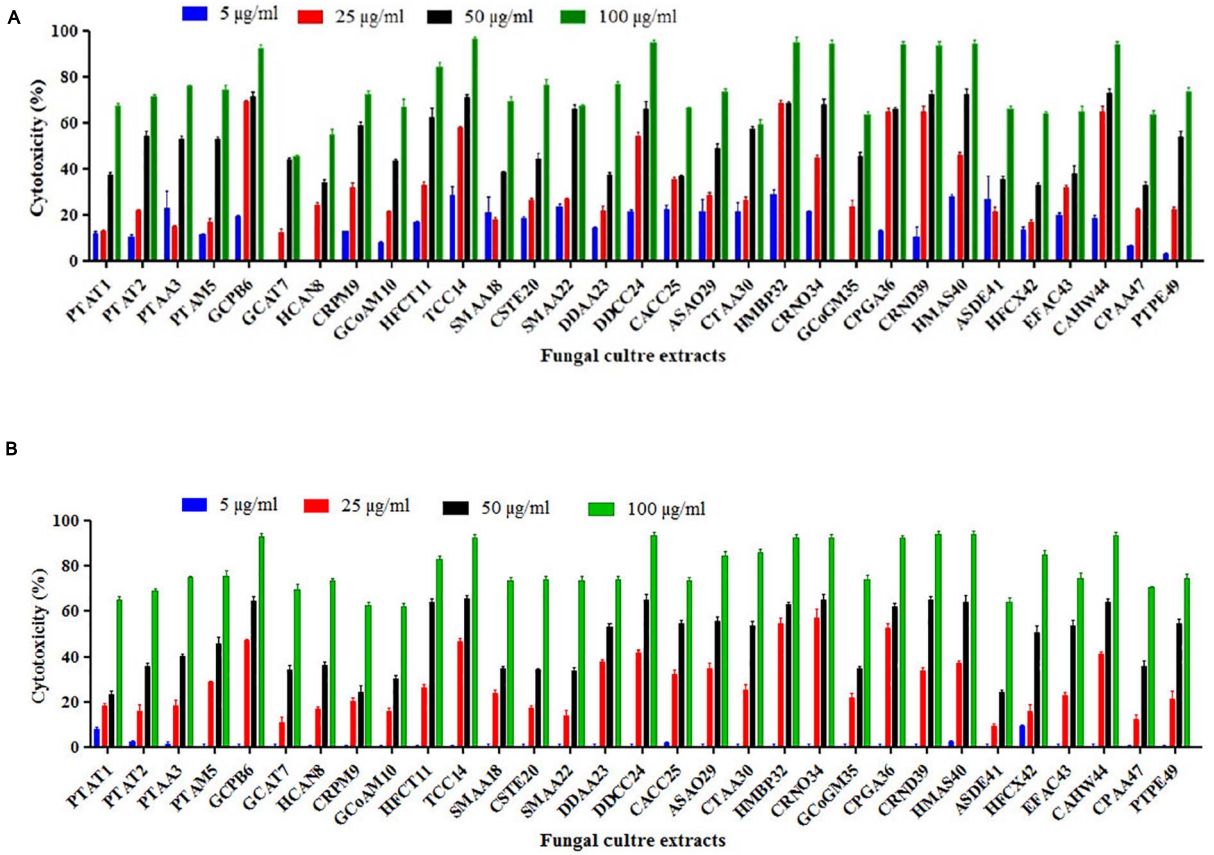

FIGURE 2 | (A,B) *In vitro* cytotoxicity of fungal ethyl acetate extracts on human cancer cells HeLa and A431.

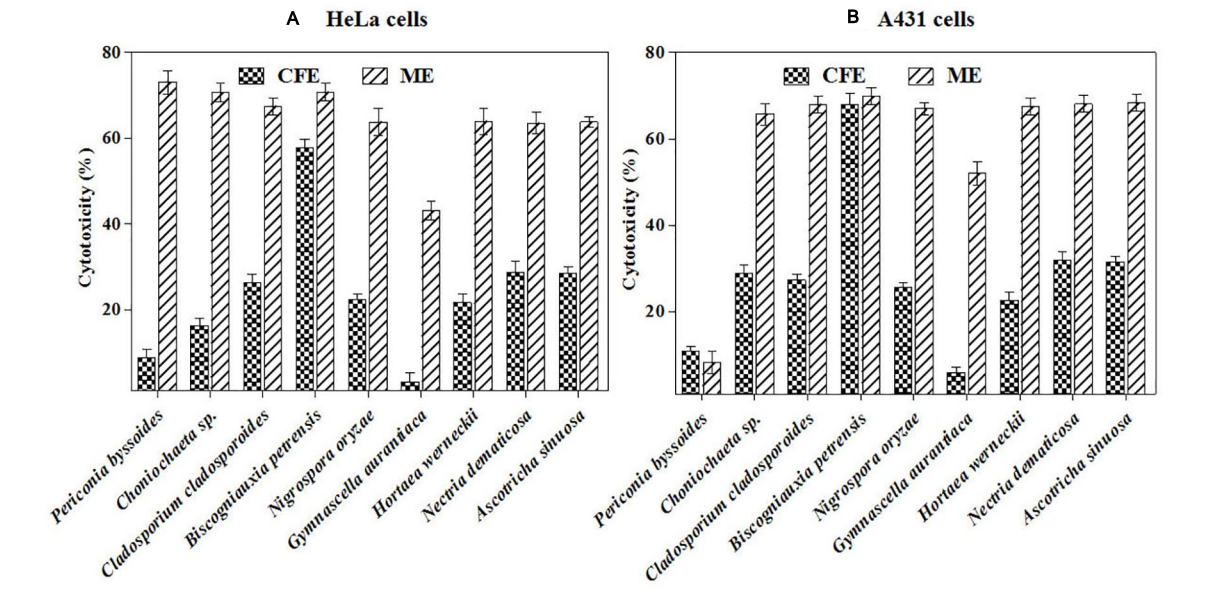

FIGURE 3 | (A,B) *In vitro* cytotoxicity of selected fungal culture filtrates and mycelia extracts against A431 **(A)** and HeLa **(B)** cancer cell line.

TABLE 2 | Host algae and their respective endophytic fungi with CFU and NCBI accession number.

Marine Algae	Gracilaria crassa	Halimeda crasilis	Caulerpa racemosa	Caulerpa scafeliformis	Chaetomorpha antenina	Caulerpa taxifolia	Halimeda macroloba	Caulerpa peltata	Enteromorpha flexuosa	Turbinaria conoides	Sargassum myriocystum	Stochospermum marginatum	Dictyota dichotama	Padina tetrastomatica	Gracilaria corticata	Hracilaria corticata	Acanthophora spicifera	Champia parvula	Total CFU	CFU%	NCBI accession number
Endophytic fungi																					
Ascomycota																					
Gymnascella aurantiaca (CPGA36)	–	–	1	–	–	–	–	–	–	–	–	–	–	–	–	–	–	3	4	1.17	MH748175
Cladosporium xantochromaticum (HFCX42)	–	–	–	–	–	–	1	–	–	–	–	–	–	–	–	5	–	–	6	1.7	MH748179
Amesia atrobrunnea (SMAA18)	–	–	–	–	–	–	–	–	1	–	6	–	–	–	–	–	–	–	7	2.06	MH748152
Amesia atrobrunnea (PTAA3)	–	–	–	–	–	–	–	–	–	–	–	–	–	3	–	–	–	1	4	1.17	MH748153
Periconia byssoides (GCPB6)	–	–	–	–	–	–	2	–	–	–	–	–	–	–	7	–	–	–	9	2.65	MH748157
Ascotricha chartarum (EFAC43)	–	–	–	–	–	–	–	1	5	1	–	–	–	–	–	–	–	–	7	2.06	MH748180
Nectria dematicosa (CRND39)	–	–	–	–	–	3	–	–	–	–	–	–	1	–	–	–	–	–	4	1.17	MH748176
Ascotricha sinuosa (HMAS40)	–	–	–	–	–	–	6	–	–	–	–	–	–	1	–	–	1	–	8	2.35	MH748177
Cladosporium tenuissimum (HFCT11)	–	–	–	–	–	–	–	1	–	–	–	–	–	–	–	3			4	1.17	MH748170
Cladosporium tenuissimum (CACC25)	4	–	–	–	12	–	–	–	–	–	1	–	–	–	–	–	–	–	17	5.01	MH748162
Cladosporium cladosporioides (DDCC24)	–	–	4	–	–	–	2	–	–	–	–	–	19	–	1	–	–	–	29	8.55	MH748169
Hortaea werneckii (CAHW44)		1	–	–	8	–	–	1	1	–	–	–	–	–	–	–	–	–	11	3.24	MH748181
Gliomastix murorum (GCoGM35)	–	–	–	–	–	–	–	–	2	–	–	–	–	–	4	–	–	–	6	1.76	MH748174
Basidiomycetes																					
Daldinia eschscholtzii (ASDE41)	–	–	–	–	–	1	–	–	2	2	–	–	–	–	–	–	13		18	5.30	MH748178
Hyphomycetes																					
Trichoderma erinaceum (CSTE20)	–	–	–	7	–	–	–	–	–	–	–	–	1	–	–	–	–	1	9	2.65	MH748164
Alternaria alternata (DDAA23)	–	1	–	–	–	–	–	–	–	1	–	6	11	–	–	4	–	–	23	6.78	MH748168
Aspergillus amoenus (CPAA47)	–	–	–	–	–	–	–	4	–	–	1	–	–	–	–	–	–	–	5	1.47	MH748182
Aspergillus tubingensis (GCAT7)	9	–	–	–	1	–	–	–	–	2	–	–	–	–	–	–	–	–	12	3.53	MH748158
Aspergillus terreus (PTAT20)	–	–	–	–	–	2	–	–	–	–	–	1	–	8	–	1	–	–	12	3.53	MH748155
Aspergillus ochraceopetaliformis (ASAO29)	3	–	–	1	–	–	–	–	–	–	–	–	–	–		–	14		18	5.30	MH748171
Aspergillus amstelodami (GCoAM10)	–	–	–	–	–	–	1	–	–	–	–	–	–	–	7	–	–	2	10	2.94	MH748161
Aspergillus amstelodami (PTAM5)	–	–	1	–	1	–	–	–	1	–	1	–	–	9	–	1	–	1	15	4.42	MH748156
Aspergillus niger (HCAN8)	–	13	–	–	–	–	–	2	–	–	–	–	–	–	1	–	–	–	16	4.71	MH748159
Aspergillus tamari (PTAT1)	1	–	–	–	1	–	–	–	–	–	–	–	–	11	–	–	2	–	15	4.42	MH748154
Coniochaeta sp. (TCC14)	–	–	–	–	–	–	–	–	–	2	–	–	–	–	–	–	–	–	2	0.58	MH748163
Biscogniauxia petrensis (HMBP32)	–	–	–	–	–	–	7	–	1	–	–	–	–	–	–	–	–	1	9	2.65	MK073011
Nigrospora oryzae (CRNO34)	–	–		3	–	–	–	–	–	–	–	–	1	–	–	1	–	–	5	1.47	MH748173
Periconia elaeidis (PTPC49)	1	–	–	–	–	–	1	–	–	–	–	–	–	3	–	–	–	–	5	1.47	MH748183
Coelomycetes																					
Phoma moricola (CRPM9)	–	–	4	–	–	–	–	1	–	–	–	–	–	–	–	–	–	–	5	1.47	MH748160
Aplosporella artocarpi (CTAA30)	–	1	–	–	1	14	–	–	–	1	–	4	–	–	–	–	3	–	24	7.07	MH748172
Aplosporella artocarpi (SMAA22)	–	–	–	1	–	–	–	–	–	–	–	17	–	–	–	1	–	1	20	5.89	MH748167

Apoptotic Properties of Ethyl Acetate Extract From *B. petrensis*

Live/Dead Assay

The mycelial and culture filtrate ethyl acetate extracts of *B. petrensis* were tested on HeLa using the PI live/dead assay. The percentage of dead cells increased from 23 to 52% and from 34 to 60% in BpCFE- and BpME-treated cells, respectively. This indicated a dose-dependent effect of *B. petrensis* extracts when compared with the untreated (control) cells, showing 1% cytotoxicity and 45% cell death in paclitaxel-treated cells (**Figure 6**).

Effect of Fungal Extract on Mitochondrial Membrane Potential in Cancer Cells

The MMP loss is an essential event in the mitochondrial pathway of apoptosis and can be measured using the cationic dye JC-1. The loss of MMP was observed in HeLa cells when treated

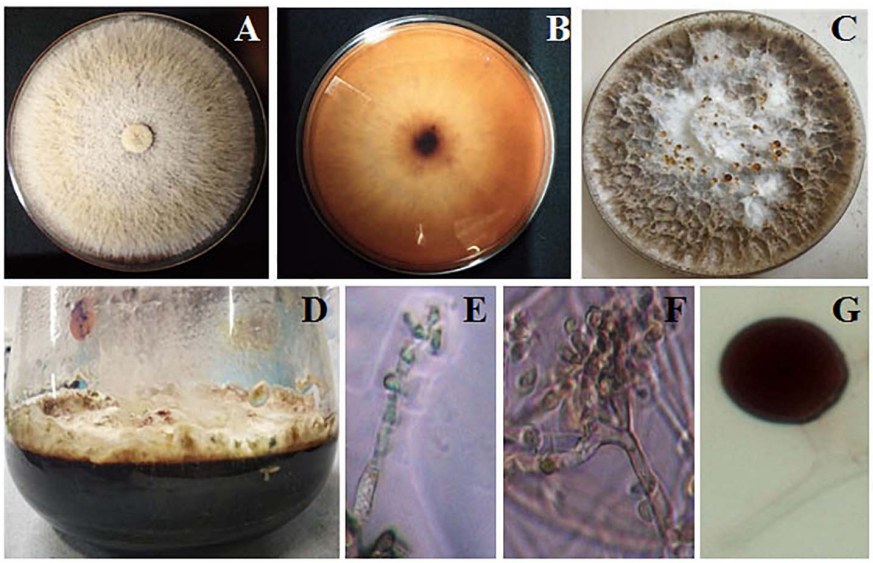

FIGURE 4 | Morphological observation of *Biscogniauxia petrensis*. The colonies at 7 days of inoculation on potato dextrose agar (PDA) plate front **(A)** and rear **(B)** view, respectively. **(C)** Appearance of red droplets at 10–14 days of growth on PDA plate. **(D)** Growth of *B. petrensis* in PDYEB at 21 days of culture. **(E–G)** Light microscopy image of the *B. petrensis* spores (×40 magnification) and microscopy image of chlamydospore.

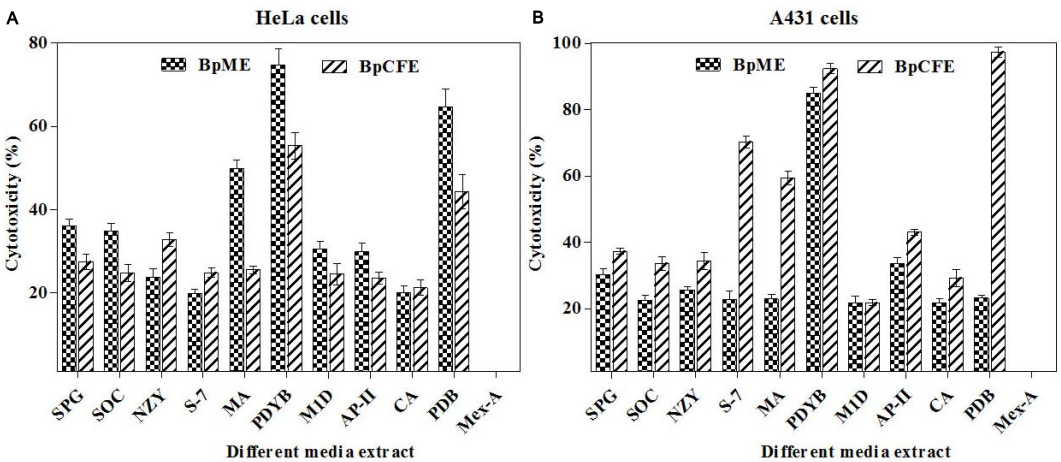

FIGURE 5 | Cytotoxic effects of *B. petrensis* culture extracts grown in different media on HeLa **(A)** and A431 **(B)** at 25 μg/ml.

with mycelial and culture filtrate EtOH extracts with two different concentrations. According to the results (**Figure 7**), the apoptotic cell death due to MMP loss increased from 25 to 43% in BpCFE-treated HeLa cells and from 18 to 45% in the case of BpME-treated cells at 25 and 50 μg/ml, respectively. In comparison, the untreated cells that were considered as control showed only 3.22% cell death; the 2,4-DNP-treated cells that served as positive control exhibited 54.61% cell death due to MMP loss.

Effect of *B. petrensis* Ethyl Acetate Extracts on Cell Cycle

To examine the effect of ethyl acetate extract on cell cycle progression, the phase distribution of cells was assessed after treating the HeLa cells with BpCFE and BpME at two different concentrations for 12 h. There was a gradual increase in the percentage of cells in the sub-G1 phase from 24.29 to 47.59% in BpCFE and from 26.80 to 50.38% in BpME when treated with 25 and 50 μg/ml, respectively. The results showed a concentration-dependent accumulation of cells in the sub-G1 phase, which clearly indicates a sub-G1 phase arrest induced by the ethyl acetate extracts of *B. petrensis* (**Figure 8**).

Bioactive Compounds From *Biscogniauxia petrensis* Extracts

To trace out the active compounds present in the crude extract, the BpME and BpCFE ethyl acetate extracts were separated by

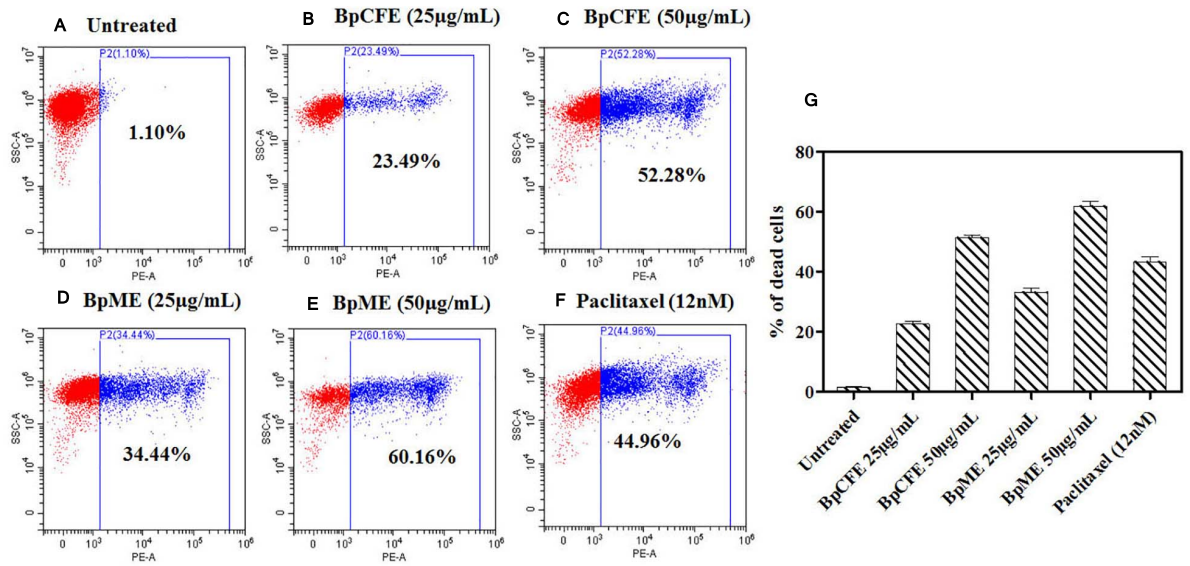

FIGURE 6 | Cytotoxic effect of Bp culture extracts on HeLa cells and estimated using PI staining by FACS analysis. **(A)** Untreated **(B)** culture filtrate extract (25 µg/ml), **(C)** culture filtrate extract (50 µg/ml), **(D)** mycelial extract (25 µg/ml), **(E)** mycelial extract (50 µg/ml), **(F)** paclitaxel (12 nM), and **(G)** bar diagram representing the distribution of cell death. The data are results from three independent experiments.

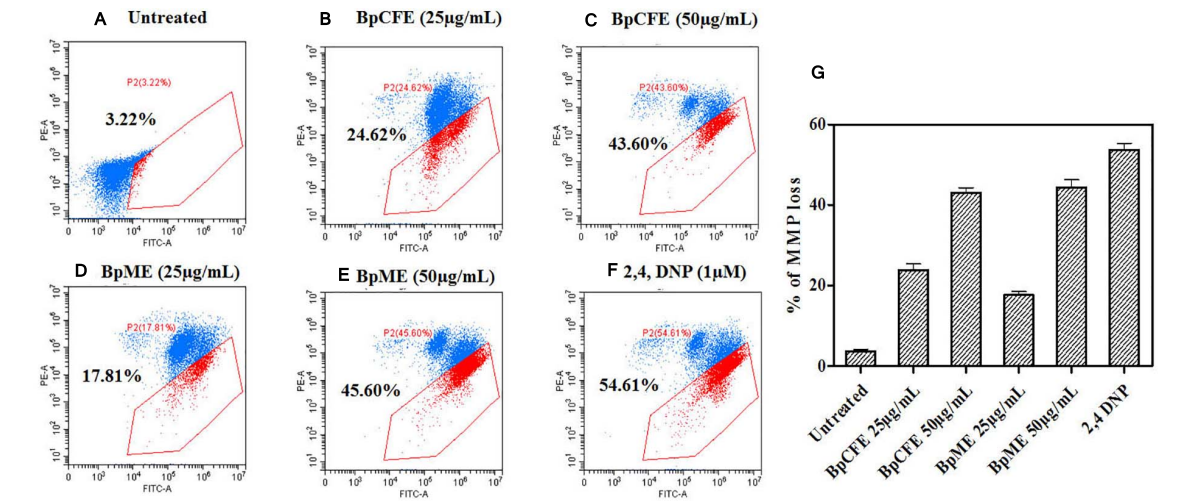

FIGURE 7 | Determination of apoptosis through loss of mitochondrial membrane potential in HeLa cells induced by Bp culture extract and quantified by JC-1 monomer percentage. **(A)** Untreated **(B)** culture filtrate extract (25 µg/ml), **(C)** culture filtrate extract (50 µg/ml), **(D)** mycelial extract (25 µg/ml), **(E)** mycelial extract (50 µg/ml), **(F)** 2,4-DNP, and **(G)** statistical analysis of loss of mitochondrial membrane potential acquired in a flow cytometer. The experiments were conducted three times, and results are obtained from mean ± SD.

preaparative thin-layer chromatography. The R_f values of all the bands, along with their properties (**Supplementary Figure 6**), are mentioned in **Supplementary Tables 4A,B**. The cytotoxicity of each fraction was assessed by an MTT assay (**Supplementary Figures 7A,B**). Interestingly, four fractions, namely, C2 and C5 (from BpCFE) and M3 and M4 (from BpME), displayed significant cytotoxicity against all the four cancer cell lines (HeLa, A431, HepG2, and MCF7); there was no detectable effect on non-cancerous cells (HEK) (**Figure 9**). The results also indicated that the remaining fractions obtained from mycelia extract (16) and culture extract (12) showed a prominent cytotoxic activity against the cancer cells used in this study but also exhibited toxic effects on non-cancerous cells (HEK).

The purified active principles C2, C5, M3, and M4 were tested for their purity, all of which possess R_f values of 0.88, 0.71, 0.66, and 0.61, respectively, with single pure spots TLC (**Supplementary Figure 8**). In addition, purity was further analyzed by HPLC, with C2, C5, M3, and M4 active compounds exhibiting a single peak with Rt values of 2.31, 4.74, 8.35, and 2.54, respectively (**Supplementary Figure 9**).

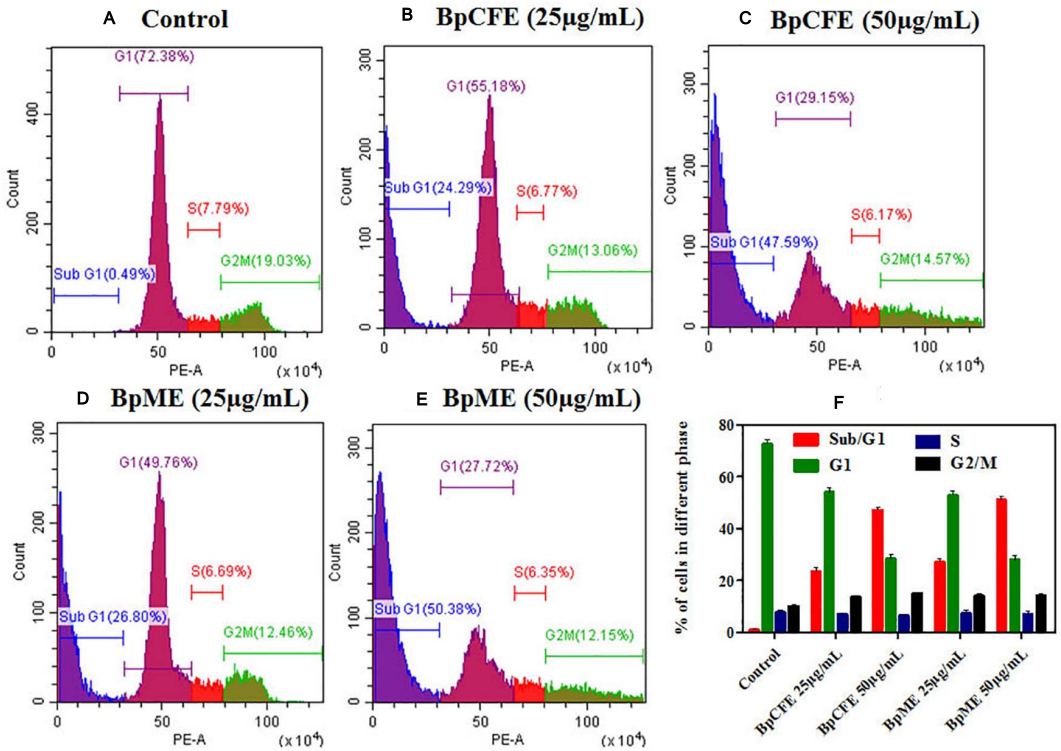

FIGURE 8 | Cell cycle analysis of HeLa cells treated with Bp culture extract estimated using propidium iodide staining by flow cytometry analysis. **(A)** Untreated **(B)** culture filtrate extract (25 µg/ml), **(C)** culture filtrate extract (50 µg/ml), **(D)** mycelial extract (25 µg/ml), and **(E)** mycelial extract (50 µg/ml). **(F)** Statistical analysis showing the percentage of cell cycle in each phase. The experiments were conducted three times, and results are obtained from mean ± SD.

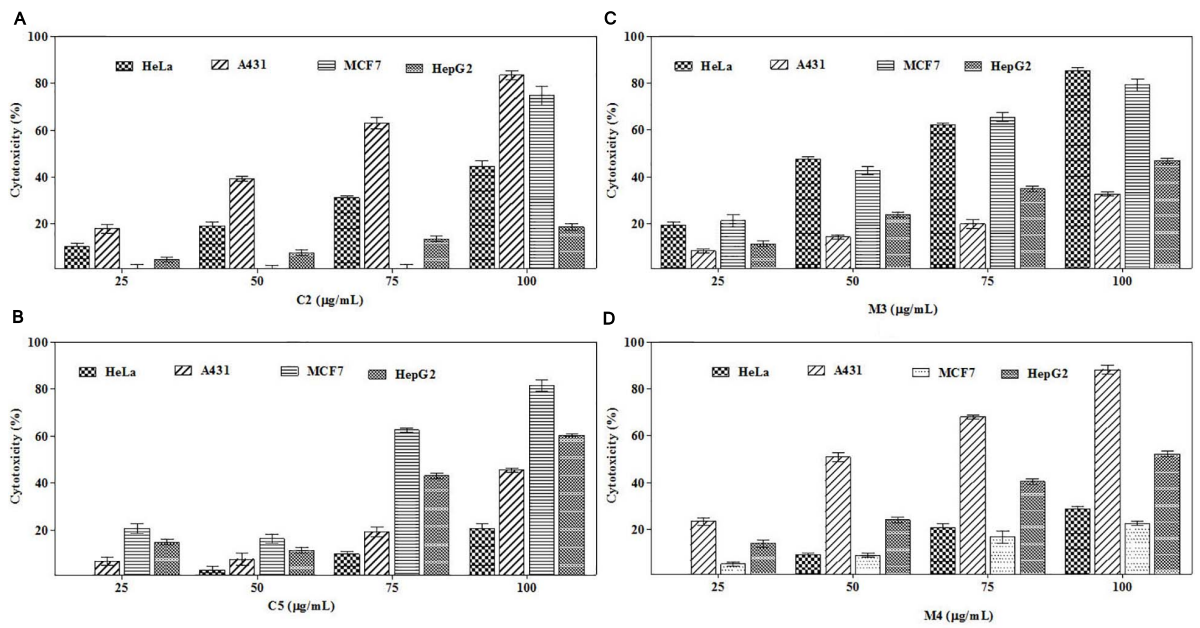

FIGURE 9 | Cytotoxic effects of purified bioactive fractions from *B. petrensis* culture extracts. The cytotoxic effect was determined against HeLa, A431, MCF-7, and HepG2 cancer cell lines with different concentrations of bioactive fractions: **(A)** C2, **(B)** C5, **(C)** M3, and **(D)** M4.

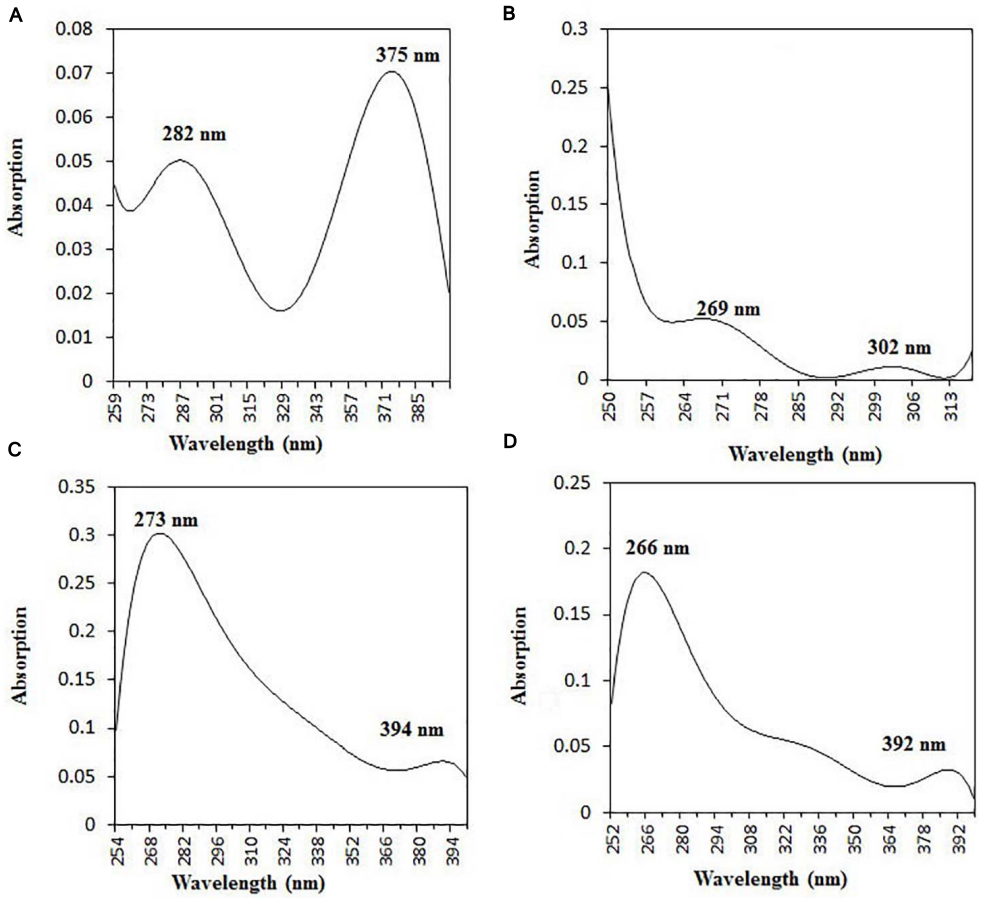

FIGURE 10 | UV–vis absorbance spectra of purified bioactive fractions from *B. petrensis* culture extracts. The UV–visible spectrum of bioactive fraction showed two main absorption peaks at λ.282 and λ.375 for C2 **(A)**, λ.269 and λ.302 for C5 **(B)**, λ.273 and λ.394 for M3 **(C)**, and λ.266 and λ.392 for M4 **(D)**.

The C2, C5, M3, and M4 fractions were identified using ultraviolet–visible spectrophotometry to observe the transition type experienced by the electrons of these isolated compounds. The ultraviolet spectrum of C2 showed maximum absorbance (λ_{max}) at 263 and 270 nm, while for C3 it was at 222 and 244 nm. The λ_{max} values of M2 and M3 were observed to be at 222 and 244 nm and at 350–385 nm, respectively (**Figure 10**). The liquid chromatogram profile peak of the *B. petrensis* culture filtrate and mycelial extract displayed Rt values of 33.31, 10.13, 27.9, and 13.4 for the purified bioactive fractions C2, C5, M3, and M4, respectively, corresponding to the fungal extract Rt values of 33.31, 10.14, 33.31, and 13.7 (**Figures 11**, **12**). The purified bioactive compounds were subjected to ESI–MS/MS to determine their molecular mass and fragmentation pattern. The bioactive metabolites C2, C5, M3, and M4 showed a mass of 212.02, 185.11, 229.08, and 185.11 m/z, respectively (**Figures 11**, **12**). Furthermore, their MS/MS data were analyzed through the MetFrag library to find similarity matches, and these were identified as 2-(1,3-benzothiazol-2-ylsulfanyl)ethanol, 5-cyclohexyl-1-oxido-triazolidin-4-one, 3-hydroxy-7-propyl-naphthalene-2-carboxylic acid, and 2,2-bis(azidomethyl)butan-1-ol for C2, C5, M3, and M4, respectively. The information on the corresponding molecular formulae, determined based on MetFrag analysis, is mentioned in **Supplementary Table 5**.

DISCUSSION

Marine organisms comprise approximately half of the total biodiversity on earth and constitute one of the greatest sources for anticancer therapeutics (Munro et al., 1999; Faulkner, 2002). Among marine organisms, fungi are a group of biotechnologically valuable and remarkable cradle of bioactive secondary metabolites; however, they are less explored in comparison to terrestrial fungi (Deshmukh et al., 2018). A few studies have investigated marine algae and algae-associated endophytic fungal cytotoxic compounds such as gliotoxin, cytochalasin B, and demethoxyfumitremorgin (Hwang et al., 2013; Nguyen et al., 2013; Kim et al., 2017). In a very recent study, our group had documented the cytotoxic properties of marine algae-associated endophytic fungi from Kerala and Goa (Kumari et al., 2018; Kamat et al., 2020). There are many reports mentioning the diversity and bioactivity,

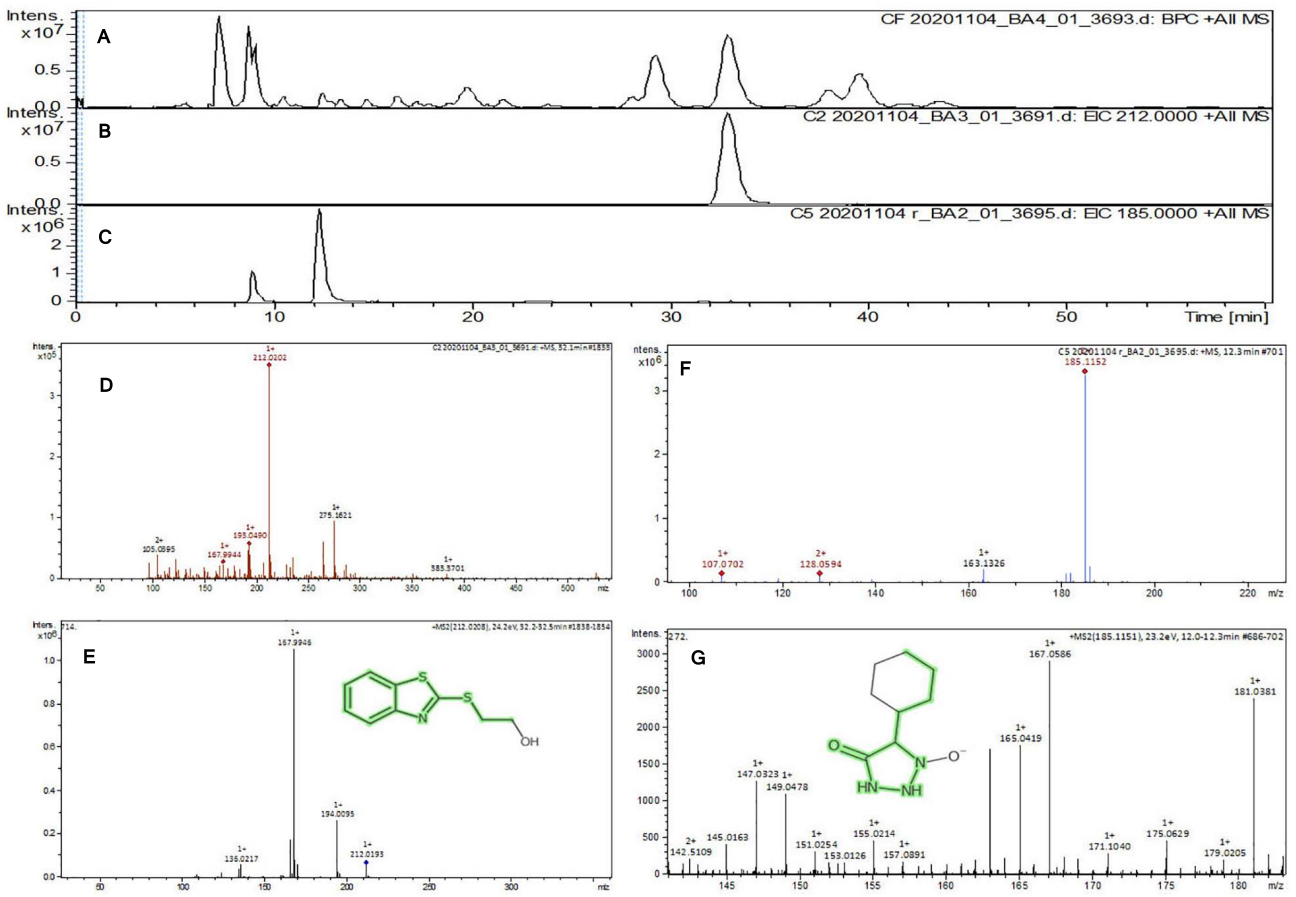

FIGURE 11 | Liquid chromatogram profile from culture filtrate extract of *B. petrensis* **(A)**, liquid chromatogram profile of purified C2 fraction **(B)**, and C5 fraction **(C)**. The LC peak at Rt 33.31 and 10.13 displaying the purified bioactive fractions C2 and C5 corresponding to fungal culture filtrate extract Rt 33.31 and 10.14, respectively **(A–C)**. The mass spectrum displaying the feature m/z 212.02, 185.11 $[M+H]^+$ of compounds 2-(1,3-benzothiazol-2-ylsulfanyl)ethanol and 5-cyclohexyl-1-oxido-triazolidin-4-one obtained a similar characteristic feature of molecular mass in CFE with a positive ion mode **(D–G)**.

like insecticidal, antibacterial, and antioxidant properties, of endophytic fungal secondary metabolites from the region of Rameswaram (Thirunavukkarasu et al., 2012), but no one has explored the anticancer activity. At this junction, the present study focuses on the diversity of marine endophytic fungi harbored inside macro-algae from the same region, especially highlighting the cytotoxic potential of their secondary metabolites. In the current study, 31 endophytic fungal strains were isolated from 18 different host algae that were collected from under-explored marine habitats of Gulf of Mannar at Rameswaram to find out their cytotoxic potential. It was observed that *Aspergillus* was the dominant genus of endophytic fungi among 17 genera, representing seven species (highest) out of 27 different species. The *Aspergillus* colonies were isolated from all three groups (green, brown, and red) of algae. Suryanarayanan et al. (2010) have also reported that the genus *Aspergillus* dominated the endophyte assemblage of marine algae in the coast of Tamil Nadu. Another study reported *Aspergillus* sp. as dominating all other marine-derived endophytic fungi (Sarasan et al., 2017). The results of the current study comprise all the classes of fungi such as Ascomycetes (13), Basidiomycetes (1), Hyphomycetes (14), and Coelomycetes (3).

In the preliminary screening of ethyl acetate extracts, nine fungi showed 60% notable cytotoxicity, whereas 22 fungal total extracts exhibited 30–50%. A study reported four out of 11 mangrove-associated endophytic fungi as showing cytotoxicity (cell viability, < 50%) against T47D cells (Handayani et al., 2019). The current study highlights the mycelial extract of *B. petrensis*, showing 70% cytotoxicity in HeLa as well as A431 cells, with the culture filtrate extracts showing 60 and 70% at 25 μg/ml. Similar results were reported by Nursid et al. (2020), indicating that mycelium extracts have stronger cytotoxicity than the culture filtrate extracts. Recently, *B. petrensis* isolated from red algae was reported to exhibit a cytotoxic activity against A549 and K562 cells from ethyl acetate extracts with CC_{50} values of 13.5 and 3.5 μg/ml, respectively (Ma et al., 2020); this confirms that potential active constituents are present in the culture extracts. However, media optimization, impact of different solvent extracts, and the apoptotic activity of the extracts and cytotoxic metabolites in *B. petrensis* have remained unexplored.

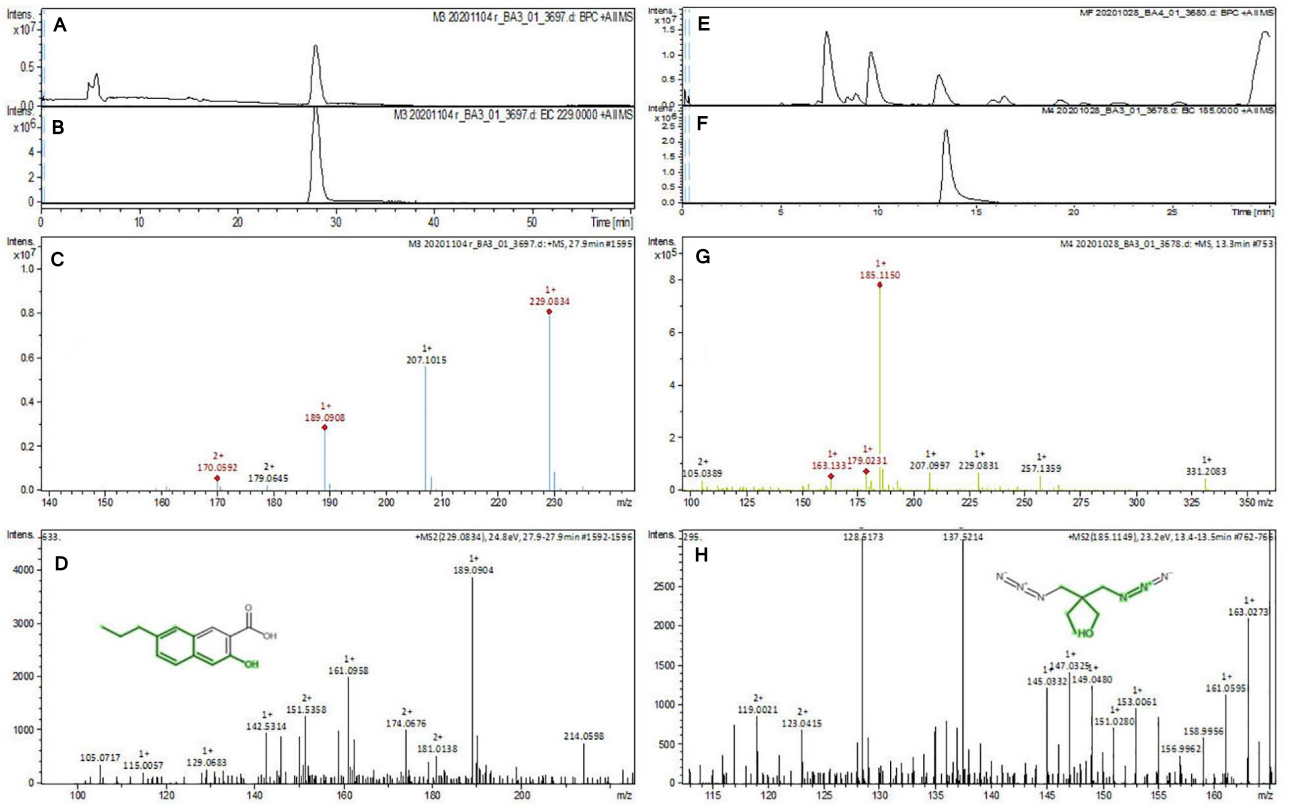

FIGURE 12 | Liquid chromatogram profile from culture filtrate extract of *B. petrensis* **(A)** and liquid chromatogram profile of purified M3 fraction **(B)** and M4 fraction **(C)**. The LC peak at Rt 27.9 and 13.4 displaying the purified bioactive fractions M3 and M4 corresponding to fungal culture filtrate extract Rt 33.31 and 13.7, respectively **(A,B,E,F)**. The mass spectrum displaying the feature m/z 229.08, 185.11 $[M+H]^+$ of compounds 3-hydroxy-7-propyl-naphthalene-2-carboxylic acid and 2,2-bis(azidomethyl)butan-1-ol obtained a similar characteristic feature of molecular mass in ME with a positive ion mode **(C,D,G,H)**.

The addition of one or more nutrients achieved substantial differences in the production of secondary metabolites (Frisvad, 2012; VanderMolen et al., 2013). This present study reports the production of cytotoxic secondary metabolites with nutrient availability by using different media. The PDYEB medium culture extract showed significant cytotoxicity, followed by the PDB, M1D, and S7 media culture extracts. In the past, the production of penicillin was seen to increase when the culture media were optimized from the *Penicillium* species (Dayalan et al., 2011). Various organic polar and non-polar solvents have been used to extract the bioactive compounds from microorganisms (de Felício et al., 2015; Ahsan et al., 2017). In the present study, the optimization of organic solvents for the extraction of cytotoxic secondary metabolites was studied, which enhanced the cytotoxic properties of ethyl acetate extracts. Similar results have been well established from studies of marine algae-associated endophytic fungus, which possess a cytotoxic activity (de Felício et al., 2015). A study showed the apoptotic activity of demethoxyfumitremorgin, which was isolated from a marine algae-associated fungus (Kim et al., 2017). Unlike the study by Ma et al. (2020), the present investigation shows (for the first time) that the *B. petrensis* fungal extract induces apoptosis (PI live/dead assay, loss of mitochondrial membrane potential, and cell cycle analysis), resulting in dose-dependent cell death in HeLa cells. The measurement of MMP loss by JC-1 indicated a high percentage of cell death at high concentrations of fungal extract. Similar observations were reported from macro-algae-associated endophytic fungi (Kumari et al., 2018; Kamat et al., 2020; Sajna et al., 2020).

The flow cytometry analysis revealed a sub-G1 phase arrest in HeLa cells after treatment with mycelia and culture filtrate extracts. Arora et al. (2016) have also reported fungal extract-induced sub-G1 phase arrest. Interestingly, anticancer agents (linalool and subamolide E) also induce cell death by leading to the activation of DNA damage checkpoints and sub-G1 phase cell cycle arrest (Wang et al., 2011; Sun et al., 2015). The fungal secondary metabolic profiling remains uncharacterized to recognize the bioactive compounds contributing to the cytotoxic and apoptotic activities exhibited by BpME and BpCE from *B. petrensis*. Forty-two fractions were separated from the culture filtrate and mycelial extract by preparative TLC and tested on cancer cell lines HeLa, A431, MCF-7, and HepG2 and non-cancer HEK cells by the MTT assay. All the fractions were found to inhibit the proliferation of cancer cells. Four fractions, namely, C2, C5, M3, and M4, exhibited significant cytotoxicity against all cancer cells; compared to the other fractions, they did not show

a cytotoxic activity in non-cancerous HEK. A previous study showed that four preparative TLC fractions of the *Aspergillus ochraceus* extract inhibit growth in HeLa cells (Nadumane et al., 2013). In the current study, results of the MTT assay led the authors to isolate four compounds, namely, C1 and C2 (from BpCFE) and M2 and M3 (from BpME), with significant cytotoxicity; these were further characterized by spectrometry. The fractions C2, C5, M3, and M4 displayed single spots with characteristics of light orange, yellow, dark blue, and dark orange colors under a UV 365 lamp with R_f values of 0.88, 0.70, 0.71, and 0.66, respectively. The highest cytotoxicity was exhibited by the fraction M3 with CC_{50} value of 65 μg/ml, followed by C2, C5, and M4. The pure compound in the fractions C2, C5, M3, and M4 was soluble in methanol and had an UV λ-maximum at 375, 269, 273, and 266 nm, respectively. This guided the authors to select these four compounds for further studies. The mass and preliminary structures of these compounds were interpreted from the database using the m/z ratio obtained from LC–ESI–MS/MS (Tapfuma et al., 2019). From the matches with a score value of 1 (MetFrag), the names were confirmed as 2-(1,3-benzothiazol-2-ylsulfanyl)ethanol, 5-cyclohexyl-1-oxido-triazolidin-4-one, 3-hydroxy-7-propyl-naphthalene-2-carboxylic acid, and 2,2-bis(azidomethyl)butan-1-ol for C2, C5, M,3 and M4, respectively. Since the purified bioactive compounds from these fungal organic extracts exhibited the best cytotoxic activities, there is a promising use of these agents in cancer therapeutics.

CONCLUSION

The rate of cancer occurrence has increased, with serious side effects due to chemotherapy and multidrug resistance. This has led to the search for novel and effective anticancer molecules from endophytic fungi. In this study, the authors have reported 31 marine algae-associated endophytic fungi from Rameswaram, India, for the first time, that show a cytotoxic activity against cancer cell lines. Among the fungi, *B. petrensis* extract exhibited significant cytotoxic and apoptotic effects. This is the first report of *B. petrensis* for its growth and media optimization to enhance cytotoxicity and apoptotic effects with loss of mitochondrial membrane potential. In the future, the purified cytotoxic compounds will be characterized with detailed structures, mode of action in cancer cells, and mouse models.

DATA AVAILABILITY STATEMENT

The datasets presented in this study can be found in online repositories. The names of the repository/repositories and accession number(s) can be found below: https://www.ncbi.nlm.nih.gov/, MH748175, MH748179, MH748152, MH748153, MH748157, MH748180, MH748176, MH748177, MH748170, MH748162, MH748169, MH748181, MH748174, MH748178, MH748164, MH748168, MH748182, MH748158, MH748155, MH748171, MH748161, MH748156, MH748159, MH748154, MH748163, MK073011, MH748173, MH748183, MH748160, MH748172, and MH748167.

AUTHOR CONTRIBUTIONS

JC conceived the idea. SS and KS did the sampling, designed and performed the experiments, analyzed the data, and wrote the manuscript. All the authors reviewed the manuscript.

FUNDING

This study was supported by a grant from the Department of Biotechnology, Govt. of India, New Delhi (ref. no. BT/PR/14569).

ACKNOWLEDGMENTS

The authors thank the FACS and LCMS facility of the Division of Biological Sciences, Indian Institute of Science, Bangalore. The authors are thankful to the DBT-IISc partnership program and the DST-FIST and UGC special assistance program for financial support. SS thanks CSIR for her SRF fellowship and KS thanks the Indian Institute of Science, Bangalore, for his IISc research associate fellowship. The authors deeply acknowledge Dr. Murugan for his help in the collection and identification of marine algal samples at the location and Dr. Balendra Sah for his help during the collection. The authors thank Prof. Kartik Shanker and Dr. Aniruddha Marathe, CES, IISc, for their help and suggestions in calculating the diversity indices. The authors are very much thankful to the late Prof. T. Ramasarma and Dr. Deepika Prasad for their valuable comments and suggestions on this manuscript. The authors also acknowledge Mr. Jagabandhu Sahoo, research scholar in the Department of Organic Chemistry, IISc, for the UV–visible analysis.

SUPPLEMENTARY MATERIAL

The Supplementary Material for this article can be found online at: https://www.frontiersin.org/articles/10.3389/fmicb.2021.650177/full#supplementary-material

Supplementary Figure 1 | Marine algae: green (GCSS, HCSS, CRSS, CSSS, CASS, CTSS, HMSS, CPeSS, and EFSS), brown (PTSS, TCSS, SMSS, SMaSS, DDSS), and red (GCSS, HFSS, ASSS, S) collected from four different coastal regions of Rameswaram, Tamil Nadu, India.

Supplementary Figure 2 | PCR product of fungal ITS 1 and ITS 2 regions on 1% agarose gel.

Supplementary Figure 3 | Phylogenetic tree of endophytic fungi obtained from marine macro-algae based on ITS regions. The phylogenetic tree was constructed using the maximum parsimony method. A bootstrap value of 100% showed that each genus was distinguished by a monophyletic group in different subclades from the outgroup.

Supplementary Figure 4 | (A) Fungal extract yields from mycelia, culture filtrate, and total culture of the nine potent fungi. **(B)** Fungal biomass (mycelial dry weight) of the nine potent fungi.

Supplementary Figure 5 | Cytotoxic effects of different solvents, namely, ethyl acetate, dichloromethane, chloroform, hexane, and diethyl ether extracts of *B. petrensis* grown in PDYEB medium. **(A)** Total extract, **(B)** culture filtrate extract, and **(C)** mycelial extract on HeLa and A431 cells at 25 μg/ml.

Supplementary Figure 6 | Thin-layer chromatography (TLC) profile of *B. petrensis* mycelia (1) and culture filtrate (2) extracts. **(A)** Analytical TLC plate (sample loaded, 100 μg) and **(B)** preparative TLC plate (sample loaded, 1.6 mg).

Supplementary Figure 7 | (A) Cytotoxic effects of purified metabolites of BpME on different human cancer cell lines. **(B)** Cytotoxic effects of purified metabolites of BpCFE on different human cancer cell lines.

Supplementary Figure 8 | Thin-layer chromatography profile of purified active principles M3, M4 and C2, C5 (sample loaded, 10 μg) obtained from BpME and BpCFE, respectively.

Supplementary Figure 9 | (A) High-performance liquid chromatography (HPLC) profile of M3 and M4 compounds in comparison with mycelial extract. **(B)** HPLC profile of C2 and C5 compounds in comparison with culture filtrate extract.

Supplementary Table 1 | Composition of different media used in this study (all media mentioned below are without agar served as broth media).

Supplementary Table 2 | Species richness and diversity indices of marine endophytic fungi obtained from green, brown, and red algae.

Supplementary Table 3 | The 50% cytotoxic concentration (CC_{50}) value of marine endophytic fungal extract against cancer cell lines HeLa, A431, and healthy cells (HEK).

Supplementary Table 4 | (A) Thin-layer chromatography band character and retention factor (R_f) value of the mycelia extract of *B. petrensis*. **(B)** Thin-layer chromatography band character and retention factor (R_f) value of the culture filtrate extract of *B. petrensis*.

Supplementary Table 5 | The putative identifications of bioactive compounds compared with direct Mass-based search selected peaks in MetFrag data base.

REFERENCES

Ahsan, T., Chen, J., Zhao, X., Irfan, M., and Wu, Y. (2017). Extraction and identification of bioactive compounds (eicosane and dibutyl phthalate) produced by *Streptomyces* strain KX852460 for the biological control of *Rhizoctonia solani* AG-3 strain KX852461 to control target spot disease in tobacco leaf. *AMB Express* 7:54. doi: 10.1186/s13568-017-0351-z

Altschul, S. F., Gish, W., Miller, W., Myers, E. W., and Lipman, D. J. (1990). Basic local alignment search tool. *J. Mol. Biol.* 215, 403–410. doi: 10.1016/S0022-2836(05)80360-2

Aly, A. H., Debbab, A., and Proksch, P. (2011). Fungal endophytes: unique plant inhabitants with great promises. *Appl. Microbiol. Biotechnol.* 90, 1829–1845. doi: 10.1007/s00253-011-3270-y

Arora, D., Sharma, N., Singamaneni, V., Sharma, V., Kushwaha, M., Abrol, V., et al. (2016). Isolation and characterization of bioactive metabolites from *Xylaria psidii*, an endophytic fungus of the medicinal plant *Aegle marmelos* and their role in mitochondrial dependent apoptosis against pancreatic cancer cells. *Phytomedicine* 23, 1312–1320. doi: 10.1016/j.phymed.2016.07.004

Bhagyaraj, I., and Kunchithapatham, V. R. (2016). Diversity and distribution of seaweeds in the shores and water lagoons of Chennai and Rameshwaram coastal areas, South Eastern coast of India. *Biodivers. J.* 7, 923–934.

Blunt, J. W., Copp, B. R., Keyzers, R. A., Munro, M. H. G., and Prinsep, M. R. (2017). Marine natural products. *Nat. Prod. Rep.* 34, 235–294. doi: 10.1039/c4np00144c

Bode, H. B., Bethe, B., Hofs, R., and Zeeck, A. (2002). Big effects from small changes: possible ways to explore nature's chemical diversity. *Chem. Bio. Chem.* 3, 619–627. doi: 10.1002/1439-7633(20020703)3

Chakravarthi, B. V., Sujay, R., Kuriakose, G. C., and Jayabaskaran, C. (2013). Inhibition of cancer cell proliferation and apoptosis-inducing activity of fungal taxol and its precursor baccatin III purified from endophytic *Fusarium solani*. *Cancer Cell Int.* 13:105. doi: 10.1186/1475-2867-13-105

Colwell, R. K., and Elsensohn, J. E. (2014). EstimateS turns 20: statistical estimation of species richness and shared species from samples, with non-parametric extrapolation. *Ecography* 37, 609–613. doi: 10.1111/ecog.00814

Cossarizza, A., Baccarani-Contri, M., Kalashnikova, G., and Franceschi, C. (1993). A new method for the cytofluorimetric analysis of mitochondrial membrane potential using the J-aggregate forming lipophilic cation 5,5',6,6'-tetrachloro-1,1',3,3'-tetraethylbenzimidazolcarbocyanine iodide (JC-1). *Biochem. Biophys. Res. Commun.* 197, 40–45. doi: 10.1006/bbrc.1993.2438

Dayalan, S. A., Darwin, P., and Prakash, S. (2011). Comparative study on production, purification of Penicillin by *Penicillium chrysogenum* isolated from soil and citrus samples. *Asian Pac. J. Trop. Biomed.* 1, 15–19. doi: 10.1016/S2221-1691(11)60061-0

de. Felício, R., Pavão, G. B., de Oliveira, A. L. L., Erbert, C., Conti, R., Pupo, M. T., et al. (2015). Antibacterial, antifungal and cytotoxic activities exhibited by endophytic fungi from the Brazilian marine red alga *Bostrychia tenella* (Ceramiales). *Rev. Bras. Farmacogn.* 25:641650. doi: 10.1016/j.bjp.2015.08.003

Debbab, A., Aly, A. H., and Proksch, P. (2011). Bioactive secondary metabolites from endophytes and associated marine derived fungi. *Fungal Divers.* 49, 1–12. doi: 10.1007/s13225-011-0114-0

Deshmukh, S. K., Prakash, V., and Ranjan, N. (2017). Marine fungi: a source of potential anticancer compounds. *Front. Microbiol.* 8:2536.

Deshmukh, S. K., Prakash, V., and Ranjan, N. (2018). Marine fungi: a source of potential anticancer compounds. *Front. Microbiol.* 8:2536. doi: 10.3389/fmicb.2017.02536

Dhayanithy, G., Subban, K., and Chelliah, J. (2019). Diversity and biological activities of endophytic fungi associated with *Catharanthus roseus*. *BMC Microbiol.* 19:22. doi: 10.1186/s12866-019-1386-x

Faulkner, D. J. (2002). Marine natural products. *Nat. Prod. Rep.* 19, 1–48. doi: 10.1039/b009029h

Frisvad, J. C. (2012). "Media and Growth Conditions for Induction of Secondary Metabolite Production," in *Fungal Secondary Metabolism. Methods in Molecular Biology (Methods and Protocols)*, Vol. 944, eds N. Keller and G. Turner (Totowa, NJ: Humana Press), doi: 10.1007/978-1-62703-122-6_3

Gouda, S., Das, G., Sen, S., Shin, H. S., and Patra, J. K. (2016). Endophytes: a treasure house of bioactive compounds of medicinal importance. *Front. Microbiol.* 7:1538. doi: 10.3389/fmicb.2016.01538

Guo, B., Wang, Y., Sun, X., and Tang, K. (2008). Bioactive natural products from endophytes: a review. *Appl. Biochem. Microbiol.* 44, 136–142. doi: 10.1134/S0003683808020026

Handayani, D., Sandrawati, N., Nestianda, O., Ruslan, R., Fajrina, A., and Tallei, T. E. (2019). Cytotoxic and antimicrobial activities of ethyl acetate extract of mangrove plant *Scyphiphora hydrophyllacea* C. F. Gaertn—associated fungi. *J. Appl. Pharm. Sci.* 9, 075–079. doi: 10.7324/JAPS.2019.90610

Holler, U., Wright, A. D., Matthee, G. F., Gabrielle, M. K., Draeger, S., Aust, H. J., et al. (2000). Fungi from marine sponges: diversity, biological activity and secondary metabolites. *Mycol. Res.* 104, 1354–1365. doi: 10.1017/s0953756200003117

Hwang, J., Yi, M., Zhang, X., Xu, Y., Jung, J. H., and Kim, D. K. (2013). Cytochalasin B induces apoptosis through the mitochondrial apoptotic pathway in HeLa human cervical carcinoma cells. *Oncol. Rep.* 30, 1929–1935. doi: 10.3892/or.2013.2617

Imhoff, J. F. (2016). Natural products from marine fungi-still an underrepresented resource. *Mar. Drugs* 14, 19. doi: 10.3390/md14010019

Jeewon, R., Luckhun, A. B., Bhoyroo, V., Sadeer, N. B., Mahomoodally, F. M., Rampadarath, S., et al. (2019). "Pharmaceutical Potential of Marine Fungal Endophytes," in *Endophytes and Secondary Metabolites Phytochemistry*, ed. S. Jha (Cham: Springer), doi: 10.1007/978-3-319-90484-9_6

Jones, E. B. G. (2011). Fifty years of marine mycology. *Fungal Divers.* 50:73. doi: 10.1007/s13225-011-0119-8

Kamat, S., Kumari, M., Taritla, S., and Jayabaskaran, C. (2020). Endophytic fungi of marine alga from Konkan Coast, India- a rich source of bioactive material. *Front. Mar. Sci.* 7:31. doi: 10.3389/fmars.2020.00031

Kim, Y. S., Kim, S. K., and Park, S. J. (2017). Apoptotic effect of demethoxyfumitremorgin C from marine fungus Aspergillus fumigatus

on PC3 human prostate cancer cells. *Chem. Biol. Interact.* 269, 18–24. doi: 10.1016/j.cbi.2017.03.015

Kjer, J., Debbab, A., Aly, A. H., and Proksch, P. (2010). Methods for isolation of marine-derived endophytic fungi and their bioactive secondary products. *Nat. Protoc.* 5, 479–490. doi: 10.1038/nprot.2009.233

Kumari, M., Taritla, S., Sharma, S., and Jayabaskaran, C. (2018). Antiproliferative and antioxidative bioactive compounds in extracts of marine-derived endophytic fungus *Talaromyces purpureogenus*. *Front. Microbiol.* 9:1777. doi: 10.3389/fmicb.2018.01777

Ma, X., Nontachaiyapoom, S., Hyde, K., Jeewon, R., Doilom, M., Chomnunti, P., et al. (2020). *Biscogniauxia dendrobii* sp. nov. and *B. petrensis* from Dendrobium orchids and the first report of cytotoxicity (towards A549 and K562) of *B. petrensis* (MFLUCC 14-0151) in vitro. *S. Afr. J. Bot.* 134, 382–393. doi: 10.1016/j.sajb.2020.06.022

Molinski, T. F., Dalisay, D. S., Lievens, S. L., and Saludes, J. P. (2009). Drug development from marine natural products. *Nat. Rev. Drug Discov.* 8, 69–85. doi: 10.1038/nrd2487

Moller, E. M., Bahnweg, G., Sandermann, H., and Geiger, H. H. (1992). A simple and efficient protocol for isolation of high molecular weight DNA from filamentous fungi, fruit bodies, and infected plant tissues. *Nucleic Acids Res.* 20, 6115–6116. doi: 10.1093/nar/20.22.6115

Mosmann, T. (1983). Rapid colorimetric assay for cellular growth and survival: application to proliferation and cytotoxicity assays. *J. Immunol. Methods* 65, 55–63. doi: 10.1016/0022-1759(83)90303-4

Munro, M. H., Blunt, J. W., Dumdei, E. J., Hickford, S. J., Lill, R. E., Li, S., et al. (1999). The discovery and development of marine compounds with pharmaceutical potential. *J. Biotechnol.* 70, 15–25. doi: 10.1016/s0168-1656(99)00052-8

Nadumane, V. K., Venkat, P., Pal, A., Dharod, H., Shukla, M., and Prashanthi, K. (2013). A novel metabolite from *Aspergillus ochraceus* JGI 25 showing cytotoxicity to HeLa cells. *Indian J. Pharm. Sci.* 7:507. doi: 10.4103/0250-474X.122834

Nagai, H., and Kim, Y. H. (2017). Cancer prevention from the perspective of global cancer burden patterns. *J. Thorac. Dis.* 9, 448–451. doi: 10.21037/jtd.2017.02.75

Nguyen, V. T., Lee, J. S., Qian, Z. J., Li, Y. X., Kim, K. N., Heo, S. J., et al. (2013). Gliotoxin isolated from marine fungus *Aspergillus* sp. induces apoptosis of human cervical cancer and chondrosarcoma cells. *Mar. Drugs* 12–1, 69–87. doi: 10.3390/md12010069

Nursid, M., Dewi, A. S., Maya, D., and Priyanti. (2020). Cytotoxicity of marine-derived fungi collected from Kepulauan Seribu Marine National Park. *IOP Conf. Ser. Earth Environ. Sci.* 404:012006. doi: 10.1088/1755-1315/404/1/012006

Pietra, F. (1997). Secondary metabolites from marine microorganisms: bacteria, protozoa, algae and fungi. Achievements and prospects. *Nat. Prod. Rep.* 14, 453–464. doi: 10.1039/np9971400453

Sajna, K. V., Kamat, S., and Jayabaskaran, C. (2020). Antiproliferative role of secondary metabolites from *Aspergillus unguis* AG 1.1 (G) isolated from marine macroalgae *Enteromorpha* sp. by inducing intracellular ROS production and mitochondrial membrane potential loss leading to apoptosis. *Front. Mar. Sci.* 7:543523. doi: 10.3389/fmars.2020.543523

Sarasan, M., Job, N., Puthumana, J., Ravinesh, R., Prabhakaran, M. P., Thomas, L. C., et al. (2020). Exploration and profiling of hidden endophytic mycota of marine macroalgae with potential drug leads. *FEMS Microbiol. Lett.* 367, 1–9. doi: 10.1093/femsle/fnaa078

Sarasan, M., Puthumana, J., Job, N., Han, J., Lee, J. S., and Philip, R. (2017). Marine algicolous endophytic fungi–a promising drug resource of the era. *J. Microbiol. Biotechnol.* 27, 1039–1052. doi: 10.4014/jmb.1701.01036

Schulz, B., and Boyle, C. (2005). The endophytic continuum. *Mycol. Res.* 109(Pt. 6), 661–686. doi: 10.1017/s095375620500273x

Shirley, H. J., Jamieson, M. L., Brimble, M. A., and Bray, C. D. (2018). A new family of sesterterpenoids isolated around the Pacific Rim. *Nat. Prod. Rep.* 35, 210–219. doi: 10.1039/C7NP00049A

Sowmya, P. R., Arathi, B. P., Vijay, K., Baskaran, V., and Lakshminarayana, R. (2015). Role of different vehicles in carotenoids delivery and their influence on cell viability, cell cycle progression, and induction of apoptosis in HeLa cells. *Mol. Cell. Biochem.* 406, 245–253. doi: 10.1007/s11010-015-2442-y

Strobel, G., and Daisy, B. (2003). Bioprospecting for microbial endophytes and their natural products. *Microbiol. Mol. Biol. Rev.* 67, 491–502. doi: 10.1128/mmbr.67.4.491-502.2003

Sun, X., Wang, S. M., Li, T., and Yang, Y. (2015). Anticancer activity of linalool terpenoid: apoptosis induction and cell cycle arrest in prostate cancer cells. *Trop. J. Pharm. Res.* 14, 619–625. doi: 10.4314/TJPR.V14I4.9

Suryanarayanan, T. S., Venkatachalam, A., Thirunavukkarasu, N., Ravishankar, J. P., Doble, M., and Geetha, V. (2010). Internal mycobiota of marine macroalgae from the Tamilnadu coast: distribution, diversity and biotechnological potential. *Bot. Mar.* 53, 457–468. doi: 10.1515/bot.2010.045

Tamura, K., Stecher, G., Peterson, D., Filipski, A., and Kumar, S. (2013). MEGA6: molecular evolutionary genetics analysis version 6.0. *Mol. Biol. Evol.* 30, 2725–2729. doi: 10.1093/molbev/mst197

Tapfuma, K. I., Mekuto, L., Makatini, M. M., and Mavumengwana, V. (2019). The LC-QTOF-MS/MS analysis data of detected metabolites from the crude extract of *Datura stramonium* leaves. *Data Br.* 25, 1–4. doi: 10.1016/j.dib.2019.104094

Thirunavukkarasu, N., Jahnes, B., Broadstock, A., Rajulu, M. B. G., Murali, T. S., Gopalan, V., et al. (2015). Screening marine-derived endophytic fungi for xylan-degrading enzymes. *Curr. Sci.* 109, 112–120.

Thirunavukkarasu, N., Suryanarayanan, T. S., Girivasan, K. P., Venkatachalam, A., Geetha, V., Ravishankar, J. P., et al. (2012). Fungal symbionts of marine sponges from Rameswaram, southern India: species composition and bioactive metabolites. *Fungal Divers.* 55, 37–46. doi: 10.1007/s13225-011-0137-6

VanderMolen, K. M., Raja, H. A., El-Elimat, T., and Oberlies, N. H. (2013). Evaluation of culture media for the production of secondary metabolites in a natural products screening program. *AMB Express* 3:71. doi: 10.1186/2191-0855-3-71

Venkatachalam, A., Govinda, R. M. B., Thirunavukkarasu, N., and Suryanarayanan, T. S. (2015a). Endophytic fungi of marine algae and seagrasses: a novel source of chitin modifying enzymes. *Mycosphere* 6, 345–355. doi: 10.5943/mycosphere/6/3/10

Venkatachalam, A., Thirunavukkarasu, N., and Suryanarayanan, T. S. (2015b). Distribution and diversity of endophytes in seagrasses. *Fungal Ecol.* 13, 60–65. doi: 10.1016/j.funeco.2014.07.003

Wang, H. M., Chiu, C. C., Wu, P. F., and Chen, C. Y. (2011). Subamolide E from *Cinnamomum subavenium* induces Sub-G1 cell-cycle arrest and caspase-dependent apoptosis and reduces the migration ability of human melanoma cells. *J. Agric. Food Chem.* 59, 8187–8192. doi: 10.1021/jf2018929

White, T. J., Bruns, T., Lee, S., and Taylor, J. (1990). Amplification and direct sequencing of fungal ribosomal RNA genes for phylogenetics. *PCR Protoc. Guide Methods Appl.* 18, 315–322. doi: 10.1016/b978-0-12-372180-8.50042-1

Wright, G. D. (2019). Unlocking the potential of natural products in drug discovery. *Microb. Biotechnol.* 12, 55–57. doi: 10.1111/1751-7915.13351

Zhang, P., Li, X., and Wang, B. G. (2016). Secondary metabolites from the marine algal-derived endophytic fungi: chemical diversity and biological activity. *Planta Med.* 82, 832–842. doi: 10.1055/s-0042-103496

Conflict of Interest: The authors declare that the research was conducted in the absence of any commercial or financial relationships that could be construed as a potential conflict of interest.

frontiers in Microbiology

ORIGINAL RESEARCH
published: 09 July 2021
doi: 10.3389/fmicb.2021.710364

Indole-Terpenoids With Anti-inflammatory Activities From *Penicillium* sp. HFF16 Associated With the Rhizosphere Soil of *Cynanchum bungei* Decne

Guojun Pan[1], Yanfen Zhao[1], Shuang Ren[1], Fengyang Liu[1], Qicai Xu[1], Weibin Pan[2], Tongtao Yang[3], Mingtian Yang[1], Xinru Zhang[1], Chuanyue Peng[1], Gangping Hao[1], Fandong Kong[2], Liman Zhou[2] and Na Xiao[3,4]**

[1] College of Life Sciences, Shandong First Medical University & Shandong Academy of Medical Sciences, Tai'an, China, [2] Key Laboratory of Chemistry and Engineering of Forest Products, State Ethnic Affairs Commission, Guangxi Key Laboratory of Chemistry and Engineering of Forest Products, Guangxi Collaborative Innovation Center for Chemistry and Engineering of Forest Products, School of Chemistry and Chemical Engineering, Guangxi University for Nationalities, Nanning, China, [3] State Key Laboratory of Crop Biology, College of Agronomy, Shandong Agriculture University, Tai'an, China, [4] State Key Laboratory of Natural Medicines, China Pharmaceutical University, Nanjing, China

Four new indole-terpenoids **(1–4)** named encindolene A, 18-*O*-methyl-encindolene A, encindolene B, and encindolene C, as well as three known analogs **(5–7)**, were isolated from the fungus *Penicillium* sp. HFF16 from the rhizosphere soil of *Cynanchum bungei* Decne. The structures of compounds including absolute configurations were elucidated by spectroscopic data and electronic circular dichroism (ECD) analysis. Anti-inflammatory activity evaluation revealed that compounds **1–7** inhibit the production of nitric oxide with IC_{50} values of 79.4, 49.7, 81.3, 40.2, 86.7, 90.1, and 54.4 μM, respectively, and decrease the levels of tumor necrosis factor-α, interleukin-6 contents in lipopolysaccharide-induced RAW264.7 macrophages.

Keywords: fungus, *Penicillium* sp. HFF16, indole-terpenoids, anti-inflammatory activity, *Cynanchum bungei* Decne

OPEN ACCESS

Edited by:
Paola Angelini,
University of Perugia, Italy

Reviewed by:
Deli Chen,
Chinese Academy of Medical Sciences and Peking Union Medical College, China
Xin Li,
Zhejiang University, China
Duqiang Luo,
Hebei University, China

***Correspondence:**
Liman Zhou
zhouliman88@126.com
Na Xiao
xiaona198707@126.com

Specialty section:
This article was submitted to Microbiotechnology, a section of the journal Frontiers in Microbiology

Received: *18 May 2021*
Accepted: *11 June 2021*
Published: *09 July 2021*

Citation:
Pan G, Zhao Y, Ren S, Liu F, Xu Q, Pan W, Yang T, Yang M, Zhang X, Peng C, Hao G, Kong F, Zhou L and Xiao N (2021) Indole-Terpenoids With Anti-inflammatory Activities From Penicillium sp. HFF16 Associated With the Rhizosphere Soil of Cynanchum bungei Decne. Front. Microbiol. 12:710364. doi: 10.3389/fmicb.2021.710364

INTRODUCTION

The paxilline-type indole-terpenoids are one of the largest classes of fungal indole-terpenoids with diverse structures. Typical representatives of such compounds include paxilline (Springer et al., 1975), thiersinines (Li et al., 2002), lolicines (Munday-Finch et al., 1998), shearinines (Belofsky and Gloer, 1995), and penerpenes (Kong et al., 2019). Many of these compounds have significant bioactivities, such as antibacterial, and anti-inflammatory activities. Inflammation, as a protective response of living tissues to injury and infection and stress, involves a wide variety of physiological and pathological processes (Medzhitov, 2008). During the process, if acute inflammatory response fails to eliminate stimuli, it will devolve a chronic inflammation response, which is associated with many diseases, including asthma, cancer, stroke, and obesity (Zhong and Shi, 2019). The chronic inflammation response is characterized by secretion of nitric oxide (NO) and proinflammatory

cytokines such as tumor necrosis factor-α (TNF-α) and interleukin-6 (IL-6) (Medzhitov, 2008). Therefore, finding novel and effective anti-inflammatory compounds is urgently required.

In search of new compounds with anti-inflammatory activity, the secondary metabolites produced by *Penicillium* sp. HFF16 isolated from the rhizosphere soil of *Cynanchum bungei* Decne. in Mount Tai, East China, were investigated, which resulted in the isolation and identification of four new indole-terpenoids (**1–4**) named encindolene A, 18-*O*-methyl-encindolene A, encindolene B, and encindolene C, along with three known analogs including 7α-hydroxy-13-desoxy paxilline (**5**) (Peter and Christopher, 1994), 7-methoxypaxilline (**6**) (Ariantari et al., 2019), and paspalitrem C (**7**) (Dorner et al., 1984; **Figure 1**), which were isolated and identified. All of the compounds exhibited moderate inhibitory effects on the production of NO and proinflammatory cytokines (TNF-α and IL-6) in RAW264.7 macrophages stimulated by lipopolysaccharide (LPS). Herein, the isolation, structural elucidation, and bioactivities of these compounds were described.

MATERIALS AND METHODS

General Experimental Procedures

Optical rotations were measured on a JASCO P-1020 digital polarimeter, and UV spectra were measured

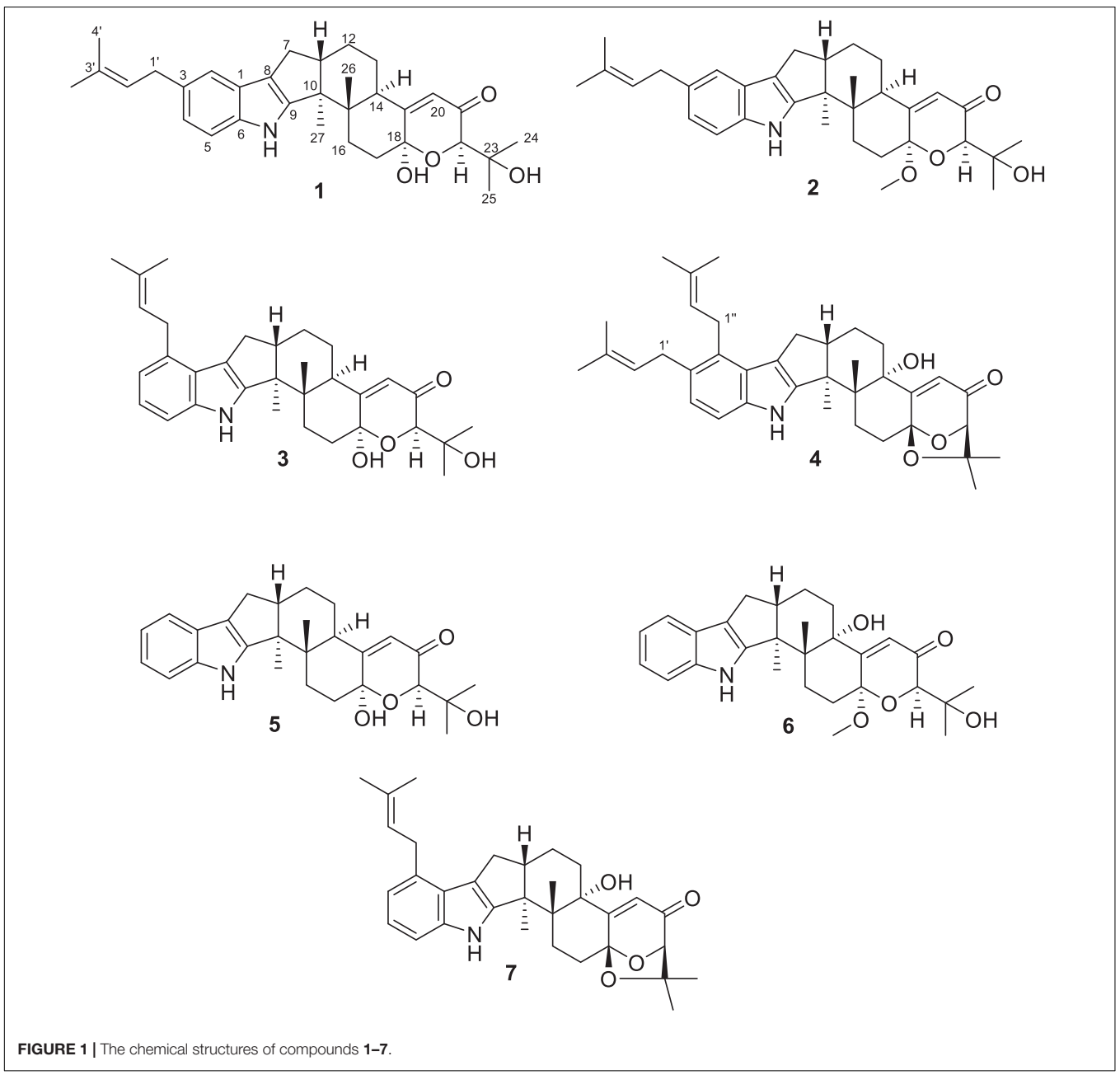

FIGURE 1 | The chemical structures of compounds **1–7**.

on a Beckman DU 640 spectrophotometer. Electronic circular dichroism (ECD) data were collected using a JASCO J-715 spectropolarimeter. NMR spectra were recorded on a Bruckmercury Plus-400 or a JNM-ECZR-500 spectrometers with TMS as an internal standard. High-resolution electrospray ionization mass spectrometry (HRESIMS) spectra were recorded with a Micromass Autospec-Uitima-TOF. Semipreparative high-performance liquid chromatography (HPLC) was carried out using an ODS column (YMC-pack ODS-A, 10 × 250 mm, 5 μm, 4 ml/min). Thin layer chromatography (TLC) and column chromatography (CC) were performed on plates precoated with silica gel GF_{254} (10–40 μm, Yantai Jiangyou Silicone Development Co., Ltd.).

Fungal Material and Fermentation

The fungus *Penicillium* sp. HFF16 was isolated from the rhizosphere soil of *Cynanchum bungei* Decne. in Mount Tai, China, in May 2020. After grinding, the sample (1.0 g) was diluted to 10^{-2} g/ml with sterile H_2O, 100 μl of which was deposited on Bengal red medium (maltose 20 g, monosodium glutamate 10 g, glucose 10 g, yeast extract 3 g, corn pulp 1 g, mannitol 20 g, sodium chloride 0.3 g, potassium dihydrogen phosphate 0.5 g, agar 20 g per liter of tap water) plate containing chloramphenicol (200 μg/ml) as a bacterial inhibitor. A single colony was transferred onto another PDA plate and was identified according to its morphological characteristics and ITS gene sequences (**Supplementary Material**). The data presented in the study are deposited in the GenBank, accession

TABLE 1 | The ^1H (400 MHz) and ^{13}C NMR (100 MHz) data of compounds **1–3** in CD_3OD.

Position	1		2		3	
	δ_C	δ_H (*J* in Hz)	δ_C	δ_H (*J* in Hz)	δ_C	δ_H (*J* in Hz)
1	126.3, C		126.3, C		125.4, C	
2	118.0,CH	7.08, s	118.0, CH	7.07, s	133.5, C	
3	133.2, C		133.2, C		119.2, CH	6.70, d (8.0)
4	121.8, CH	6.81, d (7.9)	121.8, CH	6.80, d (7.9)	121.3, CH	6.88, t (8.0)
5	112.5, CH	7.18, d (7.9)	112.4, CH	7.18, d (7.9)	110.6, CH	7.12, d (8.0)
6	140.6, C		140.6, C		142.0, C	
7	28.1, CH_2	2.34, dd (10.7, 12.9)	28.1, CH_2	2.36, dd (10.7, 13.3)	30.2, CH_2	2.51, dd (12.8, 14.9)
		2.65, dd (7.0, 12.9)		2.66, dd (7.0, 13.3)		2.82, overlap
8	117.8, C		117.8, C		117.5, C	
9	151.1, C		151.0, C		150.3, C	
10	51.6, C		51.6, C		51.4, C	
11	50.3, CH	2.74, m	50.4, CH	2.81, m	50.5, CH	2.85, overlap
12	25.3, CH_2	1.75, overlap	25.4, CH_2	1.80, overlap	25.3, CH_2	1.81, m
		1.73, overlap		1.78, overlap		1.68, m
13	26.7, CH_2	1.43, m	26.8, CH_2	1.31, m	26.8, CH_2	1.42, m
		1.61, m		1.64, m		1.71, m
14	43.3, CH	2.80, m	43.4, CH	2.80, m	43.3, C	2.84, m
15	43.8, C		43.5, C		43.9, C	
16	31.9, CH_2	1.88, m	31.4, CH_2	1.88, m	31.8, CH_2	1.952, m
		2.23, m		2.04, m		2.25, m
17	37.1, CH_2	2.13, m	29.9, CH_2	2.49, m	37.1, CH_2	2.15, m
		2.13, m		1.90, m		2.15, m
18	95.0, C		98.1, C		95.0, C	
19	168.1, C		167.0, C		168.1, C	
20	122.7, CH	5.71, s	122.8, CH	5.74, s	122.7, CH	5.74, s
21	199.8, C		198.6, C		199.8, C	
22	78.2, CH	4.20, s	78.5, CH	4.02, s	78.2, CH	4.20, s
23	73.4, C		73.2, C		73.4, C	
24	25.2, CH_3	1.27, s	25.4, CH_3	1.30, s	25.2, CH_3	1.27, s
25	26.6, CH_3	1.28, s	26.3, CH_3	1.30, s	26.6, CH_3	1.28, s
26	15.7, CH_3	0.91, s	15.9, CH_3	0.99, s	15.7, CH_3	0.98, s
27	14.8, CH_3	1.07, s	14.8, CH_3	1.07, s	14.8, CH_3	1.09, s
27–OCH_3			49.6, CH_3	3.41, s		
1′	35.5, CH_2	3.36, d (7.4)	35.5, CH_2	3.36, d (7.0)	31.8, CH_2	3.56, d (7.4)
2′	126.2, CH	5.36, t (7.4)	126.3, CH	5.35, t (7.4)	125.6, CH	5.35, t (7.4)
3′	131.8, C		131.8, C		132.1, C	
4′	17.9, CH_3	1.74, overlap	17.9, CH_3	1.74, overlap	18.1, CH_3	1.76, s
5′	26.0, CH_3	1.74, overlap	26.0, CH_3	1.74, overlap	25.9, CH_3	1.73, s

number (MZ165618). A reference culture of *Penicillium* sp. HFF16 maintained at –80°C was deposited in our laboratory. The isolate was cultured on plates of PDA medium at 28°C for 4 days. Plugs of agar supporting mycelium growth were cut and transferred aseptically to 7 × 250-ml Erlenmeyer flasks each containing 100 ml of liquid medium (potato 200 g, glucose 20 g per liter of tap water) and cultured at 28°C at 150 RPM for 3 days. The seed liquid was inoculated aseptically into 140 × 1,000-ml Erlenmeyer flasks each containing rice medium (80 g rice, 100 ml tap water) at 0.5% inoculation amount and incubated at room temperature under static conditions for 35 days.

Extraction and Isolation

The cultures (11.2 kg) were then extracted into EtOAc (40 L) by soaking overnight. The extraction was repeated three times. The combined EtOAc extracts were dried under vacuum to produce 38.2 g of extract. The EtOAc extract was subjected to a silica gel VLC column, eluting with a stepwise gradient of 0, 9, 11, 15, 20, 30, 50, and 100% EtOAc in petroleum ether (v/v) to give seven fractions (Fr. 1-7). Fraction 2 (2.3 g) was applied to ODS silica gel with gradient elution of MeOH-H_2O (1:5, 2:3, 3:2, 4:1, and 1:0) to yield five subfractions (Fr. 2–1–Fr. 2–4). Fr. 2–4 (66 mg) was purified using semiprep HPLC (isocratic system 90% MeOH/H_2O, v/v) to give compounds **7** (t_R 9.86 min; 14 mg) and **4** (t_R 16.41 min; 5.4 mg). Fraction 5 (7.3 g) was applied to ODS silica gel with gradient elution of MeOH-H_2O (1:5, 2:3, 3:2, 4:1, and 1:0) to yield four subfractions (Fr. 5–1–Fr. 5–6). Fr. 5–1 (256 mg) was further purified using semiprep HPLC (isocratic system 90% MeOH/H_2O, v/v) to give compound **5** (t_R 6.0 min; 4.7 mg). Fr. 5–2 (306 mg) was further purified using semiprep HPLC (isocratic system 90% MeOH/H_2O, v/v) to give compounds **6** (t_R 8.4 min; 9.2 mg), **3** (t_R 10.5 min; 6.2 mg), and **1** (t_R 11.5 min; 5.3 mg). Fr. 5–3 (56 mg) was further purified using semiprep HPLC (isocratic system 90% MeOH/H_2O, v/v) to give compound **2** (t_R 16.0 min; 3.7 mg).

*Encindolene A (**1**)*: white powder; [α]25 D–31 (*c* 0.1, MeOH); UV (MeOH) λ_{max} (log ε): 289 (2.85) and 237 (3.46) nm; ECD (0.25 mM, MeOH) λ_{max} 218 (–14.85), 242 (–8.04), 258 (+ 4.52), and 307 (+ 1.16) nm. ^{1}H and ^{13}C NMR data (**Table 1**); HRESIMS *m/z* 526.2902 $[M + Na]^+$ (calcd for $C_{32}H_{41}NO_4Na$, 526.2928).

*18-O-methyl-encindolene A (**2**)*: white powder; [α]25 D–25 (*c* 0.1, MeOH); UV (MeOH) λ_{max} (log ε): 284 (2.89) and 237 (3.51) nm; ECD (0.24 mM, MeOH) λ_{max} 216 (–12.32), 243 (–9.41), 259 (+ 2.75), and 308 (+ 1.35) nm. ^{1}H and ^{13}C NMR d*18-O-methyl-encindolene A (**2**)*: white powder; [α]25 D–25 (*c* 0.1, MeOH); UV (MeOH) λ_{max} (log ε): 284 (2.89) and 237 (3.51) nm; ECD (0.24 mM, MeOH) λ_{max} 216 (–12.32), 243 (–9.41), 259 (+ 2.75), and 308 (+ 1.35) nm. ^{1}H and ^{13}C NMR data (**Table 1**); ^{1}H and ^{13}C NMR data (**Table 1**); HRESIMS *m/z* 540.3078 $[M + Na]^+$ (calcd for $C_{33}H_{43}NO_4Na$, 540.3084).

*Encindolene B (**3**)*: white powder; [α]25 D–16 (*c* 0.1, MeOH); UV (MeOH) λ_{max} (log ε): 287 (2.73) and 235 (3.31) nm; ECD (1.2 mM, MeOH) λ_{max} 2*Encindolene B (**3**)*: white powder; [α]25 D–16 (*c* 0.1, MeOH); UV (MeOH) λ_{max} (log ε): 287 (2.73) and 235 (3.31) nm; ECD (1.2 mM, MeOH) λ_{max} 216 (–9.10), 239 (–11.19), 258 (+ 2.27), and 286 (+ 0.94) nm. ^{1}H and ^{13}C NMR data (**Table 1**); HRESIMS *m/z* 526.2903 $[M + Na]^+$ (calcd for $C_{32}H_{41}NO_4Na$, 526.2928).

*Encindolene C (**4**)*: white powder; [α]25 D + 98 (*c* 0.1, MeOH); UV (MeOH) λ_{max} (log ε): 285*Encindolene C (**4**)*: white powder; [α]25 D + 98 (*c* 0.1, MeOH); UV (MeOH) λ_{max} (log ε): 285 (3.02)

TABLE 2 | The ^{1}H (400 MHz) and ^{13}C NMR (100 MHz) data of compound **4** in CD_3OD.

Position	4	
	δ_C	δ_H (*J* in Hz)
1	126.6, C	
2	130.7,C	
3	130.4, C	
4	123.0, CH	6.75, d (7.9)
5	110.6, CH	7.05, d (7.9)
6	140.6, C	
7	30.6, CH_2	2.48, dd (11.3, 12.9)
		2.75, overlap
8	116.3, C	
9	153.4, C	
10	52.5, C	
11	50.1, CH	2.79, m
12	22.3, CH_2	2.04, overlap
		1.94, overlap
13	26.7, CH_2	2.62, m
		1.90, m
14	77.9, C	
15	40.8, C	
16	27.6, CH_2	1.88, m
		2.23, m
17	29.4, CH_2	2.82, m
		1.99, m
18	106.2, C	
19	172.4, C	
20	118.2, CH	5.80, s
21	199.4, C	
22	89.1, CH	4.29, s
23	79.4, C	
24	23.4, CH_3	1.13, s
25	29.2, CH_3	1.41, s
26	23.8, CH_3	1.22, s
27	16.6, CH_3	1.36, s
1′	32.3, CH_2	3.31, overlap
2′	126.5, CH	5.22, t (7.2)
3′	130.7, C	
4′	18.0, CH_3	1.72, s
5′	26.0, CH_3	1.70, s
1″	30.1, CH_2	3.55, m
2″	126.4, CH	5.11, t (7.2)
3″	131.1, C	
4″	18.3, CH_3	1.78, s
5″	25.9, CH_3	1.68, s

*1.68,make sure all **Supplementary Files** are cited. Please also provide captions for these files, if relevant. Note that ALL **Supplementary Files** will be deposited to FigShare and receive a DOI. Notify us of any previously deposited material. Please provide the meaning of "*,#" specified in **Figure 5**.*

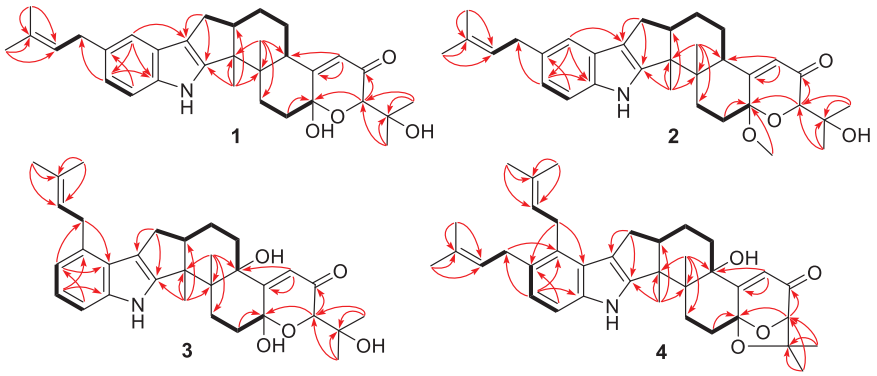

FIGURE 2 | Selected HMBC and COZY correlations of **1–4**.

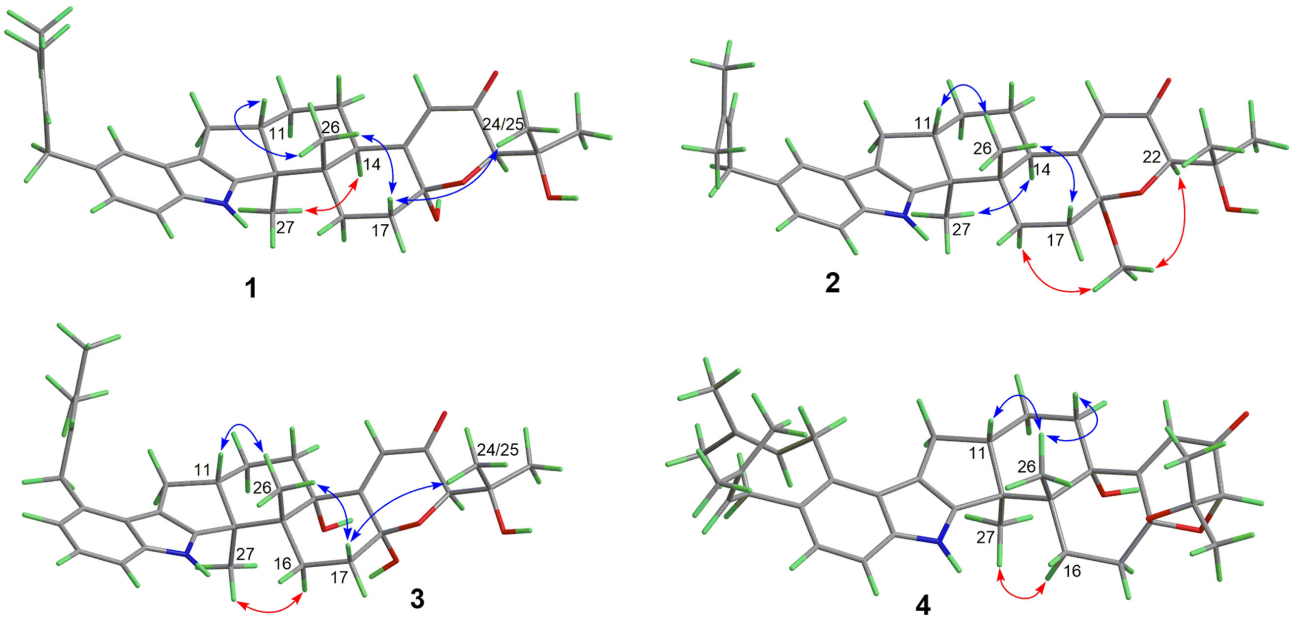

FIGURE 3 | Selected NOESY correlations of **1–4**.

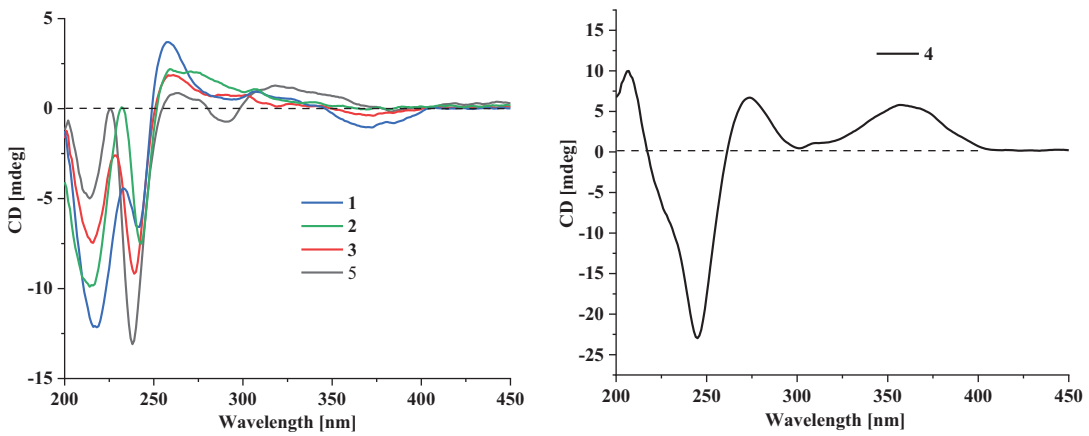

FIGURE 4 | The experimental ECD curves of **1–5**.

and 237 (3.54) nm; ECD (0.22 mM, MeOH) λ_{max} 207 (+ 13.75), 245 (–31.6), 274 (+ 9.23), and 357 (+ 7.98) nm. ^{1}H and ^{13}C NMR data (**Table 2**); HRESIMS *m/z* 570.3581 $[M + H]^+$ (calcd for $C_{37}H_{48}NO_4Na$, 570.3578).

Cell viability of the test compounds were detected using MTT assay (Pan et al., 2021). RAW264.7 cells (Type Culture Collection of the Chinese Academy of Sciences, Shanghai, China) were cultured in DMEM supplemented with 10% fetal bovine serum (Gibco, United States) at 37°C in a 5% CO_2 incubator. Cells were seeded in a 96-well plate at a concentration of 8×10^5 cells/well and treated with LPS (5 μg/ml) and various concentrations of test compounds (1–200 μM) for 24 h. After that, MTT solution (10 μl) was added and incubated at 37°C for 4 h. The purple crystals dissolved with dimethylsulfoxide (150 μl) were added, and the absorbance value was measured by a microplate reader at 570 nm.

Measurement of NO, TNF-α, and IL-6 Production

RAW264.7 cells were seeded in a 96-well plate at a concentration of 8×10^5 cells/well. After incubation, cells were pretreated with the test compounds with different dose (20–160 μM) and then stimulated with LPS (5 μg/ml) for 24 h. The NO concentration in culture medium was calculated by the commercial kit (Jiancheng, Nanjing, China) according to the manufacturer's instruction. The TNF-α and IL-6 levels were determined using ELISA (Xiao et al., 2017). In brief, the cells were incubated with the test compounds (50 μM) in the presence or absence of LPS (5 μg/ml). After incubation for 24 h, the supernatant was detected for TNF-α and IL–6 at 450 nm. All data were expressed as the mean ± SD from at least three independent experiments.

RESULTS AND DISCUSSION

Structure Elucidation of Compounds

Compound **1** has a molecular formula $C_{32}H_{41}NO_4$ as established from its HRESIMS and ^{13}C NMR data (**Supplementary Table 1**). The ^{1}H and ^{13}C NMR data of **1** (**Table 1**), with the aid of a heteronuclear single quantum coherence (HSQC) spectrum, showed a total of 32 carbon signals comprising 1 ketone carbonyl, 12 olefinic or aromatic carbons with 5 protonated, 6 sp^3 methylenes, 3 sp^3 methines with 1 oxygenated, 4 sp^3 non-protonated carbons with 2 oxygenated, and 6 methyls. These data are quite similar to those of 7α-hydroxy-13-desoxy paxilline (**5**) with the main differences being the presence of additional signals ($\delta_{C/H}$ 35.3/3.36, 126.2/5.36, 131.8, 17.9/1.74, and 26.0/1.74) corresponding to an isopentene group in the NMR data of **1**. Besides, unlike that of **5**, only three aromatic protons resonating into an ABX system were observed in the ^{1}H NMR data of **1**, indicating that the C–3 or C–4 of **1** was substituted. The above data suggested that **1** was a prenylated derivative of **5**. COZY correlations (**Figure 2**) of H_2-1′/H-2′ as well as HMBC correlations (**Figure 2**) from H_3-4′ and H_3-5′ to C-3′ and C-2′ and from H_2–1′ to C–2, C–3, and C–4 confirmed the presence of an isopentene group at C–3. The remaining substructure was deduced to be the same as that of **5** by their similar NMR chemical shifts, which was further corroborated by detailed analysis of the two-dimensional NMR data (**Figure 2**) of **1**. NOESY correlations (**Figure 3**) of H_3–24(25)/H–17/H_3–26/H–11 suggested the same face of these protons, while NOESY correlation of H_3–27/H–14 indicated that they were on the face opposite to H_3–26. The absolute configuration of **1** was determined to be the same as that of **5** by their similar ECD curves (**Figure 4**). Accordingly, compound **1** was assigned as a new indole-terpenoid and named as encindolene A.

Compound **2** was determined to have the molecular formula $C_{33}H_{43}NO_4$ based on the positive HRESIMS data, containing an additional methyl substituent in comparison with **1**. The NMR spectra of **2** were closely related to those of **1** except for the appearance of an additional methoxy group at $\delta_{C/H}$ 49.6/3.41. The location of this methoxy group at C-18 in **2** was confirmed by the HMBC correlation (**Figure 2**) from its protons to C-18 (δ_C 98.1). Thus, compound **2** was elucidated as 18-*O*-methyl-sperindolene A according to compound **1**. The relative and absolute configurations of **2** were determined to be the same as **1** by NOESY correlations (**Figure 3**) of H-22/MeO-18/H-16, H_3–27/H–14, and H–11/H_3–26/H–17, as

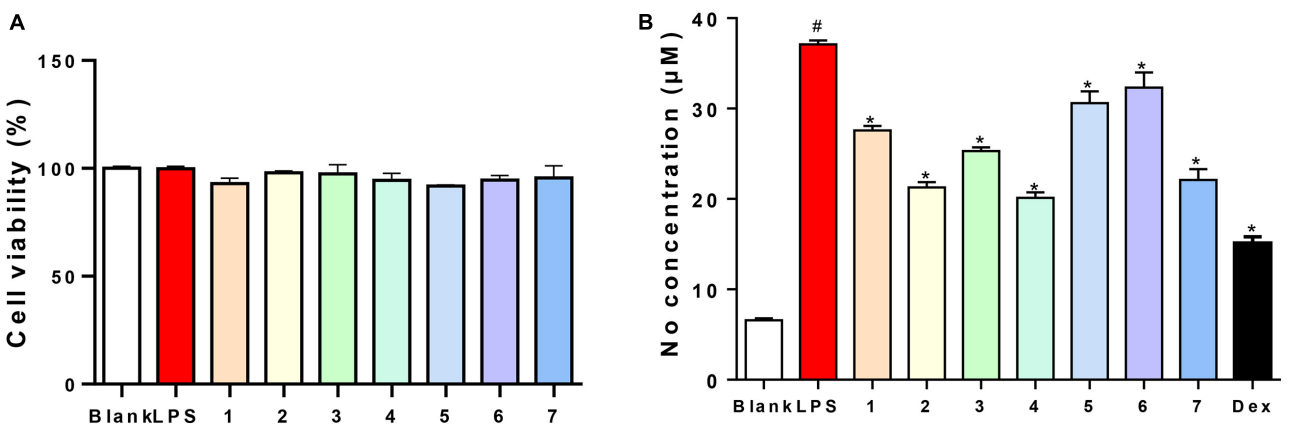

FIGURE 5 | Viability effects and NO inhibitory activities of compounds 1–7 **(A)**: 200 μM; **(B)**: 40 μM) on RAW264.7 cells.

well as the comparison of the ECD curve of **1** with that of **2** (**Figure 4**).

Compound **3** possessed the molecular formula $C_{32}H_{41}NO_5$ as determined by HRESIMS data. The ^{1}H-NMR, ^{13}C-NMR, and HSQC data of **3** were quite similar to those of **1**. However, three continuous proton signals at δ_H 6.70, 6.88, and 7.12 instead of an ABX coupling system as in **1** were shown in the aromatic region of the ^{1}H-NMR of **3**, implying the position of the isopentene group at C-2 or C-5. HMBC correlations (**Figure 2**) from H-1′ to C-1, C-2, and C-3 demonstrated the position of the isopentene group at C-2. The relative configuration of 3 was assigned to be the same as that of **1** by ROESY correlations (**Figure 3**) of H–24(25)/H–17/H_3–26/H–11 and H_3–27/H–14. The ECD curve (**Figure 4**) of **3** is very similar to those of **1** and **2**, leading to the assignment of the absolute configuration of **3** as shown in **Figure 1**.

The HRESIMS data for **4** showed an ion peak at *m*/*z* 570.3581 $[M + H]^+$, indicating the molecular formula $C_{37}H_{47}NO_4$. The UV absorption at 237 and 285 nm suggested that **4** was also an indole-terpenoid. The ^{13}C NMR data of **4** are very similar to that of paspalitrem C (**7**) (Dorner et al., 1984) except for the presence of five additional signals at $\delta_{C/H}$ 30.1/3.55, 126.4/5.11, 131.1, 18.3/1.78, and 25.9/1.68 corresponding to an isopentene group, as deduced from HMBC correlations from H_3–4″ and H_3–5″ to C-3″ and C-2″ and COZY correlations of H-2″ and H_2–1″. Besides, unlike that of compound 7, the ^{1}H NMR spectrum of **4** showed the presence of only two proton signals (δ_H 6.75 and 7.05) in the aromatic region, which are coupled to each other. This suggested the location of the above isopentene group at C-2. HMBC correlations (**Figure 2**) from H_2–1″ to C-1, C-2, and C-3 further corroborated this deduction. The remaining substructure was determined to be the same as that of **7** by detailed analysis of the HMBC and COSY data (**Figure 2**). The relative configuration of compound **4** was also deduced to be the same as that of **7** by their nearly identical 1D NMR chemical shifts of C-7 to C-27 and was further confirmed by NOE correlations (**Figure 3**) of H–11/H_3–26/H–13 and H_3–27/H–16. The ECD curve of **4** showed strong positive Cotton effects (CEs) around 210, 275, and 325 nm (**Figure 4**). These data were very similar to those of shearilicine (Ariantari et al., 2019), a previously described analog bearing similar carbon skeleton as that of **4**, thus leading to the assignment of the absolute configuration of **4**.

Anti-inflammatory and Antibacterial Activities Assay

The antibacterial activities of all of the isolated compounds against *Staphylococcus aureus* and *Escherichia coli* were evaluated using the twofold dilution assay (Song et al., 2021). The results showed that all of the compounds were inactive. Compounds **1–7** were also non-cytotoxic to RAW264.7 cells at the concentration of 200 μM by MTT assay (**Figure 5A**). NO production was used as an indicator to evaluate the anti-inflammatory activity of **1–7**. All of the compounds showed varying degrees of inhibitory activities on the production of NO in LPS-stimulated RAW264.7 cells, with IC_{50} values of 79.4, 49.7, 81.3, 40.2, 86.7, 90.1, and 54.4 μM, respectively, while 13.30 μM for dexamethasone, a positive control. Based on this, compounds **1–7** (40 μM) could suppress NO overproduction in cells (**Figure 5B**). To further confirm the anti-inflammatory activities, the effects of compounds **1–7** on the production of proinflammatory cytokines (TNF-α and IL-6) in LPS-induced RAW264.7 cells were evaluated. All the compounds showed moderate inhibitory effects on the production of TNF-α and IL-6 production at the concentration of 50 μM, with compound **4** showing the strongest effect (**Figure 6**).

CONCLUSION

In summary, from the fungus *Penicillium* sp. HFF16, seven indole-terpenoids including four new were isolated and identified. These compounds could inhibit NO, TNF-α, and IL-6 production without affecting the cell viability in LPS-stimulated RAW264.7 macrophages. These results further demonstrated that fungi from medicinal plants are an abundant source of new bioactive products with medicinal use.

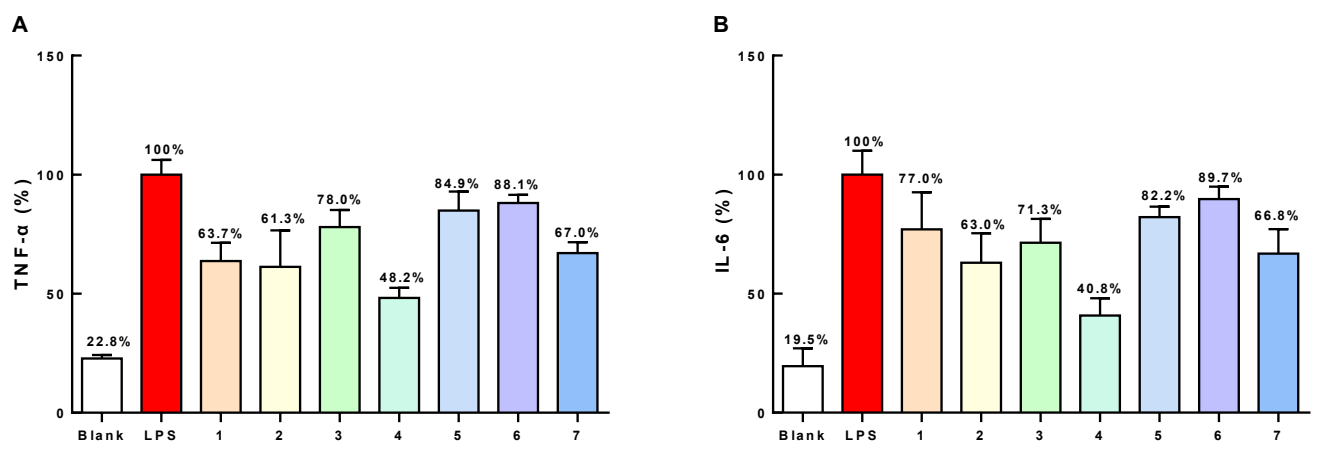

FIGURE 6 | The inhibitory effects on TNF-α **(A)** and IL-6 **(B)** production of compounds 1–7 (50 μM) on RAW264.7 cells.

DATA AVAILABILITY STATEMENT

The datasets presented in this study can be found in online repositories. The names of the repository/repositories and accession number(s) can be found below: GenBank, MZ165618.

AUTHOR CONTRIBUTIONS

GP conceived and designed the experiments and was involved in isolation of compounds. YZ, SR, FL, QX, and XZ contributed to isolation of compounds. WP contributed to the collection of physical data of compounds. MY, CP, and GH performed genetic manipulation, strain fermentation, and extraction. TY contributed to the collection of the NMR data of compounds. FK revised the manuscript. LZ supervised the work and prepared the manuscript. NX contributed to bioactivity assay and revised the manuscript. All authors contributed to the article and approved the submitted version.

FUNDING

This work was financially supported by the Natural Science Foundation of Shandong Province (No. ZR2019BH080), the National Natural Science Foundation of China (No. 82004014), the Open Project of State Key Laboratory of Natural Medicines (No. SKLNMKF202001), the Medical and Health Project of Shndong Province (No. 202001060294), the Science and Technology Innovation Development Project of Tai'an City (No. 2020NS059), and the Specific Research Project of Guangxi for Research Bases and Talents (No. AD18126005).

SUPPLEMENTARY MATERIAL

The Supplementary Material for this article can be found online at: https://www.frontiersin.org/articles/10.3389/fmicb.2021.710364/full#supplementary-material

REFERENCES

Ariantari, N. P., Ancheeva, E., Wang, C., Mándi, A., Knedel, T. O., Kurtán, T., et al. (2019). Indole diterpenoids from an endophytic *Penicillium* sp. *J. Nat. Prod.* 82, 1412–1423. doi: 10.1021/acs.jnatprod.8b00723

Belofsky, G. N., and Gloer, J. B. (1995). Antiinsectan alkaloids: shearinines A-C and a new paxilline derivative from the ascostromata of *Eupenicillium shearii*. *Tetrahedron* 51, 3959–3968. doi: 10.1016/0040-4020(95)00138-X

Dorner, J. W., Cole, R. J., Cox, R. H., and Cunfer, B. M. (1984). Paspalitrem C, a new metabolite from sclerotia of *Claviceps paspali*. *J. Agric. Food Chem.* 32, 1069–1071. doi: 10.1021/jf00125a033

Kong, F. D., Fan, P., Zhou, L. M., Ma, Q. Y., Xie, Q. Y., Zheng, H. Z., et al. (2019). Penerpenes A-D, Four indole terpenoids with potent protein tyrosine phosphatase inhibitory activity from the marine-derived fungus *Penicillium* sp. KFD28. *Org. Lett.* 21, 4864–4867. doi: 10.1021/acs.orglett.9b01751

Li, C., Gloer, J. B., Wicklow, D. T., and Dowd, P. F. (2002). Thiersinines A and B: novel antiinsectan indole diterpenoids from a new fungicolous *Penicillium Species* (NRRL 28147). *Org. Lett.* 4, 3095–3098. doi: 10.1021/ol026424a

Medzhitov, R. (2008). Origin and physiological roles of inflammation. *Nature* 454, 428–435. doi: 10.1038/nature07201

Munday-Finch, S. C., Wilkins, A. L., and Miles, C. O. J. (1998). Isolation of Lolicine A, Lolicine B, Lolitriol, and Lolitrem N from loliumperenne infected with *Neotyphodium lolii* and evidence for the natural occurrence of 31-Epilolitrem N and 31-Epilolitrem F. *Agric. Food Chem.* 46, 590–598. doi: 10.1021/jf9706787

Pan, G. J., Li, Y. L., Che, X. Y., Tian, D., Han, W. J., Wang, Z. M., et al. (2021). New Thio-compounds and monoterpenes with anti-inflammatory activities from the fungus *Aspergillus* sp. CYH26. *Front. Microbiol.* 12:668938. doi: 10.3389/fmicb.2021.668938

Peter, G. M., and Christopher, M. W. (1994). Biosynthesis and transformation of tremorgenic indolediterpenoids by *Penicillium paxilli* and *Acremonium lolii*. *Phytochemistry* 36, 1209–1217. doi: 10.1016/S0031-9422(00)89639-9

Song, M., Liu, Y., Li, T., Liu, X., Hao, Z., Ding, S., et al. (2021). Plant natural flavonoids against multidrug resistant pathogens. *Adv. Sci.* (Weinh) e2100749. doi: 10.1002/advs.202100749

Springer, J. P., Clardy, J., Wells, J. M., Cole, R. J., and Kirksey, J. W. (1975). The structure of paxilline, a tremorgenic metabolite of *Penicillium paxilli* bainier. *Tetrahedron Lett.* 16, 2531–2534. doi: 10.1016/S0040-4039(00)75170-7

Xiao, N., Yang, L. L., Yang, Y. L., Liu, L. W., Li, J., Liu, B. L., et al. (2017). Ginsenoside Rg5 inhibits succinate-associated lipolysis in adipose tissue and prevents muscle insulin resistance. *Front. Pharmacol.* 8:43. doi: 10.3389/fphar.2017.00043

Zhong, J., and Shi, G. (2019). Editorial: regulation of inflammation in chronic disease. *Front. Immunol.* 10:737. doi: 10.3389/fimmu.2019.00737

Conflict of Interest: The authors declare that the research was conducted in the absence of any commercial or financial relationships that could be construed as a potential conflict of interest.

frontiers in Microbiology

REVIEW
published: 23 July 2021
doi: 10.3389/fmicb.2021.723828

Trichoderma: A Treasure House of Structurally Diverse Secondary Metabolites With Medicinal Importance

Jian-Long Zhang[1,2,3†], Wen-Li Tang[2†], Qing-Rong Huang[1,4], You-Zhi Li[2], Mao-Lian Wei[2], Lin-Lin Jiang[1,2,3,5], Chong Liu[1], Xin Yu[1,2,4], Hong-Wei Zhu[1,2,3,5], Guo-Zhong Chen[1,3,4] and Xing-Xiao Zhang[1,3,4]*

[1] School of Life Sciences, Ludong University, Yantai, China, [2] Shandong Provincial Key Laboratory of Quality Safty Monitoring and Risk Assessment for Animal Products, Jinan, China, [3] Shandong Aquaculture Environmental Control Engineering Laboratory, Yantai, China, [4] Yantai Key Laboratory of Animal Pathogenetic Microbiology and Immunology, Yantai, China, [5] Yantai Research Institute for Replacing Old Growth Drivers with New Ones, Yantai, China

OPEN ACCESS

Edited by:
Paola Angelini, University of Perugia, Italy

Reviewed by:
Andreas Lazaros Chryssafidis, University of the State of Santa Catarina, Brazil
Wanping Chen, Georg-August-Universität Göttingen, Germany
Laith Khalil Tawfeeq Al-Ani, Universiti Sains Malaysia, Malaysia
Vivek Sharma, Chandigarh University, India

***Correspondence:**
Xing-Xiao Zhang
zhangxingxiao@ldu.edu.cn

† These authors have contributed equally to this work

Specialty section:
This article was submitted to Microbiotechnology, a section of the journal Frontiers in Microbiology

Received: *11 June 2021*
Accepted: *28 June 2021*
Published: *23 July 2021*

Citation:
Zhang J-L, Tang W-L, Huang Q-R, Li Y-Z, Wei M-L, Jiang L-L, Liu C, Yu X, Zhu H-W, Chen G-Z and Zhang X-X (2021) Trichoderma: A Treasure House of Structurally Diverse Secondary Metabolites With Medicinal Importance. Front. Microbiol. 12:723828. doi: 10.3389/fmicb.2021.723828

Fungi play an irreplaceable role in drug discovery in the course of human history, as they possess unique abilities to synthesize diverse specialized metabolites with significant medicinal potential. *Trichoderma* are well-studied filamentous fungi generally observed in nature, which are widely marketed as biocontrol agents. The secondary metabolites produced by *Trichoderma* have gained extensive attention since they possess attractive chemical structures with remarkable biological activities. A large number of metabolites have been isolated from *Trichoderma* species in recent years. A previous review by Reino et al. summarized 186 compounds isolated from *Trichoderma* as well as their biological activities up to 2008. To update the relevant list of reviews of secondary metabolites produced from *Trichoderma* sp., we provide a comprehensive overview in regard to the newly described metabolites of *Trichoderma* from the beginning of 2009 to the end of 2020, with emphasis on their chemistry and various bioactivities. A total of 203 compounds with considerable bioactivities are included in this review, which is worth expecting for the discovery of new drug leads and agrochemicals in the foreseeable future. Moreover, new strategies for discovering secondary metabolites of *Trichoderma* in recent years are also discussed herein.

Keywords: *Trichoderma*, secondary metabolites, chemical diversity, biological activity, bioactive compounds

INTRODUCTION

Trichoderma is a fungal genus that was first described in 1794 (Persoon, 1794). This genus is well adapted to various ecological niches and is ubiquitous in most types of soils, roots, and foliar environments. *Trichoderma* species are beneficial for their commercial enzymes, plant growth-accelerating abilities, and biocontrol of plant diseases, indicating their promising industrial, agricultural, and medicinal potential (Cai et al., 2013; Bhardwaj and Kumar, 2017; McMullin et al., 2017). Globally, *Trichoderma* has proved to achieve great success as effective biological control drugs (Keswani et al., 2014). Many *Trichoderma* species, such as *T. harzianum*,

T. hamatum, *T. asperellum*, *T. atroviride*, *T. koningii*, *T. virens*, and *T. viride*, are lucratively used as potent biocontrol agents worldwide (Bhardwaj and Kumar, 2017). These fungal species exhibit outstanding biocontrol capability against pathogenic microorganisms either through indirect (scrambling for nutrients, changing the ambient conditions, stimulating plant growth and defense responses) or direct (mycoparasitism) mechanisms (Bhardwaj and Kumar, 2017). Moreover, in addition to ecological effects, it is well known that *Trichoderma* can produce secondary metabolites that not only participate in signal transduction but also go through communications with various organisms (Keswani et al., 2014; Zeilinger et al., 2016). It is also believed that the successes of *Trichoderma* as biocontrol drugs are, at least partially, due to their capacity to secrete abundant secondary metabolites (Zeilinger et al., 2016).

Fungi play an irreplaceable role in the drug discovery in the course of human history, as they possess unique abilities to synthesize diverse secondary metabolites with significant medical potential (Li X.Q. et al., 2020). The discovery of penicillin from the filamentous fungal species *Penicillium* was a milestone in pharmaceutical research (Fleming, 1929). Since then, chemical studies regarding fungal secondary metabolites have become a research hotspot (Zhang P. et al., 2020). A large number of fungal secondary metabolites have been discovered, many of which have potential as drug leads (Newman and Cragg, 2016). The fungal species belonging to *Penicillium* and *Talaromyces* are representative flora, with many secondary metabolites possessing intriguing chemical skeletons and bioactivities characterized from these species (Frisvad, 2014). For the genus *Trichoderma*, more than 1000 metabolites have been isolated from *Trichoderma* in recent years (Zeilinger et al., 2016). Accordingly, many reviews on various aspects of *Trichoderma*, not only for the chemical diversity of metabolites but also for the various bioactivities and their potential applications, have been published. Zeilinger et al. (2016) reviewed the selected *Trichoderma*-derived secondary metabolites and gave an all-round summary of genomic analysis and putative gene clusters involved in biosynthesis. Keswani et al. (2014) listed targeted metabolites of *Trichoderma* and pointed out the utilization potentiality in multifarious areas, especially in agriculture. As mentioned above, *Trichoderma* is a well-known biocontrol agent that is used globally. Since many *Trichoderma* species are some of the most prominent producers of anti-phytopathogenic secondary metabolites, Khan et al. (2020) exhibited 45 fungicidal secondary metabolites of *Trichoderma* sp. along with the structural overview, biosynthesis pathway, and action mechanism. Moreover, Reino et al. (2008) systematically summarized the metabolites of *Trichoderma* and their bioactivities. As of 2008, a total of 186 compounds and 269 references were cited, including a detailed study of the activities of biocontrol mechanisms (Reino et al., 2008). Herein, in order to update the relevant list of reviews of secondary metabolites of *Trichoderma* sp., we provide a comprehensive overview in regard to the newly described metabolites of *Trichoderma* from the beginning of 2009 to the end of 2020, with emphasis on their chemistry and various bioactivities. Moreover, new strategies for discovering secondary metabolites of *Trichoderma* in recent years have also been discussed.

LITERATURE SEARCH

To retrieve literature published up to 2020, an in-depth inspection was performed (Zhang P. et al., 2020). The key words of "*Trichoderma*" and "secondary metabolites" were used to search for related literatures in Web of Science, with the times pan from 2009 to 2020 (**Supplementary Figure 1**). Additionally, other platforms such as Crossref, Google Scholar, Elsevier, and Springer Link were also searched at the same time. The retrieved articles were categorized according to natural product chemistry. In all, 63 records in the context of natural product research were retained and assessed to present this review. A total of 203 compounds were found from *Trichoderma* from 2009 to 2020. It should be pointed out that some omissions were inevitable during the literature search. However, with the greatest effort, we have demonstrated almost all of the relevant research herein.

CHEMICAL DIVERSITY

Terpenoids

Trichothecene Sesquiterpenes

Trichothecenes, which are primarily produced by several genera of fungi, are sesquiterpene-based compounds possessing a tricyclic 12,13-epoxytrichothec-9-ene skeleton (Takahashi-Ando et al., 2020). Structurally, trichothecenes are classified into different families of nivalenols, neosolaniols, isotrichodermins, calonectrins, trichothecene, and trichobreols based on the substitution pattern. To date, more than 200 trichothecene derivatives have been discovered (Shi Z.Z. et al., 2020; Takahashi-Ando et al., 2020). The structures of trichothecenes isolated from *Trichoderma* species are listed in **Figure 1**. Eight newly discovered trichothecenes, trichodermarins G–N (**1**–**8**), and six known trichothecenes, trichodermol (**9**), trichodermin (**10**), trichoderminol (**11**), trichodermarin A (**12**) and trichodermarin B (**13**), and 2,4,12-trihydroxyapotrichothecene (**14**), were isolated from *Trichoderma brevicompactum* ADL-9-2, which was obtained as an endophyte of marine algae *Chondria tenuissima* (Shi Z.Z. et al., 2020). Trichodermarin N (**8**), featuring a 2'-*N*-acetylglucosaminyl moiety, represented the first aminoglycoside-bearing trichothecene. Chemical investigations of the marine fungus *Trichoderma* cf. *brevicompactum* TPU199 fermented with NaI afforded three new trichothecenes, trichobreols A–C (**15**–**17**) (Yamazaki et al., 2020a). Interestingly, **15** can be produced under the original culture conditions (seawater medium), whereas compounds **16** and **17** were found only under NaI-containing culture conditions. Additionally, isolation of the same fungus yielded two new trichothecenes, trichobreols D (**18**) and E (**19**) (Yamazaki et al., 2020b). Harzianums A (**20**) and B (**21**), two trichothecenes linked with octa-2,4,6-trienedioyl moiety, were isolated from the biofertilizer fungus *T. brevicompactum* (CGMCC19618) (Yin et al., 2020). From a marine fungus *Trichoderma longibrachiatum*, three trichothecenes, trichothecinol A (**22**), 8-deoxy-trichothecin (**23**), and trichothecinol B (**24**) were yielded (Du et al., 2020).

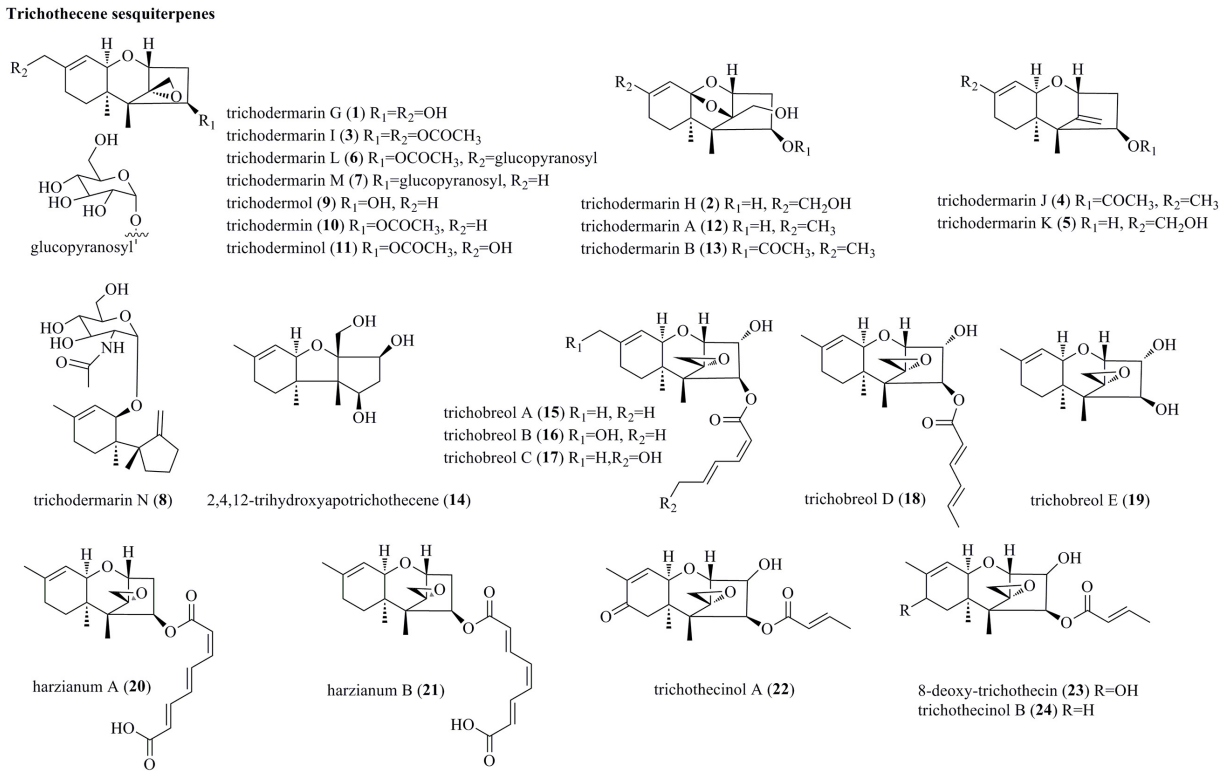

FIGURE 1 | Trichothecene sesquiterpenes produced by *Trichoderma* species (**1–24**).

Carotane Sesquiterpenes

From the marine-derived fungus *T. virens* Y13-3, eight undescribed carotane sesquiterpenes, trichocarotins A–H (**25**–**32**), along with the known compounds CAF-603 (**33**), trichocarane B (**34**), 7-β-hydroxy CAF-603 (**35**), and trichocarane A (**36**), were discovered (**Figure 2**) (Shi et al., 2018a). Carotane sesquiterpenes are commonly found in plants. However, only approximately 10 compounds have been isolated from filamentous fungi, representing a rare class of fungal metabolites (Shi et al., 2018a).

Cadinane Sesquiterpenes

A new example of a cadinane-skeletoned sesquiterpene, trichocadinin A (**37**), containing a previously unrecognized site of an exocyclic olefin functionality at C-10, was obtained from the marine-derived fungus *T. virens* Y13-3 (Shi et al., 2018a). This is the first time to report cadinane sesquiterpenes from *Trichoderma*. three new cadinane-type sesquiterpenes, i.e., trichodermaloids A–C (**38**–**40**), and three known ones, i.e., aspergilloid G (**41**), rhinomilisin E (**42**), and rhinomilisin G (**43**), were characterized from the marine sponge-derived fungus *Trichoderma* sp. SM16 (Cui et al., 2020).

Cyclonerane Sesquiterpenes

Induced by a chemical epigenetic manipulation strategy, a new cyclonerane, 3,7,11-trihydroxy-cycloneran (**44**), was produced by the marine fungus *T. harzianum* (XS-20090075), which was isolated from soft corals (Shi T. et al., 2020). Cycloneranes having a monocyclic skeleton are reported to be produced from various fungal genera, such as *Trichoderma*, *Aspergillus*, *Fusarium*, *Paecilomyces*, and *Trichothesium*. Based on previous findings, the five-membered ring of all the isolated cyclonerane sesquiterpenes featured the same relative configuration (Liu X.H. et al., 2020). However, chromatographic separation of the marine fungus *Trichoderma citrinoviride* A-WH-20-3 yielded two undescribed cycloneranes, (10*E*)-isocyclonerotriol (**45**) and (10*Z*)-isocyclonerotriol (**46**), which were characterized as the first example with an isomerized ring in cycloneranes (Liu X.H. et al., 2020). New cycloneranes, 11-methoxy-9-cycloneren-3,7-diol (**47**), methyl 3,7-dihydroxy-15-cycloneranate (**50**), and 10-cycloneren-3,5,7-triol (**51**), as well as two structurally related cycloneranes, 9-cycloneren-3,7,11-triol (**48**) and (–)-cyclonerodiol (**49**), were obtained from *T. harzianum* X-5, an endophyte of the marine alga *Laminaria japonica* (Song et al., 2018). Biosynthetically, **47** and **50** may be produced through *O*-methylation during the fermentation process. Two previously reported cycloneranes, i.e., 10-cycloneren-3,5,7-triol (**51**) and 10(*E*)-cyclonerotriol (**52**), were obtained from *T. longibrachiatum*, an endophyte of the highly halophile *Suaeda glauca* (Du et al., 2020).

Drimane Sesquiterpenes

Chemical exploration of an endophyte *Trichoderma* sp. 1212-03 from *Daedaleopsis tricolor* yielded three new drimane

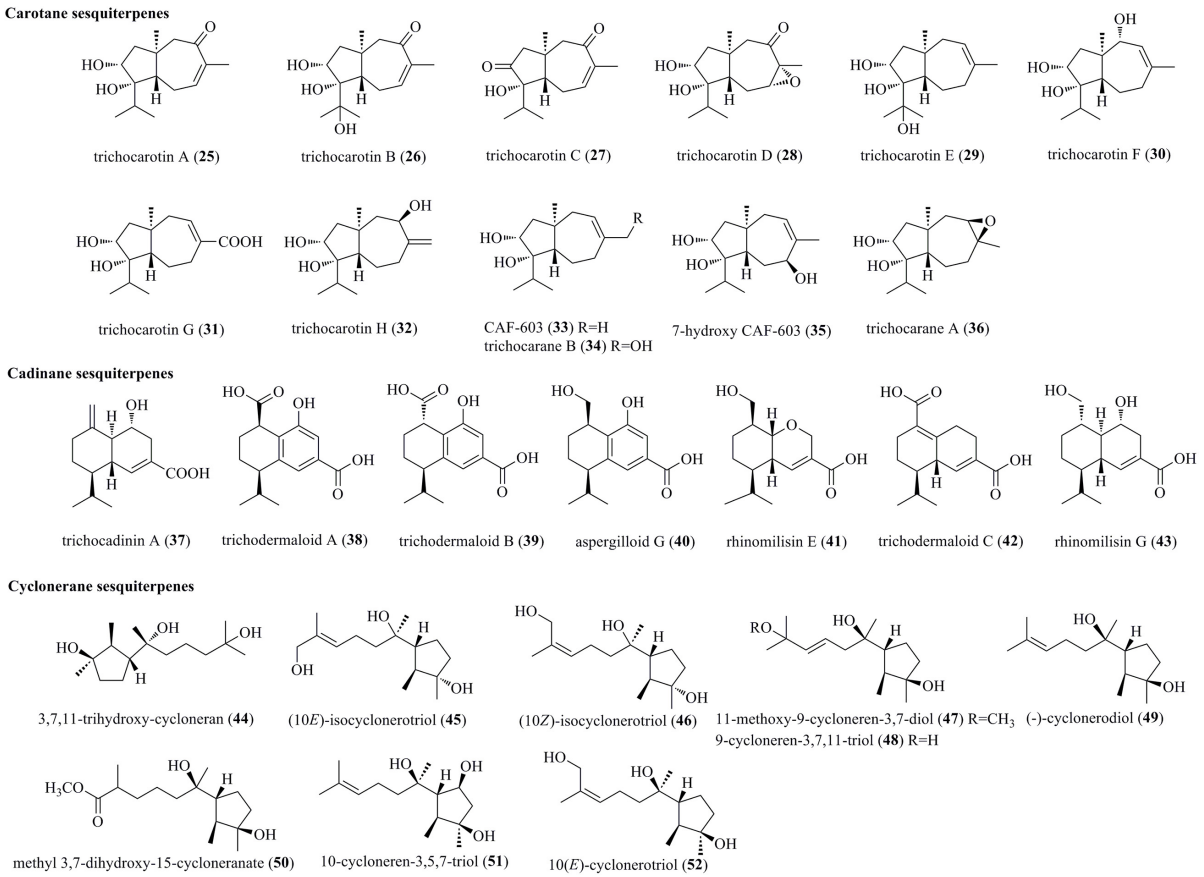

FIGURE 2 | Carotane, cadinane, and cyclonerane sesquiterpenes produced by *Trichoderma* species (**25–52**).

sesquiterpenes, i.e., neomacrophorins I (**53**), II (**54**), and III (**55**) (**Figure 3**) (Hirose et al., 2014). They belong to macrophorins and drimane sesquiterpene-linked cyclohexenone epoxides but feature a hydroxyl in the drimene skeleton and a 5′,6′-α-epoxide in quinone functionality. Furthermore, six novel neomacrophorins, i.e., 3-deoxyneomacrophorin IV (**56**), 3-oxoneomacrophorins I (**57**) and II (**58**), neomacrophorin VII (**59**), 5′-epimacrophorin B (**60**), and 5′-deoxyneomacrophorin IV (**61**), as well as four novel premacrophorin congeners, i.e., premacrophorin III (**62**), premacrophorindiol (**63**), premacrophorintriols I (**64**), and II (**65**), were isolated from the same fungus (Nishiyama et al., 2019). These molecules possessed 2,3-epoxybenzoquinone (**56** and **57**) or 2,3-epoxybenzosemiquinol substructures (**58**–**60** and **62**–**64**). Premacrophorins **62**–**65** carried acyclic isoprenoid side chains biosynthetically derived from neomacrophorins in the early stage, rather than the common drimane skeleton.

Other Sesquiterpenes

Co-culture of the mangrove endophytic fungus *Trichoderma* sp. 307 and aquatic pathogenic bacterium *Acinetobacter johnsonii* B2 afforded two undescribed furan-type isoeremophilane sesquiterpenes, microsphaeropsisins B (**66**) and C (**67**) (Zhang et al., 2017). It is believed that both of them were derived from *Trichoderma* sp. rather than induced by the coculture. 8-Acoren-3,11-diol (**68**), trichoacorenol (**69**), and trichoacorenol B (**70**) were isolated from marine-derived *T. harzianum* X-5, and they were structurally characterized as acorane sesquiterpenes (Song et al., 2018). Trichodermene A (**71**), an unusual norsesquiterpene with a novel tricyclic-6/5/5-[4.3.1.$0^{1,6}$]-decane framework, was characterized to originate from *T. longibrachiatum* (Du et al., 2020). Two new sesquiterpenes, i.e., trichoderiols A (**72**) and B (**73**), were produced by *T. atroviride* S361, an endophyte of *Cephalotaxus fortunei* (Zheng et al., 2011). Compounds **72** and **73** were structurally characterized as 2-oxabicyclo[2,1]heptane derivatives. New cuparenes, i.e., trichocuparins A (**74**) and B (**75**), were obtained from *T. brevicompactum* ADL-9-2, which was isolated from marine algae *C. tenuissima* (Shi Z.Z. et al., 2020). Compounds **74** and **75** are rare cuparenes with a cyclopentylcyclohexane unit. Three new sesquiterpenes, i.e., Trichodones A–C (**76**–**78**), were isolated from *T. asperellum* residing in *Panax notoginseng* (Ding et al., 2012a). The new sesquiterpenes possess the same skeleton as juvabione. However, the diol groups in compounds **76**–**78** were different from those of known juvabione analogs. Fermentation of *T. atroviride*, an endophyte of *Lycoris radiate*, afforded a new sesquiterpene, atrichodermone C (**79**) (Zhou et al., 2017). Chemical study of the marine sponge-associated fungus

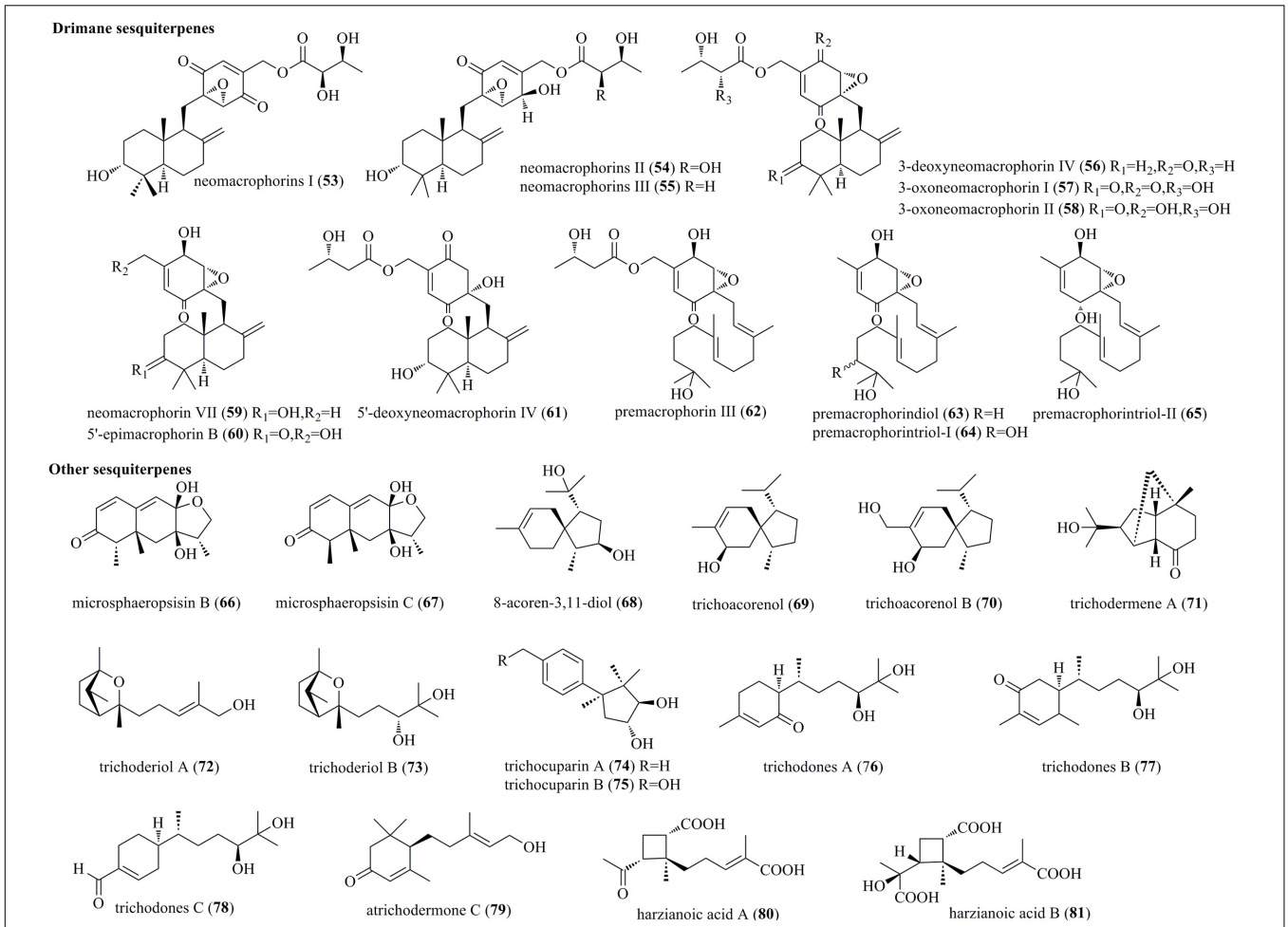

FIGURE 3 | Drimane and other sesquiterpenes produced by *Trichoderma* species (**53–81**).

T. harzianum LZDX-32-08 yielded two new structurally unique sesquiterpenes, i.e., harzianoic acids A (**80**) and B (**81**) (Li et al., 2019). Interestingly, **80** and **81** had a cyclobutane framework, which was biogenetically derived from an unusual isoprenoid pathway.

Harziane Diterpenes

Harziane diterpenes, typically possessing a 4/7/5/6-fused tetracyclic framework, have been reported exclusively from various *Trichoderma* species (**Figure 4**). Five undescribed harziane diterpenes, i.e., harzianols F–J (**82–86**), and three previously reported diterpenes, i.e., 3*S*-hydroxyharzianone (**87**), harziandione (**88**), and harzianol A (**89**), were isolated from the endophyte *T. atroviride* B7 of *Colquhounia coccinea* var. *mollis* (Li W.Y. et al., 2020). Deoxytrichodermaerin (**90**), an undescribed harziane lactone, was isolated from an endophyte *T. longibrachiatum* A-WH-20-2 of marine algae *Laurencia okamurai* (Zou et al., 2021). A new harziane diterpenoid, harzianone E (**91**), was obtained from the soft coral-sourced *T. harzianum* (XS-20090075) by chemical epigenetic manipulation strategy (Shi T. et al., 2020). A new harziane diterpene, 3*R*-hydroxy-9*R*,10*R*-dihydroharzianone (**92**), was produced by *T. harzianum* X-5 (Song et al., 2018). Two undescribed harzianes, i.e., (9*R*,10*R*)-dihydro-harzianone (**93**) and harzianelactone (**94**), were produced by *Trichoderma* sp. Xy24 from mangrove plant *Xylocarpus granatum* (Zhang et al., 2016). Chemical investigations on the marine fungus *T. harzianum* XS-20090075 yielded diverse harzianes, including two undescribed harziane lactones, i.e., harzianelactones A and B (**95** and **96**), as well as five new lactones, i.e., harzianones A–D (**97–100**) and harziane (**101**) (Zhao et al., 2019). Finally, a new diterpenoid lactone, trichodermaerin (**102**), was isolated from *Trichoderma erinaceum* derived from *Acanthaster planci* (Xie et al., 2013).

Other Diterpenes

Citrinovirin (**103**), a rare norditerpene, was produced by an endophyte *T. citrinoviride* cf-27 (Liang et al., 2016). Compound **103** possessed a perhydroazulene ring system, which was synthesized by a unique biogenetic pathway including demethylation, cyclization, oxidation, and S_N2 reaction with Walden inversion. A new proharziane-type diterpene,

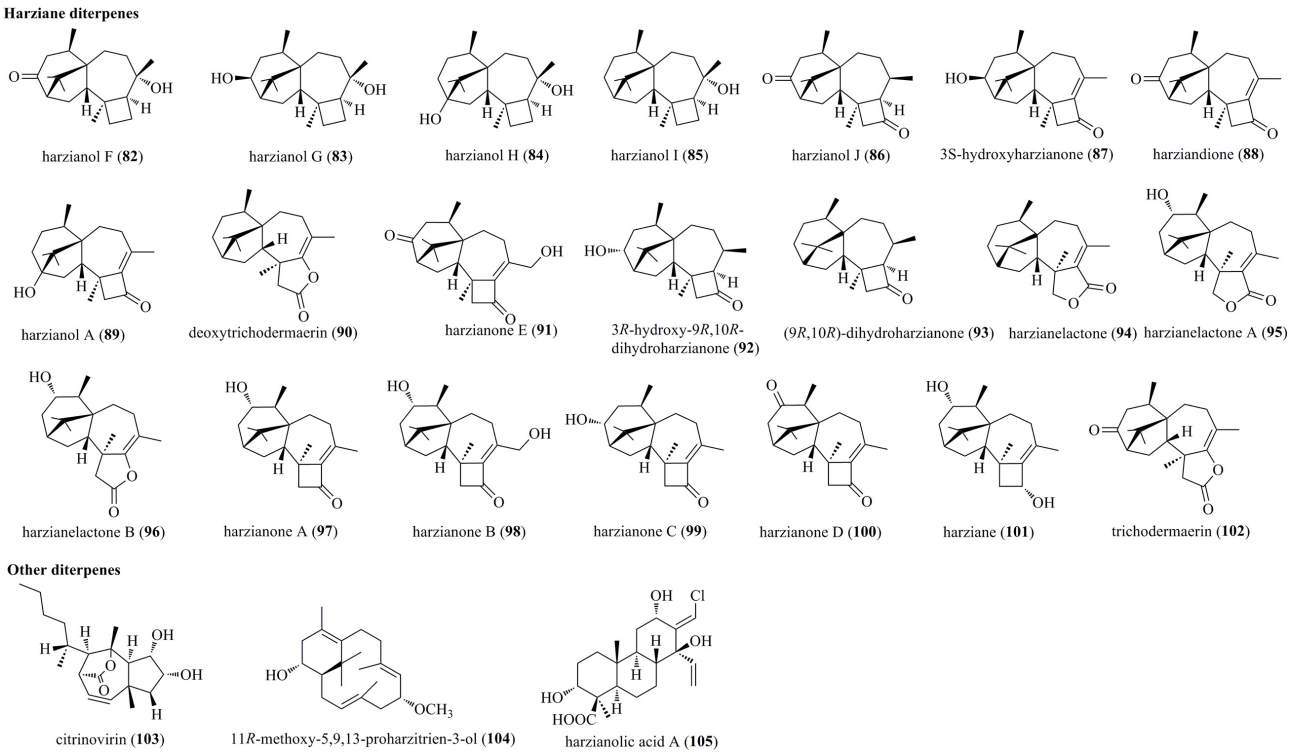

FIGURE 4 | Harziane and other diterpenes produced by *Trichoderma* species (**82–105**).

11*R*-methoxy-5,9,13-proharzitrien-3-ol (**104**), was characterized from the marine algicolous fungus *T. harzianum* X-5 (Song et al., 2018). **104** and harzianes were structurally related diterpenes. Harzianolic acid A (**105**), characterized as a novel chlorinated cleistanthane diterpenoid, was isolated from the marine fungal strain *T. harzianum* (XS-20090075) (Shi T. et al., 2020). Tricyclic diterpenoids categorized to cleistanthanes were reported from *Trichoderma* for the first time.

Cyclopeptides

Bioassay-guided fractionation of the plant endophytic fungus *T. harzianum* KZ-20 afforded four new cyclodepsipeptides belonging to the destruxin family, i.e., trichodestruxins A–D (**106–109**), and two previously reported derivative, i.e., destruxin E2 chlorohydrin (**110**) and destruxin A2 (**111**) (**Figure 5**) (Liu Z. et al., 2020). Destruxins represent rare cyclic hexadepsipeptides. Structurally, new compound **107** possessed hydroxy acid fragments of the 2,4,5-trihydroxypentanoic acid unit, while **106** and **108** had a β-methylproline moiety. Homodestcardin (**112**), trichomide B (**113**), and homodestruxin B (**114**), characterized as cyclohexadepsipeptides of the trichomide series, were produced by *T. longibrachiatum* (Du et al., 2020). Finally, cyclopeptides PF1022F (**115**) and halobacillin (**116**) were obtained from the endophyte *T. asperellum* (Ding et al., 2012a).

Diketopiperazines

The marine fungus *Trichoderma* sp. TPU199 is a producer of a series of diketopiperazines (**117–127**) (**Figure 6**) (Yamazaki et al., 2020a). Initially, this fungal strain was found to produce pretrichodermamide A (**117**), gliovirin (**118**), and trichodermamide A (**119**). **117** and **118** possessed an unusual epipolythiodiketopiperazine (ETP) skeleton. Then, this strain with sodium halides added to the culture medium afforded the halogenated gliovirin-type ETPs DC1149B (**120**), DC1149R (**122**), and iododithiobrevamide (**123**). Subsequently, chlorotrithiobrevamide (**124**), the first trisulfide derivative in the type of ETP, was characterized. Furthermore, a highly modified dipeptide, dithioaspergillazine A (**125**), was obtained after the long time cultivation. Finally, two undescribed ETPs, i.e., 5-*epi*-pretrichodermamide A (**126**) and 5-*epi*-trithiopretrichodermamide A (**127**), were characterized under NaI-containing culture conditions. Pretrichodermamide G (**128**) was established as a 1,2-oxazadecaline ETP, and it was identified from the endophyte *T. harzianum* of *Zingiber officinale* (Harwoko et al., 2021). A rare heterocyclic dipeptide, i.e., trichodermamide G (**129**), and a biogenetically related metabolite aspergillazin A (**130**) were produced by the marine-sourced *T. harzianum* D13 (Zhao et al., 2020). Notably, **129** and **130** were novel ETP derivatives with the sulfur bridge locating at different positions. Dehydroxymethylbis(dethio)bis(methylthio)gliotoxin (**131**) and (3*S*,6*R*)-6-(para-hydroxybenzyl)-1,4-dimethyl-3,6-bis(methylthio)piperazine-2,5-dione (**132**), which were structurally characterized as two undescribed sulfurated diketopiperazines, were produced by an algicolous isolate of *T. virens* Y13-3 (Shi et al., 2018b). The fungal strain *T. asperellum* A-YMD-9-2 from *Gracilaria verrucosa* produced an undescribed

Cyclopeptides

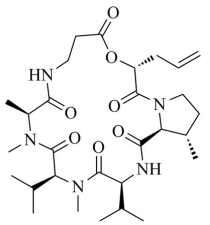

trichodestruxin A (**106**)

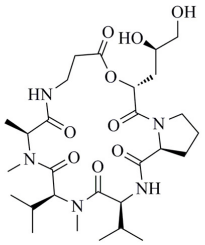

trichodestruxin B (**107**)

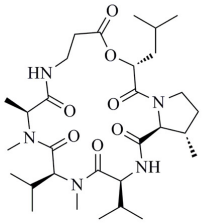

trichodestruxin C (**108**)

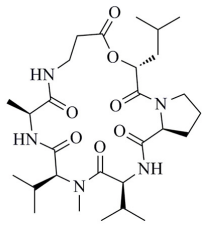

trichodestruxin D (**109**)

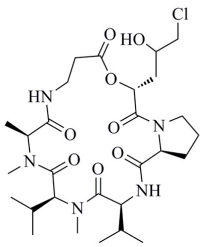

destruxin E2 chlorohydrin (**110**)

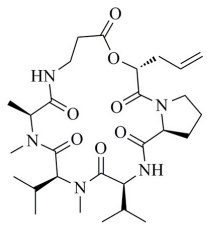

destruxin A2 (**111**)

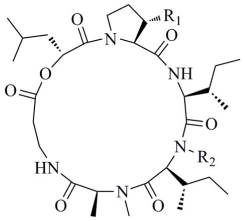

homodestcardin (**112**) R_1=CH_3, R_2=CH_3
trichomide B (**113**) R_1=CH_3, R_2=H
homodestruxin B (**114**) R_1=H, R_2=CH_3

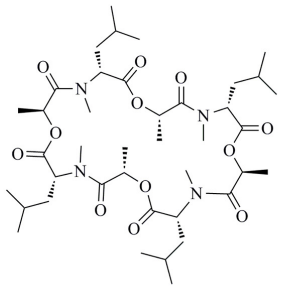

PF1022F (**115**)

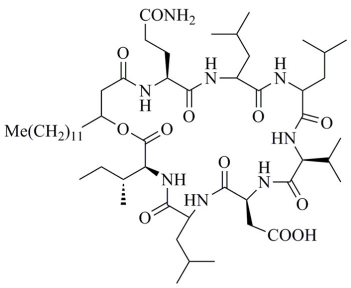

halobacillin (**116**)

FIGURE 5 | Cyclopeptides produced by *Trichoderma* species (**106–116**).

Diketopiperazines

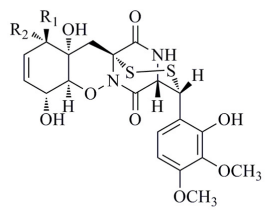

pretrichodermamide A (**117**) R_1=OH, R_2=H
DC1149B (**120**) R_1=Cl, R_2=H
DC1149R (**122**) R_1=Br, R_2=H
iododithiobrevamide (**123**) R_1=I, R_2=H
5-*epi*-pretrichodermamide A (**126**) R_1=H, R_2=OH

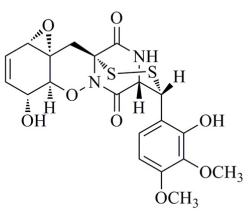

gliovirin (**118**)

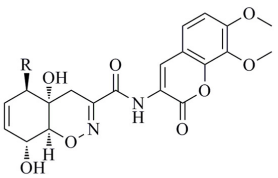

trichodermamide A (**119**) R=OH
trichodermamide B (**121**) R=Cl

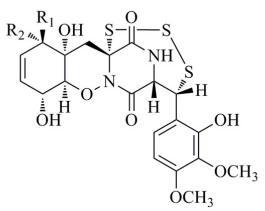

chlorotrithiobrevamide (**124**) R_1=Cl, R_2=H
5-epi-trithiopretrichodermamide A (**127**) R_1=H, R_2=OH

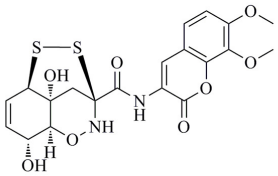

dithioaspergillazine A (**125**)

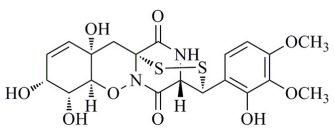

pretrichodermamide G (**128**)

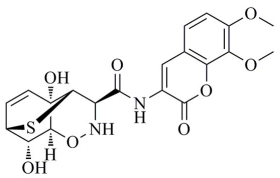

trichodermamide G (**129**)

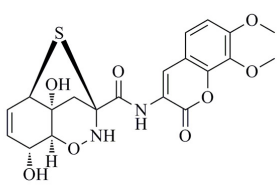

aspergillazin A (**130**)

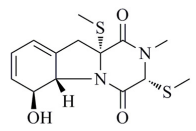

dehydroxymethylbis(dethio)bis
(methylthio)gliotoxin (**131**)

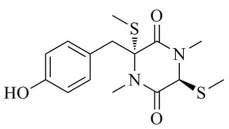

(3*S*,6*R*)-6-(para-hydroxybenzyl)-1,4-
dimethyl-3,6-bis(methylthio)piperazine-2,5-dione (**132**)

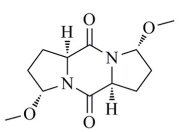

cyclo(L-5-MeOPro-L-5-MeO-Pro) (**133**)

FIGURE 6 | Diketopiperazines produced by *Trichoderma* species (**117–133**).

symmetric diketopiperazine, cyclo(L-5-MeO-Pro-L-5-MeO-Pro) (**133**) (Song et al., 2020).

Alkaloids and Other Nitrogen-Containing Compounds

Chemical survey of *T. virens* FKI-7573 generated an undescribed N-containing compound, i.e., trichothioneic acid (**134**) (**Figure 7**) (Miyano et al., 2020). **134** contained a heptelidic acid and an L-ergothioneine substructure. Ethyl 2-bromo-4-chloroquinoline-3-carboxylate (**135**) was produced by the soft coral-sourced *T. harzianum* (XS-20090075) in Czapek's medium (Yu et al., 2021). **135** was the first halogenated quinoline derivative from *Trichoderma*. Trichoderamides A (**136**) and B (**137**), isolated as stereoisomers originating from the PKS-NRPS mixed pathway, were isolated from *T. gamsii*, an endophyte of *P. notoginseng* (Ding et al., 2015). Two rare pyridones, i.e., trichodins A (**138**) and B (**139**), were identified from *Trichoderma* sp. strain MF106 from the Greenland Seas (Wu et al., 2014). Harzianic acid (**140**), a nitrogen heterocyclic siderophore, was isolated from *T. harzianum* M10 (Vinale et al., 2013). **140** was identified as 2-hydroxy-2-[4-(1-hydroxy-octa-2,4-dienylidene)-1-methyl-3,5-dioxopyrrolidin-2-ylmethyl]-3-methyl-butyric acid. Atrichodermone A (**141**) was a unique compound with a dimeric cyclopentenone framework that was discovered from the endophytic fungal strain *T. atroviride* (Zhou et al., 2017). **141** was the first example of a 3-amino-5-hydroxy-5-vinyl-2-cyclopenten-1-one dimer. Two nitrogen-containing cyclonerane sesquiterpene derivatives, 5′-acetoxy-deoxycyclonerin B (**142**) and 5′-acetoxy-deoxycyclonerin D (**143**), were obtained from the marine fungus *T. asperellum* A-YMD-9-2 (Song et al., 2020).

Polyketides

Naphthalene Derivatives

An undescribed naphthalene, trichoharzin B (**144**), a natural product, methyl-trichoharzin (**145**), and the known trichoharzin (**146**) and eujavanicol A (**147**) were produced by the marine fungus *T. harzianum* XS-20090075 (**Figure 8**) (Yu et al., 2021). **144**–**146** were characterized as new polyketides with an alkylated decalin framework and esterified with a rare acyl group. Trichoharzianol (**148**) was identified from a fungal strain of *T. harzianum* F031 (Jeerapong et al., 2015). **148** was reported as a new decalin derivative bearing a 3-hydroxypropionyl moiety, a 1-methylpropyl moiety, and an acetonide moiety. Trichodermic acid A (**149**) and B (**150**) were isolated from an endophytic fungus *T. spirale*, and characterized as new octahydronaphthalene derivatives (Li et al., 2012).

Octaketides

Five new polyketides, *ent*-koninginin A (**151**), 1,6-di-*epi*-koninginin A (**152**), 15-hydroxykoninginin A (**153**), 10-deacetylkoningiopisin D (**154**), and koninginin T (**155**), along with two previously reported derivatives, koninginin L (**156**) and trichoketide A (**157**), were produced by *Trichoderma koningiopsis* QA-3 (Shi et al., 2017). Compounds **151**–**153** were characterized as tricyclic polyketides with an octahydrochromene skeleton. Koninginins I (**158**), J (**159**) and K (**160**), which were structurally characterized as new koninginin-type compounds, were produced by *T. neokongii* 8722 (Zhou et al., 2014). Chemical study of the marine-derived fungus *T. koningii* afforded five new polyketides, 7-*O*-methylkoninginin D (**161**) and trichodermaketones A–D (**162**–**165**) (Song et al., 2010). **162** and **163** represented unprecedented tricyclic polyketides having a bistetrafuran skeleton. Trichoketides A (**166**) and B (**167**), two undescribed octaketides, were isolated from *Trichoderma* sp. TPU1237 (Yamazaki et al., 2015). **166** and **167** were epimers at the α-position of the dihydrofuran ring. Finally, koninginins L (**156**) (herein reported as a new compound) and M (**168**) were isolated from solid fermentation of *T. koningii* 8662 (Lang et al., 2015). A series of koninginins were reported from *Trichoderma* species, but only in koninginins L (**156**) and M (**168**) was an oxygen bridge located between the C-10 and C-7 positions.

Cytochalasans

Cytochalasans are a kind of novel fungal metabolic products, with more than 100 cytochalasans being reported to date. These metabolites contain a polycyclic skeleton and an isoindole moiety, which was fused with one macrocyclic ring (Ding et al., 2012c). Two highly complicated pentacyclic cytochalasans, trichoderone A (**169**) and trichoderone B (**170**), together with three previously reported cytochalasans, aspochalasins D (**171**), J (**172**), and I (**173**), were obtained from *T. gamsii* from *P. notoginseng* (**Figure 9**) (Ding et al., 2012c). **169** possessed a highly functionalized 7/6/6/5/5 pentacyclic skeleton, while **170** contained the unusual 6/5/6/6/5 pentacyclic framework. Furthermore, two undescribed cytochalasans, trichalasins C (**174**) and D (**175**), as well as three known cytochalasans, aspochalasins D (**171**), M (**176**), and P (**177**), were obtained from the abovementioned strain *T. gamsii* (Ding et al., 2012b).

Other Polyketides

An undescribed cyclopentenone, atrichodermone B (**178**), was isolated from endophytic *T. atroviride* (Zhou et al., 2017). A newly discovered cyclopentenone, 5-hydroxycyclopeni cillone (**179**), was produced by the marine-sourced *Trichoderma* sp. HPQJ-34 (Fang et al., 2017). **179** possessed a 3-substituted 4,5-dihydroxy-2,5-dimethylcyclopent-2-enone skeleton. Two previously reported unsaturated lactones, xylogibloactones A (**180**) and B (**181**), were found from the marine fungus *T. harzianum* (XS-20090075) (Yu et al., 2021). Compounds **180** and **181** had a C_9 polyketide framework with a γ-lactone moiety. Trichoderpyrone (**182**), a novel cyclopentenone-pyrone mixed polyketide, was produced by *T. gamsii* (Chen et al., 2017). **182** had two individual ring systems, i.e., a 3-aminocyclopent-2-*en*-1-one moiety and a 4-hydroxy-6-methyl-2*H*-pyran-2-one moiety, which were derived from a mixed biosynthetic pathway. Trichoderone (**183**), a new cyclopentenone, was obtained from the marine *Trichoderma* sp. (You et al., 2010). Compounds **184** and **185**, characterized as two new isocoumarin derivatives with a butanetriol residue, were isolated from the endophytic fungus *T. harzianum* Fes1712 (Ding et al., 2019). Trichophenol A (**186**), which was identified as a new isocoumarin derivative with a 6,8-dihydroxyisocoumarin moiety, was isolated from *T. citrinoviride* A-WH-20-3 (Liu X.H. et al., 2020). Previously described metabolites,

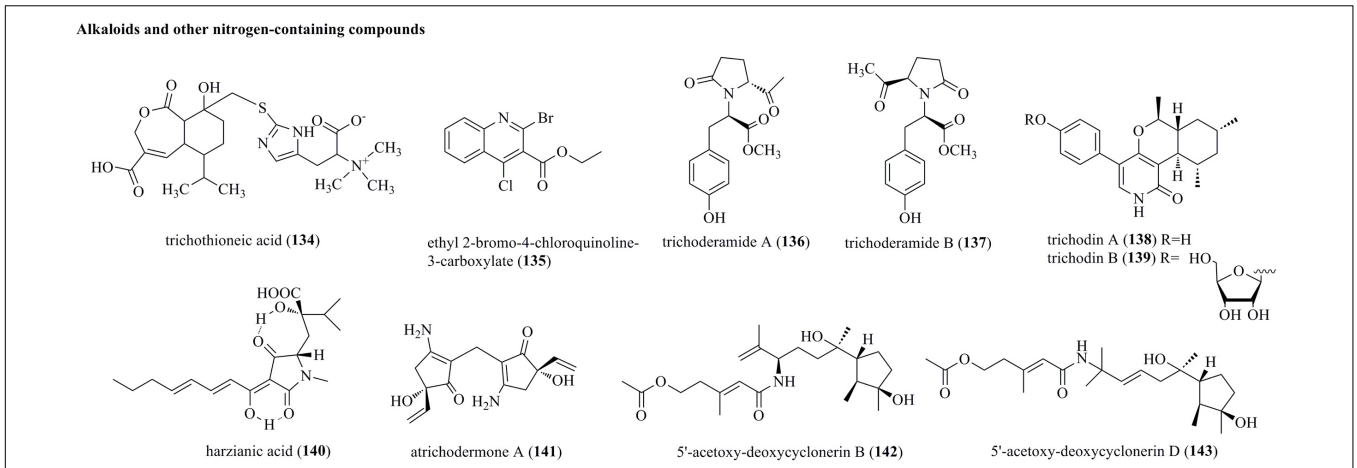

FIGURE 7 | Alkaloids and other nitrogen-containing compounds produced by *Trichoderma* species (**134–143**).

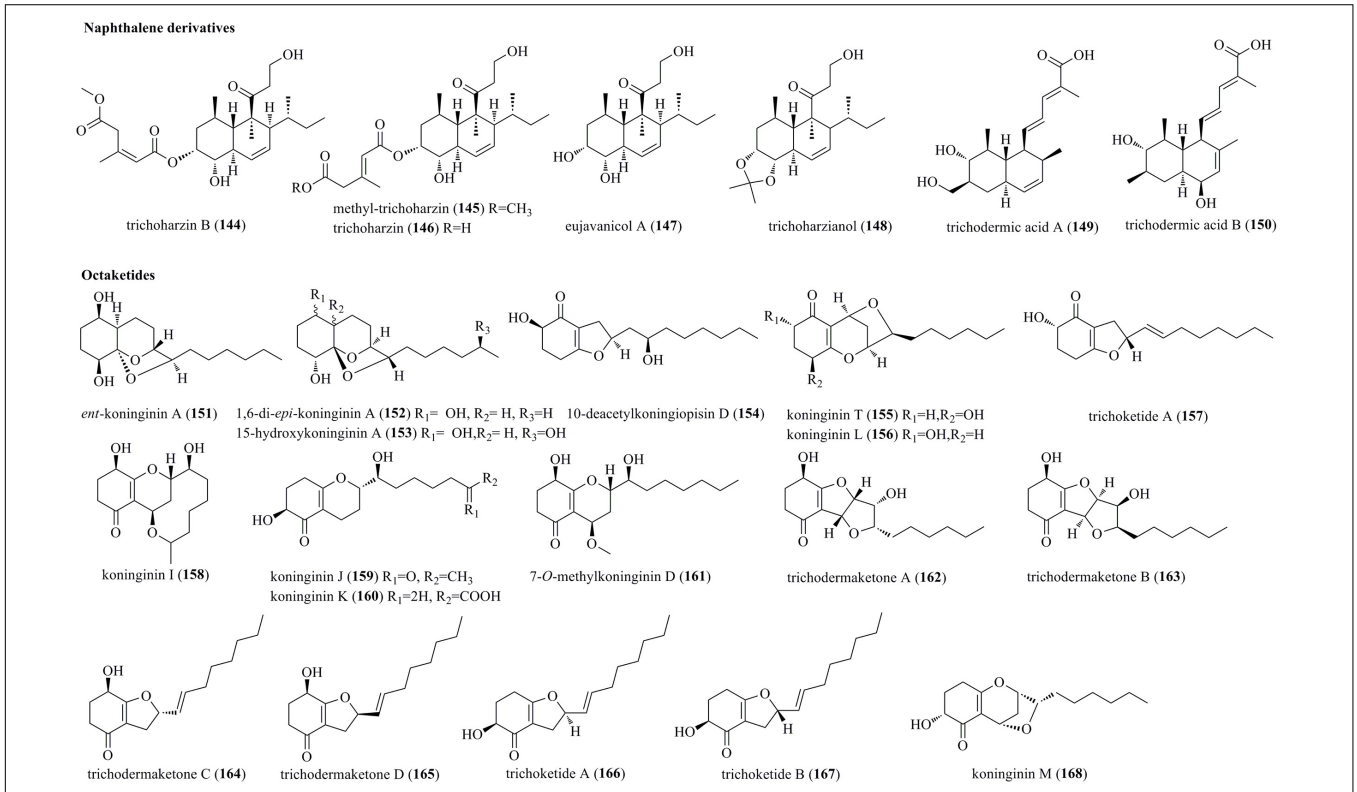

FIGURE 8 | Naphthalene and octaketide derivatives produced by *Trichoderma* species (**144–168**).

5-hydroxy-3-hydroxymethyl-2-methyl-7-methoxychromone (**187**) and 4,6-dihydroxy-5-methylphthalide (**188**), were produced by the fungus *T. harzianum* F031 (Jeerapong et al., 2015). Two structurally new polyketides (**189** and **190**) with a 1-hydroxyhepta/methoxyhepta-3,5-dien-2-one moiety were produced in the transformant of *Trichoderma afroharzianum* (Ding et al., 2020). Two undescribed azaphilone derivatives, azaphilones D (**191**) and E (**192**), were obtained from dragonfly associated *T. harzianum* QTYC77 (Zhang S. et al., 2020). A new 10-membered lactone cremenolide (**193**), elucidated as but-2-enoic acid 7-acetoxy-6-hydroxy-2-methyl-10-oxo-5,6,7,8,9,10-hexahydro-2*H*-oxecin-5-yl ester, was isolated from cultural filtrates of *Trichoderma cremeum* (Vinale et al., 2016). Two undescribed polyketides, (3*R*,7*R*)-7-hydroxy-de-*O*-methyllasiodiplodin (**194**) and (3*R*)-5-oxo-de-*O*-methyllasiodiplodin (**195**), were isolated from the cocultivation of *Trichoderma* sp. 307 and *A. johnsonii* B2 (Zhang et al., 2017). An undescribed polyketide, nafuredin C (**196**), and

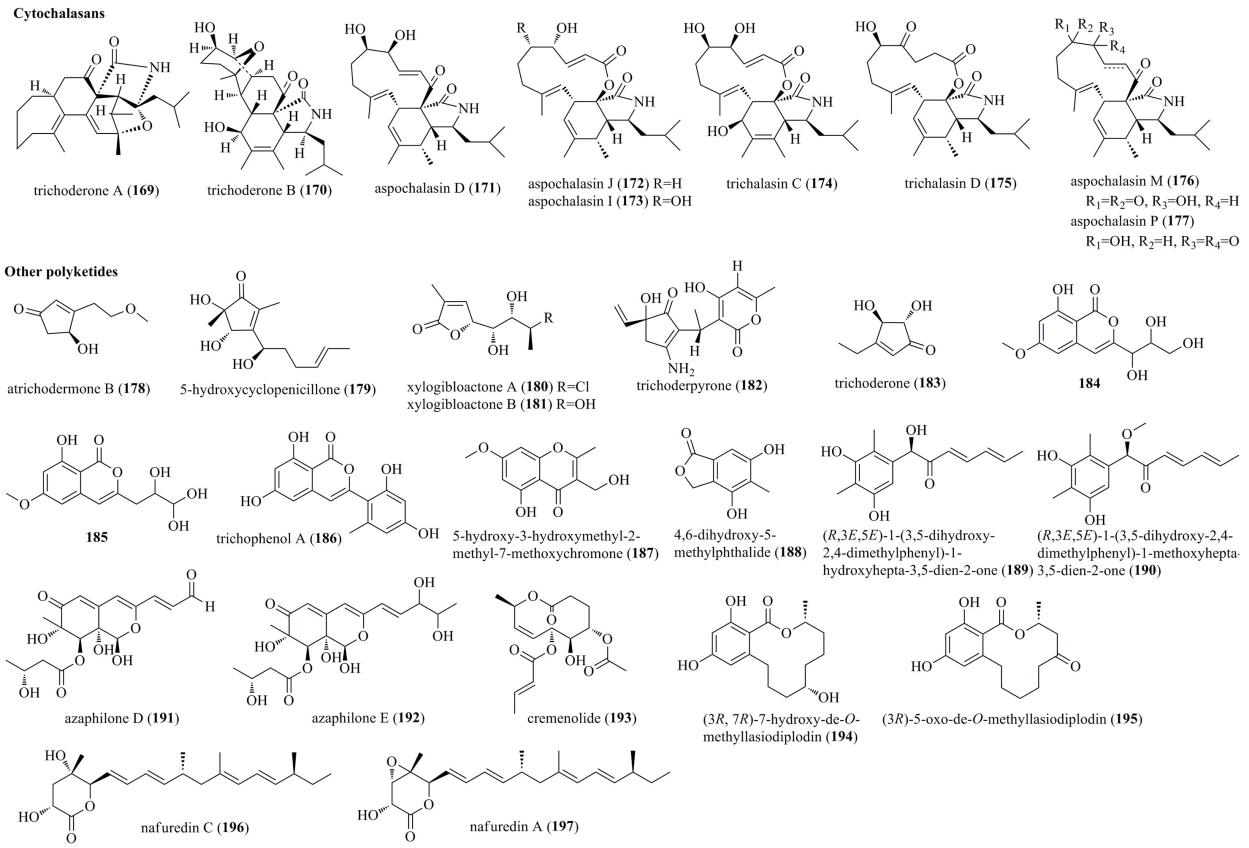

FIGURE 9 | Cytochalasans and other polyketides produced by *Trichoderma* species (**169–197**).

the known nafuredin A (**197**), were produced by marine fungus *T. harzianum* D13 (Zhao et al., 2020).

Other Compounds

Two new sulfur compounds, designated thioporidiols A (**198**) and B (**199**), were produced by a culture broth of *T. polypori* FKI-7382 (**Figure 10**) (Matsuo et al., 2020). Both of them were determined to be C13 lipid structures with an *N*-acetylcysteine moiety. A chemical investigation of the endophytic fungus *T. polyalthiae* offered two diphenyl ethers, Violaceol I (**200**) and II (**201**). Notably, both of them were characterized from *Trichoderma* for the first time (Nuankeaw et al., 2020). Trichodenols A (**202**) and B (**203**), two new compounds with 4-(2-hydroxyethyl) phenol moieties, were isolated from an endophyte *T. gamsii* (Ding et al., 2015).

NEW STRATEGIES FOR DISCOVERING SECONDARY METABOLITES OF *TRICHODERMA*

Recent fungal genome sequencing indicated that the majority of biosynthetic gene clusters (BGCs) associated with secondary metabolites are cryptic (transcriptionally silent) or expressed at very low levels under general laboratory conditions (Ren et al., 2017). Therefore, despite a large number of secondary metabolites being characterized from *Trichoderma*, genome sequencing revealed that there were more BGCs than we discovered, especially in filamentous fungi. These findings suggested that those silent metabolic pathways urgently need to be stimulated, which may lead to the discovery of novel metabolites with attractive functions. To activate cryptic biosynthetic pathways, many innovative approaches, such as cultivation-based approaches, metabolomic profiling, and genome mining-based molecular approaches, have been developed in recent years. These new approaches were accomplished with various degrees of success. The following are typical examples of searching for secondary metabolites of *Trichoderma* induced by cultivation regulation, cocultivation, chemical epigenetic manipulation, and transcript regulation, as shown in **Figure 11**.

The marine-derived fungus *Trichoderma* sp. TPU199 was found to produce a series of diketopiperazines under different conditions (**Figure 12**) (Yamazaki et al., 2020a). Chemical investigations of this fungal strain under ordinary culture conditions led to the discovery of compounds **169**–**177**. Then, this fungus produced the halogenated gliovirin-type ETPs **120** (Cl derivative of **117**), **122** (Br derivative of **117**), and **123** (I derivative of **177**) when added with NaCl, NaBr, and NaI in culture medium, respectively. Moreover, TPU199 supplemented

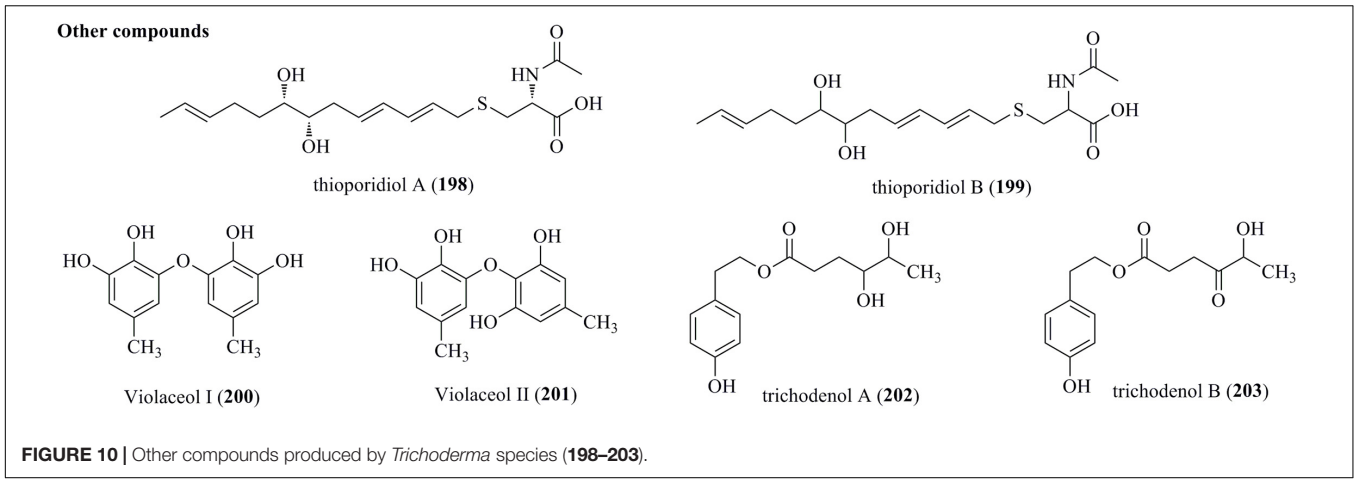

FIGURE 10 | Other compounds produced by *Trichoderma* species (**198–203**).

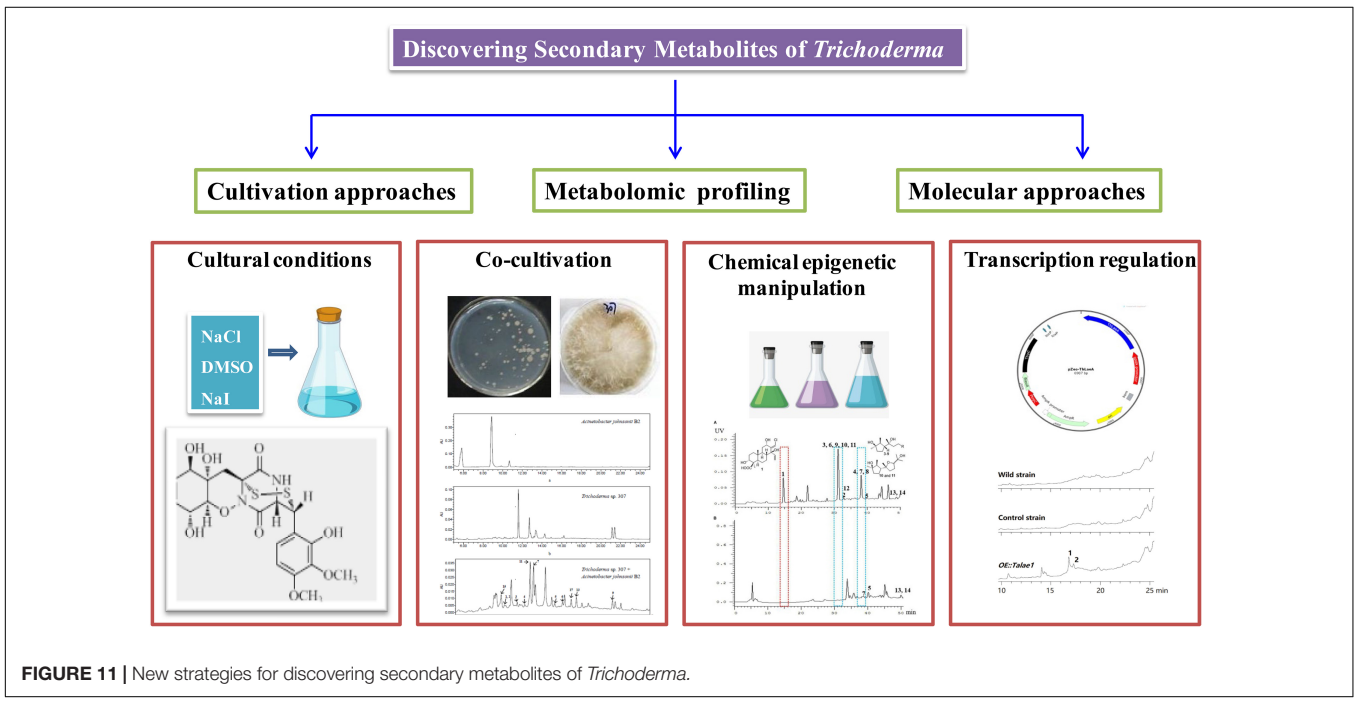

FIGURE 11 | New strategies for discovering secondary metabolites of *Trichoderma*.

with DMSO yielded **124**, a new trithio derivative of **120**. A continuous study indicated that, with the long time cultivation, an undescribed modified dipeptide **125** was obtained. Finally, two undescribed ETPs **126** and **127** were characterized under NaI-containing culture conditions. It is undoubtedly proven that changing the culture conditions can activate cryptic metabolic pathways.

Microorganism coculture based on microbial interspecies competition is an efficient path to stimulate cryptic BGCs. Cocultivation of *Trichoderma* sp. 307 and pathogenic bacterium *A. johnsonii* B2 yielded two undescribed sesquiterpenes (**66** and **67**) and de-*O*-methyllasiodiplodin (**194** and **195**) (Zhang et al., 2017). HPLC analysis indicated that they were derived from *Trichoderma* sp. rather than by the coculture. Chemical epigenetic manipulation has also proven to be an effective method to activate cryptic BGCs. Therefore, it was applied to the marine fungal strain *T. harzianum* XS-20090075 to mine its potential to synthesize secondary metabolites (Shi T. et al., 2020). A histone deacetylase inhibitor, sodium butyrate at 10 μM, significantly changed its metabolic profile and gave rise to three undescribed terpenoids, including a cleistanthane **105**, a harziane diterpenoid **91**, and a cyclonerane sesquiterpenoid **44**. Interestingly, harziane diterpenoids were the dominant metabolites from this fungal strain under ordinary culture conditions, indicating the production of harzianes as the dominant metabolic pathway. In this study, the production of harzianes was hampered due to chemical epigenetic manipulation. In contrast, the biosynthetic pathways of cleistanthanes and cycloneranes were successfully activated, leading to the isolation of the new cleistanthane diterpenoid **105** and a series of cyclonerane sesquiterpenoids (**44** and other known cycloneranes). This is the first report of

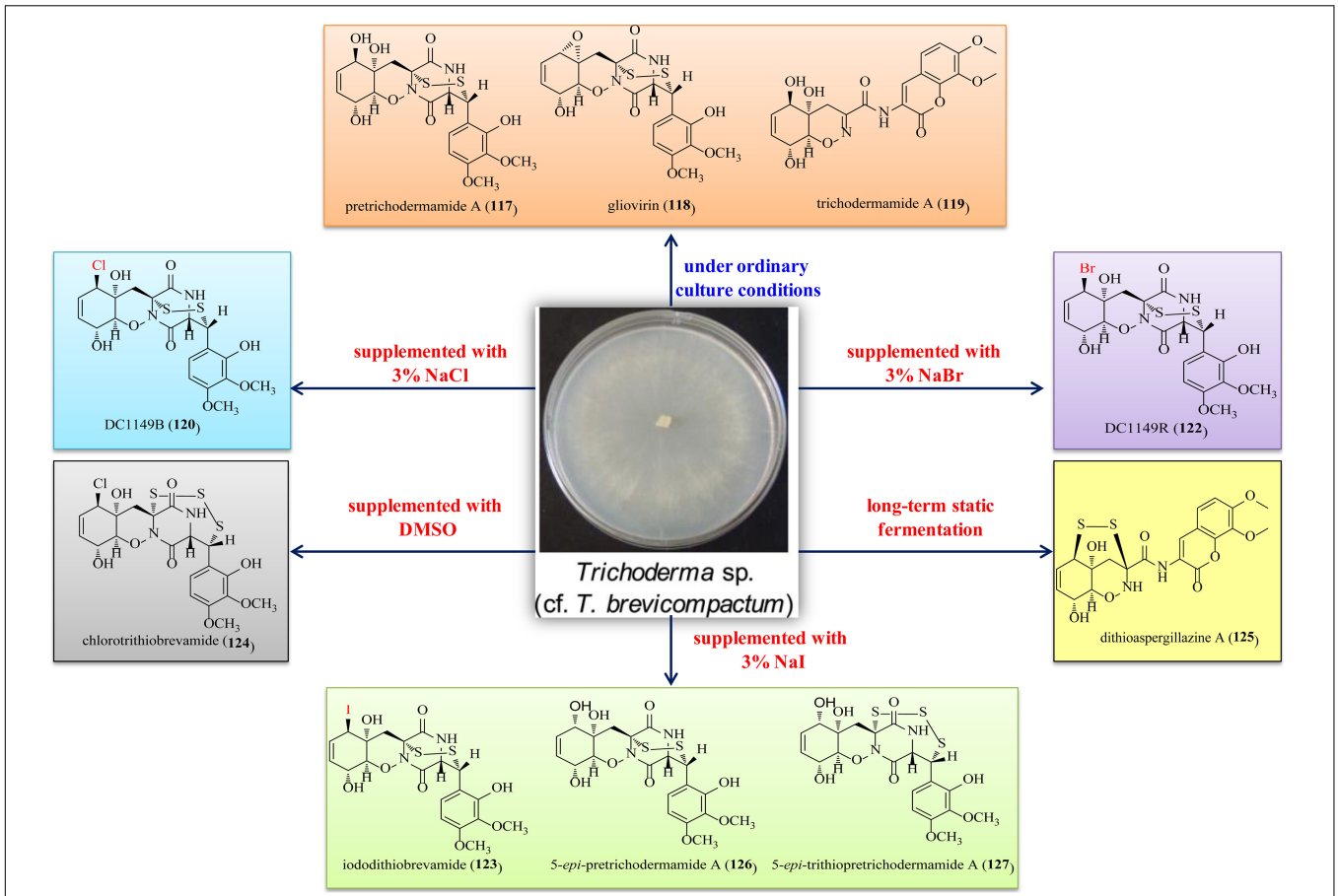

FIGURE 12 | Diketopiperazines produced by *Trichoderma* sp. TPU199 under different conditions.

cleistanthane diterpenoids isolated from *Trichoderma* species. This study provided solid example to show that it is efficient to activate the silent genes of *Trichoderma* species by chemical epigenetic manipulation.

The transcriptional control has also proven to be an effective approach. To activate the chemical potential of the endophytic fungus *T. afroharzianum*, a *laeA*-like gene overexpression transformant was built (Ding et al., 2020). Further chemical investigation of this transformant successfully yielded two new antifungal polyketides (**189** and **190**). This study indicated that transcriptional control could be a considerable strategy in activating more secondary metabolites and enhancing the silent potential metabolism of *Trichoderma* species.

BIOLOGICAL ACTIVITIES

The producing fungus, environmental source, and bioactivities of compounds **1**–**203** are listed in **Table 1**. As shown in **Table 1**, most compounds possess various moderate to potent biological activities. Among them, antimicrobial, antimicroalgal, and anticancer activities represent dominant bioactivities to assess the pharmacological potential of these natural products. Detailed descriptions of these metabolites with promising biological activities are described as follows.

Antimicrobial Activities

Isolated trichothecene derivatives **1**–**14** were assayed for antifungal activity against *Botrytis cinerea*, *Cochliobolus miyabeanus*, *Fusarium oxysporum* f. sp. *cucumerium*, *F. oxysporum* f. sp. *niveum*, and *Phomopsis asparagi* (Shi Z.Z. et al., 2020). Compounds **1**–**3** and **9**–**11** displayed promising antifungal activity with MICs of 4.0–64 μg/mL. Among them, **10** was the most active, while compounds **4**, **5**, **8**, and **12**–**14** were inactive. Structure–activity relationships (SAR) among these trichothecenes indicated that the acetoxy and methyl functionalities (compound **10**) were necessary, while the epoxide moiety and the ether linkage were other possibilities (Shi Z.Z. et al., 2020). Compounds **15**–**17** showed antifungal activities against *Candida albicans* and *Cryptococcus neoformans*, with MICs of 1.6–50 μg/mL (Yamazaki et al., 2020a). In the same way, compounds **18** and **19** were active, with MICs of 6.3, 12.5, and 25 μg/mL, respectively (Yamazaki et al., 2020b). Apparently, the diene group and 2′*Z*-configuration play an important role in antifungal activities. Trichothecenes **22** and **23** showed significant activities toward the soil-borne phytopathogens *Colletotrichum*

TABLE 1 | The producing strain, environmental source, and biological activities of compounds **1**–**203**.

Compounds	Producing Strain	Environment Source	Biological Activities	References
Trichodermarins G–N (**1**–**8**), trichodermol (**9**), trichodermin (**10**), trichoderminol (**11**), trichodermarins A (**12**) and B (**13**), 2,4,12-trihydroxyapotrichothecene (**14**)	*T. brevicompactum* A-DL-9-2	Isolated from the marine red alga *Chondria tenuissima* collected from Dalian, China	Potent antifungal and antimicroalgal activities	Shi Z.Z. et al., 2020
Trichobreols A–C (**15**–**17**)	*T.* cf. *brevicompactum* TPU199	Isolated from an unidentified red alga, collected at the coral reef in Palau	Antifungal activity	Yamazaki et al., 2020a
Trichobreols D (**18**) and E (**19**)	*T.* cf. *brevicompactum* TPU199	Isolated from an unidentified red alga, collected at the coral reef in Palau	Antifungal activity	Yamazaki et al., 2020b
Harzianums A (**20**) and B (**21**)	*T. brevicompactum* (CGMCC19618)	Isolated from soil	Potent herbicidal activity	Yin et al., 2020
Trichothecinol A (**22**), 8-deoxy-trichothecin (**23**), trichothecinol B (**24**)	*T. longibrachiatum*	Isolated from the root of *Suaeda glauca*, a highly halophile plant	Potent antifungal activity	Du et al., 2020
Trichocarotins A–H (**25**–**32**), CAF-603 (**33**), trichocarane B (**34**), 7-β-hydroxy CAF-603 (**35**), trichocarane A (**36**), trichocadinin A (**37**)	*T. virens* Y13-3	Isolated from the surface of the marine red alga *Gracilaria vermiculophylla* collected from Yantai, China	Potent antimicroalgal activity	Shi et al., 2018a
Trichodermaloids A–C (**38**–**40**), aspergilloid G (**41**), rhinomilisin E (**42**), rhinomilisin G (**43**)	*Trichoderma* sp. SM 16	Isolated from a marine sponge *Dysidea* sp. collected from the Xisha Islands	Moderate anticancer activity	Cui et al., 2020
3,7,11-trihydroxy-cycloneran (**44**)	*T. harzianum* (XS-20090075)	Isolated from fresh tissue of an unidentified soft coral collected from Xisha Islands	No obvious antibacterial activity	Shi T. et al., 2020
(10*E*)-isocyclonerotriol (**45**), (10*Z*)-isocyclonerotriol (**46**)	*T. citrinoviride* A-WH-20-3	Isolated from the inner tissue of the red alga *Laurencia okamurai*	Moderate antimicroalgal activity	Liu X.H. et al., 2020
11-methoxy-9-cycloneren-3,7-diol (**47**), 9-cycloneren-3,7,11-triol (**48**), (–)-cyclonerodiol (**49**), methyl 3,7-dihydroxy-15-cycloneranate (**50**), 10-cycloneren-3,5,7-triol (**51**)	*T. harzianum* X-5	Isolated from the marine brown alga *Laminaria japonica*	Moderate to potent antimicroalgal activity	Song et al., 2018
10-cycloneren-3,5,7-triol (**51**), 10(*E*)-cyclonerotriol (**52**)	*T. longibrachiatum*	Isolated from the root of *Suaeda glauca*, a highly halophile plant	Moderate nematicidal activity	Du et al., 2020
Neomacrophorins I (**53**), II (**54**), III (**55**)	*Trichoderma* sp. 1212-03	Isolated from *Daedaleopsis tricolor* in Shirakami Mountains area	Moderate antifungal and anticancer activities	Hirose et al., 2014
3-deoxyneomacrophorin IV (**56**), 3-oxoneomacrophorin I (**57**), 3-oxoneomacrophorin II (**58**), neomacrophorin VII (**59**), 5′-epimacrophorin B (**60**), 5′-deoxyneomacrophorin IV (**61**), premacrophorin III (**62**), premacrophorindiol (**63**), premacrophorintriol-I (**64**), premacrophorintriol-II (**65**)	*Trichoderma* sp. 1212-03	Isolated from *Daedaleopsis tricolor* in Shirakami Mountains area	Moderate to potent anticancer activity	Nishiyama et al., 2019
Microsphaeropsisins B (**66**), C (**67**)	*Trichoderma* sp. 307	Isolated from the stem bark of mangrove *Clerodendrum inerme*	Weak α-glucosidase inhibitory activity	Zhang et al., 2017
8-acoren-3,11-diol (**68**), trichoacorenol (**69**), trichoacorenol B (**70**)	*T. harzianum* X-5	Isolated from the marine brown alga *L. japonica*	Moderate antimicroalgal activity	Song et al., 2018
Trichodermene A (**71**)	*T. longibrachiatum*	Isolated from the root of *Suaeda glauca*, a highly halophile plant	Potent antifungal activity	Du et al., 2020
Trichoderiols A (**72**), B (**73**)	*T. atroviride* S361	Isolated from the bark of *Cephalotaxus fortune*	Potent anti-inflammatory activity	Zheng et al., 2011
Trichocuparins A (**74**), B (**75**)	*T. brevicompactum* A-DL-9-2	Isolated from the marine red alga *Chondria tenuissima*	No obvious antifungal activity	Shi Z.Z. et al., 2020
Trichodones A (**76**), B (**77**), C (**78**)	*T. asperellum*	Isolated from the traditional Chinese medicinal plant *Panax notoginseng*	No obvious antibacterial activity	Ding et al., 2012a
Atrichodermone C (**79**)	*T. atroviride*	Isolated from the bulb of *Lycoris radiate*	No obvious anti-inflammatory and cytotoxic activities	Zhou et al., 2017

(Continued)

TABLE 1 | Continued

Compounds	Producing Strain	Environment Source	Biological Activities	References
Harzianoic acids A (**80**), B (**81**)	*T. harzianum* LZDX-32-08	Isolated from the marine sponge *Xestospongia testudinaria*	Moderate anti-HCV activity	Li et al., 2019
Harzianols F–J (**82**–**86**), 3*S*-hydroxyharzianone (**87**), harziandione (**88**), harzianol A (**89**),	*T. atroviride* B7	Isolated from the healthy flowers of *Colquhounia coccinea* var. *mollis*	Potent antibacterial activity and moderate cytotoxicity	Li W.Y. et al., 2020
Deoxytrichodermaerin (**90**)	*T. longibrachiatum* A-WH-20-2	Isolated from marine red alga *L. okamurai*	Potent antimicroalgal activity	Zou et al., 2021
Harzianone E (**91**)	*T. harzianum* (XS-20090075)	Isolated from an unidentified soft coral	Weak antibacterial activity	Shi T. et al., 2020
3*R*-hydroxy-9*R*,10*R*-dihydroharzianone (**92**)	*T. harzianum* X-5	Isolated from the marine brown alga *L. japonica*	Moderate antimicroalgal activity	Song et al., 2018
(9*R*,10*R*)-dihydro-harzianone (**93**), harzianelactone (**94**)	*Trichoderma* sp. Xy24	Isolated from mangrove plant *Xylocarpus granatum*	Moderate anticancer activity	Zhang et al., 2016
Harzianelactones A, B (**95**, **96**), harzianones A–D (**97**–**100**), harziane (**101**)	*T. harzianum* XS-20090075	Isolated from the inner part of an unidentified soft coral	Potent phytotoxicity	Zhao et al., 2019
Trichodermaerin (**102**)	*T. erinaceum* 2011F1-1	Isolated from the inner tissue of the sea star *Acanthaster planci*	No cytotoxic activity	Xie et al., 2013
Citrinovirin (**103**)	*T. citrinoviride* cf-27	Isolated from the marine brown alga	Moderate antibacterial activity	Liang et al., 2016
11*R*-methoxy-5,9,13-proharzitrien-3-ol (**104**)	*T. harzianum* X-5	Isolated from the marine brown alga *L. japonica*	Potent antimicroalgal activity	Song et al., 2018
Harzianolic acid A (**105**)	*T. harzianum* (XS-20090075)	Isolated from an unidentified soft coral	No antibacterial activity	Shi T. et al., 2020
Trichodestruxins A–D (**106**–**109**), destruxin E2 chlorohydrin (**110**), destruxin A2 (**111**)	*T. harzianum* KZ-20	Isolated from the inner tissue of fruit of *Physalis angulata* L.	Moderate to potent anticancer activity	Liu Z. et al., 2020
Homodestcardin (**112**), trichomide B (**113**), homodestruxin B (**114**)	*T. longibrachiatum*	Isolated from the root of *Suaeda glauca*	Moderate nematicidal activity	Du et al., 2020
Cyclopeptides PF1022F (**115**), halobacillin (**116**)	*T. asperellum*	Isolated from *P. notoginseng*	Weak antibacterial activity	Ding et al., 2012a
Pretrichodermamide A (**117**), gliovirin (**118**), trichodermamide A (**119**), DC1149B (**120**), DC1149R (**122**), iododithiobrevamide (**123**), chlorotrithiobrevamide (**124**), dithioaspergillazine A (**125**), 5-*epi*-pretrichodermamide A (**126**), 5-*epi*-trithiopretrichodermamide A (**127**)	*T.* cf. *brevicompactum* TPU199	Isolated from an unidentified red alga, collected at the coral reef in Palau	Untested activity	Yamazaki et al., 2020a
Pretrichodermamide G (**128**)	*T. harzianum*	Isolated from the medicinal plant *Zingiber officinale*	No obvious activity	Harwoko et al., 2021
Trichodermamide G (**129**), aspergillazin A (**130**)	*T. harzianum* D13	Isolated from the mangrove plant *Excoecaria agallocha*	Untested activity	Zhao et al., 2020
Dehydroxymethylbis(dethio)bis(methylthio) gliotoxin (**131**), (3*S*,6*R*)-6-(para-hydroxybenzyl)-1,4-dimethyl-3,6-bis(methylthio)piperazine-2,5-dione (**132**)	*T. virens* Y13-3	Isolated from the surface of the marine red alga *G vermiculophylla*	No obvious activity	Shi et al., 2018b
Cyclo(L-5-MeO-Pro-L-5-MeO-Pro) (**133**)	*T. asperellum* A-YMD-9-2	Isolated from the marine marcroalga *Gracilaria verrucosa*	No obvious activity	Song et al., 2020
Trichothioneic acid (**134**)	*T. virens* FKI-7573	Isolated from a soil sample collected in Obihiro, Japan	Potent antioxidant activity	Miyano et al., 2020
Ethyl 2-bromo-4-chloroquinoline-3-carboxylate (**135**)	*T. harzianum* (XS-20090075)	Isolated from an unidentified soft coral from the Xisha Islands	No obvious activity	Yu et al., 2021
Trichoderamides A (**136**) and B (**137**)	*T. gamsii*	Isolated from the traditional Chinese medicinal plant *P. notoginseng*	No obvious cytotoxic activity	Ding et al., 2015
Trichodins A (**138**) and B (**139**)	*Trichoderma* sp. Strain MF106	Isolated from a Greenland Sea (Fram Strait) sample	Moderate antimicrobial activity	Wu et al., 2014
Harzianic acid (**140**)	*T. harzianum* M10	Source was not given	Potent plant growth promotion activity	Vinale et al., 2013

(Continued)

TABLE 1 | Continued

Compounds	Producing Strain	Environment Source	Biological Activities	References
Atrichodermone A (**141**)	*T. atroviride*	Isolated from the bulb of *L. radiate*	No obvious anti-inflammatory and cytotoxic activities	Zhou et al., 2017
5′-acetoxy-deoxycyclonerin B (**142**), 5′-acetoxy-deoxycyclonerin D (**143**)	*T. asperellum* A-YMD-9-2	Isolated from the marine marcroalga *G. verrucosa*	No obvious activity	Song et al., 2020
Trichoharzin B (**144**), methyl-trichoharzin (**145**), trichoharzin (**146**), eujavanicol A (**147**)	*T. harzianum* (XS-20090075)	Isolated from an unidentified soft coral from the Xisha Islands	Moderate antifouling activity	Yu et al., 2021
Trichoharzianol (**148**)	*T. harzianum* F031	Isolated from soil collected in Suphanburi, Thailand	Moderate antifungal activity	Jeerapong et al., 2015
Trichodermic acid A (**149**), trichodermic acid B (**150**)	*T. spirale*	Isolated from the medicinal plant *Aquilaria sinensis*	Untested activity	Li et al., 2012
ent-koninginin A (**151**), 1,6-di-*epi*-koninginin A (**152**), 15-hydroxykoninginin A (**153**), 10-deacetylkoningiopisin D (**154**), koninginin T (**155**), koninginin L (**156**), trichoketide A (**157**)	*T. koningiopsis* QA-3	Isolated from the inner tissue of *Artemisia argyi* that was collected from Qichun, China	Moderate antibacterial activity	Shi et al., 2017
Koninginins I (**158**), J (**159**) and K (**160**)	*T. neokongii* 8722	Source was not given	No obvious antifungal activity	Zhou et al., 2014
7-*O*-methylkoninginin D (**161**), trichodermaketones A–D (**162**–**165**)	*T. koningii*	Isolated from marine mud of the South China Sea	No obvious antifungal activity	Song et al., 2010
Trichoketides A (**166**) and B (**167**)	*Trichoderma* sp. TPU1237	Isolated from a seawater sample collected at Aomori, Japan	Moderate PTP1B inhibitory activity	Yamazaki et al., 2015
Koninginins L (**156**) and M (**168**)	*T. koningii* 8662	Source was not given	No obvious antifungal activity	Lang et al., 2015
Trichoderones A (**169**) and B (**170**), aspochalasins D (**171**), J (**172**), I (**173**)	*T. gamsii*	Isolated from the medicinal plant *P. notoginseng*	Moderate cytotoxic activity	Ding et al., 2012c
Trichalasins C (**174**), D (**175**), aspochalasins D (**171**), M (**176**), P (**177**)	*T. gamsii*	Isolated from the medicinal plant *P. notoginseng*	Moderate cytotoxic activity	Ding et al., 2012b
Atrichodermone B (**178**)	*T. atroviride*	Isolated from the bulb of *Lycoris radiate*	No obvious anti-inflammatory and cytotoxic activities	Zhou et al., 2017
5-hydroxycyclopeni cillone (**179**)	*Trichoderma* sp. HPQJ-34	Isolated from the sponge *Hymeniacidon perleve* collected from Dongji Island.	Moderate antioxidative, anti-Aβ fibrillization and neuroprotective activities	Fang et al., 2017
Xylogibloactones A (**180**) and B (**181**)	*T. harzianum* (XS-20090075)	Isolated from an unidentified soft coral from the Xisha Islands	No obvious activity	Yu et al., 2021
Trichoderpyrone (**182**)	*T. gamsii*	Isolated from the medicinal plant *P. notoginseng*	Weak cytotoxic activity	Chen et al., 2017
Trichoderone (**183**)	*Trichoderma* sp. GIBH-Mf082	Isolated from marine sediment in the South China Sea	Potent anticancer activity	You et al., 2010
184 and **185**	*T. harzianum* Fes1712	Isolated from *Ficus elastica* leaves	Moderate antibacterial activity	Ding et al., 2019
Trichophenol A (**186**)	*T. citrinoviride* A-WH-20-3	Isolated from the red alga *L. okamurai*	Moderate antimicroalgal activity	Liu X.H. et al., 2020
5-hydroxy-3-hydroxymethyl-2-methyl-7-methoxychromone (**187**), 4,6-dihydroxy-5-methylphthalide (**188**)	*T. harzianum* F031	Isolated from soil collected in Suphanburi, Thailand	No obvious antifungal activity	Jeerapong et al., 2015
(*R*,3*E*,5*E*)-1-(3,5-dihydroxy-2,4-dimethylphenyl)-1-hydroxyhepta-3,5-dien-2-one (**189**), (*R*,*3E*,*5E*)-1-(3,5-dihydroxy-2,4-dimethylphenyl)-1-methoxyhepta-3,5-dien-2-one (**190**)	*T. afroharzianum* Fes1712	Isolated from fresh leaves of *F. elastica*	Moderate antifungal activity	Ding et al., 2020
Azaphilones D (**191**) and E (**192**)	*T. harzianum* QTYC77	Isolated from the intestine of *Pantala flavescens*	Moderate antibacterial activity	Zhang S. et al., 2020
Cremenolide (**193**)	*T. cremeum* 506	Isolated from decaying wood in Central Poland	Potent antifungal and plant growth promotion activity	Vinale et al., 2016

(Continued)

TABLE 1 | Continued

Compounds	Producing Strain	Environment Source	Biological Activities	References
(3*R*,7*R*)-7-hydroxy-de-*O*-methyllasiodiplodin (**194**), (3*R*)-5-oxo-de-*O*-methyllasiodiplodin (**195**)	*Trichoderma* sp. 307	Isolated from the stem bark of mangrove *C. inerme*	Potent α-glucosidase inhibitory activity	Zhang et al., 2017
Nafuredin C (**196**), nafuredin A (**197**)	*T. harzianum* D13	Isolated from the mangrove plant *E. agallocha*	Moderate antifungal activity	Zhao et al., 2020
Thioporidiols A (**198**), B (**199**)	*T. polypori* FKI-7382	Isolated from a sediment sample collected at Omuta city	Moderate antibacterial activity	Matsuo et al., 2020
Violaceol I (**200**), Violaceol II (**201**)	*T. polyalthiae*	Source was not given	Moderate antimicrobial activity	Nuankeaw et al., 2020
Trichodenols A (**202**), B (**203**)	*T. gamsii*	Isolated from the traditional Chinese medicinal plant *P. notoginseng*	No obvious cytotoxic activity	Ding et al., 2015

The bold values are compounds numbers.

lagenarium with an MIC value of 16 μg/mL, which was stronger than that of the positive control carbendazim (MIC, 32 μg/mL) (Du et al., 2020). Furthermore, both of them showed potency against carbendazim-resistant *B. cinerea*. In contrast, compared to those of **22** and **23**, trichothecene congener **24** only showed weak effects, indicating that the hydroxyl substituted in **23** may enhance its antifungal activity. Trichothecenes are reported to possess promising antifungal, phytotoxic and cytotoxic activities. *Trichoderma*-derived trichothecenes were mainly focused on their antifungal activity in the literature above, which highlighted their potential as biocontrol agents. Drimane sesquiterpenes **53**–**55** were active against *C. miyabeanus* by inducing hyphal branching at 1.0 and 10 μg/mL (Hirose et al., 2014). The novel norsesquiterpene **71** showed potent ability against *C. lagrnarium* with an MIC of 8 μg/mL (Du et al., 2020). The new harziane diterpene harzianol I (**85**) exhibited potent effect on *Staphylococcus aureus*, *Bacillus subtilis*, and *Micrococcus luteus*, with EC_{50}s of 7.7, 7.7, and 9.9 μg/mL, respectively (Li W.Y. et al., 2020). It seemed that substitutions at C-2 and/or C-3 of harzianes may decrease their antibacterial activity. The novel norditerpene **103** inhibited *S. aureus* with an MIC of 12.4 μg/mL (Liang et al., 2016). Cyclopeptides **115** and **116** displayed weak ability against *Enterococcus faecium* with IC_{50}s of 7.30 and 5.24 μM and against *S. aureus* with IC_{50}s of 19.02 and 14.00 μM, respectively (Ding et al., 2012a). The new pyridine trichodin A (**138**) was active against *B. subtilis* (IC_{50}, 27.05 μM), *Staphylococcus epidermidis* (24.28 μM), and *C. albicans* (25.38 μM) (Wu et al., 2014). Trichoharzianol (**148**) displayed mild activity against *Colletotrichum gloeosporioides*, with an MIC value of 128 μg/mL (Jeerapong et al., 2015). Polyketides **151** and **157** showed moderate activity against *Escherichia coli*, *Edwardsiella tarda*, *Vibrio anguillarum*, and *Vibrio parahaemolyticus*, with MICs of 8–64 μg/mL (Shi et al., 2017). Trichodermaketone A (**162**) was inactive against *C. albicans* (MIC > 125 μg/mL). However, it was active at 125 μg/mL when treated with 0.05 μg/mL ketoconazole (Song et al., 2010). New isocoumarins **184** and **185** exhibited growth inhibitory activity against *E. coli* with an MIC of 32 μg/mL (Ding et al., 2019). Polyketides **189** and **190** exhibited selective antifungal activity toward *B. cinerea*, *F. oxysporum*, and *C. lagenarium*, with MICs of 8–32 μg/mL (Ding et al., 2020). The new azaphilone **191** displayed moderate effect on *S. aureus* and *B. subtilis* with disc diameters of the zone of inhibition of 7.3 and 7.0 mm (Zhang S. et al., 2020). The new 10-membered lactone **193** significantly inhibited *F. oxysporum*, *B. cinerea*, and *Rhizoctonia solani* (Vinale et al., 2016). Nafuredins **196** and **197** showed strong activity against *Magnaporthe oryzae*, with MICs of 8.63 and 17.4 μM, respectively (Zhao et al., 2020).

Antimicroalgal Activities

The antimicroalgal activity against marine phytoplankton (*Amphidinium carterae*, *Heterocapsa circularisquama*, *Heterosigma akashiwo*, and *Prorocentrum donghaiense*) of trichothecene derivatives **1**–**14** was evaluated. Notably, **10** featured the strongest effect, with IC_{50}s of 1.7, 0.82, 0.91, and 1.4 μg/mL (Shi Z.Z. et al., 2020). Carotane sesquiterpenes **27**–**29**, **32**, and **36** exhibited strong activity against several phytoplankton, with IC_{50}s of 0.24–1.2 μg/mL (Shi et al., 2018a). Proposed SAR study indicated that the carbonyl, hydroxyl, and the epoxy moiety play an important role in the antimicroalgal potency of carotenes. The cyclonerane sesquiterpene **45** was more active against *Karlodinium veneficum* than **46**, with an IC_{50} of 8.1 μg/mL (Liu X.H. et al., 2020). It is interesting that, compared to their isomerized derivatives (10*E*)- and (10*Z*)-cyclonerotriol, the isomerization of the five-membered ring greatly suppressed their antimicroalgal activities (Liu X.H. et al., 2020). Cycloneranes **47**–**51** exhibited moderate to potent growth inhibition against (*Chattonella marina*, *H. akashiwo*, *K. veneficum*, and *P. donghaiense* with low μg/mL range (Song et al., 2018). Compound **47** potently inhibited *C. marina* with an IC_{50} of 0.66 μg/mL. The new acorane sesquiterpene **68** exhibited mild growth inhibition of *C. marina* (IC_{50}, 2.8 μg/mL), while the new proharziane diterpene **104** potently inhibited with IC_{50}s of 1.2–4.3 μg/mL (Song et al., 2018). Additionally, the new harziane lactone **90** possessed potent activity, with IC_{50}s of 0.53–2.7 μg/mL (Zou et al., 2021). The new isocoumarin **186** was active against *C. marina* (IC_{50}, 4.4 μg/mL), *H. akashiwo* (9.1 μg/mL), and *P. donghaiense* (5.9 μg/mL) (Liu X.H. et al., 2020).

Anticancer Activities

The cytotoxicities of cadinane sesquiterpenes **38**–**43** were evaluated against NCIH-460, NCI-H929, and SW620 cell lines (Cui et al., 2020). In contrast to the known compounds **41**–**43**,

the newly reported sesquiterpenes **38**–**40** showed more potent cytotoxicities, with IC_{50}s of 6.8–12.7 μM. Neomacrophorin I (**53**) showed cytotoxicity against human adenocarcinoma cells (COLO 201) with an IC_{50} of 46 μg/mL (Hirose et al., 2014). Neomacrophorins **56** and **61** were cytotoxic toward COLO 201 with IC_{50}s of 20.5 and 18.2 μg/mL, respectively (Nishiyama et al., 2019). From a structural point of view, the common substructure of 2′-cyclohexene-1′,4′-dione was critical for cytotoxicity. The new harziane diterpene harzianol I (**85**) was observed to exhibit moderate cytotoxicity against NCI-H1975 (IC_{50}, 58.72 μM), HepG2 (60.88 μM), and MCF-7 (53.92 μM) cell lines (Li W.Y. et al., 2020). **93** showed selective cytotoxicity toward HeLa and MCF-7, with IC_{50}s of 30.1 and 30.7 μM, respectively (Zhang et al., 2016). Cyclodepsipeptides **106**–**111** were active on HT-29, A549, and P388, with IC_{50}s of 0.7–19.1 μM (Liu Z. et al., 2020). Cytochalasans **171** and **172** showed cytotoxicity on HeLa with IC_{50}s of 5.72 and 27.4 μM, respectively, whereas **169**, **170**, and **173**–**177** were inactive (IC_{50} > 40.0 μM) (Ding et al., 2012b,c). The rare polyketide **182** displayed weak only cytotoxic activity toward A549 (IC_{50}, 16.9 μM), HepG2 (30.8 μM), and HeLa (33.9 μM) (Chen et al., 2017). Cyclopentenone **183** displayed potent cytotoxicities against A549, NCI-H460, MCF-7, MDA-MB-435, HeLa, and DU-145, whereas it was inactive toward the normal human lung fibroblast cell line (You et al., 2010). The selectivity index was more than 100, which was even more remarkable than that of cisplatin.

Phytotoxic Activities

In phytotoxicity assays, harzianums A (**20**) and B (**21**) decreased the shoot and root lengths of the dicot species *Brassica chinensis* and induced inhibitory effect of seed germination at 2 μg/mL (Yin et al., 2020). Moreover, **20** and **21** showed phytotoxicity against monocots, *Oryza sativa* and *Echinochloa crusgalli*, compared with the positive control 2,4-dichlorophenoxyacetic acid (a chlorophenoxy herbicide most commonly used worldwide). The results indicated that **20** and **21** possess potent herbicidal potential for dicotyledon and/or monocotyledon weeds. All of the isolated harzianes **95**–**101** exhibited potent phytotoxicity at 200 ppm (Zhao et al., 2019).

Other Activities

Cyclonerane sesquiterpenes **51** and **52** exhibited certain nematicidal activity against *Meloidogyne incognita*, with second-stage juvenile (J2s) lethal rates of 38.2 and 42.7% at 200 μg/mL (Du et al., 2020). Cyclodepsipeptides **112**–**114** also showed nematicidal activity against *M. incognita* (Du et al., 2020). New sesquiterpenes **72** and **73** showed potent NO scavenging effects, with IC_{50}s of 15.3 and 9.1 μM, respectively (Zheng et al., 2011). Harzianoic acids **80** and **81** exerted potency to decrease the HCV RNA with EC_{50}s of 24.5 and 20.4 μM, respectively (Li et al., 2019). Trichothioneic acid (**134**) showed OH radical-scavenging and singlet oxygen-quenching ability in a dose-dependent manner, which was equivalent to those of positive controls (Miyano et al., 2020). The activity of harzianic acid (**140**) as a plant growth promoter was evaluated (Vinale et al., 2013). Treatment with 100 or 10 μM **140** significantly affected seed germination at 4 and 5 times stronger than that of the blank control. Naphthalene derivatives **145** and **147** showed moderate antifouling potency with EC_{50}s of 29.8 and 35.6 μg/mL, respectively (Yu et al., 2021). The new de-*O*-methyllasiodiplodin **194** and **195** showed strong α-glucosidase inhibitory activity with IC_{50}s of 25.8 and 54.6 μM, respectively, which were higher than acarbose (703.8 μM) (Zhang et al., 2017).

SUMMARY OF THE STUDIES

Chemical Structures

A total of 203 natural products were reported from *Trichoderma* from 2009–2020. Their chemical structures were classified into terpenoids (**1**–**24** for trichothecene sesquiterpenes, **25**–**36** for carotane sesquiterpenes, **37**–**43** for cadinane sesquiterpenes, **44**–**52** for cyclonerane sesquiterpenes, **53**–**65** for drimane sesquiterpenes, **66**–**81** for other sesquiterpenes, **82**–**102** for harziane diterpenes, and **103**–**105** for other diterpenes), cyclopeptides (**104**–**116**), diketopiperazines (**117**–**133**), alkaloids and other nitrogen-containing compounds (**134**–**143**), polyketides (**144**–**150** for naphthalene derivatives, **151**–**168** for octaketides, **169**–**177** for cytochalasans, and **178**–**197** for other polyketides), and other compounds (**198**–**203**) according to their putative biogenetic sources. As shown in **Figure 13A**, 39.9% of the metabolites reported were sesquiterpenes, followed by polyketides with 26.6%. Taking diterpenes into account, terpenoids accounted for 51.72% of the obtained compounds, which indicated that species belonging to *Trichoderma* are considerable producing strains of novel terpenoids. It should be pointed out that some terpenoids, such as harzianes, are isolated exclusively from *Trichoderma* species. This review described 21 harziane diterpenes produced by *Trichoderma*. Considering their intriguing structures and bioactivities, much more attention should be devoted to this type of terpenoid in subsequent chemical studies.

Producing Strains

The genus *Trichoderma* comprises more than 340 species. Some of them are used as biocontrol agents, while some of them are promising producers of enzymes for industrial purposes. On the other hand, some *Trichoderma* species possess the unique capacity to synthesize various secondary metabolites with potent biological activities. In this review, a total of 17 identified species, including *T. harzianum*, *T. brevicompactum*, *T. virens*, *T. gamsii*, *T. atroviride*, *T. longibrachiatum*, *T. asperellum*, *T. koningiopsis*, *T. koningii*, *T. citrinoviride*, *T. neokongii*, *T. spirale*, *T. afroharzianum*, *T. polypore*, *T. polyalthiae*, *T. erinaceum*, and *T. cremeum*, are reported as the producing strains of the described metabolites. Among them, *T. harzianum* and *T. brevicompactum* were the most prolific strains, with 48 (23.76%) and 33 (16.34%) metabolites identified, respectively (**Figure 13B**). The fungus *T. harzianum* is famous for widely used biocontrol agents, and it is also considered to be a promising producer of bioactive metabolic products. *T. brevicompactum* can synthesize trichothecene-type sesquiterpenoids with potent antifungal activity and high biotechnological value. Twenty-one

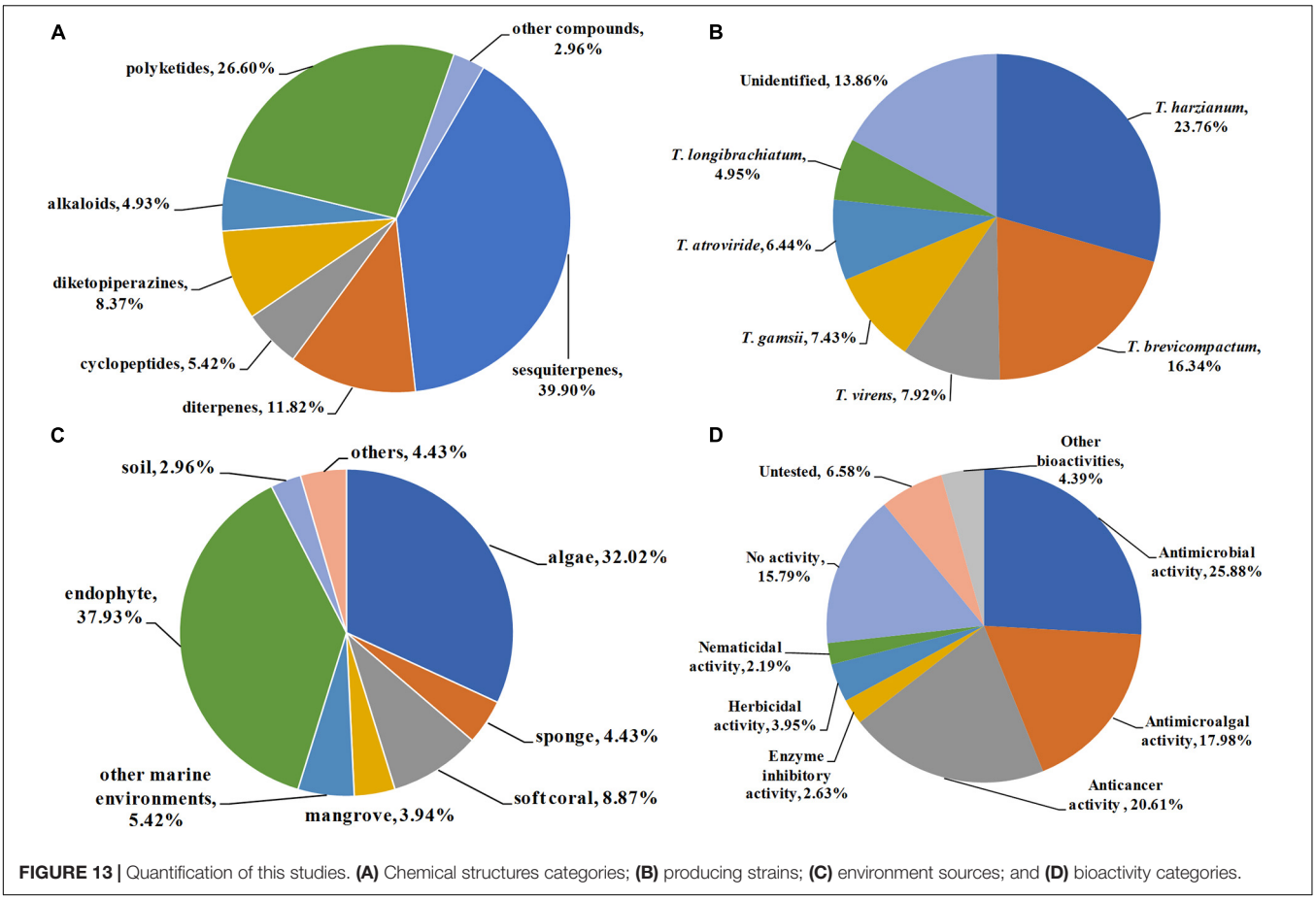

FIGURE 13 | Quantification of this studies. **(A)** Chemical structures categories; **(B)** producing strains; **(C)** environment sources; and **(D)** bioactivity categories.

novel trichothecenes (**1**–**21**) have been characterized from *T. brevicompactum*.

Environment Sources

The genus *Trichoderma* is widely distributed and has been isolated in soils, decaying wood, and endophytes in the inner tissue of host plants. Previous studies have mainly focused on terrestrial species of *Trichoderma*. However, *Trichoderma* from the marine environment are unexploited. It would be useful to examine marine-derived *Trichoderma* species since they may be induced to produce specific metabolites in hyperhaline environments. Accordingly, in recent years, increasing attention has been devoted to marine *Trichoderma*. As shown in **Figure 13C**, a total of 54.7% producing fungus were obtained from marine environments, including algae (32.02%), sponges (4.43%), soft corals (8.87), mangroves (3.94%), and other marine environments (5.42%, seawater, sediments), with 111 compounds characterized. Moreover, some fungi are obtained as endophytes from medicinal plants. Endophytic fungi, which harmoniously live in the inner tissues of their hosts without causing apparent diseases, are considered to be prolific sources of novel metabolites with remarkable pharmacological activities. It is estimated that 37.97% of these compounds were isolated from endophytic *Trichoderma*. From the above analysis, it can be concluded that marine environment and endophytes are more abundant sources of those productive strains.

Biological Activities

As discussed above, most of the presented compounds possess considerable biological activities, such as antimicrobial, antimicroalgal, anticancer, enzyme inhibitory, herbicidal, and nematicidal activities. Among them, antimicrobial (25.88%), anticancer (20.61%), and antimicroalgal (17.98%) activities were dominant in assessing the pharmacological potential of these metabolites (**Figure 13D**). It should be pointed out that a high proportion (73.40%) of the presented metabolites showed moderate to potent bioactivities. Even more importantly, a large number of them exhibit potent activities, which are higher than those of positive controls. For example, trichothecenes **22** and **23** showed higher antifungal effect on *C. lagrnarium* (MIC, 16 μg/mL) than the synthetic fungicide carbendazim (MIC, 32 μg/mL) (Du et al., 2020). Cyclopentenone **183** displayed potent cytotoxicities, whereas it was inactive toward the normal lung cell line (You et al., 2010). The selectivity index was even more remarkable than that of cisplatin, indicating **183** has high selective toxicity to cancer cell lines. Sesquiterpenes **72** and **73** showed potent NO scavenging effects (Zheng et al., 2011). These impressive bioactivities indicate that many of these compounds could be used as potential candidates for new drug discovery.

CONCLUSION

In the present review, we offer a detailed summary of recently isolated metabolites from *Trichoderma* from the beginning of 2009 to the end of 2020. As a result, a total of 203 metabolites are described herein, including their structural diversity and biological activities. Moreover, new strategies for discovering secondary metabolites of *Trichoderma* in recent years have also been discussed. *Trichoderma* has proven to be a treasure house of interesting secondary metabolites with medicinal importance. The biochemical studies of *Trichoderma* are untapped. Although a mass of metabolites have been isolated from *Trichoderma* species, the further excavation of those metabolites is worth expecting. By using new approaches to activate their silent gene clusters, including cultivation-based approaches, metabolomic profiling, and genome mining-based molecular approaches, an ever-increasing number of bioactive compounds will be obtained, which will be beneficial for the new drug discovery in the near future.

AUTHOR CONTRIBUTIONS

J-LZ and W-LT wrote this manuscript. Q-RH, Y-ZL, M-LW, L-LJ, CL, XY, H-WZ, and G-ZC collected and reorganized the literature data. X-XZ supervised the research work and revised the manuscript. All authors reviewed the manuscript.

FUNDING

This work was financially supported by the National Key Research and Development Program of China (Grant Nos. 2016YFD0501010, 2017YFD0500806, and 2018YFD0501402), the Major Agricultural Applied Technological Innovation Projects of Shandong Province (to X-XZ), the Key Research and Development Plan of Yantai (Nos. 2020XDRH101, 2021YT06000060, 2021YT06000636, and 2018XSCC045), the Natural Science Foundation of Shandong Province (Nos. ZR201911120018 and ZR2014HL061), the Yantai Research Institute for Replacing Old Growth Drivers with New Ones (Grant No. 2020XJDN001), and the Innovation Team Project for Modern Agricultural Industrious Technology System of Shandong Province (SDAIT-11-10).

SUPPLEMENTARY MATERIAL

The Supplementary Material for this article can be found online at: https://www.frontiersin.org/articles/10.3389/fmicb.2021.723828/full#supplementary-material

REFERENCES

Bhardwaj, N., and Kumar, J. (2017). Characterization of volatile secondary metabolites from *Trichoderma asperellum*. *J. Appl. Nat. Sci.* 9, 954–959. doi: 10.31018/jans.v9i2.1303

Cai, F., Yu, G., Wang, P., Wei, Z., Fu, L., Shen, Q., et al. (2013). Harzianolide, a novel plant growth regulator and systemic resistance elicitor from *Trichoderma harzianum*. *Plant Physiol. Biochem.* 73, 106–113. doi: 10.1016/j.plaphy.2013.08.011

Chen, L., Niu, S. B., Li, L., Ding, G., Yu, M., Zhang, G. S., et al. (2017). Trichoderpyrone, a unique polyketide hybrid with a cyclopentenone-pyrone skeleton from the plant endophytic fungus *Trichoderma gamsii*. *J. Nat. Prod.* 80, 1944–1947. doi: 10.1021/acs.jnatprod.7b00190

Cui, J., Shang, R. Y., Sun, M., Li, Y. X., Liu, H. Y., Lin, H. W., et al. (2020). Trichodermaloids A-C, cadinane sesquiterpenes from a marine sponge symbiotic *Trichoderma* sp. SM16 fungus. *Chem. Biodivers.* 17:e2000036. doi: 10.1002/cbdv.202000036

Ding, G., Chen, A. J., Lan, J., Zhang, H., Chen, X., Liu, X., et al. (2012a). Sesquiterpenes and cyclopeptides from the endophytic fungus *Trichoderma asperellum* SAMUELS, LIECKF. & NIRENBERG. *Chem. Biodivers.* 9, 1205–1212. doi: 10.1002/cbdv.201100185

Ding, G., Chen, L., Chen, A., Tian, X., Chen, X., Zhang, H., et al. (2012b). Trichalasins C and D from the plant endophytic fungus *Trichoderma gamsii*. *Fitoterapia* 83, 541–544. doi: 10.1016/j.fitote.2011.12.021

Ding, G., Wang, H., Li, L., Chen, A. J., Chen, L., Chen, H., et al. (2012c). Trichoderones A and B: two pentacyclic cytochalasans from the plant endophytic fungus *Trichoderma gamsii*. *Eur. J. Org. Chem.* 2012, 2516–2519. doi: 10.1002/ejoc.201200053

Ding, G., Chen, L., Zhou, C., Hong-Mei, J., Liu, Y. T., Chang, X., et al. (2015). Trichoderamides A and B, a pair of stereoisomers from the plant endophytic fungus *Trichoderma gamsii*. *J. Antibiot.* 68, 409–413. doi: 10.1038/ja.2015.1

Ding, Z., Tao, T., Wang, L., Zhao, Y., Huang, H., Zhang, D., et al. (2019). Bioprospecting of novel and bioactive metabolites from endophytic fungi isolated from rubber tree ficus elastica leaves. *J. Microbiol. Biotechnol.* 29, 731–738. doi: 10.4014/jmb.1901.01015

Ding, Z., Wang, X., Kong, F. D., Huang, H. M., Zhao, Y. N., Liu, M., et al. (2020). Overexpression of global regulator talae1 leads to the discovery of new antifungal polyketides from endophytic fungus *Trichoderma afroharzianum*. *Front. Microbiol.* 11:622785. doi: 10.3389/fmicb.2020.622785

Du, F. Y., Ju, G. L., Xiao, L., Zhou, Y. M., and Wu, X. (2020). Sesquiterpenes and cyclodepsipeptides from marine-derived fungus *Trichoderma longibrachiatum* and their antagonistic activities against soil-borne pathogens. *Mar. Drugs* 18:165. doi: 10.3390/md18030165

Fang, F., Zhao, J., Ding, L., Huang, C., Naman, C. B., He, S., et al. (2017). 5-hydroxycyclopenicillone, a new β-amyloid fibrillization inhibitor from a sponge-derived fungus *Trichoderma* sp. HPQJ-34. *Mar. Drugs* 15:260. doi: 10.3390/md15080260

Fleming, A. (1929). On the antibacterial action of cultures of a *Penicillium*, with special reference to their use in the isolation of *B. influenzae*. *Br. J. Exp. Pathol.* 10, 226–236.

Frisvad, J. C. (2014). Taxonomy, chemodiversity, and chemoconsistency of *Aspergillus*, *Penicillium*, and *Talaromyces* species. *Front. Microbiol.* 5:773. doi: 10.3389/fmicb.2014.00773

Harwoko, H., Daletos, G., Stuhldreier, F., Lee, J., Wesselborg, S., Feldbrügge, M., et al. (2021). Dithiodiketopiperazine derivatives from endophytic fungi *Trichoderma harzianum* and *Epicoccum nigrum*. *Nat. Prod. Res.* 35, 257–265. doi: 10.1080/14786419.2019.1627348

Hirose, A., Maeda, H., Tonouchi, A., Nehira, T., and Hashimoto, M. (2014). Neomacrophorin I, II, and III, novel drimenyl cyclohexanes with hydroxylated butanoates from *Trichoderma* sp. 1212-03. *Tetrahedron* 70, 1458–1463. doi: 10.1016/j.tet.2013.12.087

Jeerapong, C., Phupong, W., Bangrak, P., Intana, W., and Tuchinda, P. (2015). Trichoharzianol, a new antifungal from *Trichoderma harzianum* F031. *J. Agric. Food Chem.* 63, 3704–3708. doi: 10.1021/acs.jafc.5b01258

Keswani, C., Mishra, S., Sarma, B. K., Singh, S. P., and Singh, H. B. (2014). Unraveling the efficient applications of secondary metabolites of various *Trichoderma* spp. *Appl. Microbiol. Biotechnol.* 98, 533–544. doi: 10.1007/s00253-013-5344-5

Khan, R. A., Najeeb, S., Hussain, S., Xie, B., and Li, Y. (2020). Bioactive secondary metabolites from *Trichoderma* spp. against

phytopathogenic fungi. *Microorganisms* 8:817. doi: 10.3390/microorganisms8060817

Lang, B. Y., Li, J., Zhou, X. X., Chen, Y. H., Yang, Y. H., Li, X. N., et al. (2015). Koninginins L and M, two polyketides from *Trichoderma koningii* 8662. *Phytochem. Lett.* 11, 1–4. doi: 10.1016/j.phytol.2014.10.031

Li, B., Li, L., Peng, Z., Liu, D., Si, L., Wang, J., et al. (2019). Harzianoic acids A and B, new natural scaffolds with inhibitory effects against hepatitis C virus. *Bioorg. Med. Chem.* 27, 560–567. doi: 10.1016/j.bmc.2018.12.038

Li, D. L., Chen, Y. C., Tao, M. H., Li, H. H., and Zhang, W. M. (2012). Two new octahydronaphthalene derivatives from *Trichoderma spirale*, an endophytic fungus derived from *Aquilaria sinensis*. *Helv. Chim. Acta* 95, 805–809. doi: 10.1002/hlca.201100417

Li, W. Y., Liu, Y., Lin, Y. T., Liu, Y. C., Guo, K., Li, X. N., et al. (2020). Antibacterial harziane diterpenoids from a fungal symbiont *Trichoderma atroviride* isolated from *Colquhounia coccinea* var. mollis. *Phytochemistry* 170:112198. doi: 10.1016/j.phytochem.2019.112198

Li, X. Q., Xu, K., Liu, X. M., and Zhang, P. (2020). A systematic review on secondary metabolites of paecilomyces species: chemical diversity and biological activity. *Planta Med.* 86, 805–821. doi: 10.1055/a-1196-1906

Liang, X. R., Miao, F. P., Song, Y. P., Liu, X. H., and Ji, N. Y. (2016). Citrinovirin with a new norditerpene skeleton from the marine algicolous fungus *Trichoderma citrinoviride*. *Bioorg. Med. Chem. Lett.* 26, 5029–5031. doi: 10.1016/j.bmcl.2016.08.093

Liu, X. H., Hou, X. L., Song, Y. P., Wang, B. G., and Ji, N. Y. (2020). Cyclonerane sesquiterpenes and an isocoumarin derivative from the marine-alga-endophytic fungus *Trichoderma citrinoviride* A-WH-20-3. *Fitoterapia* 141:104469. doi: 10.1016/j.fitote.2020.104469

Liu, Z., Sun, Y., Tang, M., Sun, P., Wang, A., Hao, Y., et al. (2020). Trichodestruxins A-D: cytotoxic cyclodepsipeptides from the endophytic fungus *Trichoderma harzianum*. *J. Nat. Prod.* 83, 3635–3641. doi: 10.1021/acs.jnatprod.0c00808

Matsuo, H., Noguchi, Y., Miyano, R., Higo, M., Nonaka, K., Sunazuka, T., et al. (2020). Thioporidiols A and B: two new sulfur compounds discovered by molybdenum-catalyzed oxidation screening from *Trichoderma polypori* FKI-7382. *Antibiotics* 9:236. doi: 10.3390/antibiotics9050236

McMullin, D. R., Renaud, J. B., Barasubiye, T., Sumarah, M. W., and Miller, J. D. (2017). Metabolites of *Trichoderma* species isolated from damp building materials. *Can. J. Microbiol.* 63, 621–632. doi: 10.1139/cjm-2017-0083

Miyano, R., Matsuo, H., Mokudai, T., Noguchi, Y., Higo, M., Nonaka, K., et al. (2020). Trichothioneic acid, a new antioxidant compound produced by the fungal strain *Trichoderma virens* FKI-7573. *J. Biosci. Bioeng.* 129, 508–513. doi: 10.1016/j.jbiosc.2019.11.007

Newman, D. J., and Cragg, G. M. (2016). Natural products as sources of new drugs from 1981 to 2014. *J. Nat. Prod.* 79, 629–661. doi: 10.1021/acs.jnatprod.5b01055

Nishiyama, M., Maeda, H., Tonouchi, A., and Hashimoto, M. (2019). Neomacrophorin and premacrophorin congeners from *Trichoderma* sp. 1212-03. *Tetrahedron* 75, 2993–3000. doi: 10.1016/j.tet.2019.04.018

Nuankeaw, K., Chaiyosang, B., Suebrasri, T., Kanokmedhakul, S., Lumyong, S., and Boonlue, S. (2020). First report of secondary metabolites, Violaceol I and Violaceol II produced by endophytic fungus, *Trichoderma polyalthiae* and their antimicrobial activity. *Mycoscience* 61, 16–21. doi: 10.1016/j.myc.2019.10.001

Persoon, C. H. (1794). Neuer Versuch einer systematischen Einteilung der Schwämme. *Racodium Römer's Neues Magazin der Botanik.* 1:123.

Reino, J. L., Guerrero, R. F., Hernández-Galán, R., and Collado, I. G. (2008). Secondary metabolites from species of the biocontrol agent *Trichoderma*. *Phytochem. Rev.* 7, 89–123. doi: 10.1007/s11101-006-9032-2

Ren, H., Wang, B., and Zhao, H. (2017). Breaking the silence: new strategies for discovering novel natural products. *Curr. Opin. Biotechnol.* 48, 21–27. doi: 10.1016/j.copbio.2017.02.008

Shi, T., Shao, C. L., Liu, Y., Zhao, D. L., Cao, F., Fu, X. M., et al. (2020). Terpenoids from the coral-derived fungus *Trichoderma harzianum* (XS-20090075) induced by chemical epigenetic manipulation. *Front. Microbiol.* 11:572. doi: 10.3389/fmicb.2020.00572

Shi, X. S., Wang, D. J., Li, X. M., Li, H. L., Meng, L. H., Li, X., et al. (2017). Antimicrobial polyketides from *Trichoderma koningiopsis* QA-3, an endophytic fungus obtained from the medicinal plant *Artemisia argyi*. *RSC Adv.* 7, 51335–51342. doi: 10.1039/C7RA11122C

Shi, Z. Z., Fang, S. T., Miao, F. P., Yin, X. L., and Ji, N. Y. (2018a). Trichocarotins A-H and trichocadinin A, nine sesquiterpenes from the marine-alga-epiphytic fungus *Trichoderma virens*. *Bioorg. Chem.* 81, 319–325. doi: 10.1016/j.bioorg.2018.08.027

Shi, Z. Z., Miao, F. P., Fang, S. T., Yin, X. L., and Ji, N. Y. (2018b). Sulfurated diketopiperazines from an algicolous isolate of *Trichoderma virens*. *Phytochem. Lett.* 27, 101–104. doi: 10.1016/j.phytol.2018.07.005

Shi, Z. Z., Liu, X. H., Li, X. N., and Ji, N. Y. (2020). Antifungal and antimicroalgal trichothecene sesquiterpenes from the marine algicolous fungus *Trichoderma brevicompactum* A-DL-9-2. *J. Agric. Food Chem.* 68, 15440–15448. doi: 10.1021/acs.jafc.0c05586

Song, F., Dai, H., Tong, Y., Ren, B., Chen, C., Sun, N., et al. (2010). Trichodermaketones A–D and 7-O-methylkoninginin D from the marine fungus *Trichoderma koningii*. *J. Nat. Prod.* 73, 806–810. doi: 10.1021/np900642p

Song, Y., Miao, F., Yin, X., and Ji, N. (2020). Three nitrogen-containing metabolites from an algicolous isolate of *Trichoderma asperellum*. *Mar. Life Sci. Technol.* 2, 155–160. doi: 10.1007/s42995-020-00030-6

Song, Y. P., Fang, S. T., Miao, F. P., Yin, X. L., and Ji, N. Y. (2018). Diterpenes and sesquiterpenes from the marine algicolous fungus *Trichoderma harzianum* X-5. *J. Nat. Prod.* 81, 2553–2559. doi: 10.1021/acs.jnatprod.8b00714

Takahashi-Ando, N., Matsui, K., Suzuki, T., Sadamatsu, K., Azuhata, H., Okada, A., et al. (2020). Trichothecene biosynthesis in different fungal genera: resistance mechanisms, pathway enzymes, and their product applications. *JSM Mycotoxins* 70, 67–74. doi: 10.2520/myco.70-2-3

Vinale, F., Nigro, M., Sivasithamparam, K., Flematti, G., Ghisalberti, E. L., Ruocco, M., et al. (2013). Harzianic acid: a novel siderophore from *Trichoderma harzianum*. *FEMS Microbiol. Lett.* 347, 123–129. doi: 10.1111/1574-6968.12231

Vinale, F., Strakowska, J., Mazzei, P., Piccolo, A., Marra, R., Lombardi, N., et al. (2016). Cremenolide, a new antifungal, 10-member lactone from *Trichoderma cremeum* with plant growth promotion activity. *Nat. Prod. Res.* 30, 2575–2581. doi: 10.1080/14786419.2015.1131985

Wu, B., Oesker, V., Wiese, J., Schmaljohann, R., and Imhoff, J. F. (2014). Two new antibiotic pyridones produced by a marine fungus, *Trichoderma* sp. strain MF106. *Mar. Drugs* 12, 1208–1219. doi: 10.3390/md12031208

Xie, Z. L., Li, H. J., Wang, L. Y., Liang, W. L., Liu, W., and Lan, W. J. (2013). Trichodermaerin, a new diterpenoid lactone from the marine fungus *Trichoderma erinaceum* associated with the sea star *Acanthaster planci*. *Nat. Prod. Commun.* 8, 67–68. doi: 10.1177/1934578X1300800116

Yamazaki, H., Saito, R., Takahashi, O., Kirikoshi, R., Toraiwa, K., Iwasaki, K., et al. (2015). Trichoketides A and B, two new protein tyrosine phosphatase 1B inhibitors from the marine-derived fungus *Trichoderma* sp. *J. Antibiot.* 68, 628–632. doi: 10.1038/ja.2015.44

Yamazaki, H., Takahashi, O., Kirikoshi, R., Yagi, A., Ogasawara, T., Bunya, Y., et al. (2020a). Epipolythiodiketopiperazine and trichothecene derivatives from the NaI-containing fermentation of marine-derived *Trichoderma* cf. brevicompactum. *J. Antibiot.* 73, 559–567. doi: 10.1038/s41429-020-0314-5

Yamazaki, H., Yagi, A., Takahashi, O., Yamaguchi, Y., Saito, A., Namikoshi, M., et al. (2020b). Antifungal trichothecene sesquiterpenes obtained from the culture broth of marine-derived *Trichoderma* cf. brevicompactum and their structure-activity relationship. *Bioorg. Med. Chem. Lett.* 30:127375. doi: 10.1016/j.bmcl.2020.127375

Yin, M., Fasoyin, O. E., Wang, C., Yue, Q., Zhang, Y., Dun, B., et al. (2020). Herbicidal efficacy of harzianums produced by the biofertilizer fungus, *Trichoderma brevicompactum*. *AMB Express* 10:118. doi: 10.1186/s13568-020-01055-x

You, J., Dai, H., Chen, Z., Liu, G., He, Z., Song, F., et al. (2010). Trichoderone, a novel cytotoxic cyclopentenone and cholesta-7, 22-diene-3β, 5α, 6β-triol, with new activities from the marine-derived fungus *Trichoderma* sp. *J. Ind. Microbiol. Biotechnol.* 37, 245–252. doi: 10.1007/s10295-009-0667-z

Yu, J. Y., Shi, T., Zhou, Y., Xu, Y., Zhao, D. L., and Wang, C. Y. (2021). Naphthalene derivatives and halogenate quinoline from the coral-derived fungus *Trichoderma harzianum* (XS-20090075) through OSMAC approach. *J. Asian Nat. Prod. Res.* 23, 250–257. doi: 10.1080/10286020.2020.1729752

Zeilinger, S., Gruber, S., Bansal, R., and Mukherjee, P. K. (2016). Secondary metabolism in *Trichoderma*–chemistry meets genomics. *Fungal Biol. Rev.* 30, 74–90. doi: 10.1016/j.fbr.2016.05.001

Zhang, L., Niaz, S. I., Khan, D., Wang, Z., Zhu, Y., Zhou, H., et al. (2017). Induction of diverse bioactive secondary metabolites from the mangrove endophytic fungus *Trichoderma* sp. (strain 307) by co-cultivation with *Acinetobacter johnsonii* (strain B2). *Mar. Drugs* 15:35. doi: 10.3390/md15020035

Zhang, M., Liu, J. M., Zhao, J. L., Li, N., Chen, R. D., Xie, K. B., et al. (2016). Two new diterpenoids from the endophytic fungus *Trichoderma* sp. Xy24 isolated from mangrove plant *Xylocarpus granatum*. *Chin. Chem. Lett.* 27, 957–960. doi: 10.1016/j.cclet.2016.02.008

Zhang, P., Wei, Q., Yuan, X., and Xu, K. (2020). Newly reported alkaloids produced by marine-derived *Penicillium* species (covering 2014-2018). *Bioorg. Chem.* 99:103840. doi: 10.1016/j.bioorg.2020.103840

Zhang, S., Sun, F., Liu, L., Bao, L., Fang, W., Yin, C., et al. (2020). Dragonfly-associated *Trichoderma harzianum* QTYC77 is not only a potential biological control agent of *Fusarium oxysporum* f. sp. cucumerinum but also a source of new antibacterial agents. *J. Agric. Food Chem.* 68, 14161–14167. doi: 10.1021/acs.jafc.0c05760

Zhao, D. L., Yang, L. J., Shi, T., Wang, C. Y., Shao, C. L., and Wang, C. Y. (2019). Potent phytotoxic harziane diterpenes from a soft coral-derived strain of the fungus *Trichoderma harzianum* XS-20090075. *Sci. Rep.* 9:13345. doi: 10.1038/s41598-019-49778-7

Zhao, D. L., Zhang, X. F., Huang, R. H., Wang, D., Wang, X. Q., Li, Y. Q., et al. (2020). Antifungal nafuredin and epithiodiketopiperazine derivatives from the mangrove-derived fungus *Trichoderma harzianum* D13. *Front. Microbiol.* 11:1495. doi: 10.3389/fmicb.2020.01495

Zheng, C. J., Sun, P. X., Jin, G. L., and Qin, L. P. (2011). Sesquiterpenoids from *Trichoderma atroviride*, an endophytic fungus in *Cephalotaxus fortunei*. *Fitoterapia* 82, 1035–1038. doi: 10.1016/j.fitote.2011.06.010

Zhou, P., Wu, Z., Tan, D., Yang, J., Zhou, Q., Zeng, F., et al. (2017). Atrichodermones A–C, three new secondary metabolites from the solid culture of an endophytic fungal strain, *Trichoderma atroviride*. *Fitoterapia* 123, 18–22. doi: 10.1016/j.fitote.2017.09.012

Zhou, X. X., Li, J., Yang, Y. H., Zeng, Y., and Zhao, P. J. (2014). Three new koninginins from *Trichoderma neokongii* 8722. *Phytochem. Lett.* 8, 137–140. doi: 10.1016/j.phytol.2014.03.004

Zou, J. X., Song, Y. P., and Ji, N. Y. (2021). Deoxytrichodermaerin, a harziane lactone from the marine algicolous fungus *Trichoderma longibrachiatum* A-WH-20-2. *Nat. Prod. Res.* 35, 216–221. doi: 10.1080/14786419.2019.1622110

Conflict of Interest: The authors declare that the research was conducted in the absence of any commercial or financial relationships that could be construed as a potential conflict of interest.

Publisher's Note: All claims expressed in this article are solely those of the authors and do not necessarily represent those of their affiliated organizations, or those of the publisher, the editors and the reviewers. Any product that may be evaluated in this article, or claim that may be made by its manufacturer, is not guaranteed or endorsed by the publisher.

frontiers in Microbiology

ORIGINAL RESEARCH
published: 09 August 2021
doi: 10.3389/fmicb.2021.727670

New Enantiomers of a Nor-Bisabolane Derivative and Two New Phthalides Produced by the Marine-Derived Fungus *Penicillium chrysogenum* LD-201810

Yan Ge[1,2,3†], Wen-Li Tang[2†], Qing-Rong Huang[1,4], Mao-Lian Wei[2], You-Zhi Li[2], Lin-Lin Jiang[1,2,3], Cheng-Lin Li[5], Xin Yu[1,2,4], Hong-Wei Zhu[1,2,3], Guo-Zhong Chen[1,3,4], Jian-Long Zhang[1,2,3] and Xing-Xiao Zhang[1,3,4*]*

[1] School of Life Sciences, Ludong University, Yantai, China, [2] Shandong Provincial Key Laboratory of Quality Safty Monitoring and Risk Assessment for Animal Products, Jinan, China, [3] Shandong Aquaculture Environmental Control Engineering Laboratory, Yantai, China, [4] Yantai Key Laboratory of Animal Pathogenetic Microbiology and Immunology, Yantai, China, [5] Department of Oncology, Linyi People's Hospital, Linyi, China

OPEN ACCESS

Edited by:
Paola Angelini, University of Perugia, Italy

Reviewed by:
Hemraj Chhipa, Agriculture University, Kota, India
Xin Wu, Shenyang Pharmaceutical University, China

***Correspondence:**
Jian-Long Zhang
zhangjianlong@ldu.edu.cn
Xing-Xiao Zhang
zhangxingxiao@ldu.edu.cn

† These authors have contributed equally to this work

Specialty section:
This article was submitted to Microbiotechnology, a section of the journal Frontiers in Microbiology

Received: *19 June 2021*
Accepted: *21 July 2021*
Published: *09 August 2021*

Citation:
Ge Y, Tang W-L, Huang Q-R, Wei M-L, Li Y-Z, Jiang L-L, Li C-L, Yu X, Zhu H-W, Chen G-Z, Zhang J-L and Zhang X-X (2021) New Enantiomers of a Nor-Bisabolane Derivative and Two New Phthalides Produced by the Marine-Derived Fungus Penicillium chrysogenum LD-201810. Front. Microbiol. 12:727670. doi: 10.3389/fmicb.2021.727670

Marine-derived fungi are a treasure house for the discovery of structurally novel secondary metabolites with potential pharmaceutical value. In this study, a pair of new nor-bisabolane derivative enantiomers (±)−1 and two new phthalides (4 and 5), as well as four known metabolites, were isolated from the culture filtrate of the marine algal-derived endophytic fungus *Penicillium chrysogenum* LD-201810. Their structures were established by detailed interpretation of spectroscopic data (1D/2D NMR and ESI-MS). The optical resolution of compound (±)−1 by chiral HPLC successfully afforded individual enantiomers (+)−1 and (−)−1, and their absolute configurations were determined by TDDFT-ECD calculations. Compound (±)−1 represents the first example of bisabolane analogs with a methylsulfinyl substituent group, which is rare in natural products. All of the isolated compounds 1–7 were evaluated for their cytotoxic activity against A549, BT-549, HeLa, HepG2, MCF-7, and THP-1 cell lines, as well as for antifungal activity against four plant pathogenetic fungi (*Alternaria solani*, *Botrytis cinerea*, *Fusarium oxysporum*, and *Valsa mali*). Compound 2, a bisabolane-type sesquiterpenoid, was shown to possess excellent activity for control of *B. cinerea* with half-maximal inhibitory concentration (IC_{50}) of 13.6 μg/mL, whereas the remaining investigated compounds showed either weak or no cytotoxic/antifungal activity in this study.

Keywords: marine fungus, *Penicillium chrysogenum*, secondary metabolites, bisabolane derivatives, phthalides, antifungal activity

INTRODUCTION

Marine-derived fungi that inhabit the marine environment possess the unique metabolic pathways to produce a great diversity of bioactive secondary metabolites, which play an important role in agrochemical and pharmaceutical industries (Xu et al., 2020; Zhang et al., 2020). It is well-known that a large number of new marine natural products have been discovered and reported every year

(Carroll et al., 2021). Mining natural products with novel structures and remarkable bioactivities from marine-derived fungi is still a research hotspot.

Filamentous fungi belonging to the genus *Penicillum* are important and untapped producers of structurally diverse metabolites (Bai et al., 2019). *Penicillum* from marine environment have gained particular attention, not only due to their unusual chemical skeletons but also their significant bioactivities with pharmaceutical potential (Zhang et al., 2020). In our continuing study on bioactive metabolites of marine-derived fungi, we investigated *Penicillium chrysogenum* LD-201810, a marine alga-associated fungus isolated from the marine red alga *Grateloupia turuturu* (Jiang et al., 2020). Previous solid cultivation of this fungus on rice medium led to the isolation of a new pentaketide derivative, two new hydroxyphenylacetic acid derivatives, as well as the known bisabolane-type sesquiterpenoids and meroterpenoids (Jiang et al., 2020). Motivated by OSMAC (one strain-many compounds) strategy (Zhao et al., 2020), the fungal strain was cultivated on liquid PDB medium. A follow-up examination of this cultivation yielded a pair of new nor-bisabolane derivative enantiomers (±)−1, two previously reported bisabolenes (2 and 3), and two new phthalides (4 and 5) (**Figure 1**). The aromatic bisabolenes are a rarely found family of sesquiterpenes. Mulholland et al. firstly reported a new trisnor-bisabolane sesquiterpene boivinianin A (Mulholland et al., 2006). Then Li et al. (2015) reported the second occurrence of a new nor-bisabolane derivative, 1-hydroxyboivinianin A. Herein we reported the first example of nor-bisabolane analogs with a methylsulfinyl substituent group, which is rare in natural products. Moreover, the structure elucidation of the new phthalides (4 and 5), as well as the cytotoxicity and antifungal activity of the isolated compounds, are also described.

MATERIALS AND METHODS

General Experimental Procedures

The UV and optical rotations data were obtained on a Shimadzu UV-2700 spectrometer (Shimadzu Co., Ltd., Kyoto, Japan) and Jasco P-1020 automatic polarimeter (JASCO, Tokyo, Japan), respectively. ^{1}H (500 MHz), ^{13}C (125 MHz), and 2D NMR spectra were measured on an Agilent DD2 spectrometer (Agilent Technologies, Waldbronn, Germany). The mass spectra (ESI-MS) were measured under the positive and negative ion modes by a Waters Xevo G2-XS QTof mass spectrometer (Waters, Milford, MA, United States). Column chromatography was performed on silica gel (100–200 and 200–300 mesh, Qingdao Marine Chemical Inc., Qingdao, China), Lobar LiChroprep RP-18 (40–60 μm, Merck, Darmstadt, Germany), and on Sephadex LH-20 (Merck). Preparative TLC plates precoated with silica gel GF_{254} were purchased from Qingdao Marine Chemical Industry Company.

Fungal Material

The producing fungal strain *P. chrysogenum* LD-201810 was isolated from *Grateloupia turuturu*, a marine red alga which collected in Qingdao coastal zone. The gene sequencing in the ITS region of the rDNA (GenBank no. MT075873) was applied to identify the fungus (Jiang et al., 2020). To identify the phylogenetic location of this fungus, phylogenetic trees were constructed based on the ITS region sequences using maximum likelihood (ML) method, and the bootstrap support was calculated using 1,000 replicates. The fungus has been deposited in School of Life Sciences, Ludong University, Yantai, China.

Fermentation, Extraction, and Isolation

The selected fungal strain *P. chrysogenum* LD-201810 was cultured on potato dextrose agar (PDA) medium (Solarbio Life Sciences, Beijing) at 28°C. After 5 days, the agar blocks were cut into small pieces (0.5 × 0.5 cm), and then inoculated to 100 erlenmeyer flasks containing the liquid potato dextrose broth (PDB) medium (Solarbio Life Sciences) under static conditions at room temperature for 30 days. The culture filtrate was collected, combined, and extracted with equivoluminal EtOAc (30 L) for three times. The organic phase was subsequently dried under reduced pressure to afford 12.6 g of crude extract. Then the detailed separation process was as follows: (i) The crude extract was subjected to open silica gel column chromatography (CC) (100−200 mesh), eluted with a mixed petroleum ether (PE)−EtOAc gradient system (30:1, 10:1, 5:1, 2:1, 1:1, and 0:1) to yield six fractions (Fr. 1 to Fr. 6); (ii) Fr. 4 (2.5 g, eluted with PE−EtOAc 2:1, v/v) was re-fractionated by reversed-phase CC over Lobar LiChroprep RP-18 with a MeOH−H_2O gradient system (from 10% MeOH−H_2O to 100% MeOH, v/v) to give nine subfractions (Fr. 4.1 to Fr. 4.9); (iii) Fr. 4.3 (0.5 g, eluted with 30% MeOH−H_2O, v/v) was separated by preparative thin layer chromatography [prep.-TLC, 20 × 20 cm; developing solvents: dichloromethane (DCM)−methanol (MeOH), 20:1, v/v] to furnish the new compounds 4 (4.5 mg) and 5 (8.0 mg); (iv) Fr. 4.4 (0.8 g, eluted with 40% MeOH−H_2O, v/v) was also separated by prep.-TLC (developing solvents: DCM−MeOH, 20:1, v/v) to obtain compound 6 (12.0 mg); (v) Fr. 4.6 (0.6 g, eluted with 60% MeOH−H_2O, v/v) was repeatedly subjected to Sephadex LH-20 (MeOH) to give compound 7 (20.5 mg); (vi) Fr. 5 (1.9 g, eluted with PE−EtOAc 1:1, v/v) was subjected to Sephadex LH-20 (MeOH) to yield five subfractions (Fr. 5.1 to Fr. 5.5); (vii) Fr. 5.2 (0.8 g) was applied to silica gel CC (200–300 mesh; DCM−MeOH 20:1, v/v) to yield compounds 2 (9.6 mg) and 3 (31.8 mg); (viii) Fr. 5.3 (0.4 g) was purified by prep.-TLC (developing solvents: DCM−MeOH, 10:1, v/v) to give the racemic compound 1 (7.0 mg). Compound 1 was well resolved into the pure enantiomers (+)−1 (3.0 mg, t_R = 16.3 min) and (−)−1 (2.8 mg, t_R = 18.3 min) by HPLC using a (*R*,*R*) Whelk-O1 chiral column (10 μm; 4.6 × 250 mm; *n*-hexane-ethanol eluent 7:3, v/v; 1.0 mL/min).

Methylsulfinyl-1-hydroxyboivinianin A (±1): white amorphous powder; UV (MeOH) λ_{max} (log ε) 200 (2.65), 282 (1.52) nm; ^{1}H and ^{13}C NMR data were assigned and listed in **Table 1**; (−)-HR-ESI-MS *m/z* 267.0680 $[M - H]^-$ (calcd for $C_{13}H_{15}O_4S$, 267.0691).

(+)−1: $[\alpha]^{25}_D$ + 23.8° (c 0.05, MeOH); ECD (0.125 mg/mL, MeOH) λ_{max} (Δε) 220 (+ 1.54) nm.

(−)−1: $[\alpha]^{25}_D$ −22.2° (c 0.04, MeOH); ECD (0.125 mg/mL, MeOH) λ_{max} (Δε) 218 (−1.52) nm.

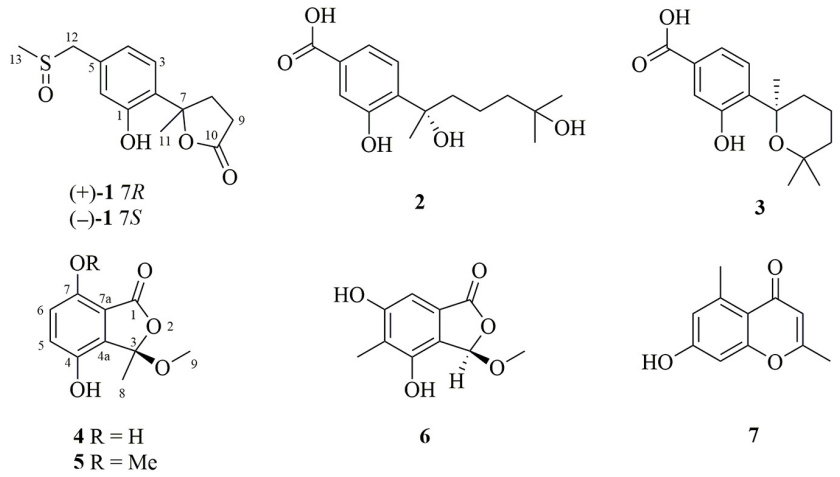

FIGURE 1 | Chemical structures of the isolated compounds 1–7 from *P. chrysogenum* LD-201810.

TABLE 1 | ^{1}H (500 MHz) and ^{13}C NMR (125 MHz) data of the new compounds 1, 4, and 5.

No.	Compound (±)-1[a]		No.	Compound 4[b]		Compound 5[b]	
	δ_H (mult, *J* in Hz)	δ_C, type		δ_H (mult, *J* in Hz)	δ_C, type	δ_H (mult, *J* in Hz)	δ_C, type
1		155.0, C	1		166.2, C		165.5, C
2		132.0, C	3		107.2, C		107.1, C
3	7.33 (d, 8.4)	126.5, CH	4		145.2, C		146.5, C
4	6.83 (d, 8.4)	122.3, CH	4a		131.3, C		132.7, C
5		132.3, C	5	7.01 (d, 8.7)	124.3, CH	7.14 (d, 8.8)	123.8, CH
6	6.82 (s)	118.9, CH	6	6.84 (d, 8.7)	119.7, CH	7.06 (d, 8.8)	115.6, CH
7		88.6, C	7		149.7, C		150.9, C
8	2.67 (m) 2.49 (m)	35.1, CH_2	7a		113.1, C		114.8, C
9	2.65 (m) 2.45 (m)	29.7, CH_2	8	1.73 (s)	24.2, CH_3	1.75 (s)	24.1, CH_3
10		179.6, C	9	2.93 (s)	51.0, CH_3	2.93 (s)	51.1, CH_3
11	1.76 (s)	26.7, CH_3	10	–	–	3.80 (s)	56.3, CH_3
12	4.07 (d, 13.0) 3.94 (d, 13.0)	59.7, CH_2					
13	2.58 (s)	37.4, CH_3					

[a] *Measured in CD_3OD.*
[b] *Measured in DMSO-d_6.*

Chrysoalide A (4): white amorphous powder; $[\alpha]^{25}_{D}$ + 31.5° (c 0.03, MeOH); UV (MeOH) λ_{max} (log ε) 216 (2.58), 239 (2.03), 330 (1.96) nm; ^{1}H and ^{13}C NMR data were assigned and listed in **Table 1**; (−)-HRESIMS *m/z* 209.0431 $[M - H]^-$ (calcd for $C_{10}H_9O_5$, 209.0450).

Chrysoalide B (5): white amorphous powder; $[\alpha]^{25}_{D}$ + 15.8° (c 0.03, MeOH); UV (MeOH) λ_{max} (log ε) 215 (2.13), 237 (1.63), 329 (1.50) nm; ^{1}H and ^{13}C NMR data were assigned and listed in **Table 1**; (−)-HRESIMS *m/z* 223.0584 $[M - H]^-$ (calcd for $C_{11}H_{11}O_5$, 223.0606).

Computational Section

The conformational search was performed by the molecular mechanics with MM + method in HyperChem 8.0 software. Next, the geometries were optimized at B3LYP/6-31G(d) level with Gaussian 09 software to afford the energy-minimized conformers (Frisch et al., 2013). The optimized conformers were subjected to TD-DFT ECD calculations at PBE0/TZVP, CAM-B3LYP/TZVP, and BH&HLYP/TZVP level. The solvent effects (MeCN) were evaluated at the same DFT level with the SCRF/PCM method.

Cytotoxic Assay

Cytotoxicity of compounds 1−7 toward A549, BT-549, HeLa, HepG2, MCF-7, and THP-1 cell lines was tested by the Cell Counting Kit-8 (CCK-8) method (Yuan et al., 2020). All of the cell lines were purchased from the Chinese Academy of Sciences Committee on Type Culture Collection Cell Bank (Shanghai,

China). The six cell lines (3.0×10^4 cells per well) were initially inoculated into 96-well plates for 24 h. Subsequently, the cells were exposed to various concentrations of tested compounds (0, 5, 10, 20, 40, 80, and 100 μg/mL). With the treatment of 24, 48, and 72 h, 10 μL of 5 g/L CCK-8 solution (CCK-8 Cell Proliferation and Cytotoxicity Assay Kit, #CA1210, Solarbio, Beijing, China) was applied to each well and the cells were cultured for 1.5 h at 37°C. Absorbance data were obtained with a microplate spectrophotometer reader (Multiskan GO, Thermo Fisher Scientific, Waltham, MA, United States) at 490 nm.

Antifungal Assay

The antifungal activities against four phytopathogenic fungi (*Alternaria solani, Botrytis cinerea, Fusarium oxysporum,* and *Valsa mali*) were evaluated in 96-well microtiter plates using a modified broth microdilution method

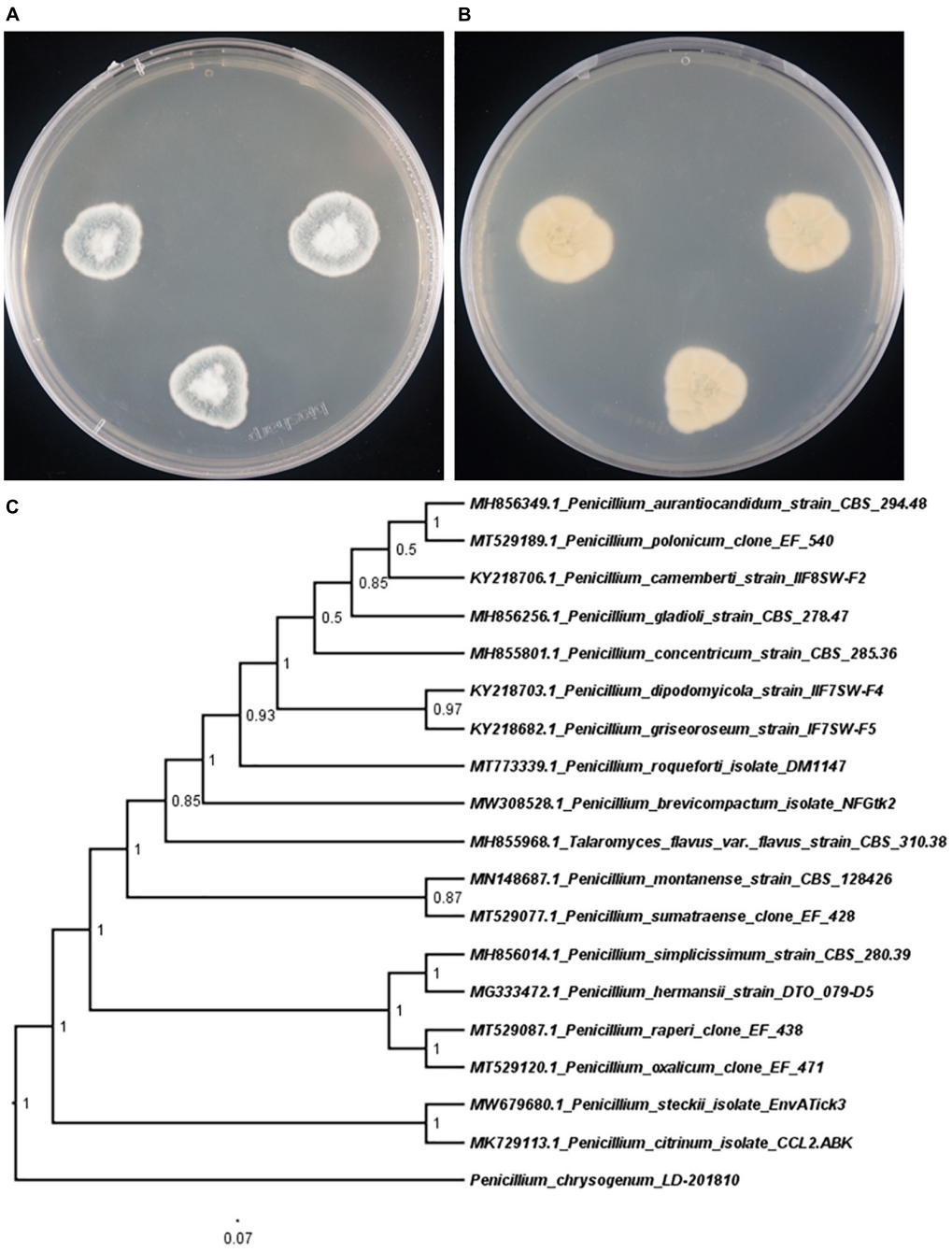

FIGURE 2 | Morphology of *P. chrysogenum* LD-201810 on PDA medium (**A**, front view; **B**, reverse view). **(C)** Neighbor-joining tree based on ITS nucleotide sequences.

(Shi et al., 2017). Carbendazim was used as a positive control. The tested compounds were added to autoclaved PDA medium to a final concentration of 3.12, 6.25, 12.5, 25, and 50 μg/mL, while 95% ethanol was treated as black control. The blocks (about 5 mm diameter) from four phytopathogenic fungi were cultured in the center of plates at 20°C. Colony diameters were measured with the cross method. The mycelial growth inhibition rate was calculated as follows, while IC_{50} values were obtained by the logarithm method.

The mycelial growth inhibition rate = (control colony diameter − treatment colony diameter)/(control colony diameter − 5) × 100%

RESULTS AND DISCUSSION

Identification of the Producing Strain

To clarify the evolutionary position of the producing strain LD-201810, we performed phylogenetic analysis based on its ITS

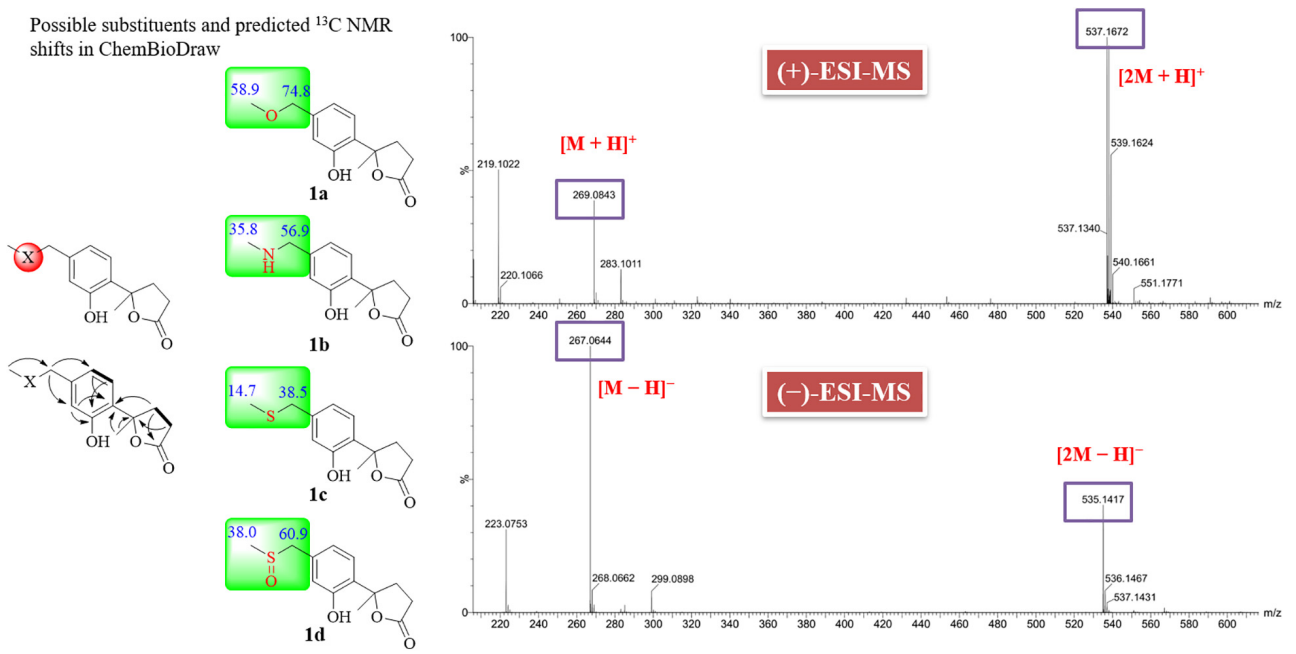

FIGURE 3 | COSY, key HMBC correlations and possible substituents of compound (±)−1.

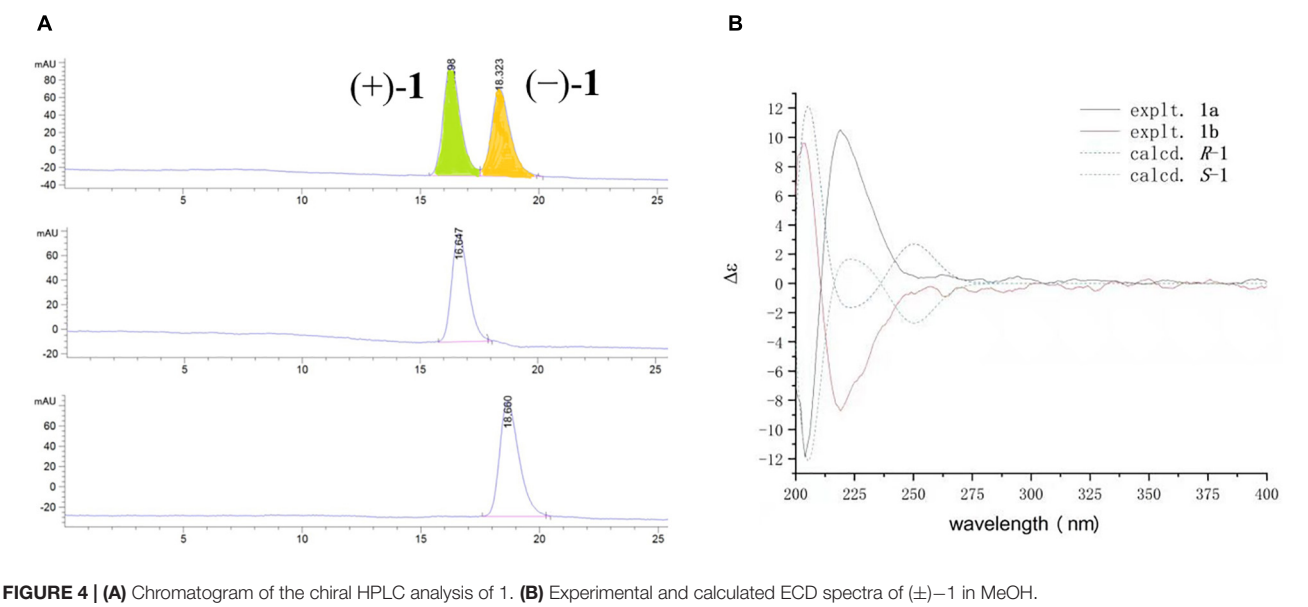

FIGURE 4 | (A) Chromatogram of the chiral HPLC analysis of 1. **(B)** Experimental and calculated ECD spectra of (±)−1 in MeOH.

sequence, together with those from other *Penicillium* species. Results indicated that the strain LD-201810 located at the basal position of the whole tree with high confidence (100%, **Figure 2**). The result demonstrated that *Penicillium chrysogenum* LD-201810 belongs to the *Penicillium* genus.

Structural Elucidation

Compound (±)−1 was a white amorphous powder (MeOH), and its molecular formula was determined to be $C_{13}H_{16}O_4S$ by negative-mode HR-ESI-MS (*m/z* 267.0680 $[M - H]^-$, calcd 267.0691). The ^{1}H NMR data for 1 (**Table 1**) clearly revealed signals of two methyl singlets at δ_H 1.76 (s, H_3-11) and 2.58 (s, H_3-13), two sets of methylene multiplets at δ_H 2.67 (m, H-8α), 2.65 (m, H-9α), 2.49 (m, H-8β), and 2.45 (m, H-9β), a pair of methylene doublets at δ_H 4.07 (d, *J* = 13.0 Hz, H-12α) and 3.94 (d, *J* = 13.0 Hz, H-12β), and three aromatic protons at δ_H 7.33 (d, *J* = 8.4 Hz, H-3), 6.83 (d, *J* = 8.4 Hz, H-4), and 6.82 (s, H-6). The ^{13}C NMR data identified 13 carbon signals that were highly resolved, categorized as two methyls, three methylenes, three sp^2 methines, and five quaternary carbons including three sp^2, one oxygenated sp^3, and one carbonyl carbon at δ_C 179.6 (C-10). Detailed analysis of the 1D and 2D NMR (**Figure 3**) spectra of 1 indicated that they were similar to those of 1-hydroxyboivinianin A, a trisnor-bisabolane derivative identified from the culture of a deep-sea sediment-derived fungus *Penicillium aculeatum* SD-321 (Li et al., 2015). By comparison of the NMR data of 1-hydroxyboivinianin A with those of 1, the main differences in 1 were the presence of an additional methylene group at δ_C 59.7 (C-12) and a distinctive methyl at δ_C 37.4 (C-13). The downfield chemical shifts of 13-CH_3 ($\delta_{H/C}$ 2.58/37.4) and 12-CH_2 (δ_C

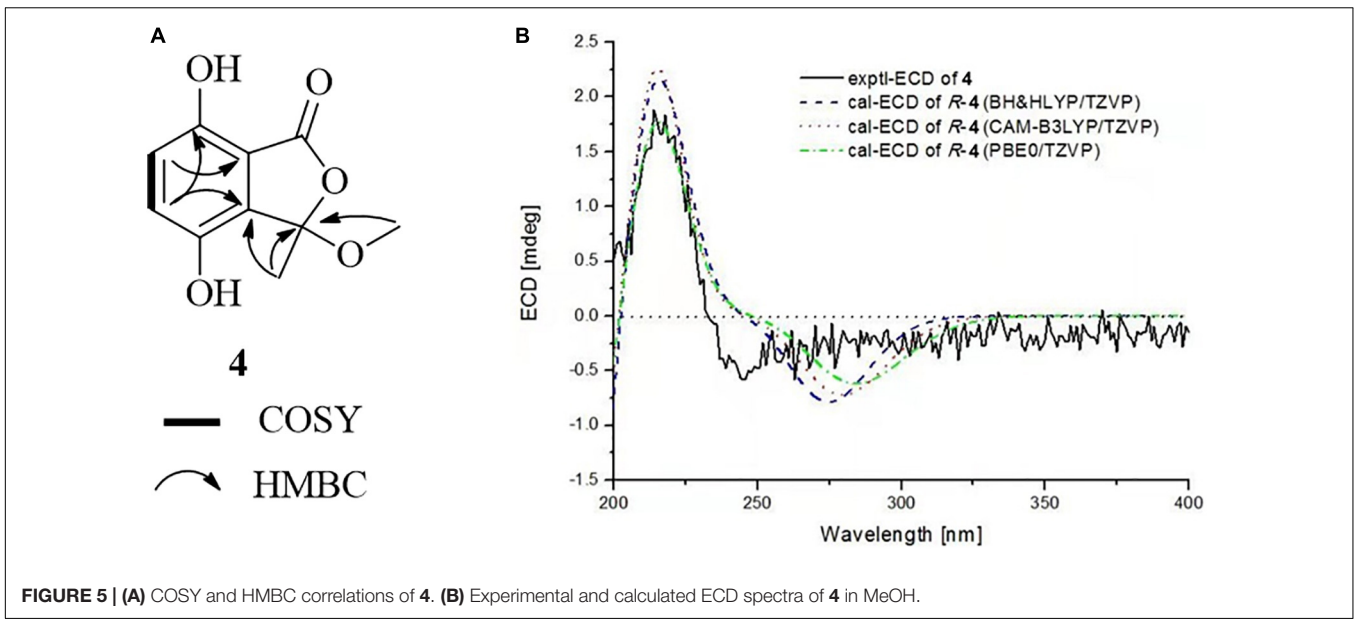

FIGURE 5 | (A) COSY and HMBC correlations of **4**. **(B)** Experimental and calculated ECD spectra of **4** in MeOH.

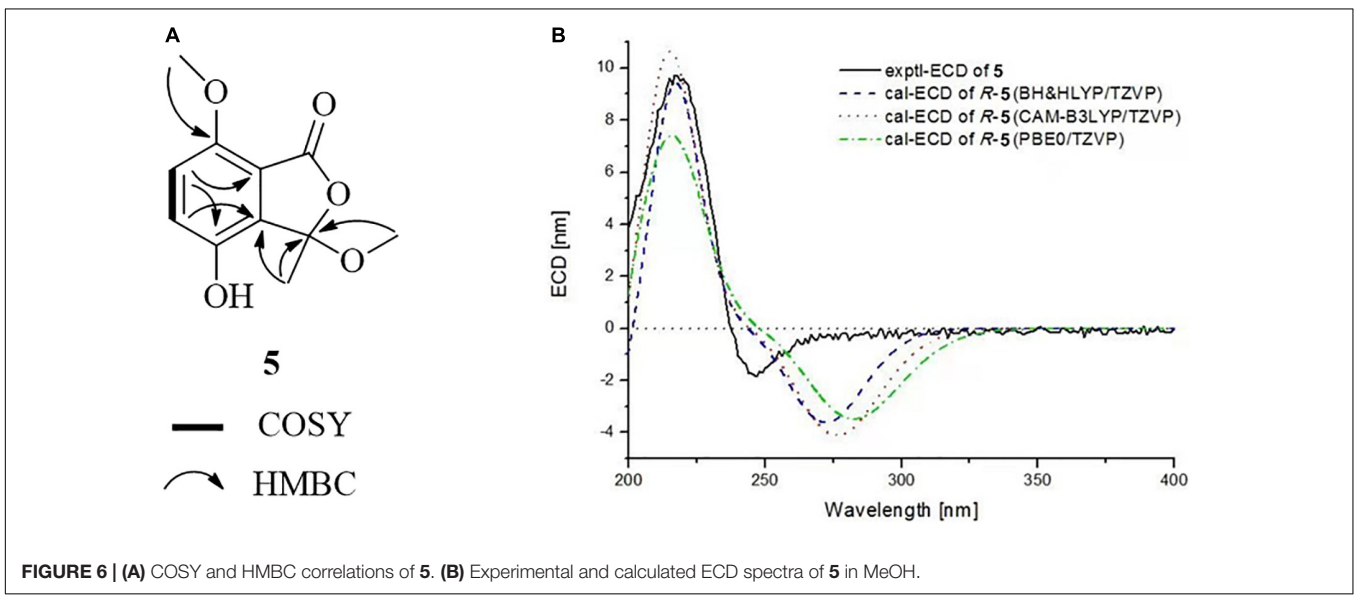

FIGURE 6 | (A) COSY and HMBC correlations of **5**. **(B)** Experimental and calculated ECD spectra of **5** in MeOH.

59.7) were ascribed to that bearing a heteroatom between them. Initially, the common-observed heteroatoms, such as oxygen (1a), nitrogen (1b), and sulfur (1c) atoms, were assumed between C-13 and C-12. However, the predicted ^{13}C NMR shifts in ChemBioDraw didn't match well with that for measured data (**Figure 3**). Furthermore, combined with positive-mode ESI-MS (*m/z* 269.0843 $[M + H]^+$ and 537.1672 $[2M + H]^+$) and negative-mode ESI-MS (*m/z* 267.0644 $[M - H]^-$ and 535.1417 $[2M - H]^-$), the molecular weight of 1 was determined as 268. In view of its molecular weight, a remaining S and O atom could be accounted for by inserting the S = O group between C-13 and C-12 to form a methylsulfinyl substituent. The predicted data for 1d were in good agreement with the authentic data. Moreover, Fu et al. reported a series of synthetic compounds with a methylsulfinyl group (Fu et al., 2020). The chemical shifts of C-12 and C-13 in 1 were accordant with those of known compounds, which further confirmed the presence of such a rare substituent in natural products. On the basis of the above discussion, the structure of compound 1 was determined as methylsulfinyl-1-hydroxyboivinianin A.

Compound 1 had only one chiral center at C-7. The zero specific rotation value and baseline ECD curve indicated its racemic nature (Meng et al., 2016). Subsequent chiral HPLC analysis of (±)−1 successfully led to the separation of the two individual enantiomers (+)−1 and (−)−1 with a ratio of approximately 1:1, which exhibited opposite optical rotations (**Figure 4A**). To determine the absolute configurations of (+)−1 and (−)−1, their ECD spectra were measured in MeOH and simulated by the time-dependent density function theory (TD-DFT) method. The experimental ECD spectrum of (+)−1 showed a positive (+220 nm) Cotton effect, whereas the experimental (−)−1 showed an almost mirror image ECD curve (**Figure 4B**). The calculated ECD curves of 7*R* and 7*S* matched the experimental ECD curves of (+)−1 and (−)−1, thus the absolute configurations of (+)−1 and (−)−1 were proposed as 7*R* and 7*S*, respectively.

Chrysoalide A (4), a white amorphous powder, was shown to possess a molecular formula of $C_{10}H_{10}O_5$ by its HR-ESI-MS (*m/z* 209.0431 $[M - H]^-$, calcd 209.0450). Its UV spectrum showed absorption peaks at 216, 239, and 330 nm, indicating the presence of a conjugated carbonyl chromophore (Phainuphong et al., 2018; Saetang et al., 2021). The ^1H NMR data for 4 (**Table 1**) showed signals of one methyl singlet at δ_H 1.73 (s, H_3-8), one methoxy singlet at δ_H 2.93 (s, H_3-9), and a pair of intercoupling aromatic protons at δ_H 7.01 (d, J = 8.7 Hz, H-5) and 6.84 (d, J = 8.7 Hz, H-6), which can be easily deduced the presence of a 1,2,3,4-tetrasubstituted benzene group. The ^{13}C NMR spectrum (**Table 1**) displayed signals for two methyls at δ_C 24.2 (C-8) and 51.0 (C-9), two sp^2 methines at δ_C 124.3 (C-5) and 119.7 (C-6), five quaternary carbons, and one ester carbonyl at δ_C 166.2 (C-1). Detailed analysis of 2D NMR data established the planar structure of 4 (**Figure 5A**). Moreover, the experimental ECD spectrum of 4 displayed a similar shape of curves and Cotton effects to those of the calculated ECD spectrum of the *R*-configuration (**Figure 5B**), which established the absolute configuration of C-3 to be *R*.

Chrysoalide B (5) was also obtained as a white amorphous powder with a molecular formula of $C_{11}H_{12}O_5$ as determined by HR-ESI-MS. The molecular weight of 5 was more than that of 4 by 14 units (CH_2). The 1D and 2D NMR spectra of 5 (**Table 1** and **Figure 6A**) suggested that it resembled 4 structurally, but possessed an additional methoxy group at $\delta_{H/C}$ 3.80/56.3. The extra methoxy group was shown to be linked to C-7, as evidenced from the HMBC correlation from 10-CH_3 to C-7. Compound 5 was elucidated as a methoxy derivative of 4. The absolute configuration of 5 was considered to be identical with that of 4 by its similar ECD curve, which gave a positive Cotton effect at 220 nm. Comparison of the experimental ECD data with those of calculated spectra further proved the above assignment (**Figure 6B**).

In addition to the new compounds, two previously reported bisabolane sesquiterpenes 2 and 3, a phthalide derivative 6, and a chromone 7, were also isolated from this fungal strain. Based on detailed spectroscopic analysis as well as by comparisons with literature data, their structures were identified as hydroxysydonic acid (2) (Hamasaki et al., 1978), sydowic acid (3) (Hamasaki et al., 1975), rubralide C (6) (Kimura et al., 2007), and 2,5-dimethyl-7-hydroxychromone (7) (Kashiwada et al., 1984).

Bioactivity of the Isolated Compounds

All of the isolated compounds were evaluated for their cytotoxicity against six different types of cancer cell lines, A549 (a human lung adenocarcinoma epithelial cell line), BT-549 (a human breast cancer cell line), HeLa (a human cervix carcinoma cell line), HepG2 (a human liver carcinoma cell line), MCF-7 (a human breast adenocarcinoma cell line), and THP-1 (a human monocytic cell line). However, none of them exhibited obvious

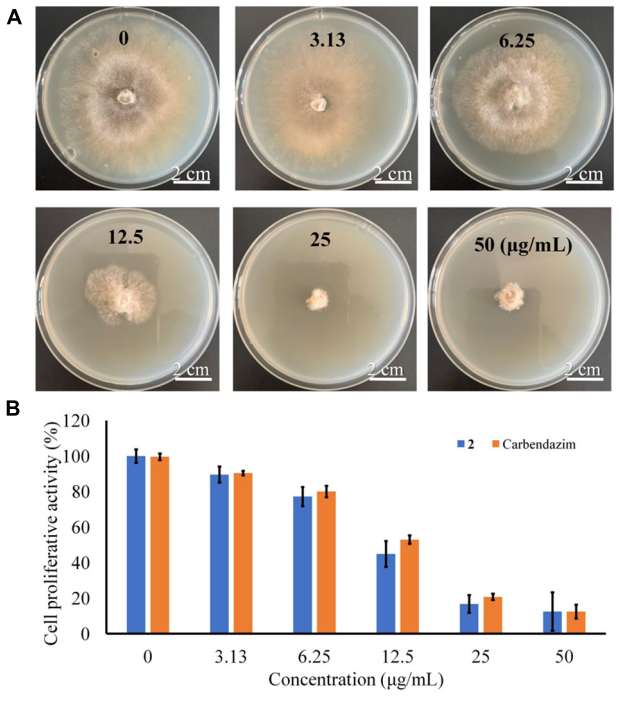

FIGURE 7 | (A) Antifungal assay against *B. cinerea* with different concentrations. **(B)** Inhibition of proliferative activity against *B. cinerea* induced by 2.

inhibitory activity at 20 μg/mL (the highest concentration tested, data were shown in **Supplementary Table 1**).

Previous studies indicated that bisabolane sesquiterpenoids and phthalides possessed promising antimicrobial activity (Li et al., 2015; Saetang et al., 2021). Marine natural products considered to be new sources of lead molecules with agrochemical significance (Oppong-Danquah et al., 2020). To discover new marine fungal agrochemicals, the isolated compounds were evaluated for antifungal activity against several plant pathogenetic fungi (*A. solani*, *B. cinerea*, *F. oxysporum*, and *V. mali*). The bisabolane-type sesquiterpenoid 2 was shown to possess excellent activity for control of *B. cinerea* with an IC_{50} value of 13.6 μg/mL (**Figure 7**) (compared with the positive control carbendazim, with an IC_{50} value of 19.2 μg/mL), whereas other compounds showed either weak or no activity (Data were shown in **Supplementary Table 2**). It should be pointed out that limited amounts of these metabolites were obtained, which prevented us to perform more biological experiments. Further study should be particularly focused on more agricultural activities, such as antifeedant and phytotoxic activities, to fully evaluate their agricultural potentials.

CONCLUSION

Marine-derived fungi have been proven to be prolific producers of secondary metabolites with potent bioactivities. In this study, chemical investigation of a marine algal-derived endophytic fungus *P. chrysogenum* LD-201810 led to the isolation and identification of a pair of new nor-bisabolane derivative enantiomers (±)−1 and two new phthalides (4 and 5), as well as four known metabolites (2, 3, 6, and 7). Compound (±)−1 represents the first example of bisabolane analogs with a methylsulfinyl substituent group, which is rare in natural products. The aromatic bisabolanes are a rarely found family of sesquiterpenes, and the discovery of (±)−1 added greatly to the diversity of this kind of molecules. The cytotoxic and antifungal activities were evaluated. Hydroxysydonic acid (2), a bisabolane-type sesquiterpenoid, showed strong inhibition against *B. cinerea*, compared with that of the positive control carbendazim. The results indicated that some marine natural products may be regarded as candidate agents of antifungal agrochemicals.

DATA AVAILABILITY STATEMENT

The original contributions presented in the study are included in the article/**Supplementary Material**, further inquiries can be directed to the corresponding authors.

AUTHOR CONTRIBUTIONS

YG and W-LT: writing—original draft preparation. Q-RH: methodology. M-LW and Y-ZL: investigation. L-LJ and C-LL: formal analysis. XY, H-WZ, and G-ZC: data curation. J-LZ and X-XZ: writing—review and editing. J-LZ: supervision. X-XZ: funding acquisition. All authors have read and agreed to the published version of the manuscript.

FUNDING

This work was funded by the National Key Research and Development Program of China (Grant Nos. 2016YFD0501010, 2017YFD0500806, and 2018YFD0501402), the Major Agricultural Applied Technological Innovation Projects of Shandong Province (to X-XZ), the Key Research and Development Plan of Yantai (Nos. 2020XDRH101, 2021YT06000060, 2021YT06000636, and 2018XSCC045), the Natural Science Foundation of Shandong Province (Nos. ZR201911120018 and ZR2014HL061), Development of Medical and Health Science and Technology in Shandong Province (No. 2016WS0224), and the Innovation Team Project for Modern Agricultural Industrious Technology System of Shandong Province (SDAIT-11-10).

SUPPLEMENTARY MATERIAL

The Supplementary Material for this article can be found online at: https://www.frontiersin.org/articles/10.3389/fmicb.2021.727670/full#supplementary-material

REFERENCES

Bai, M., Zheng, C. J., Huang, G. L., Mei, R. Q., Wang, B., Luo, Y. P., et al. (2019). Bioactive meroterpenoids and isocoumarins from the mangrove-derived fungus *Penicillium* sp. TGM112. *J. Nat. Prod.* 82, 1155–1164.

Carroll, A. R., Copp, B. R., Davis, R. A., Keyzers, R. A., and Prinsep, M. R. (2021). Marine natural products. *Nat. Prod. Rep.* 38, 362–413.

Frisch, M. J., Trucks, G. W., Schlegel, H. B., Scuseria, G. E., Robb, M. A., and Cheeseman, J. R. (2013). *Gaussian 09, Revision D.01*. Wallingford: Gaussian, Inc.

Fu, D., Dong, J., Du, H., and Xu, J. (2020). Methanesulfinylation of benzyl halides with dimethyl sulfoxide. *J. Org. Chem.* 85, 2752–2758. doi: 10.1021/acs.joc.9b03041

Hamasaki, T., Nagayama, K., and Hatsuda, Y. (1978). Two new metabolites, sydonic acid and hydroxysydonic acid from *Aspergillus sydowi*. *Agric. Biol. Chem.* 42, 37–40. doi: 10.1271/bbb1961.42.37

Hamasaki, T., Sato, Y., Hatsuda, Y., Tanabe, M., and Cary, L. W. (1975). Sydowic acid, a new metabolite from *Aspergillus sydowi*. *Tetrahedron Lett*. 16, 659–660. doi: 10.1016/s0040-4039(00)71947-2

Jiang, L. L., Tang, J. X., Bo, Y. H., Li, Y. Z., Feng, T., Zhu, H. M., et al. (2020). Cytotoxic secondary metabolites isolated from the marine alga-associated fungus *Penicillium chrysogenum* LD-201810. *Mar. Drugs* 18:276. doi: 10.3390/md18050276

Kashiwada, Y., Nonaka, G. I., and Nishioka, I. (1984). Studies on rhubarb (Rhei Rhizoma). V. isolation and characterization of chromone and chromanone derivatives. *Chem. Pharm. Bull.* 32, 3493–3500. doi: 10.1248/cpb.32.3493

Kimura, Y., Yoshinari, T., Koshino, H., Fujioka, S., Okada, K., and Shimada, A. (2007). Rubralactone, rubralides A, B and C, and rubramin produced by *Penicillium rubrum*. *Biosci. Biotechnol. Biochem.* 71, 1896–1901. doi: 10.1271/bbb.70112

Li, X. D., Li, X. M., Xu, G. M., Zhang, P., and Wang, B. G. (2015). Antimicrobial phenolic bisabolanes and related derivatives from *Penicillium aculeatum* SD-321, a deep sea sediment-derived fungus. *J. Nat. Prod.* 78, 844–849. doi: 10.1021/acs.jnatprod.5b00004

Meng, L. H., Mándi, A., Li, X. M., Liu, Y., Kurtán, T., and Wang, B. G. (2016). Isolation, stereochemical study, and antioxidant activity of benzofuranone derivatives from a mangrove-derived fungus *Eurotium rubrum* MA-150. *Chirality* 28, 581–584. doi: 10.1002/chir.22613

Mulholland, D. A., McFarland, K., and Randrianarivelojosia, M. (2006). Sesquiterpenoid derivatives from *Cipadessa boiviniana* (Meliaceae). *Biochem. Syst. Ecol.* 34, 365–369. doi: 10.1016/j.bse.2005.11.005

Oppong-Danquah, E., Budnicka, P., Blümel, M., and Tasdemir, D. (2020). Design of fungal co-cultivation based on comparative metabolomics and bioactivity for discovery of marine fungal agrochemicals. *Mar. Drugs.* 18:73. doi: 10.3390/md18020073

Phainuphong, P., Rukachaisirikul, V., Phongpaichit, S., Sakayaroj, J., Kanjanasirirat, P., Borwornpinyo, S., et al. (2018). Depsides and depsidones from the soil-derived fungus *Aspergillus unguis* PSU-RSPG204. *Tetrahedron* 74, 5691–5699. doi: 10.1016/j.tet.2018.07.059

Saetang, P., Rukachaisirikul, V., Phongpaichit, S., Preedanon, S., Sakayaroj, J., Hadsadee, S., et al. (2021). Antibacterial and antifungal polyketides from the fungus *Aspergillus unguis* PSU-MF16. *J. Nat. Prod.* 84, 1498–1506. doi: 10.1021/acs.jnatprod.0c01308

Shi, D., An, R., Zhang, W., Zhang, G., and Yu, Z. (2017). Stilbene derivatives from *Photorhabdus temperata* SN259 and their antifungal activities against phytopathogenic fungi. *J. Agric. Food Chem.* 65, 60–65.

Xu, K., Yuan, X. L., Li, C., and Li, X. D. (2020). Recent discovery of heterocyclic alkaloids from marine-derived *Aspergillus* species. *Mar. Drugs* 18:54. doi: 10.3390/md18010054

Yuan, X. L., Li, X. Q., Xu, K., Hou, X. D., Zhang, Z. F., Xue, L., et al. (2020). Transcriptome profiling and cytological assessments for identifying regulatory pathways associated with diorcinol N-induced autophagy in A3 cells. *Front. Pharmacol.* 11:570450. doi: 10.3389/fphar.2020.570450

Zhang, P., Wei, Q., Yuan, X. L., and Xu, K. (2020). Newly reported alkaloids produced by marine-derived *Penicillium* species (covering 2014–2018). *Bioorg. Chem.* 99:103840. doi: 10.1016/j.bioorg.2020.103840

Zhao, M., Guo, D. L., Liu, G. H., Fu, X., Gu, Y. C., Ding, L. S., et al. (2020). Antifungal halogenated cyclopentenones from the endophytic fungus *Saccharicola bicolor* of *Bergenia purpurascens* by the one strain-many compounds strategy. *J. Agric. Food Chem.* 68, 185–192. doi: 10.1021/acs.jafc.9b06594

Conflict of Interest: The authors declare that the research was conducted in the absence of any commercial or financial relationships that could be construed as a potential conflict of interest.

Publisher's Note: All claims expressed in this article are solely those of the authors and do not necessarily represent those of their affiliated organizations, or those of the publisher, the editors and the reviewers. Any product that may be evaluated in this article, or claim that may be made by its manufacturer, is not guaranteed or endorsed by the publisher.

frontiers in Microbiology

ORIGINAL RESEARCH
published: 23 August 2021
doi: 10.3389/fmicb.2021.727968

Screening of Key Fungal Strains in the Fermentation Process of the Chinese Medicinal Preparation "Lianzhifan Solution" Based on Metabolic Profiling and High-Throughput Sequencing Technology

Jie Xie[1], Yang Ye[1], Ze Wu[1], Xun Gou[1], Tong Peng[2], Xuegang Yuan[3], Xiangdong Yang[4], Xiaoyu Zhang[1] and Quekun Peng[5]**

[1]College of Life Sciences, Sichuan Normal University, Chengdu, China, [2]Keystonecare Technology (Chengdu) Co., Ltd., Chengdu, China, [3]Department of Anorectal Surgery, The Sixth People's Hospital of Chengdu, Chengdu, China, [4]Department of Anorectal, Chengdu Anorectal Hospital, Chengdu, China, [5]Department of Biotechnology, School of Bioscience and Technology, Chengdu Medical College, Chengdu, China

OPEN ACCESS

Edited by:
Paola Angelini, University of Perugia, Italy

Reviewed by:
Igor A. Parshikov, Institute of Applied Mechanics, Russian Academy of Sciences (RAS), Russia
Lushan Wang, Shandong University, China
Chunqiao Xiao, Wuhan Institute of Technology, China
Lilia Arely Prado Barragan, Metropolitan Autonomous University, Mexico

***Correspondence:**
Xiaoyu Zhang
zhangxy2005@126.com
orcid.org/0000-0003-0968-5969
Quekun Peng
pengquekun@163.com
orcid.org/0000-0002-4065-1137

Specialty section:
This article was submitted to Interdisciplinary Physics, a section of the journal Frontiers in Microbiology

Received: *20 June 2021*
Accepted: *21 July 2021*
Published: *23 August 2021*

Citation:
Xie J, Ye Y, Wu Z, Gou X, Peng T, Yuan X, Yang X, Zhang X and Peng Q (2021) Screening of Key Fungal Strains in the Fermentation Process of the Chinese Medicinal Preparation "Lianzhifan Solution" Based on Metabolic Profiling and High-Throughput Sequencing Technology. Front. Microbiol. 12:727968. doi: 10.3389/fmicb.2021.727968

"Lianzhifan solution" (LZF) is produced by the natural fermentation of coptis root and gardenia fruit, and it is a classic prescription for external use in anorectal department. During the fermentation process, the structural evolution of microbial communities led to significant changes in the chemical profile. In this study, we first analyzed the dynamic changes of chemical components as well as the composition and succession of microbial community during the whole fermentation process of LZF, and confirmed the changes of characteristics of nine compounds during the whole fermentation process by metabolic profile. Further analysis found that there was no significant change of alkaloids in all stages of fermentation of LZF, but there were significant changes of iridoids in the middle and late stage of fermentation by deglycosylation. Genipin gentiobioside and geniposide were converted to genipin by biotransformation, showing that deglycosylation was the main event occurring in the fermentation. The community composition and abundance of species in 10 and 19 days LZF fermentation broth were analyzed with high-throughput sequencing technology, and 16 dominant bacterial genera and 15 dominant fungal genera involved in the fermentation process were identified. Correlation analysis revealed that *Penicillium expansum* and *Aspergillus niger* involved in the fermentation were the dominant genera closely related to the dynamic changes of the deglycosylation of the main chemical components, and *P. expansum* YY-46 and *A. niger* YY-9 strains were obtained by the further fractionation. Then the monoculture fermentation process was evaluated, whereby we found that the deglycoside conversion rate of iridoid glycosides was greatly improved and the fermentation cycle was shortened by 3–4 times. This finding combined with equivalence evaluation of chemical component and pharmacodynamics to confirm that

P. expansum YY-46 and *A. niger* YY-9 strains were key strains for fermentation concoction. This study established an efficient and practical screening strategy "Microfauna communities-Chemical component-Pharmacodynamic" axis for key strain, to improve the production process and formulating good manufacturing practice (GMP) work, and it is also applicable to the whole fermentation drugs industry.

Keywords: traditional Chinese medicine fermentation, key strain screening, equivalence evaluation, chemical metabolic profiling, iridoids, high-throughput sequencing

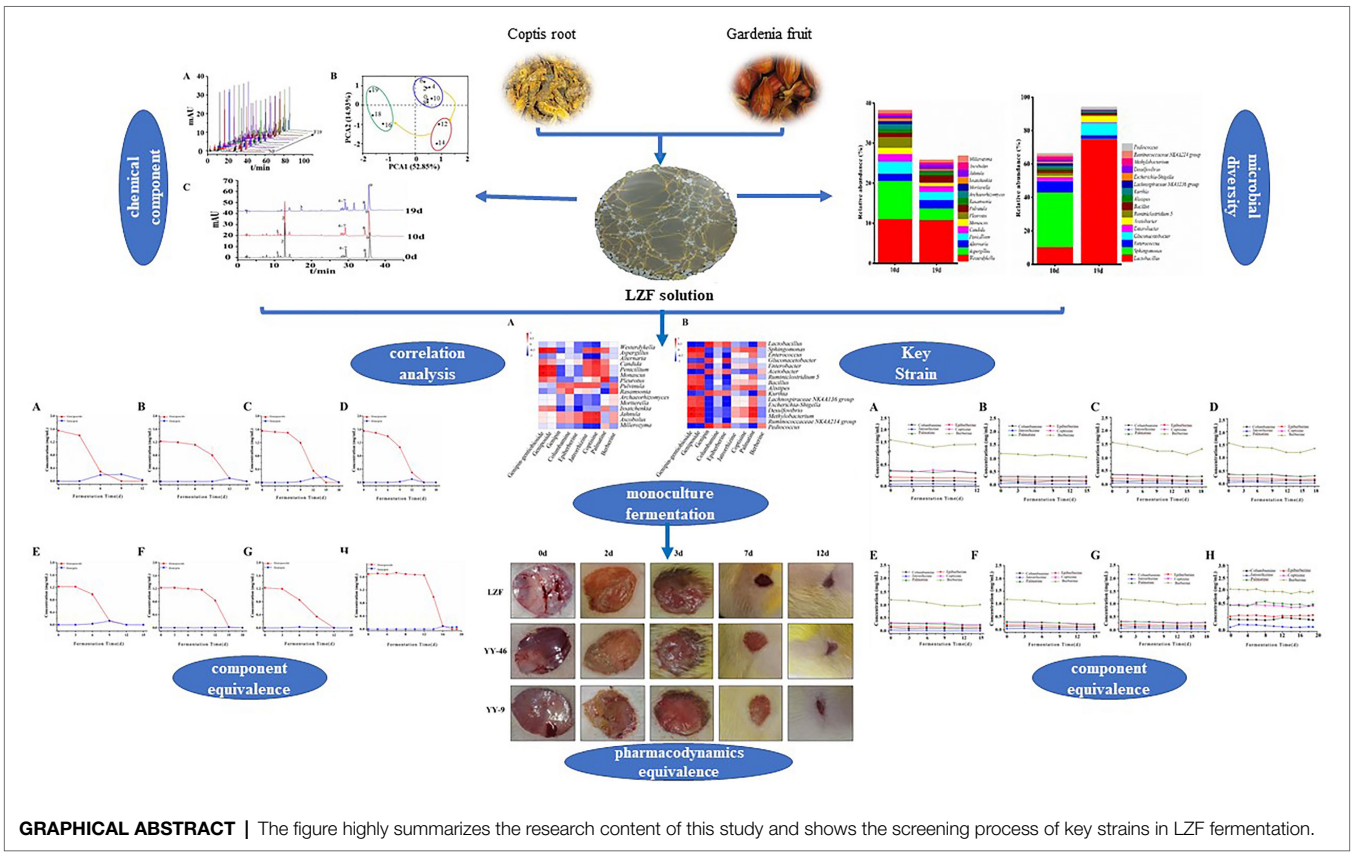

GRAPHICAL ABSTRACT | The figure highly summarizes the research content of this study and shows the screening process of key strains in LZF fermentation.

INTRODUCTION

As early as more than a 1,000 years ago, microbial fermentation has been applied to the concoction of traditional Chinese medicine (TCM) in China. Under certain environmental conditions (e.g., temperature, humidity, air, moisture, etc.) the chemical components of raw or processing drugs are transformed by microorganisms and this fermentation produces a variety of secondary metabolites (Li et al., 2020), new chemical components, or more active precursor compounds (Kim et al., 2014), and achieves new uses such as toxicity reduction and storage (Marič et al., 2019), potency enhancement (Zhang et al., 2017; Liu et al., 2018), and bioavailability improvement (Yin et al., 2017; Yim et al., 2018). Most of the traditional fermentation of TCM is natural fermentation processes using crude drugs in a natural environment with a mixture of microorganism, and it is so difficult to control the types and numbers of microorganisms involved in the fermentation environment that some "ineffective" or even "harmful" strains are involved. At the same time, this traditional fermentation method is not obviously transformation-oriented and does not control the changes of the main active ingredients of the TCM in the fermentation process. The control of the whole fermentation process generally relies only on the sensory and empirical judgment of workers. And the process lacks the support of mature, systematic and reliable scientific methods, resulting in the unstable quality of the whole traditional fermented concoction Chinese medicines, and hindering the application of large-scale production. Therefore, it is of great significance for industrial conversion of traditional processes to screen microorganisms involved in fermented concoction, to control active ingredients, to explore of the change pattern of ingredients and microorganisms and their correlation during the process of Chinese medicine concoction, and to clarify the mechanism of action of fermented concoction.

"Fermented Coptis chinensis solution," also known as "Lianzhifan Solution" (LZF), is a classic formula for external

use with a history of 3 centuries (Yuan et al., 2016). It has been used in Chengdu Anorectal Specialized Hospital for the prevention and treatment of perianal abscess, ulcerative colitis, and anorectal diseases in tens of thousands of patients. LZF consists of two herbs (coptis root and gardenia fruit) and traces of the mineral Chinese medicine alum. In fact, the coptis root is not really a root but the dried rhizome of *Coptis chinensis* Franch, a plant of the buttercup family, and the main active ingredients are alkaloids such as epiberberine, coptisine, and berberine (Dai et al., 2016); Gardenia fruit is the dried fruit of the *Gardenia jasminoides* Ellis and the main active ingredients are genoside, genipin-1-β-D-gentiobioside (Bergonzi et al., 2012). The production of LZF is an uncommon fermentation process, and the production process still strictly follows the production method determined by Mr. Jichuan Huang a 100 years ago, in which the pharmacist decocted coptis root, gardenia fruit, and alum at 100°C according to the formula, and then the medicinal solution is filtered and left to ferment in a dark and humid place for 1–3 weeks, and when the surface of the liquid shows a leopard print pattern (map spot pattern) of greenish-gray fungus and the reddish-brown color of the drug liquid, the experienced pharmacists confirm the ending point and then filter the drug solution before bottling it for clinical use. The production process is quite different from that of common topical tinctures, and is more similar to the fermentation process of soy sauce.

From the perspective of modern biotechnology, multi-strain liquid fermentation is the unique point of the production process of LZF, which is reflected in the fact that no other carbon and nitrogen sources are added. Our previous study revealed that the difference of chemical profile of different batches and different storage periods of the preparation may be related to the degree of transformation of its chemical composition by microorganisms (Ye et al., 2019). Therefore, the changes in the chemical composition of LZF are closely related to the action of microorganisms during the fermentation process. At the same time, the authors in tracking the production process of different production batches in year 2019 found that the surface microorganisms at the end of fermentation of each batch differed in morphology and color, etc. Sometimes green mold was dominant, sometimes tawny mold was dominant, but sometimes yeast film was dominant; and the fermentation time of different batches also differed: generally, 1–2 weeks in spring and summer and 2–3 weeks in autumn and winter. This difference suggests that the composition of microorganisms involved in the preparation process may vary from batch to batch, or the duration of microbial conversion may vary. The group used high-throughput sequencing technology to determine and analyze the diversity and richness of fungi during the fermentation and preparation of LZF, and found that the overall trend of the richness and diversity of fungi increased gradually with the increase of fermentation time (Yuan et al., 2018). In recent years, studies on the effect of fermentation on the microecological community structure of TCM have also been reported (Shimoyama et al., 2015; Huang et al., 2020; Qu et al., 2021). For example, some scholars have analyzed the microbial diversity of Shenqu at different fermentation times by PCR-DGGE (Liu et al., 2017). Some scholars have also used *Aspergillus* spp. to ferment cardiovascular drugs (as statins; Barrios-González et al., 2020; Al-Saman et al., 2021).

At present, LZF preparation still relies on pharmacist's personal observation and experience to control the fermentation process, which had risks of quality control and could hardly meet the good manufacturing practices (GMP) requirements for modern drug production. Therefore, it is necessary to use modern biotechnology to deeply analyze the quality control index components and dominant bacterial groups of this preparation and to identify the key strains of fermented preparations. For this purpose, this study used quantitative metabolic profile mapping to analyze the dynamic changes of chemical components during the fermentation of LZF, combined with high-throughput sequencing technology to understand the dominant microorganisms in the fermentation process. Then this study screened the strains by step-by-step isolation, and further used chemical component and bioequivalence evaluation to identify the key functional strains. This will provide important and strong scientific support for improving the traditional empirical formulation model, optimizing the formulation process, enhancing product quality and stability, and establishing GMP work.

MATERIALS AND METHODS

Materials and Reagents

Coptis root, the dried rhizome of *Coptis chinensis* Franch (batch #470330), gardenia fruit, the dried fruit of *G. jasminoides* Ellis (batch #470401), and Alunite (batch #151121) were purchased from Chengdu Kangmei Pharmaceutical Manufacturing Co., Ltd., and were identified by prof. Xiaoyu Zhang. Genipin-1-β-D-gentiobioside (Cas# 29307-60-6), Geniposide (Cas# 24512-63-8), Genipin (Cas# 6902-77-8), Columbamine (Cas# 3621-36-1), Epiberberine (Cas# 6873-09-2), Jatrorrhizine (Cas# 3621-38-3), Coptisine (Cas# 3486-66-6), Palmatine (Cas# 3486-67-7), and Berberine (Cas# 2086-83-1) were purchased from Chengdu Ruifensi Biotechnology Co., Ltd.; Chromatographic pure acetonitrile, methanol, hydrochloric acid, and phosphoric acid were purchased from Chengdu ShuoboYanchuang Science & Technology Co., Ltd.

EB (Sangon Biotech, E607322); Agarose (Sangon Biotech, A600234); PCR enzyme (KOD-401B: TOYOBO KOD-Plus-Neo DNA Polymerase); DNA marker (Takara, DL2000); TE Buffer; The primers of ITS2 region areITS3_KYO2 (5′-GATGAAGA ACGYAGYRAA-3′) and ITS4 (5′-TCCTCCGCTTATTGATA TGC-3′); The primers of 16S rDNA V4 region are 515F (5′-GTGYCAGCMGCCGCGGTAA-3′) and 806R (5′-GGACTA CHVGGGTWTCTAAT-3′; Caporaso et al., 2011); DNA Isolation Kit (MO BIO PowerSoil DNA Isolation Kit); Gel Extraction Kit (Omega); Sequencing library kit (TruSeq DNA PCR-Free Sample Prep Kit); and On-line sequencing kit (Hiseq Rapid SBS Kit V2).

Instruments and Equipments

High performance liquid chromatography (HPLC; Agilent, 1200); UPLC-PDA-ESI-MS (Waters, H-Class QDa); UV Spectrophotometer (Thermo Fisher, NanoDrop2000C BioMate3S);

E-Gel Imager (Bio-Rad, VersaDoc 5000); Centrifuge (Eppendorf, 5424R); Electrophoresis System (Bio-Rad, Powerpac Basic1645050); Fluorescent quantizer (Invitrogen, Qubit 2.0); Gel extractor (OMEGA-Biotek, Firefly NIMBUS® 96); PCR instrument (ABI, Applied Biosystems GeneAmp 9700); Sequenator (Illumina, Hiseq 2500); and Biological Analyzer (Agilent, 2100).

LZF Preparation and Sampling

The coptis root, gardenia fruit, and trace amount of the mineral Chinese medicine alum were decocted according to the formula. The filtrate was then collected in a fermentation barrel placed under the cover at room temperature for natural fermentation. Samples of the upper and lower layers of fermentation broth were taken at 0, 2, 4, 6, 8, 10, 12, 14, 16, 18, and 19 days. Around 20 ml liquid was taken with a sterile pipette from 5 cm below the liquid surface at each of the five points, and these five samples were then mixed to form the 100 ml upper fermentation broth. Then, 20 ml liquid was taken with a sterile pipette from 10 cm above the bottom of the barrel at each of the five points, and these five samples were then mixed to form the 100 ml lower fermentation broth. Finally, the upper and lower fermentation broths were mixed at ratio of 1:1.

The chromatographic analysis samples were prepared as follows: 100 μl of the mixed sample was added with 100 μl of hydrochloric acid and 9,800 μl of methanol, treated with ultrasonic for 5 min, and then filtered with 0.22 μm filter, and the chromatographic analysis sample was obtained. Finally, the chemical constituents of the solution were analyzed by HPLC and ultra performance liquid chromatography (UPLC)-MS. In addition, on 10 and 19 days of fermentation, the fermentation mixture was taken for high-throughput sequencing.

HPLC Analysis Chemical Composition Changes During the Fermentation Process of LZF

HPLC analysis was performed on an Agilent 1200 HPLC system (Agilent, United States). System control and data analysis were performed on the Chemstation Software program (version A.10.02). The separation was performed on an Eclipse column, Agilent C18 (4.6 × 250 mm, 5 μm). The binary gradient consisted of 0.1% phosphoric acid in distilled water (*v*/*v*; solvent A) and acetonitrile (solvent B), following the elution program: 0 min (5% B), 8 min (15% B), 15 min (18% B), 20 min (20% B), 30 min (25% B), and 50 min (25% B; Bian et al., 2011). A flow rate of 1 ml/min was used at 25°C, and samples (10 μl) were detected at 238 nm.

UPLC-PDA-ESI-MS Analysis of the Main Compositions

The main compositions of the LZF were analyzed using UPLC-MS (Waters H-class QDa). A Waters CORTECS UPLC T3 column (100 × 2.1 mm, 1.6 μm) was selected for the separation of the samples. The sample injection volume was 1 μl. Through a series of optimization experiments, a mobile phase was eventually adopted for the gradient elution using 25 mM ammonium formate with 0.2% formic acid (A) and acetonitrile (B); the specific conditions were: (0–1 min) 15–20% B, (1–3 min) 20% B, (3–7 min) 20–35% B, and (7–8 min) 35% B. The detection wavelength was 238 nm (scan 210–400 nM). The flow rate was 0.25 ml/min. The UPLC-MS Quadrupole Dalton (QDa; Waters Corporation) single quadrupole mass spectrometer equipped with electrospray ionization (ESI) was used to record the ESI-MS spectra. The mass spectrometer was operated in the positive and negative ionization mode. The MS analysis method was as follows: The ion spray voltage was set to −0.8 kV and +0.8 kV in the negative and positive ionization mode, respectively. The turbo-spray temperature was maintained at 600°C. The cone voltage was set at 10 and 50 ev to obtain molecular ion peak and secondary fragment, respectively. Both the nebulizer gas (gas 1) and heater gas (gas 2) were set at 50 psi, while the curtain gas was kept at 30 psi. Nitrogen was used as a nebulizer and auxiliary gas. Samples molecular weight (mw) were collected in both positive and negative modes at the same time (210–650 Da).

Analysis of Microbial

Genomic DNA was extracted *via* the MO BIO PowerSoil DNA Isolation Kit from seven samples (10 and 19 days) of the LZF according to manufacturer's protocols. The ITS2 region and the 16S rDNA V4 region of the sample were amplified by PCR instrument (9700, GeneAmp® ABI, United States; Toju et al., 2012). The purified and diluted genomic DNA as templates and universal primers ITS3 (5′-GATGAAGAACGYAGYRAA-3′), ITS4 (5′-TCCTCCGCTTATTGATATGC-3′) and 515F (5′-GTGY CAGCMGCCGCGGTAA-3′), 806R (5′-GGACTACHVGGGTWT CTAAT-3′) were used for PCR amplification (Caporaso et al., 2011). PCR products were mixed in equal density ratios. Sequencing libraries were generated *via* the TruSeq DNA PCR-Free Sample Prep Kit (Illumina, United States) following manufacturer's recommendations and index codes were added. Finally, the library was sequenced on an IlluminaHiSeq2500 platform and 250 bp paired-end reads were generated. Next-generation sequencing reads were assembled using FLASH (Magoč and Salzberg, 2011). Low quality reads were removed according to the QIIME quality control process (Caporaso et al., 2010, 2011). Sequence analyses were performed *via* Uparse software (Edgar, 2013). A 97% similarity cutoff was used to define operational taxonomic units (OTUs; Gweon et al., 2015). The representative sequences of each OTU were picked and chimeras were removed using Uchime (Edgar et al., 2011). At the same time, the fungal ITS2 region and the bacterial 16S rDNA V4 region were analyzed using the Unite database and the Silva database (Quast et al., 2012), respectively.

Isolation and Purification of Fermentation Dominant Strains

Thermal Stability Test of LZF Fermentation Broth

About 25 ml of LZF fermentation broth prepared in section "LZF Preparation and Sampling" were absorbed into 250 ml conical flask, and then treated in an autoclave at 121°C for 30 min. After cooling, 1 ml of each heat-treated sample was extracted into a 10 ml volumetric flask, which was volume fixed with methanol and filtered with a 0.22 μm filter membrane.

Samples were injected and determined according to the HPLC conditions in section "LZF Preparation and Sampling."

Isolation and Purification of the Strain

"Lianzhifan Solution" was directly used as screening medium, solid screening medium was added with appropriate amount of agar. The fermentation broth of 10 and 19 days was selected as the sample source of isolates. Around 1 ml of fermentation broth was absorbed into 25 ml of screening medium at 28 and 37°C at 120 rpm, respectively, for enrichment and culture for 3 days. Then the enrichment medium was diluted by a 10-fold gradient method according to aseptic operation. About 100 μl of diluent was evenly coated on the solid screening medium, and the plate was placed upside down at 28 and 37°C for culture. After the colony grows, single colonies with great differences are selected on each plate and purified according to colony morphology, color, and growth rate, etc., and the purified strains of bacteria and fungi were then stored in test tubes by a streaking method.

Screening of Key Strains

The appropriate number of purified strains were picked into the screening medium (LZF) and incubated at 28 and 37°C, 120 rpm shaker, respectively, and sampled every 3 days to determine the compositional changes by HPLC ($n = 3$). The key strains of fermentation were screened according to the magnitude of the conversion rate and conversion rate of gardenia glycosides.

Identification of Key Strains

Seven fungal strains obtained from the screening were subjected to genomic DNA extraction according to the instructions of the fungal DNA extraction kit. After the PCR reaction, the amplified products were detected by 1% agarose gel electrophoresis, and then sent to Biotech Bioengineering (Shanghai) for DNA sequencing analysis.

Evaluation of Virtual Equivalence of Key Strains of Monoculture Fermentation of LZF

Evaluation of the Component Equivalence

Seven fungal strains obtained from the screening were activated with Sabouraud's medium for 2 days to obtain spore suspensions. Decoct 1 L of LZF according to the recipe, take 250 ml into 500 ml conical flask, sterilize it with 121°C for 30 min, cool it and then inoculate the screened fungal strains, respectively at 10% inoculum, then 28°C, 120 rpm for monoculture fermentation. Another 250 ml of unsterilized LZF was taken into 500 ml beaker and fermented naturally at room temperature. The fermentation was detected by HPLC and set as the end point when the conversion of gardenia glycosides exceeded 95%. Then compare the difference of chemical profile between single bacteria fermentation solution and natural fermentation solution.

Evaluation of Pharmacodynamic Equivalence

The perianal abscess rat model was used to evaluate and compare the efficacy of LZF fermented by monoculture of YY46 and YY9 with the natural fermented LZF. Eighteen Wistar male rats of SPF grade, weighing 200 ± 25 g, were purchased from Chengdu Dashuo Laboratory Animal Co., Ltd., Ministry of Science and Technology Laboratory Animal Production License No.: SCXK (Chuan) 2015-030. About 2 days of acclimatization were kept 8:00–20:00 day and night, room temperature 25°C, and free feeding. Referring to the literature method (Zeng et al., 2020), a rat perianal abscess trauma model was constructed. The rats were anesthetized by intraperitoneal injection with 10% chloral hydrate (0.3 ml/100 g), fixed on the operating table, warming lamp was turned on, disinfected with iodine volt, the hair on both sides of the lower spine of the rats was removed with electric push scissors, local skin preparation was performed, one circular incision of 2 cm in diameter was made on the back of the rats, the incision was deep to the muscle layer. After hemostasis, 0.1 ml of *Escherichia coli* ($OD_{600} = 1$) was applied to the wound surface, and the wound was covered with oil gauze and dressing and fixed with medical tape.

The successful rats were divided into three groups, YY46 group, YY9 group, and LZF group. Six rats were in each group, and the drug was changed once a day, and topical administration was started at 9:00 each day. *Escherichia coli* 0.1 ml ($OD_{600} = 1$) was added dropwise to the trauma surface 0.5 h before the drug change. After rinsing the trauma with saline and iodophor at the time of drug change, 0.5 ml of drug solution was added drop by drop, respectively, and the trauma was fixed by applying drug gauze externally. The rats were continuously treated with the drug for 12 days. The rats were observed and recorded daily for feeding, body weight, wound color, wound secretion, and the degree of swelling of wound tissue.

$$\text{The healing rate} = (\text{initial wound area} - \text{unhealed wound area})/\text{original wound area} \times 100\%.$$

The healing rates of each group were counted and the differences in efficacy were compared.

Statistical Analysis

The experimental data of the components were analyzed using SPSS (Version 19.0, SPSS Inc., Chicago, IL, United States) software, HemI (Heatmap Illustrator, version 1.0) and Origin Pro 9.0 (OriginLab Corporation, MA, United States), and SIMCA (version 14.1, Umetrics, Umea, Sweden) and SPSS (Version 19.0, SPSS Inc., Chicago, IL, United States) software for compositional and microbial correlation data analysis and Python (version 3.7.1) language for graphing.

RESULTS

Analysis of Chemical Profile During the Fermentation of LZF

A preliminary analysis of the chemical profile of the fermentation process of LZF was carried out by metabolomics. The metabolic profile analysis was performed on the fermentation solution samples taken at different times in the fermentation cycle (0–19 days; **Figure 1A**), and the metabolic profile data were processed by principal component analysis (PCA) score plot (**Figure 1B**), PCA1 and PCA2 were 52.85 and 14.93%, respectively,

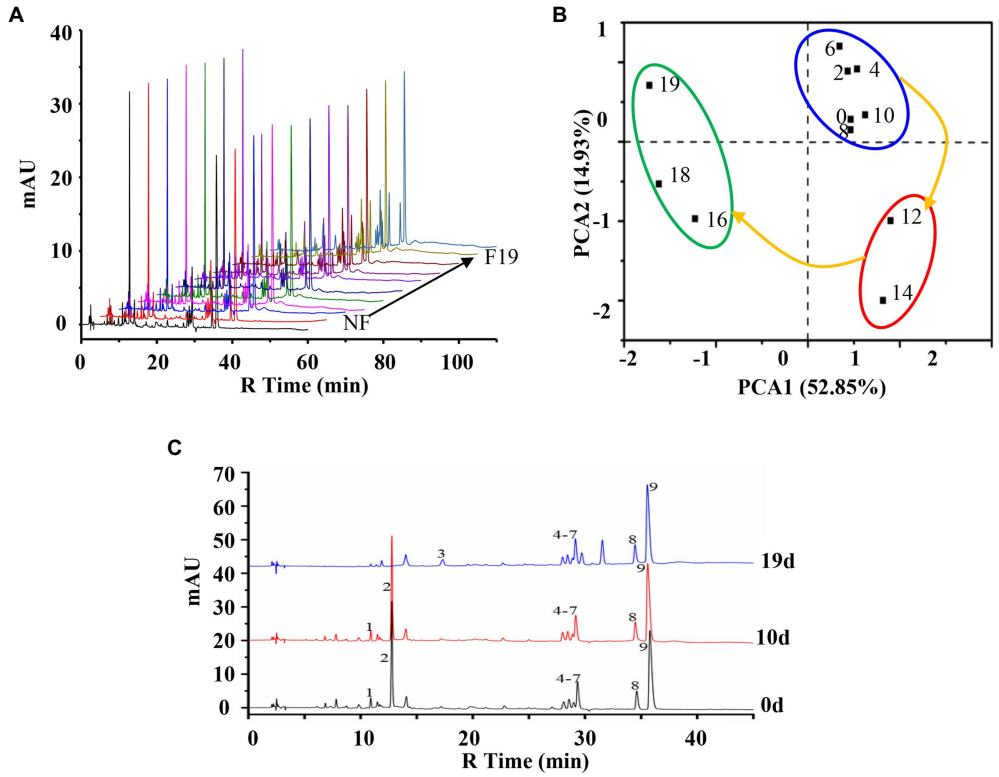

FIGURE 1 | Chemical profile analysis of the fermentation process of "Lianzhifan Solution" (LZF). **(A)** Fingerprints of metabolic profiles at different times of fermentation; **(B)** Principal component analysis (PCA) score plot; **(C)** HPLC chromatograph at 0, 10, and 19 days.

which can fully explain the differences among samples. It can be seen from the distances between different sample points that the fermentation process of LZF can be divided into three stages: early stage of fermentation (ESF; 0–10 days), medium stage of fermentation (MSF; 12–14 days), and last stage of fermentation (LSF; 16–19 days).

According to the method of peak area normalization, the chromatographic peaks of chemical components accounting for more than 2% in the fermentation broth at 0, 10 and, 19 days were counted. The results showed that there were nine main chromatographic peaks. The peak area of compounds 1 and 2 did not change significantly at the early stage of fermentation, but began to decline from the middle stage of fermentation, and gradually decreased to 0 at the later stage. Compound 3 is a newly generated component after fermentation. During the whole fermentation process, the peak area of compounds 4–9 did not change significantly, among which compound 9 had the largest peak area (**Figure 1C**).

Confirmation and Changes of the Major Chemical Components During the Fermentation of LZF

The main formulations of LZF are Coptis and Gardenia, where the main active ingredient of Coptis is benzyl isoquinoline alkaloid; the main active ingredient of Gardenia is iridoid glycosides. The main nine compounds in the solution were further confirmed by UPLC-PDA-ESI-MS method. We compared the quasi-molecular ion peaks, fragment ion peaks, and spectral features of the compounds with the reported UV spectra and mass spectral data. Nine compounds were presumed to be genipin-1-β-D-gentiobioside, geniposide, genipin, columbamine, epiberberine, jatrorrhizine, coptisine, palmatine, and berberine. The corresponding controls were then analyzed in the same way, and then the nine compounds were further confirmed by comparing the mass spectrometry data and retention times (Rtime), and the results are shown in **Figure 2**.

Compound 1: Genipin-1-β-D-gentiobioside. Molecular formula is $C_{23}H_{34}O_{15}$. Relative molecular mass is 550. In negative ion mode, ion fragmentation was *m/z* 595 $[M+CHO_2]^-$ (10 ev), *m/z* 549 $[M-H]^-$(10 ev), and the deglycoside parent nucleus (genipin) ion fragmentation *m/z* 225 (50 ev). The maximum absorption wavelength was 238.9 nm, which was consistent with control quality spectrum data.

Compound 2: Geniposide. Molecular formula is $C_{17}H_{24}O_{10}$. Relative molecular mass is 478. In negative ion mode, ion fragmentation was *m/z* 477 $[M+CHO_2]^-$(10 ev) and the deglycoside parent nucleus (genipin) ion fragmentation *m/z* 225 (50 ev). The maximum wavelength was 238.9 nm, which was consistent with the control quality spectrum data.

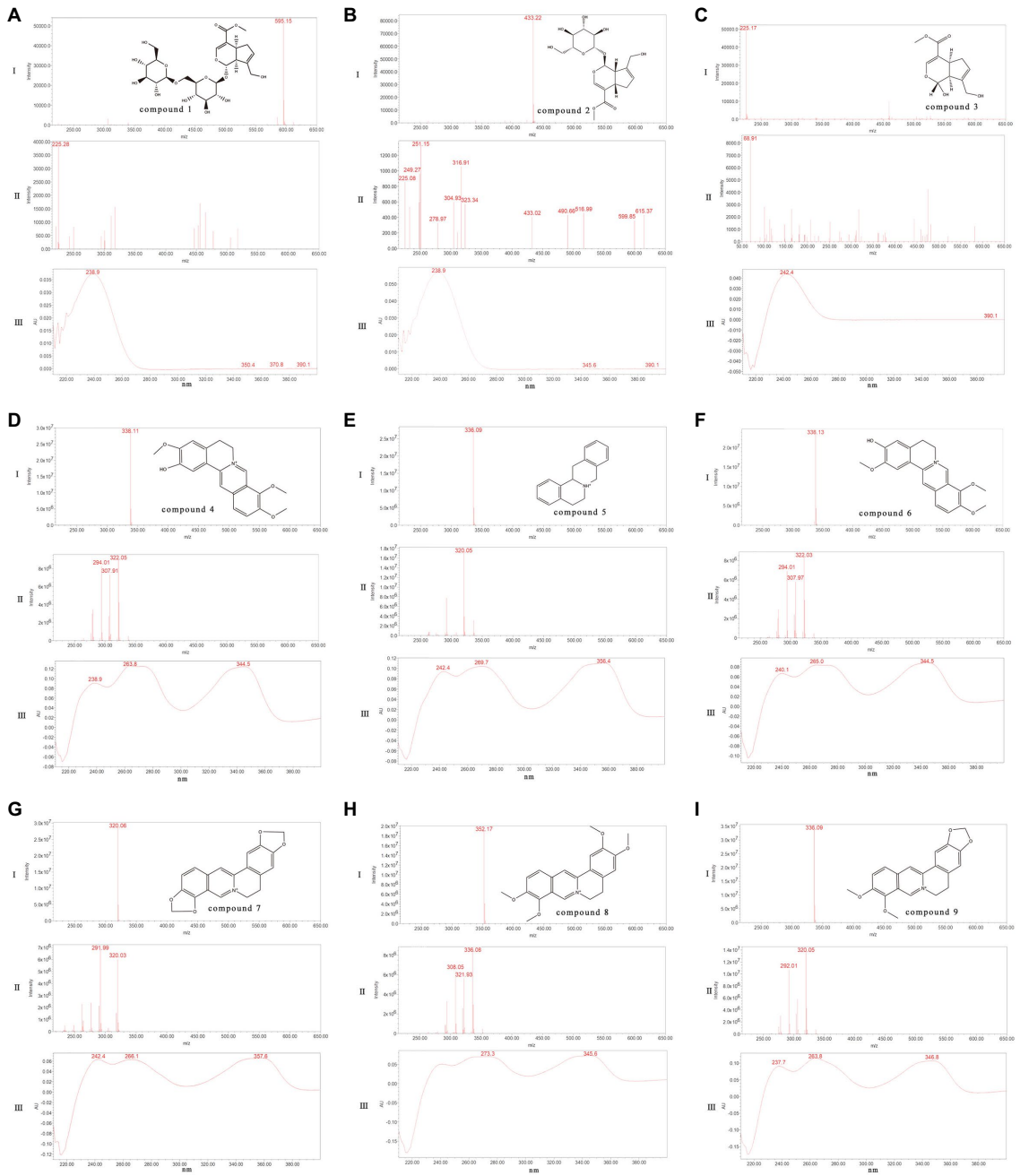

FIGURE 2 | Identification of the main chemical components in the fermentation process of LZF [I: UPLC-ESI-MS Spectrum (10 ev); II: UPLC-ESI-MS Spectrum (50 ev); III: UPLC-PDA Spectrum (210–400 nm)]. **(A)** Compound 1: Genipin-1-β-D-gentiobioside; **(B)** Compound 2: Geniposide; **(C)** Compound 3: Genipin; **(D)** Compound 4: Columbamine; **(E)** Compound 5: Epiberberine; **(F)** Compound 6: Jatrorrhizine; **(G)** Compound 7: Coptisine; **(H)** Compound 8: Palmatine; and **(I)** Compound 9: Berberine.

Compound 3: Genipin. Molecular formula is $C_{11}H_{14}O_5$. Relative molecular mass is 226. In negative ion mode, ion fragmentation was *m/z* 225 $[M\text{-}H]^-$ (10 ev), *m/z* 69 (50 ev). The maximum absorption wavelength was 244.8 nm, which was consistent with the control quality spectrum data.

Compound 4: Columbamine. Molecular formula $C_{20}H_{20}NO_4$, relative molecular mass 338. In positive ion mode, ion fragmentation was *m/z* 338 $[M]^+$ (10 ev), *m/z* 323 $[M\text{-}CH_3]^+$ (50 ev); *m/z* 308 $[M\text{-}CH_3\text{-}CH_3]^+$ (50 ev), *m/z* 294 $[M\text{-}CH_3\text{-}H\text{-}CO]^+$ (50 ev), and *m/z* 280 $[M\text{-}CH_3\text{-}CH_3\text{-}CO]^+$ (50 ev). The maximum absorption wavelength 263.8 nm (100%), 344.5 nm (99%), which were consistent with the control quality spectral data.

Compound 5: Epiberberine. Molecular formula is $C_{20}H_{18}NO_4$. Relative molecular mass is 336. In positive ion mode, ion fragmentation was *m/z* 336 $[M]^+$ (10 ev),

m/z 320 [M-CH_3]$^+$ (50 ev), *m/z* 292 [M-CH_3-H-CO]$^+$ (50 ev). The maximum absorption wavelength 269.7 nm (100%), 356.4 nm (99%), and 265.0 nm (99%), which were consistent with the data of control quality spectrum.

Compound 6: Jatrorrhizine. Molecular formula is $C_{20}H_{20}NO_4$. Relative molecular mass is 338. In positive ion mode, ion fragmentation was *m/z* 338 [M]$^+$ (10 ev), *m/z* 323 [M-CH_3]$^+$ (50 ev), *m/z* 294 [M-CH_3-H-CO]$^+$ (50 ev), and *m/z* 280 [M-CH_3-CH_3-CO]$^+$ (50 ev). The maximum absorption wavelength is 344.5 nm (100%) and 265.0 nm (99%), which were consistent with the data of control quality spectrum.

Compound 7: Coptisine. Molecular formula is $C_{19}H_{14}NO_4$, Relative molecular mass is 320. In positive ion mode, ion fragmentation was *m/z* 320 [M]$^+$ (10 ev), *m/z* 292 [M-CO]$^+$ (50 ev); *m/z* 277 [M-CH_2O-CH]$^+$ (50 ev) *m/z*, *m/z* 262 [M-CH_2O-CO]$^+$ (50 ev), and *m/z* 249 [M-CH_2O-CH-CO]$^+$ (50 ev). The maximum absorption wavelengths were 357.6 nm (100%) and 266.1 nm (99%), which were consistent with the control quality spectral data.

Compound 8: Palmatine. Molecular formula is $C_{21}H_{22}NO_4$, Relative molecular mass is 352. in positive ion mode, ion fragmentation was *m/z* 352 [M]$^+$ (10 ev), *m/z* 337 [M-CH_3]$^+$ (50 ev); *m/z* 322 [M-CH_3-CH_3]$^+$ (50 ev), *m/z* 308 [M-CH_3-H-CO]$^+$ (50 ev), and *m/z* 294 [M-CH_3-CH_3-CO]$^+$ (50 ev). The maximum absorption wavelength were 344.5 nm (100%) and 273.3 nm (100%), which were consistent with the control quality spectral data.

Compound 9: Berberine. Molecular formula is $C_{20}H_{18}NO_4$. Relative molecular mass is 336. In positive ion mode, ion fragmentation was *m/z* 336 [M]$^+$ (10 ev), *m/z* 320 [M-CH_3-H]$^+$ (50 ev); *m/z* 306 [M-CH_3-CH_3]$^+$ (50 ev), *m/z* 292 [M-CH_3-H-CO]$^+$ (50 ev), and *m/z* 278 [M-CH_3-CH_3-CO]$^+$ (50 ev). The maximum absorption wavelength were 263.8 nm (100%) and 346.8 nm (100%), which were consistent with the control quality spectrum data.

Therefore, further analysis of the characteristics of the changes of these nine compounds throughout the fermentation process showed that there was a significant biotransformation of genipin-1-*β*-D-gentiobioside and geniposide, and their content changes were not significant in the early stage of fermentation, and started to decrease from the 12 days of fermentation, and decreased to near trace levels in the final stage of fermentation (**Figure 3A**). Genipin was a newly formed composition, and started to increase from the 14 days of fermentation, and stabilized

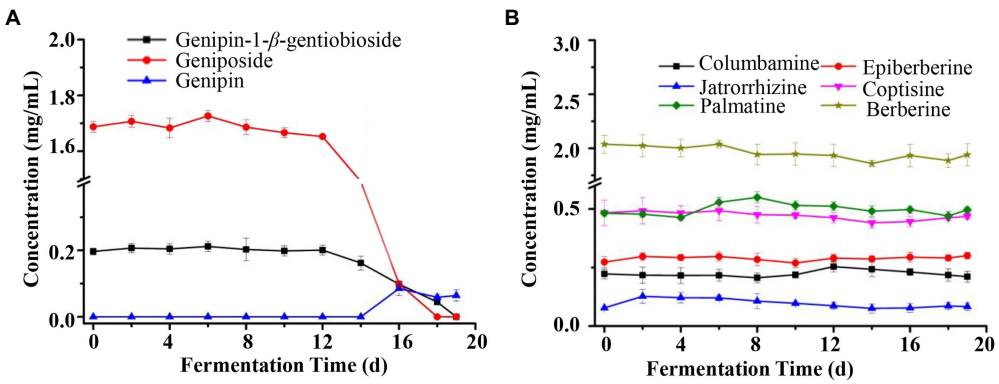

FIGURE 3 | Chemical composition dynamic changes of LZF after fermentation. **(A)** Content of iridoids (Genipin-1-β-D-gentiobioside, Geniposide, and Genipin) during fermentation of LZF; **(B)** Content of alkaloids during fermentation of LZF.

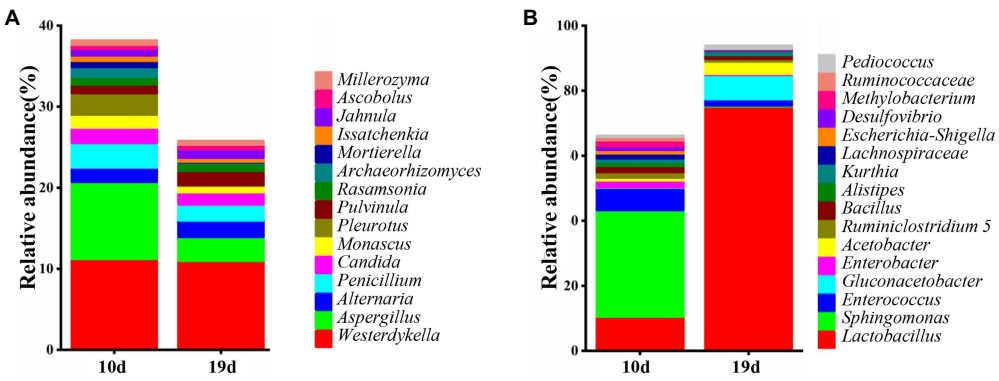

FIGURE 4 | Distribution of the fungi **(A)** and bacteria **(B)** during fermentation process.

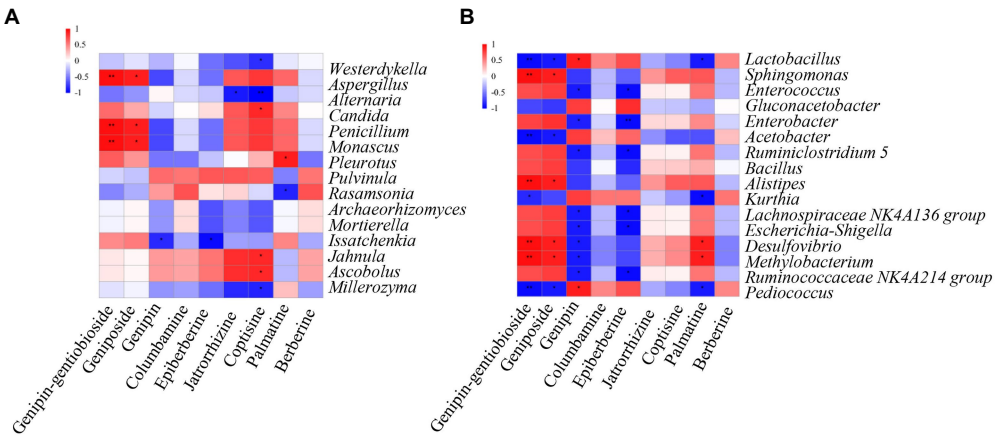

FIGURE 5 | Spearman correlation heatmap between dominant **(A)** fungal and **(B)** bacterial genera and chemical compound during LZF fermentation. The *X* and *Y* axes are chemical compound and abundant fungal and bacterial genera, respectively. The correlation coefficient (*R*) appears in different colors. The left side of the legend is the color range of different *R* values. The red color represents positive correlation and the blue color represents negative correlation. Significant values are shown as: $^{*}p > 0.01$; $^{**}p > 0.001$.

in the final stage of fermentation. This correlated with the decreasing trend of the contents of genipin-1-β-D-gentiobioside and geniposide, so genipin-1-β-D-gentiobioside and geniposide were converted into genipin by microbial conversion. At the same time, the contents of six alkaloids, including columbamine, epiberberine, jatrorrhizine, coptisine, palmatine, and berberine, did not change significantly during the whole fermentation process, with almost no obvious biotransformation (**Figure 3B**). Therefore, iridoid glycosides were the main substances of biotransformation in the fermentation process, and alkaloids were relatively stable at the initial level.

Correlation Between Dominant Microbiome and Compound Transformation in LZF Fermentation

Microorganisms can transform the main components in the fermentation, so we analyzed the dominant bacteria and fungi in the fermentation process using high-throughput sequencing technology. The community composition and abundance of species in the LZF fermentation broth at 10 and 19 days were analyzed at the genus level, and the results are shown in **Figure 4**. As can be seen, there were 15 dominant genera of fungi (relative abundance > 0.5%), which were *Westerdykella* (11.08%), *Aspergillus* (6.22%), *Alternaria* (1.91%), *Penicillium* (2.50%), *Candida* (1.70%), and *Monascus* (1.19%), *Pleurotus* (1.38%), *Pulvinula* (1.41%), *Rasamsonia* (0.96%), *Archaeorhizomyces* (0.65%), *Mortierella* (0.42%), *Issatchenkia* (0.57%), *Jahnula* (0.94%), *Ascobolus* (0.53%), and *Millerozyma* (0.52%). There were 16 dominant bacterial genera (relative abundance > 1%) and they were *Lactobacillus* (42.80%), *Sphingomonas* (16.53%), *Enterococcus* (4.40%), *Gluconacetobacter* (3.80%), *Enterobacter* (1.23%), *Acetobacter* (2.29%), *Ruminiclostridium* 5 (1.28%), *Bacillus* (1.50%), *Alistipes* (0.67%), *Kurthia* (1.20%), *Lachnospiraceae* NK4A136 group (0.87%), *Escherichia-Shigella* (0.61%), *Desulfovibrio* (0.67%), *Methylobacterium* (0.92%), *Ruminococcaceae* NK4A214 group (0.59%), and *Pediococcus* (0.71%).

To analyze the correlation between the dominant genera of LZF fermentation and compound biotransformation, we calculated Spearman correlation coefficients of 15 dominant fungal genera and 16 dominant bacterial genera with compounds and plotted Spearman correlation heat map with R software (**Figure 5**). As can be seen, the fungal genera *Aspergillus*, *Penicillium*, and *Monascus* were highly significantly positively correlated with genipin-1-β-D-gentiobioside ($p < 0.01$) and with geniposide ($p < 0.05$). Coptisine was significantly positively correlated with *Jahnula*, *Ascobolus*, and *Candida* significantly positively correlated ($p < 0.05$) and with *Westerdykella*, *Millerozyma*, and *Alternaria* significantly negatively correlated ($p < 0.05$). Bacteria were more correlated with iridoids glycosides components in LZF, *Sphingomonas*, *Alistipes*, and *Desulfovibrio*, *Methylobacterium* were highly significantly positively correlated with genipin-1-β-D-gentiobioside ($p < 0.01$) and with geniposide ($p < 0.05$); *Lactobacillus*, *Acetobacter*, and *Pediococcus* were highly significantly negatively correlated with genipin-1-β-D-gentiobioside ($p < 0.01$) and with geniposide ($p < 0.05$). Genipin was significantly positively correlated with *Lactobacillus* and *Pediococcus* significantly positively correlated ($p < 0.05$) and significantly negatively correlated ($p < 0.05$) with dominant bacteria such as *Enterococcus*, *Enterobacter*, and *Ruminiclostridium*.

Isolation and Identification of Dominant Strains

The thermal stability of the LZF pre-fermentation decoction was evaluated according to the chromatographic conditions in section "LZF Preparation and Sampling," and no chemical profile changes occurred before and after sterilization. We used this decoction as selection media to screen the transformation ability of isolated and purified bacterial and fungal strains, and artificially inoculated these strains for monoculture fermentation for 15 days after sampling to detect the changes of nine main components. The results of the chemical composition in the fermentation broth of bacterial strains were unchanged

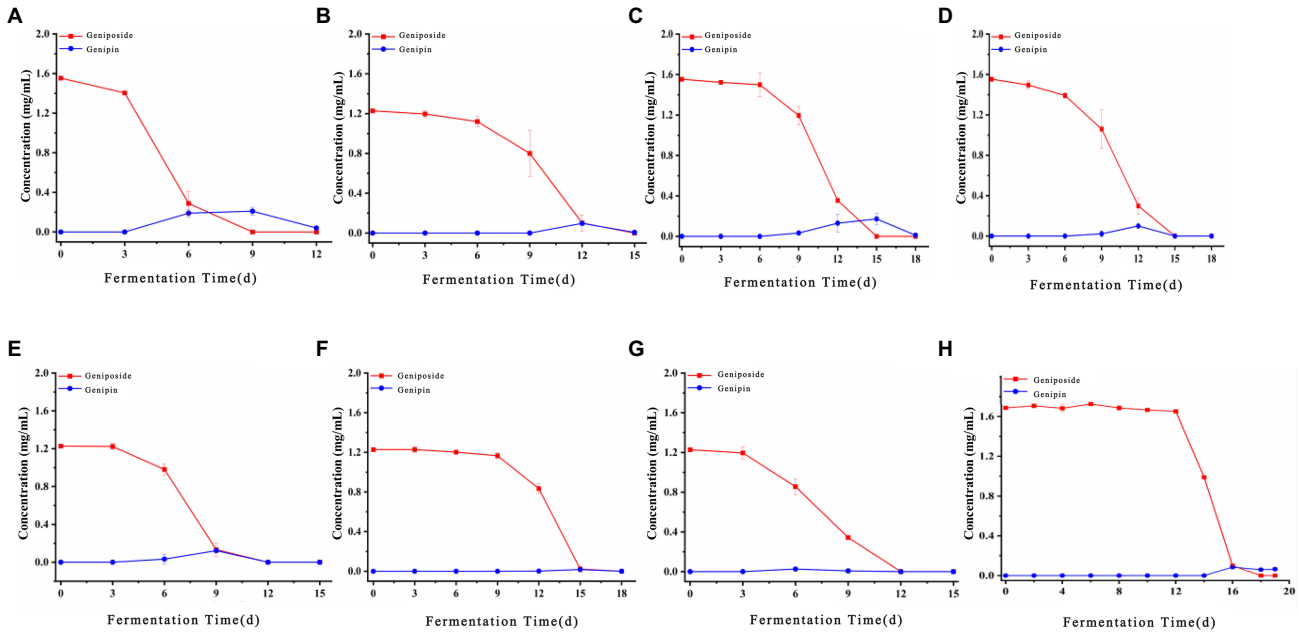

FIGURE 6 | Content of iridoids during fermentation of LZF by monoculture fermentation and natural fermentation. **(A)** *Penicillium expansum* YY-46; **(B)** *Penicillium qlabrum* YY-51; **(C)** *Aspergillus niger* YY-9; **(D)** *Aspergillus japonicus* YY-5; **(E)** *Cladosporium oxysporum* YY-19; **(F)** *Cladosporium tenuissimum* YY-23; **(G)** *Cladosporium cladosporioides* YY-34; and **(H)** natural fermentation.

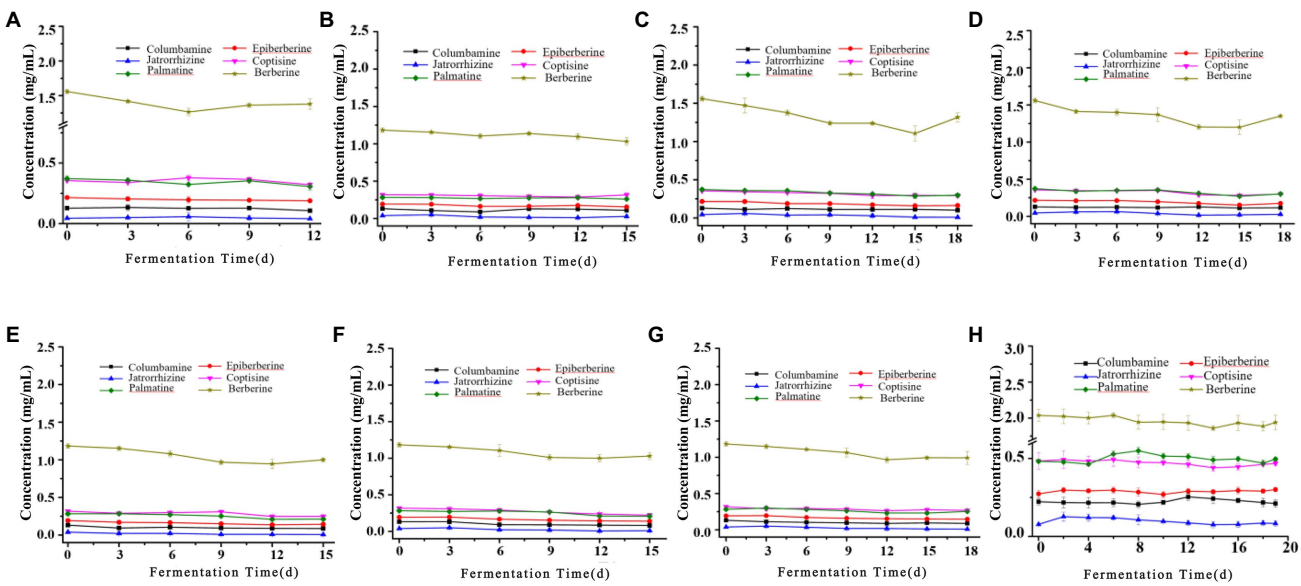

FIGURE 7 | Content of alkaloids during fermentation of LZF by monoculture fermentation and natural fermentation. **(A)** *Penicillium expansum* YY-46; **(B)** *P. qlabrum* YY-51; **(C)** *A. niger* YY-9; **(D)** *A. japonicus* YY-5; **(E)** *C. oxysporum* YY-19; **(F)** *C. tenuissimum* YY-23; **(G)** *C. cladosporioides* YY-34; and **(H)** natural fermentation.

and could not transform the iridoids, but the fermentation broth of fungal strains mostly showed changes in composition. Seven of the fungal strains (named YY-5, YY-9, YY-19, YY-23, YY-34, YY-46, and YY-51) were selected for identification by combining growth rate and conversion ability, and the results were identified as *Aspergillus japonicus* YY-5, *Aspergillus niger* YY-9, *Cladosporium oxysporum* YY-19, *Cladosporium tenuissimum* YY-23, *Cladosporium cladosporioides* YY-34, *Penicillium expansum* YY-46, and *Penicillium qlabrum* YY-51.

The biotransformation ability of seven fungal strains was further compared, as shown in **Figures 6, 7**. The dynamics of the components of the LZF fermented by *P. expansum* YY-46, *Penicillium qlabrum* YY-51, *A. niger* YY-9, and *Aspergillus japonicus* YY-5 were consistent with those of the natural

fermentation process of the solution, while the dynamics of the components of the LZF fermented by *C. oxysporum* YY-19, *C. tenuissimum* YY-23, and *C. cladosporioides* YY-34 fermentation showed some differences in compositional changes from those during natural fermentation. In terms of the biotransformation ability of gardenia glycosides, all seven strains were able to achieve 100% conversion, but the conversion rate varied among strains. *Penicillium expansum* YY-46 had the strongest transformation ability and the fastest conversion rate, and the conversion rate had reached 100% at 9 days. *Cladosporium tenuissimum* YY-23 had the slowest conversion rate, with complete conversion at 18 days. Therefore, in order of transformation rate, the transformation capacity of seven strains was *P. expansum* YY-46>*A. niger* YY-9>*A. japonicus* YY-5>*P. qlabrum* YY-51>*C. oxysporum* YY-19>*C. cladosporioides* YY34>*C. tenuissimum* YY-23. Extended *P. japonicum* YY-46 and *A. niger* YY-9 were the two fermentative strains with high transformation capacity. The results were also consistent with the correlation analysis and the observation of natural fermentation, so *P. expansum* YY-46 and *A. niger* YY-9 were identified as the key strains for the fermentation of LZF.

Evaluation of Virtual Equivalence of Key Strains of Monoculture Fermentation of LZF

Evaluation of the Composition Equivalence

About 3 L LZF was decocted according to the formula, and 250 ml was taken into a 500 ml conical flask. After sterilization at 121°C for 30 min, strains YY-46 and YY-9 were inoculated according to the aseptic operation after cooling, and then monoculture fermentation was conducted at 28°C and 120 rpm. Another 250 ml of unsterilized LZF was taken into a 500 ml beaker and fermented naturally at room temperature. Samples were taken daily and detected by HPLC. When the conversion of gardenoside exceeded 95%, it was the end point of fermentation. There were three samples in parallel in each group. Our results indicated that the fermentation ending time of YY-46 and YY-9 strains was 5 and 6 days respectively, while the fermentation ending time of natural process was 19 days (**Figure 8**). Furthermore, the metabolic profiles of LZF prepared by two kinds of single bacteria were matched with those of LZF prepared by natural method, and the similarity evaluation was carried out. The similarity between these two metabolic profiles ranged from 0.963 to 1.000. The results indicated that the chemical compositions of the solution prepared by the monoculture and the natural preparation were essentially homogeneous. However, when the inoculation amount and fermentation conditions were optimized, the conversion of iridoid glycosides by monoculture fermentation was greatly improved. The fermentation cycle of YY-46 was 5 days, which

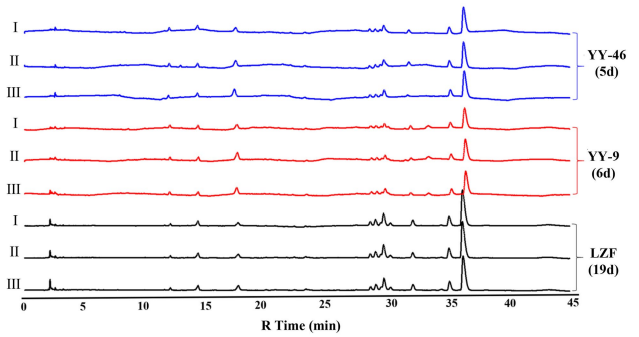

FIGURE 8 | HPLC chromatogram of chemical component equivalence evaluation (I, II, and III are parallel samples).

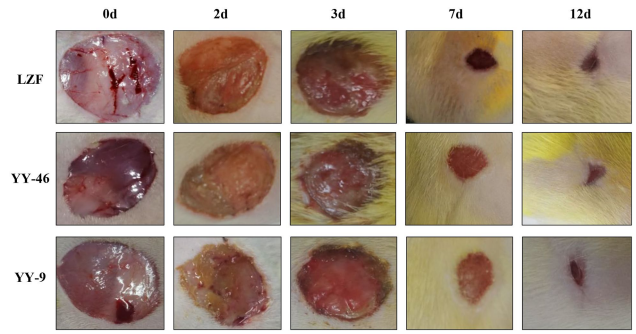

FIGURE 9 | Equivalence evaluation of pharmacodynamics in rats.

TABLE 2 | Effect of three kinds of LZF on the wound healing rate of rats ($n = 6$, $X \pm s$)

Groups	Wound healing rate (M ± *SD*%)		
	Day 3	Day 7	Day 12
LZF	23.67 ± 6.07	85.69 ± 1.51	94.28 ± 1.08
YY46	37.54 ± 3.86	85.44 ± 1.88	94.03 ± 2.79
YY9	29.22 ± 5.54	79.37 ± 6.26	92.49 ± 5.27

TABLE 1 | Similarity analysis of three kinds of LZF.

	LZF-1	LZF-2	LZF-3	YY-9-1	YY-9-2	YY-9-3	YY-64-1	YY-64-2	YY-64-3
LZF-1	1.000	0.999	0.999	0.983	0.968	0.979	0.982	0.99	0.993
LZF-2	0.999	1.000	1.000	0.98	0.964	0.976	0.980	0.988	0.994
LZF-3	0.999	1.000	1.000	0.978	0.963	0.976	0.979	0.987	0.993
YY-9-1	0.983	0.980	0.978	1.000	0.996	0.996	0.993	0.993	0.989
YY-9-2	0.968	0.964	0.963	0.996	1.000	0.995	0.990	0.986	0.979
YY-9-3	0.979	0.976	0.976	0.996	0.995	1.000	0.987	0.989	0.988
YY-64-1	0.982	0.980	0.979	0.993	0.990	0.987	1.000	0.996	0.992
YY-64-2	0.990	0.988	0.987	0.993	0.986	0.989	0.996	1.000	0.997
YY-64-3	0.993	0.994	0.993	0.989	0.979	0.988	0.992	0.997	1.000

was nearly four times shorter than natural fermentation cycle, and the fermentation cycle of YY-9 was 6 days, which was also nearly three times shorter than natural fermentation cycle. Therefore, monoculture fermentation can shorten the fermentation cycle and improve the fermentation efficiency under the condition of consistent quality, and the fermentation process for mass production can be further optimized in the later stage. The results are shown in **Table 1**.

Evaluation of Pharmacodynamics

A rat model of perianal abscess was used to evaluate and compare the efficacy of YY46, YY9, and LZF groups. Morphological observations showed that the degree of wound oozing, skin swelling, and redness around the wound edges of rats in the LZF and YY46 groups were basically the same during the treatment process, and the YY9 group showed a slightly weaker therapeutic effect than the other two groups, but there was no significant difference. At 7 days, the exudate almost disappeared, the granulation tissue started to crust and a small amount of blood leaked when crust was touched by cotton swabs in all treatment groups. At 12 days, there was no significant exudate and epithelial coverage in the treated group; the wound was smaller in the LZF and YY46 groups than in the YY9 group, as shown in **Figure 9**. After 12 days of treatment, the rats in the YY46 and LZF groups recovered better, and the wound healing rate had reached 94% by 12 days. Although, the wound healing rate of the YY9 group was lower than that of the other two groups throughout the observation period, it also reached 92% healing rate at 12 days (**Table 2**). Therefore, both of the two new preparations of monoculture fermentation with LZF could promote the healing of perianal abscess wounds in rats, and had virtual pharmacodynamic equivalence with the traditional preparation.

DISCUSSION

Natural fermentation is one of the traditional methods of processing herbal preparations and has a long history in China, while modern pharmaceutical industries commonly use monoculture fermentation for mass production of small molecule drugs (Wang et al., 2019; Zhang et al., 2021). The fermentation process is often accompanied by the change of chemical profile, but some chemical composition remains stable (Gao et al., 2020; Cai et al., 2021). We found a similar phenomenon in LZF fermentation. A variety of iridoids glycosides (compound 1 and 2) were converted to genipin (compound 3) by the action of various glycosidases secreted by microbiome, while alkaloids (compound 4–9) with antibacterial effects maintained compositional stability before and after fermentation. These results suggested the coexistence of instable and stable chemical composition in the fermentation system, and the biotransformation of instable composition should be the main event of the fermentation. Therefore, we speculate that iridoid deglycosylation is a key event in LZF fermentation.

During the fermentation process, the structural evolution of microbial communities was accompanied by significant changes in the chemical profile (An et al., 2020; Meng et al., 2021). High-throughput sequencing technology is developed to dissect microecological structures in several fields, such as food (Wu et al., 2019), healthcare (Fernanda et al., 2018), and environment (Guo et al., 2019), and it is also a frontier technology for screening microorganisms in complex microbial fermentation system. Recently, high-throughput sequencing and metabolomics have been used to predict the key strains of fermentation by correlation analysis, but researchers also believe that the predicted key strains would include culture-dependent and culture-independent strains (Xu et al., 2020, 2021). Our results showed that bacteria had a greater correlation with chemical composition in LZF fermentation than fungi did. However, when we focused on the key events of LZF fermentation and used classical screening methods, we found that fungal strains had a greater contribution to the biotransformation events than bacteria. Thus, the true key microbial strains remain to be determined and confirmed in both predictable and real fermentation systems. Therefore, only in the real fermentation system, we can obtain the identified strains by focusing on the main events of fermentation to screen the key strains.

Deglycosylation that occurs during the fermentation of LZF produces genipin, which has anti-inflammatory and antioxidant biological activities and play a role in promoting wound healing through anti-inflammatory pathways, while the hydrophilicity of iridoids glycosides is higher than the lipophilicity, thus making them difficult to exert their medicinal effects transdermally (Shanmugam et al., 2018). The deglycosylation reduce genipin's hydrophilicity and enhance its lipophilicity, so as to achieve transdermal properties to exert the pharmacodynamics effects. After obtaining two highly deglycosylated biotransformed strains, we performed monoculture fermentation to evaluate the equivalence of chemical component between the monoculture fermentation preparation and the traditional fermentation preparation. The results suggested that the monoculture fermentation preparations and the traditional fermentation had a chemical component equivalence. The new preparations also maintain the characteristics of alkaloid components stable, while making iridoids glycosides deglycosylation unstable. Therefore, we can speculate that these two strains may be the key strains in the LZF fermentation. However, the equivalence of the main chemical components of the natural medicine does not directly infer that the new preparations are equivalent to the traditional preparation in terms of biological activity. It is necessary to evaluate and validate the bioactive equivalence in the real world. Therefore, in our strategy of screening key functional strains, we added the important aspect of bioactivity equivalence evaluation as a post-verification operation step for the purpose of efficacy. The evaluation results were in accordance with expectations, and the new and traditional preparations were virtual equivalent in the treatment of perianal abscess. Therefore, by analyzing microfauna communities-chemical component in fermentation systems, and then evaluating the bioactivity of new preparations for virtual equivalence by purified strains, a "Microfauna communities-Chemical component-Pharmacodynamic" axis is formed for screening key functional strains in complex fermentation systems, which can realize a new strategy for complete combination of high-throughput screening theory and real-world reassessment.

CONCLUSION

In this study, the chemical component and bioequivalence evaluation proved that the monoculture fermentation was more effective than the natural fermentation, suggesting that this method could be used as an upgrade measure for the production process. We sought to determine whether it is possible to define a predictive strategy based on "Microfauna communities-Chemical component-Pharmacodynamic" axis that can be used to select key strains who can reduce the time of process and preserve the initial metabolites. This strategy not only provides new ideas for TCM fermentation preparation technology, but also provides an important scientific basis for improving the production process and formulating GMP work. More importantly, it is also applicable to the whole fermentation drugs industry.

Accession Number of Sequences

The sequence information from pyrosequencing has been uploaded to the European Nucleotide Archive database under the accession number PRJEB35333.

DATA AVAILABILITY STATEMENT

The datasets presented in this study can be found in online repositories. The names of the repository/repositories and accession number(s) can be found at: https://www.ebi.ac.uk/ena, PRJEB35333.

ETHICS STATEMENT

The animal study was reviewed and approved by the Ethics Committee of Sichuan Normal University.

AUTHOR CONTRIBUTIONS

JX, YY, and XZ designed the study. YY conducted the experiment, analyzed the data, and with JX drafted the manuscript. XYa and XYu provided experimental conditions. TP prepared the experimental materials. TP and QP helped to revise the manuscript. All authors contributed to the article and approved the submitted version.

FUNDING

This work was supported by the National Natural Science Foundation of China (Grants No. 32001078), the Science & Technology Department Foundation of Sichuan Province (Grant No. 2020YJ0372), and the Science and Technology Project of the Health Planning Committee of Sichuan (Grants No. 20PJ169).

ACKNOWLEDGMENTS

The authors would like to thank Du Juan (Sichuan Normal University) for HPLC assistance.

REFERENCES

Al-Saman, M., Helmy, M., Aadella, A., Wikins, M., Gobba, N., and Mahrous, H. (2021). Optimization of lovastatin production by Aspergillus terreus ATCC 10020 using solid-state fermentation and its pharmacological applications. *Biocatal. Agric. Biotechnol.* 31:101906. doi: 10.1016/j.bcab.2021.101906

An, F., Li, M., Zhao, Y., Zhang, Y., Mu, D., Hu, X., et al. (2020). Metatranscriptome-based investigation of flavor-producing core microbiota in different fermentation stages of dajiang, a traditional fermented soybean paste of Northeast China. *Food Chem.* 343:128509. doi: 10.1016/j.foodchem.2020.128509

Barrios-González, J., Pérez-Sánchez, A., and Bibián, M. (2020). New knowledge about the biosynthesis of lovastatin and its production by fermentaton of *Aspergillus terreus*. *Appl. Microbiol. Biotechnol.* 104, 8979–8998. doi: 10.1007/s00253-020-10871-x

Bergonzi, M. C., Righeschi, C., Isacchi, B., and Bilia, A. R. (2012). Identification and quantification of constituents of *Gardenia jasminoides* Ellis (Zhizi) by HPLC-DAD-ESI-MS. *Food Chem.* 134, 1199–1204. doi: 10.1016/j.foodchem.2012.02.157

Bian, B., Lowernedza, A., Song, J., Wang, H., and Brantner, A. (2011). Validation of a high performance liquid chromatography (HPLC) method for the quality control of the traditional Chinese medicine (TCM) formulation, traditional Chinese formula Huanglianjiedutang (HLJDT). *J. Med. Plant Res.* 5, 54–61. doi: 10.5897/JMPR11.086

Cai, W., Tang, F., Wang, Y., Zhang, Z., Xue, Y., Zhao, X., et al. (2021). Bacterial diversity and flavor profile of Zha-Chili, a traditional fermented food in China. *Food Res. Int.* 141:110112. doi: 10.1016/j.foodres.2021.110112

Caporaso, J. G., Kuczynski, J., Stombaugh, J., Bittinger, K., Bushman, F. D., Costello, E. K., et al. (2010). QIIME allows analysis of high-throughput community sequencing data. *Nat. Methods* 7, 335–336. doi: 10.1038/nmeth.f.303

Caporaso, J. G., Lauber, C. L., Walters, W. A., Berg-Lyons, D., Lozupone, C. A., Turnbaugh, P. J., et al. (2011). Global patterns of 16S rRNA diversity at a depth of millions of sequences per sample. *Proc. Natl. Acad. Sci. U. S. A.* 108(Suppl 1), 4516–4522. doi: 10.1073/pnas.1000080107

Dai, S. Y., Xu, B., Zhang, Y., Li, J. Y., Sun, F., Shi, X. Y., et al. (2016). Establishment and reliability evaluation of the design space for HPLC analysis of six alkaloids in *Coptis chinensis* (Huanglian) using Bayesian approach. *Chin. J. Nat. Med.* 14, 697–708. doi: 10.1016/S1875-5364(16)30083-8

Edgar, R. C. (2013). UPARSE: highly accurate OTU sequences from microbial amplicon reads. *Nat. Methods* 10, 996–998. doi: 10.1038/nmeth.2604

Edgar, R. C., Haas, B. J., Clemente, J. C., Quince, C., and Knight, R. (2011). UCHIME improves sensitivity and speed of chimera detection. *Bioinformatics* 27, 2194–2200. doi: 10.1093/bioinformatics/btr381

Fernanda, B., Pontin, L. N., Tallarico, A., Kimiko, S. I., Inés, G., Isay, S., et al. (2018). Impact of combining acerola by-product with a probiotic strain on a gut microbiome model. *Int. J. Food Sci. Nutr.* 70, 182–194. doi: 10.1080/09637486.2018.1498065

Gao, Z., Wu, Z., and Zhang, W. (2020). Effect of pit mud on bacterial community and aroma components in yellow water and their changes during the fermentation of Chinese strong-flavor liquor. *Foods* 9:372. doi: 10.3390/foods9030372

Guo, B., Liu, C., Gibson, C., and Frigon, D. (2019). Wastewater microbial community structure and functional traits change over short timescales. *Sci. Total Environ.* 662, 779–785. doi: 10.1016/j.scitotenv.2019.01.207

Gweon, H., Oliver, A., Taylor, J., Booth, T., Gibbs, M., Read, D., et al. (2015). PIPITS: an automated pipeline for analyses of fungal internal transcribed spacer sequences from the Illumina sequencing platform. *Methods Ecol. Evol.* 6, 973–980. doi: 10.1111/2041-210X.12399

Huang, P., Wang, P., Xu, J., Sun, M., Liu, X., Lin, Q., et al. (2020). Fermented traditional Chinese medicine in diet altered the composition of intestine microbiota in broiler chickens. *Res. Vet. Sci.* 135, 8–14. doi: 10.1016/j.rvsc.2020.12.021

Kim, Y. M., Choi, W. S., Kim, H. J., Lee, E. W., Park, B., Lee, H., et al. (2014). Antiulcerogenic and anticancer activities of korean red ginseng extracts bio-transformed by *Paecilomyces tenuipes*. *J. Appl. Biol. Chem.* 57, 41–45. doi: 10.3839/jabc.2014.007

Li, L., Wang, L., Fan, W. X., Jiang, Y., Zhang, C., Li, J. H., et al. (2020). The application of fermentation technology in traditional Chinese medicine: a review. *Am. J. Chin. Med.* 48, 899–921. doi: 10.1142/S0192415X20500433

Liu, T., Jia, T., Chen, J., Liu, X., Zhao, M., and Liu, P. (2017). Analysis of microbial diversity in Shenqu with different fermentation times by PCR-DGGE. *Braz. J. Microbiol.* 48, 246–250. doi: 10.1016/j.bjm.2017.01.002

Liu, Z., Tang, Y., Zhou, R., Shi, X., Zhang, H., Liu, T., et al. (2018). Bi-directional solid fermentation products of *Trametes robiniophila* Murr with Radix Isatidis inhibit proliferation and metastasis of breast cancer cells. *J. Chin. Med. Assoc.* 81, 520–530. doi: 10.1016/j.jcma.2017.12.003

Magoč, T., and Salzberg, S. L. (2011). FLASH: fast length adjustment of short reads to improve genome assemblies. *Bioinformatics* 27, 2957–2963. doi: 10.1093/bioinformatics/btr507

Marič, J., Skočaj, M., Likar, M., Sepčić, K., Cigić, I. K., Grundner, M., et al. (2019). Comparison of lovastatin, citrinin and pigment production of different *Monascus purpureus* strains grown on rice and millet. *J. Food Sci. Technol.* 56, 3364–3373. doi: 10.1007/s13197-019-03820-8

Meng, Y., Chen, X., Sun, Z., Li, Y., Chen, D., Fang, S., et al. (2021). Exploring core microbiota responsible for the production of volatile flavor compounds during the traditional fermentation of koumiss. *LWT* 135:110049. doi: 10.1016/j.lwt.2020.110049

Qu, Q., Yang, F., Zhao, C., Liu, X., Yang, P., Li, Z., et al. (2021). Effects of fermented ginseng on the gut microbiota and immunity of rats with antibiotic-associated diarrhea. *J. Ethnopharmacol.* 267:113594. doi: 10.1016/j.jep.2020.113594

Quast, C., Pruesse, E., Yilmaz, P., Gerken, J., Schweer, T., Yarza, P., et al. (2012). The SILVA ribosomal RNA gene database project: improved data processing and web-based tools. *Nucleic Acids Res.* 41, D590–D560. doi: 10.1093/nar/gks1219

Shanmugam, M. K., Shen, H., Tang, F., Arfuso, F., Rajesh, M., Wang, L., et al. (2018). Potential role of genipin in cancer therapy. *Pharmacol. Res.* 133, 195–200. doi: 10.1016/j.phrs.2018.05.007

Shimoyama, T., Takahashi, R., Kimura, M., and Fukuda, Y. (2015). Study of the mechanisms of a Japanese traditional fermented medicine in the improvement of constipation. *J. Gastroenterol. Hepatol.* 30(Suppl. 1), 53–59. doi: 10.1111/jgh.12741

Toju, H., Tanabe, A. S., Yamamoto, S., and Sato, H. (2012). High-coverage ITS primers for the DNA-based identification of ascomycetes and basidiomycetes in environmental samples. *PLoS One* 7:e40863. doi: 10.1371/journal.pone.0040863

Wang, Y., Mei, X. D., Liu, Z., Li, J., Zhang, X., Wang, S., et al. (2019). Chemical constituent profiling of *Paecilomyces cicadae* liquid fermentation for astragli radix. *Molecules* 24:2984. doi: 10.3390/molecules24162948

Wu, Q., Wang, S., Yao, N., and Xu, Y. (2019). Construction of synthetic microbiota for reproducible flavor metabolism in Chinese light aroma type liquor produced by solid-state fermentation. *Appl. Environ. Microbiol.* 85:e03090-18. doi: 10.1101/510610

Xu, X., Wu, B., Zhao, W., Lao, F., Chen, F., Liao, X., et al. (2021). Shifts in autochthonous microbial diversity and volatile metabolites during the fermentation of chili pepper (*Capsicum frutescens* L.). *Food Chem.* 335:127512. doi: 10.1016/j.foodchem.2020.127512

Xu, X., Wu, B., Zhao, W., Pang, X., Lao, F., Liao, X., et al. (2020). Correlation between autochthonous microbial communities and key odorants during the fermentation of red pepper (*Capsicum annuum* L.). *Food Microbiol.* 91:103510. doi: 10.1016/j.fm.2020.103510

Ye, Y., Zhang, X., Du, J., Xue, A., Yang, M., Xie, J., et al. (2019). Study on changes of active components in Lianzhifan solution under different storage conditions. *Chin. Tradit. Herb. Drug* 50, 106–113. doi: 10.7501/j.issn.0253-2670.2019.23.015

Yim, N. H., Gu, M. J., Park, H. R., Hwang, Y. H., and Ma, J. Y. (2018). Enhancement of neuroprotective activity of Sagunja-tang by fermentation with lactobacillus strains. *BMC Complement. Altern. Med.* 18:312. doi: 10.1186/s12906-018-2361-z

Yin, T. P., Xing, Y., Cai, L., Yu, J., Luo, P., and Ding, Z. T. (2017). A new polyketide glycoside from the rhizospheric *Clonostachys rogersoniana* associated with *Panax notoginseng*. *J. Asian Nat. Prod. Res.* 19, 1258–1263. doi: 10.1080/10286020.2017.1314271

Yuan, X., Wang, Z., Zou, L., Yang, X., Hu, H., Yu, T., et al. (2016). Study on Lianzhifan solution promoting wound healing after rat's perianal abscess. *J. Chengdu Univ. Tradit. Chin. Med.* 39, 39–43. doi: 10.13593/j.cnki.51-1501/r.2016.01.039

Yuan, X., Ye, Y., Zhao, J., Xie, J., Jin, Y., Xiao, Y., et al. (2018). Fungal community diversity changes of Lianzhifan solution during fermentation process by high-throughput sequence technology. *Chin. Tradit. Herb. Drug* 49, 4259–4268. doi: 10.7501/j.issn.0253-2670.2018.18.009

Zeng, T. T., Bin, D. H., Luo, Z., Li, K., Zheng, F. P., Cao, H., et al. (2020). Effect of Xiangpi Shengji ointment on the expression of IL-8 and TNF-α in wounds of rats after anal fistula operation. *World J. Integr. Tradit. West. Med.* 15, 634–736. doi: 10.13935/j.cnki.sjzx.200413

Zhang, Z., Li, H., Xu, T., Xu, H., He, S., Li, Z., et al. (2021). Jianqu fermentation with the isolated fungi significantly improves the immune response in immunosuppressed mice. *J. Enthnopharmacol.* 267:113512. doi: 10.1016/j.jep.2020.113512

Zhang, Y., Zhou, L., Ma, W., Shi, X., Zhang, H., and Shi, X. (2017). Bidirectional solid fermentation using *Trametes robiniophila* Murr. for enhancing efficacy and reducing toxicity of rhubarb (*Rheum palmatum* L.). *J. Tradit. Chin. Med. Sci.* 4, 306–313. doi: 10.1016/j.jtcms.2017.07.010

Conflict of Interest: TP was employed by company Keystonecare Technology (Chengdu) Co.

The remaining authors declare that the research was conducted in the absence of any commercial or financial relationships that could be construed as a potential conflict of interest.

Publisher's Note: All claims expressed in this article are solely those of the authors and do not necessarily represent those of their affiliated organizations, or those of the publisher, the editors and the reviewers. Any product that may be evaluated in this article, or claim that may be made by its manufacturer, is not guaranteed or endorsed by the publisher.

frontiers in Microbiology

ORIGINAL RESEARCH
published: 06 September 2021
doi: 10.3389/fmicb.2021.739995

Screening of Fungi for Antimycobacterial Activity Using a Medium-Throughput Bioluminescence-Based Assay

Alexander B. J. Grey[1], Melissa M. Cadelis[1,2], Yiwei Diao[1], Duckchul Park[3], Thomas Lumley[4], Bevan S. Weir[3], Brent R. Copp[2†] and Siouxsie Wiles[1†]*

[1] Bioluminescent Superbugs Lab, Department of Molecular Medicine and Pathology, School of Medical Sciences, The University of Auckland – Waipapa Taumata Rau, Auckland, New Zealand, [2] School of Chemical Sciences, The University of Auckland – Waipapa Taumata Rau, Auckland, New Zealand, [3] Manaaki Whenua – Landcare Research, Auckland, New Zealand, [4] Department of Statistics, The University of Auckland – Waipapa Taumata Rau, Auckland, New Zealand

There is a real and urgent need for new antibiotics able to kill Mycobacteria, acid-fast bacilli capable of causing multiple deadly diseases. These include members of the *Mycobacterium tuberculosis* complex, which causes the lung disease tuberculosis (TB) as well as non-tuberculous Mycobacteria (NTM) a growing cause of lung, skin, soft tissue, and other infections. Here we describe a medium-throughput bioluminescence-based pipeline to screen fungi for activity against Mycobacteria using the NTM species *Mycobacterium abscessus* and *Mycobacterium marinum.* We used this pipeline to screen 36 diverse fungal isolates from the International Collection of Microorganisms from Plants (ICMP) grown on a wide variety of nutrient-rich and nutrient-poor media and discovered that almost all the tested isolates produced considerable anti-mycobacterial activity. Our data also provides strong statistical evidence for the impact of growth media on antibacterial activity. Chemical extraction and fractionation of a subset of the ICMP isolates revealed that much of the activity we observed may be due to the production of the known anti-mycobacterial compound linoleic acid. However, we have identified several ICMP isolates that retained their anti-mycobacterial activity in non-linoleic acid containing fractions. These include isolates of *Lophodermium culmigenum*, *Pseudaegerita viridis*, and *Trametes coccinea*, as well as an unknown species of *Boeremia* and an isolate of an unknown genus and species in the family *Phanerochaetaceae*. Investigations are ongoing to identify the sources of their anti-mycobacterial activity and to determine whether any may be due to the production of novel bioactive compounds.

Keywords: mycobacteria, *Mycobacterium marinum*, *Mycobacterium abscessus*, bioluminescence, luciferase, minimum inhibitory concentration, screening, antibacterial

OPEN ACCESS

Edited by:
Paola Angelini,
University of Perugia, Italy

Reviewed by:
Joseph Oliver Falkinham,
Virginia Tech, United States
Renuka Kapoor,
Emory University, United States

***Correspondence:**
Siouxsie Wiles
s.wiles@auckland.ac.nz

† These authors have contributed equally to this work

Specialty section:
This article was submitted to Microbiotechnology, a section of the journal Frontiers in Microbiology

Received: *12 July 2021*
Accepted: *10 August 2021*
Published: *06 September 2021*

Citation:
Grey ABJ, Cadelis MM, Diao Y, Park D, Lumley T, Weir BS, Copp BR and Wiles S (2021) Screening of Fungi for Antimycobacterial Activity Using a Medium-Throughput Bioluminescence-Based Assay. Front. Microbiol. 12:739995. doi: 10.3389/fmicb.2021.739995

INTRODUCTION

There is a real and urgent need for new antibiotics able to kill Mycobacteria, acid-fast bacilli capable of causing multiple deadly diseases. Because of their slow growth and hydrophobic, lipid-rich outer membrane, treatment of mycobacterial infections can take months to years and require multiple antibiotics (Seaworth and Griffith, 2017; Pontali et al., 2019). The major mycobacterial

human pathogens are members of the *Mycobacterium tuberculosis* complex, which causes the lung disease tuberculosis (TB) (Gagneux, 2018), described by the World Health Organization as a global epidemic. Also of concern are the non-tuberculous Mycobacteria (NTM), free living opportunistic pathogens that are ubiquitous in the environment and able to cause lung, skin, and soft tissue infections (Mirsaeidi et al., 2014; Gonzalez-Santiago and Drage, 2015; Koh and Schlossberg, 2017). Almost two hundred NTM species have been identified to date, which were recently found to divide into five clades based on phylogenetic characteristics (Gupta et al., 2018). Rates of NTM infections are increasing globally, including in hospital settings (Al-Mahruqi et al., 2009; Roux et al., 2009; Moore et al., 2010; Morimoto et al., 2014; Donohue and Wymer, 2016; Donohue, 2018; Ratnatunga et al., 2020). NTM are natural inhabitants of water and their inclusion in implanted devices such as catheters, prosthetics, and pacemakers, have resulted in cases of bacteremia and disseminated infection, while NTM outbreaks have been associated with invasive procedures such as cosmetic surgeries, intramuscular injections, and tattooing (Griffin et al., 2019; Jabbour et al., 2020). Recently, some cases of pulmonary infections with *Mycobacterium chimaera* were traced back to site of manufacture of heater-cooler units routinely used during open heart surgery (Williamson et al., 2017).

Aotearoa New Zealand is an archipelago which split from the Gondwanan supercontinent approximately 85 million years ago and has since gradually become more isolated from other land masses (Wallis and Trewick, 2009). This geographical separation has led to the evolution of iconic native flora, fauna, and fungi. The Crown Research Institute Manaaki Whenua is the custodian of the International Collection of Microorganisms from Plants (ICMP) (Johnston et al., 2017). The ICMP contains over 10,000 fungal cultures derived from plants and soil from Aotearoa New Zealand and the South Pacific. The collection has a great diversity of fungal species, host substrates, and collection localities, with the earliest cultures dating from the 1960s. While the collection contains some of the fungal genera traditionally used for antibiotic production it has not been rigorously tested for antimicrobial activity against mycobacterial species. In our view, this makes the ICMP an excellent and untapped resource for antibiotic discovery.

The search for new antibiotics with activity against Mycobacteria is complicated by their slow growth, with species like *M. tuberculosis* having a doubling time of approximately 24 h. Mycobacteria also tend to clump in liquid culture due to their hydrophobic cell envelope. These properties make the two most common methods of measuring antibacterial activity, the production of zones of inhibition when grown on agar, or degree of turbidity when grown in liquid culture, slow and unreliable. Tagging bacteria with the genes that encode for luciferase-based reporters allows light to be used as a rapid surrogate marker for bacterial viability (Andreu et al., 2012). We and others have shown that bioluminescence is an excellent non-destructive real-time reporter to assay for anti-mycobacterial activity in microtiter plate formats using a luminometer (Andreu et al., 2012; Dalton et al., 2016; Early et al., 2019; Chengalroyen et al., 2020; Jain et al., 2020) or *in vivo* using sensitive imaging equipment (Andreu et al., 2013).

Here we describe a medium-throughput bioluminescence-based pipeline to screen fungi for activity against Mycobacteria using the NTM species *Mycobacterium abscessus* and *Mycobacterium marinum*. Our results indicate that many of the ICMP fungal isolates are anti-mycobacterial and have identified isolates of *Lophodermium culmigenum*, *Pseudaegerita viridis*, and *Trametes coccinea*, as well as an unknown species of *Boeremia* and an isolate of an unknown genus and species in the family *Phanerochaetaceae* as suitable for further study.

MATERIALS AND METHODS

Bacterial Strains and Growth Conditions

In this study, we used *M. abscessus* BSG301 (Cadelis et al., 2021) and *M. marinum* BSG101 (Dalton et al., 2017) which are stable bioluminescent derivatives transformed with the integrating plasmid pMV306G13ABCDE (Andreu et al., 2010). We grew mycobacterial cultures with shaking (200 rpm) in Middlebrook 7H9 broth (Fort Richard, New Zealand) supplemented with 10% Middlebrook ADC enrichment media (Fort Richard, New Zealand), 0.4% glycerol (Sigma-Aldrich, New Zealand) and 0.05% tyloxapol (Sigma-Aldrich, New Zealand). We grew *M. abscessus* at 37°C and *M. marinum* at 28°C.

Fungal Material

Fungal isolates (**Table 1**) were provided by Manaaki Whenua – Landcare Research, a New Zealand Crown Research Institute responsible for the curation of the International Collection of Microorganisms from Plants (ICMP). We stored fungal isolates individually in cryotubes at −80°C. We made freezer stocks by growing each fungus on 1.5% Potato Dextrose Agar (PDA) and excising small cubes of agar (5–6 mm in length) from the fungus' growing edge. We placed these cubes within a cryovial containing 1 mL of 10% glycerol and rested them for 1 h after which we removed the remaining liquid glycerol and stored the tubes at -80°C.

Fungal DNA Extraction and ITS Sequencing

We used a small portion of mycelium from growing fungi and extracted DNA using the REDExtract-N-Amp™ Plant PCR Kit (Sigma-Aldrich) according to the manufacturer's protocol. We diluted DNA samples five-fold and amplified using the ITS1F (5′ CTTGGTCATTTAGAGGAAGTAA 3′) and ITS4 (5′ TCCTCCGCTTATTGATATGC 3′) primer set in a 10 μl reaction volume using the REDExtract-N-Amp Plant PCR Kit (Sigma-Aldrich) according to the manufacturer's instructions. We used the following PCR conditions: initial denaturation at 94°C for 3 min, followed by 40 cycles of denaturation at 94°C for 30 s, annealing at 52°C for 30 s and extending at 72°C for 30 s. The final extension was performed at 72°C for 7 min. We checked the amplified DNA by gel electrophoresis before sequencing using an Applied Biosystems™ 3500xL Genetic

TABLE 1 | Fungal isolates used in this study.

Fungus	ICMP number	GenBank Accession	Description
Agaricales sp.	17554	MT107903	An undescribed crust fungus in the cyphellaceae – a family closely related to mushroom species but forming crust or simple hood-like fruitbodies. It was isolated in Kerikeri, New Zealand in August 2007
Aleurodiscus sp.	16336	MZ325955	*Aleurodiscus* sp. is a pinkish crust fungus. This culture was isolated from dead wood near Lake Waikaremoana, New Zealand in May 1985
Amylostereum sacratum	10158	MZ325952	*Amylostereum sacratum* is a plant pathogen causing root rot. This culture was isolated from an apple tree in Nelson, New Zealand in May 1977
Aspergillus terreus	477	MW862777	*Aspergillus terreus* is a common cosmopolitan saprotrophic soil-inhabiting fungus. This culture was isolated in September 1961 in Auckland, New Zealand from sheep's wool incubated at 30°C
Boeremia sp.	17650	MW862790	This isolate is an unknown species of *Boeremia* which are often plant pathogens. It was isolated from the surface of a mushroom in the Mamaku Plateau, New Zealand in May 1991
Cerrena zonata	16347	MW862786	*Cerrena zonata* is a white rot decay fungus of dead wood. This culture was isolated from Ngāruawāhia, New Zealand in April 1995
Chalara scabrida	20449	MK432752	*Chalara scabrida* is an endemic saprobic fungus. The culture was isolated from a living *Phormium cookianum* leaf in Mt Hutt, New Zealand in February 2014
Cunninghamella echinulata	1083	MZ325951	*Cunninghamella echinulata* is a common soil saprotroph. This culture was isolated from Auckland, New Zealand in December 1978
Cylindrobasidium sp.	16397	MZ325956	This isolate is a crust fungus in the family physlacriaceae and related to the *Armillaria* mushroom. This culture was isolated from apple wood in Auckland, New Zealand in June 1973
Dentipellis leptodon	18110	MZ325966	*Dentipellis leptodon* grows on the underside of dead wood and has dangling spines and is related to the Lion's Mane *Hericium* fungus. This culture was isolated from *Metrosideros robusta* wood in Mamaku, New Zealand in March 1984
Helicodendron triglitziense	16004	MK432688	*Helicodendron triglitziense* is an aero-aquatic species isolated from dead alder leaves in Horseshoe Lake Reserve wetland, Christchurch, New Zealand in June 2005
Hyaloscypha spinulosa	16865	MK432695	*Hyaloscypha spinulosa* is an aero-aquatic species isolated from a dead rimu twig in Pigeon Bay, New Zealand in September 2006
Hypholoma australianum	21474	MZ325972	*Hypholoma australianum* is an orange mushroom with a white stem. This culture was isolated from wood buried in soil in Otago Lakes, New Zealand in May 2016
Laetiporus portentosus	15555	MZ325953	*Laetiporus portentosus* is a soft bracket fungus, traditionally used as a tinder and wound packing material by Māori, the indigenous people of New Zealand. This culture was isolated from a beech tree in Rimutaka Forest Park, New Zealand in May 1999
Lanzia allantospora	15649	AY755334	*Lanzia allantospora* is an endemic cup fungus found on kauri wood in Northland, New Zealand in April 1992
Lauriomyces bellulus	15050	EF029218	*Lauriomyces bellulus* is a saprophytic fungus. This culture was isolated from a dead leaf of *Weinmannia racemosa* in Katikati, New Zealand in May 2003
Lentinellus pulvinulus	16586	MW862787	*Lentinellus pulvinulus* is a white rot wood decay mushroom. This culture was isolated from a dead wood in Pehitawa Kahikatea Forest Reserve, New Zealand in May 2006.
Lentinula novae-zelandiae	18003	MZ325965	*Lentinula novae-zelandiae* is a native edible "shitake" mushroom. This culture was isolated from dead wood in Dunedin, New Zealand in September 1991
Linnemannia elongate	17447	MZ325962	*Linnemannia elongate* is a Mucorales fungus. The culture was isolated from a kauri tree in Rotorua, New Zealand in January 2008
Lophodermium culmigenum	18328	MZ325968	*Lophodermium culmigenum* is a plant decay fungus. This culture was isolated from Trounson Kauri Park, Chatham Islands, New Zealand in November 1992
Metapochonia bulbillosa	18174	MZ325967	*Metapochonia bulbillosa* is an insect pathogen fungus. This culture was isolated from dead leaves of Marram grass in Lake Tennant, New Zealand in 1985
Mortierella sp.	20597	MZ325970	This isolate is an unknown species of *Mortierella*, a common Mucorales soil fungus. This culture was isolated from rotting wood from Farewell Spit, New Zealand in May 2014
Mucor laxorrhizus	20877	MZ325971	*Mucor laxorrhizus* is a Mucorales saprobe. This culture was isolated from rotten wood from a stream in St Arnaud, New Zealand in January 2015
Neodidymelliopsis sp.	11463	MW862783	This isolate is an unknown species of *Neodidymelliopsis* which are typically plant pathogens. This culture was isolated from *Pittosporum* leaves in Albany, Auckland, New Zealand in October 1991
Peniophora lycii	16714	MZ325959	*Peniophora lycii* is a crust fungus. This culture was isolated from decaying wood in Te Waiiti, New Zealand in May 2001
Phanerochaetaceae sp.	18785	MZ325969	This isolate is an unknown genus and species of crust fungi in the family *Phanerochaetaceae.* The culture was isolated from beech leaves from Matakitaki, New Zealand in December 2010
Pleurotus australis	18149	MH395972	*Pleurotus australis* is an edible wood decay mushroom. This culture was isolated from the Waitakere Ranges near Auckland, New Zealand in February 1987

(Continued)

TABLE 1 | (Continued)

Fungus	ICMP number	GenBank Accession	Description
Pleurotus purpureo-olivaceus	9630	MH395959	*Pleurotus purpureo-olivaceus* is an edible wood decay mushroom. This culture was isolated from Manapouri, New Zealand in May 1990
Pleurotus purpureo-olivaceus	17077	GQ411512	*Pleurotus purpureo-olivaceus* is an edible wood decay mushroom. This culture was isolated from the Craigieburn Range, New Zealand in May 2006
Pseudaegerita viridis	16864	MZ325960	*Pseudaegerita viridis* is an aero-aquatic species. This culture was isolated from a dead rimu twig in Pigeon Bay, New Zealand in September 2006
Stereum sp.	16953	MZ325961	This isolate is an unknown species of *Stereum*, a wood decay bracket fungus, and was isolated from Rangitoto Station, New Zealand in November 2006
Torrendiella brevisetosa	18823	JN225946	*Torrendiella brevisetosa* is a cup fungus. This culture was isolated from beech leaves in Matakitaki, New Zealand in December 2010
Trametes coccinea	13182	MW862784	*Trametes coccinea* is a wood decay bracket fungus. This culture was isolated from a dead radiata pine in Northland, New Zealand in September 1985
Umbelopsis sp.	17492	EU770239	This isolate is an unknown species of *Umbelopsis*, a Mucorales saprobe, isolated from grapevines in Whenuapai, New Zealand in April 2007
Vararia fusispora	17544	MZ325963	*Vararia fusispora* is a crust fungus. This culture was isolated from a decaying rimu branch in Owhango, New Zealand in October 2007
Xylariaceae sp.	16006	MZ325954	This isolate is an unknown genus and species of the *Xylariaceae* family that was isolated from Ahuriri Reserve, Christchurch, New Zealand in May 2005

Analyzer using both ITS1F and ITS4 primers. We trimmed and combined the sequence data using Geneious (Geneious Biologics), removed any low-quality reads and used BLAST to check fungal identification. Optimized sequence data were aligned using MEGA7 (Kumar et al., 2016).

Primary Fungal Screening

We grew fungal isolates on PDA (Fort Richard, New Zealand) prior to screening for antibacterial activity using a 24 well plate assay. Briefly, we added 0.5 mL aliquots of agar to triplicate wells of a black 24 well plate (4titude, Millennium Science, New Zealand) and allowed them to set. We obtained all media from Fort Richard (New Zealand). In addition to PDA, these comprised: Czapek Solution Agar (CSA), Czapek Yeast Extract Agar (CYA), Malt Extract Agar (MEA), Malt Yeast Extract Agar (MYA), Oatmeal Agar (OA), Rice Extract Agar (REA), and Tryptone Yeast Extract Agar (TYA). With the aid of a sterile scalpel blade, we sectioned fungal isolates grown on PDA into cubes $\leq$5 mm in diameter, and then transferred the cubes to the agar-filled wells of the 24-well plates ensuring that each cube was placed fungus-side down and touching the agar. We covered the inoculated 24-well screening plates, sealed them with parafilm, and incubated them at room temperature.

FIGURE 1 | Geographical spread of the isolation locations for the fungal isolated used in this study within the archipelago of Aotearoa New Zealand. Black dots are individual ICMP isolates.

We monitored fungal growth visually at regular intervals and recorded the time taken for them to either cover the entire well or to stop visibly growing. At twice this time, we removed a 6 mm plug of agar from each well using a biopsy punch. To screen for antibacterial activity, we resuspended *M. abscessus* BSG301 and *M. marinum* BSG101 in 0.8% Middlebrook 7H9 broth (Fort Richard, New Zealand) supplemented with 10% Middlebrook ADC enrichment media (Fort Richard, New Zealand) to a final concentration of 10^7 colony forming units (CFU)/mL for *M. abscessus* and 10^8 CFU/mL for *M. marinum*. With the aid of a pipette, we pipetted 50 μL of the bacterial-agar mixture into the cylindrical holes left after removal of the fungal-agar plugs and allowed the mixture to set. We measured bacterial luminescence at regular intervals using a Victor X-3 luminescence plate reader (PerkinElmer) with an integration time of 1 s. Between measurements, plates were covered, placed in a plastic box lined with damp paper towels, and incubated static at 37°C for *M. abscessus* and 28°C for *M. marinum*. We performed these assays three times. We have published a more detailed description of our methods on the protocol repository website protocols.io (Wiles and Grey, 2021a,b).

TABLE 2 | ICMP isolates belonging to novel fungal taxa likely endemic to Aotearoa New Zealand.

Phylum	Fungus	ICMP number	GenBank Accession	Isolation substrate and location	Isolation year
Ascomycota	*Boeremia* sp.	17650	MW862790	Isolated from the surface of a mushroom in the Mamaku Plateau	1991
	Neodidymelliopsis sp.	11463	MW862783	Isolated from *Pittosporum* leaves in Albany, Auckland	1991
	Xylariaceae sp.	16006	MZ325954	Isolated in Ahuriri Reserve, Christchurch	2005
Basidiomycota	*Agaricales* sp.	17554	MT107903	Isolated in Kerikeri, Northland	2007
	Aleurodiscus sp.	16336	MZ325955	Isolated from dead wood near Lake Waikaremoana	1985
	Cylindrobasidium sp.	16397	MZ325956	Isolated from apple wood in Auckland	1973
	Phanerochaetaceae sp.	18785	MZ325969	Isolated from beech leaves from Matakitaki	2010
	Stereum sp.	16953	MZ325961	Isolated at Rangitoto Station	2006
Mucoromycota	*Mortierella sp.*	20597	MZ325970	Isolated from rotting wood from Farewell Spit	2014
	Umbelopsis sp.	17492	EU770239	Isolated from grapevines in Whenuapai	2007

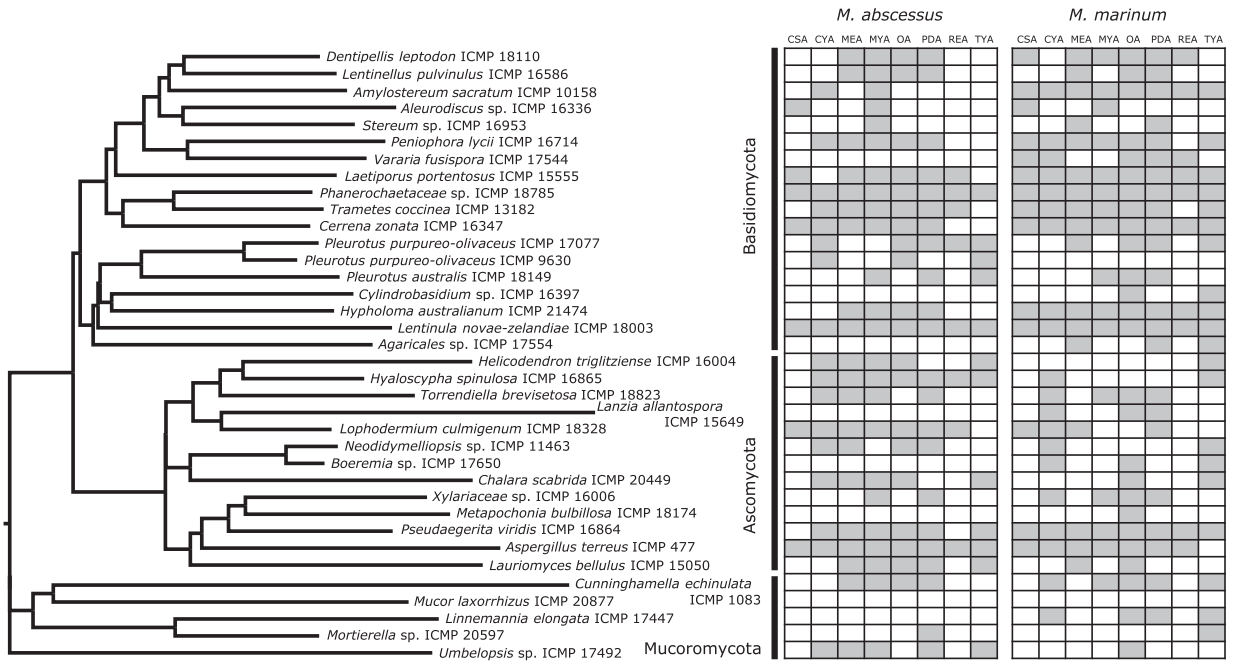

FIGURE 2 | Phylogeny and activity of ICMP isolates grown in different media against *M. abscessus* BSG301 and *M. marinum* BSG101. Active media for each isolate are shown in gray. CSA, Czapek Solution Agar; CYA, Czapek Yeast extract Agar; MEA, Malt Extract Agar; MYA, Malt Yeast extract Agar; OA, Oatmeal Agar; PDA, Potato Dextrose Agar; REA, Rice Extract Agar; TYA, Tryptone Yeast extract Agar. ICMP isolates are described as active if they caused a minimum 1-log (90%) reduction in the bioluminescence of the mycobacterial strains. The phylogenetic tree was constructed by comparing ITS sequences to those in GenBank and the phylogenetic tree was constructed using the Molecular Evolutionary Genetics Analysis version 7.0 software (MEGA7) using the neighbor-joining method and p-distance as the substitution model. Each phylogeny was tested using the bootstrap method with 500 replications.

Fungal Fermentation and Extraction

We grew fungal cultures either in liquid media or on solid media at room temperature and then freeze-dried them. We extracted the dry cultures with MeOH (Sigma-Aldrich, New Zealand) for 4 h followed by CH_2Cl_2 (Sigma-Aldrich, New Zealand) overnight. We concentrated the combined organic extracts under reduced pressure and subjected the crude extracts to C_8 reversed-phase column chromatography eluting with a gradient of H_2O/MeOH (Sigma-Aldrich, New Zealand) to afford five fractions (F1–F5). Full details are provided in **Supplementary Material**.

Extract Screening

We grew mycobacterial cultures until they reached stationary phase (approximately 3–5 days for *M. abscessus* BSG301 and 7–10 days for *M. marinum* BSG101) and then diluted these in Mueller Hinton broth II (MHB) (Fort Richard) supplemented with 10% Middlebrook ADC enrichment media and 0.05% tyloxapol to give an optical density at 600 nm (OD_{600}) of 0.001 which is the equivalent of $\sim 10^6$ bacteria per mL. We dissolved the fungal fractions in DMSO (Sigma-Aldrich, New Zealand) and added these in duplicate to the wells of a black 96-well plate (Nunc, Thermo Scientific) at doubling dilutions with a maximum concentration of 50 mg/mL. Then we added 50 μL of diluted

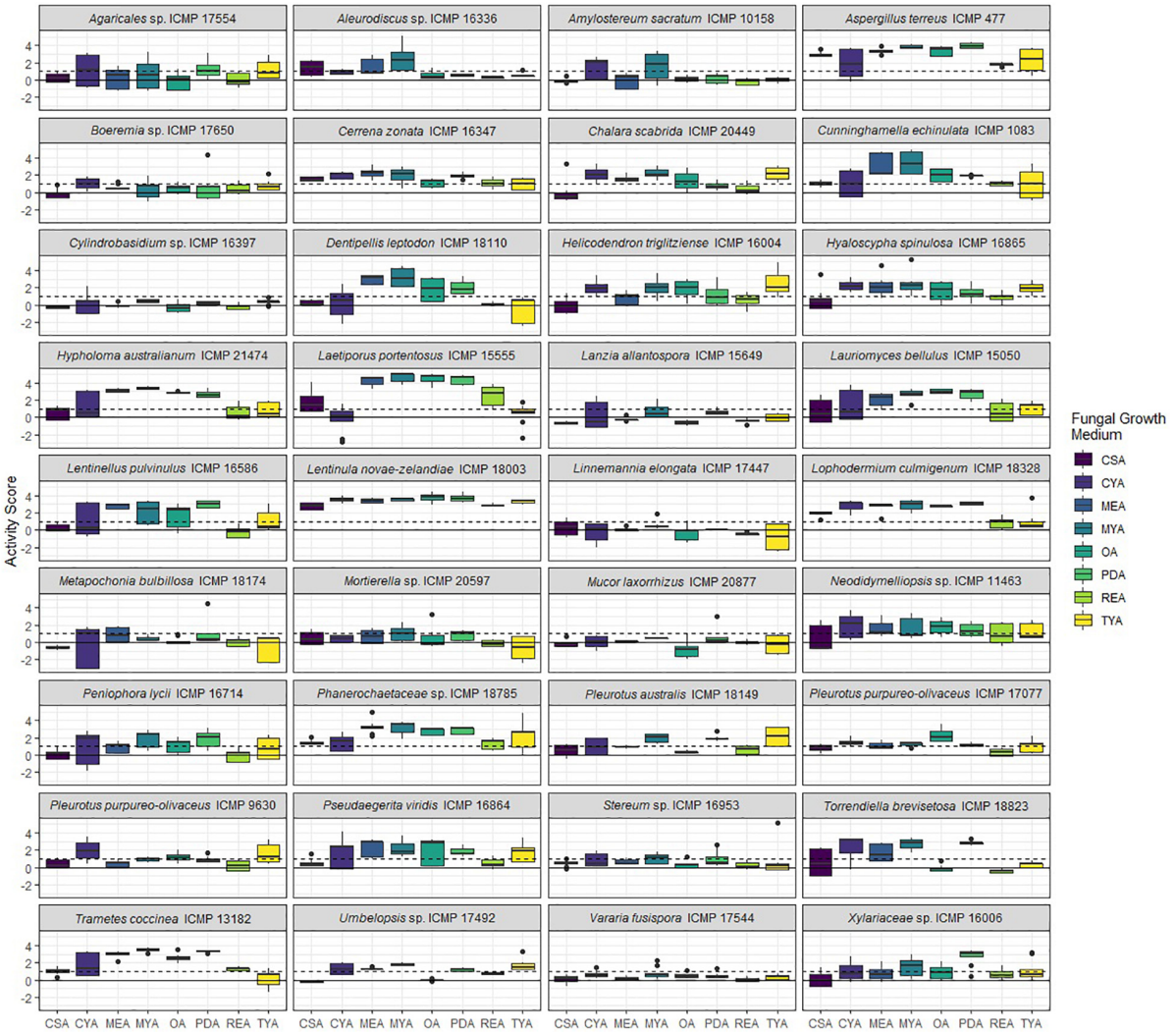

FIGURE 3 | Antibacterial activity of ICMP fungal isolates against *Mycobacterium abscessus* BSG301 when grown on different media. Data is presented as box and whisker plots of activity scores. The solid line shown at 0 is the median control value while the dotted line at 1 is the activity threshold. Scores above 1 correspond to a >90% reduction in bacterial bioluminescence compared to the corresponding no-fungi control. Similarly, an activity score above 2 means corresponds to a >99% reduction. CSA, Czapek Solution Agar; CYA, Czapek Yeast Extract Agar; MEA, Malt Extract Agar; MYA, Malt Yeast Extract Agar; OA, Oatmeal Agar; PDA, Potato Dextrose Agar; REA, Rice Extract Agar; TYA, Tryptone Yeast Extract Agar. Boxes are upper and lower quartiles with median shown. The whiskers extend up to 1.5× the inter-quartile range and any dots beyond those bounds are outliers.

bacterial culture to each well of the fraction containing plates giving final extract concentrations of 0–1000 μg/mL and a cell density of $\sim 5 \times 10^5$ CFU/mL.

We used the antibiotic rifampicin (Sigma-Aldrich, New Zealand) as a positive control at 1000 μg/mL for *M. abscessus* and 10 μg/mL for *M. marinum*. Between measurements, plates were covered, placed in a plastic box lined with damp paper towels, and incubated with shaking at 100 rpm at 37°C for *M. abscessus* and 28°C for *M. marinum*. We measured bacterial luminescence at regular intervals using a Victor X-3 luminescence plate reader (PerkinElmer) with an integration time of 1 s. We have defined the MIC as causing a 1 log reduction in light production, as previously described (Dalton et al., 2016, 2017). We have published a more detailed description of our methods on the protocol repository website protocols.io (Wiles and Grey, 2021c,d).

General Chemistry Conditions

We recorded NMR spectra using a Bruker Avance DRX-400 spectrometer or an Avance III-HD 500 spectrometer operating at 400 MHz or 500 MHz for ^{1}H nuclei and 100 MHz or 125 MHz for ^{13}C nuclei utilizing standard pulse sequences at 298 K. We recorded high resolution mass spectra on a Bruker micrOTOF QII (Bruker Daltonics, Bremen, Germany). We carried out analytical thin layer chromatography (TLC) on 0.2 mm thick plates of DC-plastikfolien Kieselgel 60 F254 (Merck). We carried out reversed-phase column chromatography on C_8 support with a pore

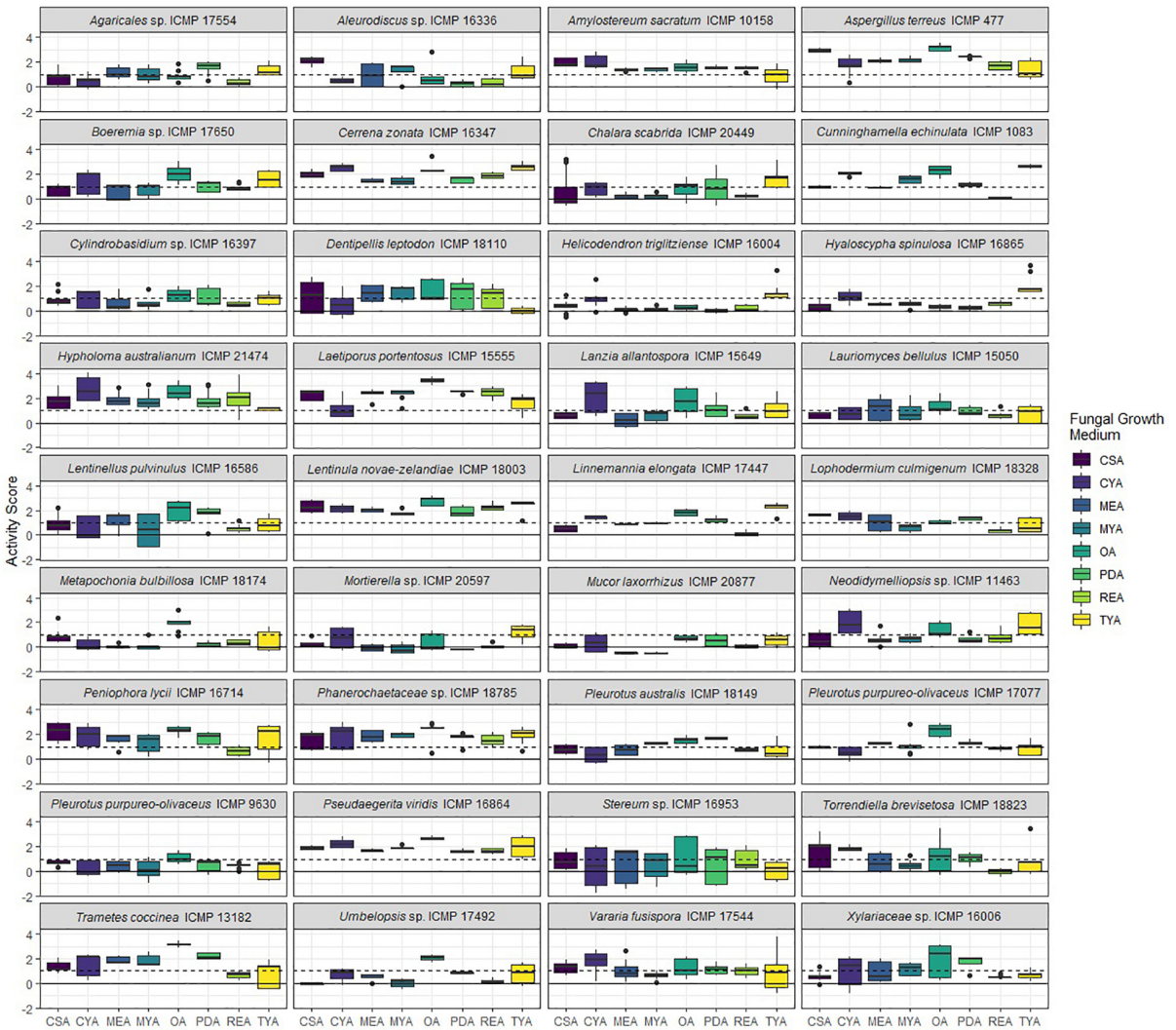

FIGURE 4 | Antibacterial activity of ICMP fungal isolates against *Mycobacterium marinum* BSG101 when grown on different media. Data is presented as box and whisker plots of activity scores. The solid line shown at 0 is the median control value while the dotted line at 1 is the activity threshold. Scores above 1 correspond to a >90% reduction in bacterial bioluminescence compared to the corresponding no-fungi control. Similarly, an activity score above 2 means corresponds to a >99% reduction. CSA, Czapek Solution Agar; CYA, Czapek Yeast Extract Agar; MEA, Malt Extract Agar; MYA, Malt Yeast Extract Agar; OA, Oatmeal Agar; PDA, Potato Dextrose Agar; REA, Rice Extract Agar; TYA, Tryptone Yeast Extract Agar. Boxes are upper and lower quartiles with median shown. The whiskers extend up to 1.5× the inter-quartile range and any dots beyond those bounds are outliers.

size of 40–63 μm (Merck). We carried out gel filtration chromatography on Sephadex LH-20 (Pharmacia). We carried out flash chromatography on Diol-bonded silica with a pore size of 40–63 micron (Merck). We used solvents that were of analytical grade or better and/or purified according to standard procedures.

Statistical Analysis

We fitted a logistic mixed model for activity with a random effect for biologic replicates. We tested the main effects and second-order interactions of the variables, using the lme4 and car packages in R (Bates et al., 2015; Fox and Weisberg, 2019; R Core Team, 2020).

RESULTS

Identification of Novel Fungal Taxa Endemic to Aotearoa New Zealand

The 36 ICMP fungal isolates used in this study were collected between 1961 and 2016 and from locations across Aotearoa New Zealand, including the North, South, and Chatham Islands (**Figure 1**). Of the 36 isolates, nine were not able to be identified as a known species and one is from both an unknown genus and species (**Table 2**). These isolates likely represent novel taxa endemic to Aotearoa New Zealand. As with the broader collection, they cover a range of isolation dates, the earliest being isolated in 1973 (*Cylindrobasidium* sp. ICMP 16397)

and the most recent in 2014 (*Mortierella* sp. ICMP 20597). They also cover a broad range of isolation locations within New Zealand, from Kerikeri in the North Island (*Agaricales* sp. ICMP 17554) to Christchurch in the South Island (*Xylariaceae* sp. ICMP 16006).

Whole Cell Screening Identified Many ICMP Fungal Isolates as Having Anti-mycobacterial Activity

We screened 36 ICMP fungal isolates for antibacterial activity against *M. abscessus* BSG301 and *M. marinum* BSG101. The isolates belong to three different fungal Phyla, and we grew them on eight different media giving us a total of 288 fungi-media combinations tested for each bacterium (**Figures 2–4**).

We measured antibacterial activity as reductions in light output of our bioluminescent mycobacterial strains over a 72-h period. We calculated activity scores by first converting the luminescence measurement at each time-point into an area under the curve (AUC) value for each well. We then divided this number by the median AUC of a sterile control plate inoculated and incubated at the same time as the fungus-containing plates. The negative log of this value corresponds to the activity score. We define a fungus-media combination as active/antibacterial if the median activity score is above 1 which corresponds to a $>$ 90% reduction in light compared to the control. Similarly, an activity score above 2 means corresponds to a $>$ 99% reduction.

We observed no consistent difference in activity by mycobacterial strain, but there is strong statistical evidence of differences in activity between media and fungal Phyla, and that these vary by mycobacterial strain (**Table 3**).

More ICMP Fungal Isolates Are Active Against *M. marinum* Than *M. abscessus*

We observed that 28/36 (77%) fungal isolates were active against *M. abscessus* when grown in at least one medium, with 130/288 (45%) fungi-medium combinations being anti-mycobacterial against this bacterium (**Figures 2**, **3**). In contrast, 34/36 (94%) fungal isolates were active against *M. marinum*, with 146/288 (51%) fungi-medium combinations being anti-mycobacterial against this bacterium (**Figures 2**, **4**). Of the two fungal isolates that were not active against *M. marinum* when grown in any of the media tested, only the Mucoromycota fungus *Mucor laxorrhizus* ICMP 20877 displayed no activity against *M. abscessus*. The second isolate, *Pleurotus purpureo-olivaceus* ICMP 9630 was active against *M. abscessus* when grown on CYA, MYA, and TYA. However, a second isolate of *P. purpureo-olivaceus* we tested, ICMP 17077, was active against both mycobacterial strains. We could discern no obvious pattern between fungal species or genus for those isolates that were only active against *M. marinum*, namely *Agaricales* sp. ICMP 17554, *Boeremia* sp. ICMP 17650, *Cylindrobasidium* sp. ICMP 16397, *Lanzia allantospora* ICMP 15649, *Linnemannia elongata* ICMP 17447, *Metapochonia bulbillosa* ICMP 18174, and *Vararia fusispora* ICMP 17544.

The fungal isolates we tested belong to three Phyla: the Basidiomycota (18 ICMP isolates), the Ascomycota (13 ICMP isolates), and the Mucoromycota (5 ICMP isolates) (**Figure 2**). We observed that the group with the most active fungi-medium combinations was the Basidiomycota (55%), followed by the Mucoromycota (52%), and then the Ascomycota (46%%) (**Figure 2**). More Basidiomycota-medium combinations were active against *M. marinum* [92/144 (64%)] (**Figures 2**, **4**) than *M. abscessus* [67/144 (47%)] (**Figures 2**, **3**). In contrast, more Ascomycota-medium combinations were active against *M. abscessus* [53/104 (51%)] (**Figures 2**, **3**) than *M. marinum* [43/104 (41%)] (**Figures 2**, **4**).

Differential Impact of Growth Medium on Anti-mycobacterial Activity

We observed that many of the ICMP fungi displayed differential activity depending on their growth medium with the majority being active on more than one medium. An isolate of the native New Zealand "shiitake" mushroom *Lentinula novae-zelandiae* (ICMP 18003) and an isolate of unknown genus and species in the family *Phanerochaetaceae* (ICMP 18785) were active against both *M. abscessus* and *M. marinum* when grown on an all 8 media (**Figures 2–4**). An isolate of *Aspergillus terreus* (ICMP 477) was also active against *M. abscessus* regardless of growth media (**Figures 2**, **4**), while *Amylostereum sacratum* ICMP 10158, *Cerrena zonata* ICMP 16347, *Hypholoma australianum* ICMP 21474, *Laetiporus portentosus* ICMP 15555, and *Pseudaegerita viridis* ICMP 16864 were active against *M. marinum* when grown on all media (**Figures 2**, **4**).

When assessing for activity against *M. abscessus*, 2/36 fungal isolates were only active when grown on one of the eight media, an unknown species of *Mortierella* (ICMP 20597) when grown on PDA and an unknown species of *Stereum* (ICMP 16953) on MYA (**Figures 2**, **3**). ICMP 20597 was also only active against *M. marinum* when grown on one of the eight media, though in this case it was TYA (**Figures 2**, **4**). Three other fungal isolates were only active against *M. marinum* when grown on one of the eight media, *Helicodendron triglitziense* ICMP 16004 on TYA, and *Metapochonia bulbillosa* ICMP 18174 and an unknown species of *Umbelopsis* (ICMP 17492) on OA (**Figures 2**, **4**).

Potato Dextrose Agar (PDA) Is the Most Active Culture Medium for Screening for Anti-mycobacterial Activity

We observed that PDA was the most active culture medium with 29/36 (80%) fungal isolates active against either bacterium (**Figure 2**). For *M. marinum*, the most active culture medium was OA, followed by PDA (24 and 23 active fungi, respectively) while for *M. abscessus* it was MYA followed by PDA (24 and 22 active fungi, respectively). We observed that isolates grown on REA and CSA were the least active, with only 14/36 isolates (39%) being active against either mycobacterium species when cultured on these media (**Figure 2**). MYA and MEA were the two media that favored *M. abscessus* activity, with 24 fungal isolates active when grown on MYA and 20 isolates active when grown on MEA, compared to 17 and 16 being active against *M. marinum*, respectively (**Figure 2**).

TABLE 3 | Analysis of Deviance Table (Type II Wald Chi^2 tests).

	Chi^2	Degrees of freedom	Significance
Fungal phyla	2.57	2	$p = 0.28$
Mycobacterial strain	3.48	1	$p = 0.06$
Fungal growth medium	273.30	7	$p < 0.0001$
Fungal Phyla × Mycobacterial strain	99.50	2	$p < 0.0001$
Fungal Phyla × fungal growth medium	117.96	14	$p < 0.0001$
Mycobacterial strain × fungal growth medium	124.95	7	$p < 0.0001$

Screening of Extracts and Fractions From ICMP Fungal Isolates for Anti-mycobacterial Activity

We prepared extracts from 41 fungus-medium combinations which were further separated into 5 fractions, designated F1–F5. Fraction F1 (100% water) is generally comprised of sugars while fraction F5 (100% methanol) contains predominantly fatty acids and sterols. Fractions F2, F3, and F4 typically contain the chemical compounds we are most interested in pursuing, with the potential to be bioactive.

We tested, at a single concentration of 1000 μg/mL, the crude extracts and fractions F1–F5 from all 41 fungus-medium combinations for activity against *M. marinum* BSG101 (**Figures 5**, **6**) and for 38 of the combinations for activity against *M. abscessus* BSG301 (**Figures 5**, **7**). As described previously, we measured antibacterial activity as reductions in light output of our bioluminescent mycobacterial strains over a 72-h period and calculated activity scores as the negative log of the ratio of the AUC values of the fungus-containing measurements and the control measurements. We define an extract/fraction as active/antibacterial if the median activity score is above 1, which corresponds to a >90% reduction in light compared to the control, as previously described. Similarly, an activity score above 2 means corresponds to a > 99% reduction.

ICMP Fungal Extracts and Fractions Retain Anti-mycobacterial Activity

We observed that only 3/38 of the fungus-medium combinations we tested for activity against *M. abscessus* BSG301 did not

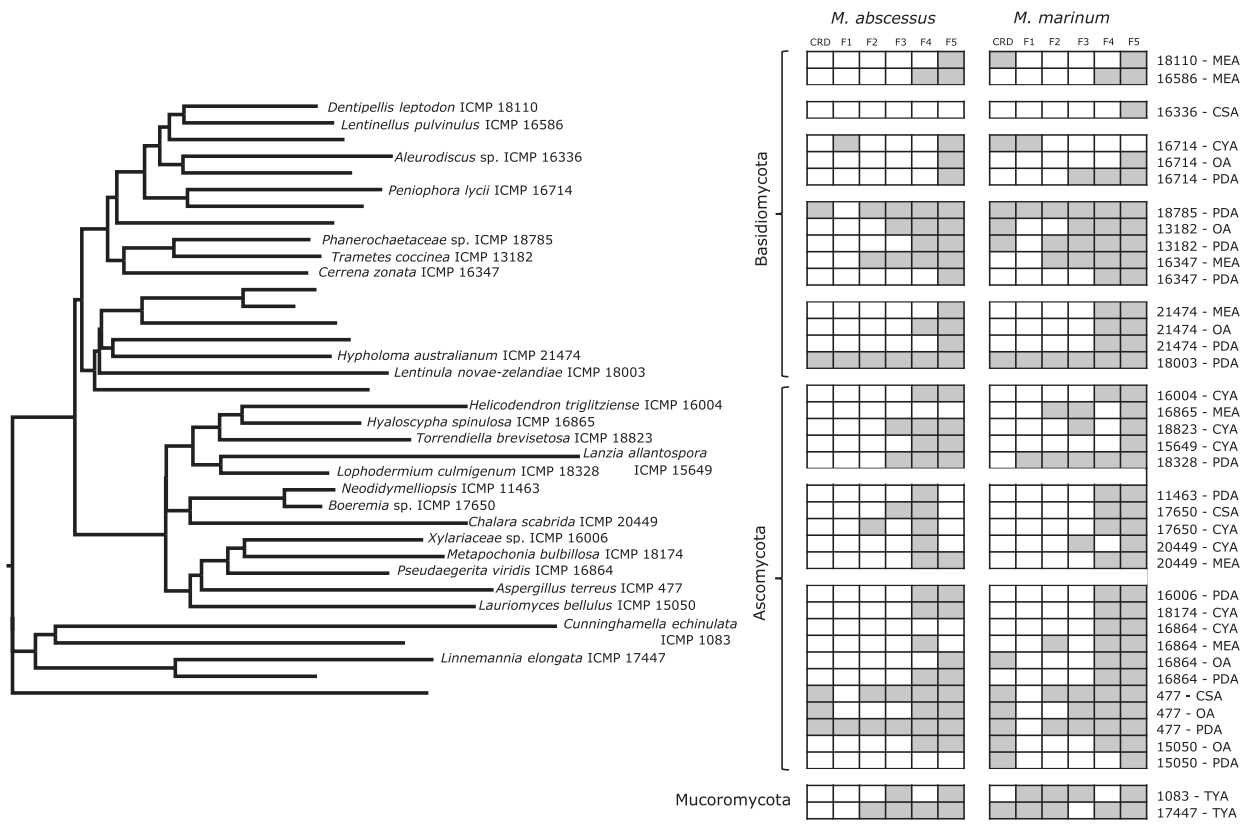

FIGURE 5 | Phylogeny and activity of crude extracts and fractions from ICMP isolates grown in different media against *M. abscessus* BSG301 and *M. marinum* BSG101. Active extracts and fractions for each isolate are shown in gray. CSA, Czapek Solution Agar; CYA, Czapek Yeast extract Agar; MEA, Malt Extract Agar; MYA, Malt Yeast extract Agar; OA, Oatmeal Agar; PDA, Potato Dextrose Agar; REA, Rice Extract Agar; TYA, Tryptone Yeast extract Agar. ICMP isolates are described as active if they caused a minimum 1-log (90%) reduction in the bioluminescence of the mycobacterial strains. The phylogenetic tree was constructed by comparing ITS sequences to those in GenBank and the phylogenetic tree was constructed using the Molecular Evolutionary Genetics Analysis version 7.0 software (MEGA7) using the neighbor-joining method and p-distance as the substitution model. Each phylogeny was tested using the bootstrap method with 500 replications.

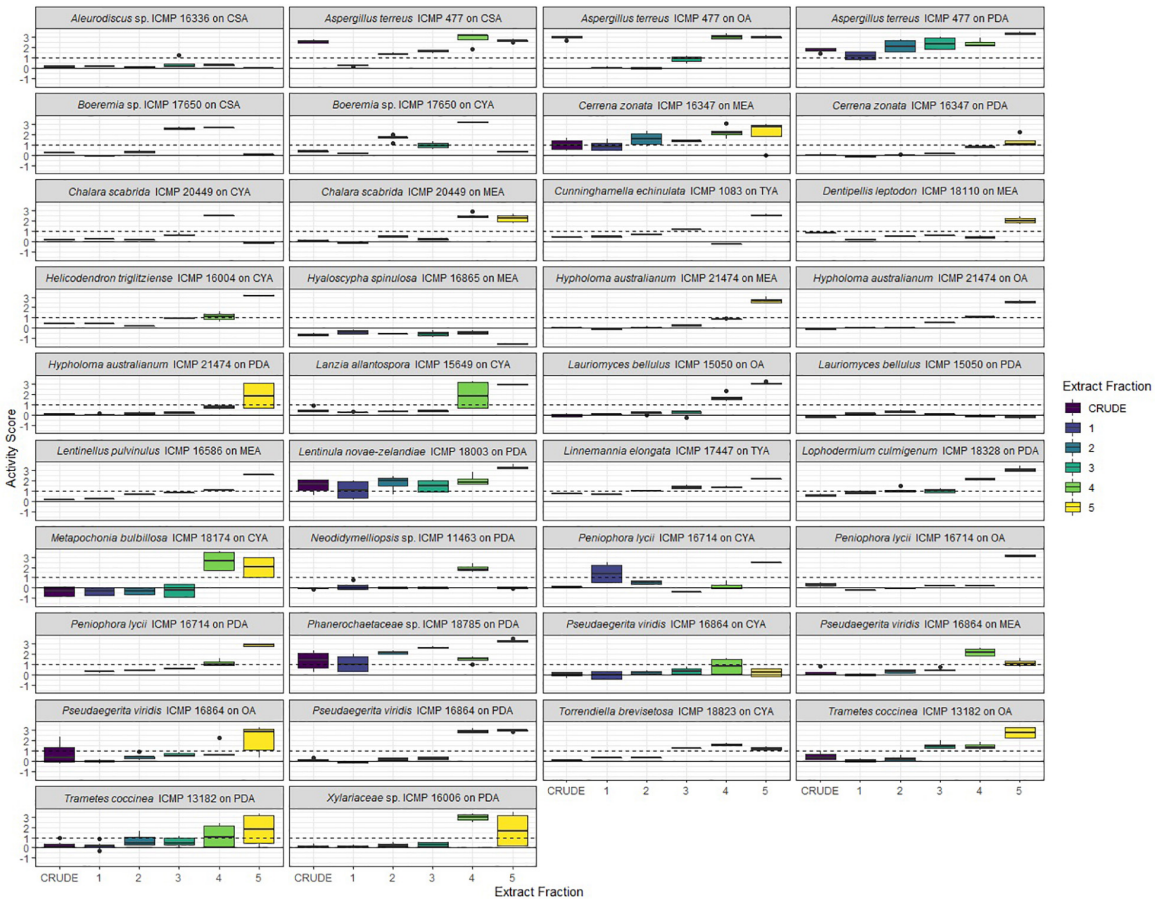

FIGURE 6 | Antibacterial activity of crude extracts and fractions 1–5 from ICMP fungal isolates against *Mycobacterium marinum* BSG101. Data is presented as box and whisker plots of activity scores. The solid line shown at 0 is the median control value while the dotted line at 1 is the activity threshold. Scores above 1 correspond to a >90% reduction in bacterial bioluminescence compared to the corresponding no-fungi control. Similarly, an activity score above 2 means corresponds to a >99% reduction. CSA, Czapek Solution Agar; CYA, Czapek Yeast Extract Agar; MEA, Malt Extract Agar; OA, Oatmeal Agar; PDA, Potato Dextrose Agar; TYA, Tryptone Yeast Extract Agar. Boxes are upper and lower quartiles with median shown. The whiskers extend up to 1.5× the inter-quartile range and any dots beyond those bounds are outliers.

retain any activity in either the crude extract or any of the 5 fractions. These belonged to *Aleurodiscus* sp. ICMP 16336 grown on CSA, *Pseudaegerita viridis* ICMP 16864 grown on CYA, and *Lauriomyces bellulus* ICMP 15050 grown on PDA (**Figures 5**, **7**). Of the remaining 14 Basidiomycota-medium combinations tested, the most active fraction was F5 [14/14 (100%)], followed by F4 [7/14 (50%)]. Four Basidiomycota-medium combinations also displayed some activity from fractions F2 and/or F3. Of the 17 Ascomycota-medium combinations we observed to be active, the most active fraction was F4 [17/17 (100%)], followed by F5 [13/17 (76%)]. Six Ascomycota-medium combinations also displayed some activity from fractions F2 and/or F3. Both Mucoromycota-medium combinations tested had multiple active fractions.

We observed that all 41 of the fungus-medium combinations we tested for activity against *M. marinum* BSG101 retained some activity in either the crude extract or at least one of the 5 fractions (**Figures 5**, **6**). Of the 18 Basidiomycota-medium combinations tested, the most active fraction was F5 [17/18 (94%)], followed by F4 [11/17 (65%)]. Seven Basidiomycota-medium combinations also displayed some activity from fractions F2 and/or F3. Like the Basidiomycota-medium combinations, of the 21 Ascomycota-medium combinations we observed to be active, the most active fraction was F5 [21/21 (100%)], followed by F4 [16/21 (76%)]. Eight Ascomycota-medium combinations also displayed some activity from fractions F2 and/or F3. Both Mucoromycota-medium combinations tested had multiple active fractions.

Linoleic Acid Is Likely the Anti-mycobacterial Compound Present in Fraction F5

Given the anti-mycobacterial activity we observed from the F5 fractions of so many of the ICMP isolates, we analyzed this fraction in more detail from four phylogenetically diverse ICMP isolates: the Basidiomycota *Aleurodiscus* sp. ICMP 16336, the Ascomycota *Hyaloscypha spinulosa* ICMP 16865 and *Lanzia allantospora* ICMP 15649, and the Mucoromycota *Cunninghamella echinulata* ICMP 1083. NMR spectroscopic and

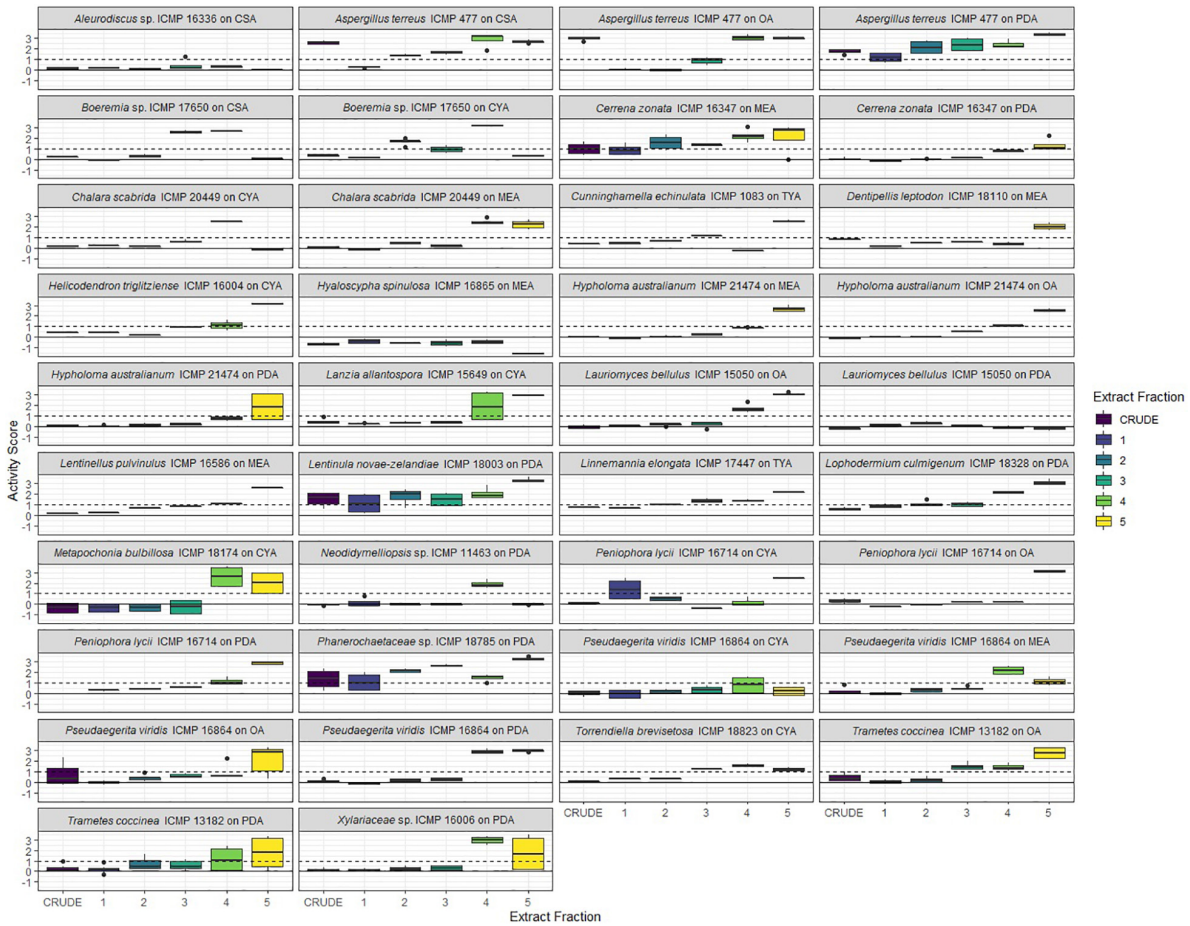

FIGURE 7 | Antibacterial activity of crude extracts and fractions 1–5 from ICMP fungal isolates against *Mycobacterium abscessus* BSG301. Data is presented as box and whisker plots of activity scores. The solid line shown at 0 is the median control value while the dotted line at 1 is the activity threshold. Scores above 1 correspond to a >90% reduction in bacterial bioluminescence compared to the corresponding no-fungi control. Similarly, an activity score above 2 means corresponds to a >99% reduction. CSA, Czapek Solution Agar; CYA, Czapek Yeast Extract Agar; MEA, Malt Extract Agar; OA, Oatmeal Agar; PDA, Potato Dextrose Agar; TYA, Tryptone Yeast Extract Agar. Boxes are upper and lower quartiles with median shown. The whiskers extend up to 1.5× the inter-quartile range and any dots beyond those bounds are outliers.

Mass spectrometric analysis confirmed the presence of linoleic acid in fraction F5 of these fungi.

Identification of Active ICMP Fungal Fractions for Further Analysis

To prioritize the most active anti-mycobacterial fungus-medium combinations for further NMR spectroscopic and Mass spectrometric analysis, we tested those fractions F2, F3, and F4 that were active at 1000 mg/mL to obtain their minimum inhibitory concentration (MIC) (**Table 4**).

Of the 31 fungus-medium combinations tested against *M. abscessus* BSG301, 11/31 (35%) F3 fractions had an MIC $\leq$ 500 μg/mL. Of these, the most active fungus-medium combinations were *Pseudaegerita viridis* ICMP 16864 grown on PDA with an MIC of 31.25 μg/mL, and *Aspergillus terreus* ICMP 477 grown on CSA, with an MIC of 125 μg/mL (**Table 4**). In contrast, only three F4 fractions and one F2 fraction had an MIC $\leq$ 500 μg/mL.

In contrast to *M. abscessus*, of the 31 fungus-medium combinations tested against *M. marinum* BSG101, the most active fractions were F4 rather than F3, with 17/31 (55%) F4 fractions having an MIC $\leq$ 500 μg/mL. Of these, the most active fungus-medium combinations were *Pseudaegerita viridis* ICMP 16864 grown on PDA and MEA, with an MIC of 31.25 and 62.5 μg/mL, respectively, and *Lophodermium culmigenum* ICMP 18328, with an MIC of 62.5 μg/mL (**Table 4**). Three F2 fractions and six F3 fractions had an MIC $\leq$ 500 μg/mL.

DISCUSSION

In this study, we describe a medium-throughput bioluminescence-based pipeline to screen fungi for activity against Mycobacteria using bioluminescent derivates of *M. abscessus* and *M. marinum* as the testing strains. We included *M. abscessus* as it is a relatively fast-growing non-tuberculous

TABLE 4 | Minimum inhibitory concentrations (MIC) of ICMP fungal fractions (F2, F3, and F4) against *M. abscessus* and *M. marinum*.

Species	ICMP	Media[1]	*M. abscessus* MIC (μg/mL)			*M. marinum* MIC (μg/mL)		
			F2	F3	F4	F2	F3	F4
Aspergillus terreus	477	CSA	1000	**125**	1000	**250**	**500**	**125**
		OA	>1000	**250**	>1000	>1000	1000	**250**
		PDA	**500**	**500**	**500**	**500**	**500**	**500**
Boeremia sp.	17650	CSA	1000	**500**	>1000	>1000	>1000	1000
		CYA	>1000	**250**	1000	>1000	>1000	**500**
Cerrena zonata	16347	MEA	1000	1000	1000	1000	1000	**500**
		PDA	>1000	>1000	>1000	>1000	>1000	1000
Chalara scabrida	20449	CYA	>1000	1000	>1000	>1000	1000	>1000
		MEA	>1000	1000	>1000	>1000	>1000	**500**
Cunninghamella echinulata	1083	TYA	1000	>1000	>1000	1000	**500**	>1000
Hypholoma australianum	21474	MEA	>1000	>1000	>1000	>1000	>1000	**500**
		OA	>1000	1000	>1000	>1000	>1000	1000
		PDA	>1000	>1000	>1000	>1000	>1000	1000
Lauriomyces bellulus	15050	OA	>1000	1000	>1000	>1000	>1000	1000
		PDA	>1000	>1000	>1000	>1000	>1000	>1000
Lentinellus pulvinulus	16586	MEA	>1000	1000	>1000	>1000	>1000	1000
Lentinula novae-zelandiae	18003	PDA	1000	1000	1000	1000	**500**	**500**
Linnemannia elongate	17447	TYA	1000	1000	1000	1000	>1000	1000
Lophodermium culmigenum	18328	PDA	1000	**500**	>1000	1000	1000	**62.5**
Metapochonia bulbillosa	18174	CYA	>1000	**250**	1000	>1000	**500**	**500**
Neodidymelliopsis sp.	11463	PDA	>1000	1000	>1000	>1000	>1000	**500**
Peniophora lycii	16714	PDA	>1000	>1000	>1000	>1000	1000	1000
Phanerochaetaceae sp.	18785	PDA	**500**	1000	1000	**500**	**250**	1000
Pseudaegerita viridis	16864	CYA	>1000	>1000	>1000	>1000	>1000	**250**
		MEA	>1000	**500**	>1000	1000	>1000	**62.5**
		OA	>1000	>1000	>1000	>1000	>1000	**250**
		PDA	>1000	**31.25**	>1000	1000	>1000	**31.25**
Torrendiella brevisetosa	18823	CYA	**500**	**500**	>1000	>1000	1000	>1000
Trametes coccinea	13182	OA	1000	1000	>1000	>1000	1000	**500**
		PDA	>1000	1000	>1000	1000	1000	**250**
Xylariaceae sp.	16006	PDA	>1000	**500**	>1000	>1000	>1000	1000

[1]*CSA, Czapek Solution Agar; CYA, Czapek Yeast Extract Agar; MEA, Malt Extract Agar; OA, Oatmeal Agar; PDA, Potato Dextrose Agar; TYA, Tryptone Yeast Extract Agar. MIC values ≤500 μg/mL are shown in bold.*

mycobacterial species and is a cause of opportunistic infections in patients with cystic fibrosis or chronic pulmonary disease, and of skin and soft tissue infections, for which treatment options are limited (To et al., 2020; Victoria et al., 2021). We also included *M. marinum* as, despite being a pathogen of fish, amphibians, and reptiles, it shares conserved virulence determinants with *M. tuberculosis* (Bouz and Al Hasawi, 2018; Ramakrishnan, 2020) and is a Biosafety Level (BSL) 2 rather than an airborne BSL 3 organism.

We screened 36 ICMP fungal isolates using our assay and discovered that almost all produced considerable anti-mycobacterial activity. This is in contrast with our experience screening ICMP isolates for activity against other human pathogens such as *Escherichia coli*, *Pseudomonas aeruginosa*, and *Staphylococcus aureus*, where we find just 5–20% of fungal isolates have some antibacterial activity (unpublished data). We also observed some differences between the two mycobacterial species, with more ICMP isolates being active against *M. marinum* than *M. abscessus*. This is not unsurprising given their different ecological niches and divergent genomes (Malhotra et al., 2017). Identification of the chemical compounds responsible may shed some further light on these differences.

Our screening pipeline involves growing fungi in 24 well plates on multiple growth media. It has previously been shown that different culture conditions can alter the expression of biosynthetic gene clusters and therefore the structural diversity and quantity of secondary metabolites produced by microorganisms, including fungi (Bills et al., 2008). For example, growing *Fusarium tricinctum* on Rice medium supplemented with fruit and vegetable juices led to the discovery of Fusarielin J (Hemphill et al., 2017) while growing *Asteromyces cruciatus* on Czapek-Dox medium with an altered nitrogen source led to the discovery of Lajollamide A (Gulder et al., 2012). We selected media that cover a broad range of carbon and nitrogen sources, as well as different pH and metal ions. We have also included media

with less chemically defined elements, including from potatoes, rice, and oatmeal. Our data provides strong statistical evidence for the impact of growth media on antibacterial activity of the ICMP fungi we tested, with some fungal isolates only active when grown on one medium and others active when grown on several, or even all. The highest proportion of ICMP isolates were active when grown on the nutritionally rich Oatmeal Agar (OA), Potato Dextrose Agar (PDA), and (MYA) while the lowest proportion were active when grown on the more nutritionally poor Rice Extract Agar (REA) and Czapek Solution Agar (CSA).

The ICMP fungi we screened in this project included isolates of several species well known to produce antimicrobial compounds. For example, *Aspergillus terreus* produces terrein (Goutam et al., 2017), maunakeanolic acid A and B (Zaman et al., 2020), and helvolic acid (Zaman et al., 2020), amongst other compounds. Chemical extraction and fractionation of a subset of the ICMP isolates revealed that much of the activity we observed may be due to the production of the known anti-mycobacterial compound linoleic acid (Kanetsuna, 1985; Choi, 2016). However, we have identified several ICMP isolates that retained their anti-mycobacterial activity in non-linoleic acid containing fractions. These include isolates of *Lophodermium culmigenum*, *Pseudaegerita viridis*, and *Trametes coccinea*, as well as an unknown species of *Boeremia* and an isolate of an unknown genus and species in the family *Phanerochaetaceae*. Investigations are ongoing to identify the sources of their anti-mycobacterial activity and to determine whether any may be due to the production of novel bioactive compounds. Species of *Lophodermium* and *Pseudaegerita* have previously been found to produce several antifungal compounds (Hosoya et al., 2007; Sumarah et al., 2011; McMullin et al., 2015), while *T. coccinea* is predicted to have secondary metabolite pathways though genomic analysis (Zhang et al., 2020).

An interesting observation we have made, is of the abundant anti-mycobacterial activity of fungi we tested in the order Polyporales. The isolates *Cerrena zonata* ICMP 16347, *Laetiporus portentosus* ICMP 15555, *Phanerochaetaceae* sp. ICMP 18785, and *T. coccinea* ICMP 13182, were active against both mycobacterial species when grown in almost all media. These fungi are bracket-like fungi with pores on the under surface. To fulfill their ecological niche of digesting moist wood, these fungi first need to colonize the wood. To do this they need to compete with other microorganisms, including bacteria, and producing antimicrobial compounds would be beneficial on this process. An alternative hypothesis could be that their antibacterial activity is a by-product of these fungi producing the peroxidases and oxidases they need to digest wood (Sulej et al., 2019). Should the activity prove not to be the result of peroxidase/oxidase production, this would suggest that focusing future screening efforts on Polyporales fungi could prove fruitful for the discovery of new antibacterial compounds.

DATA AVAILABILITY STATEMENT

The datasets presented in this study can be found in online repositories. The names of the repository/repositories and accession number(s) can be found below: https://www.ncbi.nlm.nih.gov/genbank/, MT107903, MZ325955, MZ325952, MW862777, MW862790, MW862786, MK432752, MZ325951, MZ325956, MZ325966, MK432688, MK432695, MZ325972, MZ325953, AY755334, EF029218, MW862787, MZ325965, MZ325962, MZ325968, MZ325967, MZ325970, MZ325971, MW862783, MZ325959, MZ325969, MH395972, MH395959, GQ411512, MZ325960, MZ325961, JN225946, MW862784, EU770239, MZ325963, and MZ325954 and https://figshare.com/, https://auckland.figshare.com/articles/dataset/Antibacterial_activity_of_fungal_isolates_from_the_International_Collection_of_Microorganisms_from_Plants_ICMP_against_Mycobacterium_abscessus_and_Mycobacterium_marinum_/14937894.

AUTHOR CONTRIBUTIONS

BW, BC, and SW contributed to conception and design of the study. AG, MC, YD, and DP performed the experiments. AG, MC, TL, BW, and SW were involved in data analysis. AG and SW wrote the manuscript. All authors contributed to manuscript revision, read, and approved the submitted version.

FUNDING

This work was supported by funds from Cure Kids (9102 3715810), NZ Carbon Farming (9102 3718092), Maurice Wilkins Centre for Molecular Biodiscovery (9159 3715235), and donations from the New Zealand public. BW, DP, and the ICMP culture collection were funded by the SSIF infrastructure investment fund of the New Zealand Ministry of Business, Innovation and Employment.

SUPPLEMENTARY MATERIAL

The Supplementary Material for this article can be found online at: https://www.frontiersin.org/articles/10.3389/fmicb.2021.739995/full#supplementary-material

REFERENCES

Al-Mahruqi, S. H., van Ingen, J., Al-Busaidy, S., Boeree, M. J., Al-Zadjali, S., Patel, A., et al. (2009). Clinical relevance of nontuberculous mycobacteria, Oman. *Emerg. Infect. Dis.* 15, 292–294. doi: 10.3201/eid1502.080977

Andreu, N., Fletcher, T., Krishnan, N., Wiles, S., and Robertson, B. D. (2012). Rapid measurement of antituberculosis drug activity in vitro and in macrophages using bioluminescence. *J. Antimicrob. Chemother.* 67, 404–414. doi: 10.1093/jac/dkr472

Andreu, N., Zelmer, A., Fletcher, T., Elkington, P. T., Ward, T. H., Ripoll, J., et al. (2010). Optimisation of bioluminescent reporters for use

with mycobacteria. *PLoS One* 5:e10777. doi: 10.1371/journal.pone.0010777

Andreu, N., Zelmer, A., Sampson, S. L., Ikeh, M., Bancroft, G. J., Schaible, U. E., et al. (2013). Rapid in vivo assessment of drug efficacy against *Mycobacterium* tuberculosis using an improved firefly luciferase. *J. Antimicrob. Chemother.* 68, 2118–2127. doi: 10.1093/jac/dkt155

Bates, D., Mächler, M., Bolker, B., and Walker, S. (2015). Fitting Linear mixed-effects models using lme4. *J. Stat. Softw.* 67, 1–48.

Bills, G. F., Platas, G., Fillola, A., Jiménez, M. R., Collado, J., Vicente, F., et al. (2008). Enhancement of antibiotic and secondary metabolite detection from filamentous fungi by growth on nutritional arrays. *J. Appl. Microbiol.* 104, 1644–1658. doi: 10.1111/j.1365-2672.2008.03735.x

Bouz, G., and Al Hasawi, N. (2018). The zebrafish model of tuberculosis – no lungs needed. *Crit. Rev. Microbiol.* 44, 779–792. doi: 10.1080/1040841X.2018.1523132

Cadelis, M. M., Gordon, H., Grey, A., Geese, S., Mulholland, D. R., Weir, B. S., et al. (2021). Isolation of a novel polyketide from *Neodidymelliopsis* sp. *Molecules* 26:3235. doi: 10.3390/molecules26113235

Chengalroyen, M. D., Jordaan, A., Seldon, R., Ioerger, T., Franzblau, S. G., Nasr, M., et al. (2020). Biological profiling enables rapid mechanistic classification of phenotypic screening hits and identification of KatG activation-dependent pyridine carboxamide prodrugs with activity against *Mycobacterium tuberculosis*. *Front. Cell. Infect. Microbiol.* 10:699. doi: 10.3389/fcimb.2020.582416

Choi, W. H. (2016). Evaluation of anti-tubercular activity of linolenic acid and conjugated-linoleic acid as effective inhibitors against *Mycobacterium tuberculosis*. *Asian Pac. J. Trop. Med.* 9, 125–129. doi: 10.1016/j.apjtm.2016.01.021

Dalton, J. P., Uy, B., Okuda, K. S., Hall, C. J., Denny, W. A., Crosier, P. S., et al. (2017). Screening of anti-mycobacterial compounds in a naturally infected zebrafish larvae model. *J. Antimicrob. Chemother.* 72, 421–427. doi: 10.1093/jac/dkw421

Dalton, J. P., Uy, B., Phummarin, N., Copp, B. R., Denny, W. A., Swift, S., et al. (2016). Effect of common and experimental anti-tuberculosis treatments on *Mycobacterium tuberculosis* growing as biofilms. *PeerJ* 4:e2717. doi: 10.7717/peerj.2717

Donohue, M. J. (2018). Increasing nontuberculous mycobacteria reporting rates and species diversity identified in clinical laboratory reports. *BMC Infect. Dis.* 18:163. doi: 10.1186/s12879-018-3043-7

Donohue, M. J., and Wymer, L. (2016). Increasing prevalence rate of nontuberculous mycobacteria infections in five states, 2008–2013. *Ann. Am. Thorac. Soc.* 13, 2143–2150. doi: 10.1513/AnnalsATS.201605-353OC

Early, J. V., Mullen, S., and Parish, T. (2019). A rapid, low pH, nutrient stress, assay to determine the bactericidal activity of compounds against non-replicating *Mycobacterium tuberculosis*. *PLoS One* 14:e0222970. doi: 10.1371/journal.pone.0222970

Fox, J., and Weisberg, S. (2019). *An R Companion to Applied Regression*, 3rd Edn. Thousand Oaks, CA: Sage.

Gagneux, S. (2018). Ecology and evolution of *Mycobacterium tuberculosis*. *Nat. Rev. Microbiol.* 16, 202–213. doi: 10.1038/nrmicro.2018.8

Gonzalez-Santiago, T. M., and Drage, L. A. (2015). Nontuberculous mycobacteria: skin and soft tissue infections. *Granulomat. Disord. Adult Skin* 33, 563–577. doi: 10.1016/j.det.2015.03.017

Goutam, J., Sharma, G., Tiwari, V. K., Mishra, A., Kharwar, R. N., Ramaraj, V., et al. (2017). Isolation and characterization of "Terrein" an antimicrobial and antitumor compound from endophytic fungus *Aspergillus terreus* (JAS-2) associated from *Achyranthus aspera* Varanasi, India. *Front. Microbiol.* 8:1334. doi: 10.3389/fmicb.2017.01334

Griffin, I., Schmitz, A., Oliver, C., Pritchard, S., Zhang, G., Rico, E., et al. (2019). Outbreak of tattoo-associated nontuberculous mycobacterial skin infections. *Clin. Infect. Dis.* 69, 949–955. doi: 10.1093/cid/ciy979

Gulder, T. A. M., Hong, H., Correa, J., Egereva, E., Wiese, J., Imhoff, J. F., et al. (2012). Isolation, structure elucidation and total synthesis of lajollamide A from the marine fungus *Asteromyces cruciatus*. *Mar. Drugs* 10, 2912–2935. doi: 10.3390/md10122912

Gupta, R. S., Lo, B., and Son, J. (2018). Phylogenomics and comparative genomic studies robustly support division of the Genus *Mycobacterium* into an emended Genus *Mycobacterium* and four novel genera. *Front. Microbiol.* 9:67. doi: 10.3389/fmicb.2018.00067

Hemphill, C. F. P., Sureechatchaiyan, P., Kassack, M. U., Orfali, R. S., Lin, W., Daletos, G., et al. (2017). OSMAC approach leads to new fusarielin metabolites from *Fusarium tricinctum*. *J. Antibiot. (Tokyo)* 70, 726–732. doi: 10.1038/ja.2017.21

Hosoya, T., Ohsumi, J., Hamano, K., Ono, Y., and Miura, M. (2007). *Method for Producing Cercosporamide*. Worldwide Patent No WO2007018194A1.

Jabbour, S. F., Malek, A. E., Kechichian, E. G., Tomb, R. R., and Nasr, M. W. (2020). Nontuberculous mycobacterial infections after cosmetic procedures: a systematic review and management algorithm. *Dermatol. Surg.* 46, 116–121.

Jain, P., Garing, S., Verma, D., Saranathan, R., Clute-Reinig, N., Gadwa, J., et al. (2020). Nanoluciferase reporter mycobacteriophage for sensitive and rapid detection of *Mycobacterium tuberculosis* drug susceptibility. *J. Bacteriol.* 202:e00411-20. doi: 10.1128/JB.00411-20

Johnston, P. R., Weir, B. S., and Cooper, J. A. (2017). Open data on fungi and bacterial plant pathogens in New Zealand. *Mycology* 8, 59–66. doi: 10.1080/21501203.2016.1278409

Kanetsuna, F. (1985). Bactericidal effect of fatty acids on mycobacteria, with particular reference to the suggested mechanism of intracellular killing. *Microbiol. Immunol.* 29, 127–141. doi: 10.1111/j.1348-0421.1985.tb00811.x

Koh, W.-J., and Schlossberg, D. (2017). Nontuberculous mycobacteria-overview. *Microbiol. Spectr.* 5:5.1.11. doi: 10.1128/microbiolspec.TNMI7-0024-2016

Kumar, S., Stecher, G., and Tamura, K. (2016). MEGA7: molecular evolutionary genetics analysis version 7.0 for bigger datasets. *Mol. Biol. Evol.* 33, 1870–1874.

Malhotra, S., Vedithi, S. C., and Blundell, T. L. (2017). Decoding the similarities and differences among mycobacterial species. *PLoS Negl. Trop. Dis.* 11:e0005883. doi: 10.1371/journal.pntd.0005883

McMullin, D. R., Green, B. D., and Miller, J. D. (2015). Antifungal sesquiterpenoids and macrolides from an endophytic *Lophodermium* species of *Pinus strobus*. *Phytochem. Lett.* 14, 148–152. doi: 10.1016/j.phytol.2015.10.006

Mirsaeidi, M., Farshidpour, M., Allen, M. B., Ebrahimi, G., and Falkinham, J. O. (2014). Highlight on advances in nontuberculous mycobacterial disease in North America. *BioMed Res. Int.* 2014:919474. doi: 10.1155/2014/919474

Moore, J. E., Kruijshaar, M. E., Ormerod, L. P., Drobniewski, F., and Abubakar, I. (2010). Increasing reports of non-tuberculous mycobacteria in England, Wales and Northern Ireland, 1995-2006. *BMC Public Health* 10:612. doi: 10.1186/1471-2458-10-612

Morimoto, K., Iwai, K., Uchimura, K., Okumura, M., Yoshiyama, T., Yoshimori, K., et al. (2014). A steady increase in nontuberculous mycobacteriosis mortality and estimated prevalence in Japan. *Ann. Am. Thorac. Soc.* 11, 1–8. doi: 10.1513/AnnalsATS.201303-067OC

Pontali, E., Raviglione, M. C., and Migliori, G. B. (2019). Regimens to treat multidrug-resistant tuberculosis: past, present and future perspectives. *Eur. Respir. Rev.* 28:190035. doi: 10.1183/16000617.0035-2019

R Core Team. (2020). *R: A Language And Environment for Statistical Computing*. Available online at: https://www.R-project.org/ (accessed July 12, 2021)

Ramakrishnan, L. (2020). *Mycobacterium tuberculosis* pathogenicity viewed through the lens of molecular Koch's postulates. *Curr. Opin. Microbiol.* 54, 103–110. doi: 10.1016/j.mib.2020.01.011

Ratnatunga, C. N., Lutzky, V. P., Kupz, A., Doolan, D. L., Reid, D. W., Field, M., et al. (2020). The rise of non-tuberculosis mycobacterial lung disease. *Front. Immunol.* 11:303. doi: 10.3389/fimmu.2020.00303

Roux, A.-L., Catherinot, E., Ripoll, F., Soismier, N., Macheras, E., Ravilly, S., et al. (2009). Multicenter study of prevalence of nontuberculous mycobacteria in patients with cystic fibrosis in France. *J. Clin. Microbiol.* 47, 4124–4128. doi: 10.1128/JCM.01257-09

Seaworth, B. J., and Griffith, D. E. (2017). Therapy of multidrug-resistant and extensively drug-resistant Tuberculosis. *Microbiol. Spectr.* 5, doi: 10.1128/microbiolspec.TNMI7-0042-2017

Sulej, J., Osińska-Jaroszuk, M., Jaszek, M., Grąz, M., Kutkowska, J., Pawlik, A., et al. (2019). Antimicrobial and antioxidative potential of free and immobilised cellobiose dehydrogenase isolated from wood degrading fungi. *Fungal Biol.* 123, 875–886. doi: 10.1016/j.funbio.2019.09.007

Sumarah, M. W., Kesting, J. R., Sørensen, D., and Miller, J. D. (2011). Antifungal metabolites from fungal endophytes of *Pinus strobus*. *Phytochemistry* 72, 1833–1837. doi: 10.1016/j.phytochem.2011.05.003

To, K., Cao, R., Yegiazaryan, A., Owens, J., and Venketaraman, V. (2020). General overview of nontuberculous mycobacteria opportunistic pathogens:

Mycobacterium avium and *Mycobacterium abscessus*. *J. Clin. Med.* 9:2541. doi: 10.3390/jcm9082541

Victoria, L., Gupta, A., Gómez, J. L., and Robledo, J. (2021). *Mycobacterium abscessus* complex: a review of recent developments in an emerging pathogen. *Front. Cell. Infect. Microbiol.* 11:338. doi: 10.3389/fcimb.2021.659997

Wallis, G. P., and Trewick, S. A. (2009). New Zealand phylogeography: evolution on a small continent. *Mol. Ecol.* 18, 3548–3580. doi: 10.1111/j.1365-294X.2009.04294.x

Wiles, S., and Grey, A. (2021a). *Bioluminescence-Based 24 Well Plate Assay for Screening Fungi for Activity Against Mycobacterium abscessus*. Protocols.io. Available online at: https://dx.doi.org/10.17504/protocols.io.bvqtn5wn (accessed July 12, 2021).

Wiles, S., and Grey, A. (2021b). *Bioluminescence-Based 24 Well Plate Assay For Screening Fungi for Activity Against Mycobacterium marinum*. Protocols.io. Available online at: https://dx.doi.org/10.17504/protocols.io.bvnbn5an (accessed July 12, 2021).

Wiles, S., and Grey, A. (2021c). *Bioluminescence-Based Minimum Inhibitory Concentration (MIC) Testing of Fungal Extracts Against Mycobacterium abscessus*. Protocols.io. Available online at: https://dx.doi.org/10.17504/protocols.io.bvm9n496 (accessed July 12, 2021).

Wiles, S., and Grey, A. (2021d). *Bioluminescence-based Minimum Inhibitory Concentration (MIC) Testing of Fungal Extracts Against Mycobacterium marinum*. Protocols.io. Available online at: https://dx.doi.org/10.17504/protocols.io.bvnan5ae (accessed July 12, 2021).

Williamson, D., Howden, B., and Stinear, T. (2017). *Mycobacterium chimaera* spread from heating and cooling units in heart surgery. *N. Engl. J. Med.* 376, 600–602. doi: 10.1056/NEJMc1612023

Zaman, K. A. U., Hu, Z., Wu, X., Hou, S., Saito, J., Kondratyuk, T. P., et al. (2020). NF-κB inhibitory and antibacterial helvolic and fumagillin derivatives from *Aspergillus terreus*. *J. Nat. Prod.* 83, 730–737. doi: 10.1021/acs.jnatprod.9b01190

Zhang, Y., Wang, J., Yajun, C., Zhou, M., Wang, W., Geng, M., et al. (2020). Comparative genomics uncovers the genetic diversity and synthetic biology of secondary metabolite production of *Trametes*. *Mycobiology* 48, 104–114. doi: 10.1080/12298093.2020.1725361

Conflict of Interest: The authors declare that the research was conducted in the absence of any commercial or financial relationships that could be construed as a potential conflict of interest.

Publisher's Note: All claims expressed in this article are solely those of the authors and do not necessarily represent those of their affiliated organizations, or those of the publisher, the editors and the reviewers. Any product that may be evaluated in this article, or claim that may be made by its manufacturer, is not guaranteed or endorsed by the publisher.

frontiers in Microbiology

ORIGINAL RESEARCH
published: 17 September 2021
doi: 10.3389/fmicb.2021.716523

Evaluation of the Antibacterial Activity of Crude Extracts Obtained From Cultivation of Native Endophytic Fungi Belonging to a Tropical Montane Rainforest in Colombia

*Esteban Charria-Girón[1], María C. Espinosa[1], Andrea Zapata-Montoya[1], María J. Méndez[1], Juan P. Caicedo[1], Andrés F. Dávalos[2], Beatriz E. Ferro[3], Aida M. Vasco-Palacios[4,5] and Nelson H. Caicedo[1,6]**

[1]Departamento de Ingeniería Bioquímica, Facultad de Ingeniería, Universidad Icesi, Cali, Colombia, [2]Departamento de Ciencias Biológicas, Facultad de Ciencias Naturales, Universidad Icesi, Cali, Colombia, [3]Departamento de Salud Pública y Medicina Comunitaria, Facultad de Ciencias de la Salud, Universidad Icesi, Cali, Colombia, [4]Grupo de Microbiología Ambiental - BioMicro, Escuela de Microbiología, Universidad de Antioquia (UdeA), Medellín, Colombia, [5]Asociación Colombiana de Micología (ASCOLMIC), Medellin, Colombia, [6]Centro BioInc, Universidad Icesi, Cali, Colombia

OPEN ACCESS

Edited by:
Paola Angelini,
University of Perugia, Italy

Reviewed by:
Surendra Sarsaiya,
Zunyi Medical University, China
Ravindra Prasad Aharwal,
Rani Durgavati University, India

***Correspondence:**
Nelson H. Caicedo
nhcaicedo@icesi.edu.co

Specialty section:
This article was submitted to Microbiotechnology, a section of the journal Frontiers in Microbiology

Received: 28 May 2021
Accepted: 09 August 2021
Published: 17 September 2021

Citation:
Charria-Girón E, Espinosa MC, Zapata-Montoya A, Méndez MJ, Caicedo JP, Dávalos AF, Ferro BE, Vasco-Palacios AM and Caicedo NH (2021) Evaluation of the Antibacterial Activity of Crude Extracts Obtained From Cultivation of Native Endophytic Fungi Belonging to a Tropical Montane Rainforest in Colombia. Front. Microbiol. 12:716523. doi: 10.3389/fmicb.2021.716523

Bioactive secondary metabolite production from endophytic fungi has gained a recurring research focus in recent decades as these microorganisms represent an unexplored biological niche for their diverse biotechnological potential. Despite this focus, studies involving tropical endophytes remain scarce, particularly those isolated from medicinal plants of these ecosystems. In addition, the state of the art of the pharmaceutical industry has experienced stagnation in the past 30 years, which has pushed pathogenic infections to get one step ahead, resulting in the development of resistance to existing treatments. Here, five fungal endophytes were isolated from the medicinal plant *Otoba gracilipes* (Myristicaceae), which corresponded to the genera *Xylaria* and *Diaporthe*, and screened to demonstrate the promissory potential of these microorganisms for producing bioactive secondary metabolites with broad-spectrum antibacterial activities. Thus, the evaluation of crude organic extracts obtained from the mycelia and exhaust medium allowed the elucidation of *Xylaria* sp. and *Diaporthe endophytica* potential toward providing crude extracellular extracts with promising bioactivities against reference strains of *Escherichia coli* (ATCC 25922) and *Staphylococcus aureus* (ATCC 25923), according to the determined half-maximum inhibitory concentration (IC_{50}) with values down to 3.91 and 10.50 mg/ml against each pathogen, respectively. Follow-up studies provided insights into the polarity nature of bioactive compounds in the crude extracts through bioactivity guided fractionation using a polymeric resin absorbent alternative extraction procedure. In addition, evaluation of the co-culturing methods demonstrated how this strategy can enhance endophytes biosynthetic capacity and improve their antibacterial potential with a 10-fold decrease in the IC_{50} values against both pathogens compared to the obtained values in the preliminary

evaluations of *Xylaria* sp. and *D. endophytica* crude extracts. These results support the potential of Colombian native biodiversity to provide new approaches concerning the global emergence of antibiotics resistance and future production of undiscovered compounds different from the currently used antibiotics classes and simultaneously call for the value of preserving native habitats due to their promising ecosystemic applications in the biotechnological and pharmaceutical industries.

Keywords: antibacterial activity, fungal endophytes, secondary metabolites, co-culturing strategies, *Rainforest ecosystem*

INTRODUCTION

The current health crisis that has arisen from the spread of antimicrobial resistance has become one of the major causes of death occurring worldwide, accounting for more than 700,000 deaths annually, which in turn is threatening the global community development and modern medical achievements (World Health Organization, 2019). The abovementioned points expose the pharmaceutical industry's failure to provide effective and innovative treatments to defeat multidrug-resistant (MDR) pathogens, which are increasingly becoming prevalent worldwide (Nikaido, 2009; Brown and Wright, 2016). Although the conventional approaches have proven to be effective during the last century, the most recently developed drugs are not effective against several bacteria's evolving resistance systems. This situation has resulted from the diverse mechanisms of antimicrobial resistance, which rely on the following principles: the synthesis of hydrolytic enzymes, the modification of active binding sites, decreasing antimicrobial affinity, decreasing cell-wall permeability to drugs, and the generation of efflux pumps, which transport the antimicrobial agents outside cells (Reygaert, 2018). Thus, the lack of new and effective antimicrobial agents shows the urgent need for novel sources of bioactive compounds beyond the conventional antibiotic classes (Ruddaraju et al., 2020). Historically, most antibiotics belong to a limited group of molecular scaffolds whose lifespan has been extended through several generations of synthetic modifications (Ogawara, 2021). In this way, most of the main classes of antibiotics have been discovered through systematic bioprospection of soil microbes, which led them to advance in synthetic chemistry. However, the recent advances in mycology have unearthed the biosynthetic diversity of fungi toward providing novel antibiotics in response to the new millennium crisis.

In this sense, fungal endophytes, which can survive inside plant tissues for brief or prolonged periods without producing any visible symptoms, are a promising feedstock for future antimicrobials (Gupta et al., 2020). This fact can be attributed to their extraordinary ecological relationship with the host plants, which has led to discovering novel compounds (Rambold et al., 2013; Helaly et al., 2018; Sandargo et al., 2019). This ecological interaction has provided endophytes with versatile biosynthetic pathways capable of producing previously undiscovered secondary metabolites with potentially beneficial properties and applications, including antimicrobials, antivirals, antifungals, anticarcinogens, immunosuppressants, and antioxidants (Rambold et al., 2013). In the last decade, the Ecology-Bioprospecting-Bioprocessing (EBB) research group from Universidad Icesi has focused on bioprospecting rainforests in the Valle del Cauca, Colombia, for the promotion of both the value of biodiversity and the native ecosystemic services. Recently, the EBB-research group has isolated more than 30 fungal endophytic species from *Otoba gracilipes* (Family: Myristicaceae; Common name: Otobo) with various potential applications. We explored the secondary metabolites produced by fungal endophytes of *O. gracilipes*, a tropical medicinal tree associated with a montane rainforest ecosystem, poorly explored for potential bioactive metabolites (Caicedo et al., 2019). A particular type of ecosystem that is supposed to possess an unearthed capacity to produce novel compounds in response to survival adaptation strategies acquired under the adverse conditions in these ecosystems are scarce (Sousa et al., 2016; Martinez-Klimova et al., 2017). On the other hand, a recent report indicates that *O. gracilipes* is one of seven threatened forest species in the Valley of Cauca river geographic area (Bonilla, 2020). Therefore, it is essential to continue studying the endophytic fungal diversity and its biotechnological potential on this species to preserve the value of these endangered ecosystems.

Some isolated strains belonging to the genera *Xylaria* (Xylariaceae, Xylariales, and Ascomycota) and *Diaporthe* (Diaporthaceae, Diaporthales, and Ascomycota) have been identified among the *O. gracilipes* endophytes, which have provided novel bioactive molecules in the past decade. The *Xylaria* and *Diaporthe* generas represent one of the scarcest sources of unidentified and promising secondary metabolites (Sousa et al., 2016; Helaly et al., 2018). Recent studies have demonstrated the biosynthetic capacity of *Xylaria*, providing a new source of bioactive molecules, including sesquiterpenoids, diterpenoids, diterpene glycosides, triterpene glycosides, steroids, organic nitrogenous compounds, and aromatic compounds as well as the derivatives of pyrones and polyketides (Song et al., 2014). Most of these molecules display antibacterial, antifungal, phytotoxic, anticancer, cytotoxic, and anti-inflammatory activities. Similarly, some species of *Diaporthe* can produce unique natural products with low molecular weights and a variety of bioactivities,

Abbreviations: DMSO, Dimethyl sulfoxide; EBB, Ecology-Bioprospecting-Bioprocessing; ECE, Extracellular crude extract; EtOAc, Ethyl acetate; IC_{50}, Half-maximum inhibitory concentration; LB, Luria Bertani broth; MASL, Meters above sea level; MDR, Multidrug resistant; MeOH, Methanol; OD, Optical density; PDA, Potato dextrose agar; PDB, Potato dextrose broth; YM, Yeast-maltose-glucose.

including antibacterial, anticancer, antifungal, antiviral, cytotoxic, and herbicide activities. Specifically, some endophytic strains of *Xylaria* generate compounds with antibacterial activities, such as the polyketide, mycoalexine, 3-O-methylmethylmellein, nortriterpenoid Helvolic acid (Ratnaweera et al., 2014), and the cyclopentapeptide Xylapeptide A (Xu et al., 2017); similarly, an endophytic strain of *Diaporthe* sp. produces Diaporone A, a new antibacterial secondary metabolite (Guo et al., 2020). Also, strains as *Phomopsis* sp. and *Phomopsis longicolla* S1B4 produce phomoneamide and dicerandrol A-C, respectively, which are the compounds with promissory antibacterial activity (Chepkirui and Stadler, 2017; Becker and Stadler, 2020).

On the other hand, it is well-known that, in natural ecosystems, interspecies relationship plays an important role in fungi's behavior, particularly to fungal endophytes, which interact continuously with other endophytic microorganisms and their host plants (Mani et al., 2015). Surprisingly, these interactions can lead to several biochemical changes within their metabolism, such as the regulation of silent gene clusters related to the biosynthesis of the secondary metabolite, which is presumed to be silenced under the laboratory axenic culture conditions (Brakhage et al., 2008; Deepika et al., 2016). A recent revision of strategies such as co-cultures has demonstrated its promissory potential to replicate the ecological conditions by mimicking the endophytic communities (Chagas et al., 2013). These studies have demonstrated a capacity to provide an effective platform for discovering novel compounds with diverse chemical nature and industrial applications. This hypothesis has been too evaluated with macrofungi (basidiomycetes) to investigate the expression of silent genes in symbiotic systems linked with metabolomics study. One hundred thirty-six fungi-fungi symbiotic systems were built up by co-culturing 17 strains, among which the co-culture of *Trametes versicolor* and *Ganoderma applanatum* demonstrated the strongest colouration of confrontation zones; discovering that 62 features were either newly synthesized or highly produced in this co-culture (Yao et al., 2016). Similarly, several past studies have reported that metabolites secreted during monoculture are promoted when cultured in combination with other microorganisms, increasing bioactive metabolite's productivities (Zhu et al., 2018).

In this study, the antimicrobial potential of five native fungal endophytes isolated from medicinal plant of the Colombian rainforest was assessed by evaluating their crude organic extracts against antibiotic-susceptible pathogens *Escherichia coli* (ATCC 25922, Gram-negative) and *Staphylococcus aureus* (ATCC 25923, Gram-positive). These strains were preselected from all the isolates due to they belong to well-recognized genus with ability to synthetize secondary metabolites with antimicrobial activity. Furthermore, the development of a co-culture platform between *Diaporthe endophytica* and *Xylaria* sp. was systematically investigated, where the antagonist interaction between them improved the crude extract effectivity. Similarly, an alternative extraction with a polymeric resin absorbent was used to enhance the selective capture of bioactive compounds according to their molecular weight and polarity, gaining valuable insights for future purification efforts. The presented study also emphasizes on the crucial role of systematical screening platforms in the rapid and effective prioritization of antimicrobial agents prior to chemical investigation of bioactive molecules. In some cases, the cost and investing time associated to the identification of new antimicrobial compounds could be avoid by the screening of microorganisms, which are previously known to produce specific potential antimicrobial agents into crude extracts (Caicedo et al., 2011; Santiago et al., 2021). Nonetheless, our results provide an initial step toward bioprospecting the Colombian southwestern endophyte diversity and highlight the value of preserving the native habitats owing to their promising ecosystemic applications in the biotechnological and pharmaceutical industries.

MATERIALS AND METHODS

Study Area and Collection of Plant Materials

Fresh and healthy leaves and stems of two young trees of *O. gracilipes* were collected during the dry season (November, 2019) in the Natural Reserve "La Carolina" (3°24'10.662"N, 76°36'52.774"W), Cali, Valle del Cauca, Colombia at 1,600 m.a.s.l. The plant material was collected and cut with a sterile scalpel and stored at 4°C in a sterile polyethylene bag until further use.

Endophytic Fungi Isolation

The processed material was surface-sterilized by washing thoroughly in sterile demineralized water, followed by that with 70% ethanol for 1–2 min and 3% sodium hypochlorite for 15 min (Caicedo et al., 2019). Small pieces of plant tissues were then placed on potato dextrose agar (PDA, Merck®, Darmstadt, Germany) medium at pH 6.0, which was supplemented with clindamycin (0.2 ml/100 ml) in Petri dishes and incubated at 29°C until the fungus started to grow (Prihantini and Tachibana, 2017). Pure isolates with distinct morphology were selected for further molecular identification. Each fungal strain was preserved on PDA with mineral oil and sub-cultured in the same solid media before performing genomic DNA extraction and fermentation experiments.

Molecular Identification of Endophytic Fungi

Molecular identification was conducted using the previously grown strains on PDA and incubated for 5–7 days at 29°C. The fungal DNA was extracted using the EZNA® Tissue DNA Kit (Omega Bio-Tek, Norcross, GA, United States), and the complete DNA profile was quantified (>100 ng/μl for a volume of 25 μl) using the NanoDrop Spectrophotometer 2000/2000c ND-1000 (NanoDrop, Wilmington, DE, United States). The reaction mixture contained: buffer PCR, DNTPs, $MgCl_2$, TAQ Pol, Primer F, and Primer R. The nuclear ribosomal ITS1 region was amplified with the primers ITS1 and ITS5 (White et al., 1990). DNA amplification was performed in the Swift – MiniPro Thermal Cycler (ESCO, Singapore) with an initial denaturation step for 1 min at 95°C, followed by 35 cycles of denaturation for 1 min at 95°C, annealing for 30 s at 52°C, and an extension for 30 s at 72°C. A final

extension was performed at 72°C for 5 min. The PCR products were visualized using 1% agarose gel. Purification of the products was conducted using the Wizard S.V. Gel and PCR Clean-Up System (Promega, San Luis Obispo, CA, United States) before being subjected to sequencing protocols using the Applied Biosystems® ABI Prism 3,500 Sequencers (Thermo Fisher Scientific, Waltham, MA, United States). The resulting DNA sequences were analyzed and compared with those obtained from the GenBank *via* a BLAST search. The sequences from our study were also deposited in GenBank.

All the protocols and procedures employed in this investigation were verified and approved by the appropriate institutional review committee. The specimens were kept and handled in accordance with the guidelines of the National Environmental Licensing Authority (ANLA) of Colombia, through the Framework Permit for the Collection of Specimens of Wild Species of Biological Diversity for Non-Commercial Scientific Research Purposes – Resolution 0526, May 20, 2016. Furthermore, according to the Resolution 0364, March 12, 2018, and addendum to contract No. 4 of the Framework Contract for Access to Genetic Resources and their Derivative Products No. 180 of 2018, Universidad Icesi has the acceptance to the request of Framework Contract for Access to Genetic Resources and their Derivative Products for the Program for the Study, Use, and Sustainable Use of Colombian Biodiversity.

Fermentation of Fungal Isolates

For the primary screening, endophytic fungi were cultured in 250-ml Erlenmeyer flasks containing 150 ml of potato dextrose broth (PDB) by triplicate for all five isolated strains (Rao et al., 2015). Four agar plugs of 5-mm diameter from a 7-day PDA plate were used as inoculum for each experimental unit. Flask fermentations were incubated at 29°C (pH 6.0) under orbital agitation of 90 rpm until carbon sources were depleted, according to the DNS assay for reducing sugars (Ghose, 1987). After the end of the culture period, the mycelium was separated from the fermentation broth through vacuum filtration using qualitative paper filters (0.45 μm) for further extraction procedures.

Extraction Procedures

Mycelial Organic Crude Extract

Once all the mycelia were obtained, they were subjected to maceration and breaking with glass spheres, followed by ultrasonic bath digestion with acetone (1:1 w/w) for 1 h (Surup et al., 2019) and a Soxhlet extraction with acetone (1:10 w/w) for 1 h. The resulting solution was extracted thrice in a ratio of 1:1 w/w with ethyl acetate (EtOAc) in a separation funnel. In addition, the mycelium was also extracted with EtOAc (1:5 w/w). The resulting decanted organic-phases were combined, reduced by vacuum-evaporation (40°C, 40 mbar) to 5 ml, and then vacuum-dried to finally obtain the organic crude extracts (**Figure 1**).

Extracellular Organic Crude Extract

First, the exhausted culture medium was vacuum-filtered by gradually reducing the filter pore size (From 10 to 0.22-μm). The filtrate was then concentrated to 40 ml by vacuum-evaporation (40°C, 20 mbar) and extracted thrice with EtOAc (1:1 w/w) in a separation funnel. The organic phases followed the same procedure as in section Mycelial Organic Crude Extract to finally obtain extracellular crude extracts (ECEs) as depicted in **Figure 2** (Surup et al., 2019).

In vitro Antibacterial Assays

Two bacterial strains (Test organisms) were used in this study, including a Gram-positive bacteria *S. aureus* (ATCC 25923)

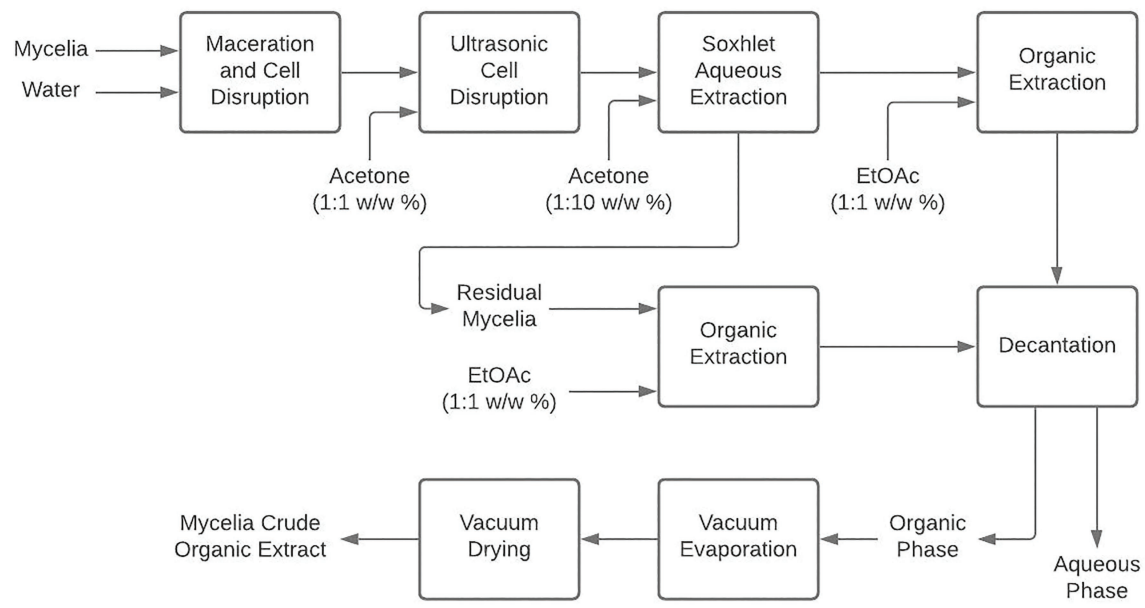

FIGURE 1 | Mycelium extraction procedure to obtain organic crude extracts from liquid cultivation of endophytic fungi.

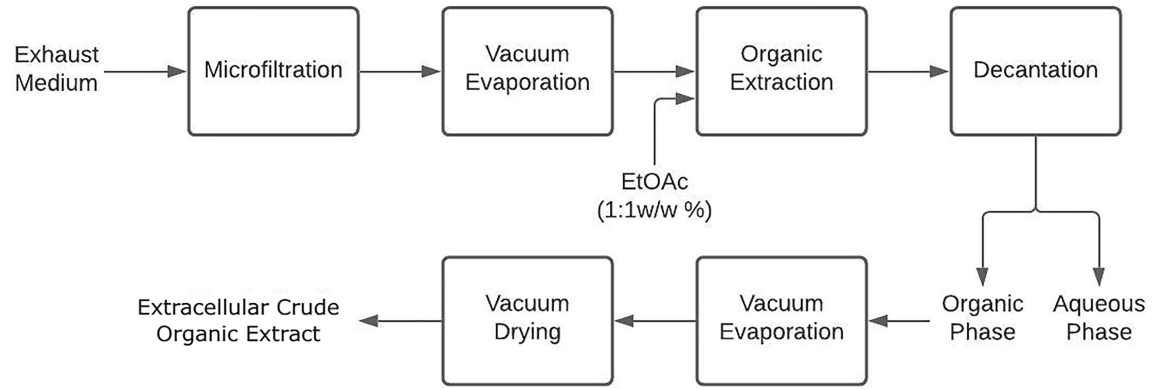

FIGURE 2 | Extracellular extraction procedure to obtain organic crude extracts from liquid cultivation of endophytic fungi.

and a Gram-negative bacteria *E. coli* (ATCC 25922). The bacterial cultures were reactivated in Luria Bertani broth medium (LB; Scharlau, Barcelona, Spain) at 37°C for 24 h, followed by streaking on LB agar medium plate and incubating for 16 h at 37°C before using in the assays.

Primary Screening for Antibacterial Activity

The antibacterial activity of organic crude extracts was evaluated against each test bacterium using a modified broth microdilution method (Caicedo et al., 2011) with four 2-fold dilutions starting from 25 mg/ml of each extract dissolved in a dimethyl sulfoxide (DMSO) solution (1% v/v). Clear round-bottomed 96-microtiter plates (Brandtech®; Essex, Connecticut, United States) were set up with the extracts to be evaluated in triplicate using LB and the broth with DMSO (1% v/v) as a negative control. Each microbial suspension was previously adjusted to an optical density (OD 620 nm) of 0.08–0.1, equivalent to 1×10^8 CFU/ml. Other dilutions were prepared with LB to yield 1×10^4 CFU/ml in the assays from this previous solution. The assay plates were then incubated at 37°C for 20 h before estimating their OD_{620} using a microplate reader (Varioskan™ LUX Thermo Scientific™, United States).

For crude extracts prioritization, the normalized responses were calculated as described by Caicedo et al. (2012). A statistical cutoff of a 0.5 normalized response at 25 mg/ml was selected in this order. Hence, the extracts that displayed a lower response than the cutoff value were scored as a positive hit. The half-maximum inhibitory concentration (IC_{50}) was determined for each selected crude extract using the Drm package from R statistical software (Ranke, 2006). Hierarchical cluster analysis (HCA) was carried out using IC_{50} values determined above to identify influential groups regarding their bioactivity. For this purpose, *clustegram* function was implemented using MATLAB® 2019b (The MathWorks, Inc.).

Extracellular Extraction Using Polymeric Resin Adsorbent

Xylaria sp. and *D. endophytica* were subjected to an alternative extracellular extraction procedure to obtain a more purified extract of each axenic culture grown on PDB. Hence, the mycelium was separated by filtration from the fermentation broth, after which the exhausted medium was extracted with polymeric resin Amberlite® XAD16N (Sigma-Aldrich, Darmstadt, Germany), previously washed with distilled water (1% w/v), methanol (1% w/v), and distilled water (0.5% w/v) again for 30 min with each solution, respectively. This method was adapted from Caicedo et al. (2011) and Narmani et al. (2018). A ratio of 0.06 g resin/ml of the exhausted media was applied and continuously mixed in an Erlenmeyer flask (100–500 ml, depending on the supernatant volumes) using agitation plates (120 rpm) at room temperature for 24 h. For the extraction, 25 ml of methanol (MeOH) and EtOAc per gram resin were added and continuously mixed for 4 h. Then, the resin was filtered, and the organic solution was reduced by vacuum-evaporation (40°C, 40 mbar) to 5 ml, and then vacuum-dried to obtain the extracts finally in Caicedo et al. (2011). These last followed the same antibacterial activity assessment procedure, which was performed for the primary screening.

Co-culturing Screening Platform

After the preliminary screening of antibacterial activity, *Xylaria* sp. and *D. endophytica,* endophytes prioritized by HCA, were selected to develop a further screening platform. In this case, first, an antagonism plate co-culture assessment between themselves and the other fungal evaluated strains was performed to identify the respective interactions through qualitative observation (Hamzah et al., 2018). Then, according to these results, co-culturing in liquid media was performed to obtain similar crude extracts for antibacterial assessments.

Antagonism Plate Assay

The antagonistic activities of the selected fungal strains were qualitatively assessed between the non-prioritized fungal strains and the two prioritized ones through a dual culture plate assay (Chagas et al., 2013). One agar plug of each strain was placed on the opposite sides of the plate, followed by incubation at 29°C for 7 days on the solid medium of Yeast-Maltose-Glucose (YM; 10 g/l malt extract, 4 g/l yeast extract, and 4 g/l D-glucose) previously adjusted to pH 6.3 (Shao et al., 2020).

Co-culture in Liquid Media

The dual culture assay between *Xylaria* sp. and *D. endophytica* was prioritized for its different liquid media studies. PDB (pH 6.0) and YM (pH 6.3) were evaluated for the selected co-culture system. Hence, each strain was individually pre-cultured in 150 ml of this medium. After proper mycelial growth, the mycelium was harvested and washed twice with a sterile solution of 0.9% w/w NaCl before inoculation in 1-L flasks containing 500 ml of each medium. Independent duplicates were incubated at 29 ± 1°C under orbital agitation of 90 rpm until all the carbon sources were depleted, according to the DNS assay for reducing sugars (Ghose, 1987). Then, the obtained ECEs were subjected to further evaluation of the antibacterial activity against the test bacteria.

Statistical Analyses

Data processing and IC_{50} determination were performed using the R (R Core Team, 2020), and the dose-response curves were produced using the ggplot2 package. The HCA was realized using the MATLAB® numerical software.

RESULTS

Molecular Identification of Endophytic Fungi

Five strains of Ascomycota isolated as endophytes of *O. gracilipes* were obtained for this study (**Figure 3**). One strain belonged to the genera *Xylaria*, while the other four strains corresponded to *Diaporthe*, respectively. Each strain was identified at the species level through amplification, sequencing, and subsequent analysis using the rDNA's ITS1 region. The sequences generated in this study were deposited in GenBank, and the associated accession numbers are indicated in **Figure 3**.

Fermentation and Extraction

The production of crude metabolites from each fungal endophyte was performed for the primary screening in PDB. Among the cultured endophytes, *Diaporthe* strains displayed a faster growth than *Xylaria* sp. In addition, the *Diaporthe* strains could consume the available carbon sources rapidly. At the same time, *Xylaria* sp. showed a more extended adaptation phase, which corresponds to the low or non-initial consumption of glucose. However, according to the iodine-starch test, this carbon source was depleted faster than glucose, suggesting this endophyte's carbon source predilection. On the other hand, *Diaporthe* endophytes consumed both the carbon sources simultaneously within a week in most cases.

On the other hand, morphological and coloration changes were observed in most of the ferementations. *Xylaria* sp. grew as pellets without coloring the fermentation broth compared to the control. In contrast, all *Diaporthe* endophytes grew as free mycelia and displayed various strain-depending colorations, where only *Diaphorte panaranensis* did not produce any coloration. *Diaporthe* sp. and *D. endophytica* exhibited a dark-brown and an orange to red colouration of the fermentation broth, respectively, in which *D. endophytica* produced colored compounds progressively as carbon sources were consumed. In the same way, *Diaphorte velutina* mycelia acquired a dark coloration and simultaneously clarified the broth, as depicted in **Figure 4**. Moreover, the mass of crude extract recovered from the exhaust medium was higher than that from the mycelial extracts. Nevertheless, the highest extraction yield of crude organic extract from the exhaust medium and the mycelium were obtained for *Xylaria* sp. (**Table 1**). Moreover, no significant differences ($p > 0.05$) were noted between the extracellular extraction yields, contrary to the mycelial extraction values. Even between the *Diaporthe* strains, different values were obtained, as depicted in **Table 1**.

Antibacterial Activity Screening

The antibacterial activities of crude organic extracts obtained from the exhaust medium and the mycelium were assessed against the antibiotic-susceptible bacteria *E. coli* (ATCC 25922) and *S. aureus* (ATCC 25923), which, according to the preliminary work, were more active than the crude metabolites obtained from aqueous extracts (data not shown). The results of antibacterial activity evaluations are summarized in **Table 2**. A reduced number of extracts were found to be effective against the gram-negative bacterium *E. coli*, with IC_{50} of 10.50 and 19.17 mg/ml. In contrast, most of the evaluated extracts displayed moderate antibacterial activity against *S. aureus*. However, the extracellular and mycelial crude organic extract from *D. endophytica* exhibited promissory antibacterial activities, with IC_{50} values of 3.91 and 3.42 mg/ml, respectively.

Hierarchical cluster analysis was later implemented to statistically identify groups with similar performance according to their IC_{50} values for each bacterium. As shown in **Figure 5A**, the ECEs from *Xylaria* sp. and *D. endophytica* were clustered under the same group. Both the extracts displayed bioactivity against both Gram-negative and Gram-positive bacteria. On the other side, the remaining extracts were clustered as extracts with antibacterial activities against *S. aureus* and those with no identified bioactivity against any bacteria under the evaluated range of concentrations. Remarkably, even when the mycelial organic extracts displayed a lower IC_{50} value than that of the ECEs, in most cases, no antibacterial activity was recorded against *E. coli* for the evaluated mycelial crude metabolites. In addition, to generate appropriate dose-response curves for the respective ECEs of the prioritized strains, a new evaluation was realized with two additional dilutions (25–0.78125 mg/ml; **Figures 5B,C**).

Extracellular Extraction Using Polymeric Resin Adsorbent

According to the primary screening, the ECEs from *Xylaria* sp. and *D. endophytica* exhibited the highest antibacterial activity. For this reason, an alternative procedure was used to recover extracellular organic metabolites with the polymeric resin Amberlite XAD-16. This resin is a non-ionic, hydrophobic, cross-linked polymer with a macro reticular structure and a

Taxa	Strain labelling	GenBank Accession Numbers	Strain morphology
Xylaria sp.	ET-18	MT992054.1	
Diaporthe sp.	ET-21	MT992057.1	
Diaporthe panoramensis	ET-24	MT992059.1	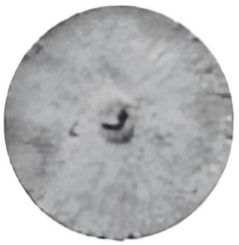
Diaporthe velutina	ET-26	MT992060.1	
Diaporthe endophytica	ET-28	MT992061.1	

FIGURE 3 | Taxonomic information of endophytic strains and mycelial growth on potato dextrose agar (PDA) after 8 days incubation at 29°C.

high surface area commonly used to select organic molecules of relatively low molecular weight.

The extraction yields obtained (indicated in **Figure 6**) with the alternative extraction procedure were lower than those obtained for both strain-extracellular crude extracts (ECEs). The elution of the resin with methanol afforded a greater than the extracted mass compared with EtOAc. However, the IC_{50} values for the methanolic fractions highlight the purification of bioactive compounds of *S. aureus*, contrary to the improved activity of the EtOAc fractions

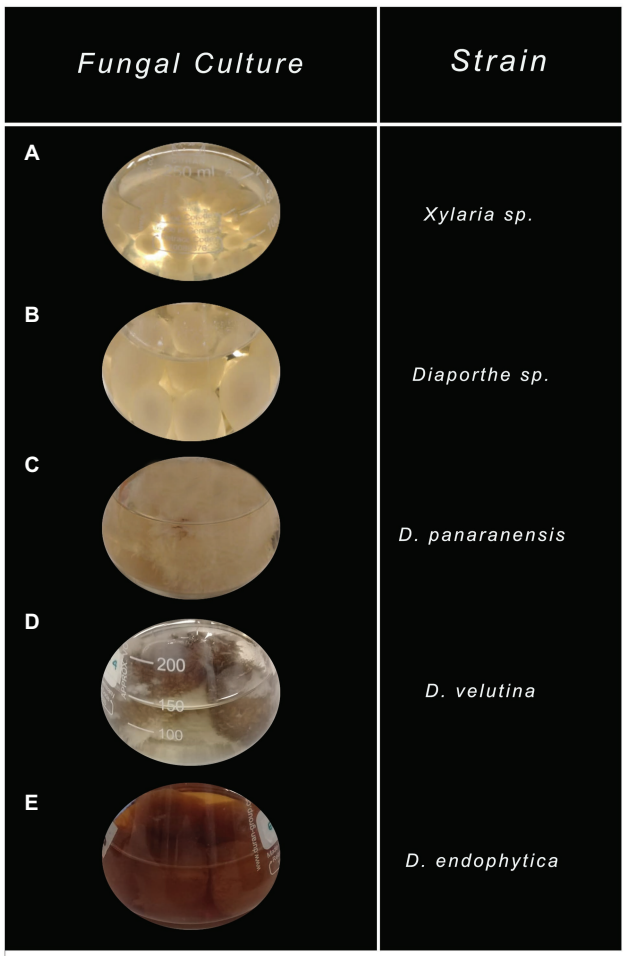

FIGURE 4 | Characteristic of endophytic fungal cultures grown on potato dextrose broth (PDB) after depleting all carbon sources. **(A)** *Xylaria* sp., **(B)** *Diaporthe* sp., **(C)** *Diaphorte panaranensis*., **(D)** *Diaporthe velutina*, and **(E)** *Diaporthe endophytica*.

TABLE 1 | Extraction yields of mycelial and ECEs from the cultivation of endophytic fungi isolated from *O. gracilipes*.

Strain	Mycelial crude extraction yield (mg crude extract/g mycelium)	Extracellular crude extraction yield (mg crude extract/g exhausted medium)
Xylaria sp.	9.3 ± 1.2	13.0 ± 1.8
Diaporthe sp.	1.5 ± 1.2	12.9 ± 1.6
Diaporthe panaranensis	8.4 ± 1.3	11.3 ± 2.5
Diaporthe velutina	1.82 ± 1.1	11.7 ± 2.8
Diaporthe endophytica	0.2 ± 0.1	12.8 ± 1.6

Each value represents the average of three independent biological replicates (n = 3).

against *E. coli*. Despite this fact, the observed activity in the respective fractions for *Xylaria* sp. against *E. coli* suggested that the alternative procedure did not effectively purify the active compounds against this pathogen (**Table 3**). Hence, the filtrate obtained after extracting the exhausted medium with the resin was extracted with EtOAc, displaying a lower IC_{50} value against *E. coli* (1.45 mg/ml).

TABLE 2 | IC_{50} for mycelial (MO) and extracellular (EO) crude organic extracts obtained from the cultivation of native fungal endophytes.

Extract	IC_{50} (mg/ml)	
	Staphylococcus aureus	*Escherichia coli*
1-MO	25	>25
1-EO	8.18	19.17
2-MO	13.66	>25
2-EO	>25	>25
3-MO	7.41	>25
3-EO	>25	>25
4-MO	3.25	>25
4-EO	>25	>25
5-MO	3.42	>25
5-EO	3.91	10.50

Xylaria sp. (1), Diaporthe sp. (2), Diaphorte panaranensis (3), Diaphorte velutina (4), and Diaphorte endophytica (5) against tested pathogens.

Co-culturing Screening Platform

Most of the novel compounds encountered during the past years continue to be discovered by classical screening platforms, either in the liquid culture or solid-state fermentation (Zhu et al., 2018; Becker and Stadler, 2020). However, current co-cultures have demonstrated an effective strategy to produce new secondary metabolites with various biotechnological applications. Herein, we implemented the dual culture of selected strains during the primary screening against the remaining evaluated endophytes to elucidate different fungal interactions between each pair of fungi and identify the secondary metabolite induction in contrast to the axenic cultures. Most of the assays on *Xylaria* sp. were confronted against a *Diaporthe* strain between the exhibited fungal interactions, with the development of a visible confrontation zone (zone line). In contrast, only the assay between *D. velutina* and *D. endophytica* displayed this type of interaction, as shown in **Figures 7C,D**. However, the dual culture between *Xylaria* sp. and *D. endophytica* as well as the dual culture of *Xylaria* sp. and *Diaporthe* sp. displayed a significant confrontation zone. The above observations suggest these models' potential to explore the effect of this type of interaction on the generation of novel secondary metabolites and their bioactivities (Bertrand et al., 2013), contrasting with the axenic cultures (**Figures 7A,B**) where these responses were not recorded. Nevertheless, *Diaporthe* sp. did not exhibit any antibacterial activity during the preliminary screening, in contrast with the case of *D. endophytica*. In contrast, the dual culture of *D. endophytica* and *D. panaranensis* exhibited a contact inhibition type interaction, thereby inducing the production of red-coloured diffusible compounds that have not been generated during the axenic culture of *D. endophytica*.

In this way, a co-culture in liquid media between *Xylaria* sp. and *D. endophytica* was performed to evaluate this strategy's performance regarding the secondary metabolites production with antibacterial activity in different liquid media. Hence, the

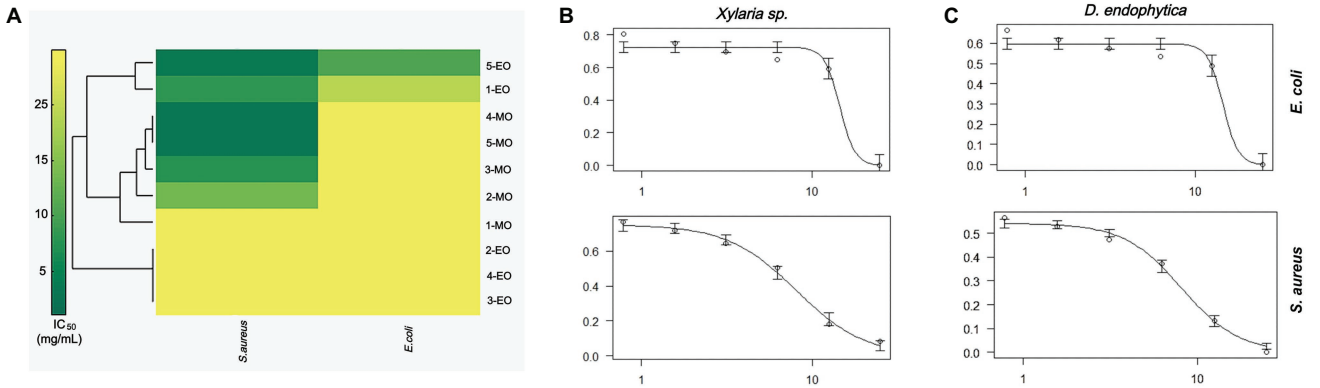

FIGURE 5 | Antibacterial activity primary screening of endophytic strains of *Otoba gracilipes* **(A)** Hierarchical cluster analysis (HCA) of half-maximum inhibitory concentration (IC_{50}) values for extracellular crude extracts (ECEs) obtained from the five fungal endophytes cultures against the evaluated pathogens. Dose-response curves were obtained for the ECEs of **(B)** *Xylaria* sp. and **(C)** *D. endophytica* against both pathogens, where the *y*-axis represents normalized response (0–1), while the *x*-axis represents extract concentration in mg/ml.

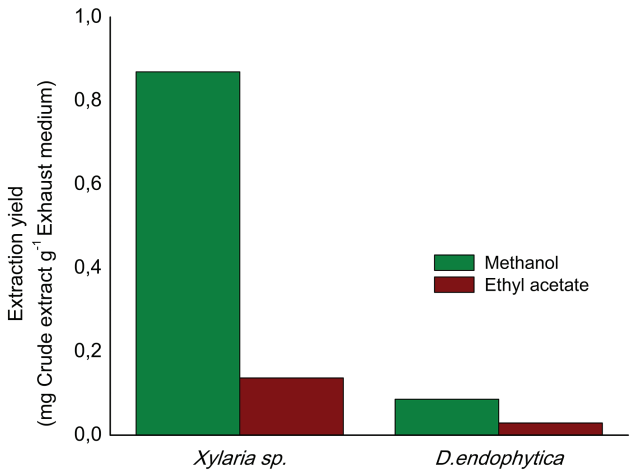

FIGURE 6 | Extraction yields obtained from the alternative extraction procedure with polymeric resin Amberlite X.A.D. 16N using as eluents: ethyl acetate (EtOAc) and methanol.

TABLE 3 | IC_{50} for fractions obtained by alternative extraction with polymeric resin Amberlite X.A.D. 16N of *Xylaria* sp. and *D. endophytica* against tested pathogens.

Strain	Eluent	IC_{50} (mg/ml)	
		Staphylococcus aureus	***Escherichia coli***
Xylaria sp.	Ethyl acetate	5.84	5.89
	Methanol	4.37	>25
D. endophytica	Ethyl acetate	1.83	0.99
	Methanol	0.86	9.27

pre-culture time for each strain was considered in terms of the substrate consumption rate. Thus, it was decided that considering the rapid growth of *D. endophytica*, 3 days for *Xylaria* sp. and 1 day for *D. endophytica* was established to ensure the optimal interaction between them. After 1 week, despite the culture medium, the color of the assay's suspensions transited from a slight red to dark brown coloration (**Figure 8**). Interestingly, the biomass production in PDB was attenuated compared to the axenic cultures of each endophyte and the same co-culture system in YM broth. In addition, different morphotypes were recorded presumably due to the interaction between fungi in PDB, where the mycelium of *D. endophytica* could not be differentiated from the *Xylaria* sp. pellets formed in the case of YM co-culture.

Moreover, the ECEs obtained from PDB exhibited more potent inhibitory activity against both pathogens than those obtained from the axenic cultures (**Table 4**). However, the IC_{50} values for each pathogen were similar, which were different from the trend obtained during the preliminary screening. Moreover, the evaluation of the YM medium improved the antibacterial activity of the co-culture system, with a 3-fold reduction in the IC_{50} value for *S. aureus* in contrast to the similar value obtained for *E. coli*.

DISCUSSION

Primary Screening

Endophytes have been proven to be a recursive source of antimicrobial compounds during the last 10 years. In addition, several studies involving endophytes isolated from the medicinal plants of tropical rainforest have led to the development of novel bioactive compounds with attractive pharmaceutical applications (Martinez-Klimova et al., 2017). In this context, no research on the antibacterial potential of the endophytic community of *O. gracilipes* has been reported (Caicedo et al., 2019). In the current study, five endophytic strains of this medicinal plant corresponding to the genera *Xylaria* and *Diaporthe* were screened for their inhibitory activity against *E. coli* and *S. aureus*. The ECEs from endophytes *Xylaria* sp. and *D. endophytica* displayed broad-spectrum activity against both the tested bacteria. Simultaneously, the mycelial crude organic extracts from the most evaluated strains were bioactive

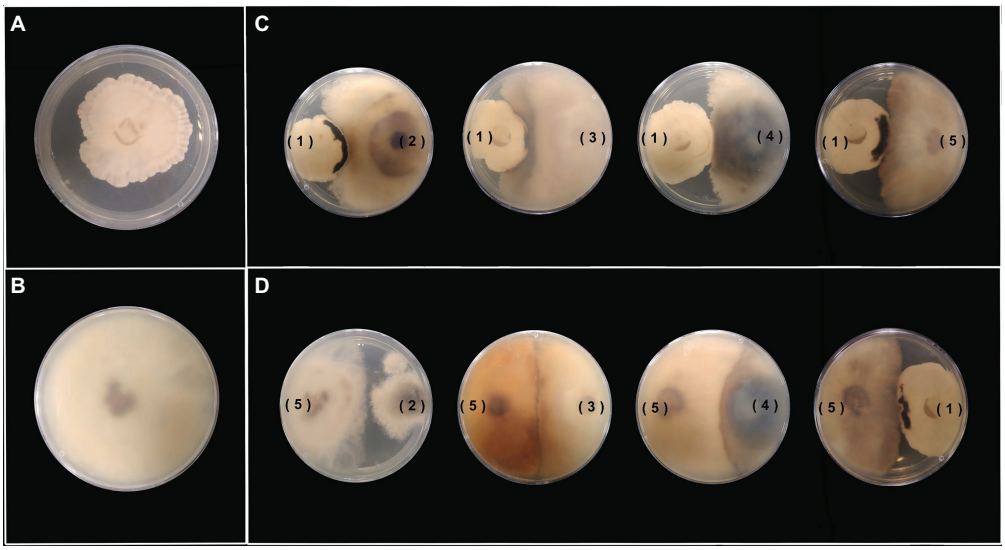

FIGURE 7 | Antagonist activity between each pair of endophytic fungal strains in YM agar. **(A,B)** Anexic culture of *Xylaria* sp. (1) and *D. endophytica* (5). **(C)** *Xylaria* sp. (1) against the four strains being assessed. **(D)** *D. endophytica* (5) against the four strains being assessed.

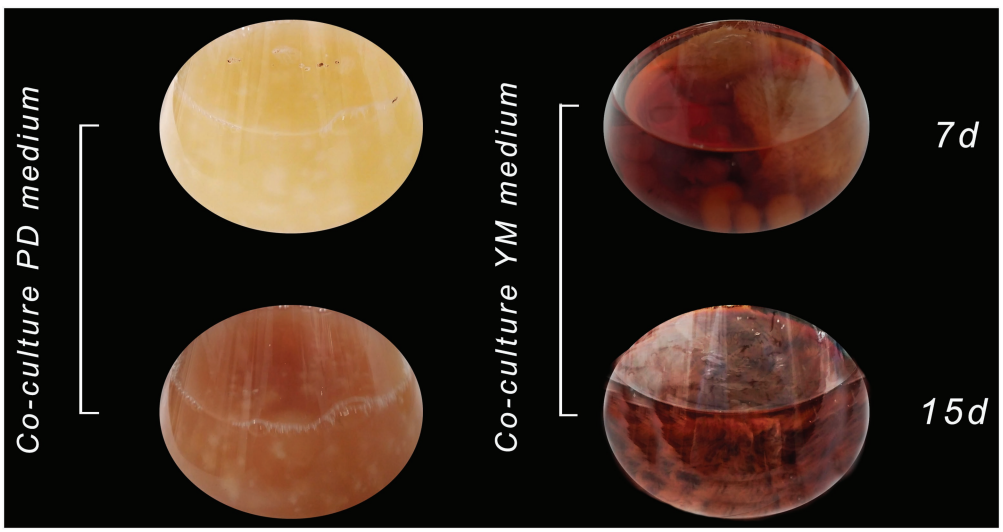

FIGURE 8 | Co-culture of *Xylaria* sp. (1) and *D. endophytica* (5) in PDB and YM broth on 7 days and 15 days of incubation.

TABLE 4 | IC_{50} for ECEs obtained from the co-culture of *Xylaria* sp. and *D. endophytica* in different media against the tested pathogens.

Medium	IC_{50} (mg/ml)	
	Staphylococcus aureus	***Escherichia coli***
PDB	1.67	1.57
YM	0.51	1.25

only against the Gram-positive bacteria. As shown in **Figure 4**, most fermentation experiments produced colored compounds, indicating that the production was affected by the culture media constituents and the evaluation conditions. Thus, the use of PDB promotes the formation of colored compounds in endophytes, as reported by several other studies (Danagoudar et al., 2017; Xu et al., 2018).

On the other hand, Rao et al. (2015) studied the impact of different culture media in the antibacterial activity of *Diaporthe liquidambaris* (Synonym: *Phomopsis liquidambaris*) and suggested the use of PDB for optimal antimicrobial activity. Interestingly, Yao et al. (2016) reported such color changes during the metabolomic study of the co-culture of *T. versicolor* and *G. applanatum*, which, in their case, represented a significant increase in the metabolic bioactivity relative to that with monocultures. Among all the evaluated strains, *D. endophytica*

exhibited a color transition during the fermentation time, which corresponded to its ECE's potent bioactivity, resulting in an organic extract with the highest potential obtained during the primary screening. In addition, even when the evaluated mycelial organic crude extracts were found bioactive only against the Gram-positive pathogen, it is noting that the obtained extraction yields are within the range of obtained values for the solid fermentation of endolichenic fungi on rice media, where also Xylariaceae species presented the highest extraction yields (Santiago et al., 2021).

During the last few decades, the increase in antimicrobial resistance has urged the need for new compounds with broad-spectrum bioactivity to provide effective treatment options to MDR bacteria (Brown and Wright, 2016). The screening of antimicrobial activity using crude extracts allows the identification of potential producer strains and, in several cases, the further isolation and identification of compounds responsible for their bioactivities. However, several reports have indicated that the individual responsible molecules can have a lower activity than the crude extract containing these molecules. This behavior suggests a synergistic effect between these molecules in the respective crude extracts (Caicedo et al., 2012; Becker and Stadler, 2020). Hence, as a selection criterion during the primary screening, identifying extracts with inhibitory activity against Gram-negative and Gram-positive bacteria was applied in the present study. Therefore, the HCA results serve as the statistical proof for selecting the ECEs of *Xylaria* sp. and *D. endophytica* for follow-up studies. Moreover, these results suggest that different bioactive metabolites can be present in the mycelium extracts than the metabolites present in the ECEs, thereby displaying broad-spectrum bioactivity.

The *Diaporthe* species predominantly produce various polyketides and cytochalasins with low molecular weight, including compounds with antibacterial activity against the MDR enteropathogenic bacteria *Shigella flexneri* and *Vibrio cholerae*, as well as other MDR pathogens such as *S. aureus* and others (Jouda et al., 2016; Chepkirui and Stadler, 2017). Furthermore, the production of terpenoids and rare compounds with broad-spectrum pharmacological bioactivity has been reported from endophytic species of this genus. Dettrakul et al. (2003) obtained the diterpenes diaportheins A and B with potent antibacterial activity against Gram-negative and Gram-positive bacteria. In the case of diaportheins B, it was reported to strongly inhibit the growth of *Mycobacterium tuberculosis* (Chepkirui and Stadler, 2017). The Diaporthe endophytic species are mainly widely distributed among different ecosystems, resulting from its secondary metabolites' chemical diversity and the capacity to interact positively with its host plant (Chepkirui and Stadler, 2017). ECEs produced by endophytes of this genus have been tested for their antibacterial activities to associate their biotechnological potential against several pathogens. In this sense, some studies have reported the antibacterial potential of diaporthe strains, with active ECEs in concentrations down to 1.25 mg/ml against susceptible *S. aureus*. In contrast, for *E. coli*, a concentration >5 mg/ml is required to show activity against this pathogen (De Azevedo Silva et al., 2018). Notably, in our study, the same trend was recorded, where the ECEs of diaporthe species were more active against the tested Gram-positive bacteria.

On the other side, the *Xylaria* species have provided several new compounds with diverse biotechnological applications during recent years, and most of the reported compounds were isolated from endophytic strains (Becker and Stadler, 2020). For instance, *Xylaria* can produce compounds with broad-spectrum activity, such as 7-amino-4-methyl coumarin, which displays antibacterial activity against 13 microorganisms, including *E. coli* and *S. aureus* (Liu et al., 2008). Despite this fact, crude EtOAc extracts of endophytic *Xylaria* strains have also been shown to be active against several bacteria at concentrations >1 mg/ml (Hamzah et al., 2018). Even when the ECEs of *Xylaria* sp. displayed a higher IC_{50} than the reported minimum inhibitory concentration values by different authors, both are not wholly comparable. The minimum inhibitory concentration is a qualitative parameter representing the minimum concentration of the extract/compound that exhibits the inhibitory activity against a pathogen (Balouiri et al., 2016). On the other hand, the IC_{50} represents a robust parameter suitable for studying antibiotic sensitivity due to its reproducibility and statistical determination.

Extracellular Extraction Using Polymeric Resin Adsorbent

The alternative extracellular extraction with Amberlite X.A.D 16 N resulted in a decreased extraction yield, which may be explained as the only organic compound of a low molecular weight to be adsorbed from the fermentation broth. Despite the above points, the obtained fractions improved the antibacterial activity, as it allowed purifying part of the crude organic metabolites responsible for the bioactivity. In the case of the methanolic fraction of *Xylaria* sp., it exhibited more vigorous antibacterial activity against *S. aureus* than its respective ECE. Moreover, the EtOAc fraction displayed moderate antibacterial activity, suggesting that, even when this eluent allowed further purification of compounds extracted by the resin, the major compounds responsible for the observed activity against *E. coli* in the ECE were not effectively extracted with this method. Notably, the resin allows capturing compounds up to 40,000 g mol^{-1}, suggesting that the recovered compounds in the obtained filtrate after extracting the fermentation broth with the resin may have a higher molecular weight than those captured with the resin alternative extraction. This hypothesis was demonstrated after evaluating the bioactivity of the EtOAc extract of this remaining solution, providing an improvement in the antibacterial activity against the Gram-negative pathogen for *Xylaria* sp.

Similarly, for *D. endophytica*, the obtained fractions significantly improved the antibacterial activity against both bacteria. Specifically, the methanolic fraction provided a better purification of the active compounds against *S. aureus*. At the same time, EtOAc promoted almost a 10-fold decrease in the IC_{50} value than the observed activity of the methanolic fraction against *E. coli*.

Co-culturing Screening Platform

Several past studies have demonstrated that co-culturing methods effectively improve the conventional screening platforms and produce unique compounds with several biotechnological applications (Bertrand et al., 2014). Herein, we developed a co-culture platform of *O. gracilipes* endophytes. For this purpose, we initially confronted the prioritized strains during a preliminary screening of antibacterial activity against the remaining evaluated fungi. Different fungal interactions were identified, but mainly pigment production was selected to indicate secondary metabolite production. Pigments produced by fungi can be attributed to different biological activities, such as antibacterial, antifungal, and herbicidal. They may be developed in response to adverse conditions or as a defence mechanism to other microbes (Hamzah et al., 2018).

In this sense, according to the significant deadlock displayed by the dual culture plate assay of *Xylaria* sp. and *D. endophytica*, we evaluated the effect of different culture media on the co-cultivation of these endophytes. We observed that when both the endophytes were cultured together in PDB, the mycelial growth was lower relative to each fungus cultured alone. This fact suggested the generation of repressing mechanisms induced by fungal interaction in this medium, but not in YM medium. Chagas et al. (2013) investigated the mixed cultivation effects on the chemical potential of endophytes isolated from the plant *Smallanthus sonchifolius*, demonstrating that, during the co-culture of *Alternaria tenuissima* with *Nigrospora sphaerica*, *A. tenuissima* produced antifungal polyketides in response to the confrontation against *N. sphaerica*. The media composition plays a significant role in the biosynthesis of secondary metabolites. In our study, two different media were evaluated for the co-culturing between *Xylaria* sp. and *D. endophytica*, where the main difference lies in the nitrogen availability. PDB appears to be a nitrogen-limited medium, which promotes a different response in terms of mycelial morphology during the co-culture compared with YM (**Figure 8**).

On the other hand, for both the evaluated media, the co-culture between *Xylaria* sp. and *D. endophytica* developed a dark brown coloration continuously. These results matched with a clear improvement of the IC_{50} values when compared to the values of each individually axenic culture. Several authors have reported that the bioactive compound production is enhanced with mixed cultures, which, in some cases, has been associated with the physiological responses as the production of coloured compounds during fermentation (Yao et al., 2016). In the current study, through the development of a co-culture platform, an improvement in the antibacterial activity was achieved in contrast to the displayed bioactivity during the preliminary screening of endophytic strains, providing almost a 10-fold reduction in the IC_{50} values relative to the lowest values of the ECEs obtained from axenic cultures. These findings together demonstrate that the same endophytic strains could display different biochemical profiles in response to the hosted interaction with other microorganisms, representing an opportunity to explore the biotechnological production of new natural products from native fungi.

CONCLUSION

This research is the first report on the antibacterial potential of crude extracts from cultivating a fungal endophytic community isolated from the medicinal plant *O. gracilipes* in tropical mountain rain forests. The primary screening of the endophytic strains revealed the potential of *D. endophytica* and *Xylaria* sp. to produce extracellular secondary metabolites with a broad-spectrum activity against *E. coli* and *S. aureus*, which are clinical importance microorganisms. Accordingly, follow-up studies were conducted to develop a co-culture platform between the selected strains, and an alternative extraction of the bioactive extracellular compounds was performed. Thus, the experimental results demonstrated the potential of co-culture induction to promote the antibacterial activity of the produced ECEs when compared with those from the axenic culture of respective endophytes. In addition, through the alternative extraction procedure, we could elucidate the polarity nature of the metabolites responsible for the antibacterial activity of *Xylaria* sp. against *S. aureus*, improved the activity of its ECEs for this pathogen. Consequently, this study suggests the possibilities for further investigations toward developing a valuable and reproducible platform to produce novel compounds within the Colombian natural diversity, particularly for unexplored ecosystems such as the tropical rainforest.

DATA AVAILABILITY STATEMENT

The original contributions presented in the study are included in the article/supplementary material, further inquiries can be directed to the corresponding author.

AUTHOR CONTRIBUTIONS

EC-G, ME, AZ-M, JC, and MM performed the experiments and wrote the draft manuscript. EC-G and ME performed data analyses. NC, AD, BF, and AV-P supervised the whole work. NC and AV-P edited the manuscript. All authors contributed to the article and approved the submitted version.

FUNDING

This study was supported by a grant (No: 22028) from the Ministerio de Ciencias, Tecnología e Innovación (MinCiencias), Colombia.

ACKNOWLEDGMENTS

The authors acknowledge the significant support of Andres Vargas, Cindy Zuñiga, and Samuel Diaz. The sample collection of material of *O. gracilipes* and the access to the forest were performed with the "Departamento Administrativo de Gestión Medio Ambiente-Dagma," Cali-Colombia (Catalina Silva and Sandra Franco) authorization. The genetic resource access contract from ANLA was the number RGE244-44#190.

REFERENCES

Balouiri, M., Sadiki, M., and Ibnsouda, S. K. (2016). Methods for in vitro evaluating antimicrobial activity: a review. *J. Pharm. Anal.* 6, 71–79. doi: 10.1016/j.jpha.2015.11.005

Becker, K., and Stadler, M. (2020). Recent progress in biodiversity research on the Xylariales and their secondary metabolism. *J. Antibiot.* 74, 1–23. doi: 10.1038/s41429-020-00376-0

Bertrand, S., Bohni, N., Schnee, S., Schumpp, O., Gindro, K., and Wolfender, J. L. (2014). Metabolite induction via microorganism co-culture: a potential way to enhance chemical diversity for drug discovery. *Biotechnol. Adv.* 32, 1180–1204. doi: 10.1016/j.biotechadv.2014.03.001

Bertrand, S., Schumpp, O., Bohni, N., Bujard, A., Azzollini, A., Monod, M., et al. (2013). Detection of metabolite induction in fungal co-cultures on solid media by high-throughput differential ultra-high pressure liquid chromatography-time-of-flight mass spectrometry fingerprinting. *J. Chromatogr. A* 1292, 219–228. doi: 10.1016/j.chroma.2013.01.098

Brakhage, A. A., Schuemann, J., Bergmann, S., Scherlach, K., Schroeckh, V., and Hertweck, C. (2008). "Activation of fungal silent gene clusters: a new avenue to drug discovery," in *Natural Compounds as Drugs*, eds. F. Petersen and R. Amstutz 1–12.

Brown, E. D., and Wright, G. D. (2016). Antibacterial drug discovery in the resistance era. *Nature* 529, 336–343. doi: 10.1038/nature17042

Bonilla, U. N. S. (2020). Especies forestales amenazadas en territorio de ASIESCA, comunidad de Angostura, Cauca - 2013. v1.0. Instituto de Investigaciones Ambientales del Pacifico John Von Neumann (IIAP). Dataset/Checklist.

Caicedo, N. H., Davalos, A. F., Puente, P. A., Rodríguez, A. Y., and Caicedo, P. A. (2019). Antioxidant activity of exo-metabolites produced by *Fusarium oxysporum*: an endophytic fungus isolated from leaves of *Otoba gracilipes*. *Microbiology* 8:e903. doi: 10.1002/mbo3.903

Caicedo, N. H., Heyduck-Söller, B., Fischer, U., and Thöming, J. (2011). Bioproduction of antimicrobial-compounds by using marine-filamentous cyanobacterium cultivation. *J. Appl. Phycol.* 23, 811–818. doi: 10.1007/s10811-010-9580-0

Caicedo, N. H., Kumirska, J., Neumann, J., Stolte, S., and Thöming, J. (2012). Detection of bioactive exometabolites produced by the filamentous marine cyanobacterium *Geitlerinema* sp. *Mar. Biotechnol.* 14, 436–445. doi: 10.1007/s10126-011-9424-1

Chagas, F. O., Dias, L. G., and Pupo, M. T. (2013). A mixed culture of endophytic fungi increases production of antifungal polyketides. *J. Chem. Ecol.* 39, 1335–1342. doi: 10.1007/s10886-013-0351-7

Chepkirui, C., and Stadler, M. (2017). The genus *Diaporthe*: a rich source of diverse and bioactive metabolites. *Mycol. Prog.* 16, 477–494. doi: 10.1007/s11557-017-1288-y

Danagoudar, A., Joshi, C. G., Sunil Kumar, R., Poyya, J., Nivya, T., Hulikere, M. M., et al. (2017). Molecular profiling and antioxidant as well as antibacterial potential of polyphenol producing endophytic fungus-*Aspergillus austroafricanus* CGJ-B3. *Mycology* 8, 28–38. doi: 10.1080/21501203.2017.1281358

De Azevedo Silva, F., Liotti, R. G., Ana Paula de Araújo, B., De Melo Reis, É., Passos, M. B. S., Dos Santos, E. L., et al. (2018). Diversity of cultivable fungal endophytes in *Paullinia cupana (Mart.) Ducke* and bioactivity of their secondary metabolites. *PLoS One* 13:e0195874. doi: 10.1371/journal.pone.0195874

Deepika, V. B., Murali, T. S., and Satyamoorthy, K. (2016). Modulation of genetic clusters for synthesis of bioactive molecules in fungal endophytes: a review. *Microbiol. Res.* 182, 125–140. doi: 10.1016/j.micres.2015.10.009

Dettrakul, S., Kittakoop, P., Isaka, M., Nopichai, S., Suyarnsestakorn, C., Tanticharoen, M., et al. (2003). Antimycobacterial pimarane diterpenes from the fungus *Diaporthe* sp. *Bioorg. Med. Chem. Lett.* 13, 1253–1255. doi: 10.1016/S0960-894X(03)00111-2

Ghose, T. K. (1987). Measurement of cellulase activities. *Pure Appl. Chem.* 59, 257–268. doi: 10.1351/pac198759020257

Guo, L., Niu, S., Chen, S., and Liu, L. (2020). Diaporone A, a new antibacterial secondary metabolite from the plant endophytic fungus *Diaporthe* sp. *J. Antibiot.* 73, 116–119. doi: 10.1038/s41429-019-0251-3

Gupta, S., Chaturvedi, P., Kulkarni, M. G., and Van Staden, J. (2020). A critical review on exploiting the pharmaceutical potential of plant endophytic fungi. *Biotechnol. Adv.* 39:107462. doi: 10.1016/j.biotechadv.2019.107462

Hamzah, T. N. T., Lee, S. Y., Hidayat, A., Terhem, R., Faridah-Hanum, I., and Mohamed, R. (2018). Diversity and characterization of endophytic fungi isolated from the tropical mangrove species, *Rhizophora mucronata*, and identification of potential antagonists against the soil-borne fungus, *Fusarium solani*. *Front. Microbiol.* 9:1707. doi: 10.3389/fmicb.2018.01707

Helaly, S. E., Thongbai, B., and Stadler, M. (2018). Diversity of biologically active secondary metabolites from endophytic and saprotrophic fungi of the ascomycete order *Xylariales*. *Nat. Prod. Rep.* 35, 992–1014. doi: 10.1039/C8NP00010G

Jouda, J. B., Tamokou, J.-d.-D., Mbazoa, C. D., Douala-Meli, C., Sarkar, P., Bag, P. K., et al. (2016). Antibacterial and cytotoxic cytochalasins from the endophytic fungus *Phomopsis* sp. harbored in *Garcinia kola* (Heckel) nut. *BMC Complement. Altern. Med.* 16:462. doi: 10.1186/s12906-016-1454-9

Liu, X., Dong, M., and Chen, X. (2008). Antimicrobial activity of an endophytic Xylaria sp.YX-28 and identification of its antimicrobial compound 7-amino-4-methylcoumarin. *Appl Microbiol Biotechnol.* 78, 241–247. doi: 10.1007/s00253-007-1305-1

Mani, V. M., Soundari, A. P. G., Karthiyaini, D., and Preethi, K. (2015). Bioprospecting endophytic fungi and their metabolites from medicinal tree *Aegle marmelos* in Western Ghats, India. *Mycobiology* 43, 303–310. doi: 10.5941/MYCO.2015.43.3.303

Martinez-Klimova, E., Rodríguez-Peña, K., and Sánchez, S. (2017). Endophytes as sources of antibiotics. *Biochem. Pharmacol.* 134, 1–17. doi: 10.1016/j.bcp.2016.10.010

Narmani, A., Teponno, R. B., Helaly, S. E., Arzanlou, M., and Stadler, M. (2018). Cytotoxic, anti-biofilm and antimicrobial polyketides from the plant associated fungus *Chaetosphaeronema achilleae*. *Fitoterapia* 139:104390. doi: 10.1016/j.fitote.2019.104390

Nikaido, H. (2009). Multidrug resistance in bacteria. *Annu. Rev. Biochem.* 78, 119–146. doi: 10.1146/annurev.biochem.78.082907.145923

Ogawara, H. (2021). Possible drugs for the treatment of bacterial infections in the future: anti-virulence drugs. *J. Antibiot.* 74, 24–41. doi: 10.1038/s41429-020-0344-z

Prihantini, A. I., and Tachibana, S. (2017). Antioxidant compounds produced by *Pseudocercospora* sp. E.S.L. 02, an endophytic fungus isolated from *Elaeocarpus sylvestris*. *Asian Pac. J. Trop. Biomed.* 7, 110–115. doi: 10.1016/j.apjtb.2016.11.020

Rambold, G., Stadler, M., and Begerow, D. (2013). Mycology should be recognized as a field in biology at eye level with other major disciplines: a memorandum. *Mycol. Prog.* 12, 455–463. doi: 10.1007/s11557-013-0902-x

Ranke, J. (2006). Fitting dose–response curves from bioassays and toxicity testing. *R News* 6, 7–12.

Rao, H. C. Y., Santosh, P., Rakshith, D., and Satish, S. (2015). Molecular characterization of an endophytic *Phomopsis liquidambaris* CBR-15 from *Cryptolepis buchanani* Roem. And impact of culture media on biosynthesis of antimicrobial metabolites. *3 Biotech* 5, 165–173. doi: 10.1007/s13205-014-0204-2

Ratnaweera, P. B., Williams, D. E., de Silva, E. D., Wijesundera, R. L., Dalisay, D. S., and Andersen, R. J. (2014). Helvolic acid, an antibacterial nortriterpenoid from a fungal endophyte, *Xylaria* sp. of orchid *Anoectochilus setaceus* endemic to Sri Lanka. *Mycology* 5, 23–28. doi: 10.1080/21501203.2014.892905

Reygaert, W. C. (2018). An overview of the antimicrobial resistance mechanisms of bacteria. *AIMS Microbiol.* 4, 482–501. doi: 10.3934/microbiol.2018.3.482

Ruddaraju, L. K., Pammi, S. V. N., Guntuku, G. S., Padavala, V. S., and Kolapalli, V. R. M. (2020). A review on anti-bacterials to combat resistance: from ancient era of plants and metals to present and future perspectives of green nano technological combinations. *Asian J. Pharm. Sci.* 15, 42–59. doi: 10.1016/j.ajps.2019.03.002

R Core Team (2020). R: A language and environment for statistical computing. R Foundation for Statistical Computing, Vienna, Austria. Available at: https://www.R-project.org

Sandargo, B., Chepkirui, C., Cheng, T., Chaverra-Muñoz, L., Thongbai, B., Stadler, M., et al. (2019). Biological and chemical diversity go hand in hand: basidiomycota as source of new pharmaceuticals and agrochemicals. *Biotechnol. Adv.* 37:107344. doi: 10.1016/j.biotechadv.2019.01.011

Santiago, K. A. A., Edrada-Ebel, R., Dela Cruz, T. E. E., Cheow, Y. L., and Ting, A. S. Y. (2021). Biodiscovery of potential antibacterial diagnostic metabolites from the endolichenic fungus *Xylaria venustula* using L.C.–MS-based metabolomics. *Biology* 10:191. doi: 10.3390/biology10030191

Shao, L., Marin-Felix, Y., Surup, F., Stchigel, A. M., and Stadler, M. (2020). Seven new cytotoxic and antimicrobial xanthoquinodins from jugulospora vestita. *J. Fungi* 6:188. doi: 10.3390/jof6040188

Song, F., Wu, S.-H., Zhai, Y.-Z., Xuan, Q.-C., and Wang, T. (2014). ChemInform abstract: secondary metabolites from the genus *Xylaria* and their bioactivities. *ChemInform* 45, 673–694. doi: 10.1002/chin.201430235

Sousa, J. P. B., Aguilar-Pérez, M. M., Arnold, A. E., Rios, N., Coley, P. D., Kursar, T. A., et al. (2016). Chemical constituents and their antibacterial activity from the tropical endophytic fungus *Diaporthe* sp. F2934. *J. Appl. Microbiol.* 120, 1501–1508. doi: 10.1111/jam.13132

Surup, F., Hennicke, F., Sella, N., Stroot, M., Bernecker, S., Pfütze, S., et al. (2019). New terpenoids from the fermentation broth of the edible mushroom *Cyclocybe aegerita*. *Beilstein J. Org. Chem.* 15, 1000–1007. doi: 10.3762/bjoc.15.98

White, T. J., Bruns, T., Lee, S. J. W. T., and Taylor, J. (eds.) (1990). "Amplification and direct sequencing of fungal ribosomal R.N.A. genes for phylogenetics," in *PCR Protocols: A Guide to Methods and Applications*. *Vol. 18.* (Cambridge, MA, USA: Academic Press), 315–322.

World Health Organization (2019). World Health Organization annual report 2019 WHO Country Office Lebanon: health for all. Available at: https://apps.who.int/iris/handle/10665/333249 (Accessed April 29, 2019).

Xu, W. F., Hou, X. M., Yao, F. H., Zheng, N., Li, J., Wang, C. Y., et al. (2017). Xylapeptide A, an antibacterial cyclopentapeptide with an uncommon L-pipecolinic acid moiety from the associated fungus *Xylaria* sp. (GDG-102). *Sci. Rep.* 7:6937. doi: 10.1038/s41598-017-07331-4

Xu, X. Y., Shen, X. T., Yuan, X. J., Zhou, Y. M., Fan, H., Zhu, L. P., et al. (2018). Metabolomics investigation of an association of induced features and corresponding fungus during the co-culture of *Trametes versicolor* and *Ganoderma applanatum*. *Front. Microbiol.* 8:2647. doi: 10.3389/fmicb.2017.02647

Yao, L., Zhu, L. P., Xu, X. Y., Tan, L. L., Sadilek, M., Fan, H., et al. (2016). Discovery of novel xylosides in co-culture of basidiomycetes *Trametes versicolor* and *Ganoderma applanatum* by integrated metabolomics and bioinformatics. *Sci. Rep.* 6:33237. doi: 10.1038/srep33237

Zhu, J., Yan, L., Xu, X., Zhang, Y., Shi, J., Jiang, C., et al. (2018). Strategies to enhance the production of pinoresinol and its glucosides by endophytic fungus (*Phomopsis* sp. XP-8) isolated from Tu-chung bark. *AMB Express* 8:55. doi: 10.1186/s13568-018-0584-5

Conflict of Interest: The authors declare that the research was conducted in the absence of any commercial or financial relationships that could be construed as a potential conflict of interest.

Publisher's Note: All claims expressed in this article are solely those of the authors and do not necessarily represent those of their affiliated organizations, or those of the publisher, the editors and the reviewers. Any product that may be evaluated in this article, or claim that may be made by its manufacturer, is not guaranteed or endorsed by the publisher.

frontiers in Microbiology

ORIGINAL RESEARCH
published: 27 September 2021
doi: 10.3389/fmicb.2021.730807

New Tetramic Acid Derivatives From the Deep-Sea-Derived Fungus *Penicillium* sp. SCSIO06868 With SARS-CoV-2 M^{pro} Inhibitory Activity Evaluation

Xiaoyan Pang[1,2,3], Weihao Chen[1], Xin Wang[4], Xuefeng Zhou[1,2], Bin Yang[1,2], Xinpeng Tian[1,2], Junfeng Wang[1,2], Shihai Xu[3]* and Yonghong Liu[1,2]**

[1] CAS Key Laboratory of Tropical Marine Bio-Resources and Ecology, Guangdong Key Laboratory of Marine Materia Medica, South China Sea Institute of Oceanology, Chinese Academy of Sciences (CAS), Guangzhou, China, [2] Sanya Institute of Oceanology, SCSIO, Yazhou Scientific Bay, Sanya, China, [3] College of Chemistry and Materials Science, Jinan University, Guangzhou, China, [4] Center for Innovative Marine Drug Screening and Evaluation, School of Medicine and Pharmacy, Ocean University of China, Qingdao, China

OPEN ACCESS

Edited by:
Paola Angelini,
University of Perugia, Italy

Reviewed by:
Fadia S. Youssef,
Ain Shams University, Egypt
Anas Shamsi,
Jamia Millia Islamia, India

***Correspondence:**
Junfeng Wang
wangjunfeng@scsio.ac.cn
Shihai Xu
txush@jnu.edu.cn
Yonghong Liu
yonghongliu@scsio.ac.cn

Specialty section:
This article was submitted to Microbiotechnology, a section of the journal Frontiers in Microbiology

Received: 25 June 2021
Accepted: 27 August 2021
Published: 27 September 2021

Citation:
Pang X, Chen W, Wang X, Zhou X, Yang B, Tian X, Wang J, Xu S and Liu Y (2021) New Tetramic Acid Derivatives From the Deep-Sea-Derived Fungus Penicillium sp. SCSIO06868 With SARS-CoV-2 M^{pro} Inhibitory Activity Evaluation. Front. Microbiol. 12:730807. doi: 10.3389/fmicb.2021.730807

Three new tetramic acid derivatives (**1**–**3**) and a new polyketide (**4**) along with eight known compounds (**5**–**12**) were isolated from cultures of the deep-sea-derived fungus *Penicillium* sp. SCSIO06868. Four new structures were elucidated by analysis of one-dimensional/two-dimensional nuclear magnetic resonance (NMR) data and high-resolution electrospray ionization mass spectrometry. Their absolute configurations were established by X-ray crystallography analysis and comparison of the experimental and reported electronic circular dichroism (ECD) values or specific optical rotation. Compound **3** exhibited potent, selective inhibitory activities against *Staphylococcus aureus* and methicillin-resistant *S. aureus* with minimum inhibitory concentration values of both 2.5 μg/ml. Also, compound **3** showed weak antiviral activity against severe acute respiratory syndrome coronavirus 2 main protease, which was responsible for the coronavirus disease 2019 pandemic.

Keywords: deep-sea-derived fungus, *Penicillium* sp., secondary metabolites, antibacterial, antiviral

INTRODUCTION

Natural products bearing a tetramic acid structural fragment (pyrrolidine-2,4-dione) are isolated from various terrestrial and marine organisms, such as bacteria, cyanobacteria, fungi, and sponges (Mo et al., 2014; Jiang et al., 2020). Tetramic acids showed a remarkable diversity of bioactivities, including antitumor (Lin et al., 2008; Fan et al., 2020), antiviral (Sun et al., 2015), antibacterial (Nord et al., 2020; Wingen et al., 2020), larvicidal (Mao et al., 2019), and herbicidal (Schrey et al., 2019) activities (Schobert and Schlenk, 2008; Mo et al., 2014; Jiang et al., 2020). Among the different marine sources, marine fungi mainly containing *Aspergillus*, *Penicillium*, and *Cladosporium* species are the dominant sources of the rapidly increasing numbers of tetramic acids (Jiang et al., 2020). With the development of sampling techniques and the possibility to culture organisms from deep-sea even in conventional standard microbiological laboratories, deep-sea-derived fungi have recently received a wide concern as a new area

for bioprospecting (Jin et al., 2016; Pang et al., 2020). As part of our ongoing research for bioactive secondary metabolites from deep-sea-derived fungi (Chen et al., 2016; Wang et al., 2016; Pang et al., 2021), the fungus *Penicillium* sp. SCSIO06868 was studied. Three new tetramic acid derivatives (**1**–**3**) and a new polyketide (**4**) along with eight known compounds (**5**–**12**) (**Figure 1**) were isolated from the deep-sea-derived fungus *Penicillium* sp. SCSIO06868, which was cultured on a liquid medium. The coronavirus disease 2019 (COVID-19) pandemic has left a mark in more than 180 countries, with more than 2.0 billion cases worldwide and over 4.4 million deaths in total (until August 2021). The COVID-19 is an infectious disease caused by a novel strain of coronavirus [severe acute respiratory syndrome coronavirus 2 (SARS-CoV-2)] (Zehra et al., 2020; Shamsi et al., 2021). SARS-CoV-2 main proteinase (M^{Pro}), a key protease of CoV-2, mediates viral replication and transcription. SARS-CoV-2 M^{Pro} has emerged as an attractive target for SARS-CoV-2 drug design and development (Sabbah et al., 2021). All isolated compounds (**1**–**12**) were tested for their antiviral activities against SARS-CoV-2 M^{pro} *in vitro*. Molecular docking research was performed to mimic the interactions between the bioactive compound and SARS-CoV-2 M^{pro}. Herein, we described the isolation, structure elucidation, and bioactivity evaluation of the 12 compounds.

MATERIALS AND METHODS

General Experimental Procedures

One-dimensional and two-dimensional (2D) nuclear magnetic resonance (NMR) spectra were measured on a Bruker Avance 700 MHz NMR spectrometer (Fällanden, Switzerland) with Tetramethylsilane as an internal standard. High-resolution electrospray ionization mass spectrometry (HRESIMS) data were recorded on a maXis Q-TOF mass spectrometer in positive ion mode (Bruker, Fällanden, Switzerland). Electronic circular dichroism (ECD) and ultraviolet (UV) spectra were measured with a Chirascan circular dichroism spectrometer (Applied Photophysics). Optical rotations were measured using an MCP-500 polarimeter (Anton, Austria). High-performance liquid chromatography (HPLC) was performed on Hitachi Primaide with YMC ODS SERIES column (YMC-Pack ODS-A, YMC Co. Ltd., Kyoto, 250 × 10 mm I.D., S-5 μm, 12 nm). Column chromatography was carried out on silica gel (200–300 mesh, Jiangyou Silica Gel Development Co., Yantai, China), YMC Gel ODS-A (12 nm, S-50 μm YMC, MA, United States), and Sephadex LH-20 (40–70 μm, Amersham Pharmacia Biotech AB, Uppsala, Sweden). Spots were detected under UV light by heating after spraying with the mixed solvent of saturated vanillin and 5% sulfuric acid in water. The thin layer chromatography plates with silica gel GF254 (0.4–0.5 mm, Qingdao Marine Chemical Factory, Qingdao, China) were used for analysis and preparation.

Fungal Material

The strain SCSIO06868 was isolated from the deep-sea sediment collected from the Indian Ocean (94°37.377′E; 2°59.853′S; depth 4,762 m). The internal transcribed spacer sequences of SCSIO06868 (494 base pairs, GenBank accession no. MZ277624) have 99% sequence identity to that of *Penicillium citrinum* DUCC5728 (GenBank accession no. 582768). Then, it was designated as a member of *Penicillium* sp. and named as *Penicillium* sp. SCSIO06868. The strain SCSIO06868 was stored on methylene blue agar (malt extract 15 g, agar 16 g, sea salt 10 g, water 1 L, pH 7.4–7.8) slants at 4°C and deposited at Key Laboratory of Tropical Marine Bio-resources and Ecology, Chinese Academy of Sciences.

Fermentation and Extraction

The mass fermentation of this fungus was carried out in 1-L Erlenmeyer flasks. The fungus was inoculated in a liquid medium (2% maltose, 2% mannitol, 1% monosodium glutamate, 1% glucose, 0.3% yeast extract, 0.05% monopotassium phosphate, 0.03% $MgSO_4 \cdot 7H_2O$, and 300-ml tap water/flask, 93 flasks, 28 L total) at 25°C under static condition for 35 days. After 35 days, the fermentation was soaked in ethyl acetate (500 ml/flask), and the mycelia were cut into small pieces and sonicated for 20 min. The ethyl acetate solution was concentrated under reduced pressure to gain a brown crude extract (59.0 g).

Isolation and Purification

The crude extract was subjected to silica gel column chromatography, which was eluted with dichloromethane

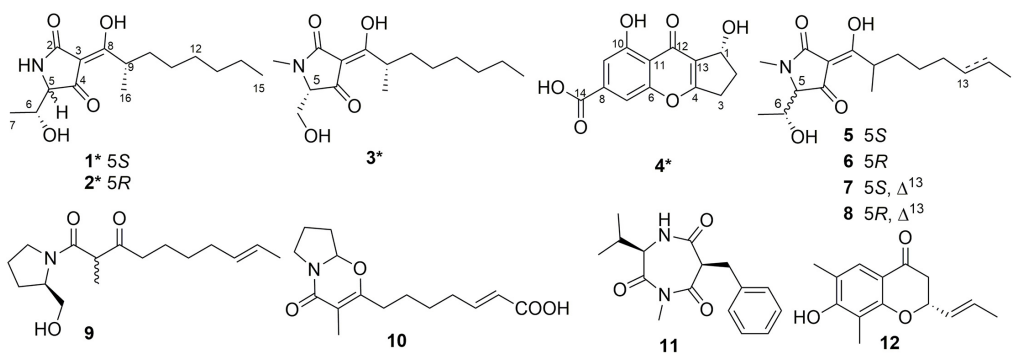

FIGURE 1 | Chemical structures of compounds **1**–**12**. *Means new compounds.

and methanol (MeOH) mixed solvent in a step gradient (100:0–5:1, *v/v*) and separated into seven fractions (Fr-1–Fr-7). Fr-1 (3.2 g) was applied to Sephadex LH-20 column eluted with MeOH, reversed-phase C_{18} medium pressure liquid chromatography (MPLC) eluted with MeOH/water (H_2O) (10:90–100:0, *v/v*), and semipreparative HPLC [72% CH_3OH/H_2O with 0.3‰ trifluoroacetic acid (TFA), 2 ml/min] to afford compounds **7** (2.2 mg, t_R = 20.2 min) and **8** (18.4 mg, t_R = 22.2 min). Fr-2 (6.3 g) was subjected to Sephadex LH-20 column eluted with MeOH, reversed-phase C_{18} MPLC eluted with MeOH/H_2O (10:90–100:0, *v/v*), and semipreparative HPLC (2 ml/min) to gain compounds **3** (4.0 mg, 54% CH_3CN/H_2O, t_R = 31.0 min), **5** (4.5 mg, 35% CH_3CN/H_2O with 0.3‰ TFA, t_R = 33.6 min), **6** (7.6 mg, 35% CH_3CN/H_2O with 0.3‰ TFA, t_R = 35.0 min), and **10** (6.4 mg, 33% CH_3CN/H_2O, t_R = 22.0 min). Fr-3 (4.6 g) was purified with Sephadex LH-20 column eluted with MeOH, reversed-phase C_{18} MPLC eluted with MeOH/H_2O (10:90–100:0, *v/v*), and semipreparative HPLC (2 ml/min) to obtain compounds **4** (2.9 mg, 72% CH_3OH/H_2O with 0.3‰ TFA, t_R = 8.2 min) and **9** (42.2 mg, 70% CH_3OH/H_2O with 0.3‰ TFA, t_R = 14.6 min). Fr-4 (3.7 g) was purified with Sephadex LH-20 column eluted with MeOH, reversed-phase C_{18} MPLC eluted with MeOH/H_2O (10:90–100:0, *v/v*), and semipreparative HPLC (75% CH_3CN/H_2O with 0.3‰ TFA, 2 ml/min) to yield compound **1** (30.5 mg, t_R = 12.2 min). Fr-5 (1.3 g) was applied to Sephadex LH-20 column eluted with MeOH, reversed-phase C-18 MPLC eluted with MeOH/H_2O (10:90–100:0, *v/v*), and semipreparative HPLC (2 ml/min) to get compounds **11** (76.5 mg, 40% CH_3CN/H_2O with 0.3‰ TFA, t_R = 11.4 min) and **12** (60% CH_3CN/H_2O, t_R = 15.2 min, 6.0 mg). Fr-6 (1.6 g) was subjected to Sephadex LH-20 column eluted with MeOH, reversed-phase C_{18} MPLC eluted with MeOH/H_2O (10:90–100:0, *v/v*), and semipreparative HPLC (75% CH_3CN/H_2O with 0.3‰ TFA, 2 ml/min) to obtain compound **2** (2.5 mg, t_R = 12.8 min).

Penicillenol G1 (**1**): Pale white solid; $[\alpha]_D^{25}$ –156.6 (*c* 0.10, MeOH); UV (MeOH) λ_{max} (log ε) 219 (3.21), and 278 (2.79) nm; ECD (1.06 mM, MeOH) λ_{max} (Δε) 209 (+ 5.26), 227 (–5.27), and 281 (−4.38) nm; ^1H and ^{13}C NMR data (**Table 1**); HRESIMS *m/z* 284.1866 $[M + H]^+$ (calcd for $C_{15}H_{26}NO_4$, 284.1856).

Penicillenol G2 (**2**): Yellowish oil; $[\alpha]_D^{25}$ + 46.0 (*c* 0.10, MeOH); UV (MeOH) λ_{max} (log ε) 242 (2.87) and 279 (3.12) nm; ECD (1.06 mM, MeOH) λ_{max} (Δε) 213 (–3.08), 238 (+ 2.50), and 271 (2.89) nm; ^1H and ^{13}C NMR data (**Table 1**); HRESIMS *m/z* 284.1862 $[M + H]^+$ (calcd for $C_{15}H_{26}NO_4$, 284.1856).

Penicillenol H (**3**): Yellow oil; $[\alpha]_D^{25}$ –21.0 (*c* 0.10, MeOH); UV (MeOH) λ_{max} (log ε) 227 (2.81) and 285 (3.04) nm; ECD (0.71 mM, MeOH) λ_{max} (Δε) 213 (2.87), 231 (–2.76), and 289 (–1.27) nm; ^1H and ^{13}C NMR data (**Table 1**); HRESIMS *m/z* 284.1858 $[M + H]^+$ (calcd for $C_{15}H_{26}NO_4$, 284.1856).

Coniochaetone N (**4**): Yellow solid powder; $[\alpha]_D^{25}$ + 46.4 (*c* 0.10, MeOH); UV (MeOH) λ_{max} (log ε) 203 (4.11), 226 (4.15), 243 (4.22), and 342 (3.56) nm; ^1H and ^{13}C NMR data (**Table 2**); HRESIMS *m/z* 285.0373 $[M + Na]^+$ (calcd for $C_{13}H_{10}NaO_6$, 285.0370).

X-Ray crystallographic analysis of penicillenol G1 (**1**): Moiety formula: $C_{15}H_{25}NO_4$ (*M* = 283.36 g/mol), colorless needle, crystal size = 0.6 × 0.03 × 0.03 mm^3, trigonal, space group C2; unit cell dimensions: *a* = 20.4710(5) Å, *b* = 4.85100(10) Å, *c* = 33.3706(10) Å, *V* = 3154.94(15) $Å^3$, *Z* = 8, ρ_{calcd} = 1.193 g cm^{-3}, *T* = 101(2) K, μ(Cu Kα) = 0.698 mm^{-1}. A total of 31,816 reflections were measured with 6,225 independent reflections (R_{int} = 0.0496, R_{sigma} = 0.0341). Final *R* indices [I > 2σ (*I*)]: R_1 = 0.0348, wR_2 = 0.0872. Final *R* indexes [all date]: R_1 = 0.0407, wR_2 = 0.0896, Flack parameter = 0.07(8). Largest diff. peak and hole = 0.18 and –0.20 $eÅ^{-3}$.

TABLE 1 | ^1H NMR (700 MHz) and ^{13}C NMR (175 MHz) data for compounds **1–3** in CD_3OD.

No.	1		2		3	
	δ_C, type	δ_H (*J* in Hz)	δ_C, type	δ_H (*J* in Hz)	δ_C, type	δ_H (*J* in Hz)
2	178.0 C		177.7 C		175.4 C	
3	102.3 C		102.8 C		102.8 C	
4	196.2 C		196.0 C		195.1 C	
5	69.0 C	3.73, brs	68.1 CH	3.94, brs	70.0 CH	3.78, brs
6	68.0 C	4.10, qd, 6.3, 2.8	68.7 CH	4.08, qd, 6.3, 3.5	59.3 CH_2	3.94, qd, 12.6, 2.8
7	20.4 CH_3	1.29, d, 7.0	17.0 CH_3	1.10, d, 6.3		
8	193.8 C		194.6 C		192.1 C	
9	37.5 CH	3.58–3.67, m	37.9 CH	3.59–3.67, m	37.2 CH	3.62–3.72, m
10	34.8 CH_2	1.66–1.74, m	34.9 CH_2	1.65–1.72, m	34.9 CH_2	1.68–1.75, m
		1.42–1.50, m		1.40–1.47, m		1.43–1.51, m
11	28.3 CH_2	1.23–1.35, m	28.4 CH_2	1.21–1.34, m	28.3 CH_2	1.23–1.37, m
12	30.3 CH_2	1.23–1.35, m	30.3 CH_2	1.21–1.34, m	30.3 CH_2	1.23–1.37, m
13	23.6 CH_2	1.23–1.35, m	23.6 CH_2	1.21–1.34, m	23.6 CH_2	1.23–1.37, m
14	32.8 CH_2	1.23–1.35, m	32.9 CH_2	1.21–1.34, m	32.9 CH_2	1.23–1.37, m
15	14.4 CH_3	0.89, t, 7.7	14.4 CH_3	0.88, t, 7.0	14.4 CH_3	0.91, t, 6.3
16	17.3 CH_3	1.16, d, 6.3	17.4 CH_3	1.14, d, 6.3	17.4 CH_3	1.17, d, 6.3
17					26.8 CH_3	3.03, s

TABLE 2 | ^{1}H NMR (700 MHz) and ^{13}C NMR (175 MHz) data for compound **4** in CD_3OD.

No.	4	
	δ_C, type	δ_H (*J* in Hz)
1	71.5 CH	5.30, d, 7.0
2	31.4 CH_2	2.45–2.53, m
		2.00, brt, 11.2
3	30.7 CH_2	3.19, dt, 17.5, 7.7
		2.89, ddd, 18.2, 9.1, 2.8
4	176.1 C	
6	158.6 C	
7	109.7 CH	7.54, brs
8	138.2 C	
9	113.1 CH	7.32, brs
10	162.3 C	
11	114.3 C	
12	182.2 C	
13	122.9 C	
14	167.9 C	

Molecular Docking Research

The molecular docking was conducted by AutoDockTools (Version 1.5.6) (Morris et al., 2008). The crystal structure of SARS-CoV-2 main protease (PDB ID: 6LU7) was retrieved from the Protein DataBank[1] (Jin et al., 2020). The structures were generated in ChemBio3D Ultra 14.0 (ChemBioOffice version 14.0), followed by an MM2 calculation to minimize the conformation energy. The original ligand and crystal water were removed before the docking calculation. The hydrogens were added to the structure of 6LU7, and Kollman united partial charges were assigned. A Lamarckian genetic algorithm was applied as a default search algorithm and set the grid box within the size of 46 × 44 × 46 Å, with the spacing of 0.375 Å. During the docking, the default parameters were used if it was not mentioned. The docking pose that had the lowest binding energy was represented as the most favorable binding conformation.

Antibacterial Activity Assay

All compounds (**1**–**12**) were tested for antibacterial activities against five pathogenic bacteria using the method of agar filter paper diffusion. Compounds that had inhibition zone were evaluated in 96-well plates using a modification of the broth microdilution method (Pang et al., 2018). Ampicillin and gentamicin were used as a positive control for Gram-positive and Gram-negative bacteria, respectively.

Antiviral Activity Assay

The antiviral activities of all compounds (**1**–**12**) against SARS-CoV-2 M^{pro} were evaluated through the method mentioned in the previous report (Li et al., 2020). Hydroxychloroquine showed potent inhibitory activity against SARS-CoV-2 M^{pro} with Ki = 0.36 μm and was used as a positive control.

[1]http://www.rcsb.org/pdb

RESULTS AND DISCUSSION

Structural Elucidation

Penicillenol G1 (**1**) possessed the elemental composition of $C_{15}H_{25}NO_4$ with 4 degrees of unsaturation as established by its ^{13}C NMR data and a protonated molecule at *m*/*z* 284.1866 in the HRESIMS spectrum. Its 1D NMR data (**Table 1**) displayed three methyls [$\delta_{C/H}$ 20.4/1.29 (d, *J* = 7.0 Hz, CH_3-7), 17.3/1.16 (d, *J* = 6.3 Hz, CH_3-16), and 14.4/0.89 (t, *J* = 7.7 Hz, CH_3-15)], three sp^3 methines [($\delta_{C/H}$ 69.0/3.73 (brs, CH-5), 68.0/4.10 (dq, *J* = 6.3, 2.8 Hz, CH-6), and 37.5/3.58–3.67 (m, CH-9)], four sp^3 methenes ($\delta_{C/H}$ 28.3–34.8/1.23–1.74), and four sp^2 non-protonated carbons (δ_C 178.0 C-2, 102.3 C-3, 196.2 C-4, and 193.8 C-8). The ^{1}H-^{1}H COSY correlations (**Figure 2**) of H_3-16/H-9/H_2-10/H_2-11 and H_3-15/H_2-14, along with four overlapping sp^3 methenes in the ^{1}H NMR, indicated the presence of a 2-isooctyl group. The ^{1}H-^{1}H COSY correlations of H_3-7/H-6/H-5 verified that there was a 1-hydroxyethyl group directly connected to C-5. Comparison of the NMR data of **1** with those of penicillenol A_1 (**5**) (Lin et al., 2008; Yoda et al., 2010) showed that they only differed by an absence of the singlet methyl in **1**. The planar structure of **1** was further confirmed by its heteronuclear multiple bond correlation (HMBC) correlations (**Figure 2**) of H-6 to C-4, H_3-7 to C-5, H_2-10 to C-8 and C-12, and H_3-16 to C-8 and C-10. The configuration of a double bond at C-3 was determined as *Z* based on that the chemical shift of acylamino (δ_C 178.0, C-2) was in a lower field than those of normal ones, which caused by the hydrogen bond between the oxygen atom at C-2 and hydroxy at C-8 (Aoki et al., 2000). Thus, the ECD of **1** (**Figure 3**) displayed a positive Cotton effect at 209 nm ($\Delta\varepsilon$ = + 18.39), a negative Cotton effect at 227 nm ($\Delta\varepsilon$ = –15.33), and a negative Cotton effect at 281 nm ($\Delta\varepsilon$ = –4.38), and the trend of which was consistent with that of **5**. Thus, the absolute configuration of C-5 in **1** was determined as *S*. Mosher's method was tried to confirm the absolute configuration of C-6 but failed. Fortunately, the single crystal of **1** was obtained, and the absolute configuration of **1** was established as 5*S*, 6*R*, 9*S* by analyzing the X-ray crystallographic data (**Figure 4**). Compound **1** was named as penicillenol G1.

The molecular formula of penicillenol G2 (**2**), which was the same as **1**, was established as $C_{15}H_{25}NO_4$ by its NMR data (**Table 1**) and a protonated molecule at *m*/*z* 284.1862 in the HRESIMS. Its NMR data were nearly the same as those of **1**, and only the chemical shifts of C-5 ($\delta_{C/H}$ 68.1/3.94, brs), C-6 [$\delta_{C/H}$ 68.7/4.08 (qd, *J* = 6.3, 3.5 Hz)], and C-7 [$\delta_{C/H}$ 17.0/1.10 (d, *J* = 6.3 Hz)] in **2** have some small differences. Compound **2** had the same planar structure with **1**, which was confirmed by the ^{1}H-^{1}H COSY and HMBC spectra (**Figure 2**). Thereby, the differences mentioned earlier might be caused by their different configurations. The ECD spectrum of **2** showed a negative Cotton effect at 213 nm ($\Delta\varepsilon$ = –3.08), a positive Cotton effect at 238 nm ($\Delta\varepsilon$ = + 2.5), and a positive Cotton effect at 271 nm ($\Delta\varepsilon$ = + 2.89), which exhibited a reverse trend with **1** and **5**, but was consistent with penicillenol A2 (**6**) (Lin et al., 2008; Sengoku et al., 2012). Therefore, the absolute configuration of C-5 in **2** was determined as *R*. Some synthetic chemists demonstrated that the

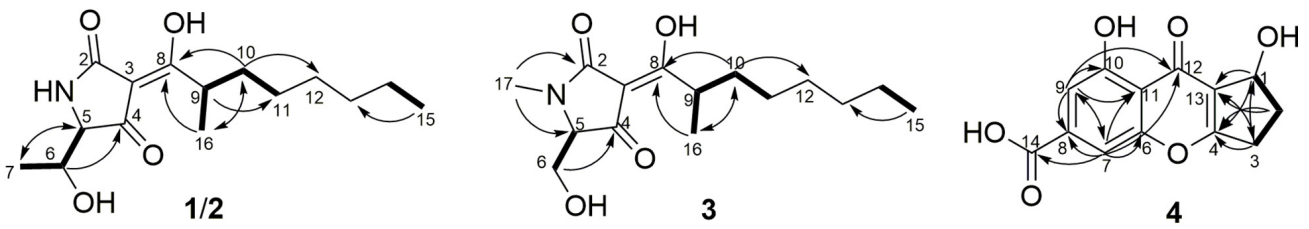

FIGURE 2 | Key ^{1}H-^{1}H COSY (—) and HMBC (→) correlations of compounds **1**–**4**.

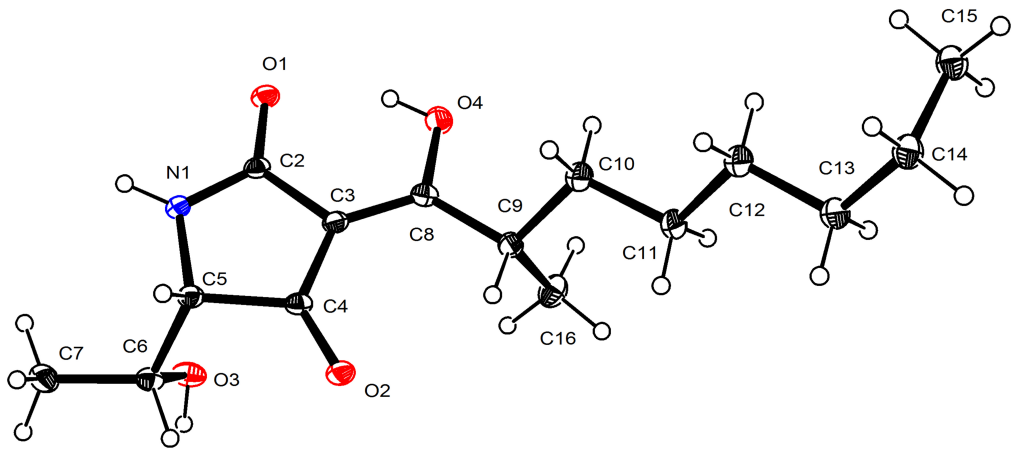

FIGURE 3 | ORTEP drawing of compound **1**.

natural penicillenol A1 (**5**) (Yoda et al., 2010), penicillenol A2 (**6**) (Sengoku et al., 2012), and penicillenol C1 (**7**) (Kempf et al., 2013) were all have the same absolute configurations of 6*R* and 9*S*, and the absolute configuration of compound **1** was also determined as 6*R* and 9*S* by the X-ray diffraction study. Thus, considering the same biosynthetic pathway (Yin et al., 2019) and comparison of the spectroscopic data with **1**, the absolute configurations of C-6 and C-9 in **2** were deduced as 6*R*, 9*S*.

Penicillenol H (**3**) was obtained as a yellow oil. The ^{13}C NMR data and a protonated molecule at *m*/*z* 284.1858 in the HRESIMS of **3** suggested that its molecular formula was $C_{15}H_{25}NO_4$ with 4 degrees of unsaturation. The NMR data (**Table 1**) of **3** were similar to those of **1**, except that the 1-hydroxyethyl group in **1** was displaced by oxygenated methylene ($\delta_{C/H}$ 59.3/3.94, qd, J = 12.6, 2.8 Hz, CH_2-6) and an *N*-methyl group ($\delta_{C/H}$ 26.8/3.03, s, CH_3-17) was added in **3**. The extinction was determined by its ^{1}H-^{1}H COSY cross-peak of H_2-6/H-5 and HMBC correlations of H_2-6 to C-4 and H_3-17 to C-2 and C-5. The planar structure of **3** was further established by its 2D NMR (**Figure 2**). The configuration of a double bond at C-3 was designated as *Z* by the chemical shift of C-2 (δ_C 178.0) (Aoki et al., 2000). The absolute configuration of C-5 and C-9 in **3** were determined as *S* and *R* same as compound **1** by their similar ECD spectrum (**Figure 3**), of which **3** showed a positive Cotton effect at 213 nm ($\Delta\varepsilon$ = + 2.87), two negative Cotton effects at 231 nm ($\Delta\varepsilon$ = – 2.76), and 289 nm ($\Delta\varepsilon$ = – 1.27), respectively. Compound **3** was named penicillenol H.

The molecular formula of compound **4** was $C_{13}H_{10}O_8$, established by its ^{13}C NMR data (**Table 2**) and a sodium adduct ion peak at *m*/*z* 285.0373 in the HRESIMS spectrum. Its ^{1}H NMR data were simple and showed two aromatic protons (δ_H 7.54, brs, CH-7; 7.32, brs, CH-9) at meta-position, an oxygenated methine (δ_H 5.30, d, J = 7.0 Hz, CH-1), and two sp^3 methylenes (δ_H 2.45–2.53, m, 2.00, brt, J = 11.2 Hz, CH_2-2; 3.19, dt,

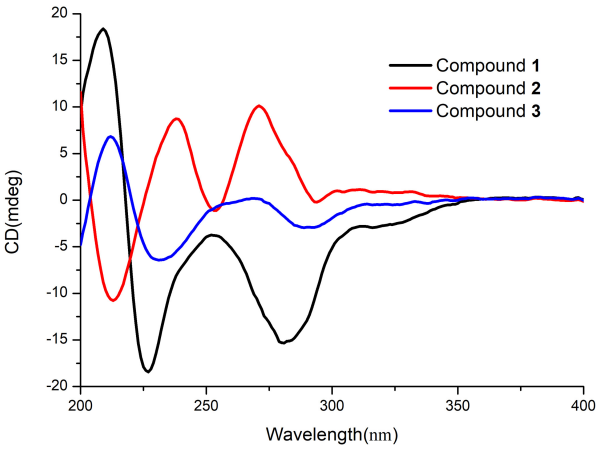

FIGURE 4 | Experimental ECD curves of compounds **1**–**3**.

J = 17.5, 7.7 Hz, 2.89, ddd, J = 18.2, 9.1, 2.8 Hz, CH_2-3). Besides the corresponding carbons (δ_C 109.7, CH-7; 113.1, CH-9; 71.5, CH-1; 34.4, CH_2-2; 30.7, CH_2-3), there were eight sp^2 non-protonated carbons in its ^{13}C NMR, which indicated the presences of an α,β-unsaturated ketone (δ_C 182.2, C-12; 122.9, C-13; 176.1, C-4) and a carboxyl (δ_C, 167.9, C-14). Its NMR data were very similar to those of coniochaetone L (Guo et al., 2019), except that the methoxy group at C-1 in coniochaetone L was replaced by hydrogen in **4**. The speculation was further confirmed by its HMBC and ^1H-^1H COSY spectra (**Figure 2**). The positive specific rotation of **4** ($[\alpha]_D^{25}$ + 46.4, MeOH) that was consistent with that of coniochaetone L ($[\alpha]_D^{25}$ + 25.3, MeOH) suggested that the configuration of C-1 was *R*. Thus, compound **4** was established as *R*-1,8-dihydroxy-9-oxo-1,2,3,9-tetrahydrocyclopenta[b]chromene-6-carboxylic acid and named as coniochaetone N.

In addition, the eight known compounds (**5**–**12**) (**Figure 1**) were identified as penicillenol A1 (**5**) (Lin et al., 2008; Yoda et al., 2010), penicillenol A2 (**6**) (Lin et al., 2008; Sengoku et al., 2012), penicillenol C1 (**7**) (Lin et al., 2008; Kempf et al., 2013), penicillenol C2 (**8**) Lin et al., 2008), scalusamide C (**9**) (Tsuda et al., 2005), (*E*)-7-(3-methyl-4-oxo-6,7,8,8a-tetrahydro-4*H*-pyrrolo[2,1-b][1,3]oxazin-2-yl)hept-2-enoic acid (**10**) (Lai et al., 2013), terretrione D (**11**) (Shaala and Youssef, 2015), and (2*R*)-2,3-dihydro-7-hydroxy-6,8-dimethyl-2-[(*E*)-prop-1-enyl] chromen-4-one (**12**) (Li et al., 2007; Zhang et al., 2019) by comparison of their physical and spectroscopic data with those in the literature.

Bioassays of Compounds

All isolated compounds (**1**–**12**) were tested for their antiviral activities against SARS-CoV-2 M^{pro} *in vitro* through the method mentioned in the reported literature (Li et al., 2020). Compound **3** showed weak inhibitory activity against M^{pro} enzyme, which was responsible for the COVID-19 pandemic. When treated with 50 μm of **3**, the relative enzyme activity of SARS-CoV-2 M^{pro} was 46.64%, and that of the positive control hydroxychloroquine was 5.28% with the same concentration. To better understand the interactions between compounds and SARS-CoV-2 M^{pro}, molecular docking research was performed to mimic the interactions between compound **3** and M^{pro} enzyme of SARS-CoV-2 (PDB ID: 6LU7) by utilizing the AutoDockTools. Molecular docking results demonstrated that compound **3** could interact with the SARS-CoV-2 M^{pro} enzyme at the entrance of the catalytic pocket, with the calculated binding affinities of –4.98 kcal/mol. The 2D binding model for **3** (**Figure 5**) showed two hydrogen bonds and two intermolecular hydrophobic interactions. Two hydrogen bonds were formed between the carbonyl group at C-4 and Thr-26, as well as between the hydroxyl group at C-6 and Thr-24. The lengths of the two hydrogen bonds were 2.0 and 1.8 Å, respectively. These results suggested that compound **3** could insert into the active site of the enzyme and bind tightly to the catalytic amino acid residues by different types of interactions to inhibit SARS-CoV-2 M^{pro}.

Compounds **1**–**12** were evaluated their antibacterial activities against five pathogenic bacteria *Escherichia coli* (ATCC 25922), *Enterococcus faecalis* (ATCC 29212), *Klebsiella pneumonia* (ATCC 13883), *Staphyloccocus aureus* (ATCC 29213), and methicillin-resistant *S. aureus* (MRSA). Compounds **1**, **3**, **5,** and **6** with 50 μg/disc showed inhibition zones against *S. aureus*. Compounds **1**, **3**, and **5** with 50 μg/disc showed an inhibition zone against MRSA (**Supplementary Figure 1**). Furthermore, their minimum inhibitory concentrations (MICs) were tested, and the results are shown in **Table 3**. Compound **3** displayed potent inhibitory activities against *S. aureus* and MRSA with MIC values of both 2.5 μg/ml. Ampicillin was used as a positive control against *S. aureus* and MRSA with MIC values of 1.56 and 0.39 μg/ml, respectively.

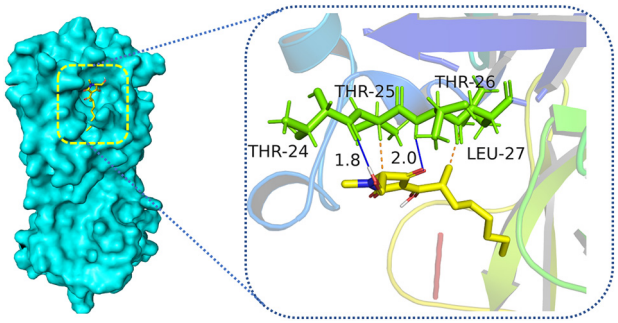

FIGURE 5 | Low-energy binding conformations the complex between compound **3** and SARS-CoV-2 M^{pro} by virtual docking. Blue solid line means hydrogen bonds, and orange dotted lines mean hydrophobic interactions.

TABLE 3 | MIC values (μg/ml) of compounds with antibacterial activities.

Compounds	*S. aureus*	MRSA
1	20	40
3	2.5	2.5
5	40	40
6	80	–
Ampicillin	1.56	0.39

CONCLUSION

In summary, we reported the isolation and identification of three new tetramic acid derivatives (**1**–**3**) and a new polyketide (**4**) along with eight known compounds (**5**–**12**) from cultures of the deep-sea-derived fungus *Penicillium* sp. SCSIO06868. The absolute configurations of new compounds were established by X-ray crystallography analysis and comparison of the experimental and reported ECD value or specific optical rotation. Compound **3** displayed potent inhibitory activities against *S. aureus* and MRSA with MIC values of both 2.5 μg/ml. Compound **3** showed weak inhibitory activity against M^{pro} enzyme of SARS-CoV-2, which was responsible for the COVID-19 pandemic. Molecular docking was performed to mimic the interactions between compound **3** and SARS-CoV-2 M^{pro}. The molecular docking results indicated that compound **3** could be

inserted into the active site of the enzyme and bind tightly to the catalytic amino acid residues by different types of interactions to inhibit SARS-CoV-2 M^{pro}.

DATA AVAILABILITY STATEMENT

The datasets presented in this study can be found in online repositories. The names of the repository/repositories and accession number (s) can be found in the article/**Supplementary Material**.

AUTHOR CONTRIBUTIONS

XP, JW, and YL contributed to conception and design of the study. XP performed the experiments, analyzed the data, and wrote the manuscript. XW performed the SARS-CoV-2 M^{pro} inhibition test. XT did the isolation of the fungus. All authors contributed to manuscript revision, review, and approved the submitted version.

FUNDING

This research was financially supported by the Finance Science and Technology Project of Hainan Province (ZDKJ202018), the National Natural Science Foundation of China (Nos. 21772210, 41776169, 41876145, and 42006084), the National Key Research and Development Program of China (No. 2019YFC0312503), the China Postdoctoral Science Foundation (No. 2019M663368), Project from the Institution of South China Sea Ecology and Environmental Engineering, CAS (No. ISEE2018PY04), and the Special Funds for Promoting Economic Development (Marine Economic Development) of Guangdong Province [Nos. GDOE (2019)A28 and (2020)037].

ACKNOWLEDGMENTS

We gratefully acknowledge the assistance of Dr. Xiao, Dr. Zheng, Ms. Sun, Ms. Zhang, and Ms. Ma in the analytical facility center of the SCSIO for recording spectroscopic data.

SUPPLEMENTARY MATERIAL

The Supplementary Material for this article can be found online at: https://www.frontiersin.org/articles/10.3389/fmicb.2021.730807/full#supplementary-material

REFERENCES

Aoki, S., Higuchi, K., Ye, Y., Satari, R., and Kobayashi, M. (2000). Melophlins A and B, novel tetramic acids reversing the phenotype of ras-transformed cells, from the marine sponge melophlus sarassinorum. *Tetrahedron* 56, 1833–1836. doi: 10.1016/S0040-4020(00)00092-2

Chen, S. T., Wang, J. F., Lin, X. P., Zhao, B. X., Wei, X. Y., Li, G. Q., et al. (2016). Chrysamides A-C, three dimeric nitrophenyl trans-epoxyamides produced by the deep-sea-derived fungus *Penicillium chrysogenum* SCSIO41001. *Org. Lett.* 18, 3650–3653. doi: 10.1021/acs.orglett.6b01699

Fan, B., Dewapriya, P., Li, F., Blumel, M., and Tasdemir, D. (2020). Pyrenosetins A-C, new decalinoylspirotetramic acid derivatives isolated by bioactivity-based molecular networking from the seaweed-derived fungus *Pyrenochaetopsis* sp. FVE-001. *Mar. Drugs* 18:47. doi: 10.3390/md18010047

Guo, C., Lin, X. P., Liao, S. R., Yang, B., Zhou, X. F., Yang, X. W., et al. (2019). Two new aromatic polyketides from a deep-sea fungus *Penicillium* sp. SCSIO 06720. *Nat. Prod. Res.* 34, 1197–1205. doi: 10.1080/14786419.2018.1553880

Jiang, M. H., Chen, S. H., Li, J., and Liu, L. (2020). The biological and chemical diversity of tetramic acid compounds from marine-derived microorganisms. *Mar. Drugs* 18:114. doi: 10.3390/md18020114

Jin, L. M., Quan, C. S., Hou, X. Y., and Fan, S. D. (2016). Potential pharmacological resources: natural bioactive compounds from marine-derived fungi. *Mar. Drugs* 14:76. doi: 10.3390/md14040076

Jin, Z. M., Du, X. Y., Xu, Y. C., Deng, Y. Q., Liu, M. Q., Zhao, Y., et al. (2020). Structure of M^{pro} from SARS-CoV-2 and discovery of its inhibitors. *Nature* 582, 289–293. doi: 10.1038/s41586-020-2223-y

Kempf, K., Raja, A., Sasse, F., and Schobert, R. (2013). Synthesis of penicillenol C1 and of a bis-azide analogue for photoaffinity labeling. *J. Org. Chem.* 78, 2455–2461. doi: 10.1021/jo3026737

Lai, D., Brotz-Oesterhelt, H., Muller, W. E. G., Wray, V., and Proksch, P. (2013). Bioactive polyketides and alkaloids from *Penicillium citrinum*, a fungal endophyte isolated from *Ocimum tenuiflorum*. *Fitoterapia* 91, 100–106. doi: 10.1016/j.fitote.2013.08.017

Li, D. H., Cai, S. X., Tian, L., Lin, Z. J., Zhu, T. J., Fang, Y. C., et al. (2007). Two new metabolites with cytotoxicities from deep-sea fungus, *Aspergillus sydowi* YHll-2. *Arch. Pharm. Res.* 33, 1051–1054. doi: 10.1007/BF02980236

Li, Z., Li, X., Huang, Y. Y., Wu, Y., Liu, R., Zhou, L., et al. (2020). Identify potent SARS-CoV-2 main protease inhibitors via accelerated free energy perturbation-based virtual screening of existing drugs. *Proc. Natl. Acad. Sci. U. S. A.* 117, 27381–27387. doi: 10.1073/pnas.2010470117

Lin, Z. J., Lu, Z. Y., Zhu, T. J., Fang, Y. C., Gu, Q. Q., and Zhu, W. M. (2008). Penicillenols from *Penicillium* sp. GQ-7, an endophytic fungus associated with *Aegiceras corniculatum*. *Chem. Pharm. Bull.* 56, 217–221.

Mao, Z. L., Wang, W. X., Su, R. X., Gu, G., Liu, Z. L., Lai, D., et al. (2019). Hyalodendrins A and B, new decalin-type tetramic acid larvicides from the endophytic fungus *Hyalodendriella* sp. Ponipodef12. *Molecules* 25:114. doi: 10.3390/molecules25010114

Mo, X. H., Li, Q. L., and Ju, J. H. (2014). Naturally occurring tetramic acid products: isolation, structure elucidation and biological activity. *RSC Adv.* 4, 50566–50593. doi: 10.1039/c4ra09047k

Morris, G. M., Huey, R., and Olson, A. J. (2008). Using AutoDock for ligand-receptor docking. *Curr. Protoc. Bioinformatics* 24, 8–14. doi: 10.1002/0471250953.bi0814s24

Nord, C., Levenfors, J. J., Bjerketorp, J., Guss, B., Oberg, B., and Broberg, A. (2020). Tetramic acid based alkaloids from *Aspergillus amoenus* Roberg strain UP197-antibiotic properties and new pyranterreones. *Nat. Prod. Res.* doi: 10.1080/14786419.2020.1855643 [Epub Online ahead of print].

Pang, X. Y., Lin, X. P., Yang, J., Zhou, X. F., Yang, B., Wang, J. F., et al. (2018). Spiro-phthalides and isocoumarins isolated from the marine-sponge-derived fungus *Setosphaeria* sp. SCSIO41009. *J. Nat. Prod.* 81, 1860–1868. doi: 10.1021/acs.jnatprod.8b00345

Pang, X. Y., Lin, X. P., Zhou, X. F., Yang, B., Tian, X. P., Wang, J. F., et al. (2020). New quinoline alkaloid and bisabolane-type sesquiterpenoid derivatives from the deep-sea-derived fungus *Aspergillus* sp. SCSIO06786. *Fitoterapia* 140:104406. doi: 10.1016/j.fitote.2019.104406

Pang, X. Y., Zhou, X. F., Lin, X. P., Yang, B., Tian, X. P., Wang, J. F., et al. (2021). Structurally various sorbicillinoids from the deep-sea sediment derived fungus

Penicillium sp. SCSIO06871. *Bioorg. Chem.* 107:104600. doi: 10.1016/j.bioorg.2020.104600

Sabbah, D. A., Hajjo, R., Bardaweel, S. K., and Zhong, H. A. (2021). An updated review on SARS-CoV-2 main proteinase (M^{Pro}): protein structure and small-molecule inhibitors. *Curr. Top. Med. Chem.* 21, 442–460. doi: 10.2174/1568026620666201207095117

Schobert, R., and Schlenk, A. (2008). Tetramic and tetronic acids: an update on new derivatives and biological aspects. *Bioorg. Med. Chem.* 16, 4203–4221. doi: 10.1016/j.bmc.2008.02.069

Schrey, H., Backenkohler, J., Kogler, H., Plaumann, M., and Spiteller, P. (2019). Aminotenuazonic acid: isolation, structure elucidation, total synthesis and herbicidal activity of a new tetramic acid from fruiting bodies of *Laccaria* species. *Chemistry* 25, 10333–10341. doi: 10.1002/chem.201901405

Sengoku, T., Nagae, Y., Ujihara, Y., Takahashi, M., and Yoda, H. (2012). A synthetic approach to diverse 3-acyltetramic acids via O- to C-acyl rearrangement and application to the total synthesis of penicillenol series. *J. Org. Chem.* 77, 4391–4401. doi: 10.1021/jo300527f

Shaala, L. A., and Youssef, D. T. (2015). Identification and bioactivity of compounds from the fungus *Penicillium* sp. CYE-87 isolated from a marine tunicate. *Mar. Drugs* 13, 1698–1709. doi: 10.3390/md13041698

Shamsi, A., Mohammad, T., Anwar, S., Amani, S., Khan, M. S., Husain, F. M., et al. (2021). Potential drug targets of SARS-CoV-2: from genomics to therapeutics. *Int. J. Biol. Macromol.* 177, 1–9. doi: 10.1016/j.ijbiomac.2021.02.071

Sun, Y. L., Wang, J., Wang, Y. F., Zhang, X. Y., Nong, X. H., Chen, M. Y., et al. (2015). Cytotoxic and antiviral tetramic acid derivatives from the deep-sea-derived fungus *Trichobotrys effuse* DFFSCS021. *Tetrahedron* 71, 9328–9332. doi: 10.1016/j.tet.2015.10.010

Tsuda, M., Sasaki, M., Mugishima, T., Komatsu, K., Sone, T., Tanaka, M., et al. (2005). Scalusamides A-C, new pyrrolidine alkaloids from the marine-derived fungus *Penicillium citrinum*. *J. Nat. Prod.* 68, 273–276. doi: 10.1021/np049661q

Wang, J. F., He, W. J., Huang, X. L., Tian, X. P., Liao, S. R., Yang, B., et al. (2016). Antifungal new oxepine-containing alkaloids and xanthones from the deep-sea-derived fungus *Aspergillus versicolor* SCSIO 05879. *J. Agric. Food Chem.* 64, 2910–2916. doi: 10.1021/acs.jafc.6b00527

Wingen, L. M., Rausch, M., Schneider, T., and Menche, D. (2020). Synthesis of tetramic acid fragments derived from *Vancoresmycin* showing inhibitory effects towards *S. aureus*. *Chem. Med. Chem.* 15, 1390–1393. doi: 10.1002/cmdc.202000241

Yin, X., Liu, Y., Pan, J., Ye, H. L., Sun, Y., Zhao, D. Y., et al. (2019). Melongenaterpenes A-L, vetispirane-type sesquiterpenoids from the roots of *Solanum melongena*. *J. Nat. Prod.* 82, 3242–3248. doi: 10.1021/acs.jnatprod.9b00206

Yoda, H., Sengoku, T., Wierzejska, J., and Takahashi, M. (2010). First stereoselective synthesis of penicillenol A1 via novel O- to C-acyl rearrangement of O-acyltetramic acid. *Synlett* 2010, 2944–2946. doi: 10.1055/s-0030-1259045

Zehra, Z., Luthra, M., Siddiqui, S. M., Shamsi, A., Gaur, N. A., and Islam, A. (2020). Corona virus versus existence of human on the earth: a computational and biophysical approach. *Int. J. Biol. Macromol.* 161, 271–281. doi: 10.1016/j.ijbiomac.2020.06.007

Zhang, P. P., Deng, Y. L., Lin, X. J., Chen, B., Li, J., Liu, H. J., et al. (2019). Anti-inflammatory mono- and dimeric sorbicillinoids from the marine-derived fungus *Trichoderma reesei* 4670. *J. Nat. Prod.* 82, 947–957. doi: 10.1021/acs.jnatprod.8b01029

Conflict of Interest: The authors declare that the research was conducted in the absence of any commercial or financial relationships that could be construed as a potential conflict of interest.

Publisher's Note: All claims expressed in this article are solely those of the authors and do not necessarily represent those of their affiliated organizations, or those of the publisher, the editors and the reviewers. Any product that may be evaluated in this article, or claim that may be made by its manufacturer, is not guaranteed or endorsed by the publisher.

frontiers in Microbiology

ORIGINAL RESEARCH
published: 01 October 2021
doi: 10.3389/fmicb.2021.730740

Lulworthinone, a New Dimeric Naphthopyrone From a Marine Fungus in the Family Lulworthiaceae With Antibacterial Activity Against Clinical Methicillin-Resistant *Staphylococcus aureus* Isolates

Marte Jenssen[1], Philip Rainsford[2], Eric Juskewitz[3], Jeanette H. Andersen[1], Espen H. Hansen[1], Johan Isaksson[2], Teppo Rämä[1] and Kine Ø. Hansen[1]*

[1] Marbio, The Norwegian College of Fishery Science, Faculty of Biosciences, Fisheries and Economics, UiT the Arctic University of Norway, Tromsø, Norway, [2] Department of Chemistry, Faculty of Science and Technology, UiT the Arctic University of Norway, Tromsø, Norway, [3] Research Group for Host Microbe Interactions, Department of Medical Biology, Faculty of Health Sciences, UiT the Arctic University of Norway, Tromsø, Norway

OPEN ACCESS

Edited by:
Carolina Elena Girometta, University of Pavia, Italy

Reviewed by:
Susan Semple, University of South Australia, Australia
Adelaide Almeida, University of Aveiro, Portugal

***Correspondence:**
Marte Jenssen
marte.jenssen@uit.no

Specialty section:
This article was submitted to Microbiotechnology, a section of the journal Frontiers in Microbiology

Received: *25 June 2021*
Accepted: *06 September 2021*
Published: *01 October 2021*

Citation:
Jenssen M, Rainsford P, Juskewitz E, Andersen JH, Hansen EH, Isaksson J, Rämä T and Hansen KØ (2021) Lulworthinone, a New Dimeric Naphthopyrone From a Marine Fungus in the Family Lulworthiaceae With Antibacterial Activity Against Clinical Methicillin-Resistant Staphylococcus aureus Isolates. Front. Microbiol. 12:730740. doi: 10.3389/fmicb.2021.730740

The emergence of drug-resistant bacteria is increasing rapidly in all parts of the world, and the need for new antibiotics is urgent. In our continuous search for new antimicrobial molecules from under-investigated Arctic marine microorganisms, a marine fungus belonging to the family Lulworthiaceae (Lulworthiales, Sordariomycetes, and Ascomycota) was studied. The fungus was isolated from driftwood, cultivated in liquid medium, and studied for its potential for producing antibacterial compounds. Through bioactivity-guided isolation, a novel sulfated biarylic naphtho-α-pyrone dimer was isolated, and its structure was elucidated by spectroscopic methods, including 1D and 2D NMR and HRMS. The compound, named lulworthinone (**1**), showed antibacterial activity against reference strains of *Staphylococcus aureus* and *Streptococcus agalactiae*, as well as several clinical MRSA isolates with MICs in the 1.56–6.25 μg/ml range. The compound also had antiproliferative activity against human melanoma, hepatocellular carcinoma, and non-malignant lung fibroblast cell lines, with IC_{50} values of 15.5, 27, and 32 μg/ml, respectively. Inhibition of bacterial biofilm formation was observed, but no eradication of established biofilm could be detected. No antifungal activity was observed against *Candida albicans*. During the isolation of **1**, the compound was observed to convert into a structural isomer, **2**, under acidic conditions. As **1** and **2** have high structural similarity, NMR data acquired for **2** were used to aid in the structure elucidation of **1**. To the best of our knowledge, lulworthinone (**1**) represents the first new bioactive secondary metabolite isolated from the marine fungal order Lulworthiales.

Keywords: antibacterial, marine fungi *sensu stricto*, Lulworthiales, lulworthinone, MRSA, natural product, mycology, natural product artifact

INTRODUCTION

Antimicrobial resistance is quickly developing as a worldwide threat, causing problems not only in the general community but also in healthcare facilities. Infections caused by methicillin-resistant *Staphylococcus aureus* (MRSA) has become a worldwide health menace (WHO, 2014). There is an urgent need to develop new antibiotics to fight these resistant microbes. The fungal kingdom has historically played an important role in the discovery and development of antibiotics and other drugs against non-infective diseases (Demain, 2014). The penicillins and cephalosporins are examples of important antibiotics isolated from fungi (Demain, 2014), from the genera *Penicillium* and *Sarocladium* (one syn. *Cephalosporium*), respectively. In marine natural product discovery, the genera *Aspergillus* and *Penicillium* have proven to be the most prolific producers of new compounds with biological activities (Imhoff, 2016). As the focus of marine natural product discovery has been on mold fungi belonging to the few genera mentioned above, the strictly marine clades of fungi remain understudied (Overy et al., 2014).

One of the understudied marine clades include the fungal order Lulworthiales from which no secondary metabolites have been reported since the discovery of the type genus and species, *Lulworthia fucicola*, in the beginning of the twentieth century (Sutherland, 1915). The order Lulworthiales was established in 2000 to accommodate the new family Lulworthiaceae in the class Sordariomycetes (Kohlmeyer et al., 2000). More recently, a new subclass, Lulworthiomycetidae, was described containing the orders Lulworthiales and Koralionastetales (Maharachchikumbura et al., 2015). Lulworthiaceae is the sole family in the Lulworthiales order, and Lulworthiaceae spp. are regarded as strictly marine species, which include the following genera: *Cumulospora*, *Halazoon*, *Hydea*, *Kohlmeyerella*, *Lulwoana*, *Lulworthia*, *Lindra*, *Matsusporium*, and *Moleospora* (Poli et al., 2020). Recently, a novel genus was introduced to the Lulworthiaceae, *Paralulworthia*, with two new species described, *Paralulworthia gigaspora* and *Paralulworthia posidoniae* (Poli et al., 2020). Hyde et al. (2020) also included the following genera in the family: *Haloguignardia*, *Lolwoidea*, *Moromyces*, *Orbimyces*, *Rostrupiella*, and *Sammeyersia*.

Fungi in the family Lulworthiaceae have been isolated from a variety of substrates and environments. Some examples include corals (Góes-Neto et al., 2020), plants located in salt marches (Calado et al., 2019), seagrass (Poli et al., 2020), Portuguese marinas (Azevedo et al., 2017), sandy beaches of the Cozumel island in Mexico (Velez et al., 2015), brown seaweed (Zuccaro et al., 2008), and driftwood (Rämä et al., 2014). The distribution of Lulworthiales fungi in marine habitats has been studied throughout the history of marine mycology (Johnson, 1958; Kohlmeyer et al., 2000; Koch et al., 2007; Rämä et al., 2014; Azevedo et al., 2017; Góes-Neto et al., 2020), but the biosynthetic potential of these fungi has not been investigated, most likely due to the special knowledge required for their isolation (Overy et al., 2019) and low growth rates.

In this paper, we report the isolation of a new antibacterial compound, lulworthinone (**1**), from a liquid culture of a marine fungus belonging to Lulworthiaceae (isolate 067bN1.2). We elucidate the structure of **1** and study its bioactivity against prokaryotic and eukaryotic cells with focus on antibacterial activity against clinical MRSA isolates. Compound **1** represents the first secondary metabolite reported from this order of fungi, and to the best of our knowledge, the first biarylic dimeric naphtho-α-pyrone substituted with a sulfate group. Initially, the compound was isolated using preparative HPLC under acidic conditions. As this procedure caused significant wear and tear to the equipment, the isolation was switched to flash chromatography under neutral conditions. When comparing spectroscopic data from the two samples, one isolated at neutral and one at acidic conditions, structural differences were observed. It was later determined that **1** concerts into the artifact **2** under acidic conditions.

MATERIALS AND METHODS

Biological Material and Phylogenetic Analysis of Isolate 067bN1.2

The marine fungus 067bN1.2 was isolated from a dead pine (*Pinus* sp.) collected in the splash zone in Kongsfjord, Berlevåg Norway in 2010. The isolate grew from a small wooden cube plated onto agar medium (specified below) during a campaign to study wood-inhabiting fungi of 50 intertidal and sea-floor logs along the Northern Norwegian coast, where Lulworthiales was one of the five most frequent orders isolated (Rämä et al., 2014). The fungus was subcultured and DNA sequenced, and the fungus was phylogenetically placed in the Lulworthiales order (isolate TR498 represents 067bN1.2 in Rämä et al., 2014). At the time of the publication (2014), the closest match from Blast, based on a 5.8S/large ribosomal subunit (LSU) dataset, was *Lulworthia medusa* (LSU sequence: AF195637). The following primer pairs were used for the internal transcribed spacer (ITS), LSU and small ribosomal subunit (SSU) sequencing, respectively: ITS5-ITS4 (White et al., 1990), LR0R-LR5 (Vilgalys and Hester, 1990; Rehner and Samuels, 1994), and NS1-NS4 (White et al., 1990). The ITS, LSU, and SSU sequences are deposited in GenBank under the following accessions: MW377595, MW375591, and MW375590. The mycelium of the fungus was preserved on pieces of agar in 20% glycerol solution at −80°C.

To identify the isolate 067bN1.2 growing as an asexual morph in culture and determine its systematic position within the order Lulworthiales, a phylogenetic analysis was run using a dataset consisting of nrSSU, nrITS, and nrLSU sequences. The reference sequences included in the analyses were sampled based on recent phylogenetic studies focusing on Lulworthiales (Azevedo et al., 2017; Poli et al., 2020) and retrieved from Genbank (**Supplementary Table 1**). Sequences for each gene were aligned individually using the E-INS-I and G-INS-I algorithms of MAFFT v7.388 (Katoh et al., 2002; Katoh and Standley, 2013) in Geneious Prime v.11.0.4 followed by manual adjustment. The concatenated dataset consisting of SSU, 5.8S, and LSU sequences and having a length of 2,270 nt was run through PartitionFinder v2.1.1 (Lanfear et al., 2017) to test for best-fit partitioning schemes and evolutionary models with the following settings: models MrBayes, linked branch lengths, greedy search, and AIC

and BIC model selection (Lanfear et al., 2012). This suggested three partitions with varying models: symmetrical model with equal base frequencies and gamma distributed rate variation among sites without (SYM+G) and with (SYM+I+G) invariable sites and general time reversible model with variable base frequencies and gamma distributed rate variation among sites (GTR+G). A phylogenetic analysis was set up applying suggested models using Parallel-MPI MrBayes v3.2.7a with beagle, and was run for 5,000,000 generations or until average standard deviation of split frequencies was below 0.0009 with sampling each of the 2,500 generations (Ronquist et al., 2012). In addition, RAxML in Geneious v10.2.3 was run with the same partitions under GTRCAT and GTRGAMMA using rapid-bootstrapping algorithm with 2,000 replicates with search for best scoring ML tree (Stamatakis, 2006). The resulting MrBayes tree was similar to the RAxML tree, excluding some of the basal nodes within Lulworthiaceae shown as polytomies in the MrBayes tree.

Fungal Cultivation and Extraction

For the purpose of this study, the fungal isolate was plated from glycerol stock and grown on nutrient-poor malt agar with sea salts [4 g/L malt extract (Moss Malt Extrakt, Jensen & Co AS), 40 g/L sea salts (S9883, Sigma-Aldrich), 15 g/L agar (A1296, Sigma-Aldrich) and Milli-Q® H_2O] until the growth covered the entire agar plate (approximately 40 days). Milli-Q® H_2O was produced with the in-house Milli-Q® system. One-half of the agar plate covered in mycelium was used to inoculate each liquid culture, in malt medium with added sea salts (4 g/L malt extract, 40 g/L sea salts). Two cultures of 200 ml were inoculated and incubated for 107 days at static conditions and 13°C. Before the addition of resin for extraction, mycelium was taken from the culture for inoculation of another round of cultures. The second cultivation contained four cultures with 250 ml of malt extract medium supplemented with sea salts and cultivated under the same conditions for 83 days. The total culture volume used for the extraction of **1** was 1.4 L. The cultures were extracted using Diaion HP-20 resin (13607, Supelco) and methanol (20864, HPLC grade, VWR) as described previously (Kristoffersen et al., 2018; Schneider et al., 2020). The extract was dried in a rotary evaporator at 40°C under reduced pressure and stored at −20°C.

Dereplication

As part of our ongoing search for antimicrobial compounds, extracts of marine microorganisms are fractioned into six fractions using flash chromatography, as previously described (Schneider et al., 2020). When we investigated the antibacterial potential of fractions produced from several understudied marine fungi, one fraction from isolate 067bN1.2 piqued our interest due to its antibacterial activity. In the active fraction, **1** was the dominating peak. The monoisotopic mass, calculated elemental composition and fragmentation pattern of **1** was determined using UHPLC-ESI-HRMS. UHPLC-ESI-HRMS was performed with positive ionization mode, using an Acquity I-class UPLC with an Acquity UPLC C18 column (1.7 μm, 2.1 mm × 100 mm), coupled to a PDA detector and a Vion IMS QToF (all from Waters). Compounds were eluted with a gradient over 12 min, from 10 to 90% acetonitrile (LiChrosolv, 1.00029, Supelco) with 0.1% formic acid (Sigma-Aldrich) in Milli-Q H_2O and a flow rate of 0.45 ml/min. Waters UNIFI 1.9.4 Scientific Information System was used to process and analyze the data. Elemental compositions of compounds in the samples were used to search relevant databases, such as Chemspider, in order to identify known compounds. Since the calculated elemental composition gave no hits in database searches, **1** was nominated for isolation.

Isolation of 1

Initial attempts to isolate **1** was performed using mass guided preparative HPLC. This strategy proved difficult due to extensive binding of the compound to an Atlantis Prep C18 (10 μM, 10 × 250 mm) (Waters) column, leading to inefficient isolation and column contamination. The preparative system and mobile phases used were as previously described (Schneider et al., 2020). The resulting sample (referred to as compound **2**) was later used to assist in structure elucidation of compound **1**.

To avoid wear and tear of the preparative HPLC system, attempts were made to isolate **1** using flash chromatography. The dried extract was dissolved in 90% methanol, and 2 g of Diaion HP-20SS (13615, Supelco) was added before removing the solvent under reduced pressure. Flash columns were prepared as previously described (Kristoffersen et al., 2018). The column was equilibrated using 5% methanol, before the dried extract-Diaion HP-20SS mixture was applied to the top of the column (maximum 2 g of extract per round). The fractionation was performed on a Biotage SP4™ system (Biotage) with a flow rate of 12 ml/min and a stepwise gradient from 5 to 100% methanol over 32 min. The following stepwise elution method was used: methanol:water (5:95, 25:75, 50:50, 75:25, 6 min per step, resulting in 12 fractions) followed by methanol (100% over 12 min, resulting in six fractions). The MeOH fractions were analyzed using UHPLC-ESI-HRMS. In the second fraction eluting at 100% MeOH, **1** was the dominating peak and was submitted for NMR and bioactivity analysis. The sample of **1** was therefore produced by pooling the second fraction eluting at 100% MeOH from multiple rounds of flash fractionation and drying the resulting volume under reduced pressure.

Structure Elucidation of 1

The structure of **1** was established by 1D and 2D NMR experiments. NMR spectra were acquired in DMSO-d_6 and methanol-d_3 on a Bruker Avance III HD spectrometer operating at 600 MHz for protons, equipped with an inverse TCI probe cryogenically enhanced for ^1H, ^{13}C, and ^2H. All NMR spectra were acquired at 298 K, in 3-mm solvent matched Shigemi tubes using standard pulse programs for proton, carbon, HSQC, HMBC, HMQC (J = 4–5 Hz), COSY, NOESY, ROESY and 1,1-ADEQUATE experiments with gradient selection and adiabatic versions where applicable. $^1H/^{13}C$ chemical shifts were referenced to the residual solvent peak (δ_H = 2.50 PPM, δ_C = 39.52 PPM for DMSO). All data were acquired and processed using Topspin 3.5pl7 (Bruker Biospin) including the structure elucidation module CMC-se v. 2.5.1. ^{13}C prediction was done using Mestrelabs MestReNova software version 14.2.0-26256 with the Modgraph NMRPredict Desktop. Optical rotation

data were obtained using an AA-10R automatic polarimeter (Optical Activity LTD).

Lulworthinone (**1**): green colored film. $[\alpha]^{20}_{D}$ -120 ± 0.02 (*c* 0.2 DMSO). ^{1}H and ^{13}C NMR spectroscopic data, **Supplementary Table 3**. HRESIMS *m/z* 741.2204 $[M+H]^{+}$ (calculated for $C_{37}H_{41}O_{14}S$, 741.2217).

Minimal Inhibitory Concentration Determination Against Reference Bacteria

The Minimal Inhibitory Concentration (MIC) of **1** against a panel of Gram-positive and Gram-negative reference bacteria was determined by broth microdilution, at final concentrations 0.2–100 μg/ml (twofold dilution series). The experiments were performed with three technical replicates. The panel of reference bacteria consisted of the following strains: *S. aureus* (ATCC 25923), MRSA (ATCC 33591), *Escherichia coli* (ATCC 25922), *Pseudomonas aeruginosa* (ATCC 27853), *Enterococcus faecalis* (ATCC 29212), and *Streptococcus agalactiae* (ATCC 12386), all strains from LGC Standards (Teddington). Briefly, the bacteria were inoculated from freeze stock onto blood agar plates (University Hospital of North Norway) and transferred to liquid medium for overnight incubation at 37°C. *S. aureus*, *E. coli*, and *P. aeruginosa* were grown in Brain Heart Infusion medium (BHI, 53286, Sigma-Aldrich), and *E. faecalis* and *S. agalactiae* were grown in Difco™ Mueller Hinton medium (MH, 275730, BD Biosciences). After overnight incubation in the respective media, the bacteria were brought to exponential growth by addition of fresh media, and incubated to reach a turbidity of 0.5 McFarland standard. The bacteria were diluted in their respective media 1:1,000 prior to addition. Subsequently, the bacteria were added to 96-well microtiter plates at 50 μl/well. A mixture of 50 μl of autoclaved Milli-Q® H_2O and 50 μl fresh autoclaved media was used as negative control, and 50 μl of autoclaved Milli-Q® H_2O was added to 50 μl of bacteria suspension as growth control. The compound was diluted in DMSO and autoclaved Milli-Q® H_2O (highest concentration of DMSO in the assay was 0.5%), and 50 μl was added to the bacterial suspension. Final volume in the wells was 100 μl. The plates were incubated overnight at 37°C. After incubation, growth was measured by absorbance at 600 nm with 1420 Multilabel Counter VICTOR^{3}™ (Perkin Elmer). Assay controls with gentamicin in a dilution series are routinely run, as well as routine counting of CFUs for each bacterium. For the strains where the compound displayed activity, the MIC was determined with three biological replicates each containing three technical replicates (n = 9). The lowest concentration of **1** that completely inhibited the growth of the bacteria was determined as the MIC.

To investigate if **1** had a bacteriocidal or bacteriostatic effect on *S. aureus* and *S. agalactiae*, the compound was inoculated together with the bacteria, as described above, and after overnight incubation, the inoculum was plated onto agar and incubated overnight at 37°C. The experiment was done with 12.5 and 25 μg/ml concentrations of **1** in triplicate, with two biological replicates (n = 6). Inspired by Zheng et al. (2007), we tested **1**, together with reserpine (broad spectrum efflux pump inhibitor) against the Gram-negative reference strains *E. coli* and *P. aeruginosa*. The assay was conducted as described above, with reserpine (L03506, Thermo Fisher Scientific) added to a final concentration of 20 μg/ml.

Minimal Inhibitory Concentration Determination Against Clinical Bacterial Isolates

Initial testing of **1** was conducted against a panel containing clinically relevant antibiotic-resistant bacteria: Gram-positive MRSA, vancomycin-resistant *Enterococcus faecium* (VRE), and Gram-negative bacteria resistant to extended-spectrum beta-lactamases as well as carbapenemases (ESBL-Carba) (detailed information about the clinical isolates can be found in **Supplementary Table 2**). The initial testing was conducted at one concentration, 100 μg/ml.

The final antibacterial testing of **1** was executed using the five clinical MRSA isolates and the VRE isolates (**Supplementary Table 2**). The isolates were tested by broth microdilution according to the Clinical Laboratory Standard Institute (CLSI) (2012) method MO7-A9. In brief, **1** was solubilized with 100% DMSO and diluted with autoclaved Milli-Q® H_2O to prepare a 200 μg/ml working solution. The final DMSO concentration did not exceed 1% to exclude any artificial influence on the assay. The bacterial inoculum was prepared to contain 1×10^{6} CFU/ml in cationic-adjusted BBL™ Mueller-Hinton II broth (BD). The inoculum was mixed in a 1:1 ratio with the working solution of **1** (twofold dilutions, ranging from 0.2 to 100 μg/ml) for a final amount of 5×10^{5} CFU/ml in each well of a 96-well round-bottom polypropylene plate (Greiner Bio-One GmbH). Growth control (without compound) and sterility control (without bacteria) were included for each strain. Each strain was tested in three independent biological replicates with four technical replicates on consecutive days. As quality assurance for the assay, the protocol was also performed with *E. coli* ATCC 25922 using Gentamicin (Merck Life Science) as a reference antibiotic. The 96-well plates were incubated at 37°C for 24 h without shaking. The MIC values were defined as the lowest concentration of **1** resulting in no visual bacterial growth, determined by visual inspection and 600 nm absorbance measurements with CLARIOstar plate reader (BMG LABTECH).

Inhibition of Biofilm Production and Eradication of Established Biofilm

Inhibition of biofilm production by **1** of *Staphylococcus epidermidis* (ATCC 35984, LGC Standards) was determined at final concentrations 0.2–100 μg/ml (twofold dilution series). Briefly, the bacteria were inoculated from freeze stock onto blood agar plates (University Hospital of North Norway) and transferred to tryptic soy broth (TSB, 22092, Sigma-Aldrich) for overnight incubation at 37°C. The overnight cultures were subsequently diluted 1:100 in fresh TSB with 1% glucose and added to 96-well microtiter plates, 50 μl/well. Positive control was *S. epidermidis* in fresh media with glucose, and negative control was a non-biofilm producing *Staphylococcus haemolyticus* (clinical isolate 8-7A, University Hospital of North Norway) in

fresh media with glucose. The compound was diluted in DMSO and autoclaved Milli-Q® H_2O (highest concentration of DMSO in the assay was 0.5%), and 50 μl was added to the bacterial suspension. Final volume in the wells was 100 μl. The plates were incubated at 37°C overnight. Growth inhibition of the bacterium was determined by visual inspection of the plates prior to further treatment. The bacterial suspension was poured out and the biofilm was fixated by heat, before adding 70 μl of 0.1% crystal violet solution (V5265, Sigma-Aldrich) and staining for 5 min. The crystal violet solution was removed and the wells were washed with water before the plates were dried by heat. The bound crystal violet was dissolved in 70 μl of 70% ethanol, and the presence of violet color, indicating biofilm formation, was measured at 600 nm absorbance using a 1420 Multilabel Counter VICTOR^{3TM} reader. Percent biofilm formation was calculated using the equation below. The data were visualized using GraphPad Prism 8.4.2, and the built-in ROUT method was used to detect and remove outliers from the dataset (Q = 1%).

$$\text{Percent (\%) biofilm formation} = \frac{(\text{absorbance treated wells} - \text{absorbance negative control})}{(\text{absorbance positive control} - \text{absorbance negative control})} \times 100 \quad (1)$$

To determine whether **1** could eradicate biofilm established by *S. epidermidis*, a modified biofilm inhibition assay protocol was performed. Here, the bacteria were grown overnight in a microtiter plate to allow the biofilm to be established prior to the addition of **1**. After addition of **1**, the plates are incubated overnight. Following this, the biofilm was fixated and colored and results were read as stated above. The experiment was conducted once with three technical replicates with concentrations of 0.2–100 μg/ml (twofold dilution series).

Determination of Antiproliferative Activity Toward Human Cell Lines

The antiproliferative activities of **1** was evaluated against the melanoma cell line A2058 (ATCC, CRL-11147^{TM}), the hepatocellular carcinoma cell line HepG2 (ATCC, HB-8065^{TM}), and the non-malignant lung fibroblast cell line MRC5 (ATCC, CCL-171^{TM}) in a MTS *in vitro* cell proliferation assay. The compound was tested in concentrations from 6.3 to 100 μg/ml against all cell lines, with three biological replicates each containing three technical replicates (n = 9). A2058 was cultured and assayed in Dulbecco's Modified Eagle's Medium (D-MEM, D6171, Sigma-Aldrich). HepG2 was cultured and assayed in MEM Earle's (F0325, Biochrom) supplemented with 5 ml of non-essential amino acids (K0293, Biochrom) and 1 mM sodium pyruvate (L0473, Biochrom). MRC5 was cultured and assayed in MEM Eagle (M7278, Sigma-Aldrich) supplemented with 5 ml of non-essential amino acids, 1 mM sodium pyruvate, and 0.15% (w/v) sodium bicarbonate (L1713, Biochrom). In addition, all media were supplemented with 10% fetal bovine serum (FBS, S1810, Biowest), 10 μg/ml gentamicin (A2712, Biochrom), and 5 ml of glutamine stable (200 mM per 500 ml medium, X0551, Biowest). Briefly, the cells were seeded in 96-well microtiter plates (Nunclon Delta Surface, VWR) at 2,000 cells/well for A2058, 4,000 cells/well for MRC5, and 20,000 cells/well for HepG2. After incubation for 24 h in 5% CO_2 at 37°C, the media was replaced and compound was added, generating a total volume of 100 μl/well. A2058 and MRC5 were incubated for 72 h before assaying, and HepG2 for 24 h. Subsequently, 10 μl of CellTiter 96 AQueous One Solution Reagent (G358B, Promega) was added to each well and the plates were incubated for 1 h at 37°C. Following this, the absorbance was measured at 485 nm with a DTX 880 multimode detector (Beckman Coulter). Negative controls were cells assayed with their respective cell media, and positive controls were cells treated with 10% DMSO (D4540, Sigma-Aldrich). Percent cell survival was calculated using the equation below. The data were visualized using GraphPad Prism 8.4.2 and IC_{50} was calculated. The built-in ROUT method was used to detect and remove outliers from the dataset (Q = 1%).

$$\text{Percent (\%) cell survival} : \frac{(\text{absorbance treated wells} - \text{absorbance positive control})}{(\text{absorbance negative control} - \text{absorbance positive control})} \times 100 \quad (2)$$

Minimal Inhibitory Concentration Determination Against *Candida albicans*

The MIC of **1** was determined by broth microdilution against *C. albicans* (ATCC 90028, LGC Standards), at final concentrations of 0.2–100 μg/ml (twofold dilution series). The experiment was performed as one biological replicate, with three technical replicates (n = 3). Briefly, the fungus was inoculated from freeze stock onto potato dextrose agar [24 g/L potato dextrose broth (P6685, Sigma-Aldrich), 15 g/L agar (A1296, Sigma-Aldrich)] and incubated overnight at 37°C. From the overnight culture, five to eight colonies were transferred to 5 ml of sterile 0.9% NaCl, before the cell density was adjusted to 1–5 × 10^6 cells/ml by adding 0.9% NaCl. The cell density was evaluated with 0.5 McFarland standard (Remel 0.5 McFarland Equivalence Turbidity Standard, 10026732, Thermo Fisher Scientific). The fungal suspension was further diluted 1:50, and then 1:20 (1–5 × 10^3 CFU/ml) in RPMI medium (R7755, Sigma-Aldrich) with 0.165 mol/L MOPS (M3183, Sigma-Aldrich) and 10.25 ml of L-glutamine. The compound was added to the microtiter plate together with the fungal suspension (1:1), to a final volume of 200 μl. The final concentration of fungal cells was 0.5–2.5 × 10^3 CFU/ml. Absorbance in the wells was measured with 1420 Multilabel Counter VICTOR^{3TM} right after addition of compound, after 24 h and after 48 h. The plates were incubated at 37°C. Amphotericin B was used as negative control at final concentration 8 μg/ml. Growth control contained fungal suspension and autoclaved Milli-Q® H_2O.

RESULTS

Systematic Placement of the Fungal Isolate 067bN1.2

Due to lack of distinct morphological characters of the cultured asexual morph and closely related reference sequences

in GenBank, the fungus is identified to family level, as Lulworthiaceae sp., for the purpose of this study. A phylogenetic study was carried out with 28 taxa (including outgroups and isolate 067bN1.2), all representing different species, as shown in **Figure 1**. The combined dataset of 5.8S, SSU, and LSU had an aligned length of 2,270 characters, and phylogenetic inference was estimated using both Maximum Likelihood and Bayesian Inference criteria. The isolate producing **1**, 067bN1.2, was placed on its own branch within the Lulworthiaceae, forming a sister clade to the clade including *Halazoon fuscus*, *Lulworthia medusa*, *Lulworthia* cf. *purpurea* and *Halazoon melhae*. Sequences of *Koralionastes ellipticus* were included to exclude the possibility that the isolate 067bN1.2 is part of the family Koralionastetaceae. *Koralionastes ellipticus* was placed outside of Lulworthiaceae.

Isolation and Structure Elucidation

Compound **1** was selected for isolation due to its antibacterial activity in an initial screen of fractions from several understudied marine fungi. Compound **1** was the dominating peak in the active fraction from fungal isolate 067bN1.2 Lulworthiaceae sp., and subsequently the fungus was re-cultivated, cultures were extracted, and the compound was isolated using RP flash chromatography. The extraction of 1.4 L of fungal culture yielded 1,017.2 mg of extract.

Initially, attempts were made to isolate the compound using preparative HPLC. This strategy had several drawbacks, including unfavorable behavior of the compound in the preparative column. This resulted in the compound eluting over several minutes (band broadening) and carryover. A batch of the compound was, however, retrieved using this strategy, resulting in a compound later determined to be a structural isomer and artifact of compound **1** (referred to as **2** throughout this article), produced due to the acidic conditions in the mobile phase. The structures of **1** and **2** can be seen in **Figure 2**.

Flash chromatography was better suited for the isolation of **1**. This isolation strategy yielded 63.8 mg of **1**, corresponding to a yield of ∼45 mg/L culture medium. Compound **1** was obtained as a green colored substance. The molecular formula was calculated to be $C_{37}H_{40}O_{14}S$ by UHPLC-ESI-HRMS (*m/z* 741.2204 $[M+H]^+$) (calculated as $C_{37}H_{41}O_{14}S$, 741.2217), suggesting 18 degrees of unsaturation. The low-energy collision mass spectrum of **1** can be seen in **Supplementary Figure 2**. MS signals of a neutral loss of 80 Da (ESI+) was observed, indicating the presence of a sulfate group in the structure. The UV absorption maxima were 224, 260, and 373 nm, which corresponded well with the previously published dinapinones (Kawaguchi et al., 2013). The UV-vis spectrum for **1** can be seen in **Supplementary Figure 3**. The IR spectrum of **1** displayed absorption bands for sulfoxide (S=O, 1,002 cm^{-1}), aromatic alkene (C=C, 1542 and 1,618 cm^{-1}), carbonyl (C=O, 1,645 cm^{-1}), alkane (C-H, 2,857 cm^{-1}), aromatic alkene (C-H, 2926 cm^{-1}), and hydroxyl (C-OH, 3455 cm^{-1}) bonds. After isolation, the structure of **1** (**Figure 2**) was elucidated by 1D and 2D NMR experiments (**Supplementary Figures 4–16**).

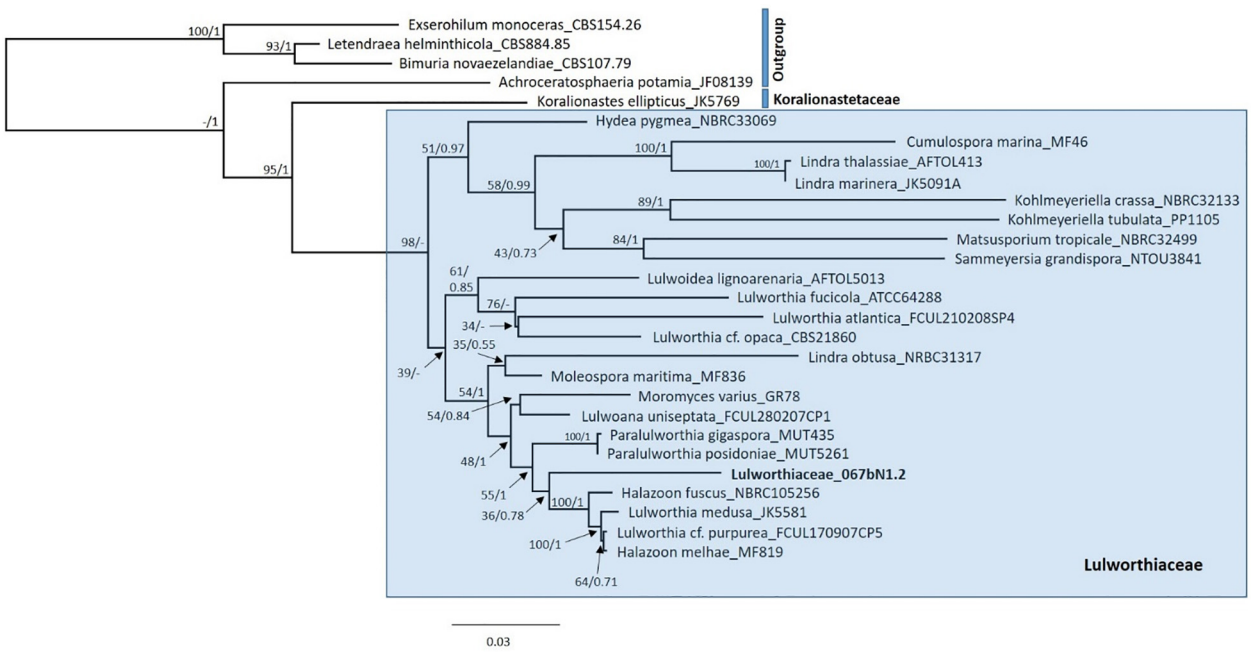

FIGURE 1 | Maximum Likelihood tree (RAxML) from the combined analysis of 5.8S, SSU, and LSU from isolates of Lulworthiaceae. One isolate from Koralionastetaceae was included, and four strains as outgroups. Node support is given as Bootstrap support values at the nodes, and posterior probabilities are included where the branching was alike (BS/PP). The isolate under investigation, Lulwortihaceae_067bN1.2, is highlighted in bold. Due to topological similarity only the ML tree is shown here containing both Bayesian posterior probabilities and Bootstrap support values. Bayesian Inference tree can be found in **Supplementary Figure 1**. – indicates that the node is missing in the Bayesian analysis. No support value is given to the node separating the outgroup taxa from the ingroup in ML analysis.

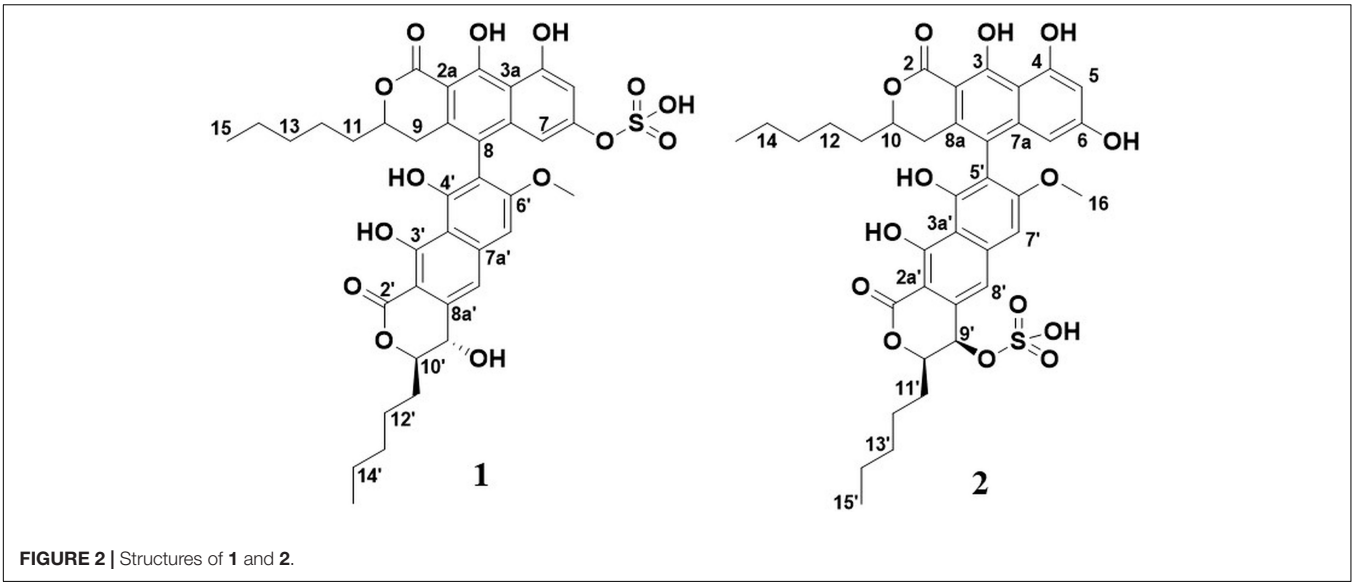

FIGURE 2 | Structures of **1** and **2**.

Initial structure elucidation was made on the sample isolated by preparative HPLC with formic acid present in the mobile phases (compound **2**). The established molecular formula suggested a highly conjugated system. The purity of **2** was estimated to be ∼80% from a quantitative proton spectrum with respect to non-solvent impurities (**Supplementary Figure 4**). Four singlet protons were identified in the aromatic region, along with three O-CH signals at ∼4.5 ppm with complex couplings along with a methoxy singlet at 3.77 ppm. Furthermore, five hydroxyl protons were identified; three between 9.5 and 10.0 ppm, and two between 13.5 and 14.0 ppm. The deshielded nature of the latter sets them apart from the other hydroxyls and suggests they may be involved in an angled intramolecular hydrogen bond, which is commonly seen for keto-enol pair configurations such as this. All 37 carbons could be identified by 1D ^{13}C NMR (**Supplementary Figure 5**), which showed **2** to contain a large number of aromatic quaternary carbons, two ester-like carbonyls, along with 10 peaks in the aliphatic region (**Table 1**).

HSQC, HMBC, and 1,1-ADEQUATE spectra (**Supplementary Figures 6, 7**) allowed the identification of two substituted napthopyrone-like moieties, as well as two five-membered aliphatic chains (denoted *C15-C11* and *C15'-C11'*, respectively), which were fully assigned using a combination of HSQC-TOCSY, TOCSY, COSY, and HMBC (**Figure 3**i). The aliphatic chains were determined to be attached at the *C10* position of the napthopyrone-like moieties by tracing the spin system into *H9* and *H9'*, respectively, and supported by multiple long-range ^{1}H-^{13}C correlations. The *C2* and *C2'* carbonyls could be directly assigned from long-range couplings from the *10*/*10'* position, but the hydroxyl carrying carbons in positions *3/3'* and *4/4'* could only be assigned through weak $^{4}J_{CH}$ correlations from the aromatic protons (**Figure 3**iii).

The *OH-4* and *OH-6* could be assigned based on NOE correlations between *OH-6* and both *H5* and *H7*, while *OH-4* only displayed correlations with *H5*. The *OH-3* and *OH-3'* are predicted to have more deshielded chemical shifts due to their proximity to the carbonyl moiety and a probable intramolecular hydrogen bond—however, it was not possible to individually distinguish *OH3* and *OH-3'* due to the absence of any correlations in NOESY, ROESY, and HMBC spectra. Thus, four fragments could initially be elucidated (**Figure 3**i). A weak $^{4}J_{C8H7'}$ correlation could be detected, linking fragment ***A*** to fragment ***B*** (**Figure 3**i) at the *C8* and *C5'* positions, respectively, and thus the only remaining ambiguity is the position of the -SO^{3-} group vis-à-vis the remaining -OH in the 9' or 4' positions. The absence of NOEs and COSY correlations between *OH-4'* and *H9'* suggests that it is positioned at *C4'* with the sulfate positioned at *C9'* (**Figure 3**ii). The $^{3}J_{HH}$ coupling constant between *H9'* and *H10'* was measured to be 2.0 Hz from line shape fitting the splitting of H9', indicating that these protons are at a significantly offset dihedral angle to one another—thus suggesting a relative R/S or S/R configuration of 9' and 10'. ^{13}C prediction was consistent with the structure of **2** (**Supplementary Figure 9**), with a mean error of 2.79 ppm between the observed and predicted ^{13}C shifts.

A second isolation where no acidic conditions were used, yielding **1**, was also examined. ^{1}H NMR revealed significantly perturbed chemical shifts as well as line broadening and heterogeneity throughout the spectra (**Supplementary Figure 11**). Multiple resonances in the carbon spectrum (**Supplementary Figures 12, 13**), especially for two resonances in the carbonyl area (presumably C3 and C3'), are heterogenous, reflecting the nuclei existing in several stable, but slightly different micro environments. The same observation is made in the proton spectrum (**Supplementary Figure 11**) for H9', OMe-6', H5, H7, 4'-OH, and 4-OH. A major difference was observed in the non-acidic preparation (**1**), compared to **2**, the presence of a 9'-OH. At ∼15 ppm, two heterogeneous OH protons were observed, deshielded by approximately 1 ppm compared to the OH-3's in the original sample preparation, while the three hydroxyls at ∼10 ppm could no longer be detected (**Supplementary Figures 8–13**). Thus, the detectable aromatic hydroxyl groups, identified as OH-4' and OH-4,

TABLE 1 | Summary of chemical shift and correlations for **2** (DMSO-d_6).

Position	δ^{13}C, type	δ^{1}H, splitting (Hz)	COSY	HMBC (^{1}H → ^{13}C)
2	171.6, C	–	–	–
2'	171.0, C	–	–	–
2a'	99.4, C	–	–	–
2a	99.2, C	–	–	–
3	162.5, C	–	–	–
3'	161.5, C	–	–	–
3a'	108.6, C	–	–	–
3a	107.5, C	–	–	–
4	159.0, C	–	–	–
4'	154.9, C	–	–	–
5'	111.7, C	–	–	–
5	102.1, CH	6.35, s	–	3, 3a, 4, 6, 7
6	161.2, C	–	–	–
6'	160.7, C	–	–	–
7a	140.6, C	–	–	–
7a'	140.1, C	–	–	–
7	100.7, CH	6.04, s	–	3, 3a, 5, 6, 8
7'	99.7, CH	7.14, s	–	3', 3a', 4', 5', 6', 8, 8'
8a'	137.4, C	–	–	–
8a	132.9, C	–	–	–
8	118.7, C	–	–	–
8'	117.5, CH	7.36, s	–	2', 3a', 4', 6', 7'a, 7', 9'
9'	65.3, CH	4.69, d (J = 2.0)	–	2a', 8', 8a', 10', 11'
9	31.0, CH2	2.59, m	10	2a, 7a, 8, 8a, 10, 11
10'	83.2, CH	4.62, ddd (J = 7.9, 6.0, 2.0)	11'	2', 8a', 9', 11', 12'
10	79.4, CH	4.56, dddd (J = 9.6, 7.4, 5.5, 4.1)	9, 11	2, 8a, 12
11	34.2, CH2	1.59, dd (J = 16.7, 9.5) 1.68, dd (J = 16.5, 4.0)	10, 12	10, 12
11'	30.0, CH2	1.85, m	10', 12'	9', 10', 12', 13'
12'	24.7, CH2	1.48, 1.52, m	11', 13'	11', 13', 14'
12	24.5, CH2	1.27, 1.36, m	11, 13	11, 13, 14
13'	31.3, CH2	1.23, m	12', 14'	11', 12', 14', 15'
13	31.6, CH2	1.36, m	12, 14	11, 12, 14, 15
14'	22.5, CH2	1.36, m	13', 15'	12', 13', 15'
14	22.4, CH2	1.24, m	15	12, 13, 15
15'	14.4, CH3	0.92, m	14'	13', 14'
15	14.3, CH3	0.82, m	14	13, 14
16	56.5, O-CH3	3.77, s	–	6'
OH3*	–	13.71, s		
OH3*	–	13.62, s		
OH4	–	9.80, s		
OH4'	–	9.51, s		
OH6	–	9.94, s		

**Ambiguous assignment.*

appeared to be involved in (stronger) hydrogen bonding, while three aromatic hydroxyls, the remaining OH-6, OH-3' and OH-3, were unaccounted for. At the same time, the majority of all other nuclei in the molecule are shielded by approximately 0.5 ppm. Together, these observations suggest that the neutral pH preparation resulted in a different molecule, **1**, that formed loose aggregates in DMSO and methanol, stabilized by both hydrogen bonding (deshielding) and stacking (shielding) interactions. Overall, worse spectral quality resulted in that the C2 and C3 from **2** could not be individually assigned in **1**, although they must correspond to the two chemical shifts of 169.4 and 173 ppm by the logic of elimination. A number of the carbons show heterogenic peaks (notably the presumed C3 and C3'), most likely as the result of through space proximity to the sulfate group and sensitivity to its different possible conformation (details in section "Discussion").

The identity of **1** was established to be identical to **2** with the only difference being that the sulfate group was attached to C6 instead of C9', supported by the loss of the OH correlating with H5 and H7, and the appearance of an OH

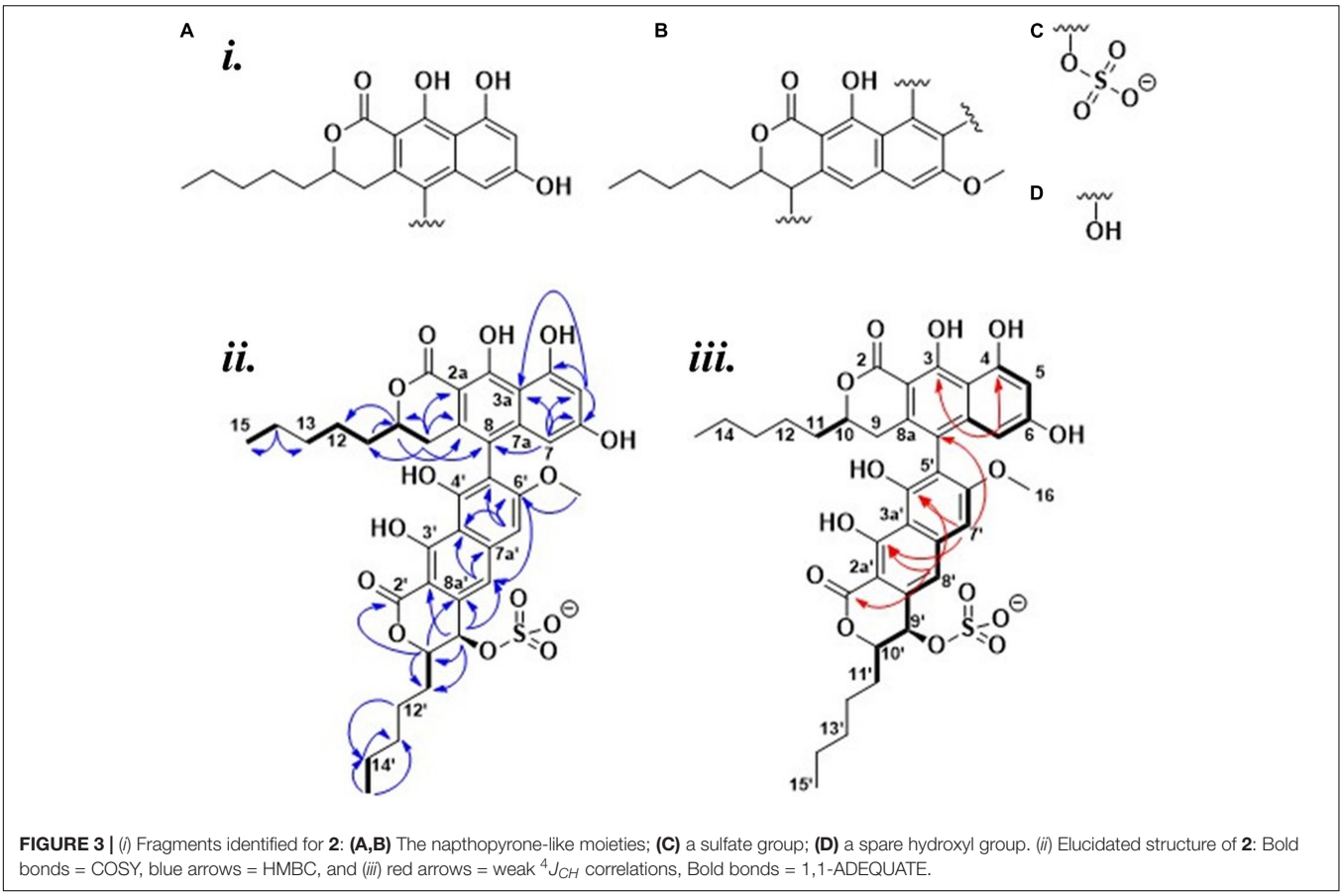

FIGURE 3 | (*i*) Fragments identified for **2**: **(A,B)** The napthopyrone-like moieties; **(C)** a sulfate group; **(D)** a spare hydroxyl group. (*ii*) Elucidated structure of **2**: Bold bonds = COSY, blue arrows = HMBC, and (*iii*) red arrows = weak $^4J_{CH}$ correlations, Bold bonds = 1,1-ADEQUATE.

correlating with H9' through a $^3J_{HH}$. There is furthermore a heterogeneity and chemical shift perturbation hotspot (vis-à-vis **2**) around the C6 position to support the assignment of a C6 sulfate. All chemical shifts and correlations are summarized in **Supplementary Table 3**. The data do not unambiguously prove whether the 3-OH's are deprotonated or if the signal is lost due to rapid exchange, but the fact that the OH-9' is observable under the same conditions is an indicium for the OH-3's to be deprotonated in **1**. No plausible resonance structures to explain the deprotonation and deshielding that does not involve the oxidation, and thus change in mass, have been found.

The non-aggregated **2** could be scavenged by lowering the pH of **1** with the addition of hydrochloric acid, upon which ^{1}H and HSQC spectra of the two samples of **2** show a great resemblance (**Supplementary Figure 10**). The molecular formula of **2** and **1** as well as the scavenged **2** were identical in the two preparations, as no change in mass was observed by high-resolution mass spectrometry.

Antibacterial Activity Against Reference and Clinical Strains

Compound **1** was tested against six reference bacteria (four Gram-positive and two Gram-negative strains). The compound was active against two of the Gram-positive reference strains, *S. aureus* and *S. agalactiae*, with MIC values of 6.25 and 12.5 μg/ml, respectively. No activity was observed against the Gram-negative strains, *E. coli* and *P. aeruginosa*, or the Gram-positive *E. faecalis* or MRSA strain (**Supplementary Table 4**). As bacterial resistance toward available antibiotics is the main challenge in future treatment of pathogenic diseases, **1** was tested against a panel of drug-resistant clinical strains (**Supplementary Table 2**). The panel included five MRSA and six VRE strains. Compound **1** was also tested in a pre-screen against four Gram-negative clinical bacterial strains: *E. coli*, *Klebsiella pneumoniae*, *Acinetobacter baumanii*, and *P. aeruginosa* (all ESBL-Carba). No activity was detected against the Gram-negative bacteria (**Supplementary Table 4**). Compound **1** showed activity against the MRSA strains with MICs in the 1.56–6.25 μg/ml (2.12–8.44 μM) range, see **Table 2**. The activity of the compound was significantly less profound against the VRE strains (MIC = 50 μg/ml or higher) (**Supplementary Table 4**).

To investigate if **1** has bacteriostatic or bacteriocidal effects on the two reference strains *S. aureus* and *S. agalactiae*, both were incubated with the compound at 12.5 and 25 μg/ml overnight and subsequently plated onto agar. For *S. aureus*, there was no growth on the plates after overnight incubation, indicating a bacteriocidal effect of **1**. For *S. agalactiae*, one of the parallels at 12.5 μg/ml (MIC of **1** against this bacterium) displayed growth on the agar plate, which was expected as visual growth could also be seen in the microtiter plate for this parallel. The remaining five parallels at this concentration, and the concentration above,

had no growth in the microtiter plates, or on agar after overnight incubation. This strongly indicates that **1** also has bacteriocidal effect on *S. agalactiae*. Compound **1** was also tested together with the efflux pump inhibitor reserpine to see if the lack of activity toward Gram-negative strains was caused by efflux of **1**, but no activity was obtained.

Inhibition of Biofilm Production and Eradication of Established Biofilm

The ability of **1** to inhibit biofilm production by *S. epidermidis* and to remove established *S. epidermidis* biofilm was assessed. In the biofilm inhibition assay, the biofilm production was completely inhibited (below 5% biofilm formation) down to 12.5 μg/ml (**Figure 4**). Clear inhibition of the bacterial growth could also be observed to 25 μg/ml by visual inspection of plates before fixation of biofilm, raising the question if the biofilm inhibition is mainly caused by growth inhibition of the bacterium. To further evaluate the potential biofilm activity, removal of established biofilm was assessed. There was no activity of **1** at concentrations up to 100 μg/ml against the established biofilm, further supporting the hypothesis that the biofilm inhibition is mainly due to growth inhibition of the bacterium.

TABLE 2 | Minimal inhibitory concentrations (MICs) of **1** against reference strains and clinical isolates.

Strain type	Strain	MIC in μg/ml
Clinical strains	*S. aureus* N315	1.56
	S. aureus 85/2082	3.13
	S. aureus NCTC 10442	3.13
	S. aureus WIS [WBG8318]	6.25
	S. aureus IHT 99040	3.13
Reference strains	*S. aureus* ATCC® 25923	6.25
	S. agalactiae ATCC® 12386	12.5

The median MIC values are reported (n = 12 for clinical isolates, n = 9 for reference strains).

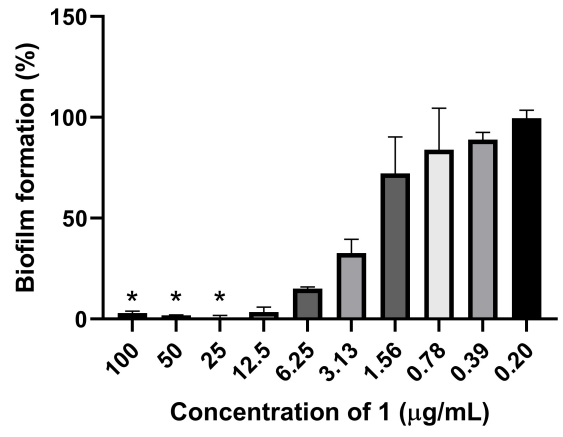

FIGURE 4 | Inhibition of bacterial biofilm formation by **1** against the biofilm producing *S. epidermidis*. *The bacterial growth was completely inhibited at compound concentrations down to 25 μg/ml.

Antiproliferative Activity Against Human Cells and Antifungal Activity

The antiproliferative activities of **1** was assessed against human melanoma cells (A2058), human non-malignant lung fibroblasts (MRC5), and human hepatocellular carcinoma cells (HepG2), in a concentration range of 6.25–100 μg/ml. The non-malignant cell line was included as a test for general toxicity, while the other cell line was included to assess possible anti-cancer activities. Antiproliferative activity was observed against all cell lines, with IC_{50} values of 15.5, 32, and 27 μg/ml against A2058, MRC5, and HepG2, respectively (**Table 3**). Compound **1** was also assayed for antifungal activity against *C. albicans* at concentrations up to 100 μg/ml, and no activity was seen.

DISCUSSION

In this study, we describe the discovery, isolation, and characterization of the new secondary metabolite lulworthinone (**1**). This novel antibacterial compound was isolated from an extract of a slow-growing marine fungus of the family Lulworthiaceae. To the best of our knowledge, this is the first reported secondary metabolite isolated from this fungal family and the order Lulworthiales. Since the isolate did not branch close to the *Lulworthia* type species, *L. fucicola* (in the *Lulworthia sensu stricto* clade) and there was a lack of support at many nodes of the phylogenetic tree, we restrained from identifying the isolate 067bN1.2 to genus and determine its identity to family level only.

A fraction of the Lulworthiaceae sp. extract was nominated for chemical investigation as it was active in an initial antibacterial screen. The content of the active Lulworthiaceae sp. fraction was dominated by **1**, whose calculated elemental composition gave no hits in database searches, indicating that the compound suspected to be responsible for the observed antibacterial activity, was novel. In the attempt to utilize preparative HPLC to isolate this compound, **2** was generated during the procedure (acidic mobile phase). As compounds **1** and **2** have the same mass, HRMS analysis did not detect the change in the positioning of the sulfate group, and the sample from the preparative HPLC isolation was characterized using NMR, believing it was **1**. As preparative HPLC was deemed inconvenient for compound isolation, flash chromatography (neutral mobile phase) was utilized to isolate sufficient amounts of **1** to conduct a thorough characterization of the compound's bioactivity. This method allows larger amounts of sample to be processed per run, but generally is less effective in separating compounds of interest from sample impurities, compared to preparative HPLC isolation. However, due to the high concentration of **1** in the extract, **1** was successfully isolated using this method. The resulting sample was submitted

TABLE 3 | Antiproliferative activity (IC_{50}) of **1** against human cell lines (*n* = 9).

Cell type	IC_{50} in μg/ml
A2058, melanoma	15.5 ± 0.6
MRC5, normal lung fibroblasts	32 ± 1
HepG2, hepatocellular carcinoma	27 ± 1

to NMR analysis to confirm its structure. The samples from both isolations were confirmed to be novel biarylic dimeric naphtho-α-pyrones substituted with a sulfate group. However, NMR analysis revealed that the sulfate group was located on different positions in the two compounds. The rearrangement was hypothesized to be catalyzed by the acidic nature of the HPLC mobile phase. This hypothesis was confirmed by subjecting **1** to acidic conditions (**Supplementary Figure 10**). The resulting sample was analyzed using NMR, confirming that **1** had indeed converted into **2**. As **2** was proven to be an artifact of **1**, all bioactivity testing was conducted using **1** isolated under neutral conditions.

The propensity of **1** to interact with itself to form higher-ordered structures, while **2** did not, offered some insight into their structural behavior in solution. In particular, the sulfate in the 6-position appeared to facilitate oligomeric aggregation, and a simple 3D model allows some speculation as to why this could be (**Figure 5**). The ground state of the naphthopyrone does not have the ability to form complementary "base pairs" with itself through hydrogen bonds between the carbonyls and hydroxyls. However, when the sulfate is in the 6-position, it can reach the C3 double OH "mismatch" in the three-dimensional structure and potentially stabilize the hydroxyls either by 4-coordnating a water molecule or a Na^+ ion together with deprotonated 3'-hydroxyls, or by directly hydrogen bonding to the protonated hydroxyls. This would provide a feasible rationale for the propensity for aggregation of **1** but not of **2**. The structural dimer model also provides a plausible explanation as to why the sulfate group would specifically and irreversibly migrate to C9' under acidic conditions even though the C9' is expected to be a less likely position for the sulfate than any other phenol position. The sulfate is in an oligomeric state involving this kind of "base pairing" positioned to be intermolecularly attacked by the OH-9' of the paired molecule, which is not possible in the monomeric state. Lowered pH is expected to ensure protonated sulfate, which would make it more susceptible for an electrophilic attack from OH-9'. If oligomeric states are indeed stabilized by the coordination of water or sodium, then lowered pH and the protonation of the 3- and 3'-oxygens would further destabilize the oligomer, which together with the lack of stabilization from the position 6 sulfate would make both the association and the reaction irreversible and trap the sulfate in the 9' position of monomeric **2** with lowered ability to self-aggregate.

Lulworthia spp. fungi have spores with end chambers containing mucus, which helps in spore attachment to surfaces (Jones, 1994). It has been observed that in liquid culture of the isolate 067bN1.2, the fungus forms a gel-like mucus, having the ability to adhere to the bottom of the culture flasks. No spores are formed in culture, and it remains unclear whether the mucus formed under cultivation of 067bN1.2 has chemical resemblance

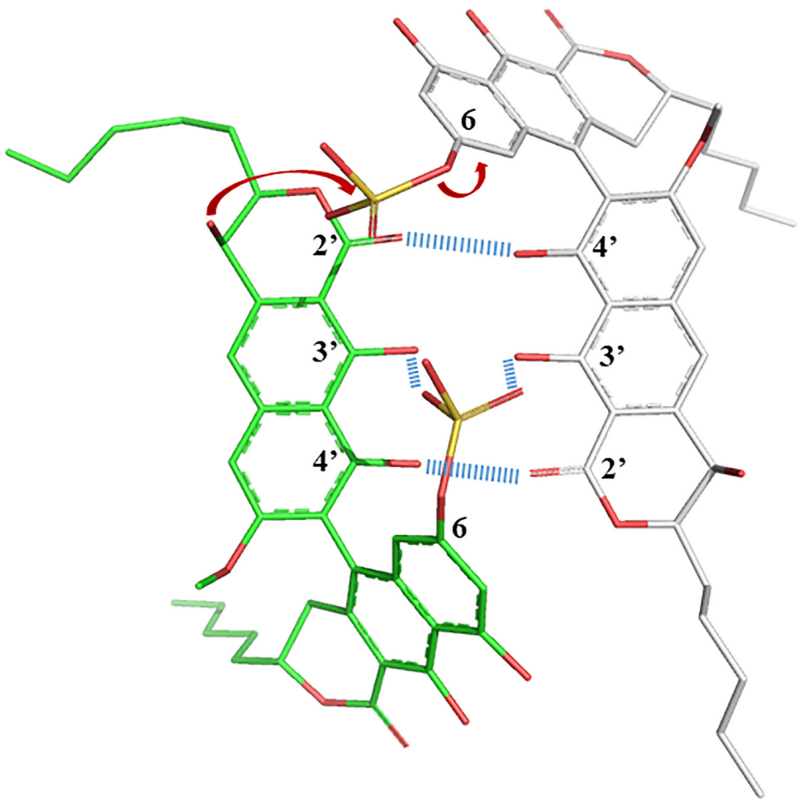

FIGURE 5 | Crude sculpted and minimized structural model of **1** displaying the sulfate potential role in stabilizing oligomerization, as well as the possibility to intermolecularly react specifically at the C-9' position to form **2** under acidic conditions.

to the mucus in end chambers of *Lulworthia* spp. spores, as it has not yet been characterized. The sheathing of mucoid by *L. medusa* has been reported in a publication from 1973, where the fungus was found and isolated from a piece of submerged pine and cultivated in bottles in media supplemented with artificial seawater (Davidson, 1973). Also in the current study, the fungus was found to adhere to the culture flask during cultivation in artificial seawater media. Davidson hypothesizes around the physiological and ecological implications of the mucoid, important in cation binding and transport, for the adhesion of other microorganisms, avoiding desiccation in intertidal regions or for the production of a matrix to concentrate exoenzymes (Davidson, 1973). Compound **1** is isolated in high yields from the fungal culture, but the ecological role of naphthopyrone-type compounds is largely unclear. The antibacterial activity of **1**, however, could indicate a protective role against pathogenic attacks, but the compound may have other types of bioactivities as well. It has been speculated that similar compounds (bis-naphthopyrones) from filamentous ascomycetes were produced to protect the fungus from predators (Xu et al., 2019). The study found that several animal predators, like woodlice, preferred feeding on fungi that had disrupted aurofusarin synthesis, and also that predation stimulated the production of aurofusarin in several *Fusarium* species (Xu et al., 2019). We have also observed marine mites feeding on fruitbody contents of Lulworthiales fungi. It is thus possible that in the natural habitat of these fungi, the naphthopyrones are produced as a means of protection.

Compound **1** was found to be a dimeric biarylic naphtho-α-pyrone substituted with a sulfate group. The naphthopyrone moiety is recurring in nature, as monomers, dimers, and trimers, and has been found from several natural sources, like plants and filamentous fungi. Naphthopyrones have also previously been isolated from organisms from the marine environment (Li et al., 2016). Compounds from this class have shown different bioactivities, among these the inhibition of triacylglycerol synthesis (Kawaguchi et al., 2013), inhibition of enzymatic activity (Zheng et al., 2007), protection against animal predators (Xu et al., 2019), antimalarial activities (Isaka et al., 2010), and antiproliferative activities (Isaka et al., 2010; Li et al., 2016). Several of these compounds have displayed antibacterial activities against Gram-positive bacteria (Suzuki et al., 1992; Wang et al., 2003; Zheng et al., 2007; Boudesocque-Delaye et al., 2015; Rivera-Chavez et al., 2019). Lu et al. (2014) defined three groups of bis-naphtho-γ-pyrones based on the diaryl bond connection between the monomers, the chaetochromin-, asperpyrone-, and nigerone-type bis-naphtho-γ-pyrones. Based on this categorization, **1** would be categorized as an asperpyrone-type bis-naphtho-α-pyrone, due to the relative placement of the oxygen atoms in the pyrone moieties. Compound **1** is substituted with a sulfate group. One of the most abundant elements in seawater is sulfur, and many sulfated compounds have been isolated from marine organisms, mostly from marine invertebrates, but also from microorganisms (Kornprobst et al., 1998; Francisca et al., 2018). Compound **1** represents, however, the first report of a dimeric naphtho-α-pyrone substituted with a sulfate group.

In the current study, **1** was broadly assessed for potential bioactivities: antibacterial activities against bacterial reference strains and clinical strains, antiproliferative activities toward a selection of human cell lines, both malignant and non-malignant, anti-fungal activity, inhibition of bacterial biofilm formation, and the eradication of established bacterial biofilm. Intriguingly, **1** showed activity against multidrug-resistant MRSA strains with MICs between 1.56 and 6.25 μg/ml (2.12–8.44 μM). In comparison, a natural product originally isolated from *Clitophilus scyphoides* (organism name at time of isolation: *Pleurotus mutilus*, Basidiomycota) pleuromutilin showed MICs in a similar range against selected reference strains (e.g., MIC = 0.66 μM against *S. aureus*, MIC = 2.64 μM against *K. pneumoniae*, and MIC = 21.13 μM against *B. subtilis*) while having significantly higher MIC values against other reference strains (e.g., MIC ≥ 100 μM against *P. aeruginosa*) (Kavanagh et al., 1951). An optimized analog of pleuromutilin, lefamulin (Xenleta®), was approved as an antibiotic drug by the US Food and Drug Administration in 2019. The herein reported MIC values thus place **1** in an activity segment, which makes it an interesting candidate for further development toward becoming a marketed antibiotic drug. In comparison to other antibacterial napthopyrones, **1** falls within the same MIC range with regard to activity toward Gram-positive bacteria. Two heterodimers, isolated from the tubers of *Pyrenacantha kaurabassana*, showed antibacterial activity against different strains of *S. aureus* with MICs in the range of 2.7–89.9 μM (Boudesocque-Delaye et al., 2015). In a recent paper from 2019, mycopyranone, a new binaphthopyranone, was isolated from the fermentation broth of *Phialemoniopsis*. The compound showed antibacterial activity against both *S. aureus* and a MRSA strain, with MICs of ≤8.7 μM against both strains (Rivera-Chavez et al., 2019). Possibly the most known naphthopyrone, viriditoxin showed MICs in the 4–8 μg/ml range against different *Staphylococcus* isolates (Wang et al., 2003).

Furthermore, the lack of activity against the Gram-negative reference and clinical strains shows the selectivity of **1** against Gram-positive bacteria. Yet, no activity or weak activity was observed against the clinical VRE isolates and the reference strain of *E. faecalis*, indicating that the activity is selective toward groups of Gram-positives, in this case *S. aureus* and *S. agalactiae*. Surprisingly, no activity was observed against the reference MRSA strain, and the reason behind this is not clear. No activity was observed for the combination of **1** and the efflux pump inhibitor reserpine, indicating that the lack of susceptibility by Gram-negatives is caused by another mechanism. In the antiproliferative activity assay, the most potent activity of **1** was observed against the melanoma cells (IC_{50} = 15.5 μg/ml). Against the non-malignant lung fibroblasts, which were included as a test for general toxicity, the compound had an IC_{50} of 32 μg/ml, which is more than five times higher than the highest MIC value against the multidrug-resistant MRSA. The concentrations where **1** did not display any toxic effect on the cells (∼100% cell survival) were 20, 12.5, and 15 μg/ml for MRC5, A2058, and HepG2, respectively. This indicates that there is little overlap between the concentration where **1** has antibacterial activity and the concentration where toxicity occurs against the human cells.

This observed difference is a good starting point when entering structure optimization, as it indicates that production of non-toxic variants of **1** can be obtained.

We isolated 45 mg/L of **1** when the Lulworthiaceae sp. fungus was grown in liquid media supplemented with sea salts. This shows that slow-growing marine fungi *sensu stricto* can produce high yields of novel compounds for chemical characterization and screening for biological activities. Compound **1** was found to be a novel sulfated dimeric naphthopyrone, and showed potent growth inhibition of multidrug-resistant MRSA with MICs down to 1.56 μg/ml, which is much lower than the IC_{50} detected against the non-malignant cell line (32 μg/ml). This study demonstrates that the family Lulworthiaceae and order Lulworthiales have biosynthetic potential to produce bioactive secondary metabolites and supports the view of Overy et al. (2014) that marine fungi *sensu stricto* should be studied for natural product discovery, despite their slow growth (Overy et al., 2014). Our study highlights the potential role of marine fungi *sensu stricto* in tackling the worldwide AMR crisis.

DATA AVAILABILITY STATEMENT

The datasets presented in this study can be found in online repositories. The names of the repository/repositories and accession number(s) can be found in the article/ **Supplementary Material**.

AUTHOR CONTRIBUTIONS

MJ was responsible for conducting experiments, data analysis, and writing and revising the draft manuscript. PR and JI were responsible for the NMR analysis of the compound and the writing related to this. EJ conducted the antibacterial testing against the clinical bacterial isolates and wrote this section in the "Materials and Methods," and contributed to the writing of the MIC results. KH assisted in writing and revision of the manuscript and contributed to the experiment design. TR did the initial isolation of the fungus and the phylogenetic analysis, contributed to the experiment design by selecting this fungus for the study, and revised the manuscript. JA and EH contributed to the conceptualization of the work, supervised the work, and revised the manuscript. All authors reviewed and approved the final manuscript.

FUNDING

This project received funding from the DigiBiotics project of the Research Council of Norway (project ID 269425), the AntiBioSpec project of UiT the Arctic University of Norway (Cristin ID 20161326), and the Centre for New Antibacterial Strategies at UiT the Arctic University of Norway (TR). The publication charges for this article have been funded by the publication fund of UiT the Arctic University of Norway.

ACKNOWLEDGMENTS

We would like to acknowledge the technical support by Kirsti Helland and Marte Albrigtsen by execution of the bioactivity assays, the contribution of Chun Li in the work with the sequencing of the genetic elements of the isolate, and Ole Christian Hagestad with his assistance in the phylogenetic analysis. We thank the Advanced Microscopy Core Facility (AMCF) of the UiT the Arctic University of Norway for the access to their devices. We would also like to acknowledge the Norwegian National Advisory Unit on Detection of Antimicrobial Resistance (K-res), University Hospital of North Norway for the VREs.

SUPPLEMENTARY MATERIAL

The Supplementary Material for this article can be found online at: https://www.frontiersin.org/articles/10.3389/fmicb.2021.730740/full#supplementary-material

REFERENCES

Azevedo, E., Barata, M., Marques, M. I., and Caeiro, M. F. (2017). Lulworthia atlantica: a new species supported by molecular phylogeny and morphological analysis. *Mycologia* 109, 287–295. doi: 10.1080/00275514.2017.1302255

Boudesocque-Delaye, L., Agostinho, D., Bodet, C., Thery-Kone, I., Allouchi, H., Gueiffier, A., et al. (2015). Antibacterial polyketide heterodimers from Pyrenacantha kaurabassana Tubers. *J. Nat. Prod.* 78, 597–603. doi: 10.1021/np5003252

Calado, M. D. L., Carvalho, L., Barata, M., and Pang, K.-L. (2019). Potential roles of marine fungi in the decomposition process of standing stems and leaves of Spartina maritima. *Mycologia* 111, 371–383. doi: 10.1080/00275514.2019.1571380

Clinical Laboratory Standard Institute (CLSI) (2012). Clinical and laboratory standards institute methods for dilution antimicrobial susceptibility tests for bacteria that grow aerobicallyapproved standard. *J. Infect. Chemother.* 18, 816–826.

Davidson, D. E. (1973). Mucoid sheath of Lulworthia medusa. *Trans. Brit.Mycol. Soc.* 60, 577–579. doi: 10.1016/S0007-1536(73)80042-7

Demain, A. L. (2014). "Valuable secondary metabolites from fungi," in *Biosynthesis and Molecular Genetics of Fungal Secondary Metabolites*, eds J. F. Martín, S. Zeilinger, and C. García-Estrada (Springer).

Francisca, C., Marta, C.-D.-S., Emília, S., Madalena, P., and Anake, K. (2018). Sulfation pathways: sources and biological activities of marine sulfated steroids. *J. Mol. Endocrinol.* 61, T211–T231. doi: 10.1530/JME-17-0252

Góes-Neto, A., Marcelino, V. R., Verbruggen, H., da Silva, F. F., and Badotti, F. (2020). Biodiversity of endolithic fungi in coral skeletons and other reef substrates revealed with 18S rDNA metabarcoding. *Coral. Reefs* 39, 229–238. doi: 10.1007/s00338-019-01880-y

Hyde, K. D., Norphanphoun, C., Maharachchikumbura, S. S. N., Bhat, D. J., Jones, E. B. G., Bundhun, D., et al. (2020). Refined families of sordariomycetes. *Mycosphere* 11:1059. doi: 10.5943/mycosphere/11/1/7

Imhoff, J. F. (2016). Natural products from marine fungistill an underrepresented resource. *Mar. Drugs* 14, 1–19. doi: 10.3390/md14010019

Isaka, M., Yangchum, A., Rachtawee, P., Komwijit, S., and Lutthisungneon, A. (2010). Hopane-type triterpenes and binaphthopyrones from the scale insect pathogenic fungus Aschersonia paraphysata BCC 11964. *J. Nat. Prod.* 73, 688–692. doi: 10.1021/np1000363

Johnson, T. W. (1958). Marine fungi. IV. *Lulworthia* and *Ceriosporopsis*. *Mycologia* 50, 151–163. doi: 10.2307/3756191

Jones, E. B. G. (1994). Fungal adhesion. *Mycol. Res.* 98, 961–981. doi: 10.1016/S0953-7562(09)80421-8

Katoh, K., and Standley, D. M. (2013). MAFFT multiple sequence alignment software version 7: improvements in performance and usability. *Mol. Biol. Evol.* 30, 772–780. doi: 10.1093/molbev/mst010

Katoh, K., Misawa, K., Kuma, K., and Miyata, T. (2002). MAFFT: a novel method for rapid multiple sequence alignment based on fast Fourier transform. *Nucleic Acids Res.* 30, 3059–3066. doi: 10.1093/nar/gkf436

Kavanagh, F., Hervey, A., and Robbins, W. J. (1951). Antibiotic substances from *Basidiomycetes*: VIII. Pleurotus Multilus (Fr.) Sacc. and Pleurotus Passeckerianus Pilat. *Proc. Natl. Acad. Sci. U.S.A.* 37, 570–574. doi: 10.1073/pnas.37.9.570

Kawaguchi, M., Uchida, R., Ohte, S., Miyachi, N., Kobayashi, K., Sato, N., et al. (2013). New dinapinone derivatives, potent inhibitors of triacylglycerol synthesis in mammalian cells, produced by *Talaromyces pinophilus* FKI-3864. *J. Antibiot.* 66, 179–189. doi: 10.1038/ja.2012.127

Koch, J., Pang, K.-L., and Jones, E. B. G. (2007). Rostrupiella danica gen. et sp. nov., a Lulworthia-like marine lignicolous species from Denmark and the USA. *Bot. Mar.* 50, 294–301. doi: 10.1515/BOT.2007.034

Kohlmeyer, J., Spatafora, J. W., and Volkmann-Kohlmeyer, B. (2000). Lulworthiales, a new order of marine Ascomycota. *Mycologia* 92, 453–458. doi: 10.2307/3761504

Kornprobst, J.-M., Sallenave, C., and Barnathan, G. (1998). Sulfated compounds from marine organisms. *Comput. Biochem. Physiol.* 119, 1–51. doi: 10.1016/S0305-0491(97)00168-5

Kristoffersen, V., Rämä, T., Isaksson, J., Andersen, J. H., Gerwick, W. H., Hansen, E., et al. (2018). Characterization of rhamnolipids produced by an Arctic marine bacterium from the *Pseudomonas* fluorescence Group. *Mar. Drugs* 16:163. doi: 10.3390/md16050163

Lanfear, R., Calcott, B., Ho, S. Y. W., and Guindon, S. (2012). PartitionFinder: combined selection of partitioning schemes and substitution models for phylogenetic analyses. *Mol. Biol. Evol.* 29, 1695–1701. doi: 10.1093/molbev/mss020

Lanfear, R., Frandsen, P. B., Wright, A. M., Senfeld, T., and Calcott, B. (2017). PartitionFinder 2: new methods for selecting partitioned models of evolution for molecular and morphological phylogenetic analyses. *Mol. Biol. Evol.* 34, 772–773. doi: 10.1093/molbev/msw260

Li, D.-H., Han, T., Guan, L.-P., Bai, J., Zhao, N., Li, Z.-L., et al. (2016). New naphthopyrones from marine-derived fungus *Aspergillus niger* 2HL-M-8 and their in vitro antiproliferative activity. *Nat. Prod. Res.* 30, 1116–1122. doi: 10.1080/14786419.2015.1043553

Lu, S., Tian, J., Sun, W., Meng, J., Wang, X., Fu, X., et al. (2014). Bis-naphtho-γ-pyrones from fungi and their bioactivities. *Molecules* 19, 7169–7188. doi: 10.3390/molecules19067169

Maharachchikumbura, S. S. N., Hyde, K. D., Jones, E. B. G., McKenzie, E. H. C., Huang, S.-K., Abdel-Wahab, M. A., et al. (2015). Towards a natural classification and backbone tree for Sordariomycetes. *Fungal. Divers.* 72:301. doi: 10.1007/s13225-015-0331-z

Overy, D. P., Bayman, P., Kerr, R. G., and Bills, G. F. (2014). An assessment of natural product discovery from marine (sensu strictu) and marine-derived fungi. *Mycology* 5, 145–167. doi: 10.1080/21501203.2014.931308

Overy, D. P., Rämä, T., Oosterhuis, R., Walker, A. K., and Pang, K.-L. (2019). The neglected marine fungi, sensu stricto, and their isolation for natural products' discovery. *Mar. Drugs* 17, 1–20. doi: 10.3390/md17010042

Poli, A., Bovio, E., Ranieri, L., Varese, G. C., and Prigione, V. (2020). Fungal diversity in the Neptune forest: Comparison of the mycobiota of *Posidonia oceanica, Flabellia petiolata*, and *Padina pavonica*. *Front. Microbiol.* 11:933. doi: 10.3389/fmicb.2020.00933

Rämä, T., Nordén, J., Davey, M. L., Mathiassen, G. H., Spatafora, J. W., and Kauserud, H. (2014). Fungi ahoy! Diversity on marine wooden substrata in the high North. *Fungal. Ecol.* 8, 46–58. doi: 10.1016/j.funeco.2013.12.002

Rehner, S. A., and Samuels, G. J. (1994). Taxonomy and phylogeny of *Gliocladium* analysed from nuclear large subunit ribosomal DNA sequences. *Mycol. Res.* 98, 625–634. doi: 10.1016/S0953-7562(09)80409-7

Rivera-Chavez, J., Caesar, L., Garcia-Salazar, J. J., Raja, H. A., Cech, N. B., Pearce, C. J., et al. (2019). Mycopyranone: a 8,8'-binaphthopyranone with potent anti-MRSA activity from the fungus *Phialemoniopsis* sp. *Tetrahedron Lett.* 60, 594–597. doi: 10.1016/j.tetlet.2019.01.029

Ronquist, F., Teslenko, M., van der Mark, P., Ayres, D. L., Darling, A., Höhna, S., et al. (2012). MrBayes 3.2: efficient Bayesian phylogenetic inference and model choice across a large model space. *Syst. Biol.* 61, 539–542. doi: 10.1093/sysbio/sys029

Schneider, Y., Jenssen, M., Isaksson, J., Hansen, K. Ø, Andersen, J. H., and Hansen, E. H. (2020). Bioactivity of serratiochelin A, a siderophore isolated from a co-culture of Serratia sp. and Shewanella sp. *Microorganisms* 8, 1–17. doi: 10.3390/microorganisms8071042

Stamatakis, A. (2006). RAxML-VI-HPC: maximum likelihood-based phylogenetic analyses with thousands of taxa and mixed models. *Bioinformatics* 22, 2688–2690. doi: 10.1093/bioinformatics/btl446

Sutherland, G. K. (1915). Additional notes on marine Pyrenomycetes. *New Phytol.* 14, 183–193. doi: 10.1111/j.1469-8137.1915.tb07185.x

Suzuki, K., Nozawa, K., Nakajima, S., Udagawa, S., and Kawai, K. (1992). Isolation and structures of antibacterial binaphtho-α-pyrones, talaroderxines A and B, from Talaromyces derxii. *Chem. Pharm. Bull.* 40, 1116–1119. doi: 10.1248/cpb.40.1116

Velez, P., González, M. C., Cifuentes, J., Rosique-Gil, E., and Hanlin, R. T. (2015). Diversity of sand inhabiting marine ascomycetes in some tourist beaches on Cozumel Island, Mexico. *Mycoscience* 56, 136–140. doi: 10.1016/j.myc.2014.04.007

Vilgalys, R., and Hester, M. (1990). Rapid genetic identification and mapping of enzymatically amplified ribosomal DNA from several Cryptococcus species. *J. Bacteriol.* 172, 4238–4246. doi: 10.1128/jb.172.8.4238-4246.1990

Wang, J., Galgoci, A., Kodali, S., Herath, K. B., Jayasuriya, H., Dorso, K., et al. (2003). Discovery of a small molecule that inhibits cell division by blocking FtsZ, a novel therapeutic target of antibiotics. *J. Biol. Chem.* 278, 44424–44428. doi: 10.1074/jbc.M307625200

White, T. J., Bruns, T., Lee, S., and Taylor, J. (1990). "Amplification and direct sequencing of fungal ribosoman RNA genes for phylogenetics," in *PCR ProtocolsA Guide to Methods and Applications*, eds M. A. Innis, D. H. Gelfand, J. J. Sninsky, and T. J. White (San Diego: Academic Press).

WHO (2014). *Antimicrobial ResistanceGlobal Report on Surveillance*. Available online at: http://www.who.int/drugresistance/documents/surveillancereport/en/. (accessed February 26, 2018).

Xu, Y., Vinas, M., Alsarrag, A., Su, L., Pfohl, K., Rohlfs, M., et al. (2019). Bis-naphthopyrone pigments protect filamentous ascomycetes from a wide range of predators. *Nat. Commun.* 10, 1–12. doi: 10.1038/s41467-019-11377-5

Zheng, C. J., Sohn, M.-J., Lee, S., Hong, Y.-S., Kwak, J.-H., and Kim, W.-G. (2007). Cephalochromin, a FabI-directed antibacterial of microbial origin. *Biochem. Biophys. Res. Commun.* 362, 1107–1112. doi: 10.1016/j.bbrc.2007.08.144

Zuccaro, A., Schoch, C. L., Spatafora, J. W., Kohlmeyer, J., Draeger, S., and Mitchell, J. I. (2008). Detection and identification of fungi intimately associated with the brown seaweed Fucus serratus. *Appl. Environ. Microbiol.* 74, 931–941. doi: 10.1128/AEM.01158-07

Conflict of Interest: The authors declare that the research was conducted in the absence of any commercial or financial relationships that could be construed as a potential conflict of interest.

Publisher's Note: All claims expressed in this article are solely those of the authors and do not necessarily represent those of their affiliated organizations, or those of the publisher, the editors and the reviewers. Any product that may be evaluated in this article, or claim that may be made by its manufacturer, is not guaranteed or endorsed by the publisher.

frontiers in Bioengineering and Biotechnology

ORIGINAL RESEARCH
published: 10 December 2021
doi: 10.3389/fbioe.2021.713840

Euglena gracilis and Its Aqueous Extract Constructed With Chitosan-Hyaluronic Acid Hydrogel Facilitate Cutaneous Wound Healing in Mice Without Inducing Excessive Inflammatory Response

Jin Li[1,2,3], Zezhou Zheng[1], Ming Du[1], Jinchun Chen[4], Hui Zhu[3], Zhangli Hu[1,2], Yanxia Zhu[4] and Jiangxin Wang[1]**

[1]*Shenzhen Key Laboratory of Marine Bioresource and Eco-Environmental Science, Shenzhen Engineering Laboratory for Marine Algal Biotechnology, Guangdong Provincial Key Laboratory for Plant Epigenetics, College of Life Sciences and Oceanography, Shenzhen University, Shenzhen, China,* [2]*Key Laboratory of Optoelectronic Devices and Systems of the Ministry of Education and Guangdong Province, College of Optoelectronic Engineering, Shenzhen University, Shenzhen, China,* [3]*College of Food Engineering and Biotechnology, Hanshan Normal University, Chaozhou, China,* [4]*Shenzhen Key Laboratory of Anti-Ageing and Regenerative Medicine, Health Science Center, Shenzhen University, Shenzhen, China*

Naturally occurring compounds isolated from the microalga *Euglena gracilis*, such as polysaccharide paramylon, exhibit antimicrobial, anti-viral, antitumor, and anti-inflammatory activities. Whether live *E. gracilis* cells and its aqueous extract accelerate burn wound healing remains to be investigated. In this study, live *E. gracilis* cells and its aqueous extract were mixed with chitosan-hyaluronic acid hydrogel (CS/HA) to form cell + CS/HA and extract + CS/HA, which were then smeared onto the deeply burned skin of mice. The efficacy of these mixtures in accelerating wound healing was assessed through wound size reduction measurement, histological and immunofluorescence analyses, and serum pro-inflammatory cytokine level (INF-γ, IL-1β, and IL-6) determination. The live *E. gracilis* cells and its aqueous extract were found to facilitate wound healing by enhancing re-epithelization and reducing fibroplasia without stimulating excessive inflammatory response. In conclusion, live *E. gracilis* cells and its aqueous extract can be potentially used to treat cutaneous wounds.

Keywords: wound healing, live Euglena gracilis cells, aqueous extract, microalgal therapeutics, chitosan-hyaluronic acid hydrogel

OPEN ACCESS

Edited by:
Paola Angelini,
University of Perugia, Italy

Reviewed by:
Vincenzo Vindigni,
University of Padua, Italy
Sheikh Fayaz Ahmad,
King Saud University, Saudi Arabia
Alexander Neef,
Consultant, Valencia, Spain
Bambang Sektiari Lukiswanto,
Airlangga University, Indonesia

****Correspondence:***
Yanxia Zhu
yanxiazhu@szu.edu.cn
Jiangxin Wang
jxwang@szu.edu.cn

Specialty section:
This article was submitted to Biomaterials, a section of the journal Frontiers in Bioengineering and Biotechnology

Received: *24 May 2021*
Accepted: *08 November 2021*
Published: *10 December 2021*

Citation:
Li J, Zheng Z, Du M, Chen J, Zhu H, Hu Z, Zhu Y and Wang J (2021) Euglena gracilis *and Its Aqueous Extract Constructed With Chitosan-Hyaluronic Acid Hydrogel Facilitate Cutaneous Wound Healing in Mice Without Inducing Excessive Inflammatory Response. Front. Bioeng. Biotechnol. 9:713840. doi: 10.3389/fbioe.2021.713840*

1 INTRODUCTION

Acute skin wounds affect individuals physically and mentally. Annually, millions of people worldwide are affected by poor wound healing after surgery, trauma, acute illness, or chronic disease conditions (Eming et al., 2014). Although skin lesions heal rapidly and efficiently within 2 weeks, epidermal appendages (e.g., sebaceous glands and hair follicles) are not regenerated at the damaged site within this period, and a connective scar with a poorly reconstituted collagen matrix can be observed (Ehrlich and Krummel 1996; Almine et al., 2012). Therefore, the major goal of wound healing biology is to induce perfect reconstruction of damaged skin parts. Although various

types of therapies have been tested to accelerate the wound healing process, optimal strategies are still being developed (Chen et al., 2018). Advances in microalgal therapeutics seem promising in promoting skin wound healing. A photoautotrophic cyanobacterium, *Synechococcus elongatus* PCC7942, accelerates wound healing by promoting angiogenesis (Yin et al., 2019). In several studies, *Euglena*-derived polysaccharide paramylon has shown promising results in tissue repair therapy (Sugiyama et al., 2010; Shibakami et al., 2013; Shibakami et al., 2015). Paramylon film accelerated skin wound healing in an animal model through its immunosuppressive effect (Yasuda et al., 2018).

Previous studies have reported that β-1,3-D-glucan modulated the Th1 and/or the Th2 cell response in experimental animals and human patients of allergic rhinitis and digestive cancers (Yoshino et al., 2000; Kirmaz et al., 2005; Ahmada et al., 2018, 2019). Leung and Bieber (2003) suggested a key role of the Th1-type cytokine interferon-γ (IFN-γ) in the chronicity of atopic dermatitis (AD) lesions of human. Oral administration of *Euglena*-derived polysaccharide paramylon inhibits the development of AD-like skin lesions in NC/Nga mice by suppressing both the T-helper (Th1) and Th 2 cell responses (Sugiyama et al., 2010). Serum levels of interleukin-4 (IL-4) and IFN-γ and IL-18 and IL-12 contents in the skin lesions were reduced. Moreover, sonicated and alkalized paramylon derived from *E. gracilis* upregulates pro-inflammatory factors (nitric oxide, tumor necrosis factor alpha, IL-6, and cyclooxygenase 2) in lymphomonocytes and has an immune-activating effect (Russo et al., 2016). Kankkunen et al. (2010) have demonstrated that paramylon as well as other large particulate β-1,3-D-glucans (curdlan, zymosan, glucan from baker's yeast *Saccharomyces cerevisiae*) are sensed by sophisticated cooperating pathways through both membrane-bound and cytosolic pattern recognition receptors (PRRs), resulting in robust activation of IL-1β-mediated inflammatory response in human primary macrophages. In this study, immunosuppressive effect of live *Euglena gracilis* cells and its aqueous extract for facilitating skin wound healing was investigated in an animal model. The expression of three important pro-inflammatory mediators of antibody responses along different pathways such as IL-6, IFN-γ, and IL-1β was evaluated.

E. gracilis is a unicellular green microalga with flagellar motility (Buetow, 1968). The presence of nutritionally crucial chemicals such as fatty acids, docosahexaenoic acid, eicosapentaenoic acid, and vitamins in *E. gracilis* implies that this alga is a valuable therapeutic resource with potential for clinical application (Kottuparambil et al., 2019; Nakashima et al., 2021). The paramylon yield from *E. gracilis* is approximately 60%–70% of the dried cells, and paramylon exhibits anti-inflammatory, antimicrobial, antioxidant, anticancer, and neuroprotective properties, as well as immune activating effects (Sakagami et al., 1991; Foltínová et al., 1994; Sugiyama et al., 2009; Russo et al., 2016; Nakashima et al., 2017; Suzuki et al., 2018; Guo et al., 2019). On the other hand, methanol or ethanol extracts of *Euglena* species (e.g., *E. viridis*, *E. gracilis,* and *E. tuba*) possess antimicrobial, antiviral, and antitumor properties (Das et al., 2005; Panja et al., 2016; Ishiguro et al., 2020). As a cosmetic or dermopharmaceutic compound, the aqueous extract of *Euglena* activates cellular metabolism and reduces the signs of aging and cutaneous fatigue (US patent US8741357B2) (Lintner et al., 2014). The author reported a decrease in deformability and an increase in cutaneous vitality of skin after 14 days treatment with 3% *Euglena* extract. Nevertheless, *E. gracilis* components, other than paramylon, stimulate the growth of *Faecalibacterium* and improve digestive health (Nakashima et al., 2021). Hence, we investigated whether live *E. gracilis* cells and its aqueous extract exert beneficial effects on skin wound healing.

Chitosan-hyaluronic acid hydrogel (CS/HA) has good biocompatibility, and therefore, it can be used as a delivery device not only for mobilizing stem cells to the injection site, but also for sustainable release of bioactive molecules or growth factors (Zhu et al., 2017). CS/HA can provide a moist environment to the wound, thereby effectively preventing tissue dehydration and cell death, enhancing the migration of inflammatory cells and growth factors, facilitating air exchange and angiogenesis, serving as a barrier for microbes, removing excessive exudate, and accelerating wound healing (Luo et al., 2010; Rudyardjo and Wijayanto, 2017). In our preliminary study, paramylon + CS/HA, extracellular vesicle + CS/HA, cell + CS/HA, and extract + CS/HA were developed by incorporating sonicated and alkalized paramylon, extracellular vesicle, live *E. gracilis* cells, and its aqueous extract into CS/HA in a 1:1 volume ratio. Sonicated and alkalized paramylon, extracellular vesicle, live *E. gracilis* cells, and its aqueous extract were uniformly distributed in CS/HA. Cells survived in CS/HA after a 24-h incubation in an illuminating incubator without shaking at 37°C (data not shown). Keeping CS/HA as the control group, the aforementioned four groups were smeared onto the deeply burned skin of mice. Wound size reduction was calculated as follows: wound size reduction (%) = $(A_0 - At)/A_0 \times 100$, where A_0 is the initial wound area and At is the wound area at day 14 after wounding (Zhang et al., 2015). Results of wound size reduction measurement revealed that cell + CS/HA and extract + CS/HA facilitated wound healing more rapidly than paramylon + CS/HA, extracellular vesicle + CS/HA, and CS/HA. In the present study, we investigate the ability of live *E. gracilis* cells and its aqueous extract to accelerate wound healing based on the results of wound size reduction measurement, histological and immunofluorescence analyses, and serum pro-inflammatory cytokine level determination. To the best of our knowledge, this is the first study to investigate the direct effect of live *E. gracilis* cells and its aqueous extract on the wound healing process.

2 MATERIALS AND METHODS

2.1 Isolation of Live *Euglena gracilis* Cells and Aqueous Extract

E. gracilis cells were grown in the EM medium under a light intensity of 100 μmol/m^2/s in an illuminating incubator without shaking at 26°C until the cells reached the stationary phase (Afiukwa and Ogbonna, 2007; Wang et al., 2018). The medium contained 1.8 g/L NH_4Cl, 0.6 g/L KH_2PO_4, 0.6 g/L $MgSO_4$, 60 mg/L urea, 0.02 g/L $CaCl_2$, 0.48 mg/L Na_2EDTA,

2 mg/L $Fe_2(SO4)_3$, 60 μl HCl, 0.01 mg/L Vb_1, 0.0005 mg/L Vb_{12}, 20 mg/L $CuSO_4{\cdot}5H_2O$, 0.4 g/L $ZnSO_4{\cdot}7H_2O$, 1.3 g/L $Co(NH_3){\cdot}H_2O$, and 1.6 g/L $MnCl_2{\cdot}4H_2O$.

The *E. gracilis* culture medium was incubated for 1 week, and then, 1 L of this medium was centrifuged at 1,000 × *g* for 4 min and collected. Cell precipitates were rinsed three times with distilled water and resuspended in 1× phosphate buffered saline (PBS) at 37°C. After cultivating the cells for 1 week, the aqueous extract was isolated from 1 L *E. gracilis* culture medium. Briefly, the culture was centrifuged at 7,000 × *g* for 3 min, and the cell pellets were rinsed three times with distilled water and then ultracentrifuged at 10,000 × *g* for 5 min three times. An ultrasonic cell pulverizer (model: JY99-IIDN, Ningbo Scientz Biotechnology Co., Ltd.) was used as an emulsified dispersion device (70% power). The precipitated cells with 20 volumes of 1× PBS were ultrasonically treated for 8 min. The device adopts a working time of 48 s and intermittent 12 s, which can effectively prevent temperature increase and improve emulsion efficiency. The cellular debris was removed using a 0.22-μm Millipore filter.

2.2 Preparation of Chitosan-Hyaluronic Acid Hydrogel

Chitosan-hyaluronic acid hydrogel was prepared according to the method of Zhu et al. (2017). Briefly, a 2% chitosan (CS, deacetylation 90%, Sigma) stock was prepared in 0.1 M hydrochloric acid, and a 10% β-glycerophosphate (GP, Sigma) stock and a 1% sodium hyaluronate (HA, 350 kDa, Huaxi Fureida) stock were prepared using distilled water. The 2% CS, 10% GP, and 1% HA solutions were subsequently mixed and maintained in a 37°C water bath before use. The hydrogel prepared with the proportions of CS:GP:HA = 5:3:2 was chosen as the optimal gel to promote cell proliferation and differentiation because it displayed good mechanical properties.

2.3 Mouse Skin Wound Model and Treatments

The Animal Research Committee of the Health Science Center of Shenzhen University approved all experimental procedures. Successful skin wound healing involves a series of events with complex cell signaling cascades that coordinate several fundamental biological processes (Martin 1997; Gurtner et al., 2008). Re-epithelialization, granulation tissue formation with collagen deposition, and successive influx of different subsets of immune cells match the classical wound healing timeline in BALB/c mice (Braiman-Wiksman et al., 2007). Briefly, 1–3 days post-wounding stage included blood-clot formation (primary clot), activation of epidermal edges, and early inflammatory response (characterized by abundance of neutrophils at the wound gap). Four to seven days post-wounding stage was marked by scab formation. Histological analysis reveals migration of the epidermal edges, selective proliferation of the early granulation tissue, and inflammatory response (lymphocytes and macrophages present in abundance). Scar detachment is observed at 8–12 days post-wounding stage. Histological results exhibit the formation of new epidermis and initiation of dermal closure. This stage is accompanied by attenuation of the inflammatory response. However, epidermal closure progresses considerably more slowly. For example, at 12 days following wounding, 40% of the wounds exhibit dermal closure (Braiman-Wiksman et al., 2007). Therefore, in the present study, we select 14 days post-wounding as the third stage. Critical events of the stepwise experimental wound healing process at 1, 7, and 14 days were probed. Wound healing did not diverge from the histomorphological features of this paradigm.

In total, 22 female 8-week-old BALB/c mice (weight: 16–20 g) were anesthetized through intraperitoneal injection of 4% chloral hydrate (1 ml/100 g). After shaving the mice, two dorsal wounds were symmetrically clipped out using a copper bar (diameter: 1 cm) punch, which was heated using a water bath at 95°C.

The mice were randomly assigned to three groups: cell + CS/HA (5×10^6 live *E. gracilis* cells mixed with CS/HA in 1:1 volume ratio), extract + CS/HA (0.05 g/ml aqueous extract from *E. gracilis* mixed with CS/HA in 1:1 volume ratio), and CS/HA (control group). A total of 42 wound sites (14 wound sites/group) were analyzed.

2.4 Histological Study

The mice were sacrificed at day 14 after wounding. For histological analyses, the skin excised from 21 dorsal wound sites (7 sites/group) was fixed in a 4% paraformaldehyde fix (PFA) solution, dehydrated with a graded alcohol series, embedded in paraffin, sectioned (section thickness: 4 μm) perpendicularly to the wound surface, and stained with hematoxylin and eosin (H&E). Masson's trichrome staining was used to determine the degree of collagen maturity.

2.5 Immunofluorescence Study

To identify vascular structures, immunofluorescence histochemistry was performed for an endothelial cell marker, CD31. For immunofluorescence staining, skin excised from the dorsal wound sites was fixed in 4% PFA (cat no. BL539A, Biosharp), dehydrated in a 30% sucrose solution, embedded in optimal cutting temperature compound (OCT), and sectioned (section thickness: 4 μm) perpendicularly to the wound surface. Tissue sections were blocked in 5% BSA for 30 min at room temperature and incubated with rabbit CD31 monoclonal antibody (1:200, ab28364, Abcam) overnight at 4°C (Zhu et al., 2021). Images were acquired using an Olympus IX81 microscope. The newly formed and mature vessels were indicated by CD31 positive staining. These newly formed vessels were counted in five random fields per section between wound edges by using ImageJ (v. 1.52) (Schneider et al., 2012).

2.6 Enzyme-Linked Immunosorbent Assay for IFN-γ, IL-1β, and IL-6

The effect of live *E. gracilis* cells and its aqueous extract was examined by investigating serum pro-inflammatory cytokine levels through enzyme-linked immunosorbent assay (ELISA). In total, 15 blood samples (5 samples/group) were obtained from the inferior vena cava of the mice under anesthesia on day 14. IL-1β (cat no. 88-7013) and IL-6 (cat no. 88-7064) levels

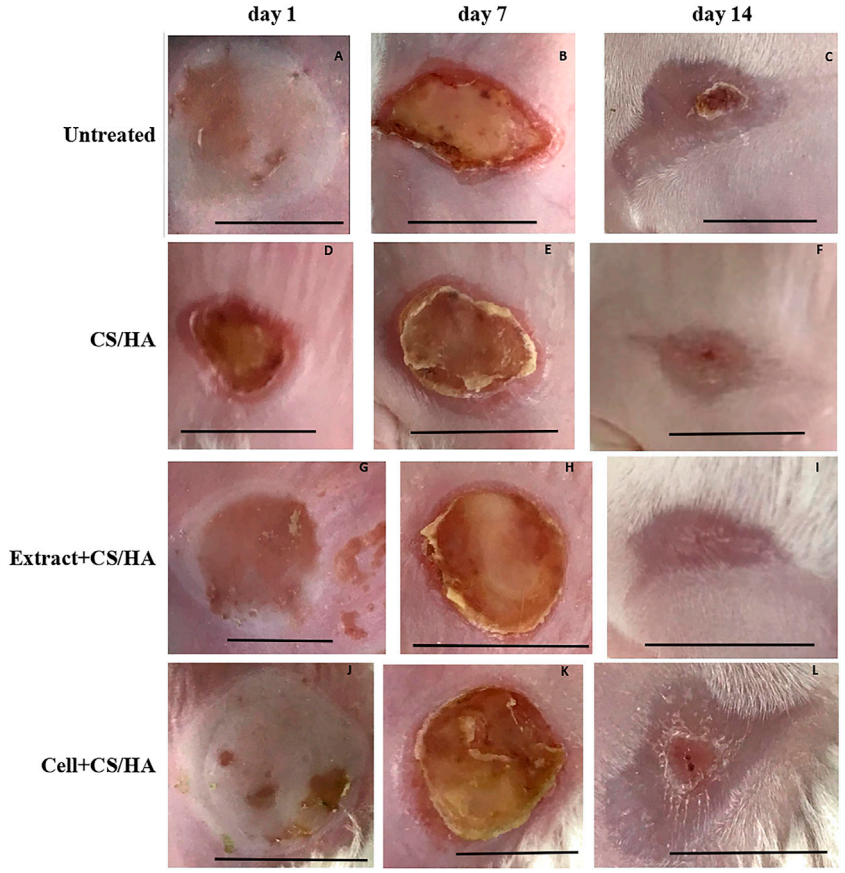

FIGURE 1 | Macroscopic appearance of wounds treated with CS/HA, extract + CS/HA, and cell + CS/HA at 1, 7, and 14 days in the mice. **(A–C)** Untreated (n = 1). **(D–F)** CS/HA (n = 7). **(H–J)** Extract + CS/HA (n = 7). **(K, L)** Cell + CS/HA (n = 7). Scale bar = 1 cm.

were measured using the ELISA Development Kit, according to the manufacturer's protocols (Multi Sciences [Lianke] Biotech Co., Ltd., Hangzhou, China). Each sample was measured in duplicate, and cytokine concentration was calculated on the basis of standard curves provided with the kits. The results are expressed in pg/ml. IFN-γ (cat no. JM-02465M1) was measured using the ELISA Development Kit, according to the manufacturer's protocols (Jingmei Biotech Co., Ltd., Yancheng, China). Because the IFN-γ level is excessively high, each sample was diluted 5-fold, and the results were multiplied by the dilution factor (5-fold). As serum available was insufficient, IL-6 concentration was detected for one sample in each group.

2.7 Statistical Analysis

Statistical significance was evaluated using GraphPad Prism (v7, GraphPad Software, Inc., La Jolla, CA, USA), and statistical analysis was performed using analysis of variance (ANOVA) followed by the Tukey's test for post-hoc analysis. p value less than 0.01 ($p < 0.01$) was considered extremely significantly different, $p < 0.05$ was statistically significant.

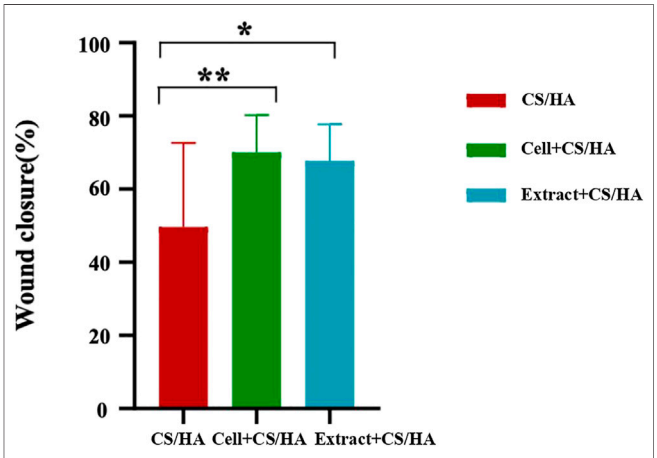

FIGURE 2 | Comparison of wound size reduction among CS/HA, extract + CS/HA, and cell + CS/HA treatments at 14 days post-wounding. Wound size reduction was significantly greater in extract + CS/HA and cell + CS/HA. Significant difference compared to CS/HA. *$p < 0.05$, **$p < 0.01$. n = 14 per group.

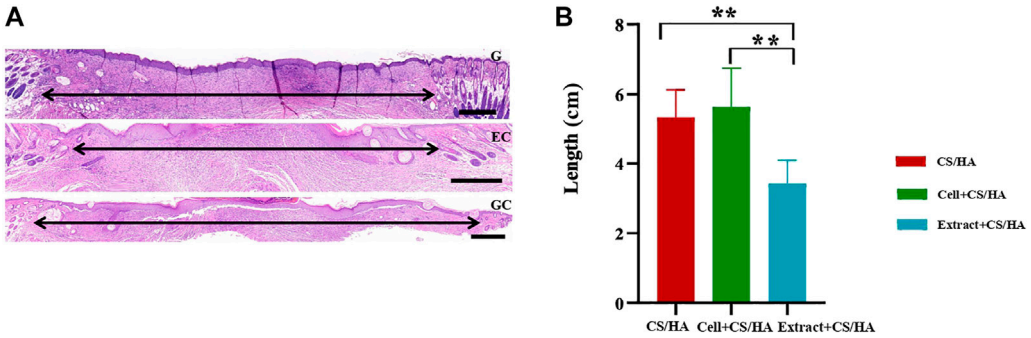

FIGURE 3 | Representative H&E-stained images of wound sections and comparison of scar length among wounds treated with CS/HA, cell + CS/HA, and extract + CS/HA at 14 days post-wounding. **(A)** Representative images of H&E-stained wound sections. Black double-headed arrows indicate the edges of scars. G: CS/HA; EC: extract + CS/HA; GC: cell + CS/HA. Scale bar = 500 μm. **(B)** Comparison of scar length after H&E staining. Wounds treated with extract + CS/HA had significantly narrower scar length than those treated with cell + CS/HA and CS/HA. Significant difference compared to CS/HA. $*p < 0.05$, $**p < 0.01$. $n = 7$ per group.

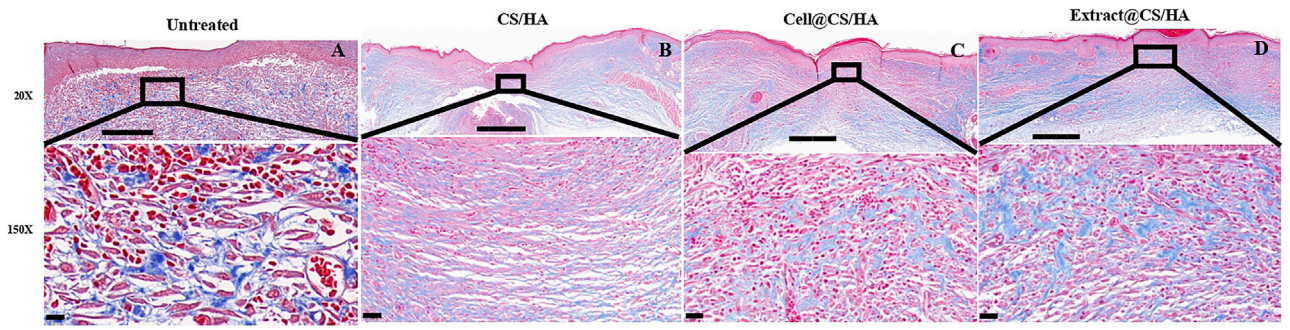

FIGURE 4 | The representative Masson's trichrome images of untreated group ($n = 1$) **(A)**, CS/HA ($n = 7$) **(B)**, extract + CS/HA ($n = 7$) **(C)**, and cell + CS/HA ($n = 7$) **(D)**. Wound tissue was stained with Masson's trichrome to access collagen content and organization at 14 days post-wounding. Scale bar: 200 μm **(top)** or 10 μm **(bottom)**.

3 RESULTS

3.1 Wound Size Reduction Was Significantly Greater in Cell + CS/HA and Extract + CS/HA

Gross observations revealed an increase in size reduction of wounds treated with cell + CS/HA and extract + CS/HA compared with those treated with CS/HA at 14 days post-wounding (**Figure 1**). Wounds treated with cell + CS/HA and extract + CS/HA exhibited a significantly greater reduction in size than those treated with CS/HA (approximately 70 and 67%, respectively, vs. 49%; **Figure 2**).

3.2 Enhanced Re-Epithelialization and Reduced Fibroplasia in Cell + CS/HA and Extract + CS/HA

Reduced scar length and increased collagen maturity were used to assess the wound healing degree (Zhang et al., 2015). Both cell + CS/HA and extract + CS/HA enhanced re-epithelialization compared with CS/HA at 14 days post-wounding (**Figure 3**). H&E staining showed that wounds treated with extract + CS/HA had significantly narrower scar length than those treated with cell + CS/HA and CS/HA (**Figure 3B**). Additionally, wounds treated with cell + CS/HA showed a larger scar length than those treated with CS/HA; however, the difference was nonsignificant (**Figure 3B**).

Dermal fibroblasts could secrete collagen and promote collagen deposition in the healing process (Li et al., 2016). In the present study, each group exhibited different amounts of collagen at 14 days post-wounding. The collagen fiber bundles were evident in the untreated group (**Figure 4A**). The application of CS/HA caused thin, undulated bundles of collagen in the scar tissue (**Figure 4B**). There was a lesser degree of fibroplasia in the extract + CS/HA and cell + CS/HA groups in comparison to the untreated group (**Figures 4C,D**).

Masson's trichrome staining showed that wounds treated with cell + CS/HA (**Figures 5A,B**) and extract + CS/HA (**Figures 5C,D**) had more newly formed vessels than those treated with CS/HA, which only exhibited epidermis and dermis formation

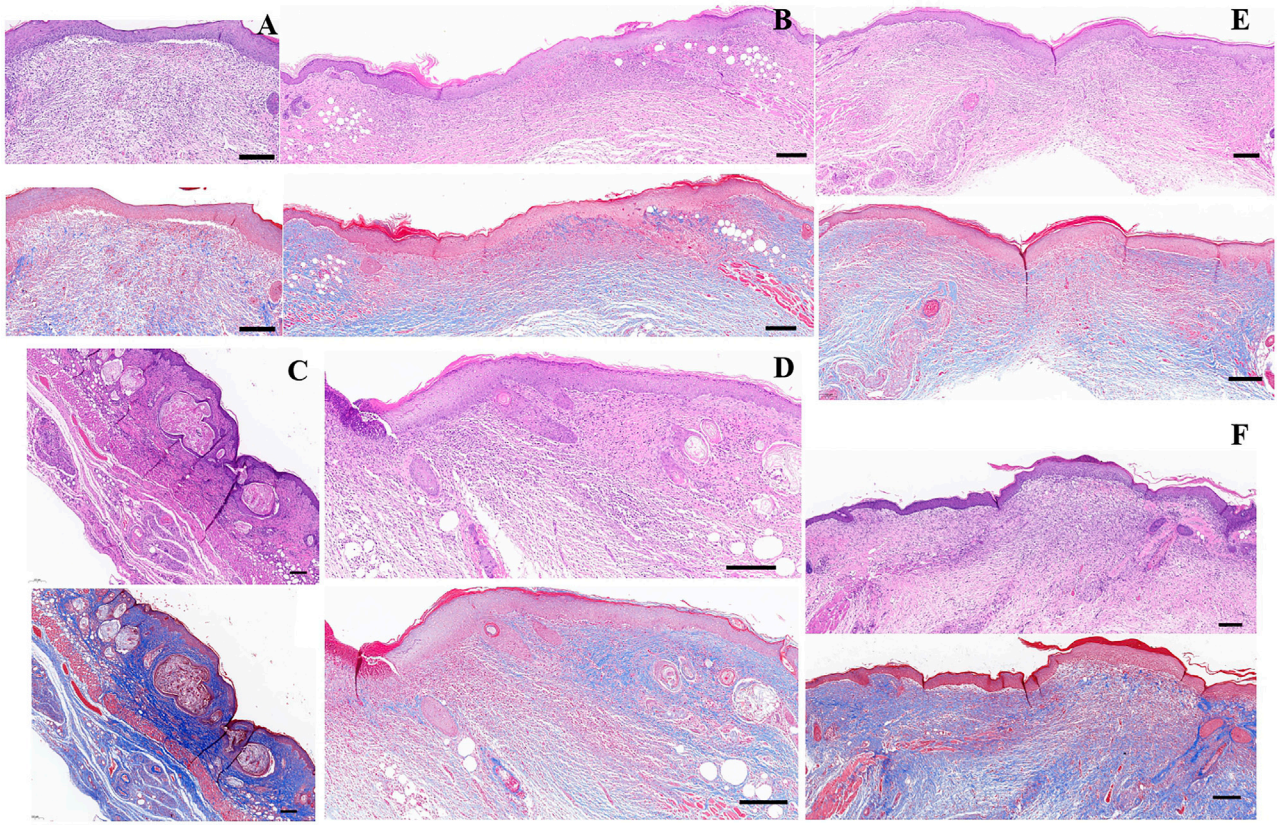

FIGURE 5 | H&E- and Masson's trichrome-stained images of wounds treated with CS/HA, extract + CS/HA, and cell + CS/HA at 14 days post-wounding. **(A)** Untreated tissue. **(B)** CS/HA. **(C,D)** Extract + CS/HA. **(E,F)** Cell + CS/HA. Scale bar = 200 μm.

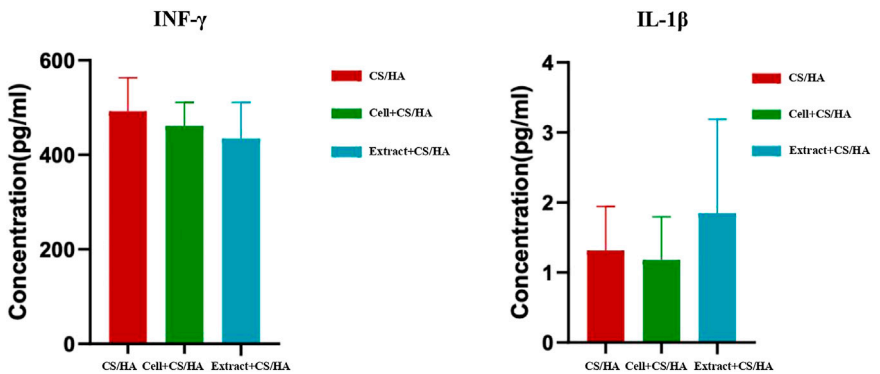

FIGURE 6 | Comparison of INF-γ and IL-1β levels among wounds treated with CS/HA, extract + CS/HA, and cell + CS/HA at 14 days post-wounding. No notable changes in INF-γ and IL-1β levels in the mice treated with cell + CS/HA and extract + CS/HA.

(**Figure 5C**). Inflammatory cells were not present in the dermis among wound sites treated with cell + CS/HA, extract + CS/HA, and CS/HA (**Figure 5**). Vascularization of newly formed tissues is essential for the wound healing process (Zhang et al., 2015). Newly formed vessels at wound sites were characterized by CD31 staining, from which average vessel densities were quantified. Herein, based on the enumeration of the newly formed vessels, no significant difference was noted in vessel density (**Supplementary Figures S1A–D**).

3.3 No Notable Changes in Cytokines (IFN-γ and IL-1β) in the Mice Treated With Cell + CS/HA and Extract + CS/HA

The effect of cell + CS/HA, extract + CS/HA, and CS/HA applications on serum pro-inflammatory cytokines in the mice was investigated through ELISA. Cell + CS/HA and extract + CS/HA did not induce notable changes in IFN-γ and IL-1β (**Figure 6**) levels. Because serum available was insufficient, IL-6 concentration was detected for one sample per group (cell + CS/HA: 2.3 pg/ml; extract + CS/HA: 2.588 pg/ml; CS/HA: 0.959 pg/ml).

4 DISCUSSION

Our study showed that live *E. gracilis* cells and its aqueous extract accelerated wound healing in the mice without inducing excessive inflammatory response. The cell + CS/HA and extract + CS/HA treatments led to greater wound size reduction and re-epithelialization, lesser degree of fibroplasia, and enhancement of new blood vessel formation in the wound bed. Both cell + CS/HA and extract + CS/HA treatments did not induce excessive inflammatory response, as revealed by no notable changes in IFN-γ and IL-1β concentrations. Moreover, inflammatory cells were not present in the dermis. Our findings that live *E. gracilis* cells and its aqueous extract facilitate wound healing without excessive immune responses are inconsistent with those obtained with paramylon of *E. gracilis*, which accelerates wound healing through its anti-inflammatory effect (Sugiyama et al., 2009; Sugiyama et al., 2010; Yasuda et al., 2018).

Live cells of cyanobacterium, *Synechococcus elongatus* PCC 7942, accelerate cutaneous wound healing by promoting angiogenesis (Yin et al., 2019). These cells exhibit the potential for wound healing primarily through the delivery of functional extracellular vesicles and not through their photosynthetic activity. Moreover, the promotion of IL-6 expression may be a mechanism for the pro-angiogenic effect and wound healing (Yin et al., 2019). As the existence of extracellular vesicles was confirmed in other microalgae (Picciotto et al., 2021), it is reasonable to propose similar mechanisms for live *Euglena* cells for skin wound healing. Additional elaborately designed experiments would provide strong evidence to support this case.

Although no study has reported the application of live *Euglena* cells, its aqueous extract in cosmetic compositions acts as an energy supplement for skin and hair follicle cells (US patent US8741357B2) (Lintner et al., 2014). The aqueous extract enables the reconstitution of the intracellular ATP pool and *de novo* synthesis of inositol 1,4,5-trisphosphate (IP3, a key molecule in the cell energy cascade), and it also triggers the release of intracellular calcium from its storage site (showing the switch of a cell from the resting state to the activated state) (US patent US8741357B2) (Lintner et al., 2014). The author also proposed that the aqueous extract of *Euglena* increases the energy supply to cells and/or tissues through the supply of phosphoinositides, which contribute to cell metabolism activation. It also stimulates the production of some biomolecules, such as ATP and calcium, in skin cells (US patent US8741357B2) (Lintner et al., 2014). Furthermore, the extract of *Euglena* species possesses a range of antimicrobial activities and/or the ability to increase cutaneous vitality (Das et al., 2005; Lintner et al., 2014). A high abundance of lipid-like, protein-like, lignin/polyphenol-like, carbohydrate-like, tannin-like compounds, and unsaturated hydrocarbon was found in the aqueous extract of light-grown *E. gracilis* cells (Lewis and Guéguen, 2020). In our laboratory, gas chromatography-mass spectrometry/mass spectrometry (GC–MS/MS) of the *Euglena* extract revealed the presence of hundreds of 2-3-amino-acid short peptides (data not shown). Short peptides have also been used as active elements for the detection of their own receptors (Pavan and Berti, 2012). For example, antimicrobial peptides (AMPs) and cell-penetrating peptides (CPPs) are used for sensing bacterial cells, antigenic peptide sequences for antibody monitoring, and peptide substrates for enzyme detection. Detailed investigations of the composition of the *Euglena* extract and their functions are being preceded to verify this hypothesis.

Signal transducer and activator of transcription 3 (STAT3) is the key mediator of both chronic inflammation and joint destruction in rheumatoid arthritis (RA). The major pro-inflammatory cytokines in RA, TNF-α, IL-6, and IL-1 induced STAT3 activation either directly or indirectly and stimulated expression of IL-6 family cytokines and receptor activator of nuclear factor kappa B ligand (RANKL) in an autocrine/paracrine manner *in vivo* and *in vitro*. Pharmacological inhibition of STAT3 also inhibited expression of RANKL in osteoblastic cells induced by IL-1β, TNF-α, and IL-6 *in vitro* as well as in the joints of a collagen-induced arthritis (CIA) model *in vivo* (Mori et al., 2011). In this study, no notable changes in IFN-γ and IL-1β concentrations were revealed by both cell + CS/HA and extract + CS/HA treatments. In addition, although IL-6 concentration was detected for one sample in each group, concentration values were similar (cell + CS/HA: 2.3 pg/ml; extract + CS/HA: 2.588 pg/ml). Thus, our data provide new insight into wound healing pathogenesis and provide evidence that inflammatory cytokines did not trigger a cytokine amplification loop.

A limitation of our study is that we did not identify the molecular mechanism underlying the pro-angiogenic and pro-wound healing effects of live *E. gracilis* cells and its aqueous extract. The molecules that mediate the different effects of live *E. gracilis* cells and its aqueous extract on the proliferation and migration of endothelial cells, keratinocytes, and fibroblasts also remain unknown. Thus, live *E. gracilis* cells and its aqueous extract may also be selectively enriched in some functional molecules that mediate their regulatory effects, although this approach requires further exploration.

Our findings suggest that live *E. gracilis* cells and its aqueous extract can facilitate wound healing without stimulating excessive

inflammatory response during the healing process. This study is the first to provide evidence for the potential of live *E. gracilis* cells and its aqueous extract in treating cutaneous wounds. The successful wound healing in mice suggests the potential use of *E. gracilis* in humans for wound care.

DATA AVAILABILITY STATEMENT

The datasets presented in this study can be found in online repositories. The names of the repository/repositories and accession number(s) can be found below: PRJNA734000.

ETHICS STATEMENT

The animal study was reviewed and approved by The Animal Research Committee of the Health Science Center of Shenzhen University.

AUTHOR CONTRIBUTIONS

JL, JW and YZ contributed to the conception and design of the study. JL, ZZ, MD, and JC conducted the experiments. JL, HZ, and ZH involved in the statistical analysis. JL wrote the first draft of the manuscript. JW, YZ and JL contributed to manuscript revision. All authors read and approved the submitted version.

ACKNOWLEDGMENTS

We would like to thank the reviewers for their insightful comments on the manuscript, as their remarks led to an improvement of the work. We would also like to thank TopEdit (www.topeditsci.com) for English language editing of this manuscript. This work was supported by the National Key R&D Program of China (2018YFA0902500, 2021YFA0910800), and the Natural Science Foundation of Guangdong Province, China (2021A1515011155) They are used for the design of the study, data collection, data analysis, and writing the manuscript, respectively.

SUPPLEMENTARY MATERIAL

The Supplementary Material for this article can be found online at: https://www.frontiersin.org/articles/10.3389/fbioe.2021.713840/full#supplementary-material

REFERENCES

Ahmad, S. F., Ansari, M. A., Nadeem, A., Bakheet, S. A., Al-Ayadhi, L. Y., Alotaibi, M. R., et al. (2018). Dysregulation of the Expression of Hla-Dr, Costimulatory Molecule, and Chemokine Receptors on Immune Cells in Children with Autism. *Int. immunopharmacology* 65, 360–365. doi:10.1016/j.intimp.2018.10.027

Ahmad, S. F., Ansari, M. A., Nadeem, A., Bakheet, S. A., Al-Ayadhi, L. Y., Alotaibi, M. R., et al. (2019). Dysregulation of T Cell Immunoglobulin and Mucin Domain 3 (TIM-3) Signaling in Peripheral Immune Cells Is Associated with Immune Dysfunction in Autistic Children. *Mol. Immunol.* 106, 77–86. doi:10.1016/j.molimm.2018.12.020

Almine, J. F., Wise, S. G., and Weiss, A. S. (2012). Elastin Signaling in Wound Repair. *Birth Defects Res. C: Embryo Today Rev.* 96, 248–257. doi:10.1002/bdrc.21016

Braiman-Wiksman, L., Solomonik, I., Spira, R., and Tennenbaum, T. (2007). Novel Insights into Wound Healing Sequence of Events. *Toxicol. Pathol.* 35, 767–779. doi:10.1080/01926230701584189

Buetow, D. E. (1968). *The Biology of Euglena*. New York, London: Academic Press.

Celestine, A. A., and James, C. O. (2007). Effects of Mixed Substrates on Growth and Vitamin Production by *Euglena Gracilis*. *Afr. J. Biotechnol.* 6, 2612–2615. doi:10.5897/AJB2007.000-2417

Chen, C.-Y., Rao, S.-S., Ren, L., Hu, X.-K., Tan, Y.-J., Hu, Y., et al. (2018). Exosomal DMBT1 from Human Urine-Derived Stem Cells Facilitates Diabetic Wound Repair by Promoting Angiogenesis. *Theranostics* 8, 1607–1623. doi:10.7150/thno.22958

Das, B. K., Pradhan, J., Pattnaik, P., Samantaray, B. R., and Samal, S. K. (2005). Production of Antibacterials from the Freshwater Alga *Euglena Viridis* (Ehren). *World J. Microbiol. Biotechnol.* 21, 45–50. doi:10.1007/s11274-004-1555-3

Ehrlich, H. P., and Krummel, T. M. (1996). Regulation of Wound Healing from a Connective Tissue Perspective. *Wound Repair Regen.* 4, 203–210. doi:10.1046/j.1524-475X.1996.40206.x

Eming, S. A., Martin, P., and Tomic-Canic, M. (2014). Wound Repair and Regeneration: Mechanisms, Signaling, and Translation. *Sci. Transl. Med.* 6, 265sr6. doi:10.1126/scitranslmed.3009337

Foltínová, P., Lahitová, N., and Ebringer, L. (1994). Antimutagenicity in *Euglena Gracilis*. *Mutat. Res. Lett.* 323, 167–171. doi:10.1016/0165-7992(94)90029-9

Guo, Q., Bi, D., Wu, M., Yu, B., Hu, L., Liu, C., et al. (2019). Immune Activation of Murine RAW264.7 Macrophages by Sonicated and Alkalized Paramylon from *Euglena Gracilis*. *BMC Microbiol.* 20, 171. doi:10.1186/s12866-020-01782-y

Gurtner, G. C., Werner, S., Barrandon, Y., and Longaker, M. T. (2008). Wound Repair and Regeneration. *Nature* 453, 314–321. doi:10.1038/nature07039

Ishiguro, S., Upreti, D., Robben, N., Burghart, R., Loyd, M., Ogun, D., et al. (2020). Water Extract from Euglena Gracilis Prevents Lung Carcinoma Growth in Mice by Attenuation of the Myeloid-Derived Cell Population. *Biomed. Pharmacother.* 127, 110166. doi:10.1016/j.biopha.2020.110166

Kankkunen, P., Teirilä, L., Rintahaka, J., Alenius, H., Wolff, H., and Matikainen, S. (2010). (1,3)-β-Glucans Activate Both Dectin-1 and NLRP3 Inflammasome in Human Macrophages. *J. Immunol.* 184, 6335–6342. doi:10.4049/jimmunol.0903019

Kirmaz, C., Bayrak, P., Yilmaz, O., and Yuksel, H. (2005). Effects of Glucan Treatment on the Th1/th2 Balance in Patients with Allergic Rhinitis: a Double-Blind Placebo-Controlled Study. *Eur. Cytokine Netw.* 16, 128–134.

Kottuparambil, S., Thankamony, R. L., and Agusti, S. (2019). *Euglena* as a Potential Natural Source of Value-Added Metabolites. A Review. *Algal Res.* 37, 154–159. doi:10.1016/j.algal.2018.11.024

Leung, D. Y., and Bieber, T. (2003). Atopic Dermatitis. *The Lancet* 361, 151–160. doi:10.1016/S0140-6736(03)12193-9

Lewis, A., and Guéguen, C. (2020). Molecular Characterization of Water Extractable Euglena Gracilis Cellular Material Composition Using Asymmetrical Flow Field-Flow Fractionation and High-Resolution Mass Spectrometry. *Anal. Bioanal. Chem.* 412, 4143–4153. doi:10.1007/s00216-020-02650-4

Li, H., Yang, L., Zhang, Y., and Gao, Z. (2016). Kaempferol Inhibits Fibroblast Collagen Synthesis, Proliferation and Activation in Hypertrophic Scar via Targeting TGF-β Receptor Type I. *Biomed. Pharmacother.* 83, 967–974. doi:10.1016/j.biopha.2016.08.011

Lintner, K., Chamberlin, C. M., Lamy, F., and Mondon, P. (2014). *Patent*. US8741357B2. 2014-06-03.

Luo, Y., Diao, H., Xia, S., Dong, L., Chen, J., and Zhang, J. (2010). A Physiologically Active Polysaccharide Hydrogel Promotes Wound Healing. *J. Biomed. Mater. Res.* 94A, 193–204. doi:10.1002/jbm.a.32711

Martin, P. (1997). Wound Healing--Aiming for Perfect Skin Regeneration. *Science* 276, 75–81. doi:10.1126/science.276.5309.75

Mori, T., Miyamoto, H., Yoshida, M., Asakawa, M., Kawasumi, T., Kobayashi, H., et al. (2011). IL-1β and TNFα-initiated IL-6-STAT3 pathway is critical in mediating inflammatory cytokines and RANKL expression in inflammatory arthritis. *Int. Immunol.* 23, 701–712.

Nakashima, A., Sasaki, K., Sasaki, D., Yasuda, K., Suzuki, K., and Kondo, A. (2021). The Alga *Euglena Gracilis* Stimulates *Faecalibacterium* in the Gut and Contributes to Increased Defecation. *Sci. Rep.* 11, 1074. doi:10.1038/s41598-020-80306-0

Nakashima, A., Suzuki, K., Asayama, Y., Konno, M., Saito, K., Yamazaki, N., et al. (2017). Oral Administration of Euglena Gracilis Z and its Carbohydrate Storage Substance Provides Survival protection against Influenza Virus Infection in Mice. *Biochem. Biophysical Res. Commun.* 494, 379–383. doi:10.1016/j.bbrc.2017.09.167

Panja, S., Ghate, N. B., and Mandal, N. (2016). A Microalga, *Euglena Tuba* Induces Apoptosis and Suppresses Metastasis in Human Lung and Breast Carcinoma Cells through ROS-Mediated Regulation of MAPKs. *Cancer Cel Int* 16, 51. doi:10.1186/s12935-016-0330-5

Pavan, S., and Berti, F. (2012). Short Peptides as Biosensor Transducers. *Anal. Bioanal. Chem.* 402, 3055–3070. doi:10.1007/s00216-011-5589-8

Picciotto, S., Barone, M. E., Fierli, D., Aranyos, A., Adamo, G., Božič, D., et al. (2021). Isolation of Extracellular Vesicles from Microalgae: towards the Production of Sustainable and Natural Nanocarriers of Bioactive Compounds. *Biomater. Sci.* 9, 2917–2930. doi:10.1039/d0bm01696a

Rudyardjo, D. I., and Wijayanto, S. (2017). The Synthesis and Characterization of Hydrogel Chitosan-Alginate with the Addition of Plasticizer Lauric Acid for Wound Dressing Application. *J. Phys. Conf. Ser.* 853, 012042–012047. doi:10.1088/1742-6596/853/1/012042

Russo, R., Barsanti, L., Evangelista, V., Frassanito, A. M., Longo, V., Pucci, L., et al. (2016). Euglena Gracilisparamylon Activates Human Lymphocytes by Upregulating Pro-inflammatory Factors. *Food Sci. Nutr.* 5, 205–214. doi:10.1002/fsn3.383

Sakagami, H., Kikuchi, K., Takeda, M., Sato, T., Ichikawa, S., Fujimaki, M., et al. (1991). Macrophage Stimulation Activity of Antimicrobial N,N-dimethylaminoethyl Paramylon. *In Vivo* 5, 101–105.

Schneider, C. A., Rasband, W. S., and Eliceiri, K. W. (2012). NIH Image to ImageJ: 25 Years of Image Analysis. *Nat. Methods* 9, 671–675. doi:10.1038/nmeth.2089

Shibakami, M., Tsubouchi, G., Nakamura, M., and Hayashi, M. (2013). Preparation of Carboxylic Acid-Bearing Polysaccharide Nanofiber Made from Euglenoid β-1,3-glucans. *Carbohydr. Polym.* 98, 95–101. doi:10.1016/j.carbpol.2013.05.026

Shibakami, M., Tsubouchi, G., Sohma, M., and Hayashi, M. (2015). Preparation of Transparent Self-Standing Thin Films Made from Acetylated Euglenoid β-1,3-glucans. *Carbohydr. Polym.* 133, 421–428. doi:10.1016/j.carbpol.2015.06.104

Sugiyama, A., Hata, S., Suzuki, K., Yoshida, E., Nakano, R., Mitra, S., et al. (2010). Oral Administration of Paramylon, a .BETA.-1,3-D-Glucan Isolated from Euglena Gracilis Z Inhibits Development of Atopic Dermatitis-like Skin Lesions in NC/Nga Mice. *J. Vet. Med. Sci.* 72, 755–763. doi:10.1292/jvms.09-0526

Sugiyama, A., Suzuki, K., Mitra, S., Arashida, R., Yoshida, E., Nakano, R., et al. (2009). Hepatoprotective Effects of Paramylon, a .BETA.-1,3-D-Glucan Isolated from Euglena Gracilis Z, on Acute Liver Injury Induced by Carbon Tetrachloride in Rats. *J. Vet. Med. Sci.* 71, 885–890. doi:10.1292/jvms.71.885

Suzuki, K., Nakashima, A., Igarashi, M., Saito, K., Konno, M., Yamazaki, N., et al. (2018). *Euglena Gracilis* Z and its Carbohydrate Storage Substance Relieve Arthritis Symptoms by Modulating Th17 Immunity. *PLoS ONE* 13, e0191462. doi:10.1371/journal.pone.0191462

Wang, Y., Seppänen-Laakso, T., Rischer, H., Wiebe, M. G., and Adrianna, I. (2018). *Euglena Gracilis* Growth and Cell Composition under Different Temperature, Light and Trophic Conditions. *PLoS ONE* 13 (4), e0195329. doi:10.1371/journal.pone.0195329

Yasuda, K., Ogushi, M., Nakashima, A., Nakano, Y., and Suzuki, K. (2018). Accelerated Wound Healing on the Skin Using a Film Dressing with β-Glucan Paramylon. *In Vivo* 32, 799–805. doi:10.21873/invivo.11231010.21873/invivo.11310

Yin, H., Chen, C.-Y., Liu, Y.-W., Tan, Y.-J., Deng, Z.-L., Yang, F., et al. (2019). *Synechococcus Elongatus* PCC7942 Secretes Extracellular Vesicles to Accelerate Cutaneous Wound Healing by Promoting Angiogenesis. *Theranostics* 9, 2678–2693. doi:10.7150/thno.31884

Yoshino, S., Tabata, T., Hazama, S., Iizuka, N., Yamamoto, K., Hirayama, M., et al. (2000). Immunoregulatory Effects of the Antitumor Polysaccharide Lentinan on Th1/Th2 Balance in Patients with Digestive Cancers. *Anticancer Res.* 20, 4707–4711.

Zhang, J., Guan, J., Niu, X., Hu, G., Guo, S., Li, Q., et al. (2015). Exosomes Released from Human Induced Pluripotent Stem Cells-Derived MSCs Facilitate Cutaneous Wound Healing by Promoting Collagen Synthesis and Angiogenesis. *J. Transl Med.* 13, 49. doi:10.1186/s12967-015-0417-0

Zhu, Y., Liao, Y., Zhang, Y., Shekh, M. I., Zhang, J., You, Z., et al. (2021). Novel Nanofibrous Membrane-supporting Stem Cell Sheets for Plasmid Delivery and Cell Activation to Accelerate Wound Healing. *Bioeng. Transl Med.* 2021, e10244. doi:10.1002/btm2.10244

Zhu, Y., Tan, J., Zhu, H., Lin, G., Yin, F., Wang, L., et al. (2017). Development of Kartogenin-Conjugated Chitosan-Hyaluronic Acid Hydrogel for Nucleus Pulposus Regeneration. *Biomater. Sci.* 5, 784–791. doi:10.1039/C7BM00001D

Conflict of Interest: The authors declare that the research was conducted in the absence of any commercial or financial relationships that could be construed as a potential conflict of interest.

Publisher's Note: All claims expressed in this article are solely those of the authors and do not necessarily represent those of their affiliated organizations, or those of the publisher, the editors, and the reviewers. Any product that may be evaluated in this article, or claim that may be made by its manufacturer, is not guaranteed or endorsed by the publisher.

frontiers in Microbiology

ORIGINAL RESEARCH
published: 10 December 2021
doi: 10.3389/fmicb.2021.743246

Extracts of Amazonian Fungi With Larvicidal Activities Against *Aedes aegypti*

Marta Rodrigues de Oliveira[1], Ricardo de Melo Katak[2], Gilvan Ferreira da Silva[3], Osvaldo Marinotti[4], Olle Terenius[5], Wanderli Pedro Tadei[1,2,6†], Afonso Duarte Leão de Souza[1,7,8] and Antonia Queiroz Lima de Souza[1,7,9]**

[1] Programa de Pós-graduação em Biodiversidade e Biotecnologia (PPG-BIONORTE), Universidade Federal do Amazonas, Manaus, Brazil, [2] Programa de Pós-graduação em Biotecnologia, Universidade Federal do Amazonas, Manaus, Brazil, [3] Embrapa Amazônia Ocidental, Manaus, Brazil, [4] MTEKPrime, Aliso Viejo, CA, United States, [5] Department of Cell and Molecular Biology, Microbiology, Uppsala University, Uppsala, Sweden, [6] Laboratório de Malária e Dengue, Instituto Nacional de Pesquisas da Amazônia, Manaus, Brazil, [7] Central Analítica – Centro de Apoio Multidisciplinar, Universidade Federal do Amazonas, Manaus, Brazil, [8] Departamento de Química, Universidade Federal do Amazonas, Manaus, Brazil, [9] Faculdade de Ciências Agrárias, Universidade Federal do Amazonas, Manaus, Brazil

OPEN ACCESS

Edited by:
Ahmed M. Abdel-Azeem, Suez Canal University, Egypt

Reviewed by:
Muniaraj Mayilsamy, Vector Control Research Centre (ICMR), India
Aunchalee Thanwisai, Naresuan University, Thailand
Elsiddig Noureldin, Saudi Center for Disease Control and Prevention (CDC), Saudi Arabia

***Correspondence:**
Marta Rodrigues de Oliveira
moliveirabiotec@gmail.com
Antonia Queiroz Lima de Souza
antoniaqueiroz@ufam.edu.br

[†] *In memoriam*

Specialty section:
This article was submitted to Microbiotechnology, a section of the journal Frontiers in Microbiology

Received: *17 July 2021*
Accepted: *28 October 2021*
Published: *10 December 2021*

Citation:
de Oliveira MR, Katak RM, da Silva GF, Marinotti O, Terenius O, Tadei WP, de Souza ADL and de Souza AQL (2021) Extracts of Amazonian Fungi With Larvicidal Activities Against Aedes aegypti. Front. Microbiol. 12:743246. doi: 10.3389/fmicb.2021.743246

The global increase in diseases transmitted by the vector *Aedes aegypti*, new and re-emerging, underscores the need for alternative and more effective methods of controlling mosquitoes. Our aim was to identify fungal strains from the Amazon rain forest that produce metabolites with larvicidal activity against *Aedes aegypti*. Thirty-six fungal strains belonging to 23 different genera of fungi, isolated from water samples collected in the state of Amazonas, Brazil were cultivated. The liquid medium was separated from the mycelium by filtration. Medium fractions were extracted with ethyl acetate and isopropanol 9:1 volume:volume, and the mycelia with ethyl acetate and methanol 1:1. The extracts were vacuum dried and the larvicidal activity was evaluated in selective bioassays containing 500 μg/ml of the dried fungal extracts. Larval mortality was evaluated up to 72 h. None of the mycelium extracts showed larvicidal activity greater than 50% at 72 h. In contrast, 15 culture medium extracts had larvicidal activity equal to or greater than 50% and eight killed more than 90% of the larvae within 72 h. These eight extracts from fungi belonging to seven different genera (*Aspergillus, Cladosporium, Trichoderma, Diaporthe, Albifimbria, Emmia,* and *Sarocladium*) were selected for the determination of LC_{50} and LC_{90}. *Albifimbria lateralis* (1160) medium extracts presented the lowest LC_{50} value (0.268 μg/ml) after 24 h exposure. *Diaporthe ueckerae* (1203) medium extracts presented the lowest value of LC_{90} (2.928 μg/ml) at 24 h, the lowest values of LC_{50} (0.108 μg/ml) and LC_{90} (0.894 μg/ml) at 48 h and also at 72 h (LC_{50} = 0.062 μg/ml and LC_{90} = 0.476 μg/ml). Extracts from *Al. lateralis* (1160) and *D. ueckerae* (1203) showed potential for developing new, naturally derived products, to be applied in integrated vector management programs against *Ae. aegypti*.

Keywords: biological control, arbovirus, *Aedes aegypti*, larvicidal activity, metabolites

INTRODUCTION

Aedes aegypti mosquitoes are the main vectors of arboviruses such as those that cause dengue, chikungunya, and Zika illnesses (Consoli and Oliveira, 1994; de Oliveira Barbosa Bitencourt et al., 2021). These diseases have occupied a prominent position in public health in several countries of the Americas, including Brazil where the occurrence of all these arboviruses has been recorded simultaneously since 2015 (Saúde and Saúde, 2016).

In 2014, chikungunya fever was first recorded in Brazil and spread rapidly throughout the country (Araújo et al., 2020). A short time later, Zika virus was detected in northeastern Brazil in 2015 (Possas et al., 2017). In 2016, the country reached a peak of cases, with more than 215 thousand estimated cases of Zika (Saúde and Saúde, 2018), which resulted in thousands of cases of neonatal microcephaly (Zanotto and Leite, 2018). Dengue is characterized as one of the main arboviruses with worldwide outbreaks occurring in the Americas, Africa, the Middle East, Asia, and the Pacific Islands. About 3.9 billion people in 129 countries are at risk of infection by the dengue virus, a notable increase from previous decades, partially explained by the improvement of records and recognition of the disease burden by governments (WHO, 2020). According to the Pan American Health Organization, the highest number of dengue cases ever reported globally was in 2019. Brazil alone reported about 2.2 million cases in 2019, representing 70% of the total recorded in the Americas (PAHO, 2020).

Since specific antiviral drugs and effective vaccines against these arboviruses are not available, measures to curb the transmission of these diseases remain focused on vector control, mostly through the elimination of breeding sites and the use of chemical insecticides (Zara et al., 2016). However, the frequent use of chemical insecticides is toxic to the environment and has resulted in the selection of insecticide-resistant mosquito populations (Seetharaman et al., 2018; Araújo et al., 2020). It is therefore urgently necessary to explore new approaches to control these vectors.

Fungal secondary metabolites constitute a rich source of bioactive molecules (Daniel et al., 2017), potentially useful for mosquito control. More specifically, fungi isolated from aquatic habitats are a rich and unexplored source of new natural products. In order to adapt and survive in the aquatic environment, fungi accumulate unique bioactive secondary metabolites, not found in terrestrial environments (Bhakuni and Rawat, 2006; Imhoff, 2016).

The Amazon rainforest contains ∼ 25% of the world's terrestrial biodiversity (Malhi et al., 2008), including microorganisms potentially useful for *A. aegypti* control programs. In this work, we explored the larvicidal potential of the fungi isolated from the aquatic environments of the Amazon region. Our results suggest the possibility of utilizing fungi-derived extracts and/or their metabolites as part of integrated vector management programs.

MATERIALS AND METHODS

Production of the Fungal Extracts

Fungi Isolation and Identification

Thirty-six fungi were isolated from water samples collected in the municipalities of Coari (muddy water) and São Gabriel da Cachoeira (black water), in the state of Amazonas, Brazil, using standard microbiological techniques. Water samples were collected at the following four sites: (a) Coari/C1 – dam (4° 06′ 43.7″ S 63° 07′ 43.6″ W), (b) Coari/C2 – natural lake (4° 06′ 56.6″ S 63° 08′ 34.4″ W), (c) São Gabriel da Cachoeira/S3 – fish farm (0° 6′ 54.873″ S 67° 5′ 12.859″ W), and (d) São Gabriel da Cachoeira/S4 – natural lake (0° 7′ 6.866″ S 67° 4′ 24.576″ W). Isolated fungi were preserved in glycerol 20%, at −80°C and stored in the collection of microorganisms of the Laboratory of Bioassays and Microorganisms of the Amazon at the Federal University of Amazonas (LabMicrA/UFAM). All fungi were registered in the Brazilian National System of Genetic Heritage Management and Associated Traditional Knowledge (SisGen) under the number AD64E07. The fungal strains were identified according to their unique deposit code in the LabMicrA/UFAM collection. Taxonomic identification of the strains was carried out in a previous study (Oliveira, 2021) and was based on the DNA sequences of the internal transcribed spacer region (ITS2) and macro- and micro morphological characters (Hanlin and Ulloa, 1988; Hawksworth et al., 1995; Dugan, 2006).

Fungal Extract Preparation

Each isolate was first inoculated in Petri dishes containing a PDA + L semi-solid culture medium (200 g/l potato, 20 g/l dextrose and 15 g/l agar and 2 g/l yeast extract). Three fragments of the mycelium of the fungi (three-point inoculation) were sown at equidistant points and cultivated at 26°C for 8 days to confirm the purity of the preserved samples. Then a single fragment of each fungus was transferred into a new Petri dish (central point) containing the PDA + L medium and grown under the same conditions used previously. Then, five fragments of 1 cm^2 of each fungus were inoculated in 300 ml of PD + L liquid culture medium (200 g/l potato, 20 g/l dextrose, and 2 g/l yeast extract) under sterile conditions (Souza et al., 2004). The samples were prepared in quintuplicate, including the media control and kept in static mode at 26°C in the absence of light.

Glucose and pH measurements of all samples were carried out every 3 days using test strips (Uriclin 10). The optimal time of cultivation of each strain was established as the time needed for total consumption of the glucose provided in the fresh medium. The cultured liquid medium was then vacuum filtered and separated from the mycelium. The culture liquid, totalizing a final volume of 1.1 l for each fungus, was partitioned, so an organic mixture, immiscible with water, was required. The partitioning process was done in a separating funnel with a mixture of ethyl acetate (AcOEt) and isopropanol (iPr-OH) 9:1 volume/volume (v/v) three times, using each time 300 ml of the solvent mixture.

The mycelium extraction was an immersion process. The solvent mixture used polar and non-polarized directed metabolites. The mycelium fraction was soaked with a mixture of methanol (MeOH) and AcOEt 1:1 (v/v) for 48 h and was then filtered to obtain the first extract. The mycelium was soaked twice more for 24 h and the extracts were combined with the first one. Each liquid and mycelial extracts obtained were concentrated in a rotary evaporator (Tecnal®), under reduced pressure with a vacuum pump and at 45°C. Dried extracts were weighed and stored in a desiccator with activated silica.

Rearing *Aedes aegypti*

Field collected *Aedes aegypti* eggs (F0) (Manaus, Brazil, February 2018) were placed in containers with water for hatching. The larvae were reared in a plastic tray containing distilled water, and the water was changed every 2 days. The larvae were fed daily with a mixture of rat food (Teklad Global 18%) and cat food (Whiskas®) at a ratio of 1:1 until they reached the pupal stage and were then transferred to plastic cups containing 50 ml of water, which were placed in mosquito rearing cages (30 cm × 30 cm × 30 cm) for the emergence of adult mosquitoes. *Aedes aegypti* taxonomic identification was confirmed by morphological examination of the emerging adults (Forattini, 2002).

Adults were fed with 10% sucrose solution soaked in cotton balls, and twice a week, the females were fed with blood by placing anesthetized hamsters (*Mesocricetus auratus*) on top of the entomological cage for 30 min, according to the protocol authorized by the Ethics Committee for the Use of Animals – CEUA (CEUA, opinion No. 054/2018). Plastic cups with 100 ml of water with partially immersed strip of filter paper were available for egg laying. The paper strips with laid eggs (F1) were dried for 2–3 days then placed in distilled water for hatching. The hatched larvae were again maintained in the same way as described before. Third instar larvae of the second generation (F2) were used for the larvicidal bioassays. All mosquitoes were kept under controlled conditions of temperature of 26 ± 2°C and relative humidity of 75 ± 5%, with a photoperiod of 12:12 h (light/dark), as recommended by the WHO (2005).

Larvicidal Bioassays

The selective and quantitative bioassays followed the criteria established by Dulmage et al. (1990) and the WHO (2005) with minor modifications. All bioassays were conducted under temperature, humidity, and photoperiod-controlled conditions, as previously mentioned.

Selective bioassays were performed in triplicate using 50 ml plastic cups containing 10 ml of distilled water, ten 3rd instar larvae, powdered rat food (Teklad Global 18%) and 500 μg/ml of the fungal extract. All tested samples were solubilized in dimethyl sulfoxide (DMSO; Thermo Fisher Scientific). Mortality readings were recorded at 24, 48, and 72 h after exposure to the fungal extracts (Danga et al., 2014). The extracts that presented mortality equal to or greater than 90% in the selective bioassay were chosen to perform quantitative bioassays and determine lethal concentrations able to kill 50% (LC_{50}) or 90% of the larvae (LC_{90}).

To determine LC_{50} and LC_{90} values, larvae were exposed to eight different concentrations of the fungal extracts, ranging from 0.01 to 250 μg/ml. Each concentration was tested in quintuplicate with three repetitions. All assays were conducted in plastic cups with a capacity of 110 ml, containing 20 ml of distilled water, powdered food, twenty 3rd instar larvae and the quantity corresponding to each concentration of fungal extract tested. DMSO as the negative control and Temephos (Pestanal Sigma-Aldrich) as the positive control were used at the same concentrations as the extracts. DMSO (maximum volume of DMSO in the assay – 0.1 ml) did not cause mortality in any of the tested concentrations and Temephos (500 μg/ml) killed 100% of the larvae in the selective bioassay.

Statistical Analysis

The mortality data obtained in the bioassays were submitted to Probit analysis $p \leq 0.05$ (Finney, 1952), using the statistical software Polo Plus (LeOra Software, CA, United States; Haddad, 1998). Lethal concentrations and the confidence interval (95% CI) were calculated using the Lilliefors normality test (K), analysis of variance (ANOVA), a multiple comparison test ($p \leq 0.05$) and the Student's *t* test using BioStat 5.3 for Windows software (Ayres et al., 2007).

RESULTS

In this study, 36 isolates belonging to 23 genera of fungi were analyzed regarding their ability to produce mosquito larvicidal compounds. Extracts from isolated strain were obtained from both mycelium and culture liquid medium fractions of the cultures. The growth time of the fungi until no glucose was detected in the medium ranged from 17 to 85 days. The pH of the cultures ranged from 6 to 7.5 in comparison to the pH of 5.5 in the control (non-inoculated medium). The extracts obtained from the liquid medium presented yielded between 82 and 724 mg, after extraction and drying procedures. Mycelium extracts from fungi strains 1132 and 1126 yielded 256 and 5872 mg, respectively, being the lowest and the highest obtained values (**Table 1**).

Seven mycelium extracts originating from fungi belonging to six genera (*Aspergillus, Cladosporium, Fusarium, Diaporthe, Talaromyces,* and *Trichoderma*) caused larval mortality from 3.3 to 43.3%, and none presented mortality equal to or greater than 50% up to 72 h of exposure (**Supplementary Table 1**). Larvicidal activity equal to or greater than 50% was observed in 15 of the 36 extracts of liquid medium; six liquid medium extracts belonging to five genera (*Albifimbria, Aspergillus, Diaporthe, Emmia,* and *Sorocladium*) killed 100% of the larvae within 72 h.

Eight extracts (from strains 1126, 1132, 1133, 1160, 1203, 1232, 1242, and 1266) showed larvicidal activity equal to or greater than 50% at 24 h, four (1244, 1246, 1248, and 1280) resulted in 50% mortality only at 48 h and three extracts (1184, 1240, and 1283) caused 50% mortality only at 72 h of exposure. Six extracts caused 100% larval mortality, three (1160, 1203, and 1242) in

TABLE 1 | Crude extracts of 36 fungi isolated from aquatic environments in the Amazonian municipalities of Coari and São Gabriel da Cachoeira used in the larvicidal tests against *Aedes aegypti*.

Tested lineage	GenBank accession numbers	Taxonomic identification	Cultivation time (days)	pH	Glucose	Extract yield (mg)	
						Liquid medium	Mycelium
1160	MZ781268	*Albifimbria lateralis* ^{C1}	50	6.5	0	120	820
1283	MZ781299	*Aspergillus hortai* ^{C1}	17	6.5	0	724	2577
1126	MZ781261	*Aspergillus* sp. ^{C1}	24	6.5	0	254	5872
1169	MZ781272	*Chrysoporthe* sp. ^{C1}	18	6.5	0	260	1624
1132	MZ781262	*Cladosporium* sp. ^{C1}	17	7	0	134	256
1135	MZ781264	*Cladosporium* sp. ^{C1}	17	6.5	0	177	334
1098	MZ781256	*Cytospora* sp. ^{C2}	52	6	0	180	628
1106	MZ781257	*Cytospora* sp. ^{C2}	41	6	0	443	3123
1203	MZ781276	*Diaporthe ueckerae* ^{S4}	41	6	0	249	2298
1242	MZ781281	*Diaporthe ueckerae* ^{S4}	28	7	0	152	872
1232	MZ781279	*Emmia* sp. ^{S4}	52	7.5	0	161	1128
1248	MZ781286	*Epicoccum latusicollum* ^{C1}	24	6.5	0	134	2564
1240	MZ781280	*Eutypella* sp. ^{S4}	41	6.5	0	221	3393
1262	MZ781291	*Fusarium oxysporum* ^{C1}	24	6.5	0	82	1559
1280	MZ781298	*Fusarium oxysporum* ^{C1}	24	6.5	0	98	959
1085	MZ781250	*Fusarium* sp. ^{S4}	27	7	0	90	1430
1277	MZ781297	*Hongkongmyces* sp. ^{S4}	72	6.5	0	92	439
1273	MZ781296	*Hyphodermella* sp. ^{C1}	67	6	0	85	547
1205	MZ781277	*Hypomontagnella monticulosa* ^{C1}	72	8	0	258	750
1082	MZ781248	*Microsphaeropsis arundinis*^{C1}	52	7.5	0	129	947
1079	MZ781246	*Nigrograna chromolaenae* ^{C1}	55	6.5	0	117	2840
1123	MZ781259	Ochronis sp. ^{C1}	28	6.5	0	149	540
1083	MZ781249	*Paraconiothyrium estuarinum* ^{C1}	28	6.5	0	129	2830
1184	MZ781274	*Paraconiothyrium estuarinum* ^{S4}	63	6.5	0	140	2019
1265	MZ781293	*Paraconiothyrium estuarinum* ^{C1}	27	7	0	138	1850
1080	MZ781247	*Paraconiothyrium* sp. ^{S4}	28	6	0	132	1985
1245	MZ781283	*Penicillium citreosulfuratum*^{S4}	35	6	0	250	838
1266	MZ781294	*Sorocladium* sp. ^{C2}	80	6.5	0	92	645
1089	MZ781252	*Striaticonidium synnematum* ^{S3}	31	7.5	0	205	1025
1263	MZ781292	*Talaromyces amestolkiae* ^{C2}	18	6	0	250	3028
1087	MZ781251	*Talaromyces* sp. ^{C2}	50	6.5	0	268	820
1244	MZ781282	*Talaromyces* sp. ^{S4}	80	6.5	0	262	901
1246	MZ781284	*Talaromyces* sp. ^{S4}	17	6	0	127	1292
1247	MZ781285	*Trametes menziesii* ^{C2}	35	6	0	158	2870
1133	MZ781263	*Trichoderma atroviride* ^{C2}	80	7.5	0	134	2109
1136	MZ781265	*Trichoderma atroviride* ^{C2}	85	6	0	223	334
		Control (culture medium)	80	5.5	2000	201	–

The water samples were collected at the following four sites: (a) ^{C1} Coari – dam; (b) ^{C2} Coari – natural lake; (c) ^{S3} São Gabriel da Cachoeira – fish rearing pond; and (d) ^{S4} São Gabriel da Cachoeira – natural lake. GenBank accession numbers are nucleotide sequences of approximately 700 bp including the internal transcribed spacers (ITS1-5.8S-ITS2). Cultivation time is the time needed for total consumption of the glucose provided in the fresh medium. Extract yield is the dry weight of extracted metabolites.

less than 24 h, two (1126 and 1266) at 48 h and one (1232) at 72 h (**Figure 1**).

Extracts with larvicidal activity equal to or greater than 90% (*Albifimbria lateralis* 1160, *Aspergillus* sp. 1126, *Cladosporium* sp. 1132, *D. ueckerae* 1203 and 1242, *Emmia* sp. 1232, *Sorocladium* sp. 1266, and *Trichoderma atroviride* 1133) were further studied and LC_{50} and LC_{90} values determined (**Figure 1** and **Supplementary Table 1**).

Overall, the liquid medium extracts from *Al. lateralis* 1160 and *D. ueckerae* 1203 showed the best results, with highest mortality rates and lowest LC values. The extract of the strain 1160 (*Al. lateralis*) presented the lowest LC_{50} (0.268 μg/ml) at 24 h. The extract of the 1203 strain (*D. ueckerae*) had the lowest LC_{90} (2.928 μg/ml) at 24 h. Furthermore, *D. ueckerae* 1203 extracts had the lowest LC_{50} (0.108 μg/ml) and LC_{90} (0.894 μg/ml) at 48 h, and at 72 h with an LC_{50} of 0.062 μg/ml and an LC_{90} of 0.476 μg/ml (**Table 2**).

DISCUSSION

The public health importance of *Ae. aegypti* in tropical regions has attracted the attention of local authorities and the World Health Organization due to the wide geographical

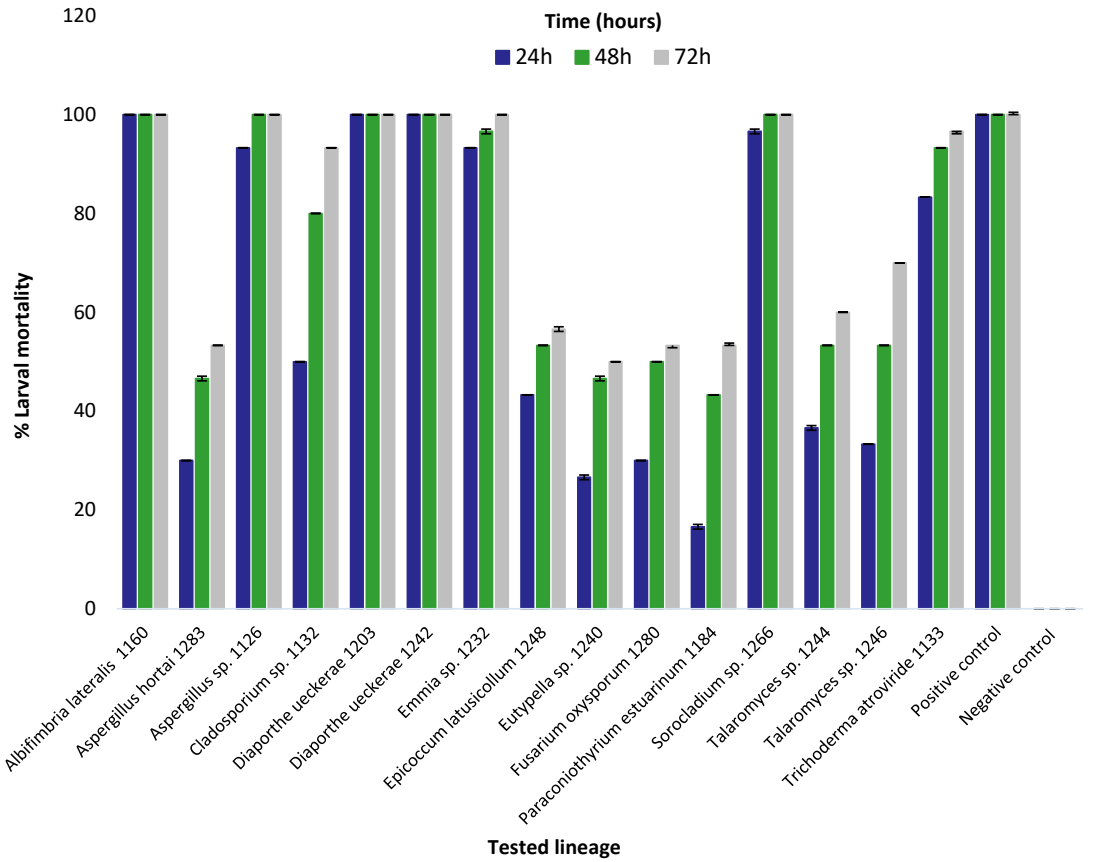

FIGURE 1 | Percentage of mortality of 3rd instar *Aedes aegypti* larvae exposed to liquid medium extracts obtained from strains of fungi isolated from Amazonian aquatic environments. Mortality was assessed after 24, 48, and 72 h of exposure to fungal extract at a concentration of 500 μg/ml. Error bars represent standard deviation. Positive control (Temephos) and Negative control (dimethyl sulfoxide).

distribution and severity of diseases transmitted by these mosquitoes in the last decades, especially dengue, chikungunya, and Zika (Rodrigues-Alves et al., 2020). As such, there is a growing interest in new insecticides and larvicides capable of controlling this vector. Naturally derived insecticides have been pursued as potentially less toxic alternatives, aiming at reducing environmental pollution and preventing the selection of mosquitoes resistant to chemical insecticides (Al-Mekhlafi, 2017; Araújo et al., 2020).

For the control of *Ae. aegypti,* insecticides are frequently applied directly in natural bodies of water and/or artificial containers, usually located closely or kept inside human households. Therefore, the use of natural, potentially less-toxic, insecticides is desirable from both environmental and social perspectives. This work investigated for the first time extracts of fungi isolated from aquatic habitats of the Amazon region in order to identify fungal lineages that can produce larvicidal bioactive metabolites against *Ae. aegypti*.

Following the protocols described here, none of the mycelium extracts showed larvicidal activity resulting in mortality rates above 50% within 72 h. However, 15 extracts from the liquid culture medium resulted in more than 50% mortality. Six killed 100% of the larvae within 72 h and three of these were lethal in less than 24 h, resembling the positive control Temephos. These results demonstrate that some of the isolated fungal strains secrete metabolites with larvicidal activity against *Ae. aegypti*.

The fungi tested in this study were subjected to the similar cultivation conditions. However, cultivation times varied for each fungal strain. To avoid differences in nutrient availability, we used total glucose consumption in the culture medium as determinant of the cultivation time length. Fungi growth styles and physical, chemical and biological factors, among others, influence development time and the production of bioactive metabolites (Kavanagh, 2011; Costa and Nahas, 2012). Species-specific traits explain the difference in cultivation time and biological activities among the isolated fungi studied in our work.

Mosquito larvicidal activities of the mycelial extracts and the liquid culture medium extracts, have been described for other fungi such as *Stereum* sp. (JO5289) (Chirchir et al., 2013), *Beauveria bassiana* (UNI 40) (Daniel et al., 2017), *Trametes* sp. (Waweru et al., 2017), *Pestalotiopsis virgulata* and *Pycnoporus sanguineus* (Bücker et al., 2013). However, the LC_{50} values revealed in our work are lower than those previously published, such as *Metarhizium anisopliae*

TABLE 2 | Lethal larvicidal concentration of liquid culture medium extracts obtained from fungal strains against 3rd instar *Aedes aegypti* larvae.

Tested lineage	LC_{50} μg/ml (CI 95%)	LC_{90} μg/ml (CI 95%)	χ^2	Df	Slope ± SE
24 h					
Tp	0.025 (0.003–0.063)ae	1.161 (0.647–3.364)a	6.9432	5	0.768 ± 0.075
1126	0.872 (0.200–3.956)abd	67.251 (9.676–0.228E + 06)ac	2.8009	2	0.679 ± 0.066
1132	0.459 (0.043–1.057)abd	74.117 (11.419–0.152E + 07)ac	3.9608	3	0.580 ± 0.057
1133	0.463 (0.367–0.586)bh	10.940 (6.789–20.553)bc	1.000	6	0.933 ± 0.060
1160	*0.268 (0.211–0.332)cdf	3.384 (2.429–5.223)ac	2.995	5	1.164 ± 0.061
1203	0.461 (0.123–0.789)adb	*2.928 (1.565–12.543)ac	9.5913	3	1.597 ± 0.065
1232	0.372 (0.087–0.731)adh	26.304 (6.548–35.519)ac	7.6254	4	0.693 ± 0.054
1242	0.427 (0.029–0.839)ah	67.918 (15.092–68.770)ac	0.460	2	0.582 ± 0.078
1266	1.904 (1.288–3.317)ef	205.87 (53.346–272.74)ac	0.961	4	0.630 ± 0.053
48 h					
Tp	0.016 (0.002–0.038)a	0.322 (0.203–0.555)a	5.3850	5	0.979 ± 0.111
1126	0.337 (0.191–0.489)ab	6.293 (3.826–14.549)a	1.922	2	1.009 ± 0.069
1132	0.170 (0.026–0.351)ab	9.896 (3.537–20.621)a	6.3742	4	0.726 ± 0.057
1133	0.142 (0.050–0.253)ab	3.261 (1.548–15.627)a	12.854	5	0.942 ± 0.063
1160	0.123 (0.058–0.195)b	1.106 (0.666–2.735)a	13.497	5	1.345 ± 0.083
1203	*0.108 (0.062–0.157)b	*0.894 (0.604–1.637)a	8.1443	5	1.397 ± 0.091
1232	0.206 (0.030–0.412)b	2.876 (1.302412–35.975)a	15.328	4	1.119 ± 0.074
1242	0.140 (0.078–0.211)b	12.095 (5.974–37.560)a	1.821	5	0.662 ± 0.056
1266	0.391 (0.295–0.505)c	10.825 (6.378–22.952)a	3.846	5	0.889 ± 0.091
72 h					
Tp	0.025 (0.009–0.041)a	0.141 (0.107–0.185)a	2.532	5	1.694 ± 0.280
1126	0.120 (0.053–0.198)a	5.877 (3.351–15.174)a	1.393	4	0.759 ± 0.059
1132	0.079 (0.033–0.132)a	1.387 (0.847–3.138)a	7.5183	5	1.028 ± 0.074
1133	0.070 (0.023–0.126)a	0.890 (0.531–2.237)a	11.466	5	1.163 ± 0.086
1160	0.088 (0.055–0.122)a	0.692 (0.506–1.074)a	5.2154	5	1.434 ± 0.101
1203	*0.062 (0.024–0.103)a	*0.476 (0.315–0.941)a	10.131	5	1.453 ± 0.121
1232	0.096 (0.031–0.172)a	1.292 (0.713–4.132)a	14.264	5	1.134 ± 0.077
1242	0.088 (0.030–0.159)a	2.119 (1.139–6.806)a	9.3874	5	0.928 ± 0.068
1266	0.180 (0.101–0.269)a	2.216 (1.307–5.364)a	9.8043	5	1.174 ± 0.101

*The LC_{50} and LC_{90} were determined at 24, 48, and 72 h after exposure to fungal extracts. LC, lethal concentration; CI, confidence interval; χ^2-chi, square; Df, degrees of freedom; SE, standard error. Equal letters (a, b, c, etc.) do not differ in the probability level of 5% ($p > 0.05$), Tp, Temephos (positive control). The lowest LC values for each time evaluated are shaded in gray and marked with *.*

(LC_{50} = 59.83 μg/ml, Vivekanandhan et al., 2020), *B. bassiana* (LC_{50} = 1.230 μg/ml, Daniel et al., 2017), and *Aspergillus terreus* (LC_{50} = 80.407 μg/ml, Ragavendran and Natarajan, 2015), indicating the potency of the metabolites obtained from the strains tested in our study.

It is worth noting that to date there have been no reports of biological activities against insect species of metabolites produced by fungal strains of the species *Al. lateralis, D. ueckerae,* and *Emmia* sp. For the first time, lineages of these species of fungi with larvicidal activity against *Ae. aegypti* have been identified.

The genus *Albifimbria* consists of four species, i.e., *Al. lateralis*, *Albifimbria terrestris, Albifimbria verrucaria,* and *Albifimbria viridis*, which are usually found in soil, leaves, fruits, and in the air (Lombard et al., 2016). The species *Albifimbria lateralis* (Lombard et al., 2016) has been recently described and needs better investigation regarding the production of secondary metabolites, though our investigation indicates promising applications of this fungus species in vector control. Metabolites produced by *Al. verrucaria* exhibit antimicrobial activities (Zou et al., 2011) and bioherbicidal activities (Walker and Tilley, 1997) and are considered to be a potential biocontrol agent against the fungus *Botrytis cinerea* in grapes (Li et al., 2019).

The species *D. ueckerae* was described by Udayanga et al. (2015). Its occurrence in Brazil was identified by Soares et al. (2018) who isolated this species of fungus from *Costus spiralis* (Jacq.) Roscoe (Costaceae), a plant native to the Amazon region used in traditional medicine. Fungal species of the genus *Diaporthe* are known to be a rich source of secondary metabolites (Chepkirui and Stadler, 2017).

Currently, 106 compounds derived from *Diaporthe* exhibiting biological activities, such as cytotoxic, antifungal, antibacterial, antiviral, antioxidant, anti-inflammatory, phytotoxic, antiparasitic, and herbicidic activities, have been studied (Ash et al., 2010; Meepagala et al., 2018; Xu et al., 2021). Two cyclohexeneoxidediones, phyllostine acetate (1) and phyllostine (2), from the fungus *Diaporthe miriciae*, showed insecticidal activity against *Plutella xylostella* larvae (Ratnaweera et al., 2020). Meepagala et al. (2018) isolated a compound from the liquid medium extract of *Diaporthe eres*, identified as 3,4-dihydro-8-hydroxy-3,5-dimethylisocoumarin (1), which has larvicidal activity against *Ae. aegypti*.

In addition, other fungi from different genera such as *Beauveria*, *Fusarium*, *Metarhizium*, *Neosartorya*, and *Paecilomyces*, also produce compounds with insecticidal activity such as beauvericin, gliotoxin, enniatin, oosporein, destruxins, cytochalasins, etc (Vyas et al., 2007; Masi et al., 2017; Berestetskiy and Hu, 2021).

CONCLUSION

This study is the first to evaluate aquatic fungi strains from the Amazon for their ability of producing mosquito larvicidal metabolites. Our findings open opportunities for the development of new larvicides that may be used as mosquito control agents. Crude fungal extracts, such as those studied here, are a complex mixture of different classes of molecules. The process of fractionation and purification of raw extracts guided by bioactivity (Chirchir et al., 2013) is necessary for the isolation and characterization of the chemical compounds responsible for the larvicidal activities observed in our work. Further studies are needed to characterize the active larvicidal metabolites produced by these fungi and define their mechanisms of action.

DATA AVAILABILITY STATEMENT

The original contributions presented in the study are included in the article/**Supplementary Material**, further inquiries can be directed to the corresponding authors.

AUTHOR CONTRIBUTIONS

MO, WT, ADS, and AQS designed the study. MO, ADS, and AQS performed the production of fungal extracts, analyzed the results, and wrote the manuscript. MO and RK reared mosquitoes and carried out bioassays. MO, GS, OM, OT, ADS, and AQS supervised and finalized the manuscript. All authors read and approved the final manuscript.

FUNDING

This study was financed in part by the Coordenação de Aperfeiçoamento de Pessoal de Nível Superior – Brazil (CAPES) – Finance Code 001, by the project Pró-Amazônia: Biodiversidade e Sustentabilidade (process number 23038.009442/2013-12) and FAPEAM. This study is part of the doctoral thesis of MO (Universidade Federal do Amazonas).

ACKNOWLEDGMENTS

We would like to thank the Graduate Program in Biodiversity and Biotechnology – PPG-BIONORTE, for MO's thesis opportunity, as also the Embrapa Western Amazon/EMBRAPA, Malaria and Dengue Laboratory of the National Institute for Amazonian Research – INPA, and LabMicrA laboratory of the Central Analítica – CAM/ UFAM, for the necessary spaces and equipment to the development of the work.

SUPPLEMENTARY MATERIAL

The Supplementary Material for this article can be found online at: https://www.frontiersin.org/articles/10.3389/fmicb.2021.743246/full#supplementary-material

REFERENCES

Al-Mekhlafi, F. A. (2017). Larvicidal activity of some fungal extracts on *Aedes caspius* and *Culex pipiens* (Diptera: Culicidae). *Entomol. Res.* 47, 388–393. doi: 10.1111/1748-5967.12235

Araújo, I. F., Loureiro, H. A., Marinho, V. H. S., Neves, F. B., Sarquis, R. S. F., Faustino, S. M. M., et al. (2020). Larvicidal activity of the methanolic, hydroethanolic and hexanic extracts from *Acmella oleracea*, solubilized with silk fibroin, against *Aedes aegypti*. *Biocatal. Agric. Biotechnol.* 24:101550. doi: 10.1016/j.bcab.2020.101550

Ash, G. J., Stodart, B., Sakuanrungsirikul, S., Anschaw, E., Crump, N., Hailstones, D., et al. (2010). Genetic characterization of a novel *Phomopsis sp*., a putative biocontrol agent for *Carthamus lanatus*. *Mycologia* 102, 54–61. doi: 10.3852/08-198

Ayres, M., Ayres, J. R. M., Ayres, D. L., and dos Santos, A. (2007). *Aplicações Estatísticas Nas Áreas Das Ciências Biológicas e Médicas*. Belém: BioEstat.

Berestetskiy, A., and Hu, Q. (2021). The chemical ecology approach to reveal fungal metabolites for arthropod pest management. *Microorganisms* 9:1379. doi: 10.3390/microorganisms9071379

Bhakuni, D. S., and Rawat, D. S. (2006). *Bioactive Marine Natural Products*. Berlin: Springer Science & Business Media.

Bücker, A., Bucker, N. C. F., Souza, A. Q., Gama, A. M., Rodrigues-Filho, E., Costa, F. M., et al. (2013). Larvicidal effects of endophytic and basidiomycete fungus extracts on *Aedes* and *Anopheles larvae* (Diptera, Culicidae). *Rev. Soc. Bras. Med. Trop.* 46, 411–419. doi: 10.1590/0037-8682-0063-2013

Chepkirui, C., and Stadler, M. (2017). The genus *Diaporthe*: a rich source of diverse and bioactive metabolites. *Mycol. Prog.* 16, 477–494. doi: 10.1007/s11557-017-1288-y

Chirchir, D. K., Ouma, R. B. O., Cheplogoi, P. K., and Omolo, J. O. (2013). Larvicidal activity of extracellular secondary metabolites from a Stereum species Hill ex Pers.(JO5289) against the dengue fever mosquito, Aedes aegypti (Linn)(Diptera: Culicidae). *Afr. J. Biotechnol.* 12, 6302–6309.

Consoli, R. A. G. B., and Oliveira, R. L. (1994). *Principais Mosquitos de Importância Sanitária no Brasil*. Available online at: http://books.scielo.org/id/th (accessed November 15, 2020).

Costa, B. D. O., and Nahas, E. (2012). Growth and enzymatic responses of phytopathogenic fungi to glucose in culture media and soil. *Braz. J. Microbiol.* 43, 332–340. doi: 10.1590/S1517-83822012000100039

Danga, Y. S. P., Nukenine, E. N., Younoussa, L., and Esimone, C. O. (2014). Phytochemicals and larvicidal activity of *Plectranthus glandulosus* (Lamiaceae) leaf extracts against *Anopheles gambiae*, *Aedes aegypti* and *Culex quinquefasciatus* (Diptera: Culicidae). *Int. J. Pure Appl. Zool.* 2, 160–171.

Daniel, J. F. S., Silva, A. A., Nakagawa, D. H., Medeiros, L. S., Carvalho, M. G., Tavares, L. J., et al. (2017). Larvicidal activity of *Beauveria bassiana* extracts against *Aedes aegypti* and identification of Beauvericins. *J. Braz. Chem. Soc.* 28, 1003–1013. doi: 10.21577/0103-5053.20160253

de Oliveira Barbosa Bitencourt, R., Reis Dos Santos Mallet, J., Mesquita, E., Silva Gôlo, P., Fiorotti, J., Rita Elias Pinheiro Bittencourt, V., et al. (2021). Larvicidal activity, route of interaction and ultrastructural changes in *Aedes aegypti* exposed to entomopathogenic fungi. *Acta Trop.* 213:105732. doi: 10.1016/j.actatropica.2020.105732

Dugan, F. M. (2006). *The Identification of Fungi. An Illustrated Introduction with Keys, Glossary, and Guide to Literature*. Saint Paul, MIN: The American Phytopathological Society.

Dulmage, H. T., Yousten, A. A., Singer, S., and Lacey, L. A. (1990). *Guidelines for Production of Bacillus Thuringiensis H-14 and Bacillus Sphaericus*. Available online at: https://apps.who.int/iris/handle/10665/61645 (accessed May 18, 2020).

Finney, D. J. (1952). *Probit Analysis: A Statistical Treatment of the Sigmoid Response Curve*. Cambridge: Cambridge university press.

Forattini, O. P. (2002). *Culicidologia Médica*, Vol. 2. São Paulo: EDUSP.

Haddad, M. D. L. (1998). *Utilização do Polo-PC Para Análise de Probit. Controle Microbiano de Insetos*. Piracicaba: FEALQ, 999–1013.

Hanlin, R. T., and Ulloa, M. (1988). *Atlas of Introductory Mycology*, 2nd Edn. Winston-Salem: Hunter Textbooks. Inc.

Hawksworth, D. L., Kirk, P. M., Sutton, B. C., and Pegler, D. N. (1995). *Ainsworth & Bisby's Dictionary of the Fungi*, 8th Edn. Oxfordshire: Oxford University Press.

Imhoff, J. F. (2016). Natural products from marine fungi–still an underrepresented resource. *Mar. Drugs* 14:19. doi: 10.3390/md14010019

Kavanagh, K. (ed.) (2011). *Fungi: biology and applications*, 2nd Edn. Hoboken, NJ: John Wiley & Sons.

Li, Z., Chang, P., Gao, L., and Wang, X. (2019). The endophytic fungus albifimbria verrucaria from wild grape as an antagonist of botrytis cinerea and other grape pathogens. *Phytopathology* 110, 843–850. doi: 10.1094/PHYTO-09-19-0347-R

Lombard, L., Houbraken, J., Decock, C., Samson, R. A., Meijer, M., Réblová, M., et al. (2016). Generic hyper-diversity in Stachybotriaceae. *Persoonia* 36, 156–246. doi: 10.3767/003158516X691582

Malhi, Y., Roberts, J. T., Betts, R. A., Killeen, T. J., Li, W., and Nobre, C. A. (2008). Climate change, deforestation, and the fate of the amazon. *Science* 319, 169–172. doi: 10.1126/science.1146961

Masi, M., Cimmino, A., Tabanca, N., Becnel, J. J., Bloomquist, J. R., and Evidente, A. (2017). A survey of bacterial, fungal and plant metabolites against *Aedes aegypti* (Diptera: Culicidae), the vector of yellow and dengue fevers and Zika virus. *Open Chem.* 15, 156–166.

Meepagala, K. M., Estep, A. S., Clausen, B. M., and Becnel, J. J. (2018). Mosquitocidal activity of a naturally occurring isochroman and synthetic analogs from the plant pathogenic fungus, diaporthe eres against *Aedes aegypti* (Diptera: Culicidae). *J. Med. Entomol.* 55, 969–974. doi: 10.1093/jme/tjy016

Oliveira, M. R. (2021). *Potencial da Biodiversidade Fúngica Cultivável de Habitats Aquáticos da Região Amazônica Para o Controle de Doenças Infecciosas*. Ph.D. thesis. Manaus: Universidade Federal do Amazonas.

PAHO (2020). *Pan American Health Organization/World Health Organization. Epidemiological Update: Dengue*. Washington, DC: PAHO.

Possas, C., Brasil, P., Marzochi, M. C., Tanuri, A., Martins, R. M., Marques, E. T., et al. (2017). Zika puzzle in Brazil: peculiar conditions of viral introduction and dissemination - a review. *Mem. Inst. Oswaldo Cruz* 112, 319–327. doi: 10.1590/0074-02760160510

Ragavendran, C., and Natarajan, D. (2015). Insecticidal potency of *Aspergillus terreus* against larvae and pupae of three mosquito species *Anopheles stephensi*, *Culex quinquefasciatus*, and *Aedes aegypti*. *Environ. Sci. Pollut. Res.* 22, 17224–17237. doi: 10.1007/s11356-015-4961-1

Ratnaweera, P. B., Jayasundara, J. M. N. M., Herath, H. H. M. S. D., Williams, D. E., Rajapaksha, S. U., Nishantha, K. M. D. W. P., et al. (2020). Antifeedant, contact toxicity and oviposition deterrent effects of phyllostine acetate and phyllostine isolated from the endophytic fungus *Diaporthe miriciae* against *Plutella xylostella* larvae. *Pest. Manag. Sci.* 76, 1541–1548. doi: 10.1002/ps.5673

Rodrigues-Alves, M. L., Melo-Júnior, O. A., de, O., Silveira, P., Mariano, R. M., da, S., et al. (2020). Historical perspective and biotechnological trends to block arboviruses transmission by controlling *Aedes aegypti* mosquitos using different approaches. *Front. Med.* 7:275. doi: 10.3389/fmed.2020.00275

Saúde, M. D., and Saúde, S. (2016). *Boletim Epidemiológico. Monitoramento dos Casos de Dengue, Febre de Chikungunya e Febre Pelo Vírus Zika até a Semana Epidemiológica 52, 2015*. Available online at: https://antigo.saude.gov.br/images/pdf/2016/janeiro/15/svs2016-be003-dengue-se52.pdf (accessed November 18, 2020).

Saúde, M. D., and Saúde, S. (2018). *Boletim Epidemiológico 47: Situação Epidemiológica da Infecção Pelo Vírus Zika no Brasil, de 2015 a 2017*. Available online at: https://antigo.saude.gov.br/images/pdf/2018/novembro/12/2018-034.pdf (accessed November 15, 2020).

Seetharaman, P. K., Chandrasekaran, R., Gnanasekar, S., Chandrakasan, G., Gupta, M., Manikandan, D. B., et al. (2018). Antimicrobial and larvicidal activity of eco-friendly silver nanoparticles synthesized from endophytic fungi *Phomopsis liquidambaris*. *Biocat. Agric. Biotechnol.* 16, 22–30. doi: 10.1016/j.bcab.2018.07.006

Soares, D. A., Oliveira, D. P., Santos, T. T., Marson, P. G., and Pimenta, R. S. (2018). Multiloci identification of *Diaporthe* fungi isolated from the medicinal plant *Costus spiralis* (Jacq.) Roscoe (Costaceae). *J. Appl. Microbiol.* 125, 172–180. doi: 10.1111/jam.13769

Souza, A. Q. L., Souza, A. D. L., Astolfi Filho, S., Pinheiro, M. L. B., Sarquis, M. I., de, M., et al. (2004). Antimicrobial activity of endophytic fungi isolated from amazonian toxic plants: *Palicourea longiflora* (aubl.) rich and *Strychnos cogens* bentham. *Acta Amazon.* 34, 185–195.

Udayanga, D., Castlebury, L. A., Rossman, A. Y., Chukeatirote, E., and Hyde, K. D. (2015). The *Diaporthe sojae* species complex: phylogenetic re-assessment of pathogens associated with soybean, cucurbits and other field crops. *Fungal Biol.* 119, 383–407. doi: 10.1016/j.funbio.2014.10.009

Vivekanandhan, P., Bedini, S., and Shivakumar, M. S. (2020). Isolation and identification of entomopathogenic fungus from Eastern Ghats of South Indian forest soil and their efficacy as biopesticide for mosquito control. *Parasitol. Int.* 76:102099. doi: 10.1016/j.parint.2020.102099

Vyas, N., Dua, K. K., and Prakash, S. (2007). Efficacy of *Lagenidium giganteum* metabolites on mosquito larvae with reference to nontarget organisms. *Parasitol. Res.* 101, 385–390. doi: 10.1007/s00436-007-0496-9

Walker, H. L., and Tilley, A. M. (1997). Evaluation of an isolate of *Myrothecium verrucaria* from sicklepod (Senna obtusifolia) as a potential mycoherbicide agent. *Biol. Control* 10, 104–112. doi: 10.1006/bcon.1997.0559

Waweru, A. W., Omolo, J. O., Cheplogoi, P. K., and Njue, A. W. (2017). Mosquito larvicidal trihydroxylindene derivative from submerged cultures of trametes species. *Afr. J. Biotechnol.* 16, 1457–1460.

WHO (2005). *Guidelines for Laboratory and Field Testing of Mosquito Larvicides*. Available online at: https://apps.who.int/iris/handle/10665/69101 (accessed October 12, 2020).

WHO (2020). *Dengue and Severe Dengue*. Available online at: https://www.who.int/news-room/fact-sheets/detail/dengue-and-severe-dengue (accessed April 20, 2021)

Xu, T.-C., Lu, Y.-H., Wang, J.-F., Song, Z.-Q., Hou, Y.-G., Liu, S.-S., et al. (2021). Bioactive secondary metabolites of the genus *Diaporthe* and *Anamorph Phomopsis* from terrestrial and marine habitats and endophytes: 2010–2019. *Microorganisms* 9:217. doi: 10.3390/microorganisms9020217

Zanotto, P. M. A., and Leite, L. C. C. (2018). The challenges imposed by dengue, zika, and chikungunya to Brazil. *Front. Immunol.* 9:1964. doi: 10.3389/fimmu.2018.01964

Zara, A. L., de, S. A., Santos, S. M. D., Fernandes-Oliveira, E. S., Carvalho, R. G., and Coelho, G. E. (2016). [*Aedes aegypti* control strategies: a review]. *Epidemiol. Serv. Saude* 25, 391–404. doi: 10.5123/S1679-49742016000200017

Zou, X., Niu, S., Ren, J., Li, E., Liu, X., and Che, Y. (2011). Verrucamides A–D, antibacterial cyclopeptides from *Myrothecium verrucaria*. *J. Nat. Prod.* 74, 1111–1116. doi: 10.1021/np200050r

Conflict of Interest: The authors declare that the research was conducted in the absence of any commercial or financial relationships that could be construed as a potential conflict of interest.

Publisher's Note: All claims expressed in this article are solely those of the authors and do not necessarily represent those of their affiliated organizations, or those of the publisher, the editors and the reviewers. Any product that may be evaluated in this article, or claim that may be made by its manufacturer, is not guaranteed or endorsed by the publisher.

Advantages of publishing in Frontiers

OPEN ACCESS
Articles are free to read for greatest visibility and readership

FAST PUBLICATION
Around 90 days from submission to decision

HIGH QUALITY PEER-REVIEW
Rigorous, collaborative, and constructive peer-review

TRANSPARENT PEER-REVIEW
Editors and reviewers acknowledged by name on published articles

Frontiers
Avenue du Tribunal-Fédéral 34
1005 Lausanne | Switzerland

Visit us: www.frontiersin.org
Contact us: frontiersin.org/about/contact

REPRODUCIBILITY OF RESEARCH
Support open data and methods to enhance research reproducibility

DIGITAL PUBLISHING
Articles designed for optimal readership across devices

FOLLOW US
@frontiersin

IMPACT METRICS
Advanced article metrics track visibility across digital media

EXTENSIVE PROMOTION
Marketing and promotion of impactful research

LOOP RESEARCH NETWORK
Our network increases your article's readership